



**A University of Sussex PhD thesis**

Available online via Sussex Research Online:

<http://sro.sussex.ac.uk/>

This thesis is protected by copyright which belongs to the author.

This thesis cannot be reproduced or quoted extensively from without first obtaining permission in writing from the Author

The content must not be changed in any way or sold commercially in any format or medium without the formal permission of the Author

When referring to this work, full bibliographic details including the author, title, awarding institution and date of the thesis must be given

Please visit Sussex Research Online for more information and further details

# Characterization of single vesicle recycling kinetics and other presynaptic properties at small central terminals

Milena Maria Wagner

Submitted for the degree of Doctor of Philosophy  
University of Sussex

September 2016

## Declaration

I hereby declare that this thesis has not been and will not be, submitted in whole or in part to another University for the award of any other degree.

Signature:

Milena Maria Wagner

**This thesis is dedicated to the loving memory of my father  
Dariusz Wagner (1961-1997).**

“Do not go gentle into that good night,  
Old age should burn and rave at close of day;  
Rage, rage against the dying of the light”

*Dylan Thomas*



## Acknowledgements

I wish to express my gratitude to my principal supervisor Kevin Staras for his help, advice and guidance throughout my PhD. Thank you for imparting your knowledge and expertise on the subject, and for keeping my wild experimental ideas in check. I would also like to thank my secondary supervisors Guy Richards for his advice and helpful comments, and Louise Serpell who is a great inspiration to me, and whose support helped me to get through times of self-doubt.

I am also grateful to Freya Crawford, Arjuna Ratnayaka and Vincenzo Marra, for sharing with me their laboratory know-how at the early stages of my PhD, and to Julian Thorpe for his assistance with electron microscopy. Thank you to George Kemenes for trusting me with his EMCCD camera.

It's been an absolute pleasure to share the laboratory with Catherine Smith and Stephanie Rey, with whom I made a strong and valued bond over the past years. Thank you for being great friends, engaging scientific and non-scientific conversations (with more of the latter), for helping to nurture my madness and for your support in the lab. My time at Sussex wouldn't be so enjoyable without my wonderful friends and colleagues: Kate Fennell, Karen Marshall, Devkee Vadukul, Mahmoud Bukar Maina, and Luca Biasetti with whom I shared the office and my scientific journey. Also, thank you to all the colleagues in the bouldering group. I will fondly reminisce our struggles at the wall.

Finally, I would like to express my gratitude to those closest to my heart. Thank you to all my friends, especially Francesca Arena and Haden Callow, for being there for me, letting me to go on about my life and for always offering consolation when needed. I am eternally grateful to my mum and grandma for their unconditional love, support and patience throughout all my studies; for always being there for me and for enabling and encouraging me to do things that I am passionate about. I would like to thank my future parents in law for their love, support and kindness during this stressful time. To my fiancée, Jon Fowler, thank you for all your love and support, for inspiring me every day with your ideas, and for nurturing the creative part of me and the spirit of adventure. You have been an extremely important part of this and I could not imagine doing PhD without you by my side.

I am truly grateful to you all!

# University of Sussex

Milena Maria Wagner

Submitted for the degree of Doctor of Philosophy

## Characterization of single vesicle recycling kinetics and other presynaptic properties at small central terminals

### Abstract

Sustained neural activity critically relies on the ongoing function of small central synapses. In particular, activity-driven fusion and recycling of neurotransmitter-filled vesicles at presynaptic terminals are key processes responsible for information transfer. Despite the fact that vesicle exocytosis and endocytosis are of great interest, the mechanisms of their regulation are still poorly understood. Moreover, hippocampal synapses exhibit high levels of variability in their structure and function, but the basis for this remains unclear. The aim of this work was to investigate these fundamental properties and establish key rules of regulation. Specifically, we wanted to test whether the timing of endocytosis of single synaptic vesicles was characteristic at individual boutons, and to investigate structural and molecular properties of synapses that underlie their particular behaviour. To explore this, we used a variety of optical imaging techniques in rat hippocampal neurons based on acutely applied probes such as FM1-43 dye, fluorescently tagged antibodies and genetically encoded reporters of presynaptic function, as well as ultrastructural readouts using electron microscopy. We found that although the timing of vesicle retrieval, measured with the optical reporter sypHy2x, was highly variable across the population of synapses, individual boutons showed signature endocytic kinetics. We also uncovered the properties of synapses that determine this behaviour, and demonstrated that these could be modulated, leading to predictable changes in the timing of recycling. These findings offer new insights into the rules that govern the function of presynaptic terminals. A second related objective examined whether amyloid beta, the misfolding protein implicated in Alzheimer's disease, causes changes that are detrimental for efficient vesicle recycling. We showed that oligomeric amyloid beta 1-42 impaired endocytosis and disrupted other related presynaptic processes. We suggest that vesicle recycling mechanisms are important target substrates in Alzheimer's disease providing potential new avenues for development of therapeutic approaches.

## Table of Contents

Declaration .....	2
Acknowledgements.....	4
Abstract .....	5
Table of Contents .....	6
List of Figures .....	10
Abbreviations.....	13

### CHAPTER 1

<b>1 INTRODUCTION .....</b>	<b>15</b>
<b>1.1 Neurons and synapses: building blocks of the nervous system .....</b>	<b>15</b>
<b>1.2 Synapse structure .....</b>	<b>16</b>
1.2.1 The presynaptic terminal .....	18
1.2.1.1 Ultrastructure and organization .....	18
1.2.1.2 Molecular composition and protein sorting .....	21
<b>1.3 Synaptic vesicle cycle .....</b>	<b>26</b>
1.3.1 Synaptic vesicle exocytosis .....	27
1.3.1.1 Variation in quantal size .....	29
1.3.2 Synaptic vesicle endocytosis.....	31
1.3.2.1 Clathrin-mediated endocytosis .....	32
1.3.2.2 Kiss-and-run endocytosis.....	34
1.3.2.3 Ultrafast endocytosis and bulk endocytosis.....	36
1.3.2.4 Kinetics of endocytosis and the predominant mode of endocytosis at hippocampal synapses.....	37
1.3.3 Exocytosis-endocytosis coupling.....	39
1.3.4 Synaptic vesicle identity .....	41
<b>1.4 Synaptic vesicle pools .....</b>	<b>43</b>
1.4.1 Regulation of vesicle pool sizes .....	45
<b>1.5 Presynaptic dysfunction in disease .....</b>	<b>48</b>
1.5.1 Alzheimer's disease and presynaptic function .....	49
<b>1.6 Tools for monitoring presynaptic function .....</b>	<b>50</b>
1.6.1 Acutely applied probes .....	51
1.6.1.1 FM dyes.....	51
1.6.1.2 Fluorescently tagged antibody - sytI-Oyster550 .....	53
1.6.2 Genetically encoded fluorescence probes .....	53
1.6.2.1 sypHy .....	54
1.6.2.2 vGlut1-pHluorin.....	55
1.6.2.3 syGCaMP .....	55
1.6.2.4 iGluSnFR .....	57
<b>1.7 Aims.....</b>	<b>58</b>

### CHAPTER 2

<b>2 METHODS AND MATERIALS .....</b>	<b>60</b>
<b>2.1 Animal Handling .....</b>	<b>60</b>
<b>2.2 Dissociated rat hippocampal cell culture.....</b>	<b>60</b>
2.2.1 Coverslip preparation and plating astrocyte feeder layer .....	61
2.2.2 Dissection .....	62

2.2.3 Culturing hippocampal neurons .....	63
<b>2.3 Transfection of hippocampal neurons .....</b>	<b>64</b>
<b>2.4 Infection of hippocampal neurons with AAV-based constructs.....</b>	<b>66</b>
<b>2.5 Plasmid DNA amplification and purification.....</b>	<b>67</b>
<b>2.6 Imaging system .....</b>	<b>69</b>
<b>2.7 Field stimulation .....</b>	<b>70</b>
2.7.1 Calibration of stimulation intensity .....	71
<b>2.8 FM1-43 and live antibody labelling protocols .....</b>	<b>75</b>
<b>2.9 Measuring synaptic vesicle pool sizes .....</b>	<b>76</b>
<b>2.10 Pharmacological disturbance of endocytic kinetics .....</b>	<b>78</b>
<b>2.11 Immunocytochemistry.....</b>	<b>78</b>
<b>2.12 Electron microscopy .....</b>	<b>80</b>
2.12.1 Fixation .....	81
2.12.2 Photoconversion of DAB .....	81
2.12.3 Sample preparation for electron microscopy.....	82
2.12.4 Region identification and serial sectioning .....	82
2.12.5 Imaging .....	83
<b>2.13 Image analysis .....</b>	<b>83</b>
2.13.1 Fluorescence.....	83
2.13.2 TEM micrographs.....	84
<b>2.14 Amyloid Beta preparation .....</b>	<b>85</b>
<b>2.15 Statistical analysis.....</b>	<b>86</b>

## CHAPTER 3

### 3 ESTABLISHING IMAGING METHODS USED FOR STUDYING FUNCTION OF PRESYNAPTIC TERMINALS.....

<b>3.1 Introduction.....</b>	<b>88</b>
<b>3.2 Fluorescent tools used to readout properties of recycling vesicles.....</b>	<b>89</b>
3.2.1 Culturing primary hippocampal neurons .....	89
3.2.2 Labelling of synapses with FM1-43 dye.....	92
3.2.3 Functional readout using FM1-43 dye .....	94
3.2.4 Labelling of synapses with sytl-Oyster550.....	96
<b>3.3 Genetically encoded probes of synaptic function.....</b>	<b>100</b>
3.3.1 Readout of synaptic vesicle exo and endocytosis with sypHy2x.....	100
3.3.1.1 Comparison of sypHy1x, sypHy2x and sypHy4x constructs.....	103
3.3.2 Measuring exo- and endocytosis at excitatory synapses using vGlu1-pHluorin .....	106
3.3.3 SyGCaMP6f allows to monitor presynaptic Ca <sup>2+</sup> influx .....	107
3.3.4 Detecting glutamate release with iGluSnFR .....	110
<b>3.4 Discussion .....</b>	<b>113</b>
3.4.1 The use of acutely applied fluorescence probes in hippocampal neurons .....	113
3.4.2 Genetically encoded reporters of synaptic function .....	116
3.4.2.1 Measuring synaptic vesicle recycling .....	116
3.4.2.2 Monitoring of glutamate release and presynaptic Ca <sup>2+</sup> influx.....	119
3.4.3 Other available tools for studying presynaptic function .....	120

**CHAPTER 4**

<b>4 CHARACTERIZATION OF SINGLE VESICLE ENDOCYTOSIS.....</b>	<b>123</b>
<b>4.1 Introduction.....</b>	<b>124</b>
<b>4.2 Heterogeneity in the timing of synaptic vesicle endocytosis amongst synapses.....</b>	<b>126</b>
4.2.1 High variability in endocytosis following RRP mobilizing stimulus.....	126
4.2.2 Examining the possible source of variability .....	130
4.2.3 High variability between synapses of the same type.....	132
<b>4.3 Synapse-specific timing of single vesicle endocytosis .....</b>	<b>136</b>
4.3.1 Visualization of single vesicle release events .....	136
4.3.2 Variability in fluorescence retrieval after stimulation evoked release events ..	140
4.3.3 Establishing method for measuring single vesicle kinetics.....	142
4.3.4 Behaviour of single vesicles at individual synapses.....	145
4.3.5 Measuring the homogeneity of behaviour of vesicles at individual synapses..	146
4.3.5.1 Point-by-point analysis .....	149
4.3.5.2 Rate analysis .....	154
4.3.6 Experimental factors that may impact on the results.....	157
<b>4.4 Discussion .....</b>	<b>161</b>
4.4.1 Variability in synaptic vesicle endocytosis .....	161
4.4.2 Synapse-specific vesicle retrieval timing .....	163
4.4.3 Establishing quantal size .....	164
4.4.4 Synapse-specific kinetics of single vesicle endocytosis.....	167

**CHAPTER 5****5 THE INVESTIGATION OF SYNAPTIC CHARACTERISTICS THAT UNDERLIE THEIR ENDOCYTIC BEHAVIOUR.....**

<b>5.1 Introduction.....</b>	<b>171</b>
<b>5.2 Properties of small and large synapses.....</b>	<b>172</b>
5.2.1 Larger synapses exhibit faster rate of endocytosis .....	172
5.2.2 Homeostatic scaling as a form of modulation of synaptic properties.....	175
5.2.2.1 Measuring synaptic vesicle pool sizes .....	175
5.2.2.2 Correlation between presynaptic size and the rate of endocytosis ....	179
5.2.2.3 Modulation of synaptic size and its effect on endocytic rate .....	181
5.2.2.4 Comparison of synapses from the same population.....	184
5.2.3 Large synapses have tendency to more variable kinetics.....	188
5.2.4 Variability in the amount of soluble protein between synapses of various sizes .....	189
<b>5.3 Modulation of synaptic behaviour with dynasore .....</b>	<b>193</b>
5.3.1 Dynasore decreases the rate of endocytosis .....	193
5.3.2 Similarity measure of synapses treated with dynasore .....	196
<b>5.4 TEM analysis of presynaptic properties .....</b>	<b>199</b>
5.4.1 Establishing loading protocols .....	200
5.4.2 TEM procedure and identification of fluorescence region on the resin block...	203
5.4.3 Visualization of sypHy2x-expressing, functional synapses at the ultrastructural level and 3D reconstruction .....	206
5.4.4 Robust method for identification of photoconverted vesicles .....	210
5.4.5 Photoconverted vesicles under different stimulation conditions .....	213

5.4.6 Ultrastructural correlates of synapse-specific behaviour .....	216
5.4.7 Difference in vesicle density between small and large synapses .....	219
<b>5.5 Discussion .....</b>	<b>222</b>
5.5.1 Synaptic size determines presynaptic properties .....	222
5.5.1.1 Rate of endocytosis scales with synaptic size .....	224
5.5.1.2 Larger synapses exhibit higher variability in their properties .....	225
5.5.2 Timing of endocytic kinetics is determined by the fission of the vesicles from the membrane .....	228
5.5.3 Density of synaptic vesicles in synapses of various sizes .....	229
5.5.4 Concluding remarks and future directions .....	231
 <b>CHAPTER 6</b>	
<b>6 THE EFFECTS OF AMYLOID BETA 1 - 42 ON FUNCTION OF PRESYNAPTIC TERMINALS.....</b>	<b>232</b>
6.1 Introduction.....	233
6.2 FM dye imaging of cells treated with 1 $\mu$ M A $\beta$ 1-42 for 24 hours .....	237
6.2.1 The effect of A $\beta$ 1-42 on the number functional presynaptic terminals.....	237
6.2.2 The effect of A $\beta$ 1-42 on synaptic function .....	239
6.3 Treatment with 1 $\mu$ M A $\beta$ 1-42 for 24 hours affects synaptic vesicle cycle .....	242
6.3.1 A $\beta$ 1-42 affects the kinetics of endocytosis.....	243
6.3.2 The effect of A $\beta$ 1-42 is more pronounced in larger responses.....	246
6.3.3 vA $\beta$ has no effect on the rate of endocytosis .....	250
6.4 24 hour treatment with 0.1 $\mu$ M A $\beta$ 1-42 had no effect on synaptic vesicles endocytosis .....	252
6.5 The effect of 1 $\mu$ M A $\beta$ 1-42 on single vesicle endocytosis.....	254
6.6 The effect of 1 $\mu$ M A $\beta$ 1-42 on stimulation evoked Ca <sup>2+</sup> influx.....	257
6.6.1 The effect of 1 $\mu$ M A $\beta$ 1-42 on Ca <sup>2+</sup> influx at larger stimulations .....	257
6.6.1.1 Sub selection of responses within the same baseline range .....	260
6.6.1.2 Sub selection of responses with the same response size .....	263
6.6.2 The effect of 1 $\mu$ M A $\beta$ 1-42 on Ca <sup>2+</sup> influx in response to minimal stimulus .....	265
6.7 Discussion .....	267
6.7.1 Oligomeric A $\beta$ 1-42 reduces the number of functional synapses .....	268
6.7.2 Oligomeric A $\beta$ 1-42 affects synaptic vesicle exocytosis .....	269
6.7.3 Oligomeric A $\beta$ 1-42 affects synaptic vesicle endocytosis .....	272
6.7.4 Model of A $\beta$ 1-42 toxicity in presynaptic terminals .....	274
6.7.5 Summary and future directions.....	276
 <b>CHAPTER 7</b>	
<b>7 GENERAL DISCUSSION .....</b>	<b>278</b>
7.1 Synapse specific timing of single vesicle retrieval kinetics .....	282
7.2 Presynaptic properties that determine kinetics of single vesicle endocytosis .....	284
7.3 Conclusions and future experiments .....	288
 Bibliography.....	290
Appendix I.....	310
Appendix II.....	317

## List of Figures

Figure 1.1 Synapse structure .....	17
Figure 1.2 3D models of organization of presynaptic proteins. ....	25
Figure 1.3 Summary of major steps in synaptic vesicle cycle.....	26
Figure 1.4 Summary of the process of synaptic vesicle exocytosis .....	28
Figure 1.5 Summary of clathrin-mediated endocytosis of synaptic vesicles .....	34
Figure 1.6 Comparison of functional fluorescence readouts of CME and kiss-and-run kinetics .....	35
Figure 1.7 Schematic summary of different modes of endocytosis at hippocampal synapses .....	39
Figure 1.8 Summary of classification of synaptic vesicle pools. ....	47
Figure 2.1 Schematic representing timeline of culturing protocol of rat hippocampal neurons. ....	61
Figure 2.2 Stimulation and imaging chamber. ....	71
Figure 2.3 Establishing optimal stimulation intensity using OGB. ....	74
Figure 2.4 Loading and imaging protocol with FM1-43 dye for labelling vesicles in the recycling pool and FM dye destaining. ....	75
Figure 2.5 The summary of the protocol measuring the size of synaptic vesicle pools. ....	77
Figure 3.1 Successful culturing of primary hippocampal neurons.....	91
Figure 3.2 Visualization of hippocampal synapses loaded with FM1-43.....	93
Figure 3.3 Functional readout of synaptic vesicles exocytosis with FM1-43 .....	95
Figure 3.4 Readout of presynaptic properties with sytl-Oyster550 .....	99
Figure 3.5 Detection and measuring of synaptic responses using sypHy2x .....	103
Figure 3.6 Comparison between sypHy constructs with varied number of fused pHluorins .....	105
Figure 3.7 Detection and measuring synaptic response with vGlu-pHluorin (vGpH). ....	107
Figure 3.8 Detection of presynaptic $\text{Ca}^{2+}$ influx with syGCaMP6f .....	109
Figure 3.9 iGluSnFR allows to monitor the release of glutamate at presynaptic terminals.....	112
Figure 4.1 Variability in the kinetics of synaptic responses to 40 APs, 20 Hz stimulus (sypHy2x readouts).....	129
Figure 4.2 The rate of synaptic vesicle endocytosis does not depend on the baseline fluorescence or the response amplitude .....	131
Figure 4.3 Responses to 40 APs, 20 Hz stimulation show high variability in retrieval kinetics in the population of glutamatergic synapses.....	135
Figure 4.4 Establishing fluorescence amplitude of single vesicle release events .....	140
Figure 4.5 Variability in the synaptic responses to 4 APs stimulation .....	142
Figure 4.6 Selection of the best function describing endocytic retrieval following single vesicle fusion events.....	144
Figure 4.7 Individual synapses exhibit signature endocytosis kinetics.....	146

Figure 4.8 Quantification of similarity in single vesicle kinetics at individual boutons.	149
Figure 4.9 Quantification of similarity in single vesicle kinetics at individual boutons II	153
Figure 4.10 Quantification of the similarity in the rate of endocytosis within individual presynaptic terminals	156
Figure 4.11 Signature endocytic kinetics at individual synapses	157
Figure 4.12 Imaging and other experimental factors	160
Figure 5.1 SyHy2x baseline fluorescence reflects the size of the synapse	174
Figure 5.2 Measuring the size of RRP, recycling and total vesicle pools	178
Figure 5.3 Relationship between the synaptic size and the rate of endocytosis	181
Figure 5.4 Modulation of synaptic properties with CNQX.	184
Figure 5.5 Comparison of endocytic kinetics in limited population of synapses	187
Figure 5.6 Relationship between the size of the synapse and variability in endocytic kinetics	189
Figure 5.7. The expression of endophilin I in small and large synapses	192
Figure 5.8 The effect of 5 $\mu$ M dynasore on the kinetics of endocytosis	195
Figure 5.9 The effect of dynasore treatment on single vesicle endocytic similarity within individual synapses	198
Figure 5.10 Comparison of the level of loading FM1-43 loading following 40 APs and 10 APs stimulus	202
Figure 5.11 Selection of syHy2x expressing region for TEM analysis and its relocalization following embedding	205
Figure 5.12 Example of correlative approach allowing to visualize syHy2x expressing terminal under TEM	208
Figure 5.13 An example 3D reconstruction of a fluorescently imaged synapse	209
Figure 5.14 Identification of photoconverted vesicles on electron micrographs	212
Figure 5.15 Quantification of PC+ vesicles in 40 APs and 10 APs loaded samples	215
Figure 5.16 Ultrastructural presynaptic properties that correlate with synaptic behaviour	218
Figure 5.17 Small and large synapses differ in the density of synaptic vesicles	221
Figure 6.1 Quantification of functional boutons in A $\beta$ 1-42 treated cells.	239
Figure 6.2 A $\beta$ 1-42 affects synaptic vesicle exocytosis under 1200 APs stimulation protocol	241
Figure 6.3 The effect of 24 h 1 $\mu$ M A $\beta$ 1-42 treatment on synaptic vesicle exocytosis and endocytosis	245
Figure 6.4 Treatment with 1 $\mu$ M A $\beta$ 1-42 for 24 hours has effect on the kinetics of endocytosis only following larger responses	249
Figure 6.5 Treatment with 1 $\mu$ M vA $\beta$ for 24 hours had no effect on synaptic vesicles endocytosis	251
Figure 6.6 The effect of 24 hour 0.1 $\mu$ M A $\beta$ 1-42 treatment on synaptic vesicle exocytosis and endocytosis	253



Figure 6.7 A $\beta$ 1-42 does not affect the kinetics of endocytosis following single vesicle release events .....	256
Figure 6.8 Measurements of A $\beta$ 1-42 effect on stimulation evoked presynaptic Ca <sup>2+</sup> influx.....	259
Figure 6.9 The effect of A $\beta$ 1-42 on Ca <sup>2+</sup> influx in population of synapses of similar size .....	262
Figure 6.10 The effect of A $\beta$ 1-42 on Ca <sup>2+</sup> influx in population of synapses of similar response amplitude .....	264
Figure 6.11 A $\beta$ 1-42 leads to increased Ca <sup>2+</sup> influx in response to 4 APs stimulation.	266
Figure 6.12 Summary of signalling pathways identified to be affected in Alzheimer's Disease – "AlzPathway".....	268
Figure 7.1 Summary of presynaptic properties and correlates associated with endocytic timing at small and large synapses .....	281
Figure 7.2 Model summarising the difference in endocytic timing at small and large synapses .....	287

## Abbreviations

AD	Alzheimer 's disease
AP5	D-(-)-2-amino-5-phosphonopentanoic acid
APs	action potentials
ara-C	cytosine- $\beta$ -D-arabinofuranoside
AZ	active zone
A $\beta$	amyloid-beta peptide
baf	bafilomycin A1
BDNF	brain-derived neurotrophic factor
BME	Basal Medium Eagle
BSA	Bovine Serum Albumin
CaN	Calcineurin
CDK5	cyclin-dependent kinase 5
CME	clathrin-mediated endocytosis
CNQX	6-cyano-7-nitroquinoxaline-2,3-dione
DAB	3,3-diaminobenzidine
DIC	differential interference contrast
DMSO	dimethyl sulfoxide
EBS	external bath solution
FBS	Foetal Bovine Serum
GECIs	genetically encoded calcium indicators
GEVIs	genetically encoded voltage indicators
h	hour
HBSS	Hanks Balanced Salt Solution
HEPES	4-(2-hydroxyethyl)piperazine-1-ethanesulfonic acid
HFIP	1,1,1,3,3,3-hexafluoro-2-propanol
HRP	horseradish peroxidase
iGluSnFR	intensity based glutamate-sensing fluorescence receptor
MEPPs	miniature end plate potentials
mEPSCs	miniature excitatory postsynaptic currents
min	minute
M $\beta$ CD	methyl- $\beta$ -cyclodextrin
OGB	oregon green
PBS	Phosphate Buffered Saline
PC-	non-photoconverted vesicle

PC+	photoconverted vesicle
PDL	poly-D-lysine
PFA	paraformaldehyde
PI(4,5)P <sub>2</sub>	phosphatidylinositol 4,5-bisphosphate
PKC	protein kinase C
$p_r$	probability of release
PSD	postsynaptic density
Qdots	quantum dots
ROI	region of interest
RRP	readily releasable pool
RSRS	random synapse rate similarity
RSS	random synapse similarity
RtP	resting pool
s	second
SNARE	soluble NSF attachment receptor
STED	stimulated emission depletion
Stn2	stonin 2
STORM	stochastic optical reconstruction microscopy
SVs	synaptic vesicles
sytl	synaptotagmin I
TEM	transmission electron microscopy
TRP	total recycling pool
TTX	tetrodotoxin
v-ATPase	vacuolar proton-ATPase
vGlut	vesicular glutamate transporter
vGpH	vGlut1-pHluorin
WSRS	within synapse rate similarity
WSS	within synapse similarity

# 1 INTRODUCTION

---

## 1.1 Neurons and synapses: building blocks of the nervous system

The function of our brain, relies on the efficient transfer of information between the specialized cells called neurons, which were first described as a basic structural component of the nervous system by Santiago Ramon y Cajal (Glickstein, 2006). Neurons form highly complex, dynamic networks and communicate with each other via synapses. The term describing this anatomically distinct structure was first introduced by Charles Sherrington in 1897 and was derived from Greek words “syn” – together and “haptein” - join (Bennett, 1999). Synapses are structurally and molecularly specialized connection points which rapidly pass on signals, in the form of released neurotransmitter, from one neuron to another or from a neuron to a target tissue (e.g. muscle fibres). Synaptic dysfunction has been indicated as an underlying cause of symptoms in various neurological diseases (Marcello et al., 2012; Picconi et al., 2012; Zoghbi and Bear, 2012). Synapses not only convey the information between neurons, but are also responsive to the history of their own activity, the demands of the network, and are capable of adjusting their structure and function in various forms of plasticity (Hopf et al., 2002; O’Rourke et al., 2012; Regehr, 2012). They are therefore critical sites for the effective operation of our nervous system and hence studying their function is of great importance.

Interneuronal communication can take place via electrical or chemical synapses, nevertheless, the majority of communication in the mammalian CNS occurs via chemical synapses, on which this work focuses. The pioneering discoveries on the function of

presynaptic terminals were made in the early 1950s and 1960s in experiments on the frog neuromuscular junction. During electrophysiological measurements, the authors observed that the distribution of amplitudes of spontaneous miniature end-plate potentials (MEPPs) revealed unitary nature of synaptic responses (Del Castillo and Katz, 1954; Fatt, and Katz, 1952). This quantal nature of MEPPs was later linked to the presence at ultrastructural level of small, membranous structures in presynaptic terminals - synaptic vesicles. These two findings combined led to the formulation of the quantal hypothesis of neurotransmitter release (De Robertis and Bennett, 1955; Palay, 1956). A more direct proof of concept, that a single synaptic vesicle contains a quantum of neurotransmitter and is responsible for the smallest unitary postsynaptic response, came from studies which combined stimulation with rapid freezing of the sample for electron microscopy (Heuser and Reese, 1973; Kononenko and Haucke, 2015; Miller and Heuser, 1984). Stimulus evoked release and loading of synaptic vesicles with horseradish peroxidase (HRP), which appears as a dense product on electron micrographs, provided the evidence that synaptic vesicle membrane is recycled back into the presynaptic terminal after neurotransmitter release via clathrin-mediated endocytosis (Heuser and Reese, 1973). The following years brought about significant advances in our knowledge on the structure, molecular composition and function of synapses.

## **1.2 Synapse structure**

Despite their functional differences (O'Rourke et al., 2012), chemical synapses share similar structural characteristics: in particular, a presynaptic terminal, postsynaptic compartment and a ~15-20 nm gap called the synaptic cleft that separates the two (Fig.1.1) (De Robertis and Bennett, 1955). The presynaptic compartment is characterized by the presence of neurotransmitter filled synaptic vesicles, which are

easily identifiable in electron micrographs, and some of which are docked at the active zone (AZ) (Südhof, 2012). The postsynaptic membrane of glutamatergic synapses can be identified by the presence of electron-dense postsynaptic density (PSD), which is composed of multiple membranous and cytoplasmic proteins and neurotransmitter receptors localized in a direct apposition to the release site of SVs (Fig.1.1) (Okabe, 2007). This organization ensures efficient information transfer between pre- and postsynaptic neuron.

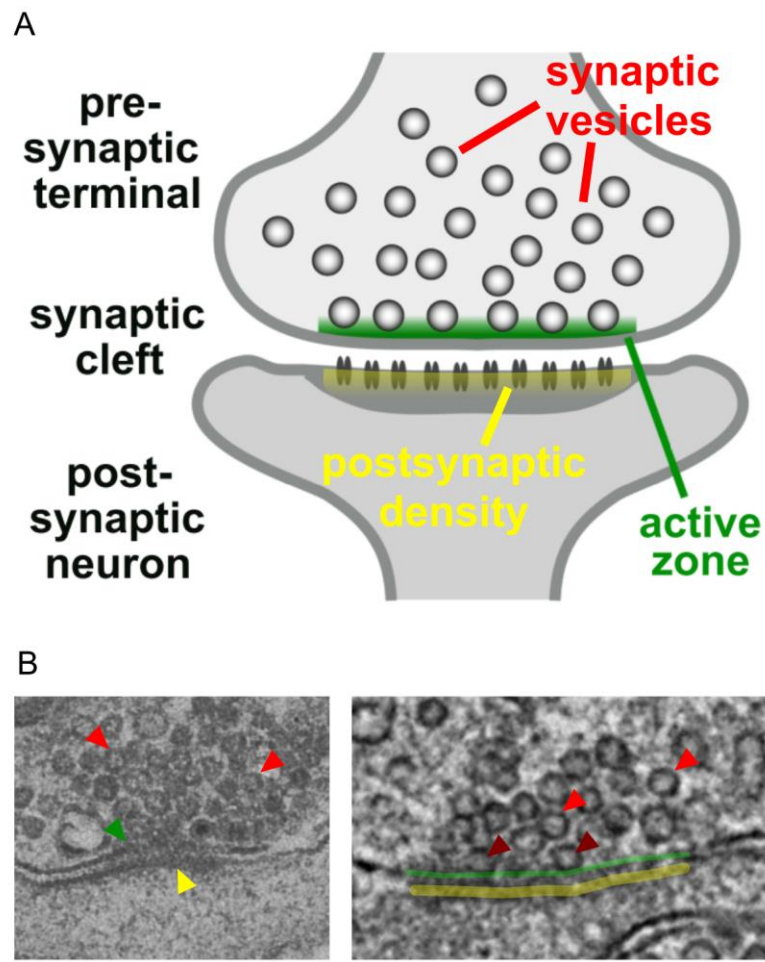


**Figure 1.1 Synapse structure.** A) Schematic showing major components of the synapse. Figure modified from (Südhof, 2012). B) Electron micrographs of hippocampal synapses. Green arrowhead and green line indicate active zone, yellow arrowhead and yellow line postsynaptic density, red arrowheads synaptic vesicles and dark red arrowheads docked synaptic vesicles. Scale bars, 100 nm.

## **1.2.1 The presynaptic terminal**

### **1.2.1.1 Ultrastructure and organization**

The most prominent ultrastructural feature of presynaptic terminals, allowing us to unequivocally recognize this cellular compartment, is the presence of small, round membranous structures – synaptic vesicles (SVs) (Fig.1.1). They were identified in the electron micrographs of synapses from frog and earthworm (De Robertis and Bennett, 1955), and also in rat tissue (Palay and Palade, 1955). These neurotransmitter filled structures release their neurotransmitter content into the synaptic cleft in an activity dependent manner. In rat hippocampal neurons the average diameter of SVs was found to be ~40 nm with an inner diameter of ~23 nm, and an overall variation in size ranging from 20 to 66 nm (Harata et al., 2001; Harris and Sultan, 1995; Schikorski and Stevens, 1997). The size of synaptic vesicles is thought to be determined by the need to accommodate structures necessary for their function. For example, vesicles which were missing glutamate transporters were found to be smaller than those expressing this protein (Daniels et al., 2006). Some of the vesicles appear to be in a direct contact with the active zone, which is in turn aligned with the PSD, and are referred to as docked vesicles (Fig.1.1). These associated with the AZ vesicles were found to be slightly smaller in diameter (23-49 nm) than the non-docked vesicles (20-60 nm) (Harris and Sultan, 1995). However, the opposite observation was made in a hippocampal preparation in a more recent study using high pressure freezing as a fixation method (Fernández-Busnadiego et al., 2010). These differences might be due to the specific experimental approach and the fixation technique used. In a study carried out by Harris & Sultan 1995, the tissue was fixed with 2% paraformaldehyde/2.5% glutaraldehyde, which might have led to the release of some of the vesicle content at the time of fixation (Harris and Weinberg, 2012). The other study on the other hand used high pressure freezing as a method of fixation (Fernández-Busnadiego et al., 2010).

The cryo-electron tomography revealed that SVs are organized into clusters of as little as 2 or up to around 50 vesicles interconnected via filamentous connectors with more than 20 such vesicle clusters per terminal (Fernández-Busnadiego et al., 2010). It has been hypothesized that the filaments that connect SVs into clusters might be composed of synapsin (Siksou et al., 2007). Indeed, synapsin was later found to be an important regulator of vesicle clustering providing link between the SVs and the actin cytoskeleton (Orenbuch et al., 2012). Nevertheless the exact composition of these connectors and the clustering mechanisms of SVs are still debated (Shupliakov et al., 2011).

Fernández-Busnadiego et al. 2010 also showed that most docked vesicles were not in a direct contact with the presynaptic membrane, as previously thought, but instead were attached to AZ via short tethers (Fernández-Busnadiego et al., 2010). On the other hand, Watanabe et al., 2013 in a technique combining optogenetic stimulation with rapid high-pressure freezing of the samples observed that vesicles were indeed in a direct contact with the plasma membrane and identified these as docked vesicles. These authors also reported the presence of vesicles which were in close apposition to the plasma membrane and attached to it via ~30 nm long tethers (Watanabe et al., 2013). The extent of the connectivity between vesicles was linked to the activity state of the synapses, with resting synapses exhibiting higher extent of clustering (Fernández-Busnadiego et al., 2010). This shows the dynamic relationship between structure and function of presynaptic terminals, and that structural adjustments that are being made depend on the activity state of the boutons.

In addition to small, neurotransmitter filled vesicles, other round membranous structures can be found at presynaptic terminals: endosomes (60 -100 nm) and large dense core vesicles (80 -120 nm). Nevertheless, these are much less abundant than the small SVs (Aravanis et al., 2003; Harris and Weinberg, 2012). Similarly, mitochondria were found in only half of the synapses in hippocampal neurons (Shepherd and Harris, 1998).



Various structural presynaptic parameters not only showed strong correlations with each other, but were also linked with the functional characteristics of presynaptic terminals. One of the most important of functional presynaptic properties, which sets the synaptic strength, is the probability of release ( $p_r$ ); that is, the likelihood of a release of a single vesicle upon the arrival of nerve impulse (Branco and Staras, 2009; Murthy et al., 1997). A detailed analysis of the relationship between the function and structure of individual hippocampal synapses, using a correlative transmission electron microscopy (TEM) approach, revealed that  $p_r$  was strongly correlated with the number of docked vesicles at the AZ (Branco et al., 2010). In another study, the number of docked vesicles was shown to scale linearly with the AZ area and the probability of release, hence  $p_r$  has also has been linked with the active zone area (Holderith et al., 2012). This can be extrapolated further. Smaller synapses (200 +) were found to have 2-6 docked vesicles, whereas larger synapses had 13-16 docked vesicles out of a total pool of 450 or more vesicles (Harris and Sultan, 1995). Taken together, larger synapses, with higher number of SVs, would be expected to display a higher  $p_r$  than the small synapses. Nevertheless, this relationship was found not true, which was attributed to the high variability in the size of recycling versus total vesicle pool at individual synapses (Branco et al., 2010). This sets the scene of an enormous complexity of the relationships between presynaptic parameters that determine their function. These structural relationships are not only valid in hippocampal synapses, but also in other systems. Detailed analysis of morphological features in ventral horn boutons revealed that many properties such as AZ number and area, mitochondrial volume or vesicle number scaled positively with synaptic size (Pierce and Mendell, 1993).

Despite the fact that these relationships between presynaptic parameters were found, the authors often commented on the large heterogeneity in the structural and functional properties within homogenous populations of synapses (Branco et al., 2010; Harris and Sultan, 1995; Holderith et al., 2012; Murthy et al., 1997; Pierce and Mendell, 1993)

highlighting the need for further exploration of function-determining presynaptic properties.

#### **1.2.1.2 Molecular composition and protein sorting**

Presynaptic terminals are not only characterized by complex structure but also by a huge abundance and variety of proteins, all serving very specific functions. Despite the fact that the role of many of the individual SVs proteins has been extensively studied, there is not much information on the overall protein composition of SVs. Three comprehensive studies in the last decade were carried out providing with a detailed analysis of the presynaptic proteins (Burré et al., 2006; Takamori et al., 2006; Wilhelm et al., 2014). Synaptosomal preparation was used in each case, allowing the determination of parameters such as copy number of a given protein per vesicle or their subcellular distribution and organization. Based on that data, 3D representations of presynaptic and vesicular architecture were created (Fig.1.2).

The analysis of the protein composition of purified synaptic vesicles with mass spectrometry revealed 410 different proteins, of which at least 80 were identified as integral membrane proteins (Takamori et al., 2006). This points towards a huge molecular diversity and complexity within these small organelles. Proteins important for exocytosis and endocytosis of synaptic vesicles were found to be present in high numbers: 70, 32, 9-14, 10, 8 and 15 copies of synaptobrevin, synaptophysin, neurotransmitter transporters, Rab3A, synapsin and synaptotagmin, respectively (Takamori et al., 2006). Nevertheless, synaptic vesicles contained only a single copy of vacuolar proton-ATPase (v-ATPase), which suggests that some vesicles might occasionally fail to contain this important for reacidification protein, and as a result lack neurotransmitter (Takamori et al., 2006).

Some proteins were shown to directly scale with certain structural components. RIM proteins, localized to AZ, are important regulators of the number of docked vesicles and for coupling of  $\text{Ca}^{2+}$  to SVs, which makes them of value for the maintenance of efficient transmitter release (Han et al., 2011). The number of RIM1/2 proteins and of voltage-gated calcium channel subunit Cav2.1 was also strongly correlated with the area of AZ (Holderith et al., 2012) demonstrating an association between the molecular composition and the structural elements. Other presynaptic proteins show strong correlation with each other and a precise ratio of the two is critical for efficient vesicle recycling. Synaptophysin and synaptobrevin form large complexes with a ratio of 1:2 and this ratio was critical for the correct trafficking of synaptobrevin to SVs and efficient synaptic performance (Gordon et al., 2016). The stoichiometry of these two proteins is also in agreement with upper mentioned copy numbers for the two proteins as reported by the Takamori et al., 2006 study. Wilhelm et al., 2014 demonstrated that the copy number of certain proteins scales linearly with synaptic size (measured against the amount of synaptophysin), whereas the copy number of others, in particular endocytic proteins, scales in an exponential manner, meaning that larger synapses have proportionally more of these proteins, than the small ones.

How is the precise copy number of various proteins maintained at presynaptic terminals and more importantly at the level of individual vesicles? This question is directly linked to the debate as to whether synaptic vesicles are recycled intact or whether some intermixing of the plasma membrane proteins occur when a new vesicle is internalized during endocytosis. This matter is discussed in section 1.3.4. Assuming that synaptic vesicles lose their identity during recycling to some extent, certain mechanisms should be in place to ensure appropriate protein sorting, allowing SVs to retain specific composition. It appears that some proteins are sorted with higher precision than others. Analysis of the intravesicular variability in protein composition was high for VAMP2/synaptobrevin 2, synaptophysin and synaptogyrin, whereas the copy number of

SV2, v-ATPase, vesicular glutamate transporter 1 (vGlut1) and synaptotagmin 1 were very uniform across vesicles (Mutch et al., 2011). It has been suggested that the proteins of which function is more redundant and replaceable by another protein are less strictly controlled than those with unique functions (Mutch et al., 2011). Certain proteins have been identified to preserve the composition of SVs. As an example, endocytic adaptor protein, stonin 2 (Stn2) was important for determining the subcellular distribution of synaptotagmin 1 (sytl) (Kononenko et al., 2013). In the absence of Stn2 in KO mice, sytl was missorted to the plasma membrane and despite the overall copy number of this protein remaining unchanged, this phenotype was associated with faster rate of endocytic retrieval of SVs in Stn2 KO neurons (Kononenko et al., 2013). The loss of Stn2 was not associated with compromised sorting of other proteins such as synaptophysin or synaptobrevin (Kononenko et al., 2013). This study shows the importance of precise control of not only copy numbers, but also subcellular distribution of proteins crucial for synaptic function. Other pairs of protein-mediated protein sorting include recruitment of VAMP2 by synaptophysin I (Pennuto et al., 2003) and localization and stabilisation of synaptotagmin by endophilin I (Schuske et al., 2003).

The complexity of protein composition of synaptic vesicles not only comes from the abundance of various proteins, but also from the presence of different isoforms. Weston et al., 2011 showed an important interaction between the 3 vGlut isoforms expressed in mammalian brain and endophilin I. Synaptic vesicles expressing vGlut1 were characterized by lower  $p_r$  due to its endophilin I binding ability and inhibition of endophilin I driven facilitation of SVs release, whereas vesicles containing vGlut2, which did not associate with endophilin, had high  $p_r$  (Weston et al., 2011). This shows how interactions between certain proteins specifically shape important aspects of presynaptic function.

Despite the structural-functional relationships discovered so far and the efforts invested into discovering the molecular composition of presynaptic terminals, the overall consensus is that presynaptic terminals show a large degree of heterogeneity in their

structure and function, and further investigation of the influence of ultrastructural diversity and molecular composition on the function is needed (Holderith et al., 2012). Proteomic analysis requires pooling together material from diverse synaptic populations and therefore does not allow to examine whether there are molecular difference between individual synapses (O'Rourke et al., 2012). Molecular diversity of synapses together with their structural characteristics might contribute to their specific behaviour and function within the network, and therefore are of great interest.

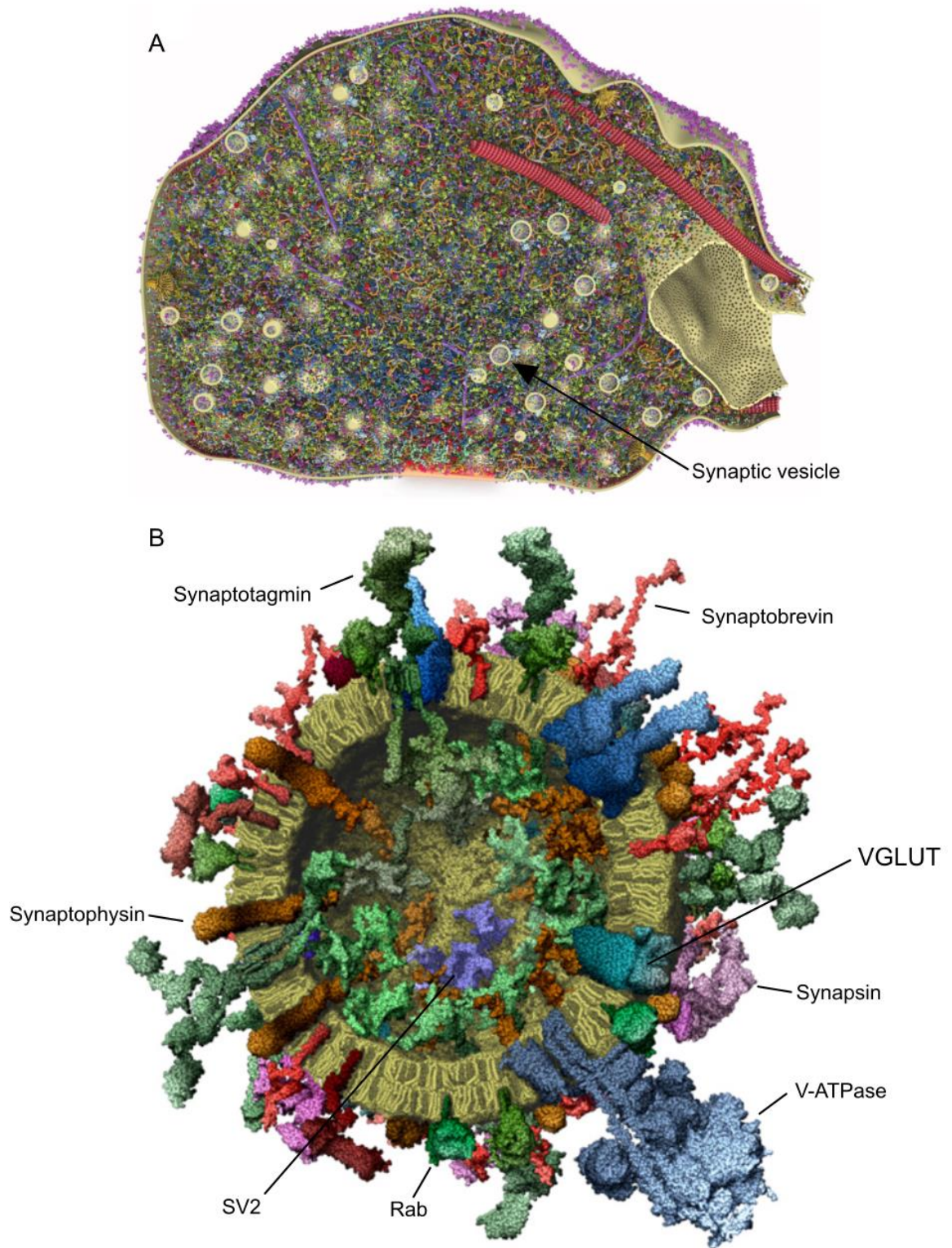


**Figure 1.2 3D models of organization of presynaptic proteins.** A) Presynaptic terminal (Figure from Wilhelm et al. 2014). B) Zoom view of a distribution of some synaptic vesicle proteins in a mid-section of SV (Figure modified from Takamori et al. 2006).

### 1.3 Synaptic vesicle cycle

The observation that synaptic vesicles recycle following their release was made in the frog neuromuscular junction. Electrophysiology was combined with electron microscopy to show that synaptic vesicles fuse with the membrane, release their neurotransmitter content and are subsequently reformed from the presynaptic membrane and stored at the terminal (Ceccarelli et al., 1973). The early studies on synaptic vesicle cycle concluded that the entire process from docking of synaptic vesicle to its availability at the active zone following endocytosis roughly takes a minute to complete (Betz and Bewick, 1992). There are two main steps in synaptic vesicle cycle: exocytosis – fusion of the SV with the plasma membrane and release of its neurotransmitter content, followed by endocytosis – reclamation of SVs via fission of presynaptic membrane and formation of new, functional vesicles (Fig.1.3).

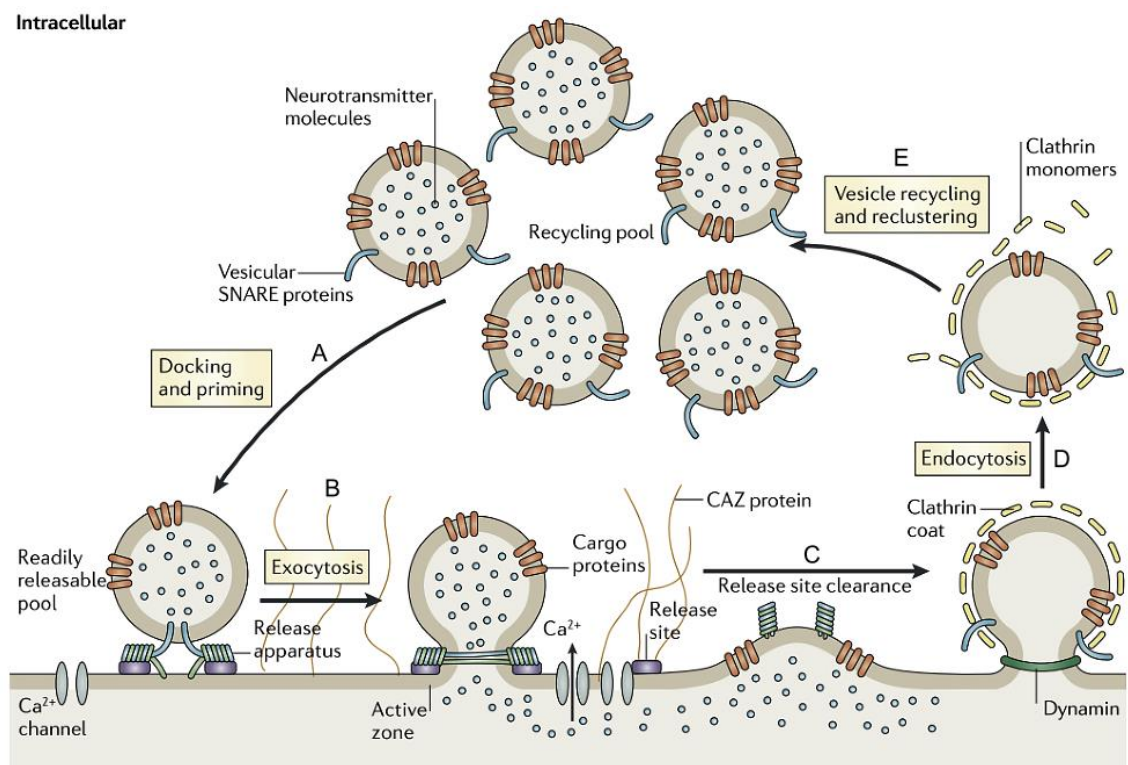


**Figure 1.3 Summary of major steps in synaptic vesicle cycle.** A) Some SVs undergo docking and later priming at the AZ. B) Influx of  $\text{Ca}^{2+}$  triggers fusion of the vesicles with the membrane and release of their neurotransmitter content. C) The vesicle membrane

collapses into the plasma membrane and it has to be cleared away from the release site to prevent clogging of the AZ with proteins. D) At a location peripheral to the AZ, new SVs vesicle are formed and reclaimed into the presynaptic terminal. E) These newly formed synaptic vesicles are reacidified and filled with neurotransmitter by specific vesicular neurotransmitter transporters and returned to the vesicle cluster. Figure modified from (Haucke et al., 2011)

### 1.3.1 Synaptic vesicle exocytosis

The exocytosis of SVs at the active zone is mediated by “soluble NSF attachment receptor proteins” (SNAREs) and Sec1/Munc18-like proteins (SM) (Südhof, 2013b). In order for the synaptic vesicle to fuse with the membrane, a helical *trans*-SNARE complex is formed between synaptic vesicle SNARE protein, synaptobrevin/VAMP, and plasma membrane SNAREs: syntaxin 1 and SNAP-25, which brings the vesicle membrane and AZ membrane in close proximity (Fig.1.4) (Rizzoli, 2014; Südhof and Rizo, 2011). It is thought that the subsequent interaction of the SM proteins with the *trans*-SNARE complex leads to the opening of the fusion pore and the release of neurotransmitter (Südhof and Rizo, 2011). The two membranes fuse, which is then followed by disassembly of the SNARE complex mediated by  $\alpha/\beta$ -SNAPs (Burgalossi et al., 2010; Haucke et al., 2011). It has been shown recently that a single SNARE complex is sufficient to drive membrane fusion (van den Bogaart et al., 2010).

Fusion of SVs and the release of neurotransmitter is preceded by 2 important steps in SVs cycle: docking and priming. These two steps ensure the presence of fusion competent vesicles at the AZ and ultrafast release of neurotransmitter in response to  $\text{Ca}^{2+}$  influx. AZ proteins RIM, RIM-BP and Munc13 have been shown to play a significant role in synaptic vesicle priming and docking (Fig.1.4) (Kaesler et al., 2011; Südhof, 2013a). RIM and RIM-BP were also shown to be crucial for localizing N- and P/Q-type  $\text{Ca}^{2+}$  channels at the active zone, in the proximity of the docked vesicles, which makes them important organizers of the site of exocytosis (Kaesler et al., 2011). The fusion of synaptic vesicles with the membrane is triggered by  $\text{Ca}^{2+}$  influx via N- and P/Q-



type  $\text{Ca}^{2+}$  channels into the presynaptic terminal (Südhof, 1995). Calcium sensor synaptotagmin, a transmembrane vesicular protein, interacts with SNARE complex, and by acting on protein complexes associated with primed vesicles initiates their fusion (Südhof, 2013a).

Despite the fact that functions of many proteins in this process have been elucidated, the exact mechanism and regulation of various steps in SVs exocytosis are to be further investigated.

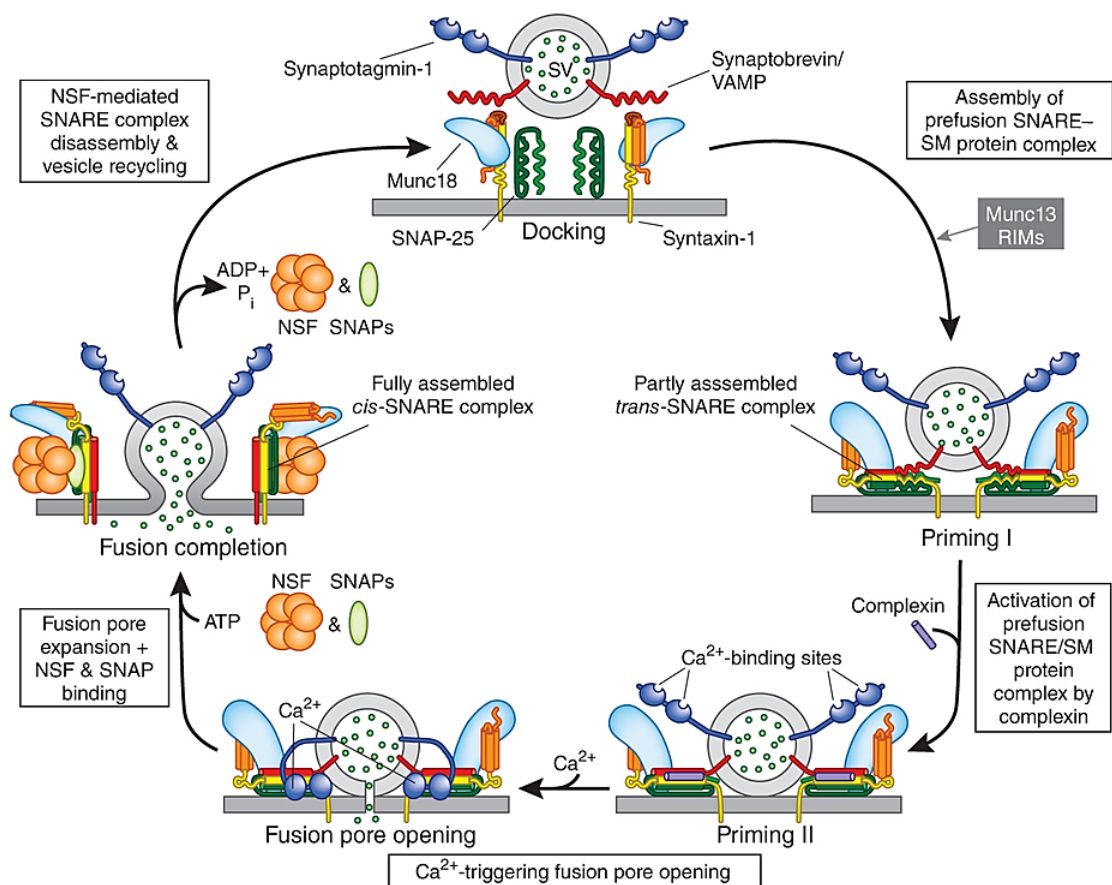


**Figure 1.4 Summary of the process of synaptic vesicle exocytosis.** Proteins crucial for consecutive steps leading to synaptic vesicle release are indicated. Figure modified from Südhof, 2013a.

### **1.3.1.1 Variation in quantal size**

Despite the fact that synaptic vesicles seemingly appear very similar ultrastructurally, a considerable variability in the size of postsynaptic responses following single vesicle release has been reported. Not only has this variability been observed across multiple boutons (Karunanithi et al., 2002), but also at the level of individual synapses (Liu and Tsien, 1995). There are many sources that can contribute to this and they can be attributed to either pre- or postsynaptic properties such as: i) the size of SVs; ii) glutamate content of SVs; iii) concentration of neurotransmitter in the synaptic cleft; iv) location of the release of SVs on the active zone; v) concentration and the number of activated receptors on the postsynaptic membrane.

Harris and Sultan, 1995 showed that SVs from the hippocampus differ in size, ranging from 20 to 66 nm in diameter, with docked vesicles mostly found to be at the bottom end of this distribution. This was associated with variation in the concentration of glutamate in individual vesicles which was estimated to be between 0.24 to 11 mM (Harris and Sultan, 1995). Nevertheless, these values were calculated from reconstructed images of hippocampal synapses and based on measurements of volumes of synaptic vesicles, therefore not providing a very accurate readout (Harris and Sultan, 1995). Another measurement of glutamate content of synaptic vesicles isolated from rat cerebral cortex revealed that individual vesicles are loaded with at least 60 mM of this neurotransmitter (Burger et al., 1989). The concentration of glutamate sufficient to saturate postsynaptic receptors in cultured hippocampal synapses was originally found to be 1.1 mM (Frerking and Wilson, 1996), suggesting, that the transmitter content of a single synaptic vesicle would be enough to achieve that. The opposite finding was made in the calyx of Held where the release of the content of single synaptic vesicles did not lead to saturation of glutamate receptors (Ishikawa et al., 2002). Subsequent electrophysiological analysis of postsynaptic currents revealed that the same applies to hippocampal synapses (Liu et

al., 1999). This indicates that the variation in postsynaptic response is likely to result from factors associated with presynaptic site.

Results based on both Monte Carlo simulation and originating from simultaneous capacitance and miniature excitatory postsynaptic currents (mEPSCs) recordings in calyx of Held, suggest that variation in the concentration of neurotransmitter in the synaptic cleft has been found to be the major contributor to the varied amplitude of postsynaptic response with the concentration of glutamate, and not the size of synaptic vesicles as such being the crucial factor for this variability (Franks et al., 2003; Wu et al., 2007). The variability in glutamate concentration might not only result from the size of individual synaptic vesicles but also from the amount of glutamate loaded into individual SVs. The level of expression of vGlut1 in mice hippocampal culture was associated with the regulation of quantal size, which was decreased in vGlut1 KO neurons but increased when vGlut1 was overexpressed (Wojcik et al., 2004). This also suggests that vesicles in wild type neurons are not filled with neurotransmitter to their maximum capacity (Wojcik et al., 2004). It has been hypothesized that the osmotic pressure resulting from neurotransmitter concentration at individual vesicles affects their size (Qu et al., 2009). However, modulation in osmolarity was not reflected in the change in size of synaptic vesicles, which demonstrates the separation between the vesicle size and neurotransmitter content in hippocampal preparation (Qu et al., 2009). The fact that synaptic vesicles are not filled to the upper limit allows for scope in dynamic regulation of the quantal size and in effect for the regulation of transmission efficiency at small central terminals.

Opposing results on the source of quantal variability were found in a study on the *Drosophila* neuromuscular junction. In this system, quantal response size was correlated with the volume of presynaptic vesicles, which suggests that vesicular size is the determinant of quantal size and that vesicle refilling with glutamate is tightly regulated with uniform concentration of this neurotransmitter being loaded into individual vesicles

(Karunanithi et al., 2002). Daniels et al. 2006 also in a study using *Drosophila* found that a single glutamate transporter was sufficient to fill a synaptic vesicle with glutamate to their maximum capacity, whereas in mice hippocampal neurons the level of refilling was closely associated with the number of vGlut1 transporters per vesicle (Wojcik et al., 2004). This highlights differences between the operation of different experimental systems.

Despite the potential experimental issues arising from this variability, multiple groups successfully established the range of fluorescence amplitudes at presynaptic terminals corresponding to single vesicle release events in live-cell imaging experiments (Balaji and Ryan, 2007; Gandhi and Stevens, 2003; Lemke, 2005; Zhu et al., 2009).

### **1.3.2 Synaptic vesicle endocytosis**

Presynaptic terminals contain a limited number of neurotransmitter filled synaptic vesicles. It is necessary that the excess membrane added during exocytosis is removed to restore membrane tension and to clear and recycle proteins. Endocytic clearance of proteins from the neuronal membrane is thought to be one of the rate limiting steps in synaptic vesicle cycle (Haucke et al., 2011). Despite the model of vesicle retrieval via clathrin-mediated endocytosis, initially proposed by Heuser and Reese in 1970s (Heuser and Reese, 1973), later studies pointed towards another recycling mechanism, without the involvement of clathrin. In this model the vesicles are thought to transiently fuse with the plasma membrane, release their content via fusion pore and to be recycled back into the terminal whilst retaining their identity (Ceccarelli et al., 1973, 1972). Later on this mechanism was referred to as 'kiss and run' (Fesce et al., 1994). Since then, 4 modes of endocytosis have been described in hippocampal neurons: i) clathrin-mediated endocytosis (CME); ii) kiss-and-run endocytosis; iii) ultrafast endocytosis; iv) bulk endocytosis. Following their endocytosis, synaptic vesicles are reacidified by v-ATPase,

which produces electron gradient needed for re-filling the vesicles with neurotransmitter (Südhof, 2004). This step is carried out by neurotransmitter-specific vesicular transporters such as vGAT for GABA or vGlut1 for glutamate (Zander et al., 2010).

### **1.3.2.1 Clathrin-mediated endocytosis**

Clathrin mediated endocytosis has been considered to be the most prevalent mechanism of SVs retrieval at presynaptic terminals. CME has been described in four (recruitment, budding, fission, uncoating) or five sequential steps (nucleation, cargo selection, coat assembly, scission and uncoating) (Fig.1.5) (McMahon and Boucrot, 2011; Schuske et al., 2003).

The presence of SV proteins on the plasma membrane, creates a nucleation site and initiates recruitment and binding of endocytic factors (McMahon and Boucrot, 2011). Phosphatidylinositol 4,5-bisphosphate  $PI(4,5)P_2$  enriched plasma membrane demarcates the binding site for these early endocytic proteins such as FCHO1/2 (Fer/Cip4 homology domain-only proteins 1 and 2), AP2 (assembly peptide 2) and AP180 (assembly protein 180) (Puchkov and Haucke, 2013). AP2 recruits further endocytic adaptors and clathrin coat composed of clathrin triskelia is formed (Rizzoli, 2014). Initially shallow clathrin coated pits mature and gradually invaginate in a process mediated by proteins containing BAR domain such as: endophilin and amphiphysin (Frost et al., 2009). These proteins in turn recruit GTPase dynamin, (Frost et al., 2009; Milosevic et al., 2011), which upon GTP hydrolysis induces the fission of a new synaptic vesicle from the membrane (Roux et al., 2006). The last step in CME is uncoating - disassembling of the clathrin coat from the newly formed synaptic vesicles. This step is facilitated by synaptojanin 1, Hsc70 and auxilin/GAK (Rizzoli, 2014). Endophilin 1, in addition to its dynamin recruiting function, has been also shown to recruit and stabilize synaptojanin to newly recycled vesicles (Schuske et al., 2003).

It is apparent from this short account on this extremely complex process that each individual step is crucial for the next stage of CME to occur. Over the years multiple proteins and lipids have been identified to be involved in the process in CME (Fig.1.5.B). The list of proteins with identified function in endocytosis exceeds 30 (McMahon and Boucrot, 2011). Our knowledge on exactly how some of the crucial steps proceed is still limited, for example, it is still debated whether dynamin driven fission of vesicles is via membrane constriction or twisting (Kononenko and Haucke, 2015; Roux et al., 2006). Nevertheless, unlike in the case with exocytosis, perturbation in expression of many of these proteins often resulted in only subtle endocytic deficiency (Dittman and Ryan, 2009). This suggests that endocytosis might proceed via a different pathway or that the function of some specific protein is somewhat redundant, and readily fulfilled by different proteins (Dittman and Ryan, 2009). However, deletion of certain proteins led to severe impairments in endocytosis. For example, accumulation of clathrin coated vesicles was observed in endophilin TKO synapses, which was accompanied by slower endocytic kinetics and early lethality in the TKO animals (Milosevic et al., 2011). On the other hand dynamin DKO, led to perinatal lethality, slower endocytic kinetics measured with vGpH and accumulation of clathrin coated pits (Raimondi et al., 2011). These results show that disturbance of any critical protein (and its isoforms) leads to severe impairment in retrieval of synaptic vesicles, with in vivo consequences.

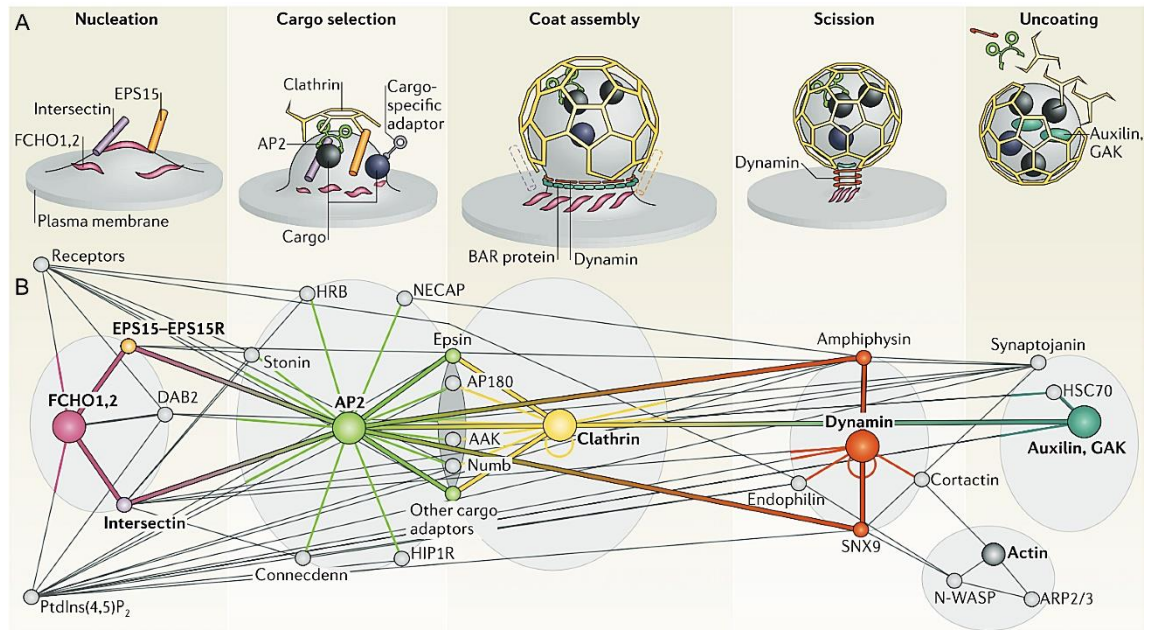


**Figure 1.5 Summary of clathrin-mediated endocytosis of synaptic vesicles.** A) Steps leading to formation of clathrin-coated vesicles and the major proteins involved. B) Network of protein-protein interactions involved in CME. The most important proteins for progression between the consecutive stages are represented with a circle. Figure modified from McMahon and Boucrot, 2011.

### 1.3.2.2 Kiss-and-run endocytosis

Unlike in CME, in kiss-and-run endocytosis, SVs are thought to maintain their identity (Harata et al., 2006). In this mode, vesicles transiently fuse with the plasma membrane, release their neurotransmitter content which is followed by an almost instantaneous closure of the fusion pore (Alabi and Tsien, 2013). Kiss-and-run has been observed using the same optical techniques that were used for monitoring CME and these include: i) FM-dyes destaining experiments (Fig.1.6.A) (Richards, 2010); ii) pHluorin based probes (Fig.1.6.B) (Zhang et al., 2009a); iii) quantum dots (Fig.1.6.C) (Zhang et al., 2009b) and in capacitance recordings (Xu et al., 2008). The optical reporters listed above are described in details in Section 1.6.

The molecular mechanisms of kiss-and-run are still very much unknown. However, an endophilin-dependent mechanism with timing corresponding to kiss-and-run was found to operate at ribbon synapses without the involvement of clathrin and AP2 (Llobet et al., 2011). One of the most puzzling aspects of kiss-and-run is the mechanism that would prevent the fusion of the vesicles with the plasma membrane following the formation of the fusion pore. The hypothesis is that the fusion promoting force resulting from zippering of the SNARE complexes at the plasma membrane might be enough for generation of the transient fusion pore as observed in kiss-and-run, but, on occasion, not enough to trigger the full fusion of the vesicles (Alabi and Tsien, 2013). In addition to this, tethers, that link individual vesicles, might restrain the primed vesicle from fully collapsing into the plasma membrane (Alabi and Tsien, 2013).

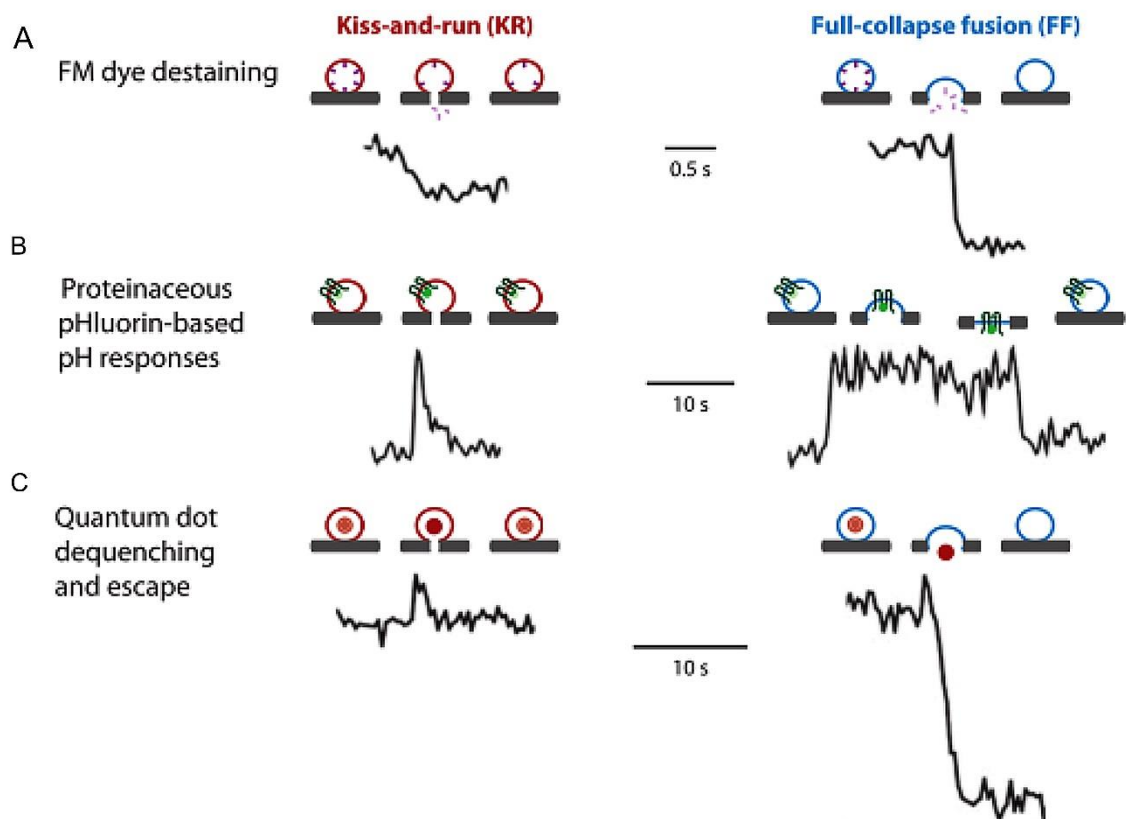


**Figure 1.6 Comparison of functional fluorescence readouts of CME and kiss-and-run kinetics.** All profiles were collected in experiments carried out on hippocampal synapses. Figure modified from Alabi & Tsien 2013.



### 1.3.2.3 Ultrafast endocytosis and bulk endocytosis

Recently another mode of endocytosis has been described. Optogenetics, with a stimulus optimized to elicit single action potential, was combined with rapid freezing and electron microscopy – ‘flash-and-freeze’ (Watanabe et al., 2013). This method allowed to fix the cells within 15 ms post stimulation and to collect the samples at various intervals post-stimulus (Watanabe et al., 2013). The full collapse of docked vesicles into the membrane was achieved within 30 ms post-stimulus (Watanabe et al., 2013). Large endocytic invaginations (~80 nm) were observed within 100 ms in the areas flanking the active zone (Watanabe et al., 2013). Individual synaptic vesicles were formed from the endosome within 5-6 s after stimulation (Watanabe et al., 2014) (Fig.1.7.C). Further investigation revealed that membrane retrieval via ultrafast endocytosis was dependent on actin polymerization, whereas clathrin was critical for the regeneration of SVs from the endosome (Watanabe et al., 2014). This mode of endocytosis differs from kiss-and-run in that SVs are not directly retrieved from the membrane, and the much faster fission rate and the lack of clathrin coat further separates it from CME.

In some aspects, bulk endocytosis might appear similar to ultrafast endocytosis. During bulk endocytosis a large portion of plasma membrane is invaginated at sites flanking the active zone. It is thought that synaptic vesicles bud-off endosomes in a clathrin-dependent manner, which is similar to ultrafast endocytosis (Kasprowicz et al., 2008; Watanabe et al., 2014). However, unlike ultrafast endocytosis, which occurs following single action potential, bulk endocytosis occurs after a very intense stimulation (Clayton and Cousin, 2009). Recently synaptotagmin-11 was found to inhibit both CME and bulk endocytosis (Wang et al., 2015), which demonstrates an overlap in the mechanism of these two processes. Nevertheless, the precise mechanism behind bulk endocytosis and its relation to ultrafast endocytosis still needs to be elucidated (Kononenko and Haucke, 2015).

#### **1.3.2.4 Kinetics of endocytosis and the predominant mode of endocytosis at hippocampal synapses**

The kinetics of these different modes of endocytosis have been measured using various techniques and tissue preparations. In hippocampal cultures the timing of CME has been reported to be ~14-20 s following single AP stimulation (Fig.1.7.B) (Balaji and Ryan, 2007; Granseth et al., 2006). Zhu et al. 2009 showed that the retrieval time can be very varied with most boutons completing the endocytosis after single vesicle release events within around 30 s mark. This and other studies also reported varied dwell times, corresponding to the time vesicles reside at the plasma membrane and perhaps time needed for the assembly of endocytic machinery, and reacidification (Balaji and Ryan, 2007; Zhu et al., 2009). Kiss-and-run on the other hand has been reported to operate within a matter of seconds (Fig.1.7.A) (Harata et al., 2006; Zhang et al., 2009b). Ultrafast endocytosis is thought to take place within milliseconds following the release, however the recovery of the synaptic vesicles from the endosomes takes at least 3 seconds, with the majority of the vesicles being recovered within 10-30 seconds post stimulus (Fig.1.7.C) (Watanabe et al., 2014).

Which mode of endocytosis is predominant at hippocampal synapses? Different types of endocytosis have been observed within the same set of synapses (Richards 2010; Zhang et al. 2009b; and different studies argue for or against predominance of CME or kiss-and-run at hippocampal synapses (Granseth et al., 2006; Smith et al., 2008; Zhang et al., 2009a). The discrepancies between studies regarding the main mode of endocytosis might simply reflect the experimental conditions and the sampling errors. Watanabe et al., 2014 showed that at room temperature, at which most imaging studies are carried out, clathrin-mediated endocytosis is a dominant form of vesicle retrieval, whereas ultrafast endocytosis was a major mode at 34°C. The mode of endocytosis might also depend on the intrinsic properties of synapses. Release probability was found

to be a determinant of the retrieval mode, with low  $p_r$  synapse preferentially recycling vesicles via kiss-and-run, whereas those with high  $p_r$  via CME (Gandhi and Stevens, 2003).  $P_r$  of individual synapses combined with stimulus frequency might determine which mode is the most likely to occur at a given synapse. During high frequency stimulation, synapses with lower  $p_r$  would be recruited which would result in an increased occurrence of kiss-and-run (Gandhi and Stevens, 2003). This leaves a lot of uncertainty as to how hippocampal synapses truly operate under physiological conditions. There has been a suggestion of a unified model. It has been proposed that synapses are capable of separating the retrieval of the membrane from the actual generation of the new synaptic vesicles depending on their activity level (Kononenko and Haucke, 2015). Calcium influx during stimulation might play an important role in determining the endocytic mode, and so SVs, can be regenerated via CME under low frequency stimulation, when the level of intracellular  $\text{Ca}^{2+}$  is relatively low; or via ultrafast endocytosis when synapses fire at high frequencies and presynaptic  $\text{Ca}^{2+}$  is high (Kononenko and Haucke, 2015). Stimulation with the same number of action potentials but at different frequencies, 5 Hz or 40 Hz, led to accumulation of either clathrin-coated pits at the membrane or a presence of large endosome-like structures (Kononenko et al., 2014), which supports the hypothesis relating the type of endocytosis used by the synapse depending on the stimulus intensity and therefore activity level of the synapse.

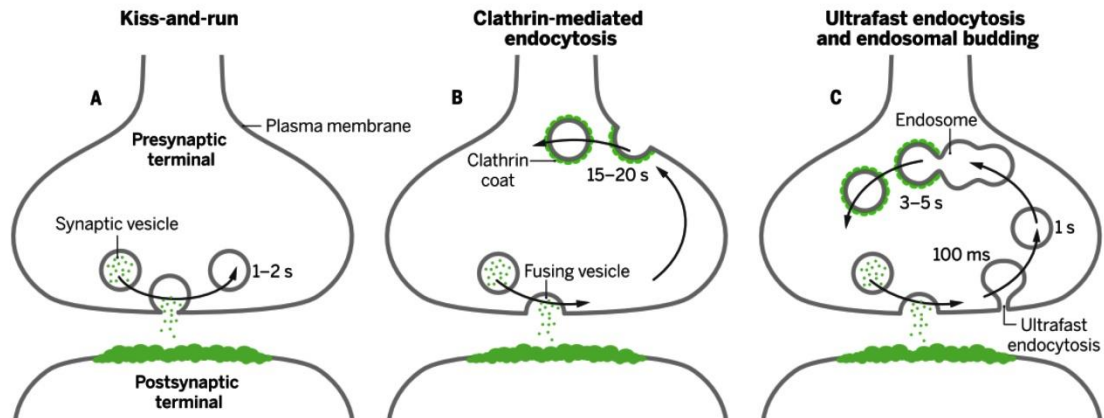


**Figure 1.7 Schematic summary of different modes of endocytosis at hippocampal synapses.** The difference in the timing of these different mechanisms is striking considering the essential role of the synapses to sustain the demands of the network. A) Vesicles transiently fuse with the plasma membrane, release neurotransmitter, which is followed by fusion pore closing. B) In CME vesicles fully collapse into the membrane, which is followed by vesicle retrieval away from the fusion site. C) Ultrafast endocytosis operates via rapid internalization of a large vesicle, which is then resolved into small synaptic vesicles in a clathrin-dependent manner. Figure modified from Watanabe, 2015.

### 1.3.3 Exocytosis-endocytosis coupling

Without stringently regulated coupling of exo- and endocytosis, an excess of SVs material at the plasma membrane would lead to gradual swelling of the terminal, change in the membrane tension and clogging-up of the release sites preventing the synapse from carrying out further release events. Mechanisms that orchestrate these two processes have to be in place in order to ensure seamless function of presynaptic terminals. Despite a lot of controversy in the subject, some mechanisms have been proposed to coordinate the timing of exo- and endocytosis.

With increased intracellular  $\text{Ca}^{2+}$  exocytic rate is also elevated, which leaves more membrane to be retrieved by endocytosis (Dittman and Ryan, 2009). Therefore, calcium is one of the candidates as an important regulator of exo-endocytic coupling.

The precise location of voltage gated  $\text{Ca}^{2+}$  channels is crucial for presynaptic operation as  $p_r$  was shown to correlate with the spatial organization of these channels in relation to releasing vesicles (Meinrenken et al., 2002). Removal of RIM1/2 resulted in a decreased density of  $\text{Ca}^{2+}$  channels at the active zone, which was accompanied by a reduction in the size of the RRP, decrease number of docked vesicles and coupling between these vesicles and  $\text{Ca}^{2+}$  (Han et al., 2011). The proximity of  $\text{Ca}^{2+}$  domain and the local level of intracellular  $\text{Ca}^{2+}$  determined whether synaptic vesicles were retrieved via fast or slow mechanism at calyx of Held (Kim and von Gersdorff, 2009). Moreover,  $\text{Ca}^{2+}$  might also modulate the activity of calcineurin, which is a  $\text{Ca}^{2+}$ /calmodulin-dependent phosphatase, which in turn might dephosphorylate various endocytic proteins such as dynamin, amphiphysin or synaptojanin, leading to the enhancement of their interactions with other proteins and an acceleration of endocytosis (Saheki and De Camilli, 2012).

Nevertheless, the role of calcium in exocytic-endocytic coupling is still debated and many contradictory findings have been made as to whether, and how calcium regulates the endocytic machinery (reviewed by Leitz & Kavalali 2015). In addition to calcium, various proteins involved in exocytosis and endocytosis have also been found to modulate this process. Synaptobrevin-2, which is one of SNARE proteins, critical for SVs fusion, was shown to play a vital role in exo-endocytic coupling (Deák et al., 2004). Hippocampal synaptobrevin-2 KO cultures were characterized by delayed endocytic retrieval time, and defects in the size and shape of SVs were observed in electron micrographs (Deák et al., 2004). The role of synaptotagmin I in exo-endocytic coupling has also been shown in synaptotagmin KO cortical neurons in which the endocytosis was threefold slower in relation to exocytosis, in comparison to the WT synapses (Nicholson-Tomishima and Ryan, 2004).

Proteins implicated in endocytosis were also shown to serve this function. Endophilin was found to directly interact with voltage-gated  $\text{Ca}^{2+}$  channels in a  $\text{Ca}^{2+}$  dependent fashion, which regulated endophilin-dynamin binding (Chen et al., 2003). This shows the

important role of this protein in coupling exo- and endocytosis in addition to its modulation of endocytosis. Other endocytic proteins implicated in coordinating the timing of exocytosis and endocytosis are synaptotagmin 11 and dynamin (Haucke et al., 2011; Wang et al., 2015). Change in mechanical forces accompanying the release of SVs might also be the trigger for endocytosis, which suggests that synapses might be equipped with some sort of tension detecting mechanism (Saheki and De Camilli, 2012).

It is apparent from this that the exocytic and endocytic machinery cooperate to efficiently clear the release site, making it available for the next rounds of release. There are two processes that are important for AZ clearance, the clearance of proteins by endocytosis and also their lateral movement within the membrane. The cytoskeletal components such as actin, intersectin, piccolo or septins, and their interactions with endocytic proteins such as dynamin might regulate and direct the diffusion of proteins away from the active zone (Haucke et al., 2011; Sakaba et al., 2013).

#### **1.3.4 Synaptic vesicle identity**

One of the pressing issues is the fate of SVs proteins following vesicle collapse into the membrane. Efficient clearance of the release site of endocytic proteins is crucial for docking of the next set of vesicles at the active zone (Hosoi et al., 2009; Kim and von Gersdorff, 2009). The main questions here are whether: i) synaptic vesicle proteins are trafficked in the plasma membrane in association with each other, creating a patch of endocytic proteins on the plasma membrane or whether they disperse; ii) proteins from newly endocytosed vesicles mix with the proteins already present at the membrane.

Studies suggest that in hippocampal neurons a significant level of intermixing between proteins residing on the plasma membrane and proteins from recently exocytosed vesicle contribute towards newly reformed vesicles (Fernández-Alfonso et al., 2006; Wienisch and Klingauf, 2006). And yet, other groups observed the opposite (Murthy and

Stevens, 1998; Opazo et al., 2010). One possibility for the discrepancy is the protein used to monitor the intermixing: synaptobrevin (Fernández-Alfonso et al., 2006; Wienisch and Klingauf, 2006), synaptophysin (Wienisch and Klingauf, 2006), synaptotagmin (Fernández-Alfonso et al. 2006; Opazo et al. 2010). As mentioned before, the level of control of protein sorting differs for different proteins (Mutch et al., 2011), and hence these 3 proteins might have been treated differently at the plasma membrane giving rise to contradictory results. Nevertheless, the proteins used in these studies overlapped and yet the groups arrived at different conclusions. The other variable is in the level of stimulation used by these studies. Opazo et al., 2010 observed that vesicles retained their identity at low stimulation level (40 APs 20 Hz), but not at 600 APs 20 Hz. The lowest stimulation in the studies that observed a high level of intermixing was 100 APs 20 Hz, which could explain the discrepancy between the results (Fernández-Alfonso et al., 2006; Wienisch and Klingauf, 2006).

It has been proposed that a patch of stranded proteins persists at the plasma membrane, and this surface population of preassembled protein complexes was referred to as readily retrievable pool (Wienisch and Klingauf, 2006). Moreover this protein pool was depleted with stimulation level larger than 40 APs 20 Hz, suggesting that it may be sufficient to replenish the size of the readily releasable pool of vesicles (RRP) (Wienisch and Klingauf, 2006). Taken together this suggests that some mechanisms are in place that prepare the synapse for efficient endocytosis and to ensure uniformity of SVs. The fact that synaptic vesicle proteins are not fully dispersed but organized into patches also fits within the framework that multiple adaptor proteins are needed to trigger endocytosis, which wouldn't be possible with single SVs proteins diffused throughout the membrane (Rizzoli, 2014).

Considering the enormous number of different proteins and their isoforms at SVs, and the fact that some of the proteins are present in just a few copy numbers suggest that mechanisms that stringently control the stoichiometry of different proteins exist. Although

overexpression of synaptophysin resulted in a higher amount of this protein stranded at the membrane, the copy number of this protein at SVs was not changed (Wienisch and Klingauf, 2006). This shows that, indeed some strict mechanisms are in place. Although the precise mechanisms have not been identified, CME-associated adaptor proteins and clathrin itself are thought to be the major players in protein sorting (Kononenko and Haucke, 2015). As mentioned before, one such protein is stonin 2, the deletion of which, led to missorting of synaptotagmin 1 and perturbed the protein composition of SVs (Kononenko et al., 2013)

## 1.4 Synaptic vesicle pools

Despite the fact that synaptic vesicles appear morphologically homogenous, different vesicle populations that share similar structural or functional characteristics have been identified and termed 'pools', which are essentially sub-classes of vesicles within the total vesicle content (Fowler and Staras, 2015). This categorisation has been widely used, providing a framework for studying presynaptic properties.

The total recycling pool (TRP) together with resting pool (RtP) constitute the entire complement of vesicles at a given synapse (Fig.1.8). The estimated size of the TRP is widely variable between boutons and values as low as 15-20% to up to >70% of the total pool of vesicles have been reported (Harata et al., 2001; Ikeda and Bekkers, 2009). Nevertheless, only a small pool or recycling vesicles (1-5%) is thought to be sufficient to sustain transmission (Denker et al., 2011a). The maintenance of a large resting fraction of synaptic vesicles at first sight seems energetically unfavourable. However, recent studies report that the vesicles from RtP are a source of soluble proteins important for vesicle recycling (Denker et al., 2011b). For example, endophilin I has been shown to be associated with synaptic vesicles in the vesicle cluster, from which it was unbound in an exocytosis-dependent manner and delivered to vesicles undergoing endocytosis (Bai et al., 2010).



The readily releasable pool (RRP) has been defined as those vesicles that are first to be exocytosed in response to the arriving action potential (Rosenmund and Stevens, 1996). Depending on the stimulation paradigm used, the size of the RRP is estimated to be 5-15 vesicles (Dobrunz and Stevens, 1997; Murthy and Stevens, 1998). Murthy et al. 2001 in a correlative microscopy experiment showed that the size of the RRP was correlated with the number of docked vesicles at individual boutons. Nevertheless, this view might not be exactly accurate as electron microscope studies, in which all vesicles in TRP were labelled never observed that all docking sites were filled with recycling vesicles only, suggesting that some docking sites were occupied by RtP vesicles (reviewed by Fowler & Staras 2015). Despite the possible controversy as to whether the docked vesicle pool represents the RRP, the number of docked vesicles was reduced in preparations fixed by high-pressure freezing within 15 ms after the onset of the stimulation and recovered within 3.8 s which corresponds well with 4.3 s measured for RRP recovery in electrophysiological study using hippocampal neurons (Pyott and Rosenmund, 2002; Watanabe et al., 2013). However, in this type of approach, different synapses are measured at each time point and perhaps the view that docked vesicle pool represents a major fraction of the RRP, but that not all RRP vesicles are docked more precisely reflects the presynaptic organization (Fowler and Staras, 2015).

The nature of the vesicles in a spontaneous vesicle pool, that is vesicles which are released in the absence of stimulation, is highly debated and various studies reported hugely conflicting results. Some studies suggested that there is a discrete pool of vesicles, most likely a subset of RtP, specifically accessed during spontaneous release (Fredj and Burrone, 2009; Sara et al., 2005). Studies with the view that spontaneous pool is a part of TRP can also be found (Groemer and Klingauf, 2007; Hua et al., 2010). Further investigation is therefore needed to establish the origin of these vesicles.

Relatively recently a new pool emerged that spans vesicles that are dynamically exchanged between synapses (Staras et al., 2010). The important feature of these

trafficking vesicles is that they can be released along the axon but also at the new 'host' synapse (Darcy et al., 2006a; Ratnayaka et al., 2011). These mobile vesicles might be important for regulation of synaptic strength by modifying the proportion of vesicles in different vesicle pools and could account for synapse-synapse variability in properties such as  $p_r$  or plasticity (Staras and Branco, 2010)

#### 1.4.1 Regulation of vesicle pool sizes

Considering the fact that presynaptic properties are correlated with the sizes of different vesicle pools, mechanisms that modulate the proportion of vesicles contributing to these pools must be in place to meet the functional demands placed upon an individual synapse. The size of the TRP and RRP has been linked with  $p_r$  at individual presynaptic boutons (Dobrunz and Stevens, 1997; Murthy et al., 2001, 1997) which attracted interest in the regulatory mechanism behind the sizes of these two pools.

RtP might not only provide a reservoir of soluble proteins but also vesicles that can be recruited into the TRP. Fluoxetine, a clinically used antidepressant drug, was shown to expand the TRP at the expense of non-recycling vesicles from RtP and therefore restored synaptic function following exhaustive stimulation (Jung et al., 2014). Similarly inhibition of cyclin-dependent kinase 5 (CDK5) with roscovitine led to increased size of the recycling fraction via recruitment of vesicles from RtP, whereas removal of calcineurin had the opposite effect (Kim and Ryan, 2010). This study provided with an important mechanisms for presynaptic homeostatic scaling via regulation of TRP size by CDK5. An NMDA-dependent form of synaptic potentiation was shown to operate via the same mechanisms - by changing the balance between the TRP and RtP (Ratnayaka et al., 2012). These studies show common mechanisms for improving synaptic strength. An increase in the RRP size at glutamatergic synapses and its refilling rate was achieved via phorbol esters mediated activation of protein kinase C (PKC) (Stevens and Sullivan,

1998; Waters and Smith, 2000). An increase in  $p_r$  accompanied by a rise in the size of RRP was induced by brain-derived neurotrophic factor (BDNF) and was attributed as a mechanism via which it modulates synaptic plasticity (Tyler et al., 2006).

Despite the fact that we have some knowledge on the factors regulating the vesicle pools fractions, what remains largely unresolved is whether synaptic vesicles that belong to a certain pool, have a specific molecular signature that ‘assigns’ them to that particular pool, and confers certain functional advantages. Some synaptic vesicles might show higher copy numbers of certain proteins than others. Recycling pool vesicles were shown to exhibit a high level of VAMP2 and vGlut1, whereas those in resting pool were characterised by an abundance of VAMP7 (Hua et al., 2011). Nevertheless, such a molecular tag in a form of membrane associated protein could only be useful if vesicles remain constant in their molecular identity, that is, there is a limited intermixing of vesicular membrane cluster with plasma membrane. Soluble proteins, such as synapsin, which in response to activity-driven calcium entry into the terminal, unbinds from the vesicles, conferring them more mobile (Kamin et al., 2010), is a candidate for being a discriminator of pool classes. Synapsin TKO neurons showed increased mobility of RrP vesicles, their increased axonal trafficking and redistribution into adjacent boutons and therefore contribution to the increased size of the superpool (Orenbuch et al., 2012). A tag for vesicles in spontaneous vesicle pool (assuming that such exists), was also identified as a soluble protein – DOC2, a calcium sensor of which deletion significantly decreased the frequency of spontaneous neurotransmission with no effect on evoked release (Crawford and Kavalali, 2015; Groffen et al., 2010; Pang et al., 2011).

This shows that some molecular ‘code’ exists behind the segregation of vesicles into the vesicle pools. In support of this, it has been shown that a larger than predicted by chance portion of vesicles from the RRP, returns to the positions close to the plasma membrane and is preferentially reused during the next RRP-mobilizing stimulation (H. Park et al., 2013; Rey et al., 2015). These preferentially reused RRP vesicles might originate from

the readily retrievable pool at the plasma membrane that might undergo some strict sorting rules ensuring consistent protein composition of these vesicles and targeting them to the RRP. Nevertheless there are still major deficits in our knowledge. One of the major challenges is posed by the enormous number of different proteins associated with SVs and limitations of the available techniques. The most pressing questions concerning molecular discrimination, nature and stability of the pools as well as relationship of these variables with the synaptic function are still to be answered. Integration of novel super-resolution imaging techniques such as stimulated emission depletion (STED) microscopy or stochastic optical reconstruction microscopy (STORM) with ultrastructural and connectivity readouts, as well as with live cell imaging, should allow us to study the molecular composition combined with functional properties of individual synapses.

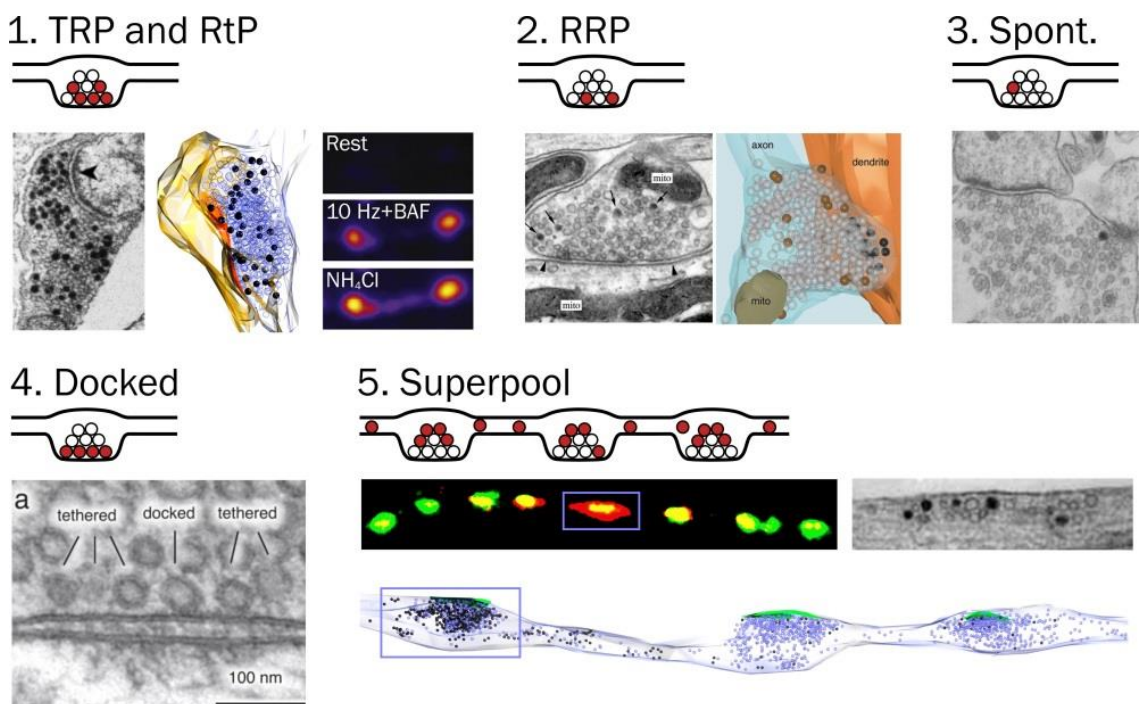


**Figure 1.8 Summary of classification of synaptic vesicle pools.** 1. Total recycling pool (TRP) and resting pool (RtP) electron micrographs showing photoconverted (dark lumen) recycling vesicles and clear vesicle from the RtP. Fluorescence panels on the right illustrate functional readout allowing to measure TRP and RtP size. 2. Functionally labelled RRP vesicles showed in electron micrograph and 3D reconstruction of a synapse. 3. Electron micrograph of spontaneous pool - HRP-labelled, dark vesicles. 4. Docked synaptic vesicles appear to be in direct contact with the membrane. 5. Superpool of vesicles that are shared between neighbouring synapses. Figure modified from Fowler & Staras 2015.

## 1.5 Presynaptic dysfunction in disease

Disturbance in the kinetics at any stage of synaptic vesicle cycle, in the balance within synaptic vesicle pools, or any changes in the expression or function of important presynaptic protein, could have detrimental effects for the function of the synapse and in effect, produce neurological symptoms and cognitive decline (Kavalali, 2006). What follows is a brief account on presynaptic factors found to be affected in neurological diseases.

Presynaptic protein,  $\alpha$ -synuclein of which soluble oligomers have been linked with pathology observed in Parkinson's disease (Stefanis, 2012), is thought to be important for the maintenance of the abundance of vesicles at presynaptic terminals; some studies also reported that it modulates neurotransmitter release thorough its interaction with SNARE complexes (Murphy et al., 2000; Stefanis, 2012). Synaptotagmin 11, which is crucial for CME and bulk endocytosis, has been identified as a susceptibility gene for schizophrenia (Wang et al., 2015). Also, analysis of post-mortem brain tissue from patients suffering from this disorder revealed modified expression patterns of genes encoding for synapsin-2 and synaptojanin, all these involved in recycling of SVs (Kavalali, 2006). Reduction in the expression of key presynaptic proteins such as synaptophysin, synaptobrevin or synapsin was reported in *in vivo* prion disease model, which coincided with the onset of behavioural abnormalities reported in this neurodegenerative disease (Gray et al., 2009). Endophilin, an important regulator of endocytic kinetics has been reported to bind to numerous proteins such as Parkin, Huntingtin and ataxin-2, all associated with neurodegenerative diseases (Milosevic et al., 2011).

Not only might the function of proteins be disturbed in various neurological disorders, but also lipids metabolism. Increasing the level of PI(4,5)P<sub>2</sub>, which is crucial for many presynaptic functions (and yet the level of which was found to be perturbed in Alzheimer's Disease), significantly improved the results of behavioural tests in

Alzheimer's Disease (AD) mice model TG2576 (McIntire et al., 2012). This elevation in PI(4,5)P2 was brought about by deletion of synaptojanin 1, a major phosphatase in the mammalian brain (McIntire et al., 2012). This shows the importance of protein-lipid interactions in synaptic homeostasis.

These examples clearly show how critical the efficient function of exocytic and endocytic machinery is for CNS performance. Identification of disease associated changes in synaptic vesicle pools and cycle might provide with novel therapeutic targets. As an example, fluoxetine, drug used to treat depression was recently shown to act via increasing the size of the recycling pool (Jung et al., 2014).

### **1.5.1 Alzheimer's disease and presynaptic function**

Alzheimer's disease is a neurodegenerative dementia, affecting a large proportion of the population over 70 years of age, clinically characterized by a progressive memory loss (Alzheimer's society, 2016). Pathologically, this disease is associated with the presence of large deposits of misfolded proteins: neurofibrillary tangles composed of phosphorylated tau, and senile plaques containing amyloid-beta peptide (A $\beta$ ) (Benilova et al., 2012). Gradual loss of synapses, proceeding the loss of neurons, has been found to be the best correlate with the cognitive decline (Serrano-Pozo et al., 2011; Walsh and Selkoe, 2007). Unlike originally thought, the synaptic deficits, loss of synapses or their dysfunction, have been linked to the toxic effects of small, soluble, oligomeric A $\beta$  species, rather than large fibrils (Murphy and LeVine III, 2010).

A $\beta$  is derived from amyloid-precursor protein (APP), via sequential cleavage of this protein carried out by  $\beta$ - and  $\gamma$ - secretases, resulting in a production of either 40 or 42 amino acid long peptide (Pimplikar, 2009). Out of the two, A $\beta$ 1-42 is thought to be more toxic, and it has been linked to a wide range of synaptic deficits (Walsh and Selkoe, 2007). Although postsynaptic effects of A $\beta$  have been extensively studied (De Felice et

al., 2007; Lambert et al., 1998; Sheng et al., 2012; Walsh et al., 2002), the presynaptic mechanisms of A $\beta$  toxicity have been given less attention, however some studies focused on this compartment in their investigation. A $\beta$  has been found to decrease the rate of synaptic vesicle endocytosis by reducing the level of dynamin, which led to redistribution of amphiphysin, which is another protein important for endocytosis (Kelly et al., 2005; Kelly and Ferreira, 2007). A similar observation on the detrimental effect of A $\beta$  on the kinetics of endocytosis was made by another group, which also exposed A $\beta$ -induced reduction in recycling vesicle pool size, accompanied by an increased resting pool fraction (J. Park et al., 2013). It has also been reported that A $\beta$  competed with VAMP2 for binding of synaptophysin, which could lead to an increased number of primed vesicles resulting in higher neurotransmitter release (Russell et al., 2012). A meta-analysis of synaptic markers associated with pre- and postsynaptic pathology, strongly indicated that presynaptic terminals were affected more in AD post-mortem brain samples, further highlighting the importance of exploring deficiency in this synaptic compartment (de Wilde et al., 2016).

Despite the fact that discoveries point toward a strong association between A $\beta$  and wide-range of synaptic dysfunctions, this is not reflected in the progress of therapeutic approaches (Amanatkar et al., 2016). It is therefore paramount to continue the search for important loci of this disease, and to consolidate the knowledge that we have gained so far in a rigorous and systematic way.

## **1.6 Tools for monitoring presynaptic function**

The very small size of presynaptic terminals and their ultrastructural components, combined with the immense speed of the processes accompanying synaptic vesicle release and recycling, pose huge technical challenges. The early studies relied on electrophysiological measurements of postsynaptic depolarizations, which provided with

a very indirect method of studying presynaptic function as it was based on the activity of postsynaptic ligand-gated ion channels (Del Castillo and Katz, 1954; Kavalali and Jorgensen, 2013). The combination of membrane capacitance measurements with recording of mEPSCs offers a powerful tool for examining the release of synaptic vesicles and the postsynaptic consequence of neurotransmitter release (Sun et al., 2002). Nevertheless, although this method is widely used in large terminals, such as calyx of Held, it is unsuitable to be performed in hippocampal terminals which are only 0.12-0.54  $\mu\text{m}$  in size (Harris and Sultan, 1995; Yang et al., 2005). Other methods for directly measuring neurotransmitter release, such as continuous amperometry, offer high temporal resolution but low selectivity due to potential contamination of the measurements with other oxidizable molecules (Benoit-Marand et al., 2007). Electron microscopy opened another avenue for examining presynaptic function and structure. Although this method allows us to explore ultrastructure in details in three dimensional reconstructions, it captures just a particular moment in the life of a synapse. Moreover, the sample has to be fixed, dehydrated and embedded, and various preparation protocols can induce different structural artefacts. The development of fluorescence markers in the early 1990s for monitoring presynaptic function allowed us to more directly study their behaviour. The techniques described below include the fluorescent probes that were used in this study. Other emerging techniques involve: quantum dots, super-resolution microscopy such as STED and STORM, and electron microscopy techniques, for example FIBSEM (focused ion beam milling scanning electron microscopy).

## **1.6.1 Acutely applied probes**

### **1.6.1.1 FM dyes**

The FM dyes were developed by Betz et al. 1992 by improving the structure of existing styryl dyes. FM dyes have an amphiphilic nature, a positively charged head group arrests



them in the outer membrane, and a lipophilic tail, of which length determines how quickly they depart from the membrane i.e. how “sticky” the dye is (Brumback et al., 2004). The more hydrophobic dyes, with longer tails, such as FM1-43, leave the membrane slower than the counterparts with shorter hydrophobic tail such as FM2-10 (Zenisek et al., 2002). Nevertheless, in comparison to other dyes, FM1-43 was among those with the highest fluorescence intensity (Wu et al., 2009). The number of double bonds between the head and the tail determines the spectral properties of FM dyes. The higher the number of the bonds, the more red shifted the dye is (FM1-43, single double bond, excitation within green spectra; FM4-64, 3 double bonds, excitation and emission red-shifted) (Brumback et al., 2004). The properties of FM dyes that made them extremely useful in studying vesicle recycling are: i) they partition into membranes which is accompanied by a large increase in fluorescence; ii) their membrane binding is reversible, meaning they can be washed off the surface of the cell and destained from the previously loaded SVs; iii) they remain in the outer portion of the membrane and are not capable of penetrating the full membrane thickness (Betz et al., 1992; Brumback et al., 2004). These properties are a result of the particular design of their structure.

Incubation of neurons with FM1-43 results in the binding of this dye to the outer leaflet of the plasma membrane. Stimulation evoked release and subsequent endocytosis of synaptic vesicles, leads to the internalization of this dye and labelling of the recycling vesicles only (Cousin, 2008). The surface dye is washed off and the remaining fluorescence corresponds to the dye trapped in the vesicles that underwent the recycling. The subsequent stimulation leads to the loss of the dye and a rapid drop in fluorescence intensity, as the dye departs from the membrane after vesicle fusion (Betz et al., 1992). Not only has FM1-43 been used to monitor the kinetics of SVs exocytosis during live imaging, but also as a means of observing recycling SVs under electron microscope. In the presence of 3,3'-diaminobenzidine (DAB) and under prolonged fluorescent illumination, an electron dense product is formed in the structures containing FM1-43,

which can be observed under the electron microscope (Darcy et al., 2006b). For this reason, FM1-43 also allows the examination of the ultrastructural properties of functional terminals and is a very valuable tool in examining structural correlates of presynaptic function (Branco et al., 2010).

#### **1.6.1.2 Fluorescently tagged antibody - sytl-Oyster550**

Another reporter used in this study is a red fluorescent marker of presynaptic terminals sytl-Oyster550, which allows to identify presynaptic boutons. Sytl-Oyster550 is an Oyster-550 labelled antibody raised against the epitope of the N-terminal domain (luminal domain) of the synaptic vesicle protein, synaptotagmin I (sytl). Synaptotagmin I is a sensor of presynaptic  $\text{Ca}^{2+}$  influx and therefore an important protein for SVs exocytosis (Südhof and Rizo, 1996). Unlike other members of the synaptotagmin family, sytl is specifically targeted to presynaptic terminals, precisely to synaptic vesicles, which makes it an ideal marker for these structures (Kang et al., 2004; Zhang et al., 2004). In a similar fashion to FM1-43, sytl-Oyster550, can be loaded into the recycling presynaptic vesicles.

#### **1.6.2 Genetically encoded fluorescence probes**

The engineering of pH-sensitive mutants of green fluorescence protein by Miesenbock et al. 1998 that can be tagged onto various presynaptic proteins, has offered the opportunity to monitor the behaviour of presynaptic terminals down to single synaptic vesicle resolution; an approach that was difficult to achieve with the acutely applied probes, such as FM1-43 dye. More importantly, these genetic constructs, allow for more specific measurement of the fluorescence signal than in the case of acute probes. That is because in these constructs pHluorin molecule is tagged onto a specific synaptic

vesicle protein in contrast to the fluorescence originating from lipid insertion of the dye as in the case of FM1-43 (Kavalali and Jorgensen, 2013).

### **1.6.2.1 sypHy**

sypHy is a genetically encoded probe developed by (Granseth et al., 2006). This construct is comprised of a super-ecliptic pHluorin molecule fused to the second intravesicular loop of synaptophysin (Granseth et al., 2006). pHluorin was developed via structure-directed combinatorial mutagenesis of green fluorescent protein leading to the development of a pH-sensitive version of GFP: fluorescence is quenched at an acidic pH and an increase in fluorescence intensity is observed at a neutral or near neutral pH (Miesenböck et al., 1998). The synaptic vesicle lumen is characterized by acidic pH (5.5) (Kavalali, 2006), when the vesicle fuses with the membrane and the luminal GFP is exposed to the extracellular environment with neutral pH, an increase in fluorescence intensity can be observed. Due to tight coupling of exocytosis and endocytosis of synaptic vesicles, as described above, SVs are recycled back into the presynaptic terminal and reacidified by vATPase. This is again reflected in the fluorescence intensity of sypHy which is re-quenched during this process. SypHy2x therefore allows to readout synaptic vesicle exocytosis and reacidification of newly formed vesicles.

Initially the pHluorin molecule was fused to synaptic vesicle protein synaptobrevin and the construct called synaptopHluorin (Miesenböck et al., 1998; Sankaranarayanan and Ryan, 2000). Nevertheless, this plasmid showed a high level of surface fluorescence and lateral diffusion of tagged protein into neighbouring axon (Granseth et al., 2006). Based on the analysis of immunofluorescence data, Granseth et al., 2006 created a new construct by fusing the pHluorin molecule to synaptophysin. This construct called sypHy, had improved properties: significantly less surface fluorescence, better signal-to-noise ratio and less lateral movement. In our study we used a modified version of this probe

which has two pHluorin molecules in the second intravesicular loop of synaptophysin (Zhu et al., 2009).

### **1.6.2.2 vGlut1-pHluorin**

Since the development of ecliptic pHluorin (Miesenböck et al., 1998), this engineered GFP has been successfully fused with various synaptic vesicle proteins such as synaptobrevin, synaptotagmin I or synaptophysin. One major difference between these probes was their surface expression resulting from the differences in the amount of these synaptic vesicle proteins on the plasma membrane at rest. SynaptopHluorin (pHluorin fused to synaptobrevin) was characterized by 15% (Sankaranarayanan and Ryan, 2000), synaptotagmin I by 23% (Fernández-Alfonso et al., 2006) and synaptophysin by 9% (Granseth et al., 2006) surface expression. A high level of baseline fluorescence is one of factors that could hinder the detection of single-vesicle fusion events. Designed specifically with this in mind, a single pHluorin was fused to vesicular glutamate transporter 1 (vGlut1) creating another reported called vGpH (Balaji and Ryan, 2007; Voglmaier et al., 2006). vGlut1 mediates glutamate uptake into SVs and is preferentially expressed over vGlut2 in hippocampal neurons (Zander et al., 2010). The surface expression of vGpH was only 2%, which is superior to proteins mentioned above, indicating that vGlut1 is targeted even more specifically to synaptic vesicles than other SVs proteins, which makes it a perfect candidate probe for single vesicle imaging (Balaji and Ryan, 2007).

### **1.6.2.3 syGCaMP**

Another group of genetically encoded probes are genetically encoded calcium indicators (GECIs). During action potential firing,  $\text{Ca}^{2+}$  enters presynaptic compartment, leads to SVs exocytosis and contributes to exo-endocytic coupling.  $\text{Ca}^{2+}$  imaging provides with a

direct, simultaneous measurement of  $\text{Ca}^{2+}$  transients within multiple presynaptic terminals which can provide with invaluable information on the function of these synapses as well as their behaviour within the network.

Synthetic  $\text{Ca}^{2+}$  indicators, such as Oregon green (OGB), offer a range of characteristics, high  $\text{Ca}^{2+}$  sensitivity and speed (Paredes et al., 2008). However, novel GECIs show several advantages over the synthetic probes. Firstly, they can be targeted to a specific cell type by being under control of cell-type specific promoter such as glial fibrillary acidic protein (GFAP) for examining  $\text{Ca}^{2+}$  transients in astrocytes (Akerboom et al., 2012). Synthetic  $\text{Ca}^{2+}$  indicators require another marker, such as sytl-Oyster550, in order to reveal the compartments of experimental interest. GECIs can be targeted to report  $\text{Ca}^{2+}$  influx into a specific cellular compartment, such as synaptic boutons (syGCaMP2) (Dreosti et al., 2009), plasma membrane or dendritic spines (Mao et al., 2008). Thirdly, GECIs also allow for efficient and long-term monitoring of  $\text{Ca}^{2+}$  in vivo (Mao et al., 2008).

The GCaMP probe is comprised of 3 main components: single, circularly permuted GFP (cGFP), calmodulin (CaM) and M13 fragment from myosin light chain kinase, which is a  $\text{Ca}^{2+}$ /CaM-binding peptide (Nakai et al., 2001). Calcium binding induces conformational change in the CaM – M13 complex which in turn leads to conformational change in cGFP and which is manifested as an increase in fluorescence intensity (Nakai et al., 2001). This original GCaMP probe (Nakai et al., 2001), has been further improved via target mutagenesis and structure-based mutagenesis resulting in sensors with much improved calcium affinity, brightness of the calcium-bound state, reporting kinetics and signal-to-noise ratio (Akerboom et al., 2012; Chen et al., 2013). These improved GECIs are therefore the probes of choice over the synthetic  $\text{Ca}^{2+}$  indicators for monitoring  $\text{Ca}^{2+}$  transients in specific cells or cellular compartments. Fusion of GCaMP with the cytoplasmic side of synaptophysin led to the expression of the construct in presynaptic terminals and therefore allowed for the detection of  $\text{Ca}^{2+}$  influx specifically into that compartment (Dreosti et al., 2009). In this study we used syGCaMP6f, which is GCaMP

variant fused with synaptophysin for presynaptic targeting and characterized by the fastest kinetics amongst GCaMP probes, and similar  $\text{Ca}^{2+}$  sensitivity to OGB (Chen et al., 2013; Dreosti et al., 2009).

#### **1.6.2.4 iGluSnFR**

In recent years yet another probe has emerged: intensity-based glutamate-sensing fluorescent reporter (iGluSnFR). As the name indicates iGluSnFR allows the detection of glutamate released from the presynaptic terminals. iGluSnFR is comprised of a circularly permuted GFP (cpGFP) fused to glutamate type 1 transporter from E coli (Marvin et al., 2013). This construct is targeted to the plasma membrane and expressed on the extracellular side thanks to another component, a transmembrane domain of platelet-derived growth factor receptor (Marvin et al., 2013). The principle working of iGluSnFR relies on ligand-induced conformational change to cpGFP. In a ligand-free state iGluSnFR fluorescence is very faint, however, glutamate binding induces conformational change within the sensor and a rapid increase in fluorescence intensity (Marvin et al., 2013). iGluSnFR was found to be uniformly distributed on extrasynaptic membrane, photostable, fast and sensitive (its signals correlated with simultaneous electrophysiological recordings) (Marvin et al., 2013). iGluSnFR under synapsin promoter was also developed in order to drive the expression only in neurons (Marvin et al., 2013).

## 1.7 Aims

From the studies presented, it is apparent that synapses in the CNS show an enormous diversity in their structural, functional and molecular properties. Despite the available information on correlations between individual parameters, very few studies attempted to consolidate the structural and molecular characteristics of individual presynaptic terminals with their functional properties.

Efficiently operating endocytosis is crucial for renewing the pool of SVs at presynaptic terminals and clearing the release site, however, the exact regulation of endocytic retrieval is unknown. Here, we do not attempt to characterize the endocytosis per se but rather to test, whether individual synapses exhibit conserved endocytic behaviour. Evidence suggests that synapses in retinal bipolar neuron are capable of retrieving vesicles with different kinetics depending on the conditions (Neves and Lagnado, 1999). This suggests that the machinery required to utilize different recycling pathways is present at individual boutons. Different endocytic mechanisms have also been identified to operate at hippocampal synapses, which indicates that these terminals are also capable of carrying out various modes of vesicle recycling (Alabi and Tsien, 2013). But what determines the selection of endocytosis mode? One possibility is that this is determined by molecular and structural characteristics of individual synapses. In various knockout experiments different presynaptic proteins have been shown to modulate the kinetics of endocytosis (Kononenko et al., 2013; Milosevic et al., 2011). Structural organization of the presynaptic terminals have also been found to underlie the functional properties of individual synapses (Branco et al., 2010; Tyler et al., 2006). Nevertheless, the relationships between various molecular and structural factors in native terminals, and the efficiency of endocytic retrieval have not been explored. The unresolved question is - to what extent can we predict the functional properties of presynaptic terminals based on their morphological characteristics and molecular composition? We hypothesized that individual synapses might exhibit a signature mode of endocytic behaviour, and the

“choice” of the path they take might result from inherent molecular or structural properties of these synapses.

The main aims of this study were:

- 1) To determine whether individual presynaptic boutons exhibit signature kinetics of retrieval of single synaptic vesicles
- 2) To identify underlying structural and molecular correlates of behaviour of individual presynaptic terminals

In the recent years evidence has been accumulated suggesting the involvement of presynaptic dysfunction in various neurological and psychiatric disorders such as Parkinson's disease, schizophrenia or autism (Südhof, 2013a). Despite the fact that impairment in postsynaptic function in Alzheimer's disease has been widely studied, the knowledge on the presynaptic component is limited. The aim of this study was to examine the effects of amyloid beta oligomers on the different components of synaptic vesicle cycle with major focus on endocytosis.



## 2 METHODS AND MATERIALS

---

### 2.1 Animal Handling

All animal handling and experimental procedures were carried in accordance with the Animals (Scientific Procedures) Act 1986. Sprague Dawley rat pups (P0-P1) were purchased from Harlan Scientific or fortnightly littered onsite.

### 2.2 Dissociated rat hippocampal cell culture

Table. 2.1.

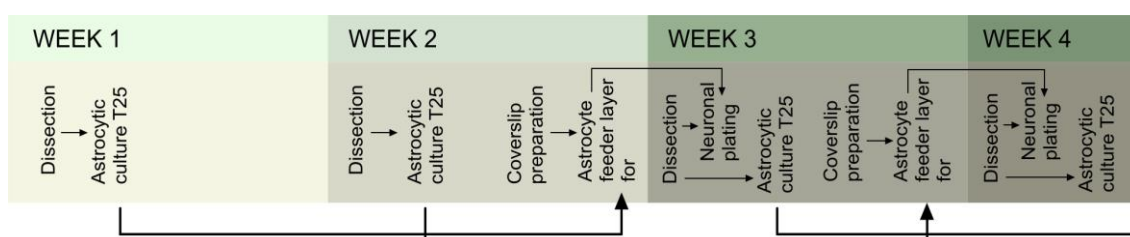
Product	Product Code	Supplier
Basal Medium Eagle (BME)	21010046	Gibco™
Foetal Bovine Serum (FBS)	10500056	Gibco™
Sodium Pyruvate (100 mM)	11360070	Gibco™
GlutaMAX™ Supplement (100X)	35050061	Gibco™
B-27 Supplement (50X), serum free	17504044	Gibco™
HEPES	H4034	Sigma-Aldrich
Glucose (45%)	G8769	Sigma-Aldrich
Penicillin-Streptomycin (100X)	P4333	Sigma-Aldrich
Hanks Balanced Salt Solution (HBSS) (10X)	14065056	Gibco™
Trypsin-EDTA (0.05%), phenol red	25300054	Gibco™
Trypan Blue Solution (0.4%)	T8154	Sigma-Aldrich
Poly-D-lysine hydrobromide	P1024	Sigma-Aldrich
Cytosine β-D-arabinofuranoside (ara-C)	C1768	Sigma-Aldrich

Table 2.2.

Solution	Composition	Storage	Used at
Poly-D-Lysine (PDL)	20 µg/ml in H <sub>2</sub> O	4 mg/ml stock at -20°C	37°C
Dissection Solution	HBSS (1x), 10 mM HEPES (1 M, pH 7.35 solution) in H <sub>2</sub> O	4°C	Ice cold
Astrocyte Growth Media	BME, 20 mM Glucose, 10 mM HEPES, 1 mM Sodium Pyruvate, 10% FBS, 1% Penicillin-Streptomycin	4°C	37°C

Neuronal Growth Media	BME, 20 mM Glucose, 10 mM HEPES, 1 mM Sodium Pyruvate, 2% FBS, 1% Penicillin-Streptomycin, 1% GlutaMAX, 2% B-27	4°C	37°C
Cytosine $\beta$ -D-arabinofuranoside (ara-C)	8.7 $\mu$ M ARA-C in Neuronal Growth Media	-20°C as 5 mM stock	37°C

Neuronal cultures were prepared using a modified version of the protocol first described by (Banker and Cowan, 1977). A two-step culturing process was employed in which hippocampal neurons were plated on top of the astrocyte feeder layer (Fig.2.1). The sections below describe in details the consecutive steps leading to viable neuronal culture.



**Figure 2.1 Schematic representing timeline of culturing protocol of rat hippocampal neurons.**

### 2.2.1 Coverslip preparation and plating astrocyte feeder layer

Circular glass coverslips (12 mm, Fisher) were sterilized in absolute ethanol and individually placed in the 8 middle wells of a 24-well plate in order to ensure even evaporation of media during culturing. The remaining outer wells were filled with sterile water. Coverslips were incubated overnight at 37°C with 20  $\mu$ g/ml PDL. The following day, wells were copiously washed with sterile H<sub>2</sub>O and coverslips were allowed to dry under the sterile hood during the preparation of astrocytes. 9-10 day old astrocytes, grown in 25 cm<sup>2</sup> flask (CLS430639, Sigma-Aldrich), were plated on these PDL coated coverslips. Cells were briefly washed with 1x sterile PBS and trypsinized at room

temperature with 0.05% Trypsin-EDTA for 5-10 minutes. Trypsin was carefully removed and replaced with 2 ml of pre-warmed astrocyte growth media (composition in Table 2.2). The flask was briskly tapped a few times in order to encourage the detachment of astrocytes from the plastic into the media. The cell suspension was carefully drawn and transferred into a 15 ml falcon tube where the cells were gently triturated a few times. The number of viable astrocytes in the suspension was calculated using haemocytometer and 0.04% trypan blue solution. Astrocytes were plated at the density of 3500-5000 cells/well which was usually equivalent to 200-500  $\mu$ l of the cell suspension. This ensured an astrocytic layer that was dense enough for favourable growth of neurons but not obstructive for imaging purposes. Diluted cell suspension was added at 0.7 ml per well and plates placed in the incubator at 37°C with 5% CO<sub>2</sub>. Astrocytes were allowed to settle in media containing 10% FBS, which promotes their growth (Ye and Sontheimer, 1998), for 4-5 days prior to plating hippocampal neurons. The source of astrocytes is described in the section below.

### **2.2.2 Dissection**

Sprague Dawley P0-P1 rat pups were sacrificed by cervical dislocation according to Schedule 1. The head was removed with the scissors and 2 incisions on both sides of the head (from the base of the skull towards the eyes) were made with fine scissors, the skull was peeled off in a single motion whilst the head was held at the base. This decreased the time between the sacrifice of the animal and tissue dissection yielding more viable cells. The brain was gently separated from the underlying tissue, lifted up with a spatula and immediately placed into a petri dish filled with ice cold dissection solution (Table 2.2). From now on the dissection was carried out under the microscope. The brain was placed dorsal side up, the olfactory bulb and cerebellum were removed and the two hemispheres were separated with a cut along the central sulcus with a sterile scalpel blade (No#22). The hemispheres were placed cortex side down (sagittal view)

and the hippocampus was gently dissected out by 'rolling it out' and separating it from the cortex. The meninges were carefully removed using fine forceps. The hippocampal tissue was then transferred into 15 ml falcon with dissection solution and kept on ice whilst the process was repeated on the other hemisphere.

### **2.2.3 Culturing hippocampal neurons**

Dissection solution was carefully removed and the dissected out hippocampus was washed three times with 2 ml of warm neuronal growth media (Table 2.2). Tissue was gently triturated in 2 ml neuronal growth medium using Gilson pipette until the suspension was uniform and there was no sign of tissue fragments. The cells were counted using a haemocytometer and 0.04% trypan blue solution. 35,000 cells per well were plated in neuronal growth medium onto the previously prepared astrocyte feeder layer (section 2.2.1). This density was optimal for imaging experiments, for which, fairly sparse neuronal networks are most desirable. Neurons were incubated at 37°C, 5% CO<sub>2</sub> until mature and used for experiments DIV 13-18. The remaining concentrated cell suspension (usually ~0.4 ml) was transferred into T25 flask and 5 ml of astrocyte growth media (Table 2.2) was added. These cells were allowed to grow for 9 -10 days following which they were transferred onto the coverslips as described in section 2.2.1. In order to prevent further astrocytic proliferation in neuronal culture, a mitotic inhibitor ara-C (final concentration 3.3 µM in neuronal growth media), was added on day 2-4 to neuronal cultures. The decision on the timing of ara-C treatment was based on the level of astrocyte confluency in the culture. It was important to provide neurons with well-established astrocytic islands supporting their growth and function.

The major factor discriminating between the growth of neurons or astrocytes in this culturing method is the concentration of FBS used. The reduction of FBS from 10% to 2%, and the addition of ara-C provides with the environment favourable for neuronal

growth, whereas 10% FBS supports astrocytic growth (Ye and Sontheimer, 1998). Also, ara-C added to neuronal culture not only inhibits proliferation of astrocytes, but was also shown to promote neurite outgrowth whilst limiting non-neuronal cells growth (Oorschot and Jones, 1986).

## 2.3 Transfection of hippocampal neurons

Table 2.3.

Product	Product code	Supplier
ProFection Mammalian Transfection System	E1200	Promega
Kynurenic acid	K3375	Sigma-Aldrich

Table 2.4.

Solution	Composition	Storage	Used at
20X Kynurenic acid	20 mM Kynurenic acid, 10 mM MgCl <sub>2</sub> , 5 mM HEPES, pH 7.5 with NaOH	-20°C	37°C
Transfection media	1 mM Kynurenic acid in 10% HEPES BME	Prepared fresh	37°C
Neuronal Growth Media	BME, 20 mM Glucose, 10 mM HEPES, 1 mM Sodium Pyruvate, 2% FBS, 1% Penicillin-Streptomycin, 1% GlutaMAX, 2% B-27	4°C	37°C

Table 2.5.

Insert	Vector	Readout	Supplier
CMV:SypHy1x	pcDNA3	Vesicle Recycling	Gift from Ruud Toonen
CMV:SypHy2x	pcDNA3	Vesicle Recycling	Gift from Ruud Toonen
CMV:SypHy4x	pcDNA3	Vesicle Recycling	Gift from Ruud Toonen
hCMV:iGluSnFR	mEGFP	Glutamate release	Gift from Leon Lagnado

Dissociated rat hippocampal neurons were transfected at DIV 6-9 using modified Ca<sup>2+</sup> phosphate protocol. It is the most widely used method for transfecting neuronal cultures due to its low toxicity and relatively high efficiency achieved with some optimization (up to 50% transfected neurons) (Micheva et al., 2003; Passafaro et al., 2003; Sun et al., 2013; Xia et al., 1996). This method relies on the endocytic uptake of DNA-Ca<sup>2+</sup> phosphate precipitate into neurons and the expression of foreign DNA in the nucleus

(Sun et al., 2013). The important factors affecting the toxicity and efficiency of this method are the even size and the amount of precipitate particles added to the cells, and the time of neuronal exposure to the precipitate (Jiang and Chen, 2007; Xia et al., 1996). The use of kynurenic acid, an inhibitor of ionotropic glutamate receptors, further reduces the neurotoxicity associated with transfection (Xia et al., 1996).

BME media containing 10% HEPES (1 M, pH 7.35) with added 1 mM kynurenic acid was used as a transfection media (Table 2.4). Conditioned media was removed from the wells, kept for later at 37°C and immediately replaced with 500 µl transfection media per well. Cells were incubated in this media for 30 min during which the transfection reactions were prepared. ProFection Mammalian Transfection System was used to deliver DNA to the neurons. 2x HEPES from this kit was pipetted into 15 ml falcon tubes and nuclease free water into Eppendorf tubes (one per reaction). 2-6 µg of plasmid DNA was added to the tubes containing nuclease free water, which was followed by the addition of  $\text{CaCl}_2$  accompanied by vigorous pipetting up and down to ensure adequate mixing. DNA suspension was pipetted dropwise into the tubes containing 2X HEPES whilst being vortexed for 30 s. This suspension was incubated for ~10 min and later added dropwise to the cells. The incubation time with the DNA- $\text{Ca}^{2+}$ -phosphate precipitate was ~45 min. Cells were washed three times with neuronal growth media (Table 2.4) and placed in 50/50 conditioned/fresh neuronal media. DNA concentration, the timing of incubation with the precipitate and the transfection day were optimized for each construct. Following transfection, fine DNA- $\text{Ca}^{2+}$ -phosphate precipitate was observed, which gradually disappeared over the next 24 h. Neurons were used for experiments at 13 -18 days *in vitro* which gave at least 4 days for expression.

## 2.4 Infection of hippocampal neurons with AAV-based constructs

Table 2.6.

Insert	Serotype	Readout	Supplier
pCAG:SypHy2x	AAV-9	Vesicle recycling	Gift from Tiago Branco
pCAG:syGCaMP6f	AAV-6	Ca <sup>2+</sup> influx	Gift from Tiago Branco
pCAG:iGluSnFR	AAV-9	Glutamate release	Penn Vector Core

Despite the fact that good efficiency of calcium phosphate transfection was achieved in our system (~30% transfected cells), and steps minimizing the stress to the neurons were employed, some level of toxicity was always observed as primary neurons are very sensitive to changes in their micro-environment (Sun et al., 2013). The use of Adeno Associated Viruses (AAV) is an alternative method for gene delivery into postmitotic cells such as hippocampal neurons. AAV virions were found to enter the cells via clathrin-mediated endocytosis and were detected in cytosol of HeLa cells within 30 min after infection and transported to the nucleus within 3-4 h post infection (Bartlett et al., 2000). There are numerous AAV serotypes which display species and tissue tropism and therefore the selection of the capsid derived from the right serotype is crucial for successful transduction (Watakabe et al., 2015). Royo et al., 2008 analysed multiple AAV serotypes for the efficiency of expression and toxicity in primary hippocampal neurons. Out of 7 serotypes tested, AAV9 exhibited no neuronal toxicity and a very high level of stable expression over time – 80% of cells displayed GFP fluorescence (Royo et al., 2008). AAV6 also showed high level of expression (72% cells) out of which 85% were neurons, making it the most neuron specific serotype (over astrocytes), nevertheless, at high doses ( $2.5 \times 10^{11}$  genome copies (GC)) AAV6 led to increased neuronal toxicity and hence had to be used at lower doses ( $2.5 \times 10^9$  GC) (Royo et al., 2008).

AAV vectors used in this study were made by Tiago Branco's lab. AAV.*sypHy2x* was based on our cDNA *sypHy2x* plasmid. AAV.*sypHy2x* or AAV.*syGCaMP6f* were added to cell culture at day 4-6 in vitro at a concentration of 0.5  $\mu$ l/well (AAV.*sypHy2x* 2.2-2.9 x

$10^{12}$  GC; AAV.*syGCaMP6f*  $2.6 \times 10^{12}$  GC) and at least 7 days were allowed to establish the expression. At these concentrations, the transduction efficiency was very satisfactory for both constructs and we did not observe any toxicity which significantly improved the experimental output in comparison to the transfected cells. Most of the initial experiments aiming to optimize the imaging system, stimulation protocols and other experimental conditions were carried out using cDNA constructs. These settings were directly transferable to the experiments using AAV-based vectors from which the majority of the data presented here originates.

## 2.5 Plasmid DNA amplification and purification.

Table 2.7.

Product	Product Code	Supplier
Tryptone	T7293	Sigma-Aldrich
Yeast extract	70161	Sigma-Aldrich
Ammonium chloride	A3920/53	ThermoFisher Scientific
Agar	L2897	Sigma-Aldrich
Kanamycin	K1377	Sigma-Aldrich
Ampicillin	A0166	Sigma-Aldrich
DH5 alpha	18263012	Invitrogen
QIAprep Spin Miniprep Kit	27115	Qiagen
Agarose	A9539	Sigma-Aldrich
50X Tris-Acetate-EDTA	B49	ThermoFisher Scientific
Ethidium Bromide	15585011	ThermoFisher Scientific
Nucleobond Xtra Midi/Maxi	740414.10	Macherey-Nagel

Table 2.8.

Solution	Composition	Storage	Used at
LB (Luria-Bertani) Broth	0.01 g/ml Tryptone, 0.005 g/ml Yeast extract, 0.01 g/ml $\text{NH}_4\text{Cl}$ in $\text{H}_2\text{O}$	21°C	37°C

Bacterial transformation was carried out in order to amplify cDNA constructs which were used for transfecting hippocampal neurons. Transformed bacteria were first inoculated on agar plates, followed by expanding the individual colonies into liquid culture. DNA was isolated in a mini-prep, allowing for the selection of the right colony for further



amplification. Bacterial culture was further increased in size and DNA was isolated and purified in a maxi-prep. Details of this process are described below.

The amplification of cDNA constructs was carried out using DH5 $\alpha$  competent cells. 1-3  $\mu$ g of cDNA was added to DH5 $\alpha$  cells, incubated on ice for 10 min and transformed into the DH5 $\alpha$  cells by a heat shock (50 s at 42°C). Following 2 min incubation on ice, SOC media was added to each tube and the mixture incubated for 1 h at 37°C in an orbital shaker (225 rpm). Transformed bacteria were diluted in LB Broth containing either kanamycin (30  $\mu$ g/ml) or ampicillin (50  $\mu$ g/ml), depending on the antibiotic resistance gene of each construct, plated onto agar plates and incubated overnight at 37°C. Single colonies were picked the next day, transferred into falcon tubes containing 5 ml of LB with the corresponding antibiotic (kanamycin or ampicillin) and incubated overnight in the orbital shaker (250 rpm, 37°C). In order to test which colony has the highest bacterial density and also to assess the integrity of the plasmid, DNA from liquid colonies was isolated using QIAprep Spin Miniprep Kit (Protocol followed: Plasmid DNA Purification using the QIAprep Spin Miniprep Kit and a Microcentrifuge). In short, bacteria were pelleted, and lysed which was followed by DNA isolation from the cell debris. The eluted DNA was run on agarose gel (0.75% agarose in 1x TAE with added 0.5  $\mu$ g/ml ethidium bromide) and imaged using a UV illuminator. Bands of the DNA isolated from the mini prep were compared against each other and against the old gel images of the construct. Any unusual pattern could indicate potential mutation and any such colony would be eliminated from further inoculation. Colonies with the brightest bands that were similar to the original construct were selected for further amplification. Following the identification of the best colony, bacteria were inoculated into conical flasks with 400 ml LB and appropriate for the construct antibiotic and incubated overnight in the orbital shaker (250 rpm, 37°C). DNA was extracted and purified using Nucleobond Xtra Midi/Maxi kit, resuspended in 150  $\mu$ l of TE buffer, measured and stored at -20°C until needed.

## 2.6 Imaging system

Table 2.9.

<b>Optimized EMCCD camera settings</b>				
Construct	Stimulation	Exposure (ms)	EM Gain	Imaging frequency (Hz)
SypHy2x	4 APs	40	40	11.2
	40 APs	40	10	11.2
syGCaMP6f	4 APs	40	20	13.5
	40 APs	40	10	13.5
vGpH	4 APs	70	60	11.2
iGluSnFR	2 APs	10	20	23.5
For all the constructs the remaining settings were as follows: binning 4 x 4, readout speed 13,000 MHz, pre-amplification gain 3.8, cooling temperature -77°C.				

All experiments were carried out on an upright microscope BX61WI using x60 1.0 NA dipping objective with the mercury lamp light source. Experimental data was collected using either charge-coupled device camera (Olympus XM10) or cooled electron multiplying charge-coupled device camera (EMCCD) (Andor Ixon) depending on the experimental needs. EMCCD camera due to its superior dynamic range, quantum efficiency and sensitivity was used for high-speed imaging of experiments aiming to image low level of fluorescence change. The camera settings were optimized for imaging of single vesicle release events and synaptic performance following small stimulation protocols with various constructs (Table 2.9). The emission and excitation filters were as follows: 480/20, 520/35 for sypHy, syGCaMP6f, iGluSnFR, FM1-43, FM1-43FX, OGB and bassoon; 470/22, 624/40 for FM4-64; 556/20, 609/54 for sytl-Oyster550; 556/20, 624/40 for endophilin I and vGlu1 and vGlu2 imaging. For the imaging of single vesicle release events a blackout curtain was mounted around the stage. The temperature in the room was kept at 23°C for all the experiments.

## 2.7 Field stimulation

Table 2.10.

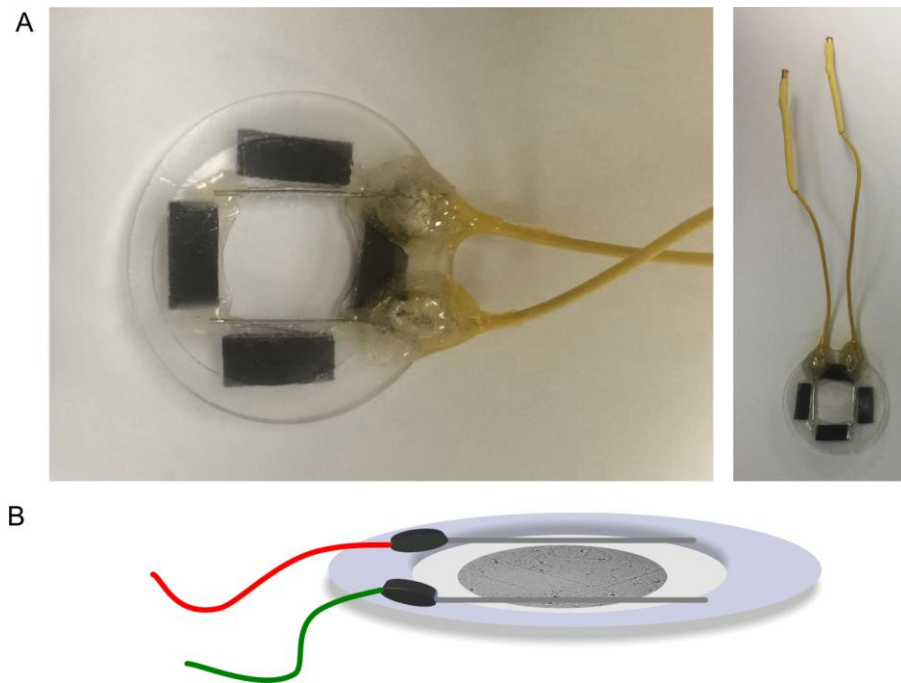
Product	Product Code	Supplier
Sodium Chloride (NaCl)	S5886	Sigma-Aldrich
Potassium Chloride (KCl)	P5404	Sigma-Aldrich
Calcium Chloride ( $\text{CaCl}_2 \cdot 2\text{H}_2\text{O}$ )	C7902	Sigma-Aldrich
Magnesium Chloride ( $\text{MgCl}_2 \cdot 6\text{H}_2\text{O}$ )	M2393	Sigma-Aldrich
D-glucose	G7021	Sigma-Aldrich
HEPES	H3784	Sigma-Aldrich
CNQX disodium salt	1045	Tocris Bioscience
D-AP5	0106	Tocris Bioscience

Table 2.11

Solution	Composition	Storage	Used at
External bath solution (EBS)	In mM: 137 NaCl, 5 KCl, 2.5 $\text{CaCl}_2$ , 1 $\text{MgCl}_2$ , 10 D-Glucose, 5 HEPES	4°C	21°C

In order to measure the activity of cultured hippocampal neurons a field stimulation was used, allowing to simultaneously induce action potential firing in all the neurons in the culture. Specifically for this purpose a custom built imaging chamber was designed, consisting of a plastic chamber with a gridded glass coverslip at the base (Fig.2.2). Two platinum wire electrodes (0.5 mm diameter) were positioned 1 cm apart, in parallel to each other, and were connected to a Grass stimulator (Astro-Med Inc, USA) for field stimulation (20 Hz, 1 ms pulse duration, 20-22.5 V – calibration shown below). The level of applied stimulation was controlled via custom-written Macromanagers scripts. Although we were able to monitor the number of action potentials delivered to the cells, the level of cellular response elicited by a given stimulus was beyond our control. Therefore from now on, when we, for example, refer to 4 action potential stimulus (4 APs), this only signifies the number of pulses delivered to the cells and not the extent of the response of the neurons. For the experimental purposes, cultured hippocampal neurons were transferred straight from the cell culture media into the stimulation chamber containing pre-warmed HEPES-buffered extracellular bath solution (EBS) supplemented with 20  $\mu\text{M}$  CNQX and 50  $\mu\text{M}$  AP5, which are AMPAR and NMDAR blockers, respectively. This

ensured that neurons were exposed to the ionic concentrations similar to their usual extracellular environment and the use of blockers prevented propagation of spontaneously generated signals and recurrent post-stimulus activity. These conditions were maintained across all the experiments unless indicated otherwise.



**Figure 2.2 Stimulation and imaging chamber.** A) Custom made imaging chamber with magnetic strips attached at the bottom for stability during imaging. B) Schematic of the chamber with the coverslip in the middle.

### 2.7.1 Calibration of stimulation intensity

Table 2.12

Product	Product Code	Supplier
Oregon Green™ 488 BAPTA -1	O-6807	Life Technologies
Sytl-Oyster550	105 011C3	SySy

A key starting point for this work was to demonstrate that observed synaptic responses resulted from a specific delivered stimulus, to calibrate the intensity of the applied

stimulus and to make sure that it is sufficient to reliably elicit synaptic response with the chamber used. Oregon Green™ 488 BAPTA -1 (OGB) was the optical reporter used for this experiment. OGB is a membrane-permeable  $\text{Ca}^{2+}$  indicator with relatively high  $\text{Ca}^{2+}$  affinity, which displays a rise in fluorescence intensity upon binding to  $\text{Ca}^{2+}$  (Paredes et al., 2008).

Cultures were incubated with 12  $\mu\text{M}$  of OGB for 2 h ( $37^\circ\text{C}$  in 5%  $\text{CO}_2$ ) allowing the passive uptake of this dye into the cultured neurons. Coverslips were then transferred into an imaging chamber and washed with EBS with blockers (section 2.7) to remove any free dye. After this, cells labelled with OGB were easily identifiable (Fig.2.3.A). The baseline fluorescence of OGB appeared very non-localized within neuronal processes (Fig.2.3.A). Therefore, in order to make sure that we read out fluorescence fluctuations resulting from stimulation driven  $\text{Ca}^{2+}$  influx, specifically at the presynaptic terminals, we loaded our samples with 1:100 sytl-Oyster550 in EBS with blockers, by applying 1200 APs, 20 Hz stimulation (stimulation and loading protocols are described in section 2.8). Sytl-Oyster550 is a fluorescently tagged anti-synaptotagmin 1 (sytl) antibody which upon applied stimulation is localized in the internal lumen of synaptic vesicles and hence marks functional presynaptic terminals. This aided the selection of the regions of interest targeting discrete synaptic terminals (Fig.2.3.A and B). OGB is not eliminated from the cells during the stimulation which allowed for multiple imaging of the same region as well as multiple regions on the same coverslip. Time lapse images were collected (12.3 Hz; 81 ms per frame) whilst 10 AP (10 Hz) stimulation was delivered with the voltage being gradually increased by increments of 5 V from 0 V to 30 V. ImageJ was used for image analysis. Regions showing robust responses to stimulation were identified based on OGB fluorescence by subtracting the fluorescence intensity of the baseline (average of 5 frames) from the fluorescence at the peak of the stimulus (average of 5 frames). This subtracted OGB image was overlaid with sytl-Oyster550 labelling to identify regions corresponding to presynaptic terminals and select ROIs (Fig 2.3.B).

There was a noticeable increase in the fluorescence intensity during the stimulus, followed by the return of the fluorescence to baseline levels (Fig.2.3.B and C). Application of stimulus at 5 V or 10 V resulted in no fluorescence increase and no synaptic response similarly to when no stimulus was applied (0 V) (n=7 regions (620 synapses), One-way ANOVA with Tukey's post-hoc analysis: 0V-5V, 0V-10V, 5V-10V,  $P > 0.9999$ ,  $P > 0.9999$  and  $P > 0.9999$ , respectively) (Fig.2.3.D). However, when the cells were subjected to 15 V stimulus an increase in fluorescence intensity followed by its decay was seen. This observable response, which exceeded baseline represents a clear stimulus-response relationship at this voltage (One-way ANOVA with Tukey's post-hoc analysis: 0V-15V, 5V-15V, 10V-15V,  $P = 0.6535$ ,  $P = 0.5962$  and  $P = 0.6017$ , respectively) (Fig.2.3.C and D). This signified that 15 V was the minimum voltage that resulted in some presynaptic  $\text{Ca}^{2+}$  influx measured by OGB. A saturation point in response amplitude was found at 20-25 V and further increases in voltage did not lead to additional rise in fluorescence amplitude. (n = 7 regions (620 synapses), One-way ANOVA with Tukey's post-hoc analysis: 15V-20V,  $P = 0.0033$ ; 20-25V,  $P = 0.4366$ ; 20V-30V,  $P = 0.4005$ ; 25-30V,  $P > 0.9999$ ).

This experiment allowed us to demonstrate stimulus-related synaptic response in our system, and to select submaximal stimulus voltage. For this particular chamber 22.5 V was used as optimal for synaptic activation. Another chamber was also used for which the optimal voltage was 20 V.

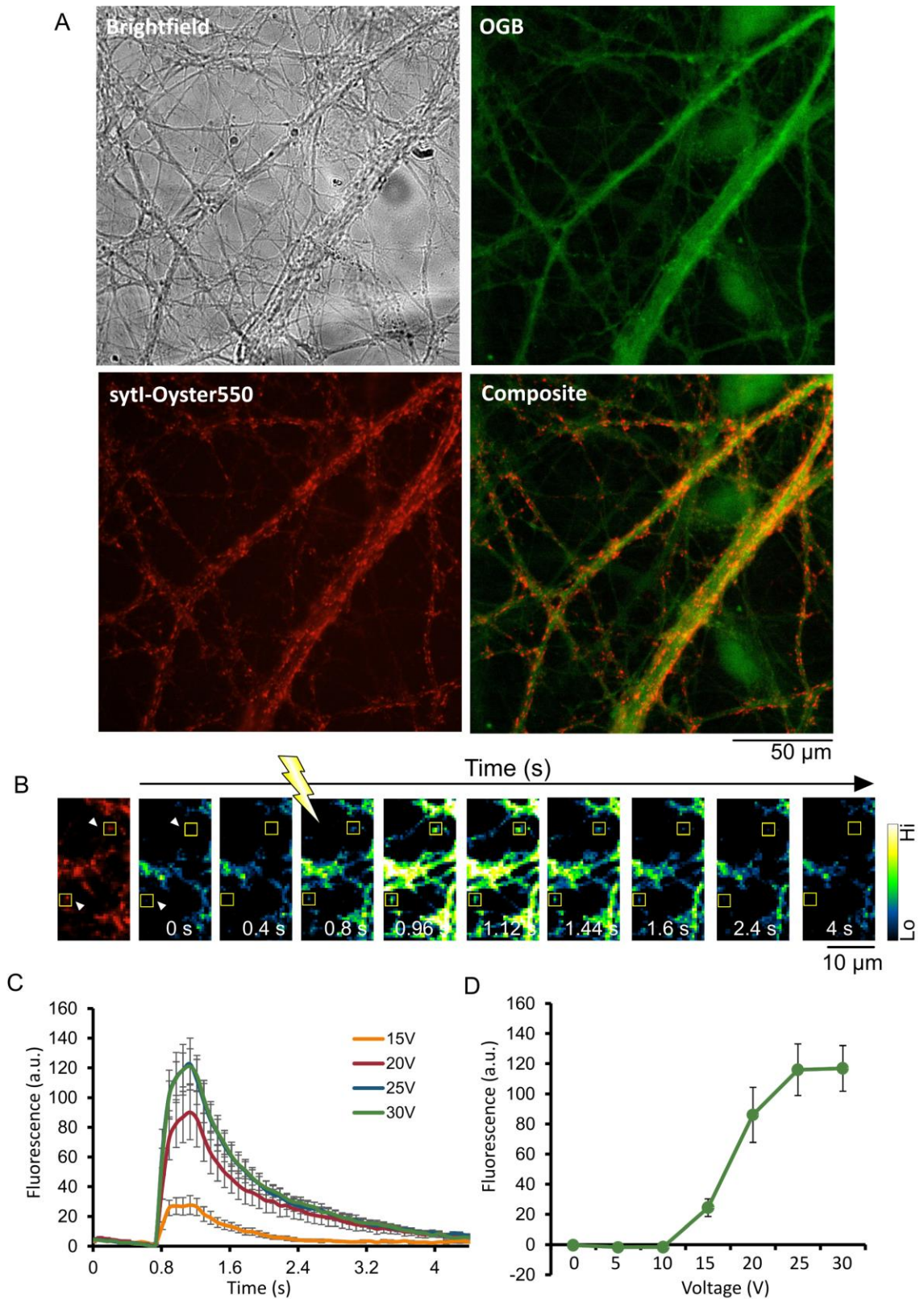


**Figure 2.3 Establishing optimal stimulation intensity using OGB.** A) Representative image of primary hippocampal culture (top left) which was incubated in the presence of OGB (top right, baseline fluorescence) and subsequently loaded with sytl-Oyster550 antibody (bottom left). Presynaptic terminals (red) are clearly identifiable against OGB background (bottom right). Images were acquired using cooled EMCCD camera ( $-77^{\circ}\text{C}$ ),

60x objective, 1x1 binning. Scale bar 50  $\mu\text{m}$ . B) Left panel shows sytl-Oyster550 fluorescence. Arrowheads indicate ROIs (2.5 x 2.5  $\mu\text{m}$ ) encapsulating example individual boutons selected for the analysis. Subsequent panels display change in OGB fluorescence in response to  $\text{Ca}^{2+}$  influx resulting from the applied stimulation (40 APs, 20 Hz). C) Mean responses of 620 presynaptic terminals to stimuli of varied voltage. Data from 3 coverslips, n=7 regions, shown as average  $\pm$  SEM. D) Quantification of  $\text{Ca}^{2+}$  influx evoked by different voltages measured as a difference between the peak fluorescence and the baseline prior to the stimulation. Stimuli at 0 V, 5 V and 10 V did not cause any rise in fluorescence (n = 7 regions, 620 synapses, One-way ANOVA with Tukey's post-hoc analysis: 0V-5V, 0V-10V, 5V-10V,  $P > 0.9999$ ,  $P > 0.9999$  and  $P > 0.9999$ , respectively). The first significant rise in fluorescence was observed at 15 V (n = 7 regions, 620 synapses, One-way ANOVA with Tukey's post-hoc analysis: 0V-15V, 5V-15V, 10V-15V,  $P = 0.6535$ ,  $P = 0.5962$  and  $P = 0.6017$ , respectively). Next incremental increase of voltage from 15 V to 20 V led to significant increase in fluorescence but any further rise in voltage, 25 V or 30 V, did not led to further change in fluorescence (n = 7 regions, 620 synapses, One-way ANOVA with Tukey's post-hoc analysis: 15V-20V,  $P = 0.0033$ ; 20-25V,  $P = 0.4366$ ; 20V-30V,  $P = 0.4005$ ; 25-30V,  $P > 0.9999$ ).

## 2.8 FM1-43 and live antibody labelling protocols

Table 2.13

Product	Product Code	Supplier
FM1-43	T35356	Life Technologies
FM1-43FX	F35355	Life Technologies
FM4-64	T3166	Life Technologies
Sytl-Oyster550	105 011C3	SySy

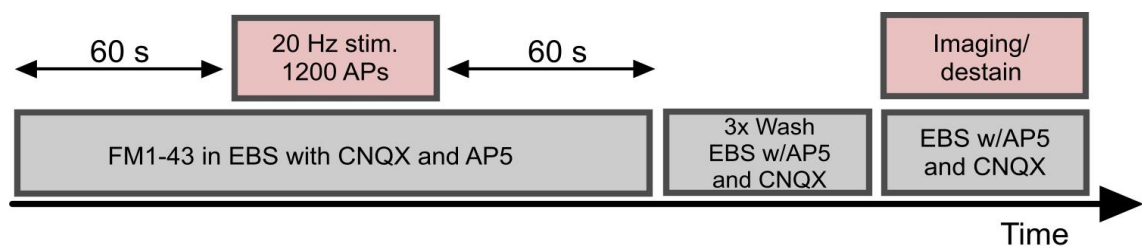


**Figure 2.4 Loading and imaging protocol with FM1-43 dye for labelling vesicles in the recycling pool and FM dye destaining.**

In order to visualize functional presynaptic terminals, coverslips with cultured hippocampal neurons were labelled with fluorescent indicators of synaptic function. Coverslips were transferred straight from culturing plates into the imaging chamber containing 0.6 ml of pre-warmed EBS with blockers (20  $\mu\text{M}$  CNQX and 50  $\mu\text{M}$  AP5). EBS solution was exchanged to EBS containing 10  $\mu\text{M}$  FM1-43 dye and the cells were



incubated for 60 s prior to the onset of the loading stimulation (Fig.2.4). A stimulus with the chosen number of action potentials was applied in order to induce exo-endocytic cycle, allowing synaptic vesicles to take up the dye. Typically 40 APs, 600 APs or 1200 APs stimulation at 20 Hz was used. Following the stimulus, the cells were kept in the presence of FM1-43 for a further minute, to permit vesicle recycling to be completed. The dye was washed at least 3 times with EBS with blockers in order to remove all traces of FM-dye from the solution and any residual dye remaining at the cell surface. The protocol summarized in Figure 2.4 represents the routine for loading all vesicles in the recycling vesicle pool. The same loading protocol was used for labelling synapses with FM1-43FX, FM4-64 and sytl-Oyster550 antibody.

## 2.9 Measuring synaptic vesicle pool sizes

Table 2.14

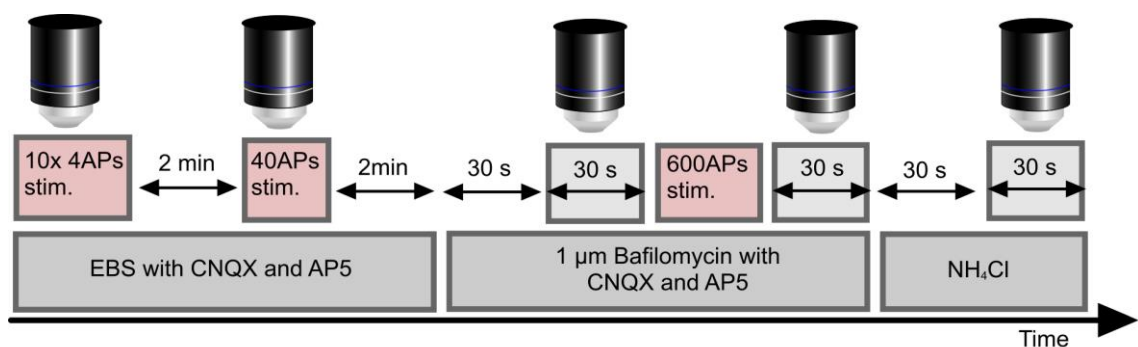
Product	Product Code	Supplier
Ammonium Chloride	A0171	Sigma-Aldrich
Bafilomycin A1	B1793	Sigma-Aldrich

Table 2.15

Solution	Composition	Storage	Used at
Ammonium chloride EBS	In mM: 50 NH <sub>4</sub> Cl, 87 NaCl, 5 KCl, 2.5 CaCl <sub>2</sub> , 1 MgCl <sub>2</sub> , 10 D-Glucose, 5 HEPES	4°C	21°C

Measurement of the sizes of distinctive vesicle pools was carried out in 3 steps based on the use of sytHy2x expressing hippocampal neurons. First, a culture was transferred to the stimulation chamber and a fluorescence region with functional synapses was identified by stimulating neurons with 10 APs, 20 Hz stimulus. Cells were stimulated 10x with 4 APs to collect data for functional analysis of presynaptic terminals. The protocol for measuring vesicle pool sizes is summarized in Figure 2.5. For readily-releasable pool (RRP), synaptic responses were imaged after 2 minutes recovery using a 40 APs, 20 Hz stimulation, which recycles this whole pool. Following another 2 min recovery, the EBS

in the chamber was replaced with 0.6 ml of EBS with blockers containing 1  $\mu$ M bafilomycin (baf), a v-ATPase blocker, which prevents reacidification of newly formed synaptic vesicles (Fernández-Alfonso and Ryan, 2004). Neurons were incubated in this drug for 30 s prior to imaging background fluorescence. Due to slow, spontaneous increase in baseline fluorescence caused by prolonged exposure to baf (Li et al., 2005), the imaging was limited to 30 s including focusing time. Stimulus of 600 APs, 20 Hz was applied to the cells in order to release the entire recycling pool, which was locked in the alkaline state in the presence of bafilomycin (Fernández-Alfonso and Ryan, 2004; Rey et al., 2015). Immediately after the end of the stimulation the sample was imaged for 30 s which allowed the measurement of the fluorescence corresponding to the size of the recycling pool. EBS-containing baf was exchanged for  $\text{NH}_4\text{Cl}$  solution by copiously washing the sample 2-3 times with  $\text{NH}_4\text{Cl}$  for 30 s to ensure the full replacement of the solution.  $\text{NH}_4\text{Cl}$  leads to neutralization of the vesicular lumen which reveals all the sypHy2x fluorescence, and enables the measurement of the total vesicle pool within the terminals. Cells were imaged for a further 30 s and the fluorescence from this final step represented the size of the total vesicle pool. All the solution exchanges were carried out with extreme care to ensure that the coverslip was not moved in the process. The timing for solution exchanges and imaging was also very strictly maintained in the consecutive experiments, to ensure highly reproducible methodology.



**Figure 2.5 Summary of the protocol measuring the size of synaptic vesicle pools.**

## 2.10 Pharmacological disturbance of endocytic kinetics

Table 2.16

Product	Product Code	Supplier
Dynasore	D7693	Sigma-Aldrich
Dimethyl sulfoxide (DMSO)	D/4121/PB08	Fisher Scientific

In order to test whether we can disrupt the endocytic kinetics of synaptic vesicles at hippocampal neurons, we used a blocker of dynamin function, Dynasore. Dynamin was shown to be involved in both clathrin dependent and independent endocytosis (Delvendahl et al., 2016; Hayashi et al., 2008; Voglmaier and Edwards, 2007). The selection of this drug therefore ensured that we targeted more than one endocytic mechanism in our experiment. AAV.*syphY2x* expressing cells were placed in a stimulation chamber with 0.6 ml EBS + blockers and imaged during 6 x 4 APs stimulation trials. Dynasore was diluted to 10  $\mu$ M in EBS with blockers (20  $\mu$ M CNQX and 50  $\mu$ M AP5) and only half of the solution was exchanged in the chamber to achieve the final concentration of 5  $\mu$ M dynasore. The cells were incubated with the drug for 10 min prior to the next round of stimulation and imaging (5 x 4 APs). The concentration of dynasore was optimized to only induce sub-threshold block of dynamin function (Macia et al., 2006; Newton et al., 2006).

## 2.11 Immunocytochemistry

Table 2.17

Product	Product Code	Supplier	Dilution used
Rabbit anti-Endophilin I antibody	159002	SySy	1:500
Rabbit anti-vGlut1 antibody	135303	SySy	1:1000
Guinea pig anti-vGlut2 antibody	135404	SySy	1:2000
Goat anti-Rabbit Alexa Fluor ® 568	175471	Abcam	1:1000
Goat anti-Guinea pig Alexa Fluor ® 568	175714	Abcam	1:1000

Table 2.18

Product	Product Code	Supplier
Paraformaldehyde (PFA) 16%	AGR1026	Agar Scientific
Triton X-100	T9284	Sigma-Aldrich
Foetal Bovine Serum (FBS)	10500056	Gibco™
Bovine Serum Albumin (BSA)	A2153	Sigma

Table 2.19

Solution	Composition	Storage	Used at
4% PFA	4 ml 4% PFA in 16 ml 1x PBS	Prepared fresh	21°C
Triton X-100 0.1%	1 µl Triton X-100 in 1 ml 1x PBS	Prepared fresh	21°C
Saturation FBS	1 ml FBS in 10 ml 1x PBS	Prepared fresh	21°C
0.1% BSA	0.01 g BSA in 10 ml 1x PBS	Prepared fresh	21°C

Antibody labelling was carried out for the purpose of identification of glutamatergic terminals and for measuring the level of endophilin I. Coverslips with cultured hippocampal neurons were transferred into imaging chamber containing EBS with blockers (20 µM CNQX and 50 µM AP-5). Regions expressing AAV.*sypHy2x* were identified and the protocols for functional readouts were carried out. Differential interference contrast (DIC) images were taken for identification of imaged region following antibody labelling. Immediately after imaging, neurons were transferred into 4% PFA, fixed for 30 min at room temperature and washed 3 times with 3x PBS. In all the following incubations, neurons were placed on a rocking platform. Cells were permeabilized with 0.1% Triton for 10 min to allow antibody penetration and after 3 washes with 1x PBS, in order to saturate non-specific binding sites, samples were incubated in 10% FBS for 20 min and washed once before adding primary antibody diluted in 0.1% BSA (for antibody dilutions refer to Table 2.15). Following 1h incubation, cells were washed 3 times with 1x PBS and incubated for 30 min with secondary antibody made up in 0.1% BSA (for concentrations refer to Table 2.15). Samples were washed 3 times with PBS 1x and either imaged immediately or mounted, stored at 4°C, and imaged within a week post-labelling.

## 2.12 Electron microscopy

Table 2.20

Product	Product Code	Supplier
Ammonium chloride	A0171	Sigma-Aldrich
Diaminobenzidine (DAB)	4170	Kem-En-Tec
DDSA	DO27	TAAB Laboratories Equipment
DMP-30	DO32	TAAB Laboratories Equipment
25% glutaraldehyde	AGR1020	Agar Scientific
Glycine	G8898	Sigma-Aldrich
MNA	M011	TAAB Laboratories Equipment
Osmium tetroxide	O012	TAAB Laboratories Equipment
16% paraformaldehyde	AGR1026	Agar Scientific
Phosphate Buffered Saline (PBS)	18912-014	Life Technologies
Potassium ferrocyanide	455989	Sigma-Aldrich
Propylene oxide	AGR1080	Agar Scientific
Sodium cacodylate	AGR1104	TAAB Laboratories Equipment
Sodium sulphate, anhydrous	798592	Sigma-Aldrich
TAAB 812	TO23	TAAB Laboratories Equipment
Tannic acid	202420050	ACROS Organics
Uranyl acetate	AGR1260A	Agar Scientific

Table 2.21

Solution	Composition	Storage	Used at
Anhydrous sodium sulphate	1% anhydrous sodium sulphate in 0.05 M cacodylate buffer	Prepared fresh	21°C
Ammonium chloride solution	100 mM in 1x PBS	4°C	21°C
DAB	1 mg/ml in 1x PBS	Prepared fresh	21°C
EPON solution	Ratio of 24 TAAB 812 : 9.5 DDSA : 16.5 MNA : 1 DMP30	Prepared fresh	21°C and 60°C
Fixative	2% paraformaldehyde, 2% glutaraldehyde in 1x PBS	Prepared fresh	21°C
Glycine	100 mM in 1x PBS	-20°C	21°C
Sodium cacodylate buffer	0.2 M sodium cacodylate in dH <sub>2</sub> O, pH 7.4 with HCl	4°C	21°C
Tannic acid	1% solution in 0.05 M sodium cacodylate	Prepared fresh	21°C
Uranyl acetate	4% uranyl acetate in 70% ethanol, vortexed for 5 min and filtered	Prepared fresh	21°C

In addition to functional readouts, hippocampal neurons were prepared for correlative ultrastructural analysis of individual presynaptic terminals. Protocol for sample preparation with some modifications was followed as previously established and described by (Darcy et al., 2006b).

### **2.12.1 Fixation**

A coverslip with 12-18 DIV hippocampal neurons expressing AAV.*sypHy2x* was etched, which helped in establishing the correct orientation of the coverslip later on during the experiment, and transferred into the imaging chamber containing EBS with blockers. Cells were imaged with 10 x 4 APs stimulation protocol to obtain functional readouts of individual presynaptic boutons. Multiple 60x and 10x DIC images were collected in order to allow relocation of the area of interest. Samples were loaded with FM1-43 FX during 10 APs, 20 Hz stimulation according to the protocol described in section 2.8. However, the sample was washed only once in order to shorten the time between the end of the experiment and fixation. Until photoconversion, great care was taken to protect the sample from the light. The coverslip was transferred straight from the imaging chamber (EBS with blockers) into fixative (2% paraformaldehyde, 2% glutaraldehyde) and incubated for 15 min at room temperature under cover. Following fixation, the coverslip was washed 3 times with 100 mM glycine and incubated in this solution for an hour. The sample was then washed for 1 min in  $\text{NH}_4\text{Cl}$  solution and copiously rinsed three times in 1x PBS.

### **2.12.2 Photoconversion of DAB**

The region of interest was relocated with the aid of DIC images taken at the end of the functional imaging of *sypHy2x*. 1x PBS solution was exchanged for 1 mg/ml DAB solution in 1x PBS in which the sample was incubated for 10 min in the dark. After that time had

elapsed, half the solution was exchanged for fresh DAB, focus was established and the sample was continuously illuminated for 10 – 15 min with a dedicated 40x NA 0.8 water immersion objective (excitation 480/20), to drive the photoconversion reaction. From this point onwards, the sample was not light sensitive anymore. After copious washing with 1x PBS the coverslip was ready for electron microscopy processing.

### **2.12.3 Sample preparation for electron microscopy**

The coverslip was transferred into 0.1 M cacodylate buffer and then placed in fixative/staining solution comprised of 1.5% potassium ferrocyanide, 1% osmium tetroxide in 0.1 M cacodylate buffer for 1 h then washed 3 times with 0.1 M cacodylate buffer. Further staining was carried out using 1% solution of tannic acid in 0.05 M for 45 min, followed by a 5 min wash in 1% anhydrous sodium sulphate in 0.05 M sodium cacodylate. The coverslip was taken through a series of dehydration steps with ethanol, each wash lasting 5 min: 1 x 50%, 2 x 70%, 2 x 90%, 3 x 100%. During the last wash with 70%, sample was stained en-bloc with 4% uranyl acetate in 70% ethanol for 30 min. The dehydrated sample was placed in 1:1 EPON/propylene oxide mix for 1 h following which it was transferred into EPON (for composition refer to Table 2.21) and incubated in the resin for 4 h. The coverslip was then placed on top of a block of pre-polymerized resin with the cells facing the EPON block, making sure that the region of interest (based on the notch in the coverslip) lay within the diameter of the block. Finally, sample was polymerized overnight at 60°C.

### **2.12.4 Region identification and serial sectioning**

Following polymerization, the coverslip was removed from the resin block by dipping it into liquid nitrogen, and discarded. This exposed the cells on the resin block, which were now easily visualized under an inverted microscope. Using DIC images from the

beginning of the experiment, the photoconverted region was identified and marked using scalpel blade (No#10A) on the resin block, which was then mounted onto a Leica EM UC7 ultramicrotome. The excess resin was carefully trimmed around the region of interest with a single-edge razor blade aiming to leave only as little surrounding resin as possible. This process was carefully monitored against the printed out image of the photoconverted region. Once trimming was completed, 60 nm serial sections were cut using a diamond knife and collected from the water boat, attached to the knife, onto a formvar coated slot grids (Agar Scientific). Serial sectioning was carried out by Catherine Smith.

### **2.12.5 Imaging**

Grids with serial sections were imaged using a JEOL 1200 transmission electron microscope with a mounted Gatan OneView camera. Depending on the intended use of the images, the micrographs were typically collected using 6000-15000x magnification.

## **2.13 Image analysis**

### **2.13.1 Fluorescence**

Fluorescence time lapse images were analysed using ImageJ. The general approach for the analysis of genetically expressed fluorescence constructs included several steps. Synapses responding to the stimulation were identified based on the subtracted image of the average baseline fluorescence before the stimulation from the average fluorescence intensity at the peak of the stimulation. Square ROIs of 2.8 x 2.8  $\mu\text{m}$  were drawn around individual responding boutons. In the protocols with repeated stimulation at least half of the trials were screened for the responding boutons. The selected ROIs were applied back to the original images and inspected for any oversaturated



regions/responses and if any identified, those ROIs were removed from the analysis. The background fluorescence was also examined and any ROIs positioned within large fluorescence regions were removed from the set. Any ROIs containing obvious moving fluorescence package were also eliminated. Once these criteria were satisfied the mean grey value was measured for the selected synapse and the readouts were transferred to Excel and saved in a format acceptable for the Matlab analysis. Details of Matlab analysis are explained under individual sections in the Results chapter. Matlab scripts were written with assistance from Prof Kevin Staras.

The analysis of FM1-43 data followed the same basic rules, with the exception of the order of image subtraction. In the case of FM1-43-labelling, the starting fluorescence is at the peak of the fluorescence, and for the analysis of destain the average of the end imaging frames was subtracted from the average of the baseline level fluorescence prior to the stimulation begin. This revealed those synapses that underwent the stimulus-evoked release of synaptic vesicles. The fluorescence puncta at the peak of fluorescence had to be fully encapsulated within the  $2.8 \times 2.8 \mu\text{m}$  ROIs, to ensure that synapses of comparable sizes are sampled. The mean grey values were measured for all ROIs in ImageJ and data transferred to Excel for further analysis. Other experiment-specific details of the analysis approach are described under the respective Results sections.

### **2.13.2 TEM micrographs**

For correlative microscopy, images of the experimental regions were identified with the aid of DIC and fluorescence images prior to the sample fixation. This allowed us to relocate the cellular process of interest. Low magnification TEM images of middle sections were taken and aligned with DIC and fluorescence images in order to identify specific synaptic boutons, which were then traced and imaged in the consecutive serial sections.

Light microscopy and TEM Images alignment was carried out in Xara Designer Pro (Xara Ltd, UK). Alignment of TEM images and their annotation was also performed in this software. More detailed measurement of presynaptic properties (total number of vesicles and synaptic volume), were extracted using Reconstruct software (Fiala, 2005). 3D reconstructions of the presynaptic terminals were also carried out in this software.

## 2.14 Amyloid Beta preparation

Table 2.22

Product	Product Code	Supplier
Recombinant A $\beta$ 1-42	A-1163-2	rPeptide
Variant A $\beta$ 1-42	Custom made	JPT
1,1,1,3,3,3-hexafluoro-2-propanol (HFIP)	52517	Sigma-Aldrich
Dry DMSO	326881000	Sigma-Aldrich
Zeba 7K MWCO	89890	Thermo Scientific

Table 2.23

Solution	Composition	Storage	Used at
HEPES buffer	10 mM HEPES, 50 mM NaCl, 1.6 mM KCl, 2 mM MgCl <sub>2</sub> , 3.5 mM CaCl <sub>2</sub> , pH to 7.4 with NaOH	4°C	21°C

Amyloid Beta 1-42 (A $\beta$ 1-42) and variant peptide (vA $\beta$ 1-42) were prepared according to the modified method developed by (Broersen et al., 2011). LoBind Eppendorfs and tips (Alpha Laboratories) were used for the preparation of these peptides. To disaggregate the peptides, 0.2 mg of A $\beta$ 1-42 and vA $\beta$ 1-42 were solubilized in 200  $\mu$ l HFIP. The vials containing the peptides were vortexed for 60 s and sonicated for 5 min in a 50/60 Hz bath sonicator. HFIP was evaporated under a low stream of nitrogen gas which resulted in dry films of A $\beta$ 1-42 and vA $\beta$ 1-42, which were next dissolved in 200  $\mu$ l dry DMSO, vortexed for 1 minute and sonicated for one minute. In the meantime, a zeba buffer-exchange column was equilibrated with HEPES buffer. Prior to addition of A $\beta$ 1-42 and vA $\beta$ 1-42 solutions, 40  $\mu$ l of HEPES buffer was added as a stack, immediately followed by the two peptides, which were eluted from the column by centrifugation at 1000 g for

2 min at 4°C into a fresh, non-stick microcentrifuge tube. Protein eluates were maintained on ice, whilst being measured using a NanoDrop spectrophotometer at 280 nm (molar absorption coefficient  $1490 \text{ M}^{-1}\text{cm}^{-1}$ ). A $\beta$ 1-42 and vA $\beta$ 1-42 were immediately diluted to 50  $\mu\text{M}$  with HEPES buffer to ensure a uniform aggregation of the peptides. Following a 2 h incubation, peptides were added to cultured neurons at 0.1  $\mu\text{M}$  or 1  $\mu\text{M}$  and HEPES buffer was added as a vehicle control.

## 2.15 Statistical analysis

Most data is presented as a mean value of a group  $\pm$  standard error of the mean, unless indicated otherwise. Typically, two-tailed Student's t-test (paired or unpaired), and one-way ANOVA with post-hoc analysis, were used to compare two or more groups, respectively. Where appropriate, the decision between parametric and nonparametric tests was made based on the normality of the data in conjunction with the sample size. The binomial test was used for the analysis of synapse similarity in Chapters 4 and 5. Pearson's correlation coefficient was used to examine the extent of relationship between two variables. Kolmogorov-Smirnov test was used for comparing distributions, and variability within data sets was measured using coefficient of variation.

# 3 ESTABLISHING IMAGING METHODS USED FOR STUDYING FUNCTION OF PRESYNAPTIC TERMINALS

---

## HIGHLIGHTS

- FM1-43 can be used for identification of functional synapses, monitoring the dynamics of synaptic vesicle pools and measuring the kinetics of synaptic vesicles exocytosis
- Sytl-Oyster550 is suitable for the identification of presynaptic terminals and measuring their size
- SypHy2x is the probe of choice for monitoring of exo- and endocytosis of single synaptic vesicles
- SyGCaMP6f can be used to measure stimulus-evoked presynaptic  $\text{Ca}^{2+}$  influx

### 3.1 Introduction

Chemical synapses in the central nervous system are highly specialized contact points between cells, and are composed of two major components: the presynaptic and postsynaptic terminal. Information transfer in the CNS relies on the generation of a postsynaptic response as a result of neurotransmitter released from synaptic vesicles. These reside at the presynaptic terminals, are organized in clusters and can be easily identified under electron microscope (Harris and Sultan, 1995; Harris and Weinberg, 2012). Despite the fact that all synaptic vesicles have a uniform ultrastructural appearance, they can be divided into distinct, functionally described vesicle pools: the readily releasable pool (RRP), recycling pool or resting pool. The way SVs are sorted into these different pools, and other parameters regulating important aspects of presynaptic function, are largely unknown. Despite a great level of heterogeneity in the behaviour of presynaptic population, the outstanding question is how and whether structural and molecular components regulate/affect the performance of the individual boutons.

Our knowledge on presynaptic terminals has been hindered, in comparison to the postsynaptic compartment, by the limits of the available techniques. However, the development of imaging tools in the last 20-25 years has provided us with new strategies for examining otherwise inaccessible presynaptic terminals of small central synapses, and broadened our understanding of their function, regulation of their performance, plasticity and disease-associated changes (Kavalali and Jorgensen, 2013; Maschi and Klyachko, 2015; Sebastião et al., 2013). However, despite this major progress there still remains uncertainty about how the properties of individual presynaptic terminals (e.g. strength, release probability or recycling kinetics) are shaped by their history, and how these properties are attuned to meet the functional needs of the network, to ensure information transmission between cells. Effective synaptic transmission relies on the efficiency of the exocytosis and endocytosis of synaptic vesicles, yet the factors that

influence these two processes are largely unexplored, and will be the major objective of this work. Given that the kinetics of recycling of multiple vesicles will mask the intricate details of the timing of this process at individual synapses, key aspect of the approach used here was to obtain measurements at the level of single vesicle release events.

The objective of this chapter was to validate available imaging probes and to identify appropriate tools for achieving the goal of imaging single vesicle recycling kinetics. The first section verifies approaches using acutely applied imaging probes: FM1-43 and sytl-Oyster550 for the purpose of detection, characterization and functional monitoring of presynaptic terminals in the remaining chapters of this thesis. The second section characterizes genetically encoded reporters of synaptic function suitable for monitoring the recycling of synaptic vesicles, presynaptic  $\text{Ca}^{2+}$  influx and glutamate release. The validation of the tools used for measuring single vesicle recycling kinetics is presented in this section and was crucial for the fulfilment of the major aims of this study (section 1.7).

## **3.2 Fluorescent tools used to readout properties of recycling vesicles**

The first objective was to establish whether we can observe functional synapses in primary hippocampal cultures. To do this we used two approaches exploiting acutely applied fluorescence markers: FM1-43 and sytl-Oyster550, which was utilized to validate the findings with FM1-43.

### **3.2.1 Culturing primary hippocampal neurons**

A key objective of this work was to establish an approach for high-sensitivity single vesicle imaging. Towards this goal, it was important to first establish viable hippocampal

cultures. Hippocampal cell culture is a universally employed system in studies, focusing on cellular and molecular function of neurons (Grabrucker et al., 2009). Precise control over plating density was one of the advantages of choosing this model for this study (Kaeck and Banker, 2006).

The dissociated rat hippocampal culture preparation used in our laboratory is a modified version of the method first developed by Banker and Cowan, 1977. As described in detail in the Methods chapter, culturing was performed in two steps: the hippocampus was dissected out from P0-P1 rat pups and plated onto an astrocyte feeder layer, which was prepared 5 days in advance. Initially, astrocytes were cultured in 10% FBS which encourages their growth (Ye and Sontheimer, 1998). Once neurons were plated, the FBS concentration was reduced to 2% and 0.6  $\mu$ M cytosine arabinoside (ara-C), a DNA synthesis inhibitor, was added to restrict astrocytic proliferation. This protocol ensured reliable, healthy and robust neuronal cultures as evidenced by Figure 3.1.A. The rationale for this two-step protocol using astrocyte pre-plating – as opposed to astrocyte-free cultures, which were also successfully trialled - was based on previous work suggesting that this feeder layer provides important structural and metabolic support to neurons (Melcangi et al., 1997). As such, the presence of astrocytes allowed us to study neurons under more physiologically relevant conditions (Anderl et al., 2009) and this was especially crucial for the analysis of the effects of A $\beta$ 1-42 (Chapter 6). Another critical factor for experimental success, was to ensure that the density was optimal; fairly low-density cultures were preferable so that individual processes could be easily resolved (Fig.3.1.A and B). Cultures were maintained in an incubator at 37°C in 5% CO<sub>2</sub> and were used at DIV 13-18, once they matured and developed synaptic connections (Grabrucker et al., 2009).

Upon maturation, a coverslip with neurons was transferred into a custom built imaging and stimulation chamber (refer to Fig.2.2) with two platinum electrodes positioned in parallel, ~1 cm apart, and the wires were connected to a Grass stimulator for field

stimulation of the culture (Fig.3.1.C). All experiments (unless indicated otherwise) were carried out in pH 7.3 external bath solution (EBS) with ionic composition, mimicking the ionic concentration of the extracellular environment, supplemented with blockers (AMPA blocker: 20  $\mu$ M CNQX; NMDAR blocker: 50  $\mu$ M AP5) to prevent repeated excitation of the network following stimulation and to limit propagation of spontaneously fired action potentials. The presence of functional presynaptic terminals was verified in experiments using FM1-43 and sytl-Oyster550, which are described below.

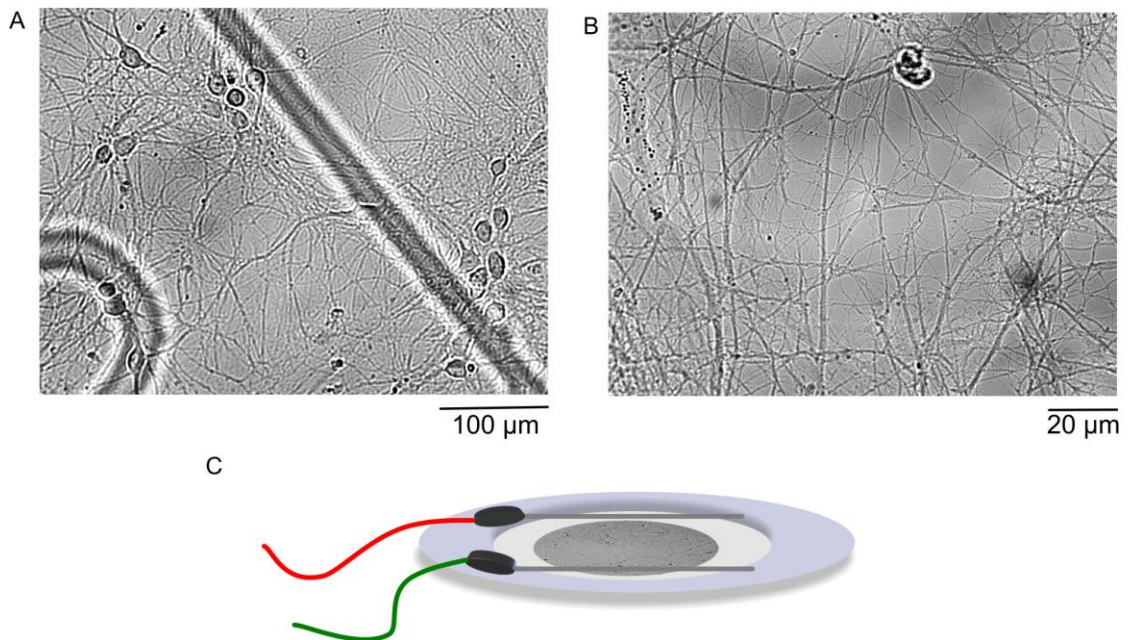


**Figure 3.1 Successful culturing of primary hippocampal neurons.** A) Primary rat hippocampal neurons in culture (DIV 14). DIC image acquired using 10x objective, 1 x 1 binning. Scale bar 100  $\mu$ m. B) Networks formed by cultured hippocampal neurons. DIC image acquired using 60x objective, 1 x 1 binning. Scale bar 20  $\mu$ m. C) Schematic showing the custom made chamber with a coverslip.



### 3.2.2 Labelling of synapses with FM1-43 dye

The development of styryl dyes by Betz and colleagues has revolutionized the study of physiology of presynaptic terminals (Betz et al., 1992). It allowed for optical monitoring of synaptic vesicle recycling in living cells. Since then FM1-43 has been used in a variety of studies examining synaptic vesicle recycling properties (Li et al., 2005; Rey et al., 2015; Ryan and Smith, 1995). In short, FM1-43 stains functional presynaptic terminals in an activity dependent fashion. It partitions into the outer leaflet of the lipid bilayer and is internalized into synaptic vesicles during the endocytic phase that follows stimulus driven exocytosis (Fig.3.2.A). The remaining FM1-43 dye can be washed off the cell surface. For a detailed description of FM1-43 structure and mechanism see Introduction.

The FM1-43 loading protocol was carried out as described in Methods 2.8. Mature hippocampal neurons (DIV 13-18) were placed in the imaging chamber, which was positioned on the stage of an upright microscope, and incubated for 60 s in the presence of 10  $\mu$ M FM1-43 dye in EBS with blockers: 20  $\mu$ M CNQX and 50  $\mu$ M AP-5. Cultures were stimulated for 30 s with 1200 APs, 20 Hz stimulation which mobilizes vesicles in the recycling pool (Ratnayaka et al., 2012). Following stimulation, an additional 60 s was allowed for the completion of endocytosis, after which the FM1-43 was washed out with fresh EBS with blockers (Fig.3.2.B). FM1-43 loaded regions of interest were then identified on the basis of fluorescence puncta present along neuronal processes (Fig.3.2.C). This clearly demonstrates the presence of functional presynaptic terminals in our hippocampal cell culture preparation, which were successfully labelled with FM1-43 dye.

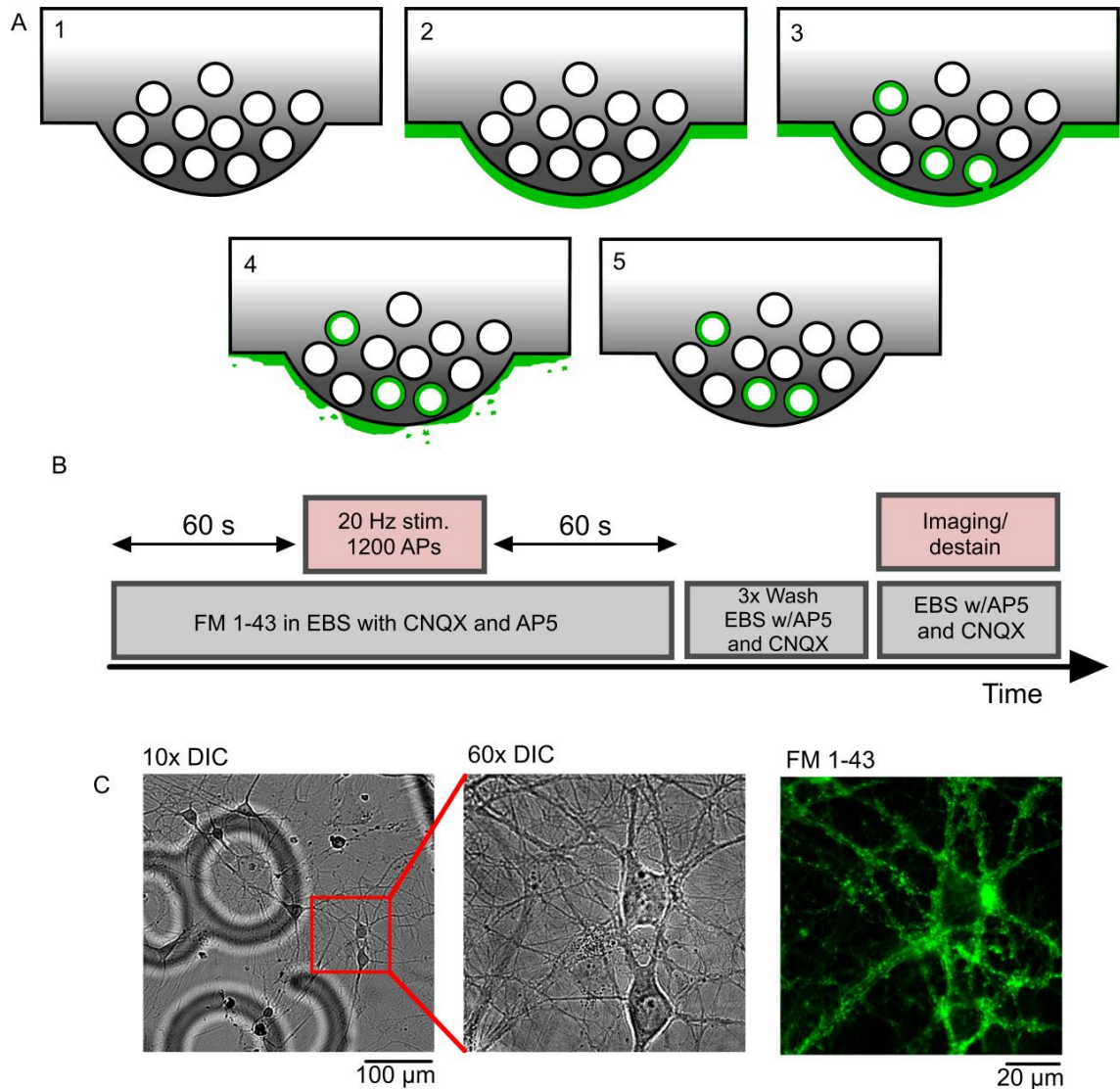


**Figure 3.2 Visualization of hippocampal synapses loaded with FM1-43.** A) Schematic representation of the labelling mechanism with FM1-43 dye. Due to its lipophilic nature, FM1-43 binds to the outer leaflet of the presynaptic membrane (1 and 2). Stimulation driven exocytosis of synaptic vesicles leads to FM1-43 uptake by subsequently endocytosing vesicles and staining of the luminal face of their membrane (3). The remaining surface dye is removed by washing with dye-free EBS solution (4) allowing to image fluorescence that originates from the labelled vesicles (5). B) Timeline illustrating the protocol followed for FM1-43 labelling of recycling vesicles. C) Example image of FM1-43 labelling following 1200 APs, 20 Hz stimulus. Punctate fluorescence represents labelled terminals.

### 3.2.3 Functional readout using FM1-43 dye

FM1-43 not only allows for identification of functional presynaptic boutons but more importantly provides an approach to monitor their function during subsequent exocytosis (Richards et al., 2005; Welzel et al., 2011). Hence, it can be used to examine the effects of various drugs, neurotoxic proteins such as A $\beta$ 1-42 (Chapter 6) or to scrutinize the behaviour of SVs in synaptic vesicle pools (Rey et al., 2015). This functional readout relies on the reversible nature of FM1-43 partitioning into the membranes, such that the dye is 'unloaded' from presynaptic terminals during stimulus-driven exocytosis of synaptic vesicles during further rounds of stimulation (Fig 3.3.A). Specifically, when the SVs are exocytosed, FM1-43 departs from the vesicular lumen into the extracellular medium and this should be observed as a decrease in fluorescence during time-lapse imaging. The amount of dye loss therefore represents the extent of SVs exocytosis.

To confirm this in our system, previously loaded cells (as described in section 3.2.2) were imaged every 1 s and stimulated with 1200 APs, 20 Hz stimulus. In order to identify stable presynaptic terminals 10 s of baseline fluorescence was recorded, followed by 60 s of stimulation (Fig.3.3.B and C). ROIs of equal size were drawn and the fluorescence level of each synapses was measured over time using ImageJ. As shown in Fig.3.3.C and D, following the initial pre-stimulus plateau, fluorescence loss was apparent with a timecourse consistent with single exponential decay. When fluorescence readouts were normalized to the baseline, it was clear that individual synapses exhibit high levels of variability in the fraction of dye loss (Fig.3.3.C). On average  $67.17 \pm 0.01\%$  of the dye was lost as a result of stimulation ( $n = 428$  synapses). The remaining fluorescence presumably corresponds to residual dye trapped in non-vesicular compartments, or potentially reflects the transfer of labelled vesicles into non-functional pools. This type of readout can be used to compare different treatment groups in terms of the dynamics of vesicle pools (Chapter 6). By fitting single exponential curves, it is possible to measure the time constant of the decay ( $\tau$ ) providing information on the kinetics of exocytosis. The

fit showed here was constrained to the average of 5 frames before the onset of the stimulation. The average destain timing as a result of 1200 APs 20 Hz stimulation of 428 successfully fitted synapses was  $9.4 \pm 0.36$  s (Fig.3.3.D).

This confirms that we can successfully load presynaptic terminals with the FM dye for the purpose of their identification and, with further stimulation, use it to assay functional properties of these synapses. This includes synaptic vesicle pool dynamics, kinetics of exocytosis, lateral mobility of vesicles, or perhaps even membrane-associated abnormalities.

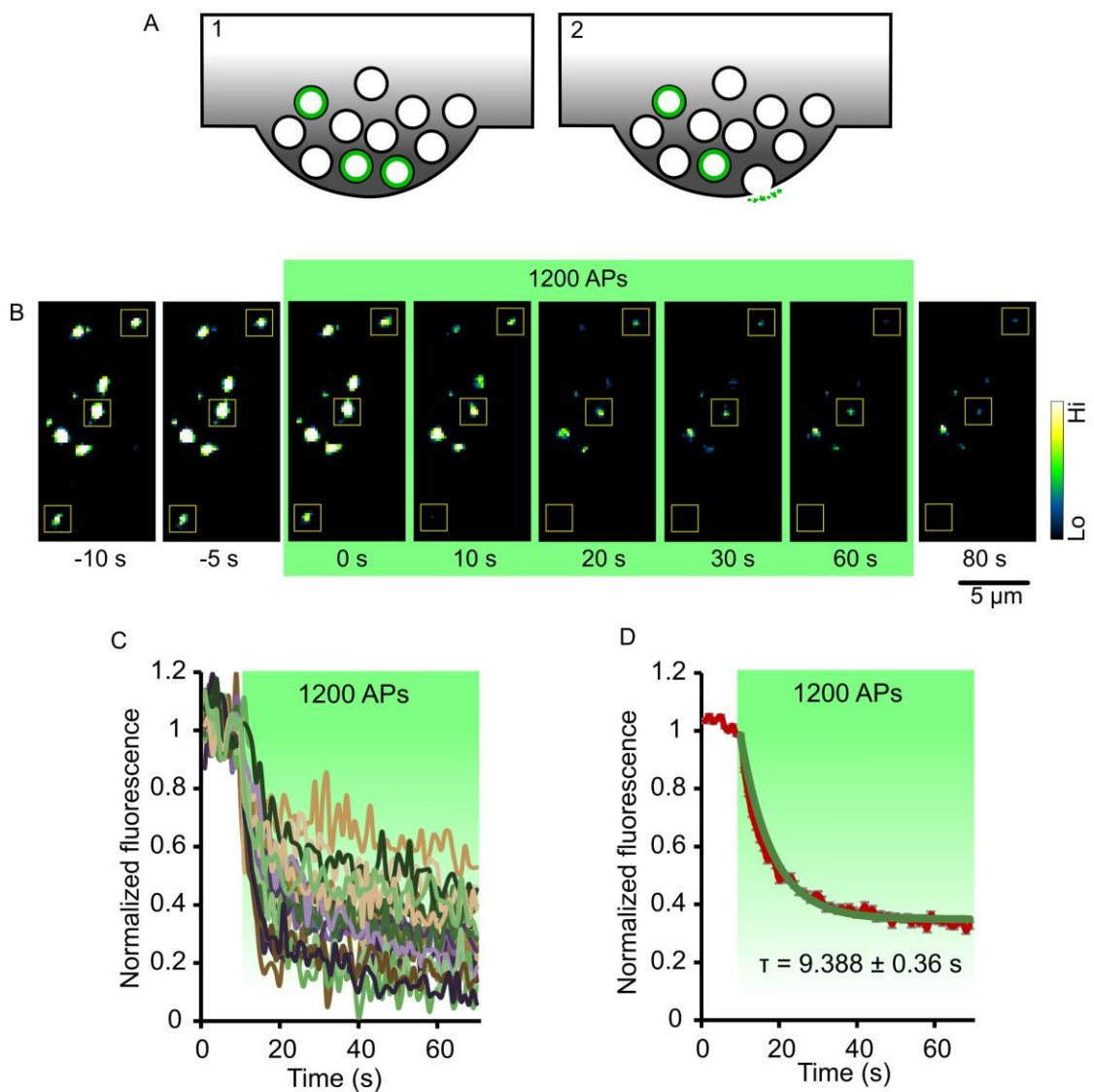


**Figure 3.3 Functional readout of synaptic vesicles exocytosis with FM1-43.** A) Schematic showing destaining of labelled synaptic vesicles. In response to applied stimulus FM1-43 is lost during vesicle exocytosis and it eventually diffuses away from

the plasma membrane into the aqueous solution. B) Images collected from time laps imaging showing decrease in fluorescence intensity resulting from FM1-43 destaining. Yellow boxes indicate example ROIs (2 x 2  $\mu\text{m}$ ). C) Quantification of the change in fluorescence level from time laps imaging. Individual curves are examples of FM1-43 destaining profiles from single synapses. D) Destaining curve allows to measure the kinetics of exocytosis: red curve is the average of 428 destain curves from individual synapses  $\pm$  SEM, green curve is a single exponential curve constrained to the fluorescence value prior to the stimulation.

### 3.2.4 Labelling of synapses with sytl-Oyster550

Sytl-Oyster550 is another acutely applied probe that can be used to label and monitor synaptic behaviour. We validated this reporter for its ability to label functional presynaptic terminals, its utilization as a marker of synaptic size that could be used in conjunction with other fluorescent probes and whether it can be used as a reporter of synaptic function in a similar fashion to FM1-43.

Sytl-Oyster550 is an antibody against synaptotagmin 1, conjugated with a fluorescent tag - Oyster550. Application of sytl-Oyster550 during stimulation leads to labelling of recycling synaptic vesicles during endocytosis and ultimately labelling of functional synapses. Following extensive washing out of the surface bound sytl-Oyster550, red, vesicle-specific punctate fluorescence can be observed, which validates the presence of functional presynaptic terminals that can be identified with this probe (Fig.3.4.A).

Due to its red tag and specificity to synaptic vesicles, sytl-Oyster550 is a widely used probe in the remaining chapters of this work in conjunction with green genetically encoded reports. We therefore carried out a pilot experiment testing whether sytl-Oyster550 can be used to monitor presynaptic properties such as relating the size of the active zone to the presynaptic size. Due to the resolution limitation of light microscopy, it is not possible to accurately quantify the size of the active zone. Nevertheless, this can be overcome by measuring the amount of fluorescently-tagged active zone specific protein. Bassoon was shown to be highly concentrated at the active zone cytomatrix (tom Dieck et al., 1998) and it has been widely used as a marker of AZ (Grabrucker et al.,

2009; Matz et al., 2010). Loading with sytl-Oyster550 at 1200 APs, 20 Hz ensures labelling of the entire recycling pool of synaptic vesicles (Ratnayaka et al., 2012). The size of the recycling pool was previously shown to correlate with the size of the synapse, measured as total vesicle pool size (Marra et al., 2012), and therefore can be used as an indirect measure of the synaptic size. The size of the active zone in an ultrastructural study, in addition to being positively correlated with the docked vesicle pool, also scaled with the synaptic volume (Murthy et al., 2001). We therefore concluded that sytl-Oyster550 from maximally loaded synapses should correlate with the size of the active zone.

We expressed GFP-tagged bassoon in primary rat hippocampal neurons. The delivery of the construct was carried out at 9 DIV, via modified calcium-phosphate transfection method (details in section 2.3). After a week of GFP-bassoon expression, cultures were labelled with sytl-Oyster550 and imaged. Cells were incubated for 1 min in the presence of 1:100 sytl-Oyster550 in EBS with blockers to prevent repeated excitation of the network (AMPA blocker: 20  $\mu$ M CNQX; NMDAR blocker: 50  $\mu$ M AP5), and then stimulated with 1200 APs at 20 Hz. The sample was kept for a further 60 s in sytl-Oyster550 in order to allow for the complete endocytic recovery of the vesicles, following which the culture was washed with EBS with blockers to remove surface bound antibody. The synapses that responded to the stimulation and taken-up sytl-Oyster550 can be clearly identified as red fluorescence puncta along neuronal processes (Fig.3.4.B). ROIs of even size were drawn around the presynaptic terminals expressing GFP-bassoon and fluorescence was quantified for both GFP-bassoon and sytl-Oyster550 using ImageJ.

The results showed that there was a strong correlation between the two measurements (Fig.3.4.C) suggesting a relationship between the AZ size and the size of the TRP (Pearson's correlation test,  $n = 27$  synapses,  $r = 0.6737$ ,  $P = 0.0001$ ) (Fig.3.4.C). We therefore established that sytl-Oyster550 is a good marker, which allows us to

quantitatively explore the properties of presynaptic terminals, in this case to relate the size of the active zone to the size of the synapse.

Having established sytl-Oyster550 as a good marker for identification of presynaptic terminals and their properties, we wanted to test whether sytl-Oyster550 can be used to measure the kinetics of exocytosis in a similar fashion of FM1-43. When subjected to 1200 APs, 20 Hz stimulation, sytl-Oyster550 fluorescence loss was observed, however, only  $37.12 \pm 0.01\%$  of the signal was lost in comparison to a 67% destain in the FM1-43 experiment (Fig.3.4.D). This high level of fluorescence retention is due to high affinity of sytl-Oyster550 to its target protein synaptotagmin I, whereas FM1-43 is characterized by fast departition from the membrane.

Despite the fact that sytl-Oyster550 is not a probe of choice for measuring synaptic vesicle cycle, it provides with a useful tool for localization of functional presynaptic terminals and measuring their size. Its photostability also offers advantage over other probes for measuring synaptic vesicle mobility (Ratnayaka et al., 2011).

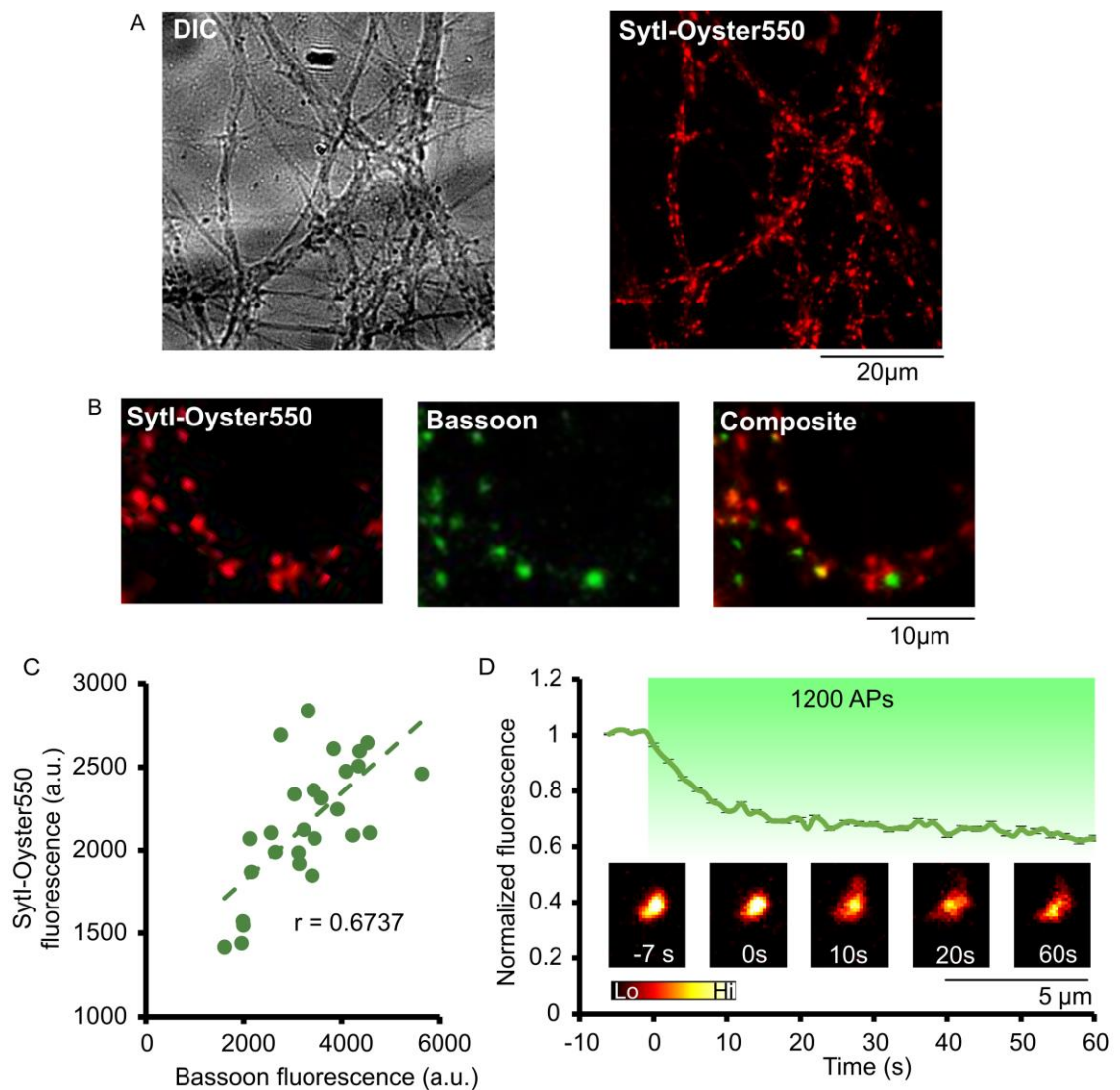


**Figure 3.4 Readout of presynaptic properties with sytl-Oyster550.** A) Bright field (left) and fluorescence (right) images of presynaptic terminals labelled with sytl-Oyster550 with stimulation of 1200 APs at 20 Hz. Images taken with 60x objective, 1x1 binning. Scale bar 20  $\mu\text{m}$ . B) Fluorescent images of sytl-Oyster550 labelled (left) and bassoon expressing neurons (middle). Bassoon expressing, responsive to stimulation terminals can be identified from the composite (right). Images taken with 60x objective, 4 x 4 bin. Scale bar 10  $\mu\text{m}$ . C) Presynaptic size, expressed as a size of recycling vesicle pool (measure of sytl-Oyster550 fluorescence), is strongly correlated with the size of the active zone (Pearson's correlation test,  $n = 27$  synapses,  $r = 0.6737$ ,  $P = 0.0001$ ). D) Stimulation driven destaining of sytl-Oyster550 from labelled presynaptic terminals. Graph represents the average destaining curve of 395 boutons  $\pm$  SEM. Stable baseline fluorescence and the decrease in fluorescence intensity upon stimulation can be observed on the panels. Scale bar 5  $\mu\text{m}$ .



### 3.3 Genetically encoded probes of synaptic function

The key aim of this work was to characterize the fundamental rules that underlie the recycling kinetics at individual presynaptic terminals. In order to achieve that goal, exocytosis and endocytosis needed to be sampled over time, which made FM1-43 and sytl-Oyster550 unsuitable for this purpose due to their destaining with each stimulation round. Tools allowing to repeatedly image vesicle recycling over multiple trials, were required for this purpose. Genetically encoded probes offer a wide range of readouts, allowing us to measure important steps of the neurotransmitter release and synaptic vesicle cycle: calcium influx, exocytosis and endocytosis of synaptic vesicles and glutamate release. In this section of the chapter we validate different genetically encoded probes, characterize and select the best tools enabling us to answer our aims of assaying recycling profiles of vesicle pools, and relating these to neurotransmission.

#### 3.3.1 Readout of synaptic vesicle exo and endocytosis with sypHy2x

SypHy2x comprises of 2 super-ecliptic pHluorin molecules fused to the second intravesicular loop of synaptophysin (Granseth et al., 2006) (Fig.3.5.A). It is a pH sensitive reporter of synaptic vesicles exocytosis and their subsequent endocytosis. These can be measured as an increase in fluorescence intensity upon vesicle fusion with the presynaptic membrane (exocytosis), and gradual fluorescence decay, which represents the reacidification of synaptic vesicles that follows their endocytosis (Fig.3.5.B). We validated this construct as a candidate for imaging and measuring synaptic vesicles recycling kinetics.

Initially, in order to introduce sypHy2x to the cells, we transfected DIV 6-8 cells using modified  $\text{Ca}^{2+}$  phosphate method (described in detail in section 2.3.). Nevertheless a viral form of sypHy2x using AAV vector, based on our cDNA construct, was made by Tiago Branco's laboratory (Cambridge). The kinetics of AAV.sypHy2x responses was

identical to cDNA plasmid, however, the cell viability and the efficiency of expression were improved based on our observations. Therefore, AAV-based sypHy2x expressing cells were used for most of the experiments shown here. Hippocampal neurons were infected on DIV 4-6 and used for experiments on days 13-18, when the expression levels were established. Figure 3.5.C shows a representative image of hippocampal culture (left) expressing AAV.sypHy2x construct (right). The change of sypHy2x fluorescence can be monitored and quantified over time (Fig.3.5.D-F). SypHy2x showed low levels of baseline fluorescence, which increased following the administration of the stimulus, in this case 40 APs, 20 Hz, and decreased again when the stimulus ceased and SVs were reacidified (Fig.3.5.D and E). In order to quantify the change in fluorescence, square ROIs of equal size were drawn based on subtracted images before and at the peak of stimulation (Fig.3.5.D). We were able to identify at least 20-100 responding boutons within a single field of view (132 x 132  $\mu\text{m}$ ) The size of the ROIs was optimized for capturing the endocytosis rather than outward movement of sypHy2x (2.8 x 2.8  $\mu\text{m}$ ) (Granseth et al., 2006) and was larger than for FM1-43 readouts (2.5 x 2.5  $\mu\text{m}$ ). It was also crucial that only individual synapses, and those with the fluorescence at the peak of the response that was completely encapsulated within the ROI boundary, were chosen for the analysis. This also helped to ensure that individual synapses and not clusters of presynaptic terminals were included in the data set. After the initial selection of ROIs, images were screened for any possible oversaturated responders or apparent moving packages, which were eliminated from the analysis. These mobile packages represent extrasynaptic vesicles exchanged between synapses (Kamin et al., 2010; Ratnayaka et al., 2011). Figure 3.6.E shows example profiles of fluorescence measured from individual boutons in response to 40 APs, 20 Hz stimulation.

Similarly to FM1-43 dye, sypHy2x allows for quantification of the kinetics of synaptic vesicle exocytosis, but additionally provides detailed information on endocytosis. The decay of normalized sypHy2x fluorescence represents the endocytosis of synaptic

vesicles, and can be fitted with single exponential curves (Fig.3.5.F). The time course of fluorescence recovery following 40 APs, 20 Hz stimulation in our system was  $\tau = 16.8 \pm 0.28$  s, which is comparable to previously reported measurement (Granseth et al., 2006).

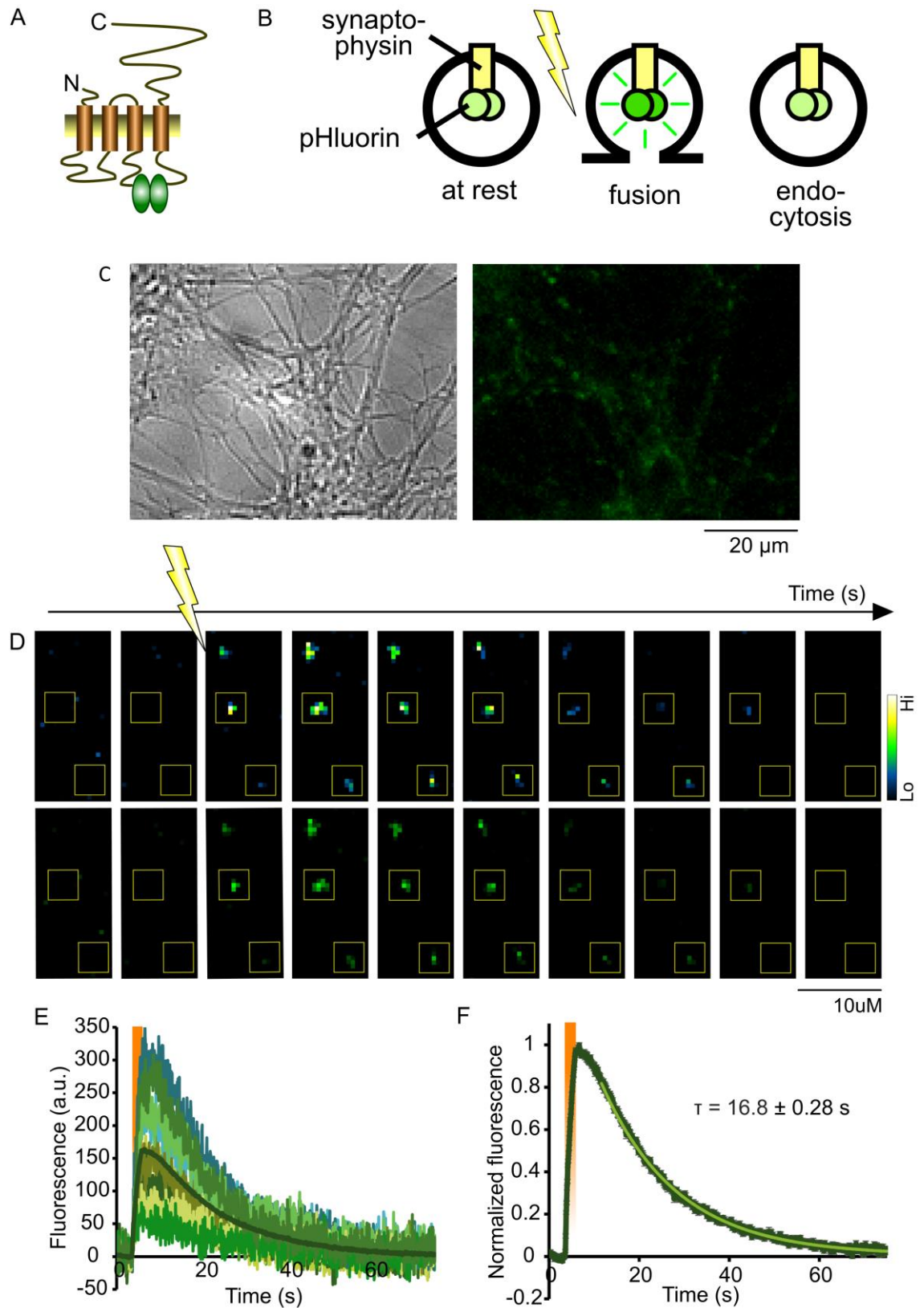


**Figure 3.5 Detection and measuring of synaptic responses using syHy2x.** A) Schematic representation of syHy2x. (Figure adapted from Zhu et al., 2009) B) Schematic representation of syHy2x mechanism of reporting synaptic vesicle cycle. At rest syHy2x is quenched inside the acidic lumen of synaptic vesicle. When SVs are released in response to the stimulation, syHluorin is exposed to the neutral pH of the extracellular environment which results in the increase of fluorescence intensity. Synaptic vesicles are then retrieved back into the presynaptic terminal. Following endocytosis newly formed vesicles are reacidified by v-ATPase which results in re-quenching and decline of syHy 2x fluorescence. C) DIC image (left) of syHy 2x expressing neuron (right, fluorescence at rest). Scale bar 20  $\mu\text{m}$ . D) Subsequent panels represent change in syHy 2x fluorescence over time in response to 40 APs at 20 Hz stimulus. Stimulation was applied at 3.5 seconds and lasted for 2 seconds. Yellow boxes encapsulate example of synaptic boutons chosen for analysis. Scale bar 10  $\mu\text{m}$ . E) Examples of fluorescence readouts from individual synapses expressing syHy2x subjected to 40 APs stimulation at 20 Hz. Dark green trace represents the average of 491 responses. Stimulus is indicated by the orange panel. F) SyHy 2x fluorescence allows to measure the kinetics of synaptic vesicle recycling. The average of 491 responses (dark green trace) reveals the kinetics of vesicles recovery of  $\tau = 16.8 \pm 0.28$  s (single exponential fit in green).

### 3.3.1.1 Comparison of syHy1x, syHy2x and syHy4x constructs

One of the main aims of this work was to establish whether individual boutons show signature recycling behaviour of single synaptic vesicles. In other words, are the vesicles at a given terminal predisposed to a certain timing of their retrieval, which is determined by the properties of that particular synapse? In order to confidently visualize the release and endocytosis of single synaptic vesicles, a probe with the best signal intensity had to be selected. Zhu, Xu, & Heinemann, 2009 used syHy4x for their study of single vesicle endocytosis after concluding its superior signal-background ratio in comparison to other constructs: synaptopHluorin, syHy1x and syHy2x.

We carried out analysis of these constructs in our cell culture system. The structural difference between syHy1x, syHy2x and syHy4x lies in the number of pHluorins in the intravesicular loop of synaptophysin (Fig.3.6.A). These constructs have one, two and four pHluorins, respectively. Responses to 40 APs, 20 Hz stimulation were recorded and measured for all three probes (Fig.3.6.B). The fluorescence amplitude was calculated by

taking the average fluorescence value at the peak of each response and subtracting the baseline fluorescence for each readout. SypHy2x showed twofold improvement in the fluorescence amplitude in comparison to sypHy1x (Fig.3.6.B and C). In this case doubling the number of pHluorins was directly translated into the extent of fluorescence amplitude multiplication.

A similar increase might have been expected when sypHy4x is compared to sypHy2x. However, that was not the case; in a previously reported study there was only ~23% improvement in the signal-background ratio between sypHy2x and sypHy4x (Zhu et al., 2009). In our hands, the fluorescence amplitude was only 15% larger in sypHy4x in relation to sypHy2x (Fig.3.6.C). We also observed that the long term health of cultures was compromised by sypHy4x construct, and fewer functional boutons were routinely identified. Based on the marginal gains in signal and concerns over cell health, the decision was made to use sypHy2x for the remainder of this study.

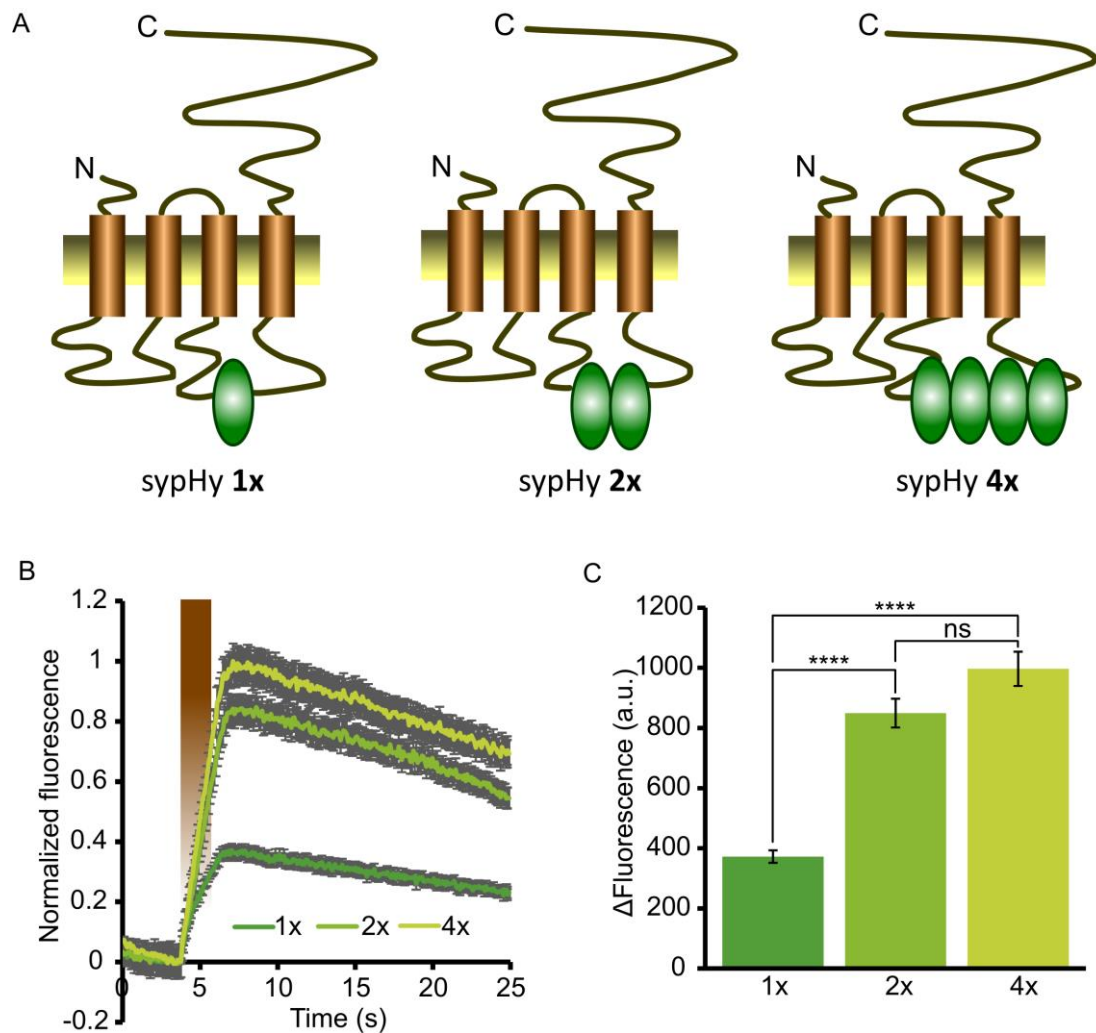


**Figure 3.6 Comparison between sypHy constructs with varied number of fused pHluorins.** A) Schematic representation of structural differences between sypHy constructs with varied number of pHluorin molecules (figure adapted from Zhu et al., 2009). B) Average sypHy signal (n = 115, n = 75, n = 108 synapses for sypHy1x, sypHy2x and sypHy4x, respectively  $\pm$  SEM) in response to 40 APs stimulus at 20 Hz (indicated by the brown panel). For all three constructs fluorescence was normalized to the signal intensity at the peak of sypHy4x response and frames before the stimulation from each data set. C) Quantification of the responses from (B) revealed significant difference between the fluorescence intensity of sypHy 1x in comparison to sypHy2x and sypHy4x (One-way ANOVA with Tukey's post-hoc analysis: sypHy1x - sypHy2x,  $P < 0.0001$ ; sypHy1x - sypHy4x,  $P < 0.0001$ ). There was no significant difference in the intensity of fluorescence between sypHy2x and sypHy4x 40 APs responses ( $P = 0.0649$ , One-way ANOVA with Tukey's post-hoc analysis). Raw, baseline subtracted data was used for quantification.

### **3.3.2 Measuring exo- and endocytosis at excitatory synapses using vGlut1-pHluorin**

Another reporter allowing to monitor synaptic vesicle release and endocytosis is vGlut1-pHluorin. Due to the fact that it has been previously successfully used to monitor single synaptic vesicles exocytosis and endocytic coupling (Balaji and Ryan, 2007), we therefore wanted to test this construct in our system. In the case of vGlut1-pHluorin, a single pHluorin molecule was fused to vesicular glutamate transporter 1. vGlut1-pHluorin (vGpH) unlike syHy2x not only allows to observe the endocytosis and exocytosis of synaptic vesicles, but allows to isolate these events to glutamate releasing terminals. In that way it provides more specific information than syHy2x in terms of the population of tested synapses.

We expressed vGpH in DIV6-8 hippocampal neurons, which were used for experiments 6-10 days after transfection. Figure 3.7. A and B show representative images of vGpH at rest and at the peak of the stimulation with 4 APs. Similarly to syHy2x data, detection of the responding synapses was carried out based on fluorescence difference between the peak of the stimulation and the baseline fluorescence. Individual responding presynaptic terminals were clearly discernible (Fig.3.7.B), and upon stimulation with 4 APs, a rise in vGpH fluorescence was observed followed by a gradual decline of the signal during reacidification (Fig.3.7.C).

Despite the advantages of vGpH, such as low surface expression and more specificity in term of the population of measured synapses, we found that the imaged responses to 4 APs were similar or even noisier than those obtained with syHy2x. The transfection efficiency and neuronal health were also more compromised with this construct. Therefore syHy2x remained the probe of choice for single vesicle imaging. Perhaps vGpH with two pHluorin molecules would have been the most optimal probe for single vesicle imaging.

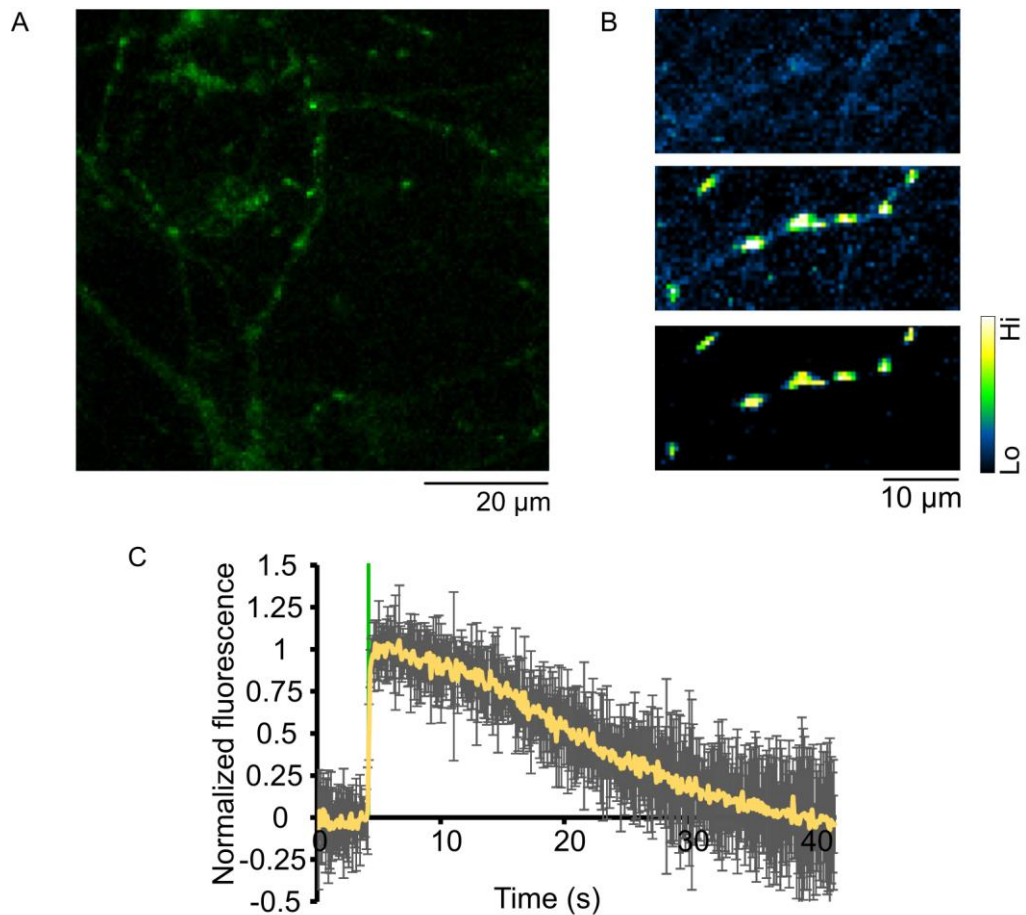


**Figure 3.7 Detection and measuring synaptic response with vGlut-pHluorin (vGpH).** A) Fluorescent image of baseline vGpH expression. Scale bar 20  $\mu\text{m}$ . B) Panels showing method used for detection of responding boutons. Baseline level of fluorescence (top panel) is subtracted from the fluorescence level at the peak of the response (middle panel). The resulting image allows for clear identification of responding presynaptic terminals (bottom panel). Scale bar 10  $\mu\text{m}$ . C) Fluorescent profile reflecting response of 119 boutons to 4 APs stimulus. Data, shown as average  $\pm$  SEM, was bleach corrected and normalized to the frames prior to and at the peak of the response. The green line indicates the length of the applied stimulus.

### 3.3.3 SyGCaMP6f allows to monitor presynaptic $\text{Ca}^{2+}$ influx

Some of the work in this project focuses on the mechanisms of the disturbance of vesicle recycling caused by neurotoxic peptide – amyloid beta. Exo-endocytic coupling is thought to be regulated by stimulus evoked presynaptic  $\text{Ca}^{2+}$  influx. The disturbance in  $\text{Ca}^{2+}$  dynamics could therefore provide with some mechanistic explanation of the abnormal timing of the endocytosis of synaptic vesicles. The aim of this experiment was



to establish the readout of presynaptic  $\text{Ca}^{2+}$  influx in response to small stimulation over multiple trials.

Neurons were infected with AAV.*syGCaMP6f* construct at DIV 4-6 and experimented on at least 10 days post infection (Construct made by Tiago Branco's laboratory at Cambridge). *syGCaMP6f* is targeted to presynaptic terminals by fusing GCaMP to cytoplasmic domain of synaptophysin. It is characterized by high sensitivity and the fastest reporting kinetics out of GCaMP family (Chen et al., 2013; Dreosti et al., 2009). Due to a low level of baseline fluorescence, the identification of expressing neurons often had to be carried out based on low level stimulus (Fig.3.8.A). In order to examine the presynaptic expression of our construct, we loaded *syGCaMP6f* expressing cells with 1:100 sytl-Oyster550 antibody (1200 APs 20 Hz stimulation; protocol as described in section 2.8 and 3.2.4). The *syGCaMP6f* and sytl-Oyster550 fluorescence co-localized well, confirming presynaptic localization of our construct (Fig.3.8.A and B).

*SyGCaMP2* was previously used to detect presynaptic calcium influx associated with single AP stimulation in primary hippocampal neurons (Dreosti et al., 2009). We therefore wanted to test if we can monitor presynaptic  $\text{Ca}^{2+}$  changes in response to 4 APs stimulus with *syGCaMP6f*. In a similar fashion to *sypHy2x* experiments, the responding boutons were identified on the basis of subtracted images, and ROIs of even size ( $2.8 \times 2.8 \mu\text{m}$ ) were drawn encapsulating responding boutons. A very sharp increase in fluorescence signal in response to stimulation was observed (Fig.3.8.C and D). *syGCaMP6f* is therefore a suitable tool allowing to measure  $\text{Ca}^{2+}$  dynamics in response to minimal stimulation.

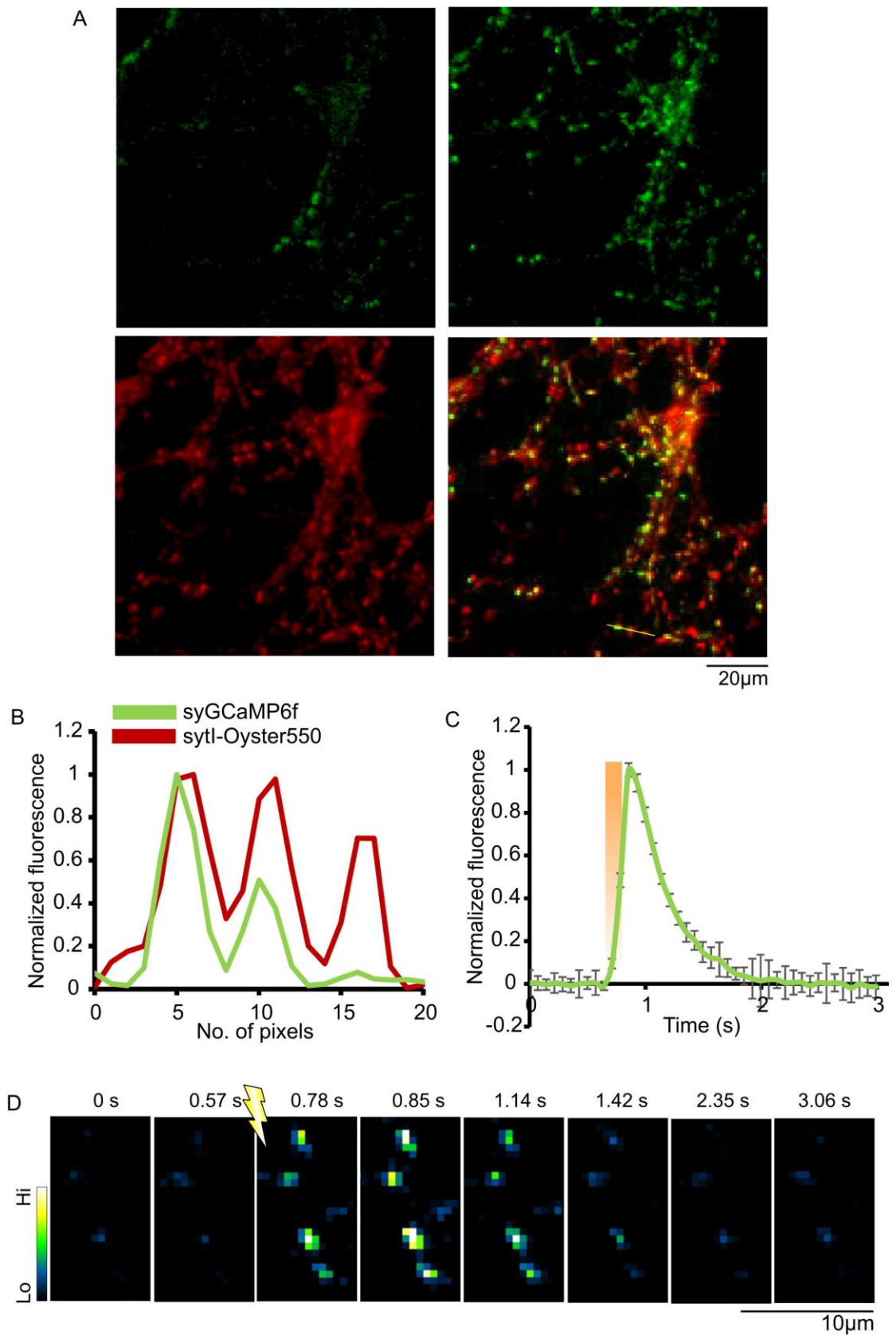


**Figure 3.8 Detection of presynaptic  $\text{Ca}^{2+}$  influx with syGCaMP6f.** A) Fluorescent image of baseline level of syGCaMP6f expression (top left) and the fluorescence level at the peak following 4 APs stimulus (top right). syGCaMP6f expressing cells were loaded with sytl-Oyster550 antibody to label presynaptic terminals (1200 APs at 20 Hz; bottom

left). Calcium influx (syGCaMP6f  $\Delta$ Fluorescence) in response to the applied stimulus can be clearly identified at the presynaptic sites (bottom right). Scale bar 20  $\mu$ m. B) Fluorescence intensity profile of syGCaMP6f and sytl-Oyster550 fluorescence measured along the yellow line on the bottom right image in A. C) Normalized mean response of 100 synaptic terminals to 4 APs stimulation  $\pm$  SEM. Orange panel indicates the length of the stimulus. D) Subsequent panels show change in syGCaMP6f fluorescence in response to 4 APs stimulation over time. Scale bar 10  $\mu$ m.

### 3.3.4 Detecting glutamate release with iGluSnFR

In this chapter so far we presented tools allowing detailed monitoring of recycling properties of synaptic vesicles (FM1-43, sypHy2x and vGpH) and the presynaptic influx of calcium (syGCaMP6f). These measurements however do not give any information regarding the actual release of neurotransmitter as a result of vesicles fusion. This is also an important measure for assaying changes in synaptic performance. A newly developed probe by (Marvin et al., 2013) provides information on this permitting a direct readout of released glutamate.

The expression of intensity-based glutamate-sensing fluorescent reporter (iGluSnFR) in our hippocampal culture, resulted in a diffuse appearance of the fluorescence at rest, with a localized increase in fluorescence amplitude as a result of stimulation (Fig.3.9.A). In order to localize functional terminals, we loaded neurons with FM4-64, a red version of FM1-43, with 1200 APs stimulation at 20 Hz. The ROIs were based on the subtracted image of iGluSnFR response to 2 APs stimulation. There was a strong correlation between FM4-64 and iGluSnFR fluorescence, indicating that the iGluSnFR signals measured were as a result of glutamate release from functional presynaptic terminals (Pearson's correlation test,  $n = 63$  synapses,  $r = 0.5486$ ,  $P < 0.0001$ ) (Fig.3.9.B). In order to test how well iGluSnFR reports the release of glutamate during small synaptic events, we stimulated our cells with 2 APs (Fig.3.9.C). There was a sharp increase in fluorescence immediately at the onset of the stimulation, and the peak of the response was reached within 42 ms. A decrease in fluorescence took place immediately after the

end of the stimulus (Fig.3.9.D). In order to test this construct for imaging the behaviour of presynaptic terminals over multiple trials, we stimulated cells 10 times in a train of 2 APs every ~2 s. We were able to observe responses of varying amplitudes as well as failures when no stimulation was delivered (Fig.3.9.E). iGluSnFR is therefore a suitable probe for detecting localization and magnitude of glutamate release at presynaptic terminals.

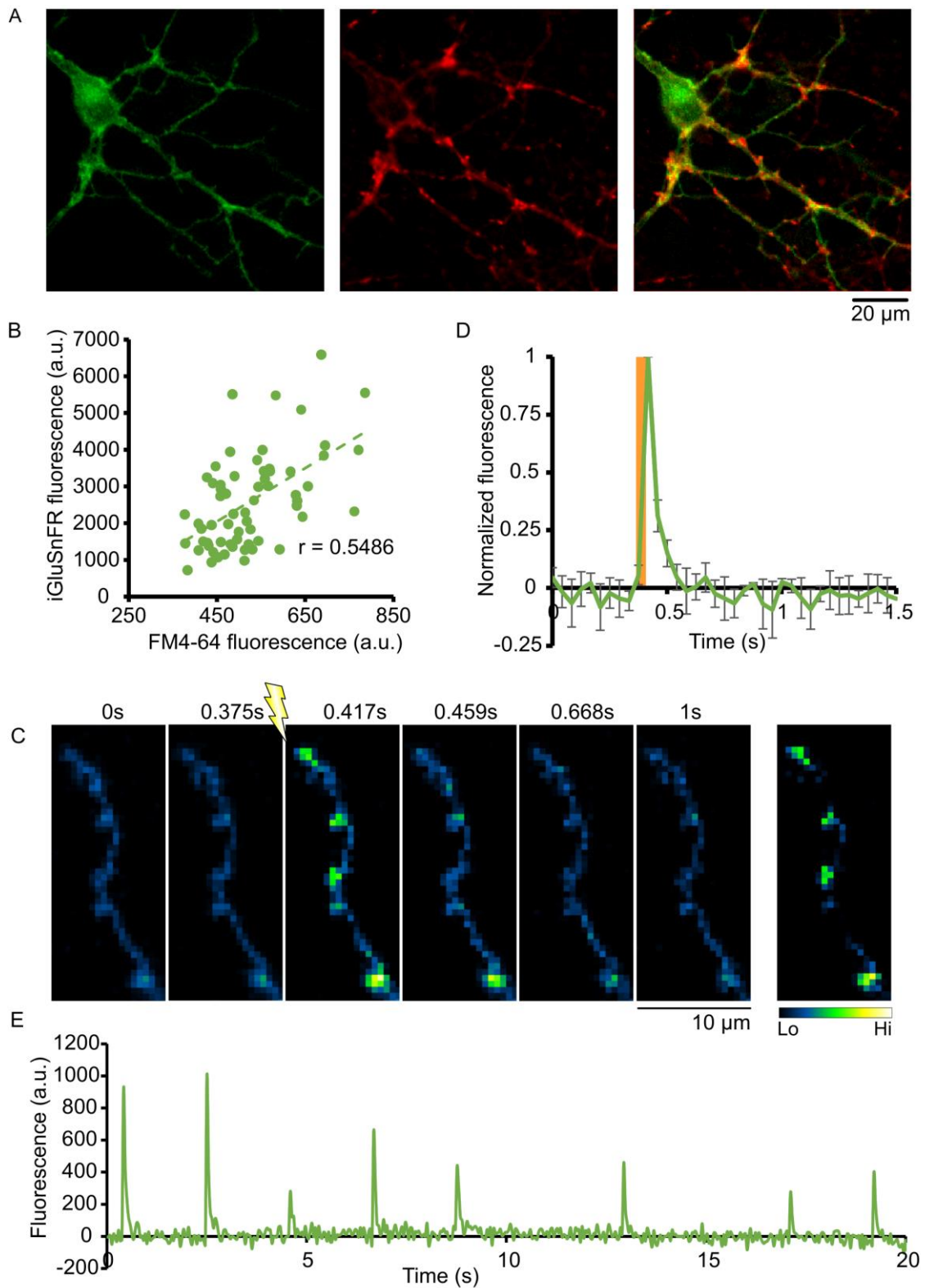


**Figure 3.9 iGluSnFR allows to monitor the release of glutamate at presynaptic terminals.** A) iGluSnFR transfected cells (top left) were loaded with FM4-64 for 60 s at 20 Hz (top right). Overlaid FM fluorescence allowed to identify iGluSnFR expression at presynaptic sites (bottom left). Scale bar 20  $\mu$ m. B) The analysis of FM fluorescence against iGluSnFR fluorescence at the peak of the response revealed correlation between the two supporting the reporting of presynaptic glutamate release (bottom right,

Pearson's correlation test,  $n = 63$  synapses,  $r = 0.5486$ ,  $P < 0.0001$ ). C) Change in iGluSnFR fluorescence in response to 2 APs stimulation can be traced on the consecutive panels. The last image represents the fluorescence baseline subtracted from the fluorescence at the peak of the stimulation, which aids the choice of responding regions. Scale bar 10  $\mu\text{m}$ . D) Average response of 3 synapses to 2 APs stimulation  $\pm$  SEM shown as change in fluorescence over time. Orange panel represents the length of the stimulation. E) Average response of synapses to a train of 10 x 2 APs stimulation trials ( $n = 11$  synapses).

### 3.4 Discussion

#### 3.4.1 The use of acutely applied fluorescence probes in hippocampal neurons

The development of styryl dyes and fluorescently labelled antibodies offered a new approach for studying function of presynaptic terminals. In turn, expanding our knowledge on principle workings of presynaptic terminals is important for dissecting disease associated or plasticity induced changes in hippocampal neurons. Hippocampal culture, used in this study, has been widely employed for this purpose due to its convenience for imaging, genetic manipulations, and dyes and drug applications (Balaji and Ryan, 2007; Evans and Cousin, 2007; Richards et al., 2005; Shields et al., 2015).

The all-encompassing objective of this chapter, was to establish the methodology for the readout of synaptic function, and to optimize the relevant approaches required to allow single vesicle imaging. The starting point was to confirm the generation of suitably healthy cultured neuronal networks, and to establish the presence of functional boutons. The ultrastructural data, combined with immunohistochemical analysis of cultured hippocampal neurons, revealed that mature excitatory synapses were observed from day 10 in culture, and characterized by a very regular developmental timeframe (Grabrucker et al., 2009). We showed in our loading experiments using FM1-43 and sytl-Oyster550 antibody, that mature, functional presynaptic terminals were present in our

culture, and that we can successfully load the synapses with these probes in an activity-dependent manner.

FM1-43 and sytl-Oyster550 antibody not only allow for the identification of presynaptic terminals in the culture, but more importantly for measuring the functional properties of individual presynaptic terminals. The time course of stimulus-driven FM1-43 destaining for mobilizing the entire recycling pool (1200 APs, 20 Hz) was  $9.4 \pm 0.36$  s (decay constant,  $\tau$ ) in our preparation. This is highly comparable with a previous study. Ratnayaka et al. 2011 reported a  $\tau = 7 \pm 1$  s under 1200 APs, 40 Hz stimulus in mature hippocampal cultures, a relevant experimental set-up to the one used in this study (Ratnayaka et al., 2011). The rate of FM1-43 destain scales with the stimulus frequency (Ratnayaka et al., 2011), hence the measurement reported in this study is well-aligned with the previously reported value.

The extent of the FM1-43 loss represents the extent of exocytosis, and therefore gives important information on the dynamics of synaptic vesicle pools. Following the endocytosis in the presence of the dye, the recycled vesicles are incorporated back into the synaptic vesicle pool. These vesicles can be either integrated into the recycling or resting pool, or transported into another bouton. In our experiment we observed a big variability in the extent of dye loss (Fig.3.3.C) suggesting that there is heterogeneity between synapses in how they partition vesicles into distinctive vesicle pools. A similar observation was made by Welzel et al., 2011 who reported that larger synapses, although characterized by bigger RP, tend to release fewer vesicles, and therefore retain more FM1-43 fluorescence, than smaller synapses. The availability of recently recycled vesicles was found to be time dependent and that their releasability increased as more time between consecutive stimulations elapsed (15 s to 90 s) (Ryan and Smith, 1995). A recent study (carried out by Milena Maria Wagner and others) also showed that only a subset of the vesicles are preferentially recycled back into the RRP, whereas the rest

takes up random positions within the pool (Rey et al., 2015). These examples illustrate how FM1-43 can be used to examine the dynamics of synaptic vesicle pools.

We tested sytl-Oyster550 antibody in a similar fashion to FM1-43 in terms of its ability to report synaptic vesicle exocytosis. We found that although sytl-Oyster550 provides with very clear labelling of presynaptic terminals, due to the high affinity of this antibody for synaptotagmin I, the activity-dependent fluorescence loss was almost half that observed with FM1-43 ( $37.12 \pm 0.01\%$  for sytl-Oyster550 and 67% for FM1-43). Nevertheless, due to its stable labelling and photostability, sytl-Oyster550 is a better probe for long term imaging, for example, during monitoring synaptic vesicle mobility (Ratnayaka et al., 2011). FM1-43, on the other hand is the probe of choice for examining the kinetics of turnover of synaptic vesicles.

Probes such as FM1-43 and sytl-Oyster550 provide information about the localization of presynaptic terminals and some readout of fundamental presynaptic properties. Nevertheless, these two reporters often rely on applying a strong loading stimuli prior to assaying their function, potentially influencing the synaptic operation being investigated. Moreover, the presence of these indicators within the terminal critically relies on exo- and endocytosis of synaptic vesicles; hence if vesicle recycling is affected by experimental conditions (neurotoxic proteins or drugs), the population of labelled vesicles might be biased towards those from synapses with higher  $p_r$ , or those belonging to a neuron that was not strongly affected. Also, these probes do not permit imaging of synaptic vesicle over multiple trials due to destaining. As such, the development of genetically encoded probes offers some major advantages in the studies of vesicle recycling, by allowing the monitoring of presynaptic properties such as synaptic vesicle recycling, calcium influx and glutamate release, without the need to first subject the sample to additional stimulation.



### **3.4.2 Genetically encoded reporters of synaptic function**

Unlike the acutely applied probes, genetically encoded reporters of synaptic function do not need to be loaded in an activity dependent fashion. They are delivered into cells via transfection or through infection with viral constructs, followed by the expression of fluorescently tagged protein. The development of these probes was possible thanks to the engineering of a pH-sensitive mutant of GFP – known as ‘pHluorin’ molecule (Miesenböck et al., 1998). Its fluorescence emission is quenched in the acidic pH of the lumen of synaptic vesicles, but significantly increases when SVs are released and intravesicular membranes are exposed to the neutral extracellular environment (Granseth et al., 2006; Miesenböck et al., 1998). AAV based viral constructs were primarily used in the present study due to their stable expression, high percentage of transduced cells and less compromised neuronal health than in the case with cDNA reporters that require transfection (Royo et al., 2008).

#### **3.4.2.1 Measuring synaptic vesicle recycling**

In this work we explored the properties of probes designed to measure the kinetics of vesicle recycling: sypHy and vGpH. One of the main objectives was to identify a probe that allows us to reliably image the exocytosis of single synaptic vesicles. vGpH, in which pHluorin molecule is attached to the vesicular glutamate transporter vGlut1, has been successfully used to image single synaptic vesicles (Balaji and Ryan, 2007). Nevertheless, in our hands the signal from vGpH was very noisy, transfection efficiency low and neuronal health compromised. We therefore turned our attention to sypHy constructs in search for the suitable tool. sypHy was developed by Granseth et al., 2006 who fused pHluorin molecule to synaptophysin. A detailed analysis of this construct by these authors revealed that sypHy was localized to synapses, did not affect exocytosis and allowed to monitor single vesicle fusion events (Granseth et al., 2006). Moreover, it

had less background fluorescence than previously developed constructs based on synaptobrevin (synaptopHluorin) (Granseth et al., 2006; Sankaranarayanan and Ryan, 2000), which is an important factor for imaging the events associated with single synaptic vesicles. The retrieval kinetics of sypHy were found to be comparable with synaptopHluorin but sypHy fluorescence exhibited less lateral movement (Granseth et al., 2006), which again makes it superior to synaptopHluorin. The kinetics of fluorescence decay is typically measured by fitting single exponential function. In our experiment, the fluorescence recovery after 40 APs 20 Hz stimulation was  $\tau = 16.8 \pm 0.28$  s. As in the case of FM1-43 (Ryan and Smith, 1995; Welzel et al., 2011; Zakharenko et al., 2001), not many papers provide their tau readouts and often rely on different stimulation intensities, but approximate comparisons are possible. Sankaranarayanan and Ryan et al., 2000 reported  $\tau$  of 10 s for 20 APs and  $\tau = 23$  s for 100 APs. Granseth et al., 2006 compared the kinetics of vesicles retrieval following stimulation ranging from 1 to 40 APs at 20 Hz and found that the endocytic kinetics were very similar within this stimulation range with an average of  $\tau = 23 \pm 1.5$  s, whereas the endocytic recovery following 400 APs, 20 Hz stimulus was 50 s (Granseth et al., 2006). Our readout is therefore in a broad agreement with these studies. The direct comparison of the kinetics between different research groups poses many problems. One possible explanation of variability between studies is the concentration of  $\text{Ca}^{2+}$  used in the external bath solution. It was demonstrated that endocytic kinetics increased with increasing extracellular calcium (Sankaranarayanan and Ryan, 2001). In our experiments  $\text{Ca}^{2+}$  concentration was 0.5 mM higher than in the two mentioned studies, which could therefore explain readout of faster kinetics. Another reason for this difference might be the temperature at which the experiments were carried out, as endocytosis is temperature dependent (Granseth and Lagnado, 2008). This highlights the importance of strict control of experimental conditions.

The timing of endocytosis in our study strongly indicates the prevalence of clathrin-mediated endocytosis (section 1.3.2). However, the main aim of this work was not to decipher the endocytic mode behind vesicle retrieval, but the properties of synapses that contribute to the determination of timing of this process at individual boutons. Hence, the actual timing of endocytosis was not the major concern here. Assuming that other modes of endocytosis, such as kiss and run, also contributed to our result, the relevant question for this study was whether a specific timing of endocytic retrieval is characteristic at individual synapses.

Having identified a synaptophysin-based probe as the reporter of choice for our study, we considered the advantages/disadvantages of different numbers of copies of pHluorin molecules in our construct, with 1, 2 or 4 pHluorin variants available. Based solely on the number of pHluorins, and the expected signal-to-noise, sypHy4x should be the best probe for monitoring single vesicle kinetics. However, despite the fact that we observed a twofold increase in response amplitude between sypHy1x and sypHy2x, there was only 15% improvement between sypHy2x and sypHy4x. Similar observations were made by Zhu et al., 2009, who also found that there was only limited improvement in the fluorescence in sypHy4x in comparison to sypHy2x. The health of cultures was compromised with sypHy4x construct and the transfection efficiency low, and therefore, we decided to use sypHy2x for future experiments.

SypHy2x not only allows to monitor the endocytosis of synaptic vesicles but also exocytosis, therefore functional information on both processes can be obtained from the same set of synapses. This is useful for examining the coupling of exo- and endocytosis (Chapter 6) or for examining endocytic curves within a given range of responses as exploited in Chapter 4.

### 3.4.2.2 Monitoring of glutamate release and presynaptic $\text{Ca}^{2+}$ influx

Despite the fact that sypHy2x should be a good indicator of the synaptic vesicle cycle, it does not provide any information on the consequence of exocytosis – the release of neurotransmitter. Until recently, the available method for measuring this was continuous amperometry or electrophysiology, which, as explained earlier, are not feasible in small central synapses. The development of iGluSnFR, a probe that permits the optical monitoring of synaptically released glutamate, opened new possibilities for studying presynaptic terminals. This probe expressed on the extracellular surface of plasma membrane, permits the translation of glutamate-receptor binding events into the fluorescence signal. As such, it provides a live readout of stimulus-evoked glutamate release and synaptic transmission (Marvin et al., 2013). iGluSnFR shows diffuse expression along the membranes, which made the localization of individual presynaptic terminals impossible. However, we showed that fluorescence ‘hot-spots’ at the peak of the stimulation overlap with the presynaptic marker FM4-64. This confirms that measured glutamate originates from synaptic boutons. The reporting kinetics of this construct is also satisfactory for our purposes (40 ms to reach the peak) as we were not aiming to resolve glutamate release events from individual action potentials, but rather to measure overall amplitude of fluorescence following the applied stimulus. Using iGluSnFR we also demonstrated that with minimal stimulus (2 APs), we evoked responses of varied amplitudes and that the fluorescence increase was stimulus-related. iGluSnFR is characterized by a very good signal-to-noise ratio as well as photostability (Marvin et al., 2013), which is also evident from our experiment. It is a relatively new tool, which so far has been successfully used to explore glutamate release at bipolar synapses in vitro and to explore cortical circuitry in mice in vivo (Borghuis et al., 2013; Xie et al., 2016).

Last but not least, in order to fully examine presynaptic function, it is crucial to measure presynaptic stimulus-evoked  $\text{Ca}^{2+}$  dynamics. Over the years, improved genetically encoded calcium indicators have been developed (summarized in the Introduction).

These constructs allow the monitoring of presynaptic  $\text{Ca}^{2+}$  influx during action potential firing as a response to delivered stimulus. Although initially GECIs, such as GCaMP, were characterized by lower sensitivity than the synthetic calcium indicators such as oregon green (OGB), recent developments have led to significant improvements in the dynamic range of these constructs, making them the probes of choice (Akerboom et al., 2012; Chen et al., 2013). For the purpose of this study we chose syGCaMP6f. This probe is presynaptically expressed, which we confirmed by loading expressing cells with sytl-Oyster550 antibody, and suitable for imaging of fast  $\text{Ca}^{2+}$  transients in response to small stimulation – 4 APs. Very low baseline fluorescence and punctate appearance of responding boutons aided the selection of responding synapses. This probe was used to investigate whether A $\beta$ 1-42 induces abnormalities in presynaptic  $\text{Ca}^{2+}$  dynamics.

### **3.4.3 Other available tools for studying presynaptic function**

Most of the available genetically encoded fluorescence probes are GFP-based, and those with red tags are inferior in comparison to their green counterparts. One example of such a construct is sypTomato which is a red tagged synaptophysin with pH sensitive red fluorescence protein pHTomato (Li and Tsien, 2012). We tested this probe in the lab as it would allow for simultaneous imaging of vesicular release with, for example, pre- or postsynaptic calcium transients, and would provide with more comprehensive data on the function of a particular synapse. Nevertheless, the responses were very difficult to observe and hence the probe was unsuitable for our purposes. Recently, an improved red version of GECIs with characteristics similar to GCaMP6 sensitivity has been developed (Dana et al., 2016), which could make possible the simultaneous imaging of  $\text{Ca}^{2+}$  transients and vesicle recycling with GFP-based probe such as sypHy2x.

Another group of reporters are genetically encoded fluorescent voltage indicators (GEVIs). Although calcium imaging can provide information on action potential

generation, it has several disadvantages. The temporal dynamics of calcium reporters are often not sufficiently fast to capture events arising from generation of individual action potentials (Peterka et al., 2011). They are also not suitable for imaging sub-threshold events (Peterka et al., 2011). The development and design of satisfactory functioning GEVIs poses several challenges some of which are: targeting the probe to the thin, two-dimensional membrane, rapid dissipation of electrical field, binding of the probe to internal membranes and intensity of emitted light (Peterka et al., 2011). Recently engineered, ArcLight overcomes this shortfall, with significantly improved signal-to-noise ratio in comparison to its predecessors, allowing to image single action potentials (Cao et al., 2013; Jin et al., 2012). We tried this probe but identification of responding cells was very cumbersome and neuronal health compromised, which prevented its use in this study. Alternative to GEVIs are high sensitivity voltage probes suitable for intracellular application such as JPW3028 used to study signal processing in axons in pyramidal neurons (Popovic et al., 2011). Nevertheless, unlike GEVIs which are expressed in multiple neurons, these dyes require delivery via a patch pipette, which largely limits the number of readouts that can be obtained in a given experiment. This approach would be irrational for the type of the experiments carried out in this study.

Alternative methods for studying vesicle recycling are emerging. Quantum dots (Qdots), which are small enough in size (12-25 nm) to fit within the lumen of synaptic vesicles, and loosely attach to neuronal membranes allowing for their endocytic uptake (Zhang et al., 2009b). These small particles with a crystal core and hydrophilic coating, are characterized by very bright photoluminescence and great photostability, making them superior to FM1-43 dyes in this regard, and exhibit pH-dependent fluorescence, similar to that of pHluorin molecules (Zhang et al., 2009b). Qdots therefore seem like the probe of choice for long term imaging of single synaptic vesicles. Indeed, they have been successfully used for this purpose, in the studies deciphering the dominant mode of endocytosis at hippocampal neurons (H. Park et al., 2013; Zhang et al., 2009b).

Nevertheless, one of the major drawbacks of this method is that Qdots exhibit 'blinking' of the fluorescence of random occurrence and duration, which can complicate interpretation of the measurements (Zhang, 2013). Moreover, Qdots have the tendency to form aggregates, which have to be removed via size exclusion column before application to neurons.

This demonstrates that the current tools have many drawbacks, but inevitably, in time the ability to optically monitor the function of presynaptic terminals will doubtless lead us to new discoveries and deeper understanding of the subject. The ability to simultaneously monitor multiple processes within the same boutons, for example  $\text{Ca}^{2+}$  influx and SVs recycling, at the level of single synaptic vesicles, is the highly desirable tool that is missing, but one that is already under development (Li et al., 2011). The improvements in photostability, signal-to-noise ratio, toxicity, specificity and reporting kinetics would all facilitate the progress in our understanding of the events accompanying the release of synaptic vesicles.

# 4 CHARACTERIZATION OF SINGLE VESICLE ENDOCYTOSIS

---

## HIGHLIGHTS

- The timing of synaptic vesicles endocytosis is highly heterogeneous within synapse populations
- Fluorescence amplitude of syHy2x corresponding to single vesicle exocytosis is established
- Individual synapses exhibit signature timing of endocytosis following single vesicle release events
- The similarity measures cannot be explained by experimental or analysis factors



## 4.1 Introduction

In the previous chapter we validated available tools for optical analysis of presynaptic function. SypHy2x was identified as the most suitable probe for our study – investigation of the timing of synaptic vesicles endocytosis and elucidating the properties of presynaptic terminals underlying them. Small central synapses show a high level of variability in their structure and function across the population of synapses (Dreosti et al., 2009; Harata et al., 2001; Ratnayaka et al., 2012). This variability is shaped by the recent history of their activity to meet the functional demands. Previous studies showed that hippocampal synapses were found to have a variable recycling pool fraction (Kim and Ryan, 2010; Marra et al., 2012; Ratnayaka et al., 2012), a high level of heterogeneity in  $p_r$  (Branco et al., 2008; Branco and Staras, 2009) and a large variation in the number of docking sites (Pulido et al., 2015). These properties are key determinants of synaptic strength. The expression of important for transmission proteins, such as Munc18, was also found to vary from synapse-to-synapse (Cijssouw et al., 2014). The expression of vGlut1 or vGlut2 isoforms on synaptic vesicles was found to be an important locus for regulation of release probability and diversity between synapses (Weston et al., 2011). Another parameter highly variable between individual boutons was the destaining kinetics of FM1-43 (Klingauf et al., 1998). Although sometimes not directly commented on by the authors, from the representative examples of fluorescence profiles, the variability in the kinetics of fluorescence decay during endocytosis from pHluorin based studies is very apparent (Balaji & Ryan, 2007; Dean et al., 2012; Gandhi & Stevens, 2003; Sankaranarayanan & Ryan, 2000; Zhu, Xu, & Heinemann, 2009). Similar observation can be made based on the example endocytic profiles generated with Qdots (Zhang et al., 2009a). Collectively, these studies demonstrate that presynaptic function is very varied, and yet the basis of this variability is still not well-understood. Defining the regulatory rules that are responsible for the behaviour of neurons and synapses is one of the major aims in neuroscience. A deep understanding of these rules could not only

contribute to our knowledge of the workings of the nervous system, but could also prompt identification of disease-associated changes in synapses in the future. We therefore decided to test the hypothesis that although there might be a high heterogeneity in the kinetics of endocytosis at the level of population of synapses, individual boutons might exhibit signature patterns of single vesicles endocytosis.

In the first section of this chapter we tested for variability in the endocytic kinetics observed after 40 APs stimulation. Of course, some temporal information might be masked through the summing of multiple vesicle recycling events. For this reason, in the second part of this chapter we decided to take the novel approach of examining variability in endocytosis following single vesicle release events.

Studies on single synaptic vesicles provided important information on many aspects of presynaptic function. Balaji and Ryan, 2007 showed that the kinetics of single synaptic vesicle endocytosis is highly variable and stochastic within a population of responses from multiple individual vesicles. The copy number of an important exocytic protein, synaptobrevin, sufficient for vesicle fusion, was deciphered in a study looking at single vesicle release events (Sinha et al., 2011). The disputed origin and properties of synaptic vesicles released during evoked or spontaneous neurotransmission were also examined by tracking the behaviour of single synaptic vesicles (Peng et al., 2012).

The quantal nature of neurotransmitter release was established from electrophysiological studies. The measurement of miniature excitatory postsynaptic current (mEPSC), which corresponds to the release of neurotransmitter content of a single synaptic vesicle, was the basis for the formulation of the hypothesis of the quantal nature of synaptic transmission (Del Castillo & Katz, 1954; Fatt, & Katz, 1952). Subsequently, capacitance measurements at presynaptic terminals combined with postsynaptic mEPSC recordings were used to monitor the fusion and endocytosis of single synaptic vesicles and to directly link these presynaptic events to the postsynaptic currents (Sun et al., 2002). Nevertheless, the available methods, which allowed these

events to be studied in larger synaptic terminals such as neuromuscular junction, Calyx of Held or retinal bipolar synapses, are substantially less useful in the small central synapses, due to the very small size and surface area of these synapses. Moreover, electrophysiological recordings do not provide information on the behaviour of individual boutons, but rather report the postsynaptic effect of the SVs release from multiple terminals and neurons. It is also important to note that the findings on the behaviour of single synaptic vesicles in these other preparations cannot always be faithfully translated to hippocampal synapses (Aravanis et al., 2003). For these reasons, the advent of powerful imaging methods and the development of optical reporters such as FM1-43, vGpH or syHy have been critical in permitting the direct monitoring of single synaptic vesicle behaviour at individual synapses, where other methods are not readily available. Single synaptic vesicles have been successfully imaged using both vGpH and syHy (Balaji and Ryan, 2007; Gandhi and Stevens, 2003; Granseth et al., 2006; Zhu et al., 2009).

The main aims of this chapter were to establish: i) the sources of variability in the kinetics of endocytosis at individual synapses; ii) whether we could determine syHy2x fluorescence amplitude corresponding to the release of single synaptic vesicle; iii) whether, despite the high level of heterogeneity in retrieval kinetics in the population, individual synapses show signature kinetics of endocytosis following single vesicle release events.

## **4.2 Heterogeneity in the timing of synaptic vesicle endocytosis amongst synapses**

### **4.2.1 High variability in endocytosis following RRP mobilizing stimulus**

We first set out to examine the variability within endocytic profiles resulting from stimulation with 40 APs at 20 Hz, an activity protocol which is known to mobilize the RRP.

For this purpose, we used *sypHy2x*, a genetically-encoded construct validated in the previous chapter. We reasoned that 40 APs would recruit sufficient vesicles to allow us to robustly visualize fluorescence changes during time-lapse imaging and provide a baseline measure of variability with good signal-to-noise.

The preparation of the cell culture, AAV.*sypHy2x* infection and experimental conditions were as described in section 3.3.1. Prior to the stimulation trials that were used for the analysis, cells were stimulated once with 40 APs and imaged. This allowed the identification of responding regions and the pre-bleaching of the sample (that is to remove the residual surface fluorescence). The following stimulation and imaging rounds were used for the analysis. ROIs of equal size were drawn around individual responding terminals and were positioned on the basis of subtracted images (peak response–baseline), which allowed for easy identification of responding boutons. The fluorescence at the peak of the response had to be fully encapsulated within the ROIs in order for the synapse to be included in the analysis.

The first striking observation in the baseline subtracted data was the variability between different boutons in the size of the responses evoked with 40 APs 20 Hz stimulation (Fig.4.1.A). This high variability in the level of the release can be caused by various factors such as  $p_r$  of individual boutons, the distribution of  $\text{Ca}^{2+}$  channels or the size of the active zone (Eggermann et al., 2011; Holderith et al., 2012; Marra et al., 2012; Matz et al., 2010). Nevertheless, the interest of this study was focused on the variability in the kinetics of endocytosis. In order to test this we fitted traces with single exponential curves constrained to the average of 3 frames following the response peak. The analysis was carried out on bleach corrected, non-normalized data. For presentation purposes, traces were normalized to the baseline and to the peak of the stimulation. Figure 4.1.B. shows 15 traces from Figure 4.1.A fitted with a single exponential curve. The high variability in the endocytic kinetics between the synapses is apparent (Coefficient of variation: 83.32%) (Fig.4.1.C and D). The analysis of the timing of endocytosis at the calyx of Held

following various stimulation intensities revealed differences in the retrieval time, depending on the frequency of action potentials and as a consequence of the number of vesicle released (Sun et al., 2002). In our case, the fluorescence amplitude represents the number of released vesicle at a given synapse, which is shown in Fig.4.1.A and which was highly variable in synapses measured. For a more detailed analysis, we therefore selected a subset of traces within a defined amplitude range, in order to examine the extent of endocytic rate variability when the amplitude of exocytosis was constrained.

All the responses were filtered according to the selected fluorescence range ( $\Delta F = 80\text{-}120$  a.u.) (Fig.4.1.E) and again fitted with single exponential decay profiles (Fig.4.1.F). The variability in tau readouts in this limited data set was still high (Coefficient of variation: 29.9%), although significantly lower than for all data ( $n = 51$  and  $331$  synapses, respectively, two-tailed unpaired Student's t-test,  $P = 0.03$ ).

These data suggest that the endocytic kinetics following the RRP mobilizing stimulus are highly variable between synapses. The lower endocytic variability within a given range of response amplitudes suggests that there is at least a partial dependency of the retrieval kinetics on the number of vesicles released. Nonetheless, even when constrained to a small range of response amplitudes, variability in endocytosis is still preserved. This implies that heterogeneity is a central feature of homogeneous synaptic populations, even under circumstances when the data are corrected for the number of vesicles released. The other conclusion to be drawn from this is that it is highly important to consider the response amplitude in experiments aiming to compare endocytic kinetics between different treatment groups when protocols leading to multivesicular release are used.

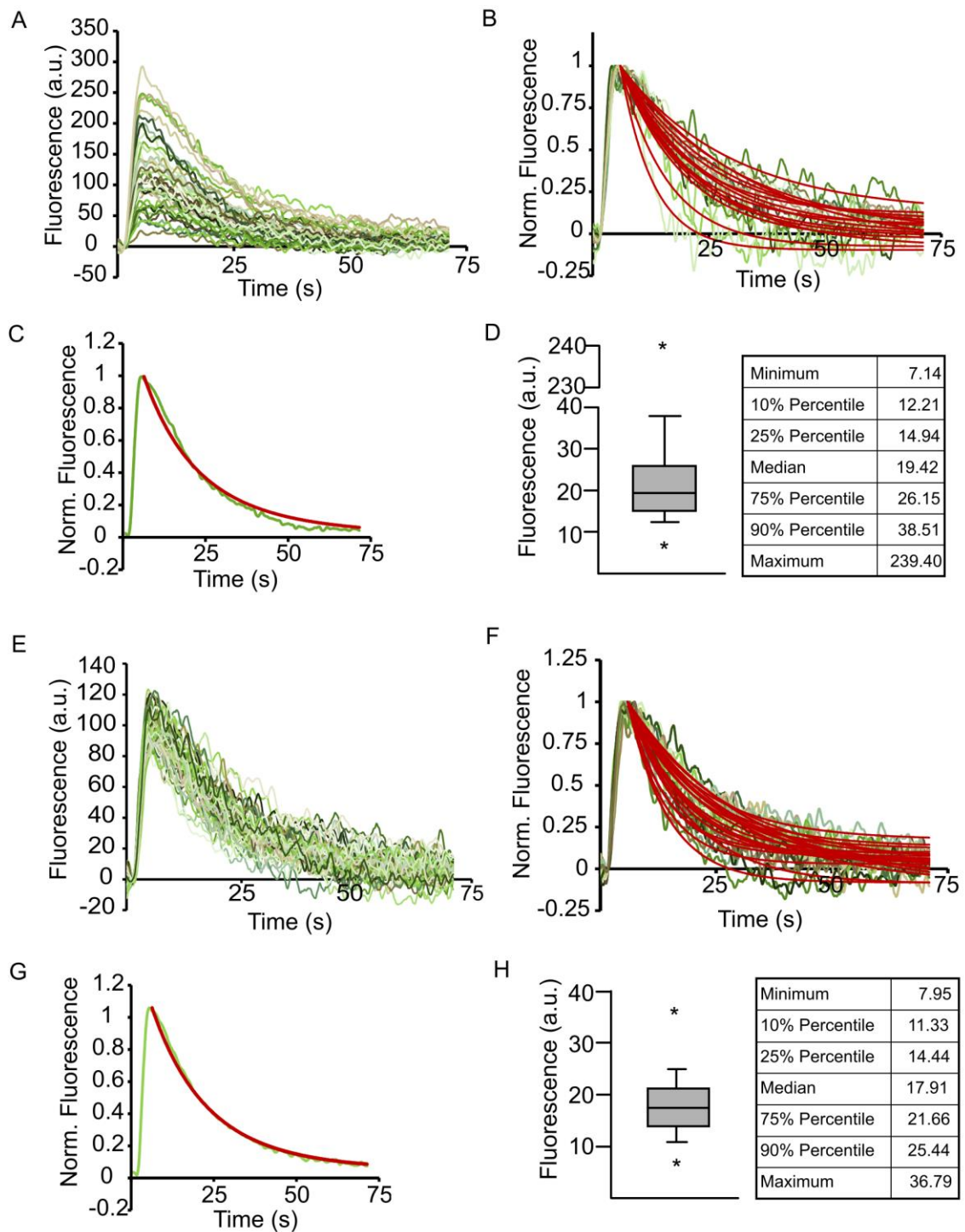


**Figure 4.1 Variability in the kinetics of synaptic responses to 40 APs, 20 Hz stimulus (sypHy2x readouts).** A) The degree of discrepancy in the size of the response of individual synapses to stimulation with 40 APs at 20 Hz (example traces from 42 synapses, 5 coverslips). B) Traces (green) were normalized between the baseline and the peak of the response and single exponential (red) was fitted to each trace revealing high variability in the kinetics of endocytosis ( $n = 15$  example synapses from 5 coverslips). C) Average kinetics of all the traces (green) fitted with single exponential (red) used for tau analysis in D ( $n = 331$  synapses from 5 coverslips). D) Whisker plot illustrating variability in tau measurements across synapses. Graphs E-H mirror A-D but

for limited range of responses. E) Responses of 57 synapses (5 experiments) to 40 APs stimulation within 80-120 fluorescence range. F) Examples of normalized traces (green) fitted with single exponential (red) ( $n = 21$  from 5 experiments). G) Average of all traces from 80-120 range (green) fitted with single exponential (red) ( $n = 51$  synapses from 5 experiments). H) Whisker plot summarizing variability in tau within the chosen range of responses ( $n = 51$  synapses from 5 experiments).

#### 4.2.2 Examining the possible source of variability

Having established that there is a variability in the rate of endocytosis following 40 APs, 20 Hz stimulus, even within data limited to the responses within a range of exocytic amplitude ( $\Delta F = 80\text{-}120$  a.u.), we wanted to test, firstly, whether this variability might be related to the bleaching rate of the baseline fluorescence, and secondly, whether the endocytic rate is varied depending on the number of vesicles released within this fluorescence range. Assuming that the size of the response had an effect on the retrieval rate, that could mean two things: i) the bleaching rate is different in case of larger responses due to more unquenched fluorescence on the surface upon vesicle release; ii) the endocytic machinery copes differently with the endocytic load when fewer or more vesicles are released. In order to examine these possibilities, we measured the slope of the baseline fluorescence prior to the onset of the stimulation and the amplitude of the responses for each analysed profile.

The same data as in Figure 4.1.G was used for this analysis. The slope of the baseline was calculated on the basis of the average of 3 frames at the beginning of imaging, which was divided by the average fluorescence just before the onset of the stimulation, and by the total number of baseline frames (40 frames, 3.6 s) (Fig.4.2.A). The amplitude of the response was calculated by subtracting the baseline fluorescence (average of 3 frames before the onset of the stimulation) from the average of 20 frames spanning the peak of the stimulation (Fig.4.2.A). Both readouts were plotted against tau measurements for each synapse (fitting described in previous section). We found that there was neither a

correlation between the rate of vesicles retrieval and the baseline bleaching rate ( $n = 51$  synapses, Pearson's correlation test,  $r = 0.1029$ ,  $P = 0.491$ ) (Fig.4.2.B), nor between the response amplitude and the tau readouts ( $n = 51$  synapses, Pearson's correlation test,  $r = 0.1130$ ,  $P = 0.4497$ ) (Fig.4.2.C) in synapses within a set range of response amplitudes ( $\Delta F_{\text{exo}} = 80\text{-}120$  a.u.).

These results suggest that the variability of the kinetics of endocytosis cannot be simply explained by the variable sybHy2x baseline fluorescence or the difference in the endocytic load resulting from the number of vesicles released by a given synapse.

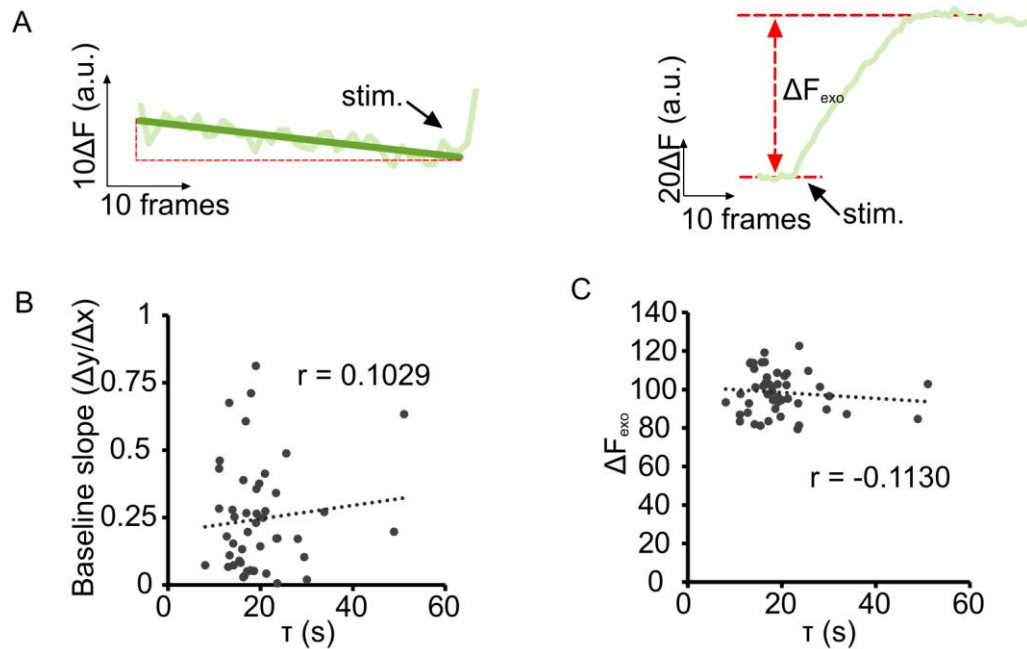


**Figure 4.2 Rate of synaptic vesicle endocytosis does not depend on the baseline fluorescence or the response amplitude.** A) Schematic illustrating methods of measurements used. The slope of the baseline was calculated by taking the average fluorescence of 3 frames at the beginning of the imaging and 3 frames before the onset of the stimulation, divided by the number of frames (left). The amplitude of the responses was found by subtracting the baseline fluorescence (average of 3 from prior to the stimulation) from the average fluorescence of 20 frames at the peak of the stimulation (right). There was no correlation between the kinetics of endocytosis and baseline slope (B,  $n = 51$  synapses, Pearson's correlation test,  $r = 0.1029$ ,  $P = 0.491$ ) and the amplitude of the response (C,  $n = 51$  synapses, Pearson's correlation test,  $r = 0.1130$ ,  $P = 0.4497$ ).



### 4.2.3 High variability between synapses of the same type

Another possibility explaining high variability in the endocytic kinetics across boutons might be heterogeneity of the population of sampled synapses. Unlike vGpH, which is only expressed in excitatory synapses (vesicles carrying vesicular glutamate transporter 1), syphHy2x does not discriminate between inhibitory and excitatory synapses. Although most synapses in hippocampal cultures are glutamatergic (Benson and Cohen, 1996; Gulyá et al., 1999), it is possible that our population contains both inhibitory and excitatory boutons and the variability is a result of the difference in the behaviour of these two populations of synapses. The proteomic analysis of the core proteins involved in vesicle docking and exocytosis showed no difference between GABAergic and glutamatergic terminals and the two populations only differed in neurotransmitter-specific enzymes and transporters (Boyken et al., 2013). Perhaps the same rule applies to endocytic proteins. Nevertheless, we wanted to test whether the population of glutamatergic synapses alone exhibits similar extent of variation in the timing of vesicle endocytosis. In order to achieve this we labelled cultures with vGlut1 and vGlut2 antibodies.

First we carried out a functional readout of endocytosis with syphHy2x expressing cells during 40 APs, 20 Hz stimulation. DIC images at 10x magnification were taken to facilitate refinding of the region of interest following antibody labelling. Immediately after imaging cultures were fixed with 4% PFA, permeabilized, blocked and co-labelled with vGlut1 and vGlut2 antibodies (1:1000 and 1:2000, respectively) (protocol in section 2.11). The reason for co-labelling comes from a study which showed that neocortical synapses in primary culture exhibited the developmental switch in the expression of these two transporters (Berry et al., 2012). The proportion of vGlut1-expressing synapses and the level of this transporter at individual synapses was gradually increasing at the expense of vGlut2 as the cells and synapses matured (Berry et al., 2012). The purpose of our experiment was to identify all glutamatergic boutons in the

preparation; hence we labelled our samples with both vGlut1 and vGlut2 antibodies and used secondary antibodies, which were both GFP-tagged. Details on the immunolabelling protocol are in section 2.11 and the results of the control experiment for the specificity of secondary antibody binding in the Appendix I, Figure 1.

Following the labelling, previously imaged sypHy2x expressing regions were relocated. The analysis showed that boutons expressing sypHy2x, responding to 40 APs, 20 Hz stimulation, were well colocalized with vGlut1 and vGlut2 fluorescence (Fig.4.3.A). The analysis of fluorescence profiles revealed a very close overlap of vGlut1 and vGlut2, and sypHy2x fluorescence (Fig.4.3.B). Despite the fact that fluorescence profile of sypHy2x before and after staining was perfectly matched in this particular experiment, due to the fact that multiple coverslips and regions had to be relocated, it often proved to be difficult to seamlessly align the images from before and after staining for the purpose of fluorescence correlation. We also tested whether sypHy2x baseline fluorescence was comparable before and after staining (Fig.4.3.B). The results in Fig.4.3.C are from the experiment where images before and after staining were perfectly overlaid. From this, it is apparent that vGlut1 and vGlut2 is well correlated with sypHy2x signal (Pearson's correlation test,  $n = 41$  synapses,  $r = 0.7493$ ,  $P < 0.0001$ ), confirming the glutamatergic nature of the analysed boutons. In order to improve the number of boutons available for the analysis, the same set of ROIs was used as in the functional part of the experiment, but ROIs were carefully adjusted for each synapse in the images following labelling to account for the shift in the regions originating from repositioning of the coverslips for imaging. This allowed us to evaluate vGlut1 and vGlut2 fluorescence against the sypHy2x fluorescence background following the labelling (Fig.4.3.D). With this result we were therefore able to confirm that all the synapses selected for functional analysis were glutamatergic (Pearson's correlation test,  $n = 154$  synapses,  $r = 0.7234$ ,  $P < 0.0001$ ) (Fig.4.3.D).

Having identified that the boutons selected for the analysis are glutamatergic we focused on the analysis of the endocytic variability within this population of synapses. As before, the endocytic kinetics of glutamatergic boutons was measured by fitting single exponential function to bleach-corrected, non-normalized 40 APs response profiles of individual synapses. The analysis revealed high variability in the timing of vesicle endocytosis within these synapses (Coefficient of variation: 38.3%) (Fig.4.3.E). In order to test whether other factors affected this variability (as described in sections above), we again filtered data according to the response amplitude and selected boutons with  $\Delta F = 80-120$  a.u. for the analysis. For visualization purposes, example profiles were normalized to the peak of their response. Although slightly lower, we still observed variability within this data set that could impact on the efficiency of function of a particular synapse (Coefficient of variation: 24%) (Fig.4.3.F. and G.). From this we can conclude that high variability of endocytic kinetics from individual synapses cannot be attributed to the difference in the nature of the synapses compared: GABAergic versus glutamatergic.

We recognize that many factors can contribute to variability in the recycling kinetics resulting from a stimulation protocol that recruits a sizeable vesicle pool, and where the precise number of released and recycled vesicles is stochastic and uncontrollable. In order to more reliably scrutinize the properties of individual synapses, we consequently decided to switch to an approach where we could examine the behaviour of single synaptic vesicles at individual presynaptic boutons. By constraining our investigation in this way, we could eliminate the variability arising from stochastic recruitment, and thus explore the inherent heterogeneity, or not, in vesicle profiles. Our approach was also designed to allow us to compare recycling kinetics across multiple trials, permitting us to test whether a particular response profile was preserved across time at individual synapses. In the next section of this chapter we first outline the rationale for the approach used for measuring endocytic kinetics of single vesicle release events and subsequently outline the principal findings.

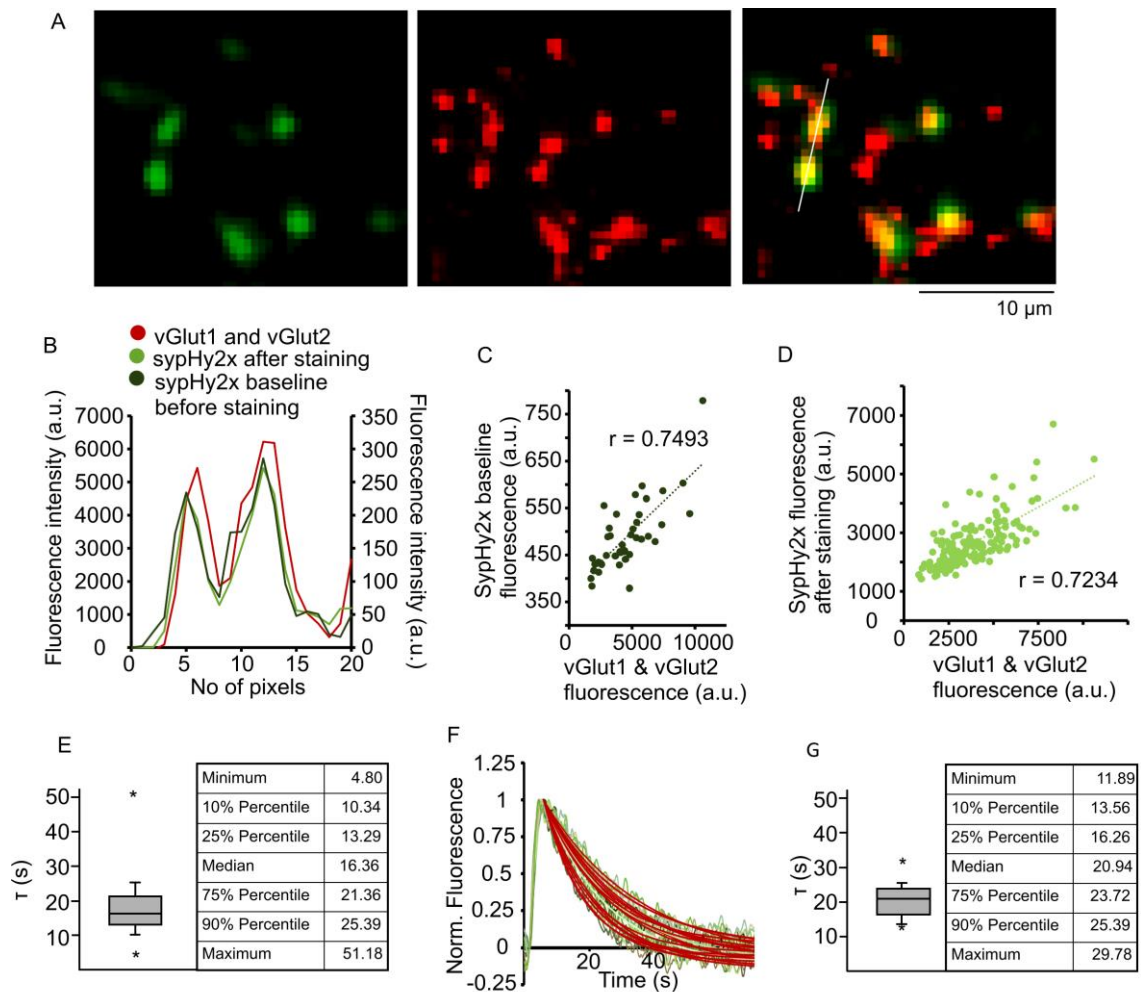


**Figure 4.3 Responses to 40 APs, 20 Hz stimulation show high variability in retrieval kinetics in the population of glutamatergic synapses.** A) Fluorescent image of sypHy2x expressing synapses (left). Background was subtracted from frames at the top of the stimulation to reveal synapses responding to 40 APs shown here. Presynaptic terminals labelled with vGlut1 and vGlut2 antibody (middle). The overlay of sypHy2 and vGlut1 and 2 fluorescence (right). The white line indicates the area for which measurement is shown in B. Scale bar 10  $\mu$ m. B) Fluorescence intensity profiles of vGlut1 and 2 staining, and sypHy2x baseline before staining and sypHy2x fluorescence after staining. C) Correlation between vGlut1 and vGlut2 fluorescence and sypHy2x baseline prior to staining (Pearson's correlation test,  $n = 41$  synapses,  $r = 0.7493$ ,  $P < 0.0001$ ) and (D) between vGlut1 and 2 and sypHy2x fluorescence after staining (Pearson's correlation test,  $n = 154$  synapses,  $r = 0.7234$ ,  $P < 0.0001$ ). E) Variability in the kinetics of endocytosis following 40 APs, 20 Hz stimulation in excitatory synapses ( $n = 159$  synapses, 3 regions from 2 coverslips). F) Examples of profiles from 19 excitatory synapses from 3 coverslips of which responses to 40 APs, 20 Hz stimulus were within 80-120  $\Delta F$  a.u. fitted with single exponential constrained to 1. G) Variability in the kinetics ( $\tau$  (s)) of synapses from 80-120  $\Delta F$  a.u. range ( $n = 36$  synapses, 3 experiments, 2 coverslips).

### 4.3 Synapse-specific timing of single vesicle endocytosis

#### 4.3.1 Visualization of single vesicle release events

Having identified high variability in endocytic kinetics following 40 APs 20 Hz stimulation, we wanted to test whether the same applies to the retrieval kinetics of single synaptic vesicles. As a starting point for this kind of approach, it is necessary to establish the signal corresponding to a single vesicle fusion event. For the purposes of this work, and in line with the assumptions made by others previously, we reason that a change in the fluorescence corresponding to vesicle fusion events conforms to a quantal distribution profile. In this way, the smallest quantal responses should correspond to single vesicle fusion profiles. A fluorescence value corresponding to single vesicle release event has been successfully determined by a few research groups in their imaging systems using: FM1-43 (Aravanis et al., 2003; Chen et al., 2008; Ryan et al., 1997), synaptopHluorin (Gandhi and Stevens, 2003), sypHy (Zhu et al., 2009), vGpH (Balaji and Ryan, 2007) and iGluSnFR (Marvin et al., 2013). The first step in this work was to establish the fluorescence value that reflects single vesicle release events in our system.

Cells were infected with *AAV.sypHy2x* viral construct. 10 days were allowed for the expression of the construct following which the cultures were used for imaging. After a suitable region was found, a culture was imaged whilst being stimulated 10 times with 4 APs 20 Hz stimulus in EBS with blockers (20  $\mu$ M CNQX, 50  $\mu$ M AP-5) (Fig.4.4.A). The stimulation with 4 action potentials was chosen based on our knowledge of the probability of release at hippocampal synapses. Although highly variable, this has been estimated to be  $0.22 \pm 0.03$  at hippocampal neurons (Branco et al., 2008), meaning that at 1 AP stimulation there is ~25% chance for a release event to occur. Therefore, by using stimulation at 4 APs, we significantly increased the likelihood of capturing a single vesicle fusion event, ultimately reducing the exposure of the sample to blue excitation light. For the purpose of analysis we discarded the first trial as a bleaching trial and used the profiles from the remaining 9 trials. The practise of pre-bleaching was previously

employed by (Gandhi and Stevens, 2003) who showed that although the fluorescence quenched in resting synaptic vesicles is not affected, pre-bleaching the sample for 2 min resulted in 90% attenuation of the background fluorescence. As the surface expression of synaptophysin is nearly half of that of synaptobrevin (refer to section 1.6.2.2), 40 seconds pre-bleaching was sufficient in our system. Longer bleaching times could have added unnecessary imaging time and resulted in the production of toxic to cells reactive oxygen species (Peterka et al., 2011). The synapses used for analysis were rigorously selected. At least 5 images from the 9 trials were screened, and the synapses had to conform to a set of pre-set rules in order to be included in the analysis: i) stable, low level baseline fluorescence puncta, ii) clear separation from the neighbouring synapse, iii) the fluorescence at the peak of the response had to be well encapsulated within the boundary of the ROI ( $2.8 \times 2.8 \mu\text{m}$ ) and not saturated.

The variation in the size of 250 example responses to the same 4 APs level of stimulation, is clearly apparent (Fig.4.4.B). Figure 4.4.C shows the behaviour of a representative synapse to the consecutive stimulation rounds. From these responses, we can fairly confidently establish how many vesicles were released in a given round of stimulation: 1, 2 or none. We found that the distribution of fluorescence amplitudes resulting from 699 events from 80 synapses, was well-described by a multiple Gaussian fit ( $P(\chi^2 \leq CV) = 1$ ,  $\chi^2$  test, d.f. = 53) (Fig.4.4.D). The first peak was located near 0 a.u. intensity and corresponds to those events that did not result in vesicle release, reflecting the noise in the baseline fluorescence. The second peak, positioned at  $\Delta F = 124.6 \pm 3.5$  a.u. reflects the responses of 1 quantum – single synaptic vesicle release events. The width of the peak was used for determining the range of 1 quantum sizes ( $\Delta F_{1Q} = 92.2$ -157 a.u.). Peaks corresponding to 2 and 3 quantum events were also clearly distinguishable. The analysis of the positions of the peaks established from the multiple Gaussian fit, shows that  $\Delta F$  increased by uniform increments of the same fundamental value, corresponding to the fluorescence resulting from single vesicle release (Pearson's

correlation test,  $r = 0.999$ ,  $P = 0.0014$ ) (Fig.4.4.D, inset). We therefore established the fluorescence amplitude corresponding to single vesicle release events in our system.

In order to confirm our result we applied the identified fluorescence amplitudes for 1 quantum and 2 quanta values to our data. Figure 4.4.E shows representative images of synaptic responses identified to be a single vesicle and 2 vesicle release events. Responses were filtered according to our values determined for 1 and 2q,  $\Delta F = 92.2$ - $157$  a.u. and  $\Delta F = 210$ - $247$  a.u., respectively. There was an apparent difference between the responses falling within the two ranges. 1q responses were also distinctly identifiable from the failures – noise within the system (Fig.4.4.F).

We showed that we were able to confidently identify the fluorescence amplitude in our system corresponding to single vesicle release events and that we were able to isolate fluorescent profiles according to their quantal size.

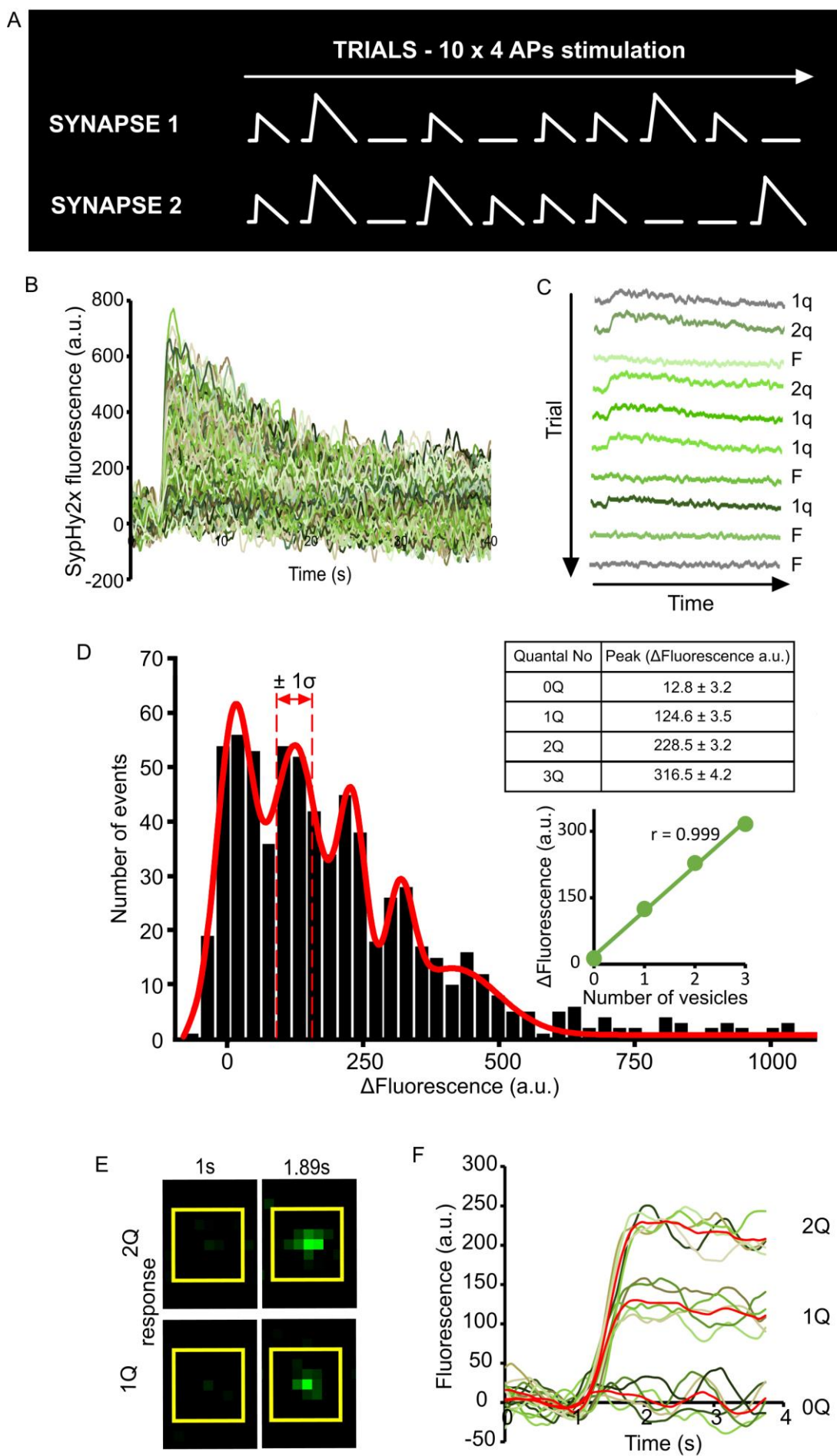




**Figure 4.4 Establishing fluorescence amplitude of single vesicle release events.**

A) Schematic represents the protocol used for data collection. Synapses were imaged whilst being stimulated 10 times with 4 APs stimulus. B) 250 fluorescent profiles resulting from 4 APs stimulation showed high variability in the size of the response. C) Responses to repeated stimulation (10 trials at 4 APs) from a single synapse reveal quantal nature of the synaptic behaviour and occasional failures to respond. D) Histogram of fluorescence amplitudes of 699 events from 80 synapses, 3 experiments. Red line represents multiple Gaussian fit revealing peaks at  $12.8 \pm 3.23$ ,  $124.6 \pm 3.48$ ,  $288.5 \pm 3.15$  and  $316.5 \pm 4.2$   $\Delta$ Fluorescence values corresponding to 0q, 1q, 2q and 3q release events (values summarized in the table;  $P(\chi^2 \leq CV) = 1$ ,  $\chi^2$  test, d.f. = 53). The width of the peak (red dashed lines) was used as a boundary for determining the size of  $\Delta$ Fluorescence range corresponding to single vesicle release (fluorescence  $124.6 \pm 32.4$ ). The position of the peaks obtained from Gaussian fit revealed that these fall as multiples of single quantal unit (Inset, Pearson's correlation test,  $r = 0.999$ ,  $P = 0.0014$ ). E) Change in fluorescence corresponding to either single or two vesicle release events. F) Examples of profiles falling within the 0q, 1q and 2q ranges. Red lines represent the averages of the profiles shown in green.

### 4.3.2 Variability in fluorescence retrieval after stimulation evoked release events

Following the observation that endocytic kinetics after 40 APs, 20 Hz stimulation are highly variable, we set out to explore whether profiles arising from 4 APs stimulation protocol reveal similar variability, and if so, to later investigate whether the kinetics of retrieval might be governed at the level of individual synapses. Variability in the endocytosis of single synaptic vesicles was previously described in a study using synaptopHluorin, where single vesicle retrieval times were classified into 3 distinct categories (Gandhi and Stevens, 2003). Others using either vGpH (Balaji and Ryan, 2007) or sypHy4x (Zhu et al., 2009) did not comment on this variability despite the fact that it is apparent from the representative traces shown in their figures.

As outlined above, we stimulated the AAV.sypHy2x-expressing hippocampal neurons 10x with 4 APs, leading to the release of small number of vesicles or failures. The histogram in Fig.4.5.A shows responses from 50 synapses, which were ordered according to the amplitude of the response. In this experiment, ~30-35% of trials resulted in failures, confirming that the logic behind using 4 APs stimulation is correct and we

were able to elicit more release events than previously reported for 1 AP stimulation ( $p_r = 0.22 \pm 0.03$  of hippocampal neurons) (Branco et al., 2008). As mentioned in section 4.2.1, only 9 trials were used for the analysis with the first trial used as a photobleaching step for the reasons described above. The heatplot in Figure 4.5.B allows us to trace the responses of individual synapses shown in Figure 4.5.A. in the subsequent trials (looking vertically), but also enables the investigation of the behaviour of synapses across an individual trial (looking horizontally). High variability of synaptic performance is very apparent from this figure. Not only is it manifested in the size of the responses, but also in the timing of endocytosis, which are depicted here by the intensity and the length of the green bars, respectively. This variability can be directly visualized in the individual endocytic profiles. Figure 4.5.C shows examples of responses from 14 synapses in 5 consecutive trials. The variability in the fluorescence amplitudes and the timing of endocytosis are apparent. A few responses from individual synapse in 4.5.C are displayed in isolation for better visualization of this (Fig.4.5.D). Taken together, these data demonstrated that high variability exists in endocytic kinetics following single vesicle release events. The next focus of this work was on characterizing the regulatory rules, if any, that specify the endocytic kinetics at individual synapses.

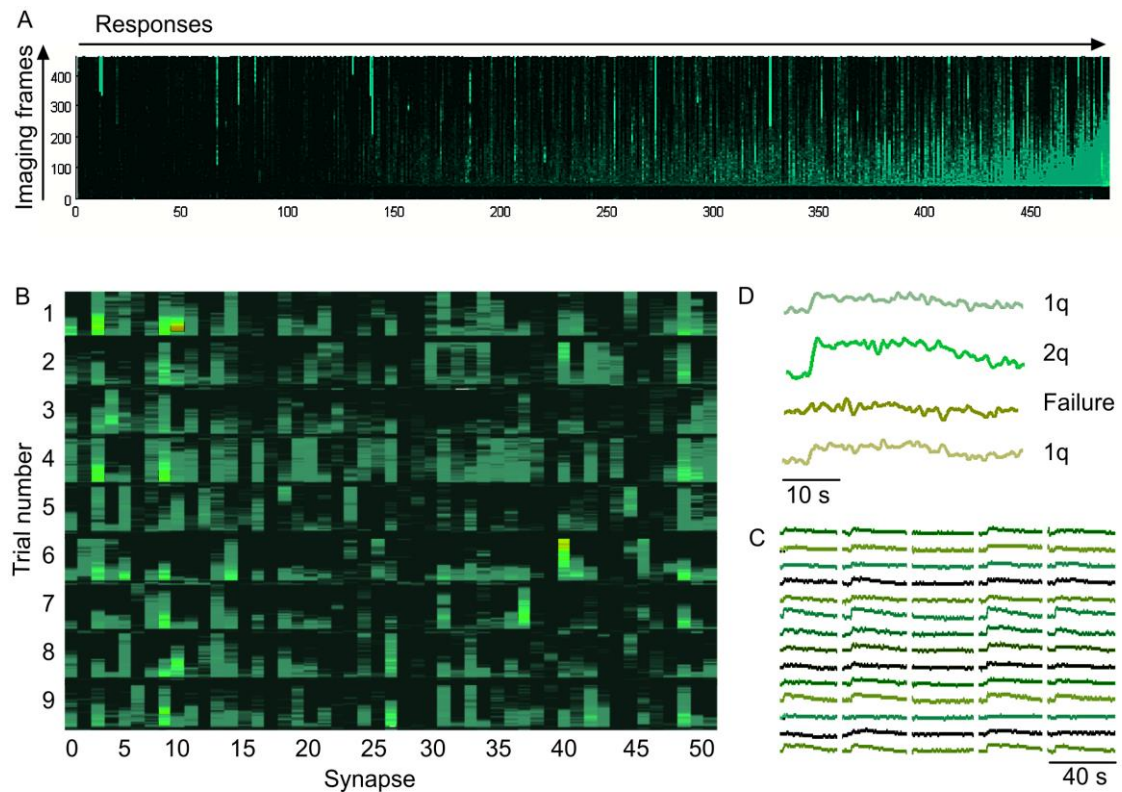


**Figure 4.5 Variability in the synaptic responses to 4 APs stimulation.** A) Heat plot summarizing responses of 50 synapses to 10 x 4 APs stimulation arranged according to the size of the response: failures on the left, largest responses on the right, dark area at the bottom is the baseline. The number of imaging frames (460) corresponds to 41 s of imaging time. B) Variability in the responses can be horizontally traced along trials or vertically along individual synapses. C and D) Examples of profiles from the same synapses over multiple trials.

### 4.3.3 Establishing method for measuring single vesicle kinetics

For the purposes of a detailed characterization, it was important to establish a method for quantifying kinetics of these single vesicle profiles. Specifically, the aim was to find a quantitative, descriptive approach to characterize and compare the kinetics of traces with different retrieval profiles. As is observed in Fig. 4.5 and in the examples in Figure 4.6.B and D, there is a huge variety in the shapes of these profiles. The challenge was to establish a quantitative approach that would encapsulate the features of these profiles and that would permit comparisons to be made between traces. We therefore trialed

different approaches to establish a suitable analysis strategy for describing profiles and the timing of fluorescence decay.

The endocytic decay of signals from pHluorin-based constructs has been typically described and measured using single exponential fits (Balaji et al., 2008; Budzinski et al., 2011; Granseth et al., 2006; Voglmaier et al., 2006; Zhao et al., 2014). Nonetheless, many of these studies are considering profiles arising from larger stimulation protocols (for example, 40 APs), where the timecourse of fluorescence change is an average product of multiple vesicles undergoing recycling. We were unsure if the same approach would be suitable for single vesicle kinetics where, as outlined above, variable profiles are readily apparent. To test this, a custom written Matlab script was used to select endocytic profiles following single vesicle release events based on the identified 1q response amplitude. We found that a single exponential decay curve was an excellent fit for the average curve of fluorescence decay arising from these 1q responses (Fig.4.6.A). However, it was clear that individual profiles were not adequately described by the same single exponential fit approach (Fig.4.6.B). To provide a better description of these profiles, we tested various functions in search for the best approach for comparing these complicated traces. All functions were fitted to the same number of frames starting from the peak of the response to the end of each profile and fits were not constrained to any values. We trialled various strategies: fitting individual profiles with single and double exponential, linear, as well as 2<sup>nd</sup> and 3<sup>rd</sup> order polynomial functions. We then calculated the  $R^2$  for each profile and averaged the values for all synapses, for each function. Where the function was not successfully converged we assigned the  $R^2$  as 0 and reported the number of unsuccessful fits (Fig.4.6.C). In the case of single and double exponential functions, a substantial fraction of profiles, 16 and 12%, respectively, could not be fitted (Fig.4.6.C). The linear fit produced a reliable fit for every trace, although this was not necessarily a perfect description of the profile in all cases. We reasoned that the simplicity of this fit and the single slope value that represented fluorescence decay would be most suitable for estimating the kinetics of traces, allowing us to preserve as many

profiles as possible and reliably evaluate the behaviour of the majority of synapses. Third order polynomial fit was, as expected, the best for describing the complex shapes observed in some traces (Fig.4.6.C and D). For this reason, we chose to use this function for our analysis of the similarity between traces since it faithfully represented all features of the profiles – important for our comparative analysis - and also allowed us to limit the basal signal noise, which would otherwise contaminate comparisons.

In summary, from this analysis we determined the most suitable functions that will be used for the analysis of behaviour of single vesicles at individual synapses: linear, for estimating the kinetics of the traces, and third order polynomial, for the analysis of the similarity of the profiles.

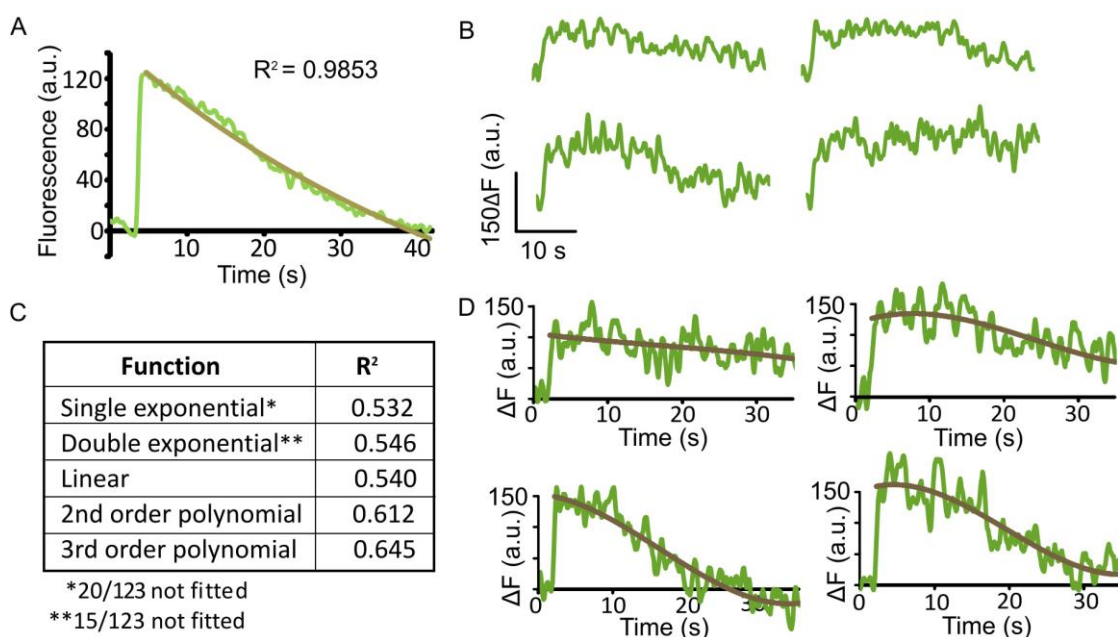


**Figure 4.6 Selection of the best function describing endocytic retrieval following single vesicle fusion events.** A) Average of 123 1q responses from 3 experiments fitted with single exponential fitted to the mean trace ( $R^2 = 0.9853$ ). B) Examples of individual single vesicle response traces that were not successfully fitted with single exponential. C) Table summarizing goodness of fit of various functions to single vesicle traces. All functions were fitted to the same number of x values and not constrained to any value ( $n = 123$  1q traces from 3 experiments). D) 3rd order polynomial function describes well the shape of the traces.

#### 4.3.4 Behaviour of single vesicles at individual synapses

Having established the fluorescence amplitude corresponding to single vesicle release events and the functions best describing the kinetics and the shape of fluorescence decay, we turned our attention to examining the endocytic profiles from individual synapses following single vesicle fusion events. The logic for this is as follows. Although our initial work reveals substantial variability across the population of synapses and trials, we wondered whether less variable responses might be observed where we limit our investigation to individual terminals. In other words, could we see evidence for 'signature' profiles at single synapses, with endocytic kinetics preserved across trials? Such an idea would offer evidence for underlying order in the apparently random fluorescent decay kinetics observed at the population level. To test this hypothesis, the protocol previously described was followed by one where AAV.*syphHy2x*-expressing cells were repeatedly stimulated with 4 APs and the single vesicle release profiles were filtered from all the responses using custom written Matlab scripts (Fig.4.7.A). Although, as expected, there was a high variability in the individual profiles (Fig.4.6.B and D), our objective was to determine if individual synapses have preserved endocytic kinetics and thus whether this heterogeneity in the population of the responses is mainly driven by the differences between synapses. We analysed our responses with a Matlab script which not only chooses the responses of a given amplitude (1q), but also fits third order polynomial function to all selected traces, and maintains the profiles assigned to their individual synapse. Thanks to this we were able to screen multiple 1q responses within individual synapses. The outcome of this approach indicated that despite the high variation between the different synapses, the timing of endocytic profiles might indeed have a synapse-specific component to it (Fig.4.7.B). This similarity of profiles from different trials, and in some cases, even complex features of these profiles, were faithfully replicated at individual synapses. The next step was to design an approach to formally

quantify this similarity of endocytic timing within a synapse versus the population of synapses.

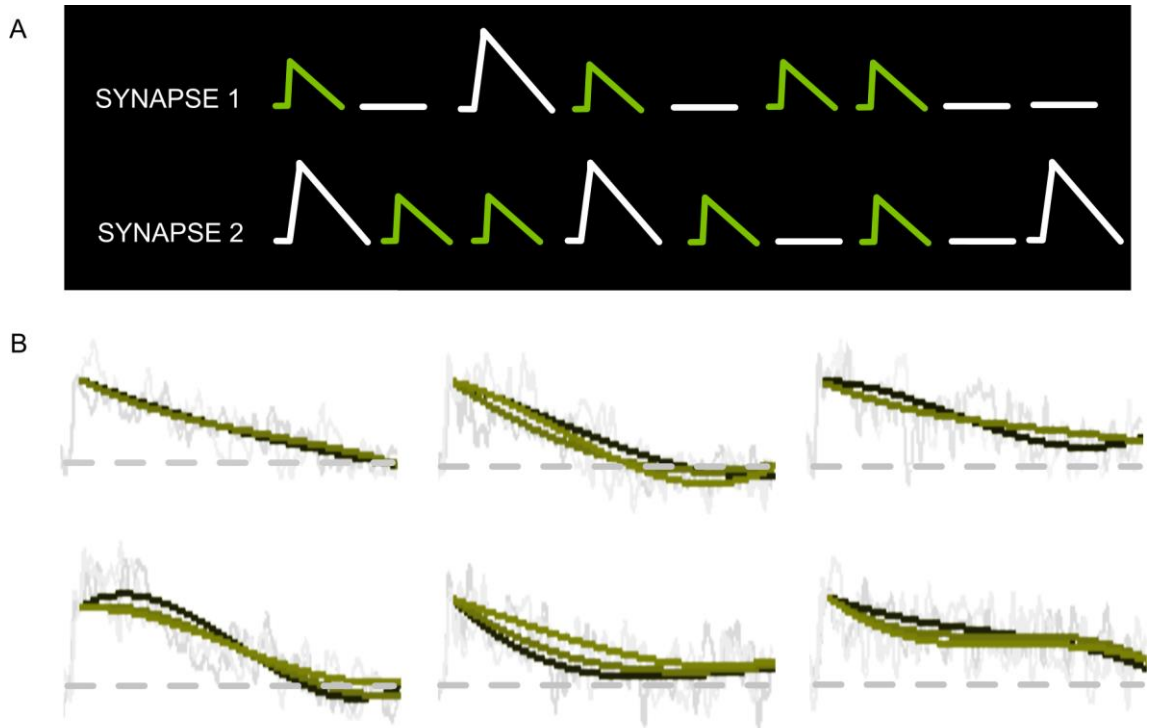


**Figure 4.7 Individual synapses exhibit signature endocytosis kinetics.** A) Cartoon representing experimental and analysis approaches. Single vesicle responses (green) at each synapse were selected from 9 x 4 APs trials. B) Examples of single vesicle responses from individual synapses (grey). All traces were fitted with 3rd order polynomial function (green) revealing varied and yet synapse-specific kinetics of endocytosis.

#### 4.3.5 Measuring the homogeneity of behaviour of vesicles at individual synapses

One of the biggest challenges of this study was to devise a reliable method for comparison of the traces at individual synapses and for comparing them to the population of the responses from multiple synaptic boutons. As shown in Figure 4.6. and 4.7. single vesicle endocytic profiles have complex, multi-step kinetics, which in many studies is obscured by averaging across all the responses. Although single vesicle profiles are clearly distinguishable from baseline signal in our imaging system, their inherently noisy

nature complicates approaches for comparing them. To circumvent this, we elected to use the 3<sup>rd</sup> order polynomial function fit, which provides a good representation of the properties of individual profiles. The next step was to establish a way of measuring the differences between these fitted profiles. We reasoned that the simplest method was to calculate point-by-point differences between 1q traces within a given synapse, and to generate an average of these giving a measure of Within Synapse Similarity (WSS). For a comparative quantification, we needed to test the WSS values obtained against similar values, calculated for all the responses in the population of other synapses; in other words, within synapse versus between-synapse analysis. Our initial approach for this between-synapse analysis was to calculate similarity for all responses from other synapses, within a given experiment, excluding the synapse in question. However, we subsequently reasoned that this approach had a major drawback. Although there is a high variability between the individual profiles, it is also very likely that multiple synapses exhibit fairly similar profiles. In this analysis we were therefore arriving at a measurement of a deviation from the average of individual profiles within the population, and so ultimately we were comparing deviation within a synapse in question to the average deviation within the population. This was not the objective of this analysis. Moreover, many synapses could have exhibited responses similar to the average response and yet have conserved characteristics, which this analysis did not pick up on.

For this reason, we designed another approach summarized in Figure 4.8.A. The rationale for this was as follows: if the vesicle retrieval time at individual boutons is stochastic, what is the likelihood that profiles with similar kinetics occur at any given synapse? In order to answer this question for each experimental synapse, we created a randomised synapse. These randomized synapses exactly matched the experimental synapse in question in terms of the number of single vesicle responses. These responses were randomly drawn from the pool of all single vesicle responses from a given experiment in our Matlab script, but excluding the responses originating from the



synapse in question. This process was repeated 100 times for each synapse and replicated for all the synapses in a given experiment. Employing this method of comparing experimental synapses to randomised synapses, we carried out two types of analysis: point-by-point analysis and rate analysis, of which results are described in the following sections

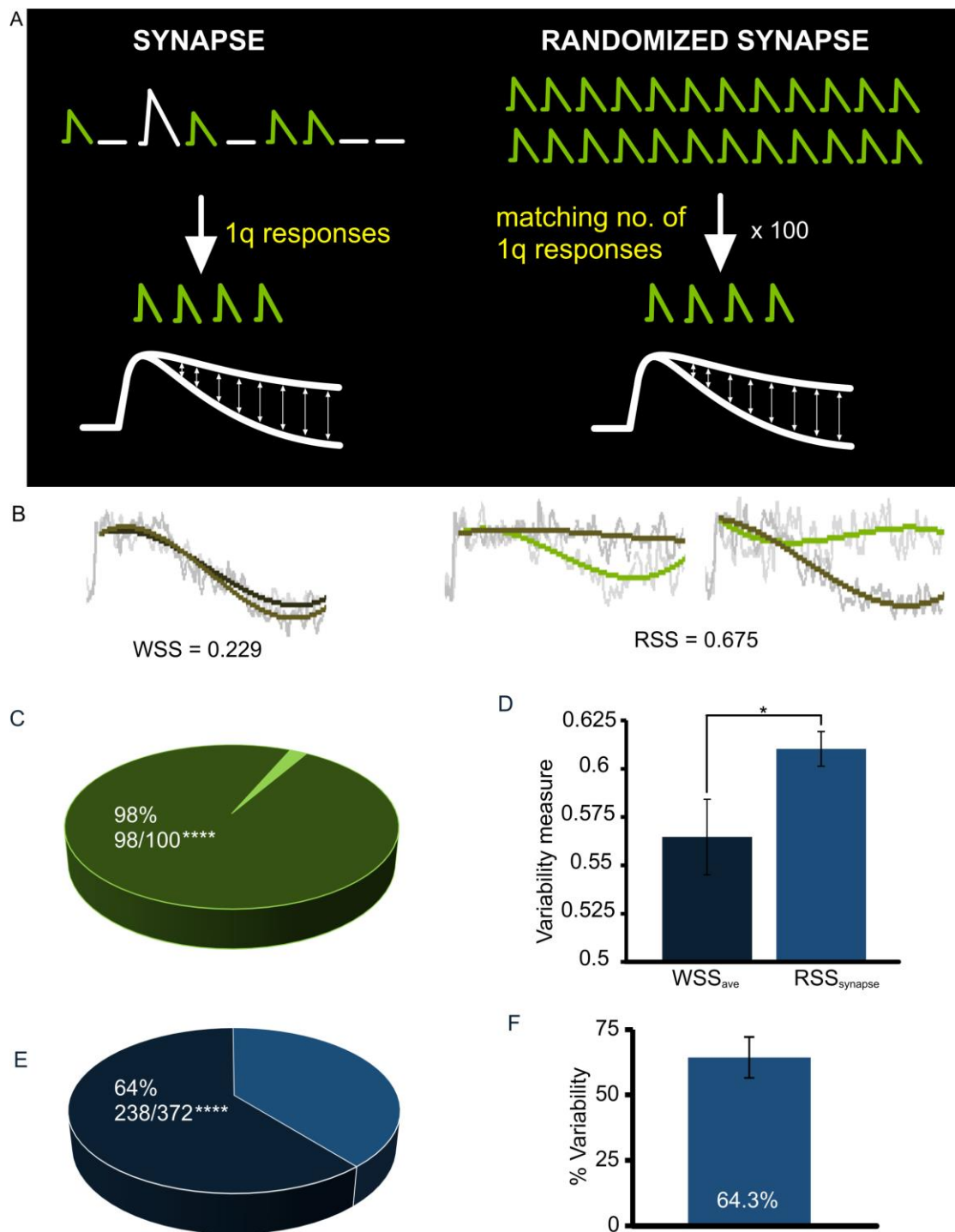


**Figure 4.8 Quantification of similarity in single vesicle kinetics at individual boutons.** A) Schematic representation of the experimental approach. For the analysis of similarity within experimental synapse, single vesicle traces were selected from all the responses from the particular synapse. Each synapse was compared to a random synapse with the same number of single vesicles responses, which were randomly drawn from other synapses from the experiment. This was repeated 100 times for each experimental synapse. Traces were fitted with 3rd order polynomial function and compared within experimental synapse and within each randomized synapse using point-by-point analysis, which allowed to establish similarity value for the two. The obtained values were used for comparison between experimental synapse and random synapse. B) Example of experimental synapse fitted with 3rd order polynomial (left) and 2 random synapses generated using 1q profiles from other experimental synapses. For the example synapse shown, within synapse similarity index ( $WSS = 0.396$ ) shows less variability between the traces in this synapse when compared to the average of similarity of 100 random, matching synapses (Random synapse similarity ( $RSS = 0.477$ )). C) Data comprising of all 1q profiles from a given experiment including single 1q profiles. 98 out of 100 trials showed higher variability in the randomized trials than in the experimental synapses (data from 25 experiments, binomial test,  $n = 100$ ,  $k = 98$ ,  $p = 0.5$ ,  $P < 0.0001$ ). D) Graph showing comparison between  $WSS$  and  $RSS$  values.  $WSS_{ave}$  shown as the average of Matlab readouts of  $WSS$  from all the synapses  $\pm$  SEM.  $RSS_{ave}$  represents the average value of  $RSS_{synapse}$ , which in turn is the average of 100  $RSS$  readouts for a given synapse  $\pm$  SEM (two-tailed paired Student's t-test,  $P = 0.024$ ,  $n = 372$  synapses from 25 experiments). E) Analysis by synapse revealed that 64% of randomized synapses were more variable than experimental synapses (data from 25 experiments, binomial test,  $n = 372$ ,  $k = 238$ ,  $p = 0.5$ ,  $P < 0.0001$ ). F)  $RSS_{ave}$  value was 64.3% higher than  $WSS_{ave}$ . Data shown as average of 372 synapses  $\pm$  SEM.

#### 4.3.5.1 Point-by-point analysis

As mentioned above, the first strategy was to carry out point-by-point analysis of the traces in experimental synapses and to compare them to the randomized synapses. Just to reiterate, single vesicle responses from our 4 APs protocol were selected according to the determined fluorescence amplitude for single vesicle exocytosis. The point-by-point difference was calculated for all responses fitted with 3<sup>rd</sup> order polynomial function within a given synapse and compared to the results from a randomised synapse, which was matched to the experimental synapse in terms of the response number. For each experimental synapse, 100 randomised iterations were created. The profiles for randomised synapses were drawn from the pool of all single vesicle responses within the experiment, and point-by-point analysis was carried out for each randomised synapse in the same fashion as in the experimental synapse (Fig.4.8.A). The rules for

the selection of traces for randomised synapses were as follows: i) traces from the synapse in question were excluded from the pool; ii) each trace could only be selected once in a given round; iii) 2 traces from the same synapse could not be selected for randomized synapse; iv) traces from synapse with only one single vesicle response were included in the pool. From this we obtained a single readout of 'within synapse similarity' (WSS) and 100 readouts for 'randomized synapse similarity' (RSS) to compare with each experimental synapse. Figure 4.8.B shows an example of experimental synapse and two randomized synapses. The smaller the value of WSS or RSS, the lesser the difference between the profiles, and thus, the bigger the similarity in endocytosis within a given synapse.

Based on our results, we carried out a series of comparisons 'by trial' and 'by synapse'. For the descriptions of the abbreviation of the particular measures refer to Appendix I, Figure 2. In the analysis 'by trial' we first calculated how many randomised trials had a higher  $RSS_{\text{trial}}$  value than  $WSS_{\text{ave}}$  obtained for experimental synapses. This analysis shows whether the similarity in the endocytic decay, as seen in the experimental synapses, can be achieved by chance. We averaged RSS values from all synapses in a given trial ( $RSS_{\text{trial}}$ ) and compared that value for each trial to the average WSS from all experimental synapses ( $WSS_{\text{ave}}$ ). Notably, our results showed that 98% of randomized trails had higher  $RSS_{\text{trial}}$  value than the  $WSS_{\text{ave}}$  readout for experimental synapses (data from 25 experiments, binomial test,  $n = 100$ ,  $k = 98$ ,  $p = 0.5$ ,  $P < 0.0001$ ). This suggests that the similarity between the profiles within a given synapses is not by chance.

We carried out another analysis of the difference in the point-by-point readout values for the experimental and randomized synapses. This result provides information about whether the overall variability within the randomized profiles is higher than in the experimental ones. We averaged the RSS readouts from 100 trials for each synapse in order to obtain a single value of variability for each randomised synapse ( $RSS_{\text{synapse}}$ ),

which we then averaged for all randomised synapses to achieve  $RSS_{ave}$ . From this we found that there was significantly higher variability within the profiles of randomised synapses than experimental ones (two-tailed paired Student's t-test,  $P = 0.024$ ,  $n = 372$  synapses from 25 experiments) (Fig.4.8.D).

An alternative way of looking at the data is 'by synapse'. Here we used the averaged RSS values from 100 trials for each randomised synapse ( $RSS_{synapse}$ ), in order to test whether randomised synapses are likely to show comparable similarity of their profiles to the experimental ones. We tested how many randomised synapses were more variable than the experimental ones. This comparison was based on WSS and  $RSS_{synapse}$  measurements. We found that 64% of randomised synapses were more variable than the experimental ones, again confirming that within synapse similarity is not an effect of a random process ( $n = 372$  synapses, data from 25 experiments, binomial test,  $n = 372$ ,  $k = 238$ ,  $p = 0.5$ ,  $P < 0.0001$ ) (Fig.4.8.E). Extension of this analysis was the comparison of the WSS and  $RSS_{synapse}$  values. In effect, we asked whether  $RSS_{synapse}$  readouts are more variable than WSS and, if so, how much more variable. Our analysis showed that  $RSS_{synapse}$  readouts yielded 64% more variability between the profiles than WSS (Fig.4.8.F), meaning that individual randomised synapses exhibited more variability between their profiles than the experimental synapses.

Taken together, these results clearly demonstrate that the properties of endocytic profiles are synapse-specific and that the comparable level of similarity cannot be achieved if the timing of vesicle retrieval was entirely stochastic at individual boutons.

We wanted to test our data by applying even more strict rules for the selection of profiles for the randomized synapses and hence we carried out two more investigations. In this analysis the rules for random picking were as indicated above, however, the traces from synapses which only exhibited one single vesicle release event were excluded from the

available drawing pool. This decision was based on the fact that these individual profiles might correspond to a non-standard population; for example, we reasoned that they could be populations of travelling vesicles or extrasynaptic release sites, rather than conventional synapses (Ratnayaka et al., 2011). As such, they might be characterized by different timing of endocytosis and add to the variability in the pool used for randomized synapses. In the first version of the analysis in which we excluded these traces, we permitted for them to be drawn only where there was no other possibility for matching randomized synapses to the experimental ones whilst conforming to the other rules described before: i) traces from the synapse in question were excluded from the pool; ii) each trace could only be selected once in a given round; iii) 2 traces from the same synapse could not be selected for randomized synapse. We carried out the same analysis as described above. In this analysis, 72 out 100 randomized trials were more variable than the experimental data (data from 25 experiments, binomial test,  $n = 100$ ,  $k = 72$ ,  $p = 0.5$ ,  $P < 0.0001$ ), 60.5% of synapses had more variable  $RSS_{\text{synapse}}$  measurement than the WSS readout for experimental synapses (data from 25 experiments, binomial test,  $n = 372$ ,  $k = 225$ ,  $p = 0.5$ ,  $P < 0.0001$ ), and randomized synapses were also 52.4% more variable than the experimental ones (Fig.4.9.A and B). As such, the same findings were still preserved.

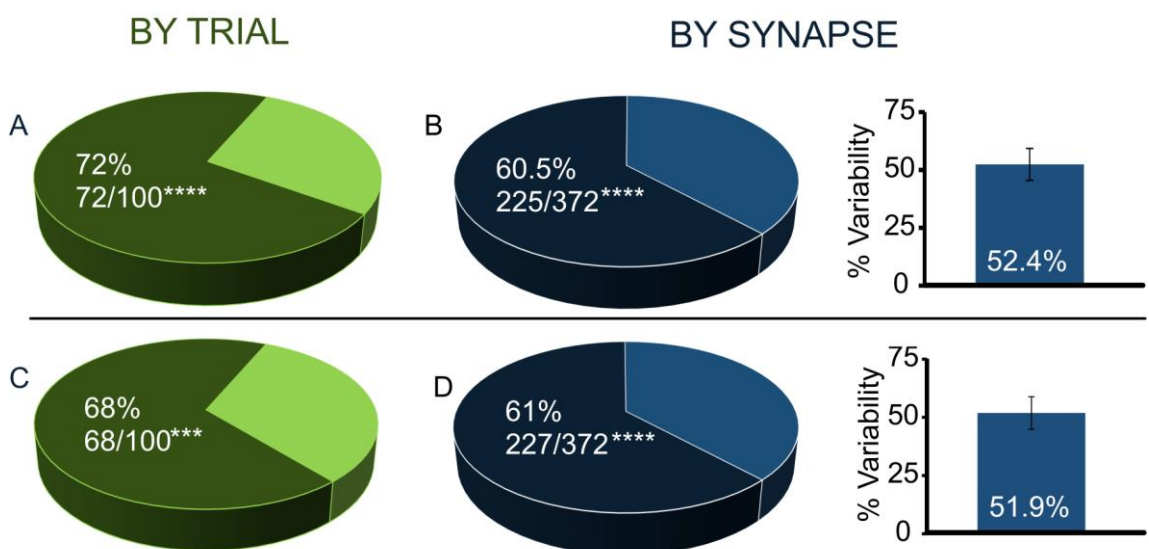


**Figure 4.9 Quantification of similarity in single vesicle kinetics at individual boutons II.** The top row comprises of data where the use 1q profiles was only allowed when all other options for drawing profiles from synapses with multiple 1q responses were exhausted. Data shown in the bottom row only includes synapses with multiple responses within 1q range. A) 72% of randomized trials showed higher variability than the experimental synapses (data from 25 experiments, binomial test,  $n = 100$ ,  $k = 72$ ,  $p = 0.5$ ,  $P < 0.0001$ ). B) Comparison of variability across synapses demonstrates 60.5% synapses from randomized group were more variable than experimental synapses (data from 25 experiments, binomial test,  $n = 372$  synapses,  $k = 225$ ,  $p = 0.5$ ,  $P < 0.0001$ ). Analysis of  $RSS_{\text{synapse}}$  and WSS showed 52.4% more variability in the profiles in the randomized group in comparison to experimental synapses. Data shown as average of 372 synapses  $\pm$  SEM. Data in C and D mimics A and B under different rules for drawing 1q profiles for randomised synapses. C) Data from 25 experiments, binomial test,  $n = 100$  iterations,  $k = 68$ ,  $p = 0.5$ ,  $P = 0.0004$ . D) Pie graph, data from 25 experiments, binomial test,  $n = 372$ ,  $k = 227$ ,  $p = 0.5$ ,  $P < 0.0001$ . Bar graph, percentage variability in  $RSS_{\text{synapse}}$  in comparison to WSSI. Data shown as average of 372 synapses  $\pm$  SEM.

In the third, and most critical analysis approach, we totally excluded synapses where there was only one single vesicle trace. To do this, we also had to amend our rule of using only a single trace from experimental synapse per randomized synapse; if this was not the case, the script could fail to random-match all the synapses due to the difference in the number of responses between synapses. This means that in some cases we could have compared 'within synapse' to other 'within synapse' values, especially in those experiments with fewer synapses, but with multiple single vesicle responses. This analysis could therefore undermine the true differences between 'within' and 'between' comparison by contaminating the random group. Nevertheless, this analysis still yielded the same outcome, and thus further added to our confidence that our observation reflects biological properties of synapses. In this case, we found that 68 out of 100 randomized trials were more variable than experimental synapses (data from 25 experiments, binomial test,  $n = 100$ ,  $k = 68$ ,  $p = 0.5$ ,  $P = 0.0004$ ), 61% of randomized synapses were more variable than the experimental ones (25 experiments, binomial test,  $n = 372$ ,  $k = 227$ ,  $p = 0.5$ ,  $P < 0.0001$ ) and the variability in randomized group was 51% higher than in the experimental group (Fig.4.9.C and D).

Taken together it can be concluded from this analysis that the similarity of endocytic profiles exhibited within individual synapses is not due to chance but that it reflects a true difference in the function between these synapses. In Chapter 5 we explore synaptic properties that may account for their conserved behaviour.

#### **4.3.5.2 Rate analysis**

In addition to our point-by-point analysis, which compares the shapes of the profiles, we also carried out analysis of the rate difference between the profiles. The point of this was not to measure the absolute kinetics of these events, since we have already discussed the challenges associated with the complex multi-element nature of the profiles seen after single vesicle responses; rather it was to reliably compare the timing of the decay at individual synapses and to compare the results to randomized population of synapses as described above. In order to do that we used the linear fit. Our goal was to maximize the number of measurements, hence we chose linear fit over more conventional single or double exponential fits, which often failed to successfully fit our traces (detailed analysis in section 4.3.3).

Randomized synapses were generated in the same way as described above, and the same analysis logic was followed, only in this case all single vesicle traces were fitted with linear fit instead of polynomial, and the difference in the slope between all the traces within experimental and randomised groups was calculated (Fig.4.10.A) The smaller the returned value (within synapse rate similarity (WSRS)), the more similar were the profiles within the tested synapse (Fig.4.10.B). This analysis was carried out based on the data set including the responses from synapses which only exhibited one single vesicle release as we felt that when these are excluded, effectively we might be comparing experimental synapses to themselves. 'By trial' analysis revealed that in 95 trials the rate difference was larger in randomized synapses than in the experimental ones (data from

25 experiments, binomial test,  $n = 100$ ,  $k = 95$ ,  $p = 0.5$ ,  $P < 0.0001$ ) (Fig.4.10.C), and in the analysis 'by synapse' we found that 62.1% of randomized synapses were more variable than the experimental synapses (data from 25 experiments, binomial test,  $n = 372$ ,  $k = 231$ ,  $p = 0.5$ ,  $P < 0.0001$ ) (Fig.4.10.D).

We also tested how the two analysis types, profile shape-based and kinetics-based analysis, compare to each other. Do synapses which have more variable profiles (higher WSS), also have more variable kinetics (higher WSRS)? The logical answer to this is that these two measurements should correlate to each other fairly well but they might not need to necessarily be perfectly matched. Even though the profiles might follow a similar shape, it is enough if one of the profiles has a slightly more steep decay in the initial stages of the retrieval, which can affect the rate difference measurement. Nevertheless, there was a strong correlation between the two measures, which in a way provides an internal control of the two approaches (Pearson's correlation test,  $n = 372$  synapses from 25 experiments,  $r = 0.755$ ,  $P < 0.0001$ ) (Fig.4.10.E).



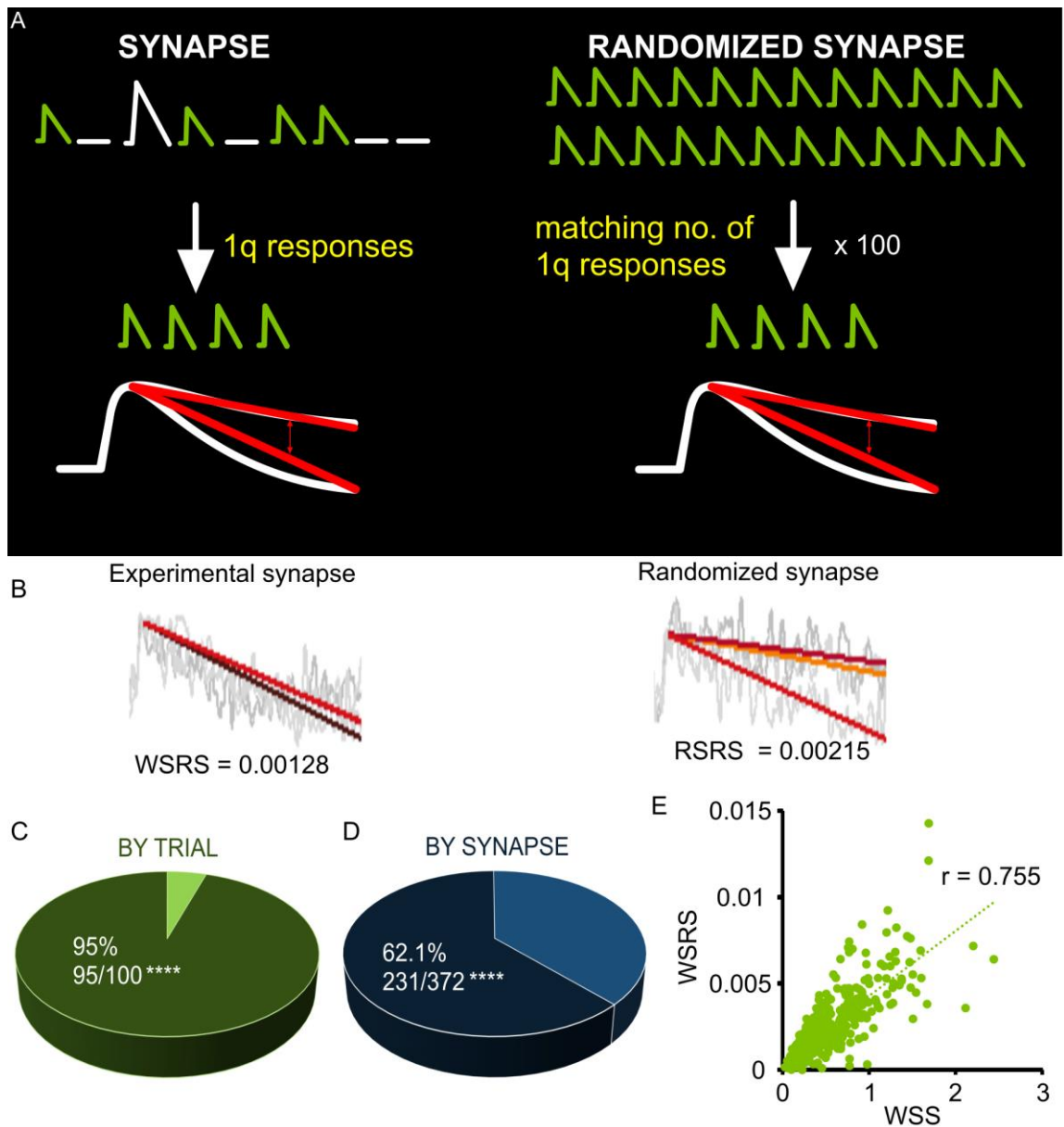


**Figure 4.10 Quantification of the similarity in the rate of endocytosis within individual presynaptic terminals.** A) Schematic representing the analysis approach. Endocytic traces from 1q responses for both experimental and randomized synapse were fitted with linear function. The difference in the slope between the fits was used as a measure of similarity. For more detailed description of the initial stages of the protocol to Figure 4.8. B) Example of experimental synapse and a randomized synapse fitted with linear fit constrained to the peak of the response. For the example synapse displayed here, within synapse rate similarity (WSRS) indicated lower variability between the profiles in comparison to the random synapse rate similarity (RSRS) generated from analysis of 100 random, matching synapses. C) 95% of randomized trials were more variable than the experimental synapses (data from 25 experiments, binomial test,  $n = 100$ ,  $k = 95$ ,  $p = 0.5$ ,  $P < 0.0001$ ). D) 62.1% of randomized synapses exhibited higher rate difference than the experimental synapse (data from 25 experiments, binomial test,  $n = 372$ ,  $k = 231$ ,  $p = 0.5$ ,  $P < 0.0001$ ). E) Strong positive correlation between the WSRS and WSS (Pearson's correlation test,  $n = 372$  synapses from 25 experiments,  $r = 0.755$ ,  $P < 0.0001$ ).

To summarize, experimental synapses exhibited higher levels of similarity in the endocytic rates at individual synapses, than the randomized synapses, which represent responses from the population of synapses, and were characterized by more variable rates of fluorescence decay (Fig.4.11). Our results therefore suggest a strong level of preservation of endocytic timing at individual presynaptic boutons, which might result from specific properties of these single synapses that will be explored in Chapter 5.

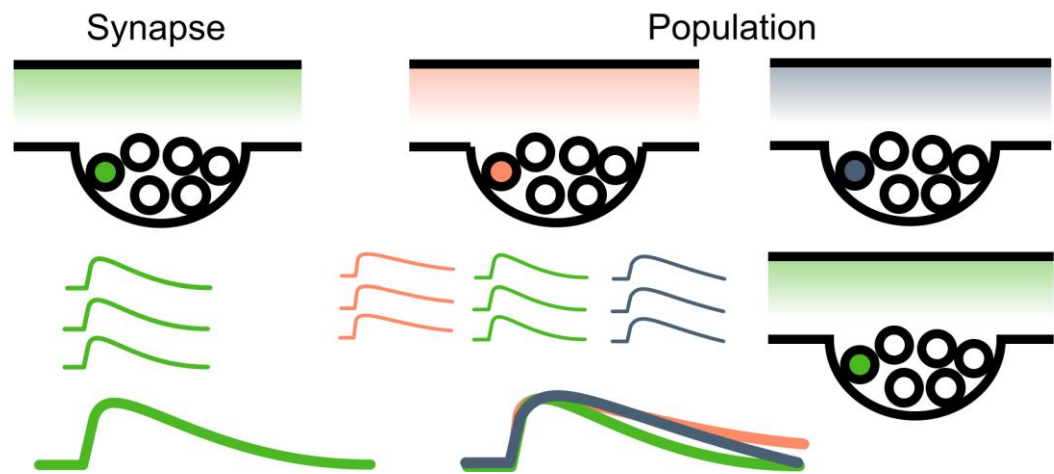


**Figure 4.11 Signature endocytic kinetics at individual synapses.** The kinetics of single vesicle responses is preserved at the level of individual synapse but varied across the population of synapses.

#### 4.3.6 Experimental factors that may impact on the results

Having established that individual synapses exhibit signature endocytic behaviour, we wanted to explore whether imaging-related factors could have influenced our results. Although neuronal cell culture is essentially two dimensional, without much depth, and despite the fact that great care was taken when focusing and choosing synapses for the analysis to make sure that only those in the middle of the focus were selected, we wanted to test whether there might be a difference in the fluorescence signal collected from

synapses that are perhaps nearer to the top of the culture (away from astrocytes) or those closer to the astrocytic layer. If yes, could this account for the differences in the population of profiles while preserving the homogeneity of fluorescence decay within a given synapse?

In order to test this we imaged cells during 4 APs stimulation whilst alternating the focus within a 4.5  $\mu\text{m}$  depth. This allowed us to image the responses from all the synapses at the top and the bottom of the focus, therefore imitating the presence of the synapses within different depths within the culture. The fluorescence at the furthest points, at the top and bottom of the focus along the profile, were selected to compare the slope of fluorescence decay between these profiles (Fig.4.12.A). These points (8 for each focus position) were normalized, and when plotted, we found that there was no difference between the slope of fluorescence values at the top and at the bottom of the focus ( $n = 8$  points, two-tailed unpaired Student's t-test,  $P = 0.987$ ) (Fig.4.12.B). This means that the position of the synapses within the focus range did not influence the shape of the profiles.

Secondly, we tested whether baseline slope has an effect on the endocytic decay. Single vesicle responses within a given synapse were fitted with linear fit between baseline frames (1-39) and immediately following the peak of the response to the end of each profile using the same Matlab script as in our similarity analysis. We found that there was no correlation between the baseline rate of fluorescence and endocytic decay rate (Pearson's correlation test,  $n = 74$  synapses from 7 experiments,  $r = 0.087$ ,  $P = 0.457$ ) (Fig.4.12.C).

Thirdly, we examined whether the amount of baseline fluorescence may have an effect on the fluorescence amplitude within the responses of 1q size. This can test for two different things: i) on the assumption that baseline level of fluorescence reflects synaptic

size (section 5.2.1.), we can check whether the quantal size in larger synapses is pushed towards the upper range of our 1q range; ii) if the baseline level only reflects the difference in the expression of sypHy2x we would expect that the fluorescence amplitude of a single vesicle release event would be larger in synapses with higher baseline level fluorescence. We calculated the average of 3 frames at the beginning of the profiles and plotted it against the fluorescence amplitude, which was calculated by subtracting the average of 3 frames just after the peak of the response and the baseline fluorescence, average of 3 frames just before the stimulus. We found that there was no correlation between the level of baseline fluorescence and the fluorescence amplitude arising from single vesicle exocytosis (Pearson's correlation test,  $n = 429$  single vesicle responses from 7 experiments,  $r < 0.0004$ ,  $P = 0.994$ ) (Fig.4.12.D).

To conclude, we showed that the shape of single endocytic profiles is not affected by the position of the synapse in culture or the accuracy of the focus, neither is it affected by the bleaching kinetics of baseline level of sypHy2x fluorescence. We also showed that fluorescence amplitude of single vesicle responses is not related to the sypHy2x baseline level fluorescence.

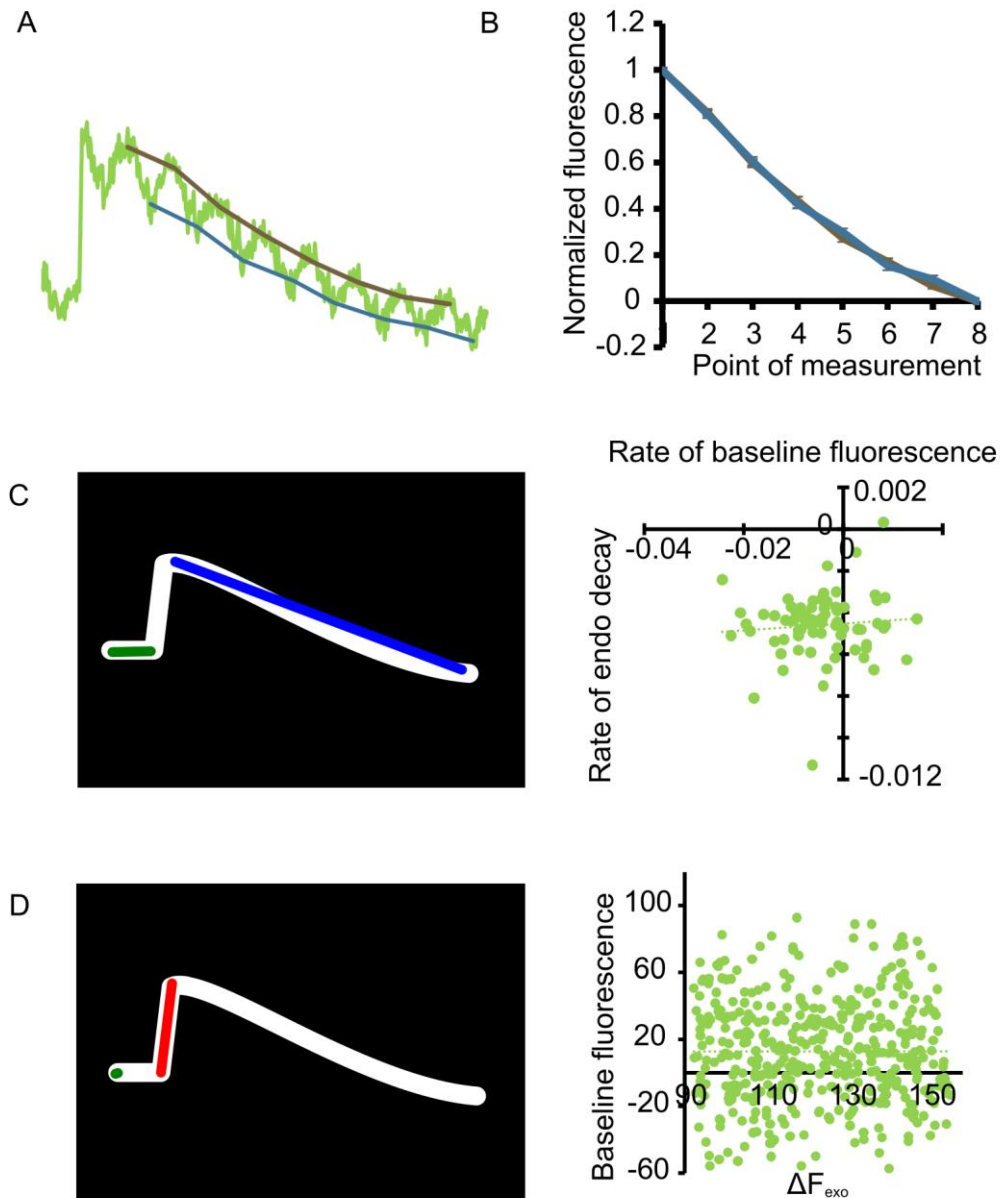


**Figure 4.12 Imaging and other experimental factors.** A) Average of responses from 42 synapses to 4 APs stimulation representing experimental and analysis design. The responding synapses were imaged with alternating focus over  $4.5 \mu\text{m}$  depth. 10 frames at the top of the focus (brown) and 5 frames at the bottom of the focus (blue) were averaged giving 8 points along the profile for each the top and the bottom of the focus. B) 3 consecutive images were analysed according to the description in A and the two traces obtained normalized. The kinetics of the decay didn't change between the bottom (blue) or the top of the focus (brown) ( $n = 126$  responses from 42 synapses  $\pm$  SEM). C) There is no significant correlation between baseline kinetics (horizontal axis) and the kinetics of the endocytosis (vertical axis) (Pearson's correlation test,  $n = 74$  synapses from 7 experiments,  $r = 0.087$ ,  $P = 0.457$ , ns). D) There is no significant relationship between the amount of baseline fluorescence (vertical axis) and the size of the response within 1q size ( $\Delta F_{\text{exo}}$  horizontal axis) (Pearson's correlation test,  $n = 429$  single vesicle responses from 7 experiments,  $r < 0.0004$ ,  $P = 0.994$ , ns).

## 4.4 Discussion

In this chapter we showed that small central synapses show a high level of variability in response amplitude to a given stimulus, and more importantly in the timing of endocytic retrieval of vesicles. We demonstrated that this variability is not associated with experimental factors and that it is not due to multiple types of synapses as it can be readily observed within a population of glutamatergic synapses. Despite the apparent variability in the timing of retrieval of single synaptic vesicles within the population of synapses, we made an important finding, namely, that individual synapses are characterized by signature retrieval profiles.

### 4.4.1 Variability in synaptic vesicle endocytosis

Individual hippocampal synapses have been shown to exhibit high variability in their properties. They have been found to differ in their structure, protein expression or distribution of calcium channels, which all shape and underlie their function (Dreosti et al., 2009; Harata et al., 2001; Michel et al., 2015). We observed in our study that profiles from populations of synapses exhibited a high level of variability in the response amplitude, which is in line with the studies cited above. This variability might result from different  $p_r$  levels of these synapses with stronger synapses releasing more vesicles in response to the same stimulation (Atwood and Karunanithi, 2002; Branco and Staras, 2009). Not only did we observe high variability in synaptic vesicle exocytosis, but also in the timing of endocytosis, which was the main interest of this study. The next relevant issue is to try and understand the source of this variability. Firstly, we should consider the nature of the reported fluorescence decay profiles with sypHy2x. SypHy2x reports the reacidification of SVs, which follows endocytic internalization of newly formed vesicles (Granseth et al., 2006). It is therefore possible that the variability in our profiles arises because of two main reasons: i) in relation to exocytosis, the onset of endocytosis

might be delayed at some synapses; ii) endocytosis proceeds immediately after release but perhaps some vesicles are reacidified with a delay. We directly address this in Chapter 5 using dynasore, a pharmacological blocker of dynamin function. The variability in the endocytic profiles has been reported before and some suggestions about the basis for this have been put forward in the literature. Balaji and Ryan, 2007, using vGpH construct (pHluorin tagged vGlut1) in hippocampal neurons showed a wide range of retrieval times following single vesicle exocytosis. They attributed this to a varied dwell time at the plasma membrane of vesicles, to be retrieved prior to their reacidification (Balaji and Ryan, 2007). Despite the fact that the average dwell time was reported to be  $\tau \sim 14$  s, the timing of individual events varied from instantaneous fluorescence decay, to no decay observed within 20 s post stimulus, perhaps indicating imperfect coupling between exo- and endocytosis (Balaji and Ryan, 2007). This, however, was not observed by Granseth et al., 2006, who saw that the sypHy2x signals always recovered following the stimulation. Gandhi and Stevens, 2003 using SpH also showed high variability in the retrieval kinetics and classified the profiles into 3 major modes. Notwithstanding, it is apparent that the variability in the profiles is more complex than just the 3 patterns described by these authors (Gandhi and Stevens, 2003). They also identified one basis for this, which was the  $p_r$  of individual terminals: synapses with a high release probability tend to use slower, clathrin mediated endocytosis, whereas those with lower  $p_r$  predominantly retrieved their vesicles via kiss-and-run (Gandhi and Stevens, 2003). The fact that the variability has been reported with 2 other construct shows that it is not an artefact of sypHy2x.

The variability in the profiles from the population of synapses might not only be due to the differences in the endocytic and reacidification kinetics, but it might also arise from sampling of synapses of either glutamatergic or GABAergic nature. These two types of synapses are known to exhibit structural and functional differences. Nevertheless, neurons in hippocampus were found to be mostly glutamatergic with only 20%

GABAergic connections (Li et al., 2005). Moreover, the analysis of the type of synapses in hippocampal culture revealed that the density of GABAergic connections was significantly higher on the somata of hippocampal cells but non-GABAergic connections dominated in the processes (Benson and Cohen, 1996; Gulyá et al., 1999). Sampling of the somatic region was avoided in our study due to a higher chance of high background fluorescence level, and a difficulty in distinguishing individual presynaptic terminals, which was very important for similarity analysis.

Although it has been reported that there was no difference in the way inhibitory and excitatory synapses recruit and sort vesicles into distinct vesicle pools following their endocytic internalization (Li et al., 2005), glutamatergic synapses expressing synaptopHluorin were found to exhibit much bigger variability in fluorescence amplitudes in response to 100 APs 20 Hz stimulation than the inhibitory synapses (Moulder et al., 2007). This was not attributable to the difference in the baseline fluorescence between the two populations, but was explained by higher variability in the recycling vesicle pool sizes at excitatory synapses (Moulder et al., 2007). The analysis of variability in vGlut1 and vGlut2-expressing synapses in our culture revealed a high level of variability in the kinetics of endocytosis within the glutamatergic population of boutons, in agreement with the study above. This provides further evidence against this variability being a result of sampling synapses of different types, but rather due to a large variability within the glutamatergic population of synapses.

#### **4.4.2 Synapse-specific vesicle retrieval timing**

Having identified this wide spread variability in the fluorescence decay, and having excluded experimental conditions as a sole source of this variability, we set out to examine whether individual presynaptic boutons might be characterized by signature retrieval profiles. Various presynaptic properties have been found to be synapse-specific,



and to undergo synapse-specific regulation. The diameter of SVs was found to be regulated at a synapse rather than neuronal level (Hu et al., 2008; Qu et al., 2009). The size of the active zone was shown to be subjected to synapse-specific regulation and was strongly correlated with the  $p_r$  at a given bouton (Matz et al., 2010). Similarly, the expression level of CDK5 at individual synapses determined the size of the recycling pool at specific terminals (Kim and Ryan, 2010). This demonstrates that individual synapses are highly predisposed/attuned to the function that they serve in a given circuitry. However, a report of cell-wide rather than synapse-specific regulation of endocytic timing can also be found. Armbruster et al., 2011, in a study on hippocampal neurons concluded that endocytic kinetics following 100 APs, 10 Hz stimulus is a cell-wide, rather than a synapse-specific property. Upon close inspection of their data, in the first example given, there is a large variability in the endocytic timing across boutons from a given cell, which is not apparent in the examples given later on. Moreover, these findings suggest that endocytosis is uncoupled from other presynaptic properties that have been shown to be determined at synapse-specific level (Armbruster and Ryan, 2011; Branco et al., 2008). In addition to this, measurement of simultaneous endocytosis of multiple vesicles might obscure the timing of their retrieval, as endocytosis might begin before all the vesicles are released, and this will make it impossible to accurately resolve the timing of fluorescence decay at individual boutons. Also, the stimulation used by Armbruster & Ryan, 2011 is largely above the usual physiologically relevant activity of these neurons. We therefore decided to explore this at the level of single vesicle retrieval. In order to do this, we first determined the fluorescence amplitude corresponding to the release of single vesicles, which itself posed some technical challenges.

#### **4.4.3 Establishing quantal size**

Despite the potential advantage of monitoring endocytosis in single vesicles, this readout presents possible challenges of interpretation, arising from the biological variability in

quantal size. As described in detail in the Introduction, the variation in the quantal response size, measured on the postsynaptic site, can result from either pre- or postsynaptic factors.

In particular, the size of synaptic vesicles is one key factor that could affect our measurements of fluorescence level corresponding to single vesicle release. Ultrastructural analysis of thousands of hippocampal SVs revealed that their diameters vary from 20 to 66 nm with an average size being  $35.2 \pm 3.4$  nm (Harris and Sultan, 1995; Schikorski and Stevens, 1997). Nevertheless, it is possible that this variability has arisen due to vesicles from different types of synapses being included in the analysis. Synapses 1b and 1a in *Drosophila* neuromuscular junction were found to have significantly different boutons specific quantal size (Karunanithi et al., 2002). Similar observations were made in excitatory synapses of CA1 region of hippocampus, where the size of SVs ranged from 34.9 to 42.8 nm and in hippocampal culture in which SVs diameter was 32.4-48.8 nm (Hu et al., 2008). This size difference equated to a 5-fold difference in the volume between the smallest and the largest vesicles, indicating a big difference for neurotransmitter storage capacity between these vesicles (Hu et al., 2008). This variability in ultrastructural measurement of vesicle size might be introduced by sampling errors and might also result from sectioning. A portion of a membrane of a given SV might appear on a neighbouring section, giving a false impression of smaller structures (Kim et al., 2000). The error in the ultrastructural evaluation of SVs size in 2D sections was found to be 9% which equates to 3.2 nm (Feuerverger et al., 2000). Nevertheless, to account for this possible variability in SVs size, the measurement of fluorescence corresponding to the release of single quantal events in our study was based on multiple Gaussian distribution of response amplitudes, with the width of the peak representing the variability in the measurements, and being used as a boundary for the quantal size. This resulted in quantal response of  $\Delta F = 124.6 \pm 26\%$  of fluorescence amplitude. This boundary is more than sufficient to cover the quantal size

variability arising due to different vesicle sizes, which was calculated to be 20% based on the data discussed above.

In the case of using sypHy2x, the variability in the quantal size might also result from the different levels of synaptophysin at individual vesicles and the expression level of this construct. Synaptophysin I accounts for 10% of total protein found in SVs, followed by synaptobrevin, with 32 molecules per vesicle (Takamori et al., 2006). This number might not only differ between vesicles in different types of synapses, but it may also vary to a certain extent between vesicles at a given synapse. However, the proteomic analysis of isolated GABAergic and glutamateric docked vesicles revealed a few differences in the protein composition between these terminal types, other than proteins specific for these neurotransmitters (Boyken et al., 2013). Similar results were reported in other studies (Takamori et al., 2000a, 2000b). This was also observed at the level of isolated synaptic vesicles from the two populations of synapses (Takamori et al., 2000b) (Takamori et al., 2000a). This indicates that the variability in quantal size is unlikely to arise due to sampling of synapses of different type. Moreover, most boutons in hippocampal preparations are glutamatergic, which further reduces this possibility. However, many presynaptic proteins have been found to be present in multiple isoforms (Jahn and Südhof, 1994). Synaptophysin II, also referred to as synaptoporin, was found to be co-expressed with synaptophysin I at hippocampal synapses, with varied distribution of the two isoforms between boutons (Singec et al., 2002). Nevertheless, the expression of synaptoporin was mostly localized to GABAergic terminals of hippocampal interneurons, whereas synaptophysin I was present in all synapse types (Singec et al., 2002). Despite all this variability, multiple groups have successfully established the fluorescence amplitude corresponding to single vesicle release events using sypHy (Granseth et al., 2006; Royle et al., 2008; Zhu et al., 2009). Numerous steps were taken in this study in order to ensure the most accurate measurement of quantal size. For the analysis, we used regions which had comparable baseline level fluorescence. The use of AAV based

construct also gave more uniform expression than cDNA construct (observation). It is also very unlikely that our fluorescence measurement for 1q represents higher magnitude of responses and their multiples. This can be concluded from the combination of the fact that we observed failures to release at 2 APs stimulation using iGluSnFR, which has very good signal-to-noise ratio and allows confident visualisation of single vesicle release events (Marvin et al., 2013), and that we also observed failures to respond with syHy2x at 4 APs stimulation level. Even under circumstances that our measurement represents higher order responses, this measurement gives the confidence that the endocytosis following release events of a similar magnitude was examined in our study. Nevertheless, the fact that the peaks in our quantal profile were evenly distributed for failures, single and double quantal events, also suggests that we were not looking at larger responses.

#### **4.4.4 Synapse-specific kinetics of single vesicle endocytosis**

Our results strongly indicate that the kinetics of retrieval of single synaptic vesicles is regulated at the level of individual synapses. We showed this in two types of analysis: point-by-point and rate analysis. In the first one the 'shapes' of profiles, and in the second one the rate of the fluorescence decay, were compared to the population of synapses with randomly picked responses. In both cases we observed that synapses exhibited signature fluorescence profiles of endocytic retrieval. How can this fidelity of single vesicle retrieval be maintained at individual synapses?

Opazo et al., 2010 reported that following 40 APs at 20 Hz stimulation (mobilizing the RRP) synaptic vesicles remained at the cell surface as a 'patch' of molecules following the exocytosis. These membrane associated protein clusters, with very limited lateral diffusion, were also retrieved as a unit to create a new vesicle (Opazo et al., 2010). This could certainly give rise to recycling kinetics of vesicles that were repeated over time at

individual boutons. These authors also observed dispersion of synaptotagmin from the retrieval site following larger stimulation (600 APs at 20 Hz). This can explain why under stronger stimulations, such as 100 APs used by Armbruster et al., 2011, the phenomenon of synapse-specific recycling was not observed. The preservation of the general structure of SVs at the membrane seems like a very energetically favourable solution, and additional proteins could be easily added to this unit. Nevertheless, other groups observed a significant level of mixing of SV proteins with those already present at the cell membrane (Fernández-Alfonso et al., 2006; Wienisch and Klingauf, 2006). These studies, however, used fairly large stimulations, with 120 APs being the lowest, which again, could influence the level of dispersion and intermixing of proteins. The same authors showed a preferential recycling of vesicles from the surface stranded pool, which was depleted with stimulation over 40 APs (Wienisch and Klingauf, 2006). This indicates the presence of a population of preassembled vesicles that are mobilized at the low stimulation level, such as in our study, and could therefore explain later similarities in their behaviour. How is the protein sorting achieved at the membrane? Although the local regulation of proteins in synapses is still not very well understood (Rizzoli, 2014), certain proteins have been implicated in this function. Stonin 2 has been found to control the sorting of SV proteins, by controlling the amount of synaptotagmin 1 at the neuronal surface, and the loss of it was associated with an increased rate of endocytosis (Kononenko et al., 2013). Studies on *Drosophila* neuromuscular junctions showed that the presynaptic protein levels are locally controlled by ubiquitin proteasome system (UPS) and this in turn had an effect on the strength of neurotransmission (Speese et al., 2003). The interaction of various proteins and regulation of endocytic kinetics will be explored in more depth in the Discussion in Chapter 5. The other possibility of how vesicles retain their molecular identity is via kiss-and-run endocytosis. However, the timing of vesicle retrieval observed in our study does not suggest that this process, which is within ms, was a predominant mode of recycling in our system (Alabi and Tsien, 2013).

One limitation of this study which deserves consideration, is the possibility that these various profiles are due to the diffusion of the GFP-tagged proteins away from the release site. It has been observed that the lateral movement of pHluorin tagged proteins was even more pronounced than that of native, untagged proteins (Opazo et al., 2010). Nevertheless, if this is a major factor giving rise to the variability of some profiles, it is surprising that these events are also consistent at a given synapse, indicating that specific protein sorting mechanisms operate at a given bouton. Not only do the kinetics of vesicle retrieval appears to be synapse-specific; Waters & Smith, 2002, in their study of the synaptic properties that influence the kinetics of vesicles release in hippocampal neurons, showed that although the destaining rates at 1 Hz were highly variable across synapses, measurements from individual boutons revealed reproducible FM1-43 fluorescence decay over repeated trials, and characteristic for a given synapse profile. As FM1-43 measurement is independent of any protein, and is known to have no toxic effects on synaptic properties, this strengthens the finding made in this study that synapse-specific mechanisms operate at individual boutons giving rise to their signature behaviour.

Future experiments, expanding the issues raised in the discussion, could involve comparing retrieval profiles at individual synapses following 2 or 3 vesicle release events and after larger stimulation paradigms (40 or 100 APs at 20 Hz) within the same set of synapses. Another interesting experiment would be to compare the similarity of behaviour of synapses, which are situated on the same axon, and of those synapses with a common dendritic target. Branco et al., 2008, demonstrated that synapses from the same axon, which shared a dendritic branch, were characterized by highly correlated  $p_r$ . Perhaps the kinetics of endocytic retrieval, in a similar fashion, is set and regulated locally in order to adapt to the demand of the network, and is highly coordinated with the postsynaptic neuron (Liu and Tsien, 1995). In the next chapter, we explore synaptic properties that may underlie the signature endocytic behaviour of individual synapses.

# 5 THE INVESTIGATION OF SYNAPTIC CHARACTERISTICS THAT UNDERLIE THEIR ENDOCYTIC BEHAVIOUR

---

## HIGHLIGHTS

- SypHy2x baseline fluorescence can be used as a measure of synaptic size
- Larger synapses exhibit faster rates of endocytosis
- The size of the total vesicle pool rather than the recycling fraction determines the kinetics of endocytosis
- Larger synapses exhibit higher variability in the timing of endocytosis
- Larger synapses have higher level of endophilin I
- Treatment with dynasore leads to homogenization of the timing of endocytosis across synapses
- Larger synapses have lower density of synaptic vesicles than the small ones

## 5.1 Introduction

In the previous chapter, it was demonstrated that properties of single vesicle response profiles were preserved across multiple trials at single synapses (sections 4.3.5.1 and 4.3.5.2). In other words, presynaptic terminals appear to be predisposed to have a particular endocytic timing, which is repeatedly expressed in the fluorescent decay profiles of retrieved vesicles after they undergo fusion. Our next goal was to determine what synaptic properties might underlie this behaviour. There are a number of possible candidate parameters which could contribute to this. This chapter explores these parameters first in further functional experiments, and then in ultrastructural correlates of synaptic function.

We hypothesized that one of the factors that might affect the endocytic kinetics is synaptic size. The basis for this is the fact that measures of synaptic ultrastructure, such as vesicle pool sizes or total vesicle numbers, have already been shown to vary between synapses, and are recognized factors influencing the efficacy of synaptic performance and processing of the information within neural networks (Branco and Staras, 2009; Welzel et al., 2011). In order to test the robustness of our results, we chronically silenced synapses, and examined whether the properties that we previously described scaled with their size. We also further examined properties of large synapses, including the expression of the important endocytic kinetics modulator – endophilin I. The question raised in Chapter 4 as to whether the variability in the kinetics between synapses reported by syHy2x is due to the difference in the kinetics of endocytic retrieval or reacidification, is also addressed here. In order to do that we used a blocker of dynamin function – dynasore.

The second half of this chapter is dedicated to ultrastructural exploration of synaptic properties that explain their behaviour. Despite the fact that functional studies provide us



with a powerful approach to monitor synapses in their native state, various properties cannot be reliably measured due to the small size of presynaptic terminals and their components. Here we addressed this limitation by carrying out ultrastructural investigation of parameters that might correlate with functional properties of individual presynaptic boutons.

## 5.2 Properties of small and large synapses

### 5.2.1 Larger synapses exhibit faster rate of endocytosis

We set out to test whether synaptic size contributes to the regulation of vesicle recycling kinetics of individual synapses as outlined in the previous chapter. We reasoned that the baseline fluorescence of sypHy2x might provide a correlate of synaptic size that we could use for the purpose of this study. In order to test this, alongside our sypHy readout, we used an independent measure of pool size based on an acutely-applied probe, sytl-Oyster550. This fluorescently tagged antibody and its principles of action are described in detail in section 3.2.4. Specifically, we loaded AAV.*sypHy2x*-expressing cells with sytl-Oyster550 in an activity-dependent manner using a saturating loading stimulus (600 APs 20 Hz) that recruits all available recycling vesicles. After labelling and washing, cultures were imaged in two colours to allow us to visualize both sypHy2x signal (green-emitting) and Oyster signal (red-emitting). From the analysis of fluorescence profile across individual boutons we found that the signals from the two probes showed good co-localization (Fig.5.1.A and B). Moreover, we found that there was a strong positive correlation between AAV.*sypHy2x* baseline and sytl-Oyster550 fluorescence size (Pearson's correlation test,  $n = 180$  synapses from 5 regions,  $r = 0.760$ ,  $P < 0.0001$ ) (Fig.5.1.C). Taken together, this provides strong justification for the use of sypHy2x baseline fluorescence as a convenient measure of synaptic size. In later sections of

Chapter 5 we also present two more methods confirming the reliability of this readout (sections 5.2.2.2 and 5.4.6).

Having confirmed a sypHy2x-based size measurement, we could now use this to investigate whether synaptic size was correlated with the recycling kinetics at individual boutons. Using our Matlab script, we selected synapses with at least 2 single vesicle responses within the defined 1q size ( $\Delta F = 92.2\text{-}157$  a.u.) for the analysis. The sypHy2x baseline fluorescence (frames 1-39, stim frame 40) from the first analysed trial was used as a measure of synaptic size. When we plotted this size measure against the rate of endocytosis, we observed a strong correlation (Pearson's correlation test,  $n = 150$  synapses from 9 experiments,  $r = -0.653$ ,  $P < 0.0001$ ) (Fig.5.1.D), suggesting that there was a clear relationship between these variables. Specifically, we found that larger synapses were characterized by faster rates of endocytic retrieval, and smaller ones, by slower rates (Fig.5.1.D and E).

From this analysis we identified an inherent characteristic of synapses, namely, that synaptic size contributes to their single vesicle behaviour. As yet, it is not clear whether these variables are correlated, perhaps through another parameter that determines both, or causal, where synaptic size dictates the timing of recycling. In order to test these alternative possibilities, we next carried out experiments to modulate the parameters associated with synaptic size. In the later sections of this chapter we consider other possibilities for how size could influence the endocytic kinetics, and examine other synaptic parameters, molecular and structural, explaining their behaviour.

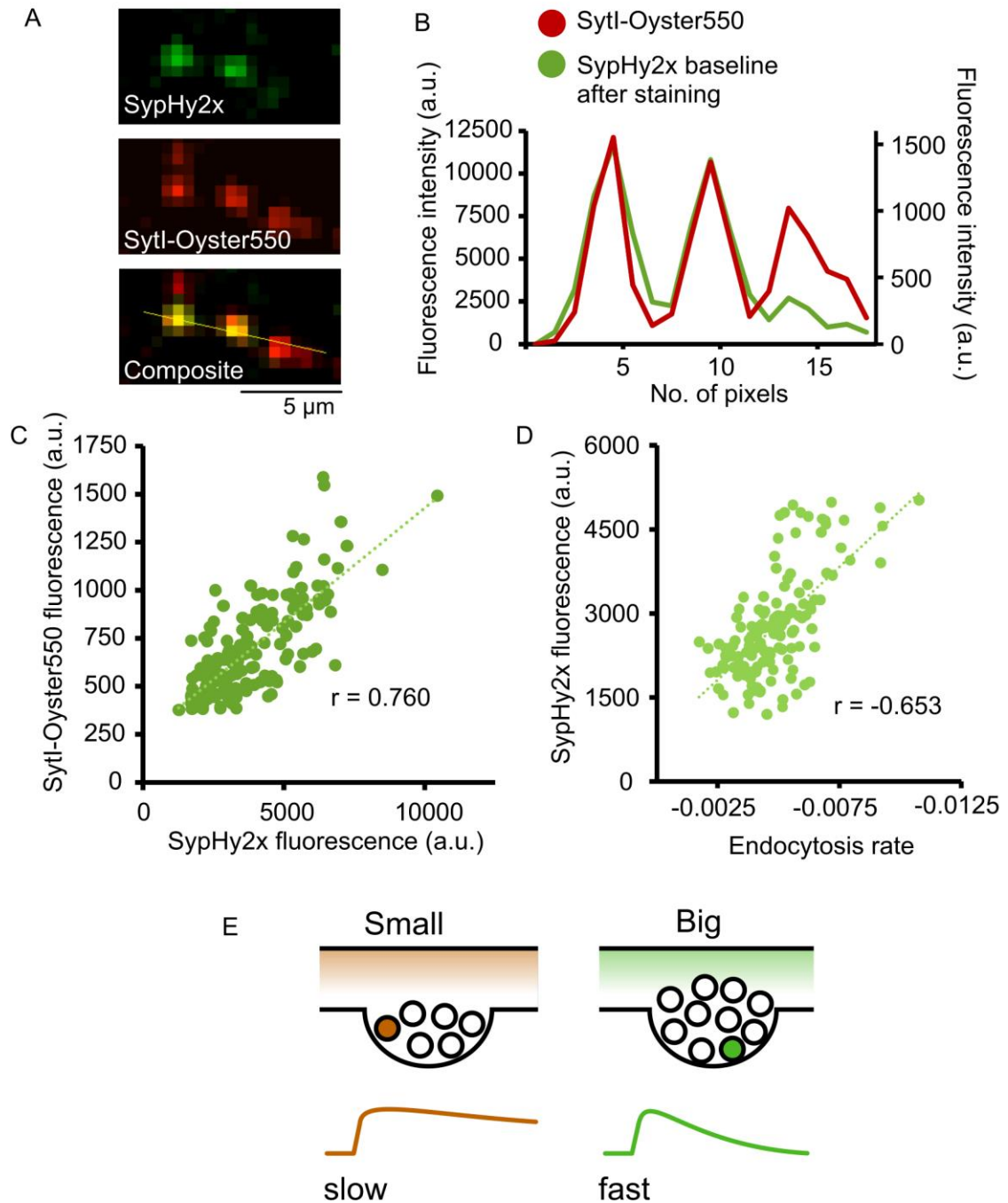


**Figure 5.1 SypHy2x baseline fluorescence reflects the size of the synapse.** A) Baseline fluorescence of sypHy2x expressing synapses (top). Synapses were loaded with sytl-Oyster550 antibody using 600 APs, 20 Hz stimulation (middle). Merged image of sypHy2x and sytl-Oyster550 fluorescence (bottom). The profile shown in B) was measured along the yellow line. Scale bar 5  $\mu$ m. B) Fluorescence intensity profiles of sypHy2x and sytl-Oyster550 fluorescence. C) Correlation between sypHy2x baseline fluorescence and sytl-Oyster550 fluorescence (Pearson's correlation test,  $n = 180$  synapses from 5 regions,  $r = 0.760$ ,  $P < 0.0001$ ). D) Strong correlation between the baseline SypHy2x fluorescence and the rate of endocytosis of single synaptic vesicle (Pearson's correlation test,  $n = 150$  synapses from 9 experiments,  $r = -0.653$ ,  $P < 0.0001$ ). E) Schematic summarizing the results: smaller synapses exhibit slower rate of endocytosis than larger synapses.

## **5.2.2 Homeostatic scaling as a form of modulation of synaptic properties**

To this point, we have identified that individual synapses have conserved endocytic timing and that larger synapses exhibit faster rates of endocytosis. In this section of Chapter 5 we investigate the robustness of this result by attempting to modulate synaptic properties and exploring their effect on synaptic function.

Disuse hypersensitivity is a form of homeostatic plasticity in central synapses which employs pharmacological block of excitatory synaptic transmission for several days, and which leads to the increase in synaptic strength of presynaptic terminals (Murthy et al., 2001). In previous work, this type of modulation, based on the use of an AMPA blocker (10  $\mu$ M NBQX, 2 days incubation) was associated with presynaptic changes in cultured hippocampal neurons in the form of increased  $p_r$  and synaptic size, and changes to other structural properties: boutons volume, total number of vesicles, number of docked vesicles, size of the active zone (Murthy et al., 2001). An increase in the size of the recycling pool was linked to the modulation in protein expression as a result of silencing with 1  $\mu$ M TTX for 72 h (Kim and Ryan, 2010). Welzel et al., 2011, also showed that a 10.5% increase in the recycling pool size in hippocampal neurons following 3 days incubation with 0.5  $\mu$ M TTX led to significant increase in the timing of exocytosis.

We decided to employ this approach in our study to test the hypothesis that the rate of endocytosis is coupled with synaptic size, and that by increasing synaptic size, we should increase the rate of endocytosis if the two variable are linked. This would be a direct test of correlation versus causality of the two key variables.

### **5.2.2.1 Measuring synaptic vesicle pool sizes**

Prior to homeostatic scaling experiments, the first step was to establish a method for measuring the size of the recycling and total vesicle pools in our cultures following

functional readouts with sypHy2x. As previously, AAV.sypHy2x-expressing cells were stimulated 10x with 4 APs (40 s apart) and after a 2 min recovery period, 40 APs 20 Hz stimulation was applied, allowing the measurement of the size of the RRP. Following another 2 min recovery period, 1  $\mu$ M bafilomycin A1 (baf) was added to the culture. Bafilomycin is a cell-permeable, potent inhibitor of v-ATPase and it acts by blocking the reacidification of newly endocytosed vesicles (Fernandez-Alfonso and Ryan, 2008), providing a readout of the amount of fluorescence signal originating from exocytosis without contamination from the endocytic phase that follows. Previous work has shown that bafilomycin does not have any effect on synaptic vesicle exocytosis or endocytosis over the timescales relevant to our work here (Sankaranarayanan and Ryan, 2001) and therefore stimulation in the presence of this drug allowed us to lock the recycling pool of vesicles in an alkaline state, and to fully evaluate its size by measuring the corresponding fluorescence. We imaged baseline baf fluorescence for 30 s following which we stimulated the cells with 600 APs 20 Hz stimulation to mobilize the recycling pool (Fig.5.2.A and B). In order to avoid the possibility of bleaching the signal, instead of imaging the sample during the stimulation, we imaged immediately after the end of the stimulation for 30 s. The timing of the experiment (imaging and washing stages) from baf application onwards was very important because of a very slow, gradual increase in baseline fluorescence resulting from baf application over longer time periods due to spontaneous alkalization (Atluri and Ryan, 2006; Sankaranarayanan and Ryan, 2001). Hence, if the timing of individual experiments was not controlled properly, the results could have been influenced by this effect of baf. Following stimulation and imaging in the presence of baf, the sample was incubated in  $\text{NH}_4\text{Cl}$ -containing bath solution. The presence of  $\text{NH}_4\text{Cl}$  neutralizes the pH of all the remaining synaptic vesicles within the terminals, providing a measure of the size of the total vesicle pool (Miesenböck et al., 1998). Following 30 s of incubation in the presence of  $\text{NH}_4\text{Cl}$ , fluorescence intensity corresponding to the total vesicle pool size was imaged for 30 s (Fig.5.2.A and B). The protocol for this experiment is summarized in Figure 5.2.A and the representative images

of synapses imaged using this protocol are shown in Figure 5.2.B. This optical method of measuring synaptic vesicle pool sizes has been widely employed in studies aiming to assess the size of the recycling fraction (Fernandez-Alfonso and Ryan, 2008; Ikeda and Bekkers, 2009) to verify the origin of fluorescence signals (Balaji and Ryan, 2007), to measure the kinetics of synaptic vesicle reacidification (Atluri and Ryan, 2006; Budzinski et al., 2011) and to confirm the expression of a newly-developed construct within synaptic vesicles (Hua et al., 2011).

This protocol allowed us to explore the relationships between different pool sizes. The fluorescence measurement spanned 2.5 s of stable fluorescence signal from imaging at each stage of the protocol: baseline, 600 APs, 20 Hz + baf (recycling pool) and  $\text{NH}_4\text{Cl}$  (total pool) was averaged for each synapse in order to obtain a readout of the pool sizes for a given synapse. The size of the RRP was calculated based on the fluorescence amplitude between the peak of the stimulation and the baseline fluorescence from 40 APs, 20 Hz stimulation. The analysis of the data showed that there was a strong correlation between the size of the recycling and total pool (Pearson's correlation test,  $n = 174$  synapses from 7 experiments,  $r = 0.756$ ,  $P < 0.0001$ ) (Fig.5.2.C). The size of the RRP was also strongly correlated with the recycling pool (Pearson's correlation test,  $n = 174$  synapses from 7 experiments,  $r = 0.736$ ,  $P < 0.0001$ ) and the total pool size (Pearson's correlation test,  $n = 174$  synapses from 7 experiments,  $r = 0.651$ ,  $P < 0.0001$ ) (Fig.5.2.D). We also explored the size of the recycling fraction using readouts for recycling and total vesicle pool size. Our data showed a high variability in the size of the recycling pool fraction between synapses with a mean value of 0.48, SD: 0.24, a very comparable value to that reported previously from research in our lab (0.49, SD: 0.16) (Ratnayaka et al., 2012) and other studies (Fernandez-Alfonso and Ryan, 2008; Kim and Ryan, 2010).

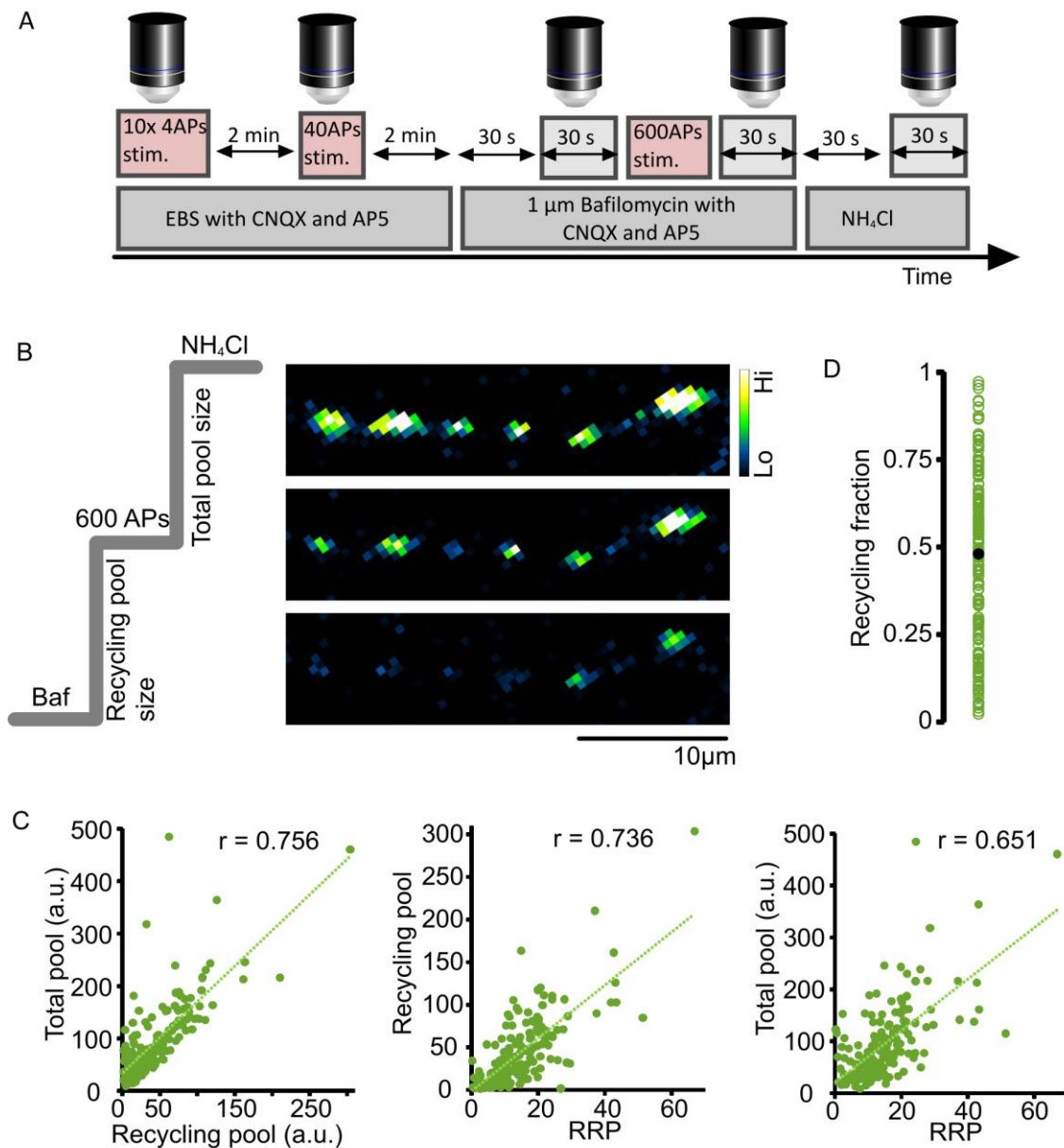


**Figure 5.2 Measuring the size of RRP, recycling and total vesicle pools.** A) Timeline illustrating the protocol followed for measuring the size of the vesicle pools. Top row shows the stimulation, timing and imaging and the bottom row shows the solutions used. B) Schematic showing the experimental steps allowing to quantify the sizes of vesicle pools and recycling fraction. Images represent fluorescence intensity at the corresponding stages of the experiment. C) The relationships between different vesicle pools. Baseline level of fluorescence for each synapse was subtracted from the readouts for total pool and recycling pool. The size of the RRP was calculated from the amplitude of the response of synapses to 40 APs stimulation. ( $n = 174$  synapses from 7 experiments, Pearson's correlation test: total pool vs RP,  $r = 0.756$ ,  $P < 0.0001$ ; RP vs RRP,  $r = 0.736$ ,  $P < 0.0001$ ; total pool vs RRP,  $r = 0.651$ ,  $P < 0.0001$ ). D) Measurement of the recycling fraction revealed high variability in this parameter between synapses. Mean recycling fraction ( $0.48 \pm 0.018$ ) is indicated by the black circle ( $n = 174$  synapses from 7 experiments).

### 5.2.2.2 Correlation between presynaptic size and the rate of endocytosis

Having established a method for measuring the size of synaptic vesicle pools, we wanted to explore the relationship between the recycling and total pool sizes in order to determine the correlation of endocytosis at individual boutons. From our sypHy2x and sytl-Oyster550 analysis, we established that sypHy2x baseline fluorescence correlates with the synaptic size and that larger synapses exhibit faster endocytic kinetics (section 5.2.1). The results from this experiment allowed us to explore this further, make new findings and to validate previous results using a different method.

The kinetics of endocytosis were measured with linear fit in synapses that underwent at least 2 single vesicle release events in response to 9 rounds of 4 APs stimulation and only these synapses were chosen for the analysis of vesicle pool sizes. The readouts of recycling and total pool were carried out according to the protocol described in the section above. First, we confirmed that the rate of endocytosis is correlated with sypHy2x baseline fluorescence in this new set of experiments (Pearson's correlation test,  $n = 116$  synapses from 6 experiments,  $r = -0.698$ ,  $P < 0.0001$ ) (Fig.5.3.A). The relationship between the size of presynaptic terminals and the kinetics of endocytosis was maintained as previously described: larger synapses exhibit a faster rate of endocytosis than small ones. In addition, we tested whether sypHy2x baseline reflects the size of the synapses by testing the relationship of this measure to the size of the total vesicle pool measured using  $\text{NH}_4\text{Cl}$ . We found a very strong correlation between the measure of total vesicle pool and sypHy2x baseline fluorescence (Pearson's correlation test,  $n = 116$  synapses from 6 experiments,  $r = 0.796$ ,  $P < 0.0001$ ) (Fig.5.3.B). This strongly confirms the rationale for using sypHy2x baseline fluorescence as a measure of synaptic size. Following this logic, the size of the total pool should correlate with the rate of endocytosis in the same manner as sypHy2x baseline fluorescence. We saw a strong positive correlation between the total vesicle pool size and the rate of endocytosis (Pearson's



correlation test,  $n = 116$  synapses from 6 experiments,  $r = -0.694$ ,  $P < 0.0001$ ) (Fig.5.3.C).

So far, we found that the kinetics of endocytosis correlated very well with the total vesicle pool size that represents the total size of the synapse, supporting the finding that the kinetics of endocytosis is influenced by the overall size of the synapse. Next, we asked whether the endocytic retrieval is dependent on the size of the recycling vesicle pool size. To reiterate the result showed in Fig.5.2.C, there was a strong correlation between the size of the total and recycling pool in this new data set (Pearson's correlation test,  $n = 116$  from 6 experiments,  $r = 0.728$ ,  $P < 0.0001$ ) (Fig.5.3.D) and hence one would expect a good relationship between the recycling pool and the endocytic rate. However, despite this relationship, there was a less robust correlation between the recycling vesicle pool size and the rate of endocytosis (Pearson's correlation test,  $n = 116$  synapses, 6 experiments,  $r = -0.398$ ,  $P < 0.0001$ ) (Fig.5.3.E). We explored the possible reason for this and found that the correlation between the recycling pool fraction, which is influenced by both the size of the recycling and total pool, and the total pool size exhibited only a moderate level of correlation (Pearson's correlation test,  $n = 116$  synapses, 6 experiments,  $r = -0.343$ ,  $P = 0.0002$ ) (Fig.5.3.F). This large variability in the relationship between these two pools gives an explanation for the limited relationship between the recycling pool and endocytic kinetics.

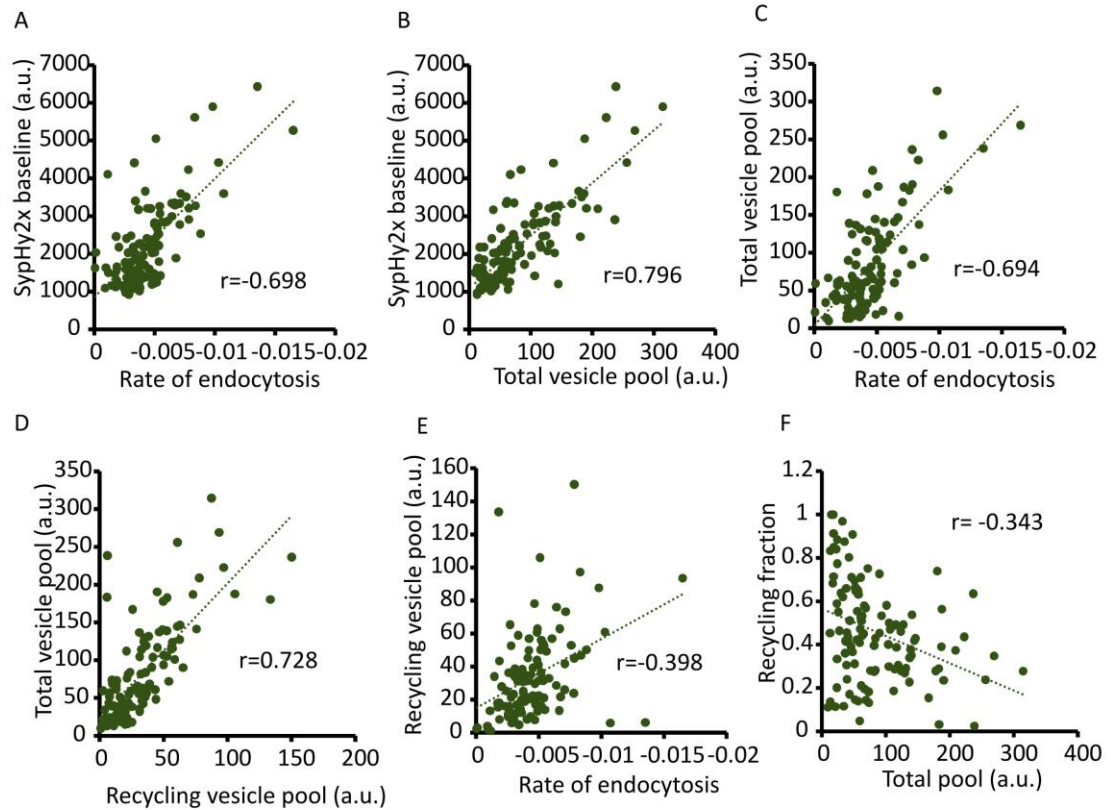


**Figure 5.3 Relationship between the synaptic size and the rate of endocytosis.** A) SypHy2x fluorescence shows strong negative correlation with the rate of endocytosis (Pearson's correlation test,  $n = 116$  synapses from 6 experiments,  $r = -0.698$ ,  $P < 0.0001$ ). B) The size of synapses expressed as the size of total vesicle pool shows strong positive correlation with the baseline sypHy2x fluorescence (Pearson's correlation test,  $n = 116$  synapses from 6 experiments,  $r = 0.796$ ,  $P < 0.0001$ ). C) Rate of endocytosis shows strong negative correlation with the total vesicle pool size (Pearson's correlation test,  $n = 116$  synapses from 6 experiments,  $r = -0.694$ ,  $P < 0.0001$ ). D) Relationship between the recycling and total vesicle pool size (Pearson's correlation test,  $n = 116$  from 6 experiments,  $r = 0.728$ ,  $P < 0.0001$ ). E) The size of the recycling pool only moderately correlates with the rate of endocytosis (Pearson's correlation test,  $n = 116$  synapses, 6 experiments,  $r = -0.398$ ,  $P < 0.0001$ ). F) There is a weak correlation between the recycling fraction and the total pool size at individual synapses (Pearson's correlation test,  $n = 116$  synapses, 6 experiments,  $r = -0.343$ ,  $P = 0.0002$ ).

### 5.2.2.3 Modulation of synaptic size and its effect on endocytic rate

Building on the data shown so far on the relationship between synaptic size and endocytic rate, this and the following section further examines the robustness of this relationship. To address the causal relationship between rate and size, we

pharmacologically silenced synapses by treating the cell culture for 3 days with 20  $\mu$ M CNQX. CNQX is an AMPA antagonist, which blocks the synaptic transmission and leads to synaptic changes associated with their disuse, such as an increase in active zone size, bouton size, number of docked vesicles or total vesicle number in the presynaptic terminals (Murthy et al., 2001). We therefore decided to employ this method to examine the causal nature of the relationship between endocytic rate and synaptic size. The hypothesis under test was that the rate of endocytic retrieval will increase along with the increase in synaptic size as a result of homeostatic plasticity.

In all synapses measured in the experiment, we saw an increase in the total pool size between the CNQX<sub>All</sub> treated group and the Control<sub>All</sub> ( $n = 435$  and  $424$  synapses for Control<sub>All</sub> and CNQX<sub>All</sub>, respectively. Two-tailed unpaired Student's t-test,  $P = 0.012$ ), and no difference in the size of the recycling pool in these two groups ( $n = 435$  and  $424$  synapses for Control<sub>All</sub> and CNQX<sub>All</sub>, respectively. Two-tailed unpaired Student's t-test,  $P = 0.14$ ) (Fig.5.4. A and B). In these measurements, we also saw that the size of the recycling fraction was smaller in CNQX<sub>All</sub> than in the Control<sub>All</sub> group ( $n = 435$  and  $424$  synapses for Control<sub>All</sub> and CNQX<sub>All</sub>, respectively. Two-tailed unpaired Student's t-test,  $P = 0.007$ ) (Fig.5.4.B and C). This result is conflicting with the effect of similar treatment reported by Kim and Ryan, 2010. In their study they saw an increase in the recycling fraction resulting from silencing (Kim and Ryan, 2010). Nevertheless, in their published results all the values were normalized to the total pool size and they didn't report whether they observed any difference in this parameter between the two treatment groups. In contrast, a parallel increase in all synaptic parameters whilst retaining the relationship between them was observed by other group (Murthy et al., 2001). We therefore reasoned that this apparently smaller size of recycling pool fraction in CNQX<sub>All</sub> group might be a result of a larger total pool size seen in the CNQX<sub>All</sub> group in our experiment. If that was the case, any possible modulation of the fraction size by CNQX becomes diluted by the increase in the total pool size. We therefore decided to explore our data in more detail.

Firstly, for the purpose of further analysis we only selected synapses that responded with at least two single vesicle release events over 9x 4 APs stimulation trials, in order to have a population with a measure of endocytic kinetics (For the legend of data processing refer to the Appendix I, Figure 3). We observed that within this population, there was no statistical difference in the sypHy2x baseline fluorescence ( $n = 157$  and  $132$  synapses for Control and CNQX, respectively. Two-tailed unpaired Student's t-test,  $P = 0.604$ ) (Fig.5.4.D) or endocytic rate between Control and CNQX ( $n = 157$  and  $132$  synapses for Control and CNQX, respectively. Two-tailed unpaired Student's t-test,  $P = 0.384$ ) (Fig.5.4.E). However, the size of the recycling pool fraction in CNQX, although not substantially, was larger in the CNQX population than in the Control ( $n = 157$  and  $132$  synapses for Control and CNQX, respectively. Two-tailed unpaired Student's t-test,  $P = 0.033$ ) (Fig.5.4.F). This shows that synapses of comparable size were characterized by a bigger recycling pool fraction in the CNQX treated group than the Control group, which confirms that our homeostatic adjustment protocol induced changes in the presynaptic characteristics is comparable with those previously reported in literature (Kim and Ryan, 2010). This also gives an indication that the endocytic rate is not dependent on the recycling fraction. Now that we established that our plasticity protocol had a desired effect, we wanted to address the main question that is the identification of synaptic properties that determined the kinetics of endocytosis.

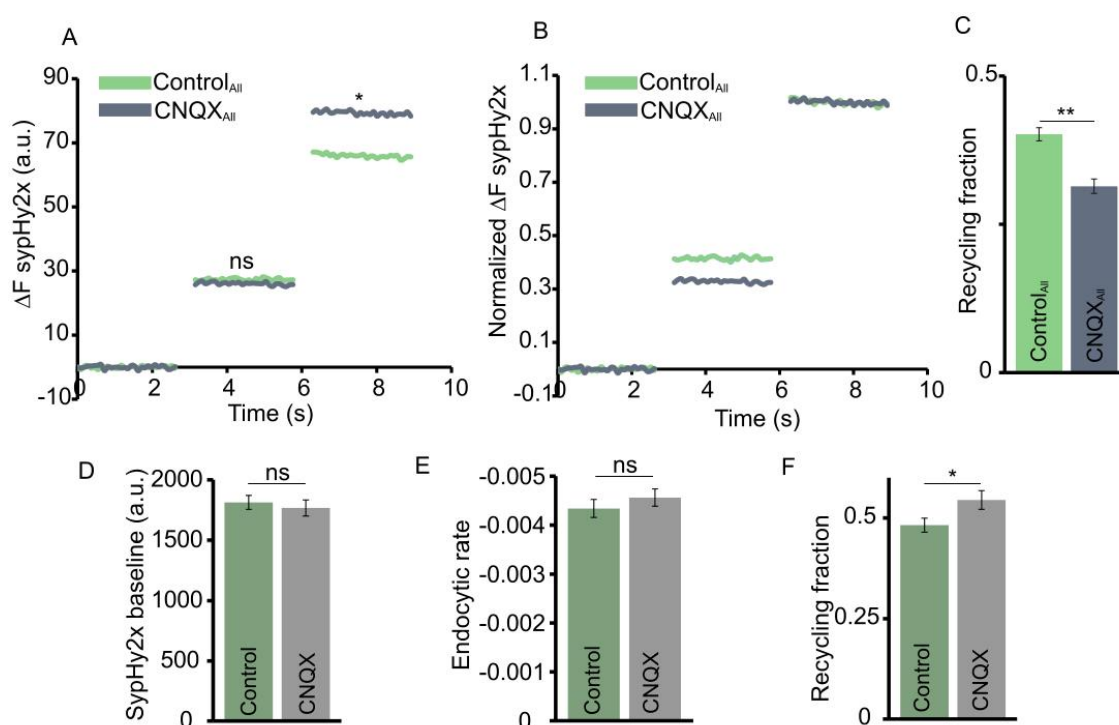


**Figure 5.4 Modulation of synaptic properties with CNQX.** A) Quantification of the size of the recycling pool and total pool according to the protocol showed in Figure 5.2 for Control and 3 days 20  $\mu$ M CNQX treated cells ( $n = 435$  and  $424$  synapses from 8 and 7 experiments for Control<sub>All</sub> and CNQX<sub>All</sub>, respectively. Two-tailed unpaired Student's t-test: recycling vesicle pool,  $P = 0.14$ ; total vesicle pool,  $P = 0.012$ ). B) Measurements of the pool sizes normalized to the total vesicle pool size for each group. C) Quantification of the recycling fraction for both treatment groups ( $n = 435$  and  $424$  synapses for Control<sub>All</sub> and CNQX<sub>All</sub>, respectively  $\pm$  SEM. Two-tailed unpaired Student's t-test,  $P = 0.007$ ). D) Comparison of sypHy2x baseline level fluorescence of synapses that responded at least twice in 9 rounds of 4 APs stimulation ( $n = 157$  and  $132$  synapses for Control and CNQX, respectively  $\pm$  SEM. Two-tailed unpaired Student's t-test,  $P = 0.604$ ). E) Summary of the rate of endocytosis of synapses in Control and CNQX groups ( $n = 157$  and  $132$  synapses for Control and CNQX, respectively  $\pm$  SEM. Two-tailed unpaired Student's t-test,  $P = 0.384$ ). F) Graph showing comparison of the recycling fraction in the two treatment groups ( $n = 157$  and  $132$  synapses for Control and CNQX, respectively. Two-tailed unpaired Student's t-test,  $P = 0.033$ ).

#### 5.2.2.4 Comparison of synapses from the same population

Before examining the relationship between endocytic kinetics and pool sizes in the two groups: control and CNQX treated, we firstly looked at our data in a different way and asked whether we can isolate two populations within control synapses and examine the

characteristics of these synapses. We examined Control data alone by splitting it into two distinct populations. We calculated median for the sypHy2x baseline fluorescence and applied that value across the data in order to obtain two populations of small and large synapses ( $n = 79$  and  $n = 78$  synapses for Control<sub>small</sub> and Control<sub>large</sub>, respectively. Kolmogorov-Smirnov test,  $P < 0.0001$ ) (Fig.5.5.A). As expected, the measurement of the size of the total pool confirmed that we isolated small and large population of synapses within the control group ( $n = 79$  and  $n = 78$  synapses for Control<sub>small</sub> and Control<sub>large</sub>, respectively. Kolmogorov-Smirnov test,  $P < 0.0001$ ) (Fig.5.5.B). Further analysis of the results showed that the small population of synapses on average was characterized by a slower rate of endocytosis than the large ones, which were 36% faster ( $n = 79$  and  $n = 78$  synapses for Control<sub>small</sub> and Control<sub>large</sub>, respectively. Two-tailed unpaired Student t-test,  $P < 0.0001$ ) (Fig.5.5.C). We also noted that small synapses were characterized by a significantly larger recycling pool fraction than the large synapses ( $n = 79$  and  $n = 78$  synapses for Control<sub>small</sub> and Control<sub>large</sub>, respectively. Two-tailed unpaired Student t-test,  $P < 0.0001$ ) (Fig.5.5.D). These results clearly show a big difference in the recycling pool fraction size within the population of synapses of different size. From this, it is again evident that the rate is highly dependent on either total vesicle pool size or the recycling fraction.

In order to further explore the relationship in the principle properties of synapses, the recycling pool fraction size and synapse size, we separated Control data based on the average size of the recycling pool fraction (those synapses over and under recycling fraction 0.482). We ended up with two populations, one of large synapses with smaller recycling fraction (Control<sub>smallFr</sub>) and another one of small synapses with a large recycling fraction (Control<sub>largeFr</sub>) ( $n = 74$  and  $83$  for Control<sub>largeFr</sub> and Control<sub>smallFr</sub>, respectively. Kolmogorov-Smirnov test: synaptic size (sypHy2x baseline fluorescence),  $P < 0.0001$ ; recycling fraction:  $P < 0.0001$ ) (Fig.5.5.E). This data shows as important relationship between synaptic size and the size of the recycling fraction.

Finally, having previously established that the endocytic kinetics either depends on the size of the total pool or the recycling fraction, we set ourselves a challenge to resolve this matter in Control and CNQX data. In light of the results above, we had to establish populations of synapses in the two groups with comparable synaptic size. Firstly, we applied the average recycling fraction from the Control group to the CNQX data in order to reveal the synapses which underwent the scaling in this parameter. We noticed, however, that the syHy2x fluorescence baseline of the Control<sub>largeFr</sub> was still larger than in the CNQX<sub>largeFr</sub> data, suggesting that the size of the synapses in the two groups was not equal ( $n = 74$  and  $70$  for Control<sub>largeFr</sub> and CNQX<sub>largeFr</sub>, respectively. Two-tailed unpaired Student's t-test,  $P = 0.007$ ). We therefore adjusted syHy2x fluorescence baseline of the Control<sub>largeFr</sub> population with a recycling pool fraction size over  $0.482$  to the baseline fluorescence level of CNQX<sub>largeFr</sub> set. We finally arrived with the population of Control synapses which were the best comparison for the CNQX<sub>largeFr</sub> data for the relationship between recycling fraction and endocytic kinetics as there was no difference in syHy2x baseline fluorescence ( $n = 57$  and  $70$  synapses for Control<sub>largeFrAdj</sub> and CNQX<sub>largeFr</sub>, respectively. Two-tailed unpaired Student's t-test,  $P = 0.967$ ), the size of the recycling ( $n = 57$  and  $70$  synapses for Control<sub>largeFrAdj</sub> and CNQX<sub>largeFr</sub>, respectively. Two-tailed unpaired Student's t-test,  $P = 0.312$ ), and total pool size ( $n = 57$  and  $70$  synapses for Control<sub>largeFrAdj</sub> and CNQX<sub>largeFr</sub>, respectively. Two-tailed unpaired Student's t-test,  $P = 0.922$ ) between the two treatment groups. Despite the significant difference between the size of the recycling fraction pool ( $n = 57$  and  $70$  synapses for Control<sub>largeFrAdj</sub> and CNQX<sub>largeFr</sub>, respectively. Two-tailed unpaired Student's t-test,  $P = 0.038$ ) (Fig.5.5.F), there was no difference in the kinetics of single vesicle endocytosis between the two groups ( $n = 57$  and  $70$  synapses for Control<sub>largeFrAdj</sub> and CNQX<sub>largeFr</sub>, respectively. Two-tailed unpaired Student's t-test,  $P=0.163$ ) (Fig.5.5.G). This suggests that the size of the recycling fraction does not influence the endocytic kinetics.

Taken together, the results indicated that: i) the size of total vesicle pool and the recycling fraction were significantly increased by CNQX treatment; ii) the kinetics of single vesicle endocytosis is not dependent on the size of the recycling fraction but on the size of the total vesicle pool; iii) smaller synapses have a larger recycling fraction than the big synapses; iv) small synapses in CNQX treated group have an even larger recycling fraction when compared to Control synapses of the same size. This unequivocally strengthens the finding that it is not the recycling pool fraction but the total vesicle pool size (and ultimately the size of the synapse) that determines the endocytic kinetics of single synaptic vesicles.

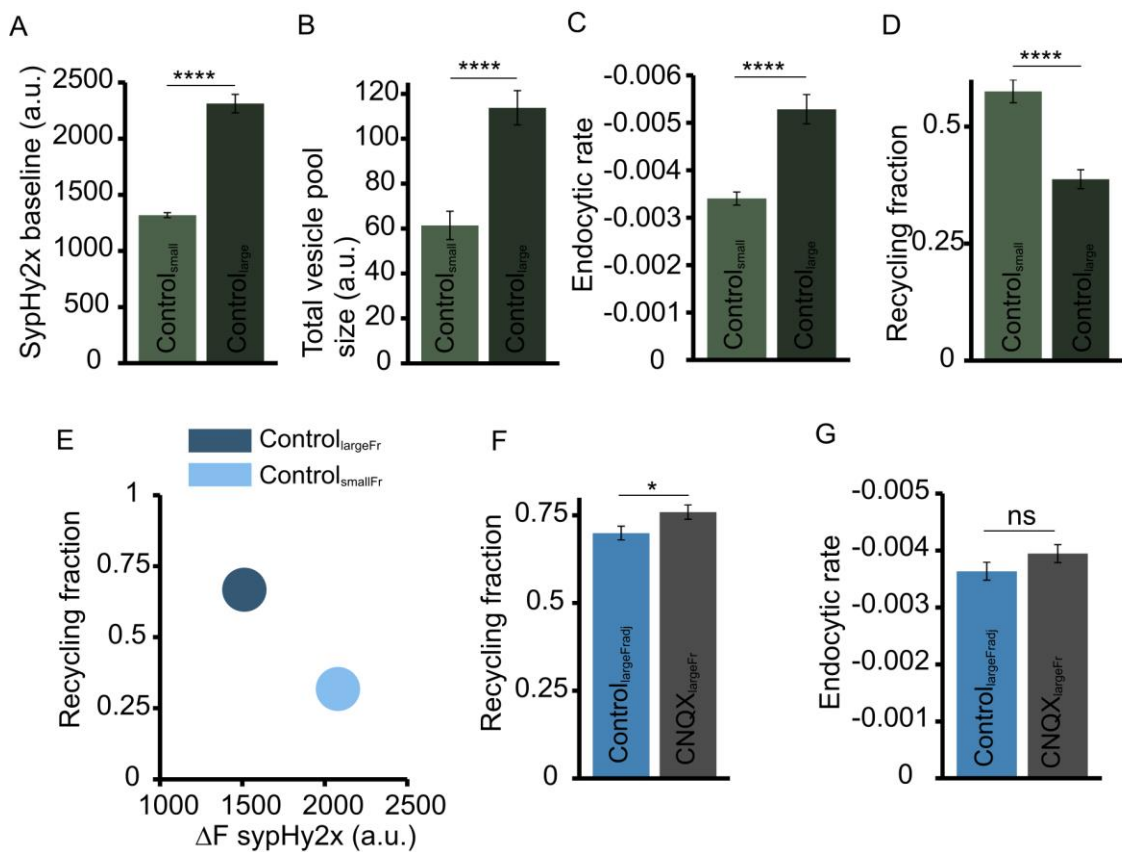


**Figure 5.5 Comparison of endocytic kinetics in limited population of synapses.** A) Comparison of the synaptic size measured on the basis of sypHy2x baseline fluorescence for Control<sub>small</sub> and Control<sub>large</sub> groups (n = 79 and n = 78 synapses for Control<sub>small</sub> and Control<sub>large</sub>, respectively. Two-tailed unpaired Student's t-test,  $P < 0.0001$ ). B) Graph showing total recycling pool size for Control<sub>small</sub> and Control<sub>large</sub> (n = 79 and n = 78 synapses for Control<sub>small</sub> and Control<sub>large</sub>, respectively. Two-tailed unpaired Student's t-test,  $P < 0.0001$ ). C) Summary of the comparison of the endocytic rate in Control<sub>small</sub> and Control<sub>large</sub> (n = 79 and n = 78 synapses for Control<sub>small</sub> and Control<sub>large</sub>, respectively. Two-tailed unpaired Student t-test,  $P < 0.0001$ ). D) Comparison of the



recycling pool fraction ( $n = 79$  and  $n = 78$  synapses for  $\text{Control}_{\text{small}}$  and  $\text{Control}_{\text{large}}$ , respectively. Two-tailed unpaired Student t-test,  $P < 0.0001$ ). E) Relationship between the synaptic size (sypHy2x baseline fluorescence) and the recycling fraction in two Control populations:  $\text{Control}_{\text{largeFr}}$  (dark blue) and  $\text{Control}_{\text{smallFr}}$  (light blue). F) Comparison of the recycling fraction between  $\text{Control}_{\text{largeFrAdj}}$  (blue) and  $\text{CNQX}_{\text{largeFr}}$  (grey) ( $n = 57$  and  $70$  synapses for  $\text{Control}_{\text{largeFrAdj}}$  and  $\text{CNQX}_{\text{largeFr}}$ , respectively. Two-tailed unpaired Student's t-test,  $P = 0.038$ ). G) Quantification of endocytic rate in  $\text{Control}_{\text{largeFrAdj}}$  and  $\text{CNQX}_{\text{largeFr}}$  ( $n = 57$  and  $70$  synapses for  $\text{Control}_{\text{largeFrAdj}}$  and  $\text{CNQX}_{\text{largeFr}}$ , respectively. Two-tailed unpaired Student's t-test,  $P = 0.163$ ).

### 5.2.3 Large synapses have tendency to more variable kinetics

So far we have shown that larger synapses exhibit a faster rate of endocytosis than small synapses. To explore other possible relationships we also considered whether variability was influenced by size. In other words, are small or large synapses more likely to have higher levels of conserved behaviour in their endocytic retrieval times, or is this an independent from size variable? To answer this question we plotted sypHy2x baseline fluorescence against the Within Synapse Similarity (WSS) readout. To reiterate, WSS measures the point-by-point differences between all the endocytic traces that follow single vesicle release events at a given synapse (for more details refer to section 4.3.5.). We found that large synapses have a strong tendency to show higher WSS readouts than small synapses, and also exhibit a large variability in the WSS values, ranging from low similarity index indicating very similar endocytic profiles to more variable readouts (Pearson's correlation test,  $n = 150$  synapses from 9 experiments,  $r = 0.45$ ,  $P < 0.0001$ ) (Fig.5.6.A). In order to test the robustness of this result we also tested whether the rate of endocytosis is correlated with the WSS. From previous analysis we know that larger synapses show a faster rate of endocytosis and therefore if larger synapses are more variable, a faster rate should also correlate with higher variability within synapse, higher WSS. As expected, we saw that synapses with faster endocytic rate had more variable WSS index scores (Pearson's correlation test,  $n = 150$  synapses from 9 experiments,  $r = -0.540$ ,  $P < 0.0001$ ) (Fig.5.6.B). From this we can conclude that large synapses are not

only faster but also that they exhibit more variability in the timing of vesicle retrieval within a given synapse.

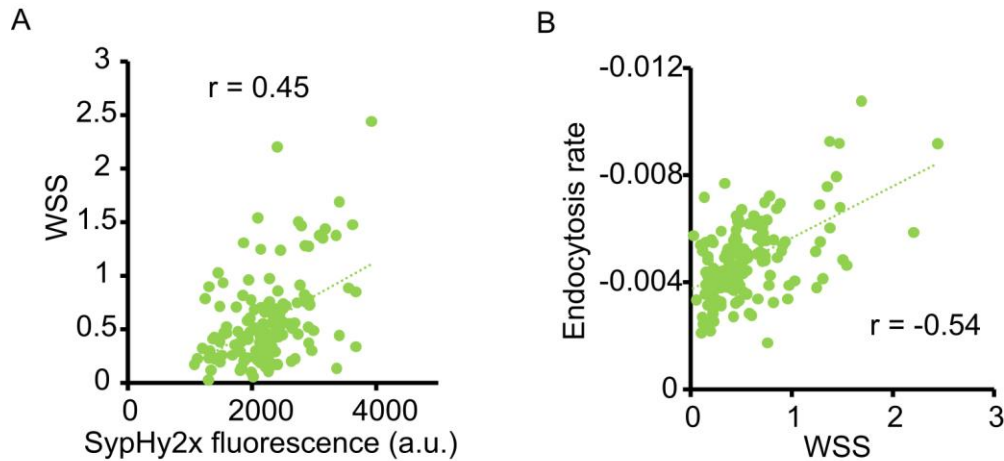


**Figure 5.6 Relationship between the size of the synapse and variability in endocytic kinetics.** A) Moderate correlation between SyHy2x baseline fluorescence and WSS (Pearson's correlation test,  $n = 150$  synapses from 9 experiments,  $r = 0.45$ ,  $P < 0.0001$ ). B) Moderate correlation between WSS and the rate of endocytosis (Pearson's correlation test,  $n = 150$  synapses from 9 experiments,  $r = -0.540$ ,  $P < 0.0001$ ).

#### 5.2.4 Variability in the amount of soluble protein between synapses of various sizes

We reasoned that the influence of size on endocytic kinetics that we have observed, might reflect the level of expression of specific endocytic factors within a terminal, which would define the properties of the endocytic waveform. We contemplated a number of possibilities and considered that one candidate in particular, endophilin, could be an important potential contributor. Endophilin I is the most abundant out of 3 endophilin isoforms expressed in the brain (Ringstad et al., 2001) and it has been previously found to be an important regulator of the kinetics of endocytosis. Despite the fact that in endophilin triple knockout mice experiments, its absence did not lead to a complete block of synaptic transmission, a severe impairment in the timing of endocytosis was observed (Milosevic et al., 2011). Most endophilin I within presynaptic terminals is bound to

synaptic vesicles; however, the soluble pool of this protein originates from adjacent vesicles from which endophilin I unbinds with an exocytosis-dependent rate (Bai et al., 2010). Major binding partners of endophilin I were identified as dynamin and synaptojanin I (Ringstad et al., 2001); and it is also thought to be an important factor in  $\text{Ca}^{2+}$ -dependent coupling of exo- and endocytosis (Haucke et al., 2011). Endophilin I is therefore an important candidate as a regulator of the timing of the synaptic vesicle cycle. Based on this, we decided to test the amount of endophilin I in our synapses in order to decipher whether the variability in this protein can underlie the observed differences in the rate between small and large synapses.

AAV.*sypHy2x*-expressing neurons were labelled with anti-endophilin I antibody (1:500) and an Alexa Fluor ® 568 secondary antibody (1:1000) (detailed protocol in section 2.11). For the control experiment for secondary antibody specificity refer to Appendix I, Figure 4. The average intensity projections of Z-stacks of 2.5  $\mu\text{m}$  in depth (10 frames x 0.25  $\mu\text{m}$ ) were generated for *sypHy2x* and endophilin fluorescence. Great care was taken to minimize the exposure of the sample to light in order to avoid photobleaching. The ROIs were selected on the basis of *sypHy2x* fluorescence as, even though most, not all synapses within a given field of view expressed the construct. A line profile of *sypHy2x* and endophilin I fluorescence showed very good overlay of the two signals, confirming that the labelling was confined to presynaptic terminals (Fig.5.7.A and B).

Next we wanted to explore the relationship between the synapse size and the amount of endophilin I. *SypHy2x* fluorescence was binned within increments of 10 a.u. and endophilin I fluorescence from corresponding boutons was averaged. We found that the relationship between the two variables was described best by an exponential function ( $R^2 = 0.86$ ) and that the correlation between the amount of endophilin and synaptic size was very strong ( $n = 24$  increments summarizing data from 1242 synapses, 11 regions, 3 coverslips. Spearman correlation test,  $r = 0.95$ ,  $P < 0.0001$ ) (Fig.5.7.C). Next, we

explored whether there were any differences between the small and large synapses in the amount of endophilin I at individual terminals. In order to do that we generated two populations of 124 small synapses (10% smallest sypHy2x baseline readouts) and 124 large synapses (10% largest sypHy2x baseline readouts). From this we saw that the level of endophilin I staining was highly variable within large synapses and it ranged from comparable levels of fluorescence as seen in small synapses to a value exceeding double the amount (Fig.5.7.D). To quantify this, we measured standard deviations for these two groups, showing that the level of fluorescence variability in large synapses was ~5.5 times larger than in small ones ( $n = 124$  synapses for both populations) (Fig.5.7.E). Another measure of variability, the coefficient of variation, was almost twice as high in large synapses versus the small ones (CV small synapses = 31.3%; CV large synapses = 59%) (Fig.5.7.F). In the previous sections, we demonstrated that larger synapses exhibited a higher rate of endocytic retrieval of synaptic vesicles than the small synapses. Here, we explored this further, expressing the endophilin I fluorescence as a function of sypHy2x baseline to find out whether large synapses have proportionally more endophilin I than small synapses. We reasoned that this could help to explain the faster endocytic rate in large versus small synapses. Data showed that large synapses, on average, had almost twice as much endophilin I as small ones, suggesting that this might be a factor for their improved endocytic performance ( $n = 124$  synapses for each group, Two-tailed unpaired Student's t-test,  $P < 0.0001$ ) (Fig.5.7.G).

These results suggest that there is higher variability of endophilin I in large synapses, which might help to explain the variability of the behaviour of these synapses. Moreover, large synapses on average exhibit higher levels of endophilin I than the small ones, proportionally to their size, which might account for their better endocytic rate. The level of endophilin I therefore does not scale linearly with the synaptic size.

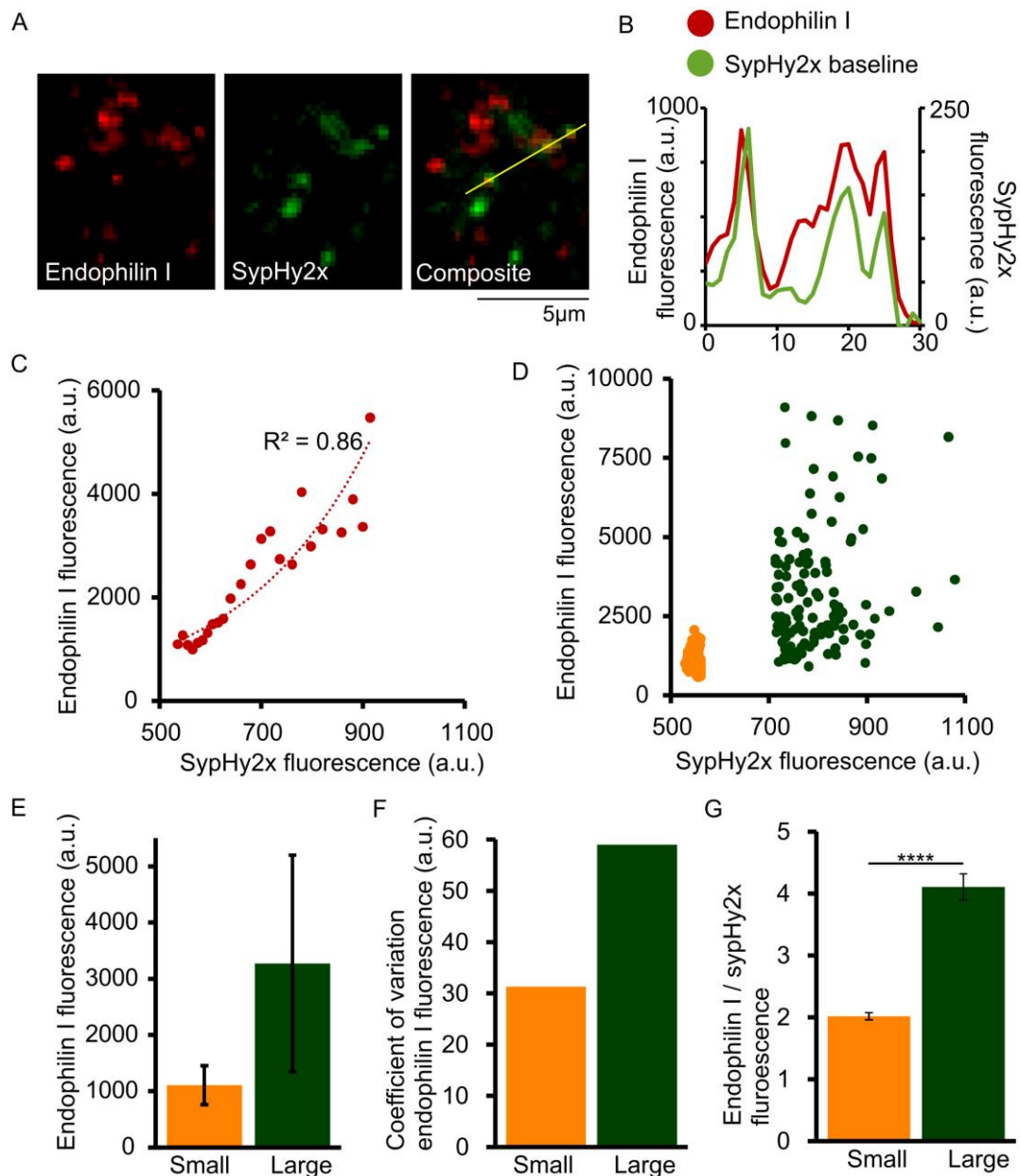


**Figure 5.7. Expression of endophilin I in small and large synapses.** A) Fluorescence images of endophilin I labelled terminals (left), sypHy2x baseline (middle) and merged image of the two (right). Yellow line indicates the ROI along which the profile shown in B was measured. Scale bar 5  $\mu$ m. B) Fluorescence intensity profiles of endophilin I and SypHy2x show overlap. C) Graph showing the relationship between synaptic size (sypHy2x) and the amount of endophilin I of which fluorescence was averaged within increments of 10 a.u. sypHy2x fluorescence ( $n = 24$  increments summarizing data from 1242 synapses, 11 regions, 3 coverslips. Exponential fit,  $R^2 = 0.86$ . Spearman correlation test,  $r = 0.95$ ,  $P < 0.0001$ ). D) Graph showing endophilin readouts for 10% smallest and 10% largest synapses as measured by sypHy2x fluorescence ( $n = 124$  synapses in each range). E) Comparison of the endophilin I variability between small and large synapses. Average of endophilin I fluorescence in the two synaptic size ranges  $\pm$  SD (SD small synapses = 346.3; SD large synapses = 1929.7). F) Coefficient of variation in the level of endophilin I in small and large synapses ( $n = 124$  synapses). G) The relationship between endophilin I and sypHy2x fluorescence in small and large synapses  $\pm$  SEM ( $n = 124$  synapses for each group, Two-tailed unpaired Student's t-test,  $P < 0.0001$ ).

### 5.3 Modulation of synaptic behaviour with dynasore

The assumption that underpins the similarity of endocytic retrieval timing at individual presynaptic terminals is that the difference within the population arises from variation in the timing of the membrane retrieval itself or reacidification kinetics at single boutons. This issue of the source of variability has been raised in Chapter 4. If the fission of the vesicles from the membrane is the main factor contributing to the observed phenomenon, then modulation of this process should result in homogenization of the responses within the population. We put this to the test by using a pharmacological block of dynamin function.

Dynamin belongs to the family of GTPases and it is an important protein for the fission of synaptic vesicles from the membrane following their internalization (section 1.3.2.1). It has been implicated in both clathrin-dependent and -independent endocytosis (Delvendahl et al., 2016; Hayashi et al., 2008; Voglmaier and Edwards, 2007). Blocking dynamin is a good test of the nature of variability in our endocytic decay profiles. In order to address this question we used a pharmacological method for disrupting dynamin function.

#### 5.3.1 Dynasore decreases the rate of endocytosis

Dynasore has been identified via a high-throughput screen as a small-molecule compound that noncompetitively inhibits GTPase activity of dynamin ( $IC_{50} = 15 \mu M$ ), effectively blocking endocytic processes (Macia et al., 2006). It is cell-permeable, and does not require a long incubation time and therefore permits the monitoring of changes associated with dynamin inhibition within a relatively short time-scale (Macia et al., 2006). In hippocampal neurons expressing sybHy, dynasore was previously shown to block endocytosis in a dose-dependent manner and to have no effect on synaptic vesicle

exocytosis (Newton et al., 2006). The ultrastructural analysis of samples treated with dynasore also revealed a higher occurrence of endocytic intermediates (invaginated, omega-shaped membranous structures) and clathrin-coated pits, which again supports the efficiency of this drug at blocking endocytosis (Newton et al., 2006). We therefore decided to use this drug in order to test the source of variation in endocytic kinetics in our system.

AAV.*syphHy2x*-expressing neurons were stimulated 6 times with the 4 APs protocol from which 5 trials were used for the analysis (first trial used for identification of responding synapses but removed from the data set as a bleaching trial). Following this set of stimulations, 5  $\mu$ M dynasore was added to the cell culture and the cultures were incubated with this drug for 10 min prior to the next set of stimulation (5 x 4 APs). The fluorescence profiles of individual synapses from all the images, before and after, were measured and the results were screened for single vesicle response events ( $\Delta F = 92.2$ -157 a.u.) using a custom-written Matlab script. The profiles for the analysis were fitted with third order polynomial functions to reflect the shape of the fluorescence decay. All single vesicle responses for both before and after dynasore groups were averaged and this revealed a slowing down effect of dynasore on the endocytic kinetics (Fig.5.8.A). Due to the fact that this figure represents all single vesicle responses, some of which might not have been from the same synapse before and after incubation of the drug, we also screened endocytic traces following single vesicle fusion events but originating from the same synapse, to confirm, that the effect is not due to different synapses being measured, but due to the effect of dynasore on individual boutons (Fig.5.8.B). In order to compare the rate of endocytosis before and after the incubation with the drug, single vesicle response traces were fitted with a linear fit and the average of the measurements of fluorescence decay from synapses that responded with at least 2 single vesicle release events before and after addition of dynasore were analysed. We found that the rate of endocytosis was decreased by  $31.8 \pm 7.1\%$  following 10 min incubation with dynasore in comparison to the endocytic kinetics before the treatment with this drug (n

= 99 not matched synapses for both groups, two-tailed unpaired Student t-test,  $P < 0.0001$ ) (Fig.5.8.C and D). These results show that dynasore was successfully used in our culture to modulate the efficiency of endocytosis. The purpose of this experiment was not to completely abolish the endocytosis, but to affect the efficiency of the endocytic machinery, which was achieved with the chosen concentration and incubation timing of dynasore used here. The next section exploits this drug to further validate the results of vesicle retrieval similarity within individual synapses.

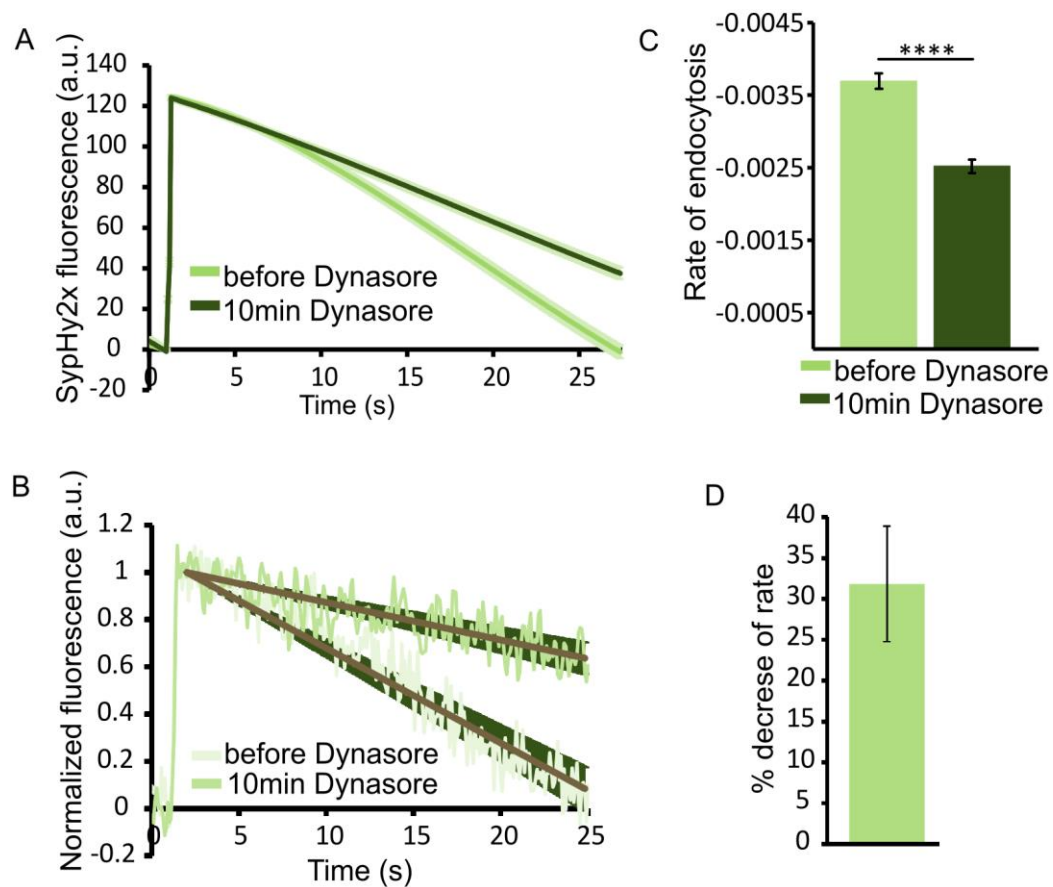


**Figure 5.8 The effect of 5  $\mu\text{M}$  dynasore on the kinetics of endocytosis.** A) Average of 1q responses before and after treatment with dynasore. Data showed as average  $\pm$  SEM (light green shade) of  $n = 327$  and  $n = 274$  1q responses before dynasore and after 10 min dynasore treatment, respectively, from 6 coverslips. B) Normalized traces from the same synapses before and after treatment. Data showed as average of 6 traces  $\pm$  SEM. Brown lines represent linear fits constrained to 1. C) Comparison of the rate of single vesicle endocytosis before and after dynasore treatment ( $n = 99$  synapses for both groups, two-tailed unpaired Student t-test,  $P < 0.0001$ ). D) The rate of endocytosis of single vesicles decreased by 31.8% in dynasore treated group ( $n = 99$  synapses for dynasore  $\pm$  SEM).



### 5.3.2 Similarity measure of synapses treated with dynasore

Our results so far show that individual synapses exhibit signature endocytic behaviour, and that we can modulate the endocytic kinetics of the retrieval of single vesicles (sections 4.3.5 and 5.3.1). From this, we formed a hypothesis that if the conservation of the endocytic kinetics within each synapse is truly due to synaptic properties that dictate their behaviour, we might, by affecting function of a protein important in endocytosis, be able to cause synapses to lose their specific characteristics and thus behave in a more homogeneous way across the population. To test this, we used the same similarity analysis method as described in detail in section 4.3.5. In short, for each experimental synapse which responded with at least 2 single vesicle responses within 5 trials before or after the addition of the drug, 100 randomised synapses were generated by drawing 1q traces from other synapses within the experiment. The average of similarity measures of 1q profiles from individual synapses ( $WSS_{ave}$ ), based on point-by-point difference between the traces was calculated and compared to the same measure in 100 randomised trials ( $RSS_{trial}$ ). DMSO at a final concentration of 0.005% was used as a control.

We found that synapses before dynasore and DMSO treatment exhibited a high level of similarity, scoring lower variability at individual synapses in 85 and 90 randomised trials, respectively (Fig.5.9.A). Following 10 min incubation with 5  $\mu$ M dynasore we observed a dramatic drop in the number of more variable randomised trials, which was not the case for the DMSO treated group (Fig.5.9.A). In other words, dynasore treated cells exhibited a 49.4% decrease in similarity within synapses, whereas it only decreased 4.4% in DMSO control (Fig.5.9.B). This result suggests that dynasore treatment led to homogenization of the endocytic kinetics across the synapses, which wasn't observed in DMSO group and was therefore unlikely to occur as a result of experimental design.

The analysis presented so far was based on synapses which were not matched in the before and after groups, meaning that some synapses that were included in the analysis

in the before group might not have had two single vesicle responses following 10 min incubation, and vice versa. We therefore identified synapses that were measured in both groups which, however, dramatically decreased the number of synapses available for the analysis (from 99 to 49). The results for DMSO control were not included due to a very small number of synapses available for analysis. Within this smaller population of before and after matched synapses, we observed an 18.6% decrease in similarity in synaptic characteristics (Fig.5.9.C). Another line of comparison came from the actual measure of similarity,  $WSS_{ave}$  and  $RSS_{ave}$ , before and after dynasore application. This was also carried out on the synapse-matched data. The results showed that  $RSS_{ave}$  was significantly larger than  $WSS_{ave}$  before the treatment with dynasore ( $n = 49$  before-and-after matched synapses. Two-tailed paired Student's t-test,  $P = 0.020$ ). This strongly indicates that, based on the same profiles, the variability in the randomly generated synapses was much larger than in experimental synapses (Fig.5.9.D). Despite the fact that the  $WSS_{ave}$  after dynasore treatment was not significantly different from  $WSS_{ave}$  before the application of the drug ( $n = 49$  synapses, two-tailed paired Student's t-test,  $P = 0.500$ ), the measurement for  $RSS_{ave}$  was significantly smaller than  $RSS_{ave}$  before the incubation with dynasore ( $n = 49$  synapses, two-tailed, paired Student's t-test,  $P < 0.0001$ ), but not different from the  $WSS_{ave}$  readouts in before and after groups ( $n = 49$  synapses, two-tailed paired Student's t-test,  $P = 0.854$  and  $P = 0.416$  for  $WSS_{ave}$  before and after, respectively) (Fig.5.9.D).

These results very strongly indicate that the modulation of the efficiency of endocytosis with dynasore led to homogenization of the kinetics of single vesicle retrieval timing amongst the synapses and therefore strengthens the findings that the conserved behaviour of individual synapses stems from the characteristic properties of individual synapses.

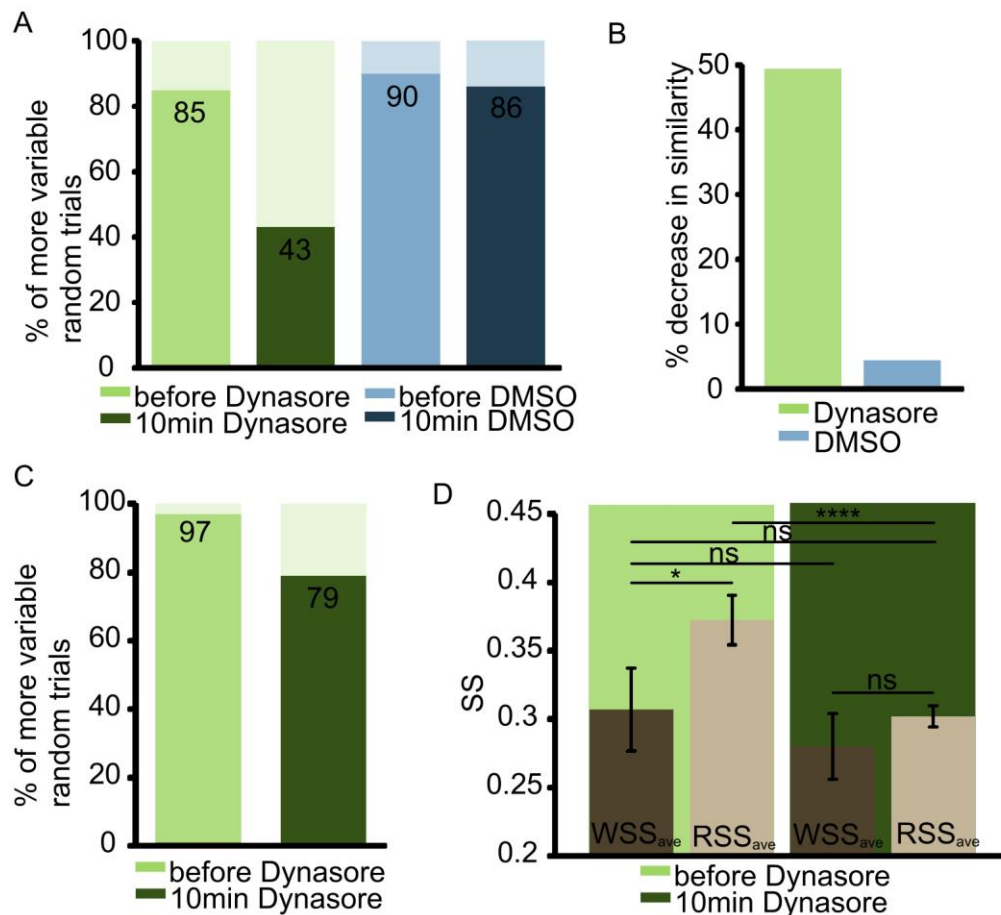


**Figure 5.9 The effect of dynasore treatment on single vesicle endocytic similarity within individual synapses.** A) Before dynasore treatment 85 out of 100 randomized trials showed higher variability in 1q profiles than the experimental synapses which decreased to 43 trials following 10 min dynasore treatment (data from 99 synapses from 6 experiments, binomial test,  $n = 100$ ,  $k = 85$ ,  $p = 0.5$ ,  $P < 0.0001$ ). Following dynasore treatment profiles from individual synapses became homogenized with the population losing their individual characteristics (data from 99 synapses from 6 experiments, binomial test,  $n = 100$ ,  $k = 43$ ,  $p = 0.5$ ,  $P = 0.193$ ). DMSO treated synapses retained their characteristics (data from 71 (before DMSO) and 64 (after DMSO) synapses from 4 experiments, binomial test: before DMSO,  $n = 100$ ,  $k = 100$ ,  $p = 0.5$ ,  $P < 0.0001$  and after 10 min DMSO,  $n = 100$ ,  $k = 86$ ,  $p = 0.5$ ,  $P < 0.0001$ ). B) There was 49.4% decrease in similarity of the endocytic behaviour of single vesicles at individual synapses observed in dynasore treated group in comparison to only 4.4% decrease in DMSO treated group. C) Only synapses that responded with at least 2 1q before dynasore treatment and after dynasore treatment were selected for analysis shown in C) and D) ( $n = 49$  from 5 experiments). DMSO control is not included due to a very small number of such synapses ( $n = 28$ ). Synapses treated with dynasore became 18.6% more similar to the population in their endocytic kinetics of single synaptic vesicles. D) Before dynasore treatment  $WSS_{ave}$  was significantly smaller than  $RSS_{ave}$  ( $n = 49$  synapses, two-tailed paired Student's t-test,  $P = 0.020$ ) but did not differ from  $WSS_{ave}$  or  $RSS_{ave}$  after 10 min dynasore ( $n = 49$  synapses, two-tailed paired Student's t-test,  $P = 0.500$  and  $P = 0.854$ , respectively). Following 10 min incubation with dynasore  $RSS_{ave}$  significantly decreased in relation to  $RSS_{ave}$  before dynasore treatment ( $n = 49$  synapses, two-tailed paired Student's t-test,  $P < 0.0001$ ) and was not significantly different from  $WSS_{ave}$  following the incubation with the drug ( $n = 49$  synapses, two-tailed paired Student's t-test,  $P = 0.416$ ).

## 5.4 TEM analysis of presynaptic properties

The readouts of presynaptic properties presented so far were solely based on functional studies of vesicle behaviour. Although these experiments provide important information on synaptic operation, the conclusions that can be drawn are limited by the lack of morphological information about individual synapses. For example, precise readouts of nanoscale parameters such as vesicle pool sizes, number of active zones and their organization, presynaptic volume, vesicle clustering densities, docked vesicle pool count, and functional vesicle pool organization, are almost completely unavailable. An approach for accessing these parameters is based on the use of electron microscopy imaging, although this is not trivial, given the need for correlative approaches to link synapses targeted in light imaging with those in embedded tissue at ultrastructural level. A major additional challenge of this type of experiment is to find an approach to link the fluorescence signal from an individual presynaptic bouton to its ultrastructure in an unambiguous way. However, this challenge can be addressed by the use of the fixable form of FM1-43 (FM1-43FX), the styryl dye introduced in Chapter 3. This dye, which is taken up into endocytosing vesicles, can be used to drive the photo-oxidation of diaminobenzidine (DAB) in the presence of intense blue excitation light. In the next sections of this chapter we further validate our stimulation protocols and fluorescence readouts with electron micrographs containing photoconverted vesicles. We established an approach for the identification of imaging of individual presynaptic terminals in a correlative manner and, more importantly, we explored ultrastructural properties of synapses with characteristic kinetic behaviour. The specific aims were: i) to check at the ultrastructural level that the number of vesicles recruited during stimulation was as expected; ii) to confirm whether *sypHy2x* baseline fluorescence reflects the size of synapses; iii) to search for characteristic ultrastructural features that align with functional synaptic properties, for example synaptic volume and the number of vesicles.

### 5.4.1 Establishing loading protocols

We first wanted to define a suitable stimulation protocol for the TEM work. In the majority of syHy2x experiments, cells were stimulated with 4 APs (median  $p_r$  at hippocampal neurons  $0.22 \pm 0.03$  (Branco et al., 2008)) in order to increase the likelihood that single release events would occur. However, we reasoned that such a protocol is not optimal for experiments where FM1-43FX loading is followed by TEM analysis. There are a number of reasons for this: first, the expectation for the number of loaded vesicles at this level of stimulation is 0-4 per synapse with a single active zone, which is the case for most hippocampal synapses (Schikorski and Stevens, 1997). This would make the localization of synapses with photoconverted vesicles (those vesicles that endocytosed in the presence of FM1-43FX) very difficult. Without full reconstructions for every synapse, this would likely favour identification of synapses with multiple PC+ vesicles. More importantly, one has to take into account the possibility of spontaneous vesicle fusion in the presence of FM1-43FX, which would falsely increase the ultrastructural readout of the number of vesicles that recycled during the applied stimulation. At this minimal stimulation level, this could have had a significant impact on the obtained readout. Also, fluorescence identification of 4 APs FM1-43-loaded synapses, although possible (Ryan et al., 1997), proved to be difficult due to the low fluorescence level of FM1-43 in comparison to syHy2x (Appendix I, Figure 5, pilot experiment). For these reasons, we therefore decided to use a stronger loading protocol based on 10 APs stimulation. 40 APs stimulation at 20 Hz was chosen as a comparison readout since it has been widely used across different studies, and is well described in the literature. The use of this stimulation level is very common due to its relevance to synaptic performance as it is thought to mobilise the vesicles in RRP (Li et al., 2005; Murthy and Stevens, 1998; Opazo et al., 2010; Schikorski and Stevens, 2001). First we wanted to confirm whether we achieved a detectable difference in the fluorescence intensity between 40 APs and 10 APs loading. The protocol used is summarized in Figure 5.10.A. Due to the

quantitative nature of this experiment, it was important to wash out any surface bound FM1-43 and hence a 10 min washing followed by 10 min incubation and another wash were carried out. The selection of boutons was critical and therefore only puncta with no other background fluorescence were selected for the analysis. The representative fluorescence images showed the apparent difference in the fluorescence intensity between the two loading groups. (Fig.5.10.B). The quantification of the signal revealed 36.6% less fluorescence in 10 APs loading group than in 40 APs loading (Fig.5.10.C). This measurement provides good reference for the comparison of the fluorescence readout with the ultrastructural results, in which the number of vesicles that underwent recycling can be visualized.

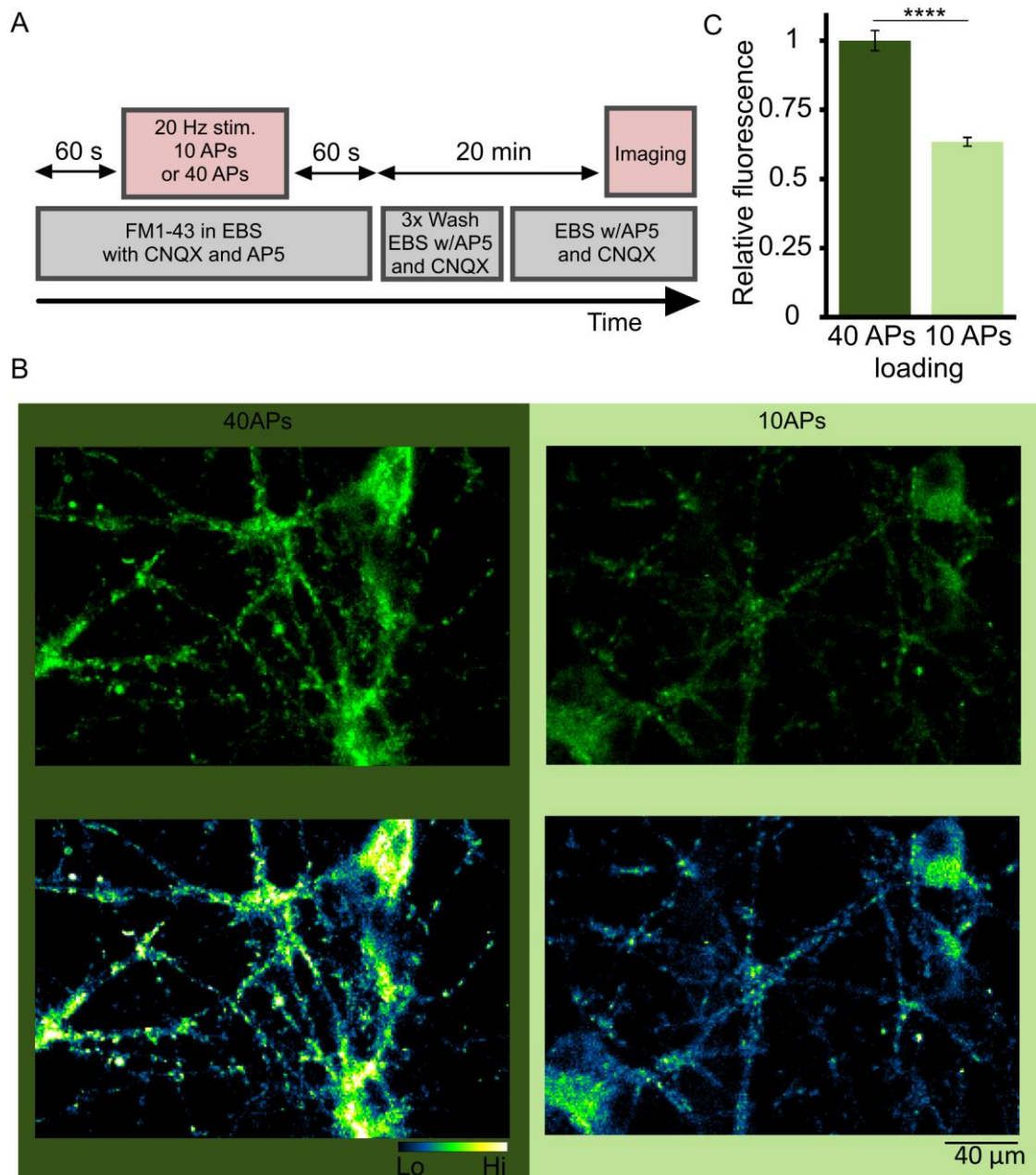


**Figure 5.10 Comparison of the level of loading FM1-43 loading following 40 APs and 10 APs stimulus.** A) Timeline demonstrating the protocol used for labelling recycling vesicles at different intensities of the stimulus. B) Images showing the difference in the level of fluorescence intensity corresponding to the level of loading. Scale bar 40  $\mu$ m. C) Quantification of fluorescence intensities of boutons loaded with either 40 APs and 10 APs reveals 36.6% less fluorescence in 10 APs loaded samples in relation to 40 APs loaded cells ( $n = 112$  and  $n = 124$  synapses for 40 APs and 10 APs loading from 2 and 3 coverslips, respectively. Two-tailed unpaired Student's t-test,  $P < 0.00001$ ).

#### **5.4.2 TEM procedure and identification of fluorescence region on the resin block**

As mentioned above, one of the most challenging aspects of correlative TEM is the relocation of the imaged region, and the even more demanding task of relocation of individual fluorescent synapses at the ultrastructural level. Approaches such as CLEM (Correlative Light-Electron Microscopy) offer a solution to this problem by allowing the imaging of the ultrastructure in the region previously examined for its function using fluorescence readouts. Recent technological advances offer the possibility of imaging fluorescence at the ultrastructural level improving the experimental output of this technique. Nevertheless, this also has its drawbacks. The preservation of GFP signals relies on the usage of minimal concentrations of heavy metals such as uranyl acetate in order to avoid quenching of the fluorescence of traditional fluorescent proteins. Heavy metals on the other hand are crucial for the preservation and good contrast of the samples at the ultrastructural level. A new, synthetic range of fluorophores is under development which will overcome the problem of GFP quenching in this method in the future (Perkovic et al., 2014).

The sample preparation was carried out according to the method described by Darcy et al., 2006 and in section 2.12. The summary of the process is shown in Figure 5.11.A. The selection of an appropriate region was crucial for this type of experiment. Following functional imaging of sypHy2x signals during 4 APs stimulation, DIC images using 4x and 10x objective were taken allowing for the later relocation of the target region (Fig.5.11.B). It was important to find a cell expressing sypHy2x with a reasonable number of functional boutons and which was positioned next to a distinguishable landmark such as a characteristic group of cells (Fig.5.11.B). This was necessary to help later relocation of the ROI. The cells were then loaded with FM1-43FX at 40 APs or 10 APs stimulation, permitting comparison with our fluorescence imaging (see previous section). One minute after the onset of stimulation, cells were rapidly fixed with 2% paraformaldehyde/2%



glutaraldehyde. The coverslip was then placed back under the microscope and the target region was relocated. Photoconversion was carried out in the presence of 1 mg/ml DAB solution during continuous illumination for 15 min under 480 nm light. This process exploits the photolabile nature of FM1-43FX and the reducing property of DAB. Free radicals are released during photoexcitation of FM1-43FX which then drive the oxidation of DAB and lead to the formation of electron dense product that can be visualized under the TEM (Branco et al., 2010; Henkel et al., 1996). This results in the dark appearance of vesicles loaded with FM1-43FX under TEM. In order to ensure that the entire ROI was illuminated, the objective used for photoconversion was 40x and therefore fully encapsulating the area imaged during functional analysis (Fig.5.11.C). The sample was prepared for TEM and embedded in EPON (for details refer to section 2.12). Following overnight polymerisation at 60°C and transfer of the cells onto the resin block, the block was searched for the ROI with the aid of DIC images taken. Once relocated, the ROI was marked and the block was trimmed as close to the ROI as possible (Fig.5.11.D). The structures showed on DIC images were clearly identifiable on the resin block which allowed for very precise positioning of the target processes and synapses (Fig 5.11.E). Ultrathin serial sections, 60 nm thick, were cut using a diamond knife and placed as a ribbon on formvar-coated grids. Sectioning was carried out by Catherine Smith. This made it possible to 3D reconstruct the target synapses and examine their architecture.

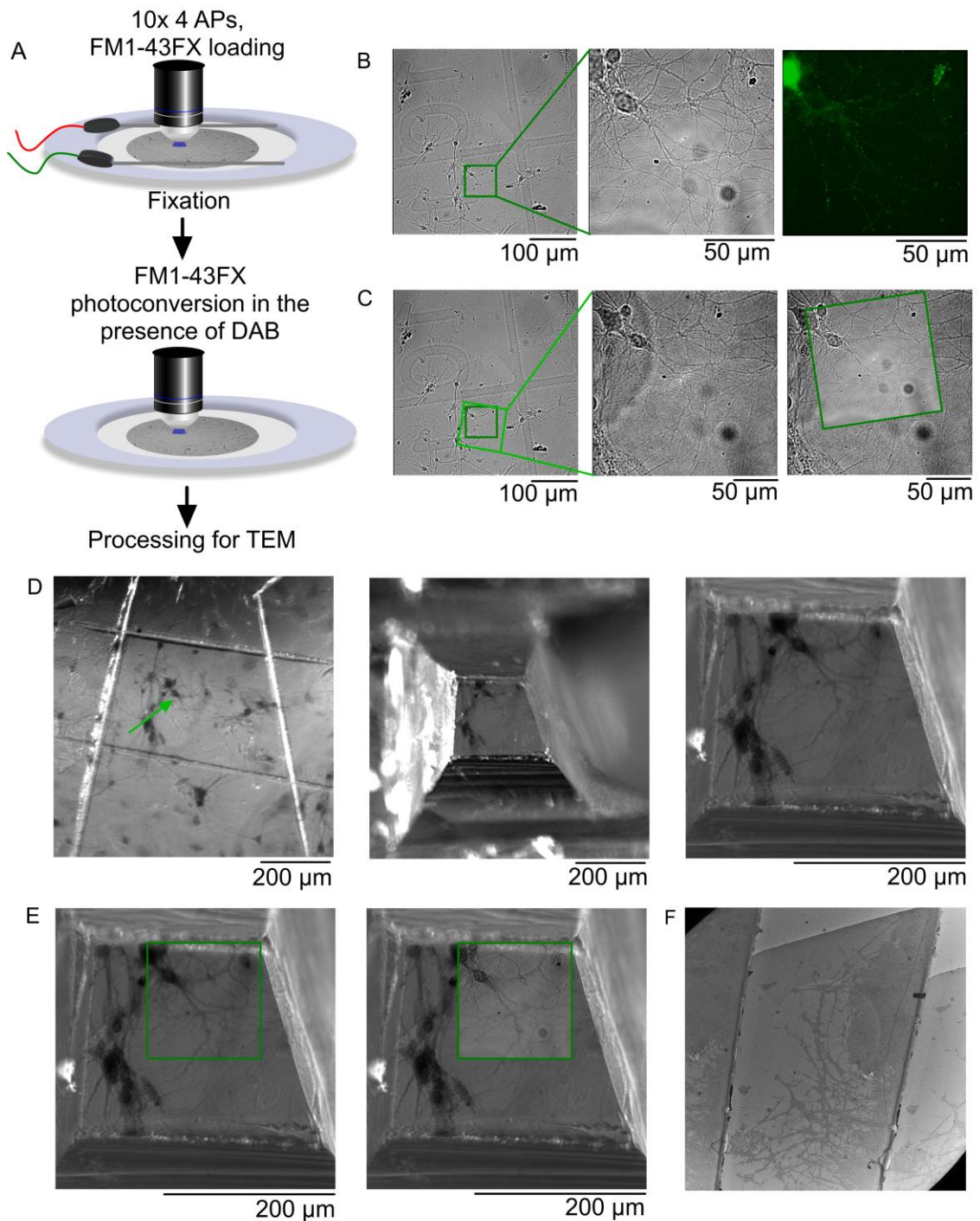


**Figure 5.11 Selection of sypHy2x expressing region for TEM analysis and its relocation following embedding.** A) Schematic representation of the protocol used. Following identification of expressing neuron, cells were imaged during 10x stimulation with 4 APs. Recycling synaptic vesicles were labelled with 10 APs or 40 APs stimulus at 20 Hz with FM1-43FX following which the cells were fixed. The ROI was relocated and the coverslips were incubated in 1 mg/ml DAB solution prior to 15 min photoconversion by irradiation with 488 nm light. Samples were prepared for TEM as described in methods section. B) 10x images were taken to facilitate relocation of the ROI. ROI indicated by green square (left). Scale bar 100 µm. Selected region with clearly visible cell body and fairly dense network (middle). Scale bar 50 µm. Fluorescence image of sypHy2x expressing synapses (right). Scale bar 50 µm. C) Relocation of ROI. Dark green square indicates ROI (60x objective) and light green square marks the photoconverted

region (40x objective) which fully encapsulates the original ROI (left and middle images). Scale bar 100  $\mu\text{m}$  (left) and 50  $\mu\text{m}$  (right). DIC image showing the relationship between the original ROI (dark green) and the photoconverted region (right). Scale bar 50  $\mu\text{m}$ . D) EPON block with embedded neurons. The target region was relocated (green arrow is pointing at the cell of interest) and the resin was marked with some margin around it (left). In preparation for sectioning the resin was trimmed closer to the target region (middle and right). Scale bars 200  $\mu\text{m}$ . E) ROI (green square) was easily identifiable on the trimmed resin block (left). Middle image shows 60x DIC image (70% transparency) of ROI perfectly matching the embedded cells. Scale bars 200  $\mu\text{m}$ . Structures of interest can be readily distinguished on the ultrathin sections (right). F) Example of ultrathin section on which cellular structures can be readily distinguished.

#### **5.4.3 Visualization of sypHy2x-expressing, functional synapses at the ultrastructural level and 3D reconstruction**

Correlative microscopy identifying individual FM1-43 labelled terminals at the ultrastructural level, has been widely used to study the relationship between structure and function of individual presynaptic terminals (Branco et al., 2010; Darcy et al., 2006a; Harata et al., 2001). Important features of presynaptic terminals emerged from these studies, which would have not been possible to be measured using other techniques or with lesser confidence. Despite the fact that the technique has been well established for ultrastructural examination of fluorescently imaged FM1-43-loaded synapses, in this study it has been attempted for the first time to scrutinize features of sypHy2x expressing boutons under the TEM. This represents another tool for deciphering characteristic features of boutons that exhibited interesting behaviour during functional sypHy2x imaging. It also provides an approach to further confirm the use of sypHy2x baseline fluorescence as a measure of synaptic size.

Following functional imaging with 10x 4 APs protocol, sypHy2x expressing neurons were loaded with 10 APs or 40 APs FM1-43Fx (protocol in Figure 5.10) fixed, photoconverted and processed for TEM as described in section 5.4.2. The cell of interest was identified and the EPON block sectioned. Subsequently the analysis of sypHy2x responses to repeated 4 APs stimulation was carried out and synapses with signature behaviour with conserved timing of vesicle retrieval were picked for the analysis. From this type of data we were able to measure the morphological parameters of these synapses (bouton

volume and total number of vesicles), which may help to explain the difference in the endocytic behaviour of individual terminals. This section shows the process of identification of one such synapse at the ultrastructural level.

A synapse of interest was identified and traced back to DIC images with the aid of fluorescence images (Fig.5.12.A-C). Following the 4 APs trials, cells were stimulated with 40 APs, 20 Hz, prior to FM1-43 loading, in order to assist with mapping of the synapse thanks to much brighter fluorescence rise than during 4 APs stimulation. From this, the area containing the synapse of interest was determined (Fig.5.12.D-G). Bright field images at 10x and 60x were used for identification of the region of interest under TEM. A very tight trimming of the block around the imaged area vastly reduced the time needed to relocate the structures. Middle sections were used for this purpose as the most representative of the overall morphology of the region. The ultrastructural images mapped perfectly on top of the DIC image (Fig.5.12.H). From this we were able to more precisely determine the area containing the synapse of interest. Figure 5.12.I shows the electron micrograph with overlaid sypHy2x fluorescence. We then took images at a higher magnification of the target area to find a seamless overlay of fluorescence over the ultrastructural image (Fig.5.12.J and K).

Once we were confident that we had identified the ultrastructural region which contains the synapse of interest, we traced this region in the remaining serial sections. This allowed the collection of consecutive images of the synapse (Fig.5.13.A). These images were meticulously aligned, and three dimensional reconstruction of the presynaptic terminal and surrounding structures was created using Reconstruct software (Fig.5.13.B). We identified the membranes surrounding the presynaptic bouton and its axon and labelled the dendritic compartment. The total number of SVs within the bouton was counted and the area of the active zone was marked out. To sum up, we developed an approach allowing the unambiguous identification of a sypHy2x-expressing synapse at an ultrastructural level.

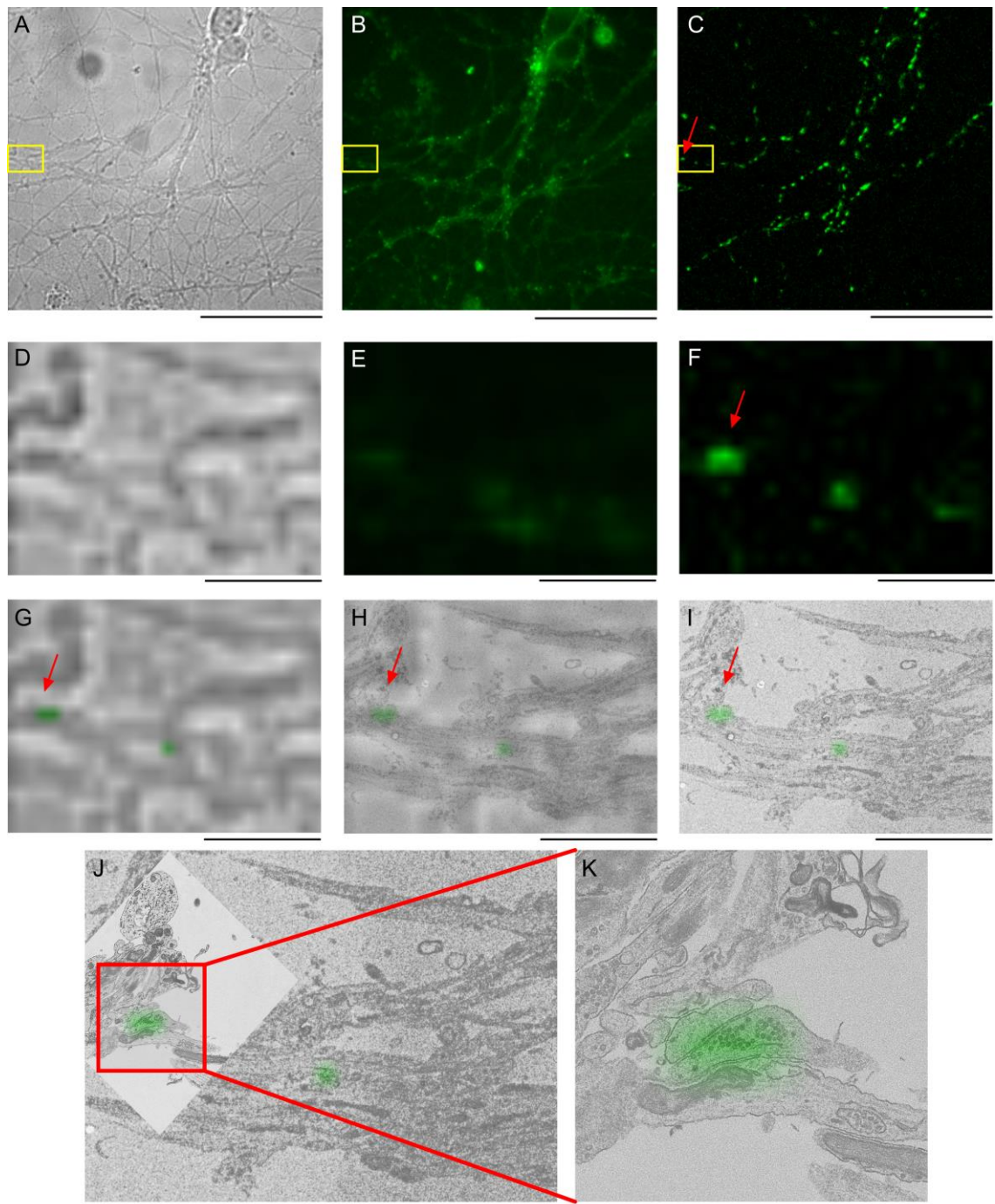


**Figure 5.12 Example of correlative approach allowing to visualize sypHy2x expressing terminal under TEM.** A-C) Light microscopy images of cell culture expressing sypHy2x. Yellow rectangle represents region encapsulating synapse of interest, which is indicated by the red arrow. Scale bar 50  $\mu\text{m}$ , A) DIC image, B) SypHy2x baseline fluorescence, C) Synaptic responses to 40 APs 20 Hz stimulation. D-F) Region of interest from the yellow box. G) Overlay of DIC and fluorescence image of the responding synapse. H) Overlay of DIC, fluorescence and ultrastructural image. I) Low magnification ultrastructural readout with overlaid fluorescence. J) Low magnification electron micrograph overlaid with higher magnification TEM image and fluorescence. Scale bar images D-J, 10  $\mu\text{m}$ . K) Magnification of fluorescence and electron micrograph overlay. Scale bar 1  $\mu\text{m}$ .



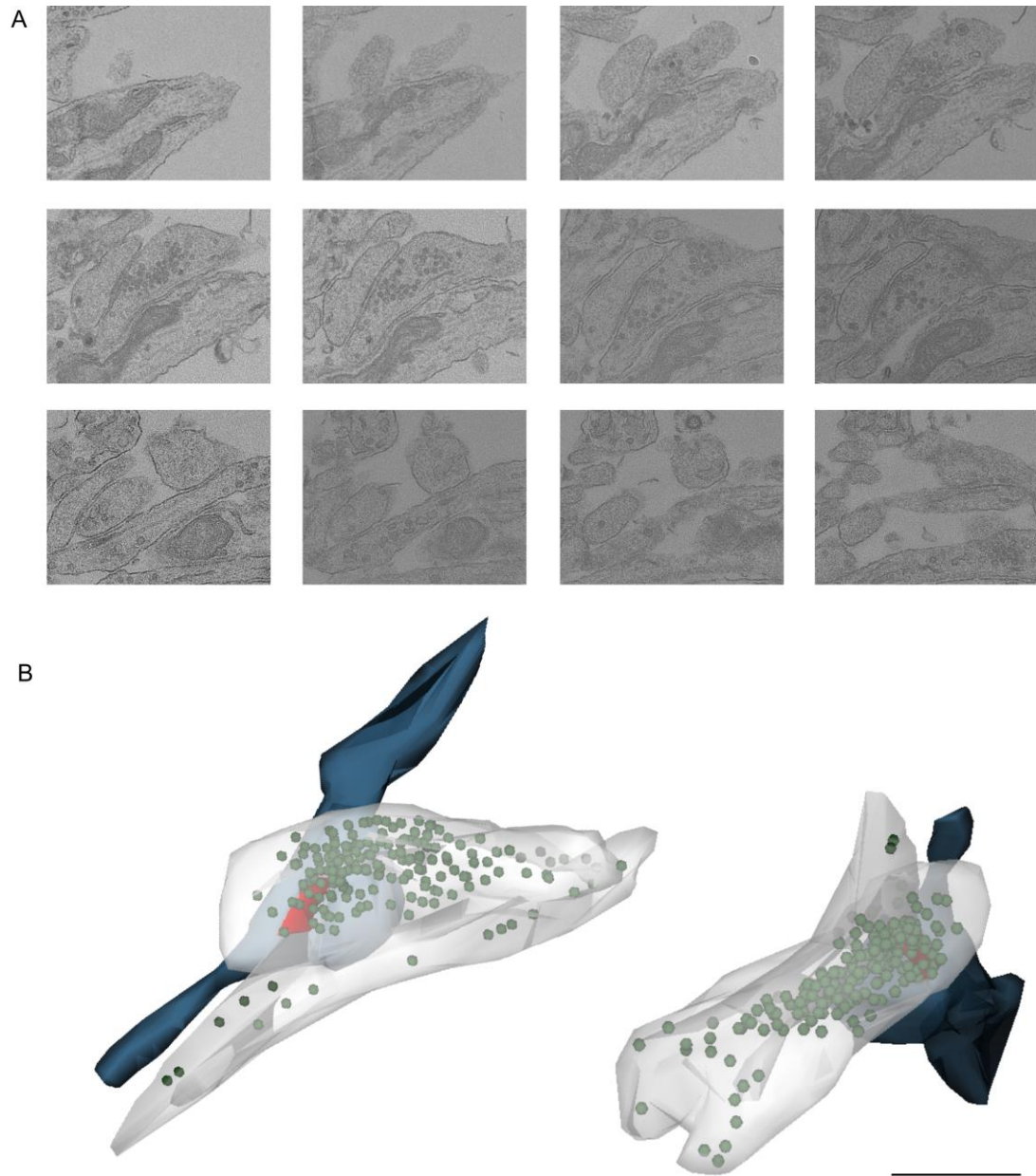


**Figure 5.13 An example 3D reconstruction of a fluorescently imaged synapse.** A) Consecutive images of the serial sections of the region containing synapse of interest. B) Three-dimensional reconstruction of the synapse. The two images show the same synapse from different perspective. The area shaded in grey represents presynaptic terminal and part of the axon. Green spheres are the synaptic vesicles. Active zone is highlighted in red. Dendrite is represented by the blue structure. Scale bar 500 nm.

#### **5.4.4 Robust method for identification of photoconverted vesicles**

The reliability of the results from photoconversion experiments heavily relies on the unambiguous identification of photoconverted vesicles. This is especially critical in this study, due to the very low level of stimulation used as every misidentified vesicle could potentially affect the results. Strict rules were therefore put in place to ensure a uniform analysis across samples. A detailed description of how to distinguish non-photoconverted from photoconverted vesicles has been previously provided by many authors (Darcy et al., 2006a; Harata et al., 2001; Schikorski and Stevens, 2001).

There was a very clear observable distinction between non-photoconverted (PC-) and (PC+) vesicles (Fig.5.14.A). The PC- vesicles were characterized by a dark membrane and a clear lumen. These were the vesicles that were not released in response to the stimulus and therefore did not take up FM1-43 dye. The lumen of PC+ vesicles appeared black and was evidently darker than the surrounding membrane (Fig.5.14.B). These electron-dense vesicles were those that underwent endocytosis in the presence of FM1-43FX, and were therefore photoconverted in the presence of DAB. The difference between PC+ and PC- vesicles can be quantified by analysing their density profiles. A line of equal length was drawn across PC+ and PC- vesicles and cross-sectional density was measured. Non-photoconverted vesicles showed an increase in density corresponding to the membrane, with a drop in the middle which reflects the vesicular lumen. Photoconverted vesicles on the other hand showed the same increase in density across the SVs membrane as PC- vesicles, but they were also characterised by a central peak with density much higher than any other point across the structure (Fig.5.14.C).

Furthermore another set of measurements were employed in order to avoid any confusion between PC+ and PC- vesicles. Lumenal densities were measured from 10 pixel diameter circular ROIs placed in the centre of the vesicle lumen. There was a clear bimodal distribution of densities with peaks at very different values for PC- and PC+ vesicles, which allows the reliable identification of these two groups of vesicles

(Fig.5.14.D). Various controls were carried out in our laboratory showing that black, photoconverted vesicles were only present in experiments with prior FM1-43FX exposure (Rey et al., 2015). Henkel et al., 1996, carried out similar control experiments to also conclude that the presence of electron dense product in SVs is specific for vesicles exposed to FM1-43.

GFP was previously reported to undergo sufficient photo-oxidation to drive DAB conversion into electron-dense product (Horstmann et al., 2013). To control for the effects of sypHy2x expression we carried out a control experiment in sypHy2x expressing cells and carried out the photoconversion protocol as normal to find that there were no photoconverted vesicles in our preparation (data not shown).

We therefore established a method for confident identification of photoconverted vesicles.



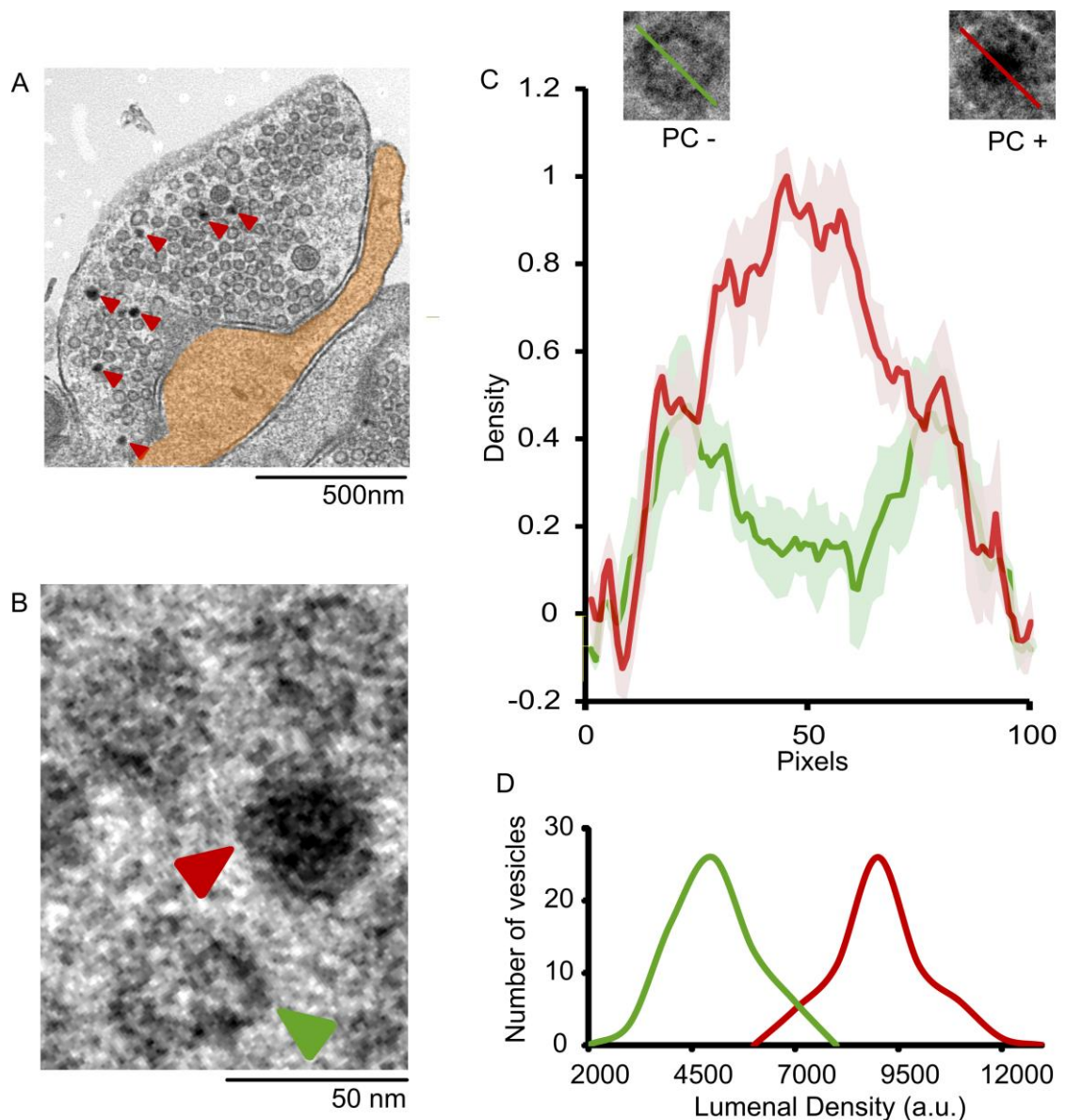


**Figure 5.14 Identification of photoconverted vesicles on electron micrographs.** A) TEM image of a sample loaded with FM1-43 dye (40 APs at 20 Hz) and subsequently photoconverted. Red arrowheads indicate all photoconverted vesicles in this presynaptic terminal. Orange shade marks postsynaptic region. Scale bar, 500 nm. B) Higher magnification image of photoconverted vesicle with dark lumen (red arrowhead) and non-photoconverted vesicle (green arrowhead). Scale bar, 50 nm. C) Density measure of the cross sections of PC- and PC+ vesicles (inset). The lumen of the PC+ is the densest area of PC + vesicle, denser than the membrane (red trace). The densest portion of the PC- vesicle is the membrane with a dip indicating the lumen of the PC- vesicle (green trace). Data showed as average of 4 vesicles for both groups  $\pm$  SEM. D) Distribution plot of luminal densities of PC- ( $n = 65$ , green trace) and PC+ ( $n = 60$  red trace) vesicles. Two clear peaks are revealed aiding identification of PC- and PC+ vesicles.

#### 5.4.5 Photoconverted vesicles under different stimulation conditions

Having established a reliable protocol for the identification of photoconverted vesicles, we next wanted to establish how well our fluorescence intensity readouts at 40 APs and 10 APs stimulation protocols (section 5.4.1) aligned with the findings from ultrastructural experiments. The size of the RRP has been estimated to comprise of 5-15 synaptic vesicles in various hippocampal preparations (Dobrunz & Stevens, 1997 ( $5 \pm 3$ , hippocampal slice); Murthy & Stevens, 1998 ( $7.7 \pm 4.4$  hippocampal cell culture); Stevens & Tsujimoto, 1995 (15, hippocampal culture)). Therefore these studies provide a good reference for the quantification of the number of mobilized quanta under 40 APs and 10 APs stimulation.

Within photoconverted regions we observed that there were few PC+ vesicles in individual synapses from 40 APs stimulation, whereas, in 10 APs loading there were mostly single PC+ vesicles in single sections (Fig.5.15.A). Due to the fact that sampling of individual sections can lead to sampling errors and overestimation of the number of photoconverted vesicles, we used 3D reconstructions of 10 APs loading for evaluation of the percentage of PC+ vesicles. We found that the percentage of photoconverted vesicles was  $3.61 \pm 1.96 \%$  ( $n = 17$  synapses). In a study with a protocol essentially identical to the one used here, the percentage of photoconverted vesicles following 40 APs, 20 Hz stimulation in 3D reconstructed synapses was 5.36% (Schikorski and Stevens, 2001). This suggests that the loading in our 10 APs protocol was 32.7% smaller than in 40 APs stimulation as reported by (Schikorski and Stevens, 2001), which is strikingly similar to the value that we reported from the fluorescence readout (Fig.5.10).

While it may seem unlikely, it is possible to mistake photoconverted vesicles with other membranous structures with round appearance. Miscounting other vesicles for PC+ could contaminate the data, hence it is important to recognize and avoid structures which deviate from  $\sim 40$  nm diameter spheres. Endosomes and large core vesicles can be mistaken for photoconverted SVs (Fig.5.15.B). However, they are not as numerous as

SVs (Harata et al., 2001) and larger than SVs (large dense core vesicles: 80-120 nm (Harris and Weinberg, 2012); endosomes: 60-100 nm (Aravanis et al., 2003). Synapses were always screened for these bigger than SVs, rounded structures, and it was ensured that they were not included in the analysis.

The outcome of these two experiments, live cell imaging and ultrastructural analysis, provides good evidence for the robustness of the experimental and analysis approaches in our system.

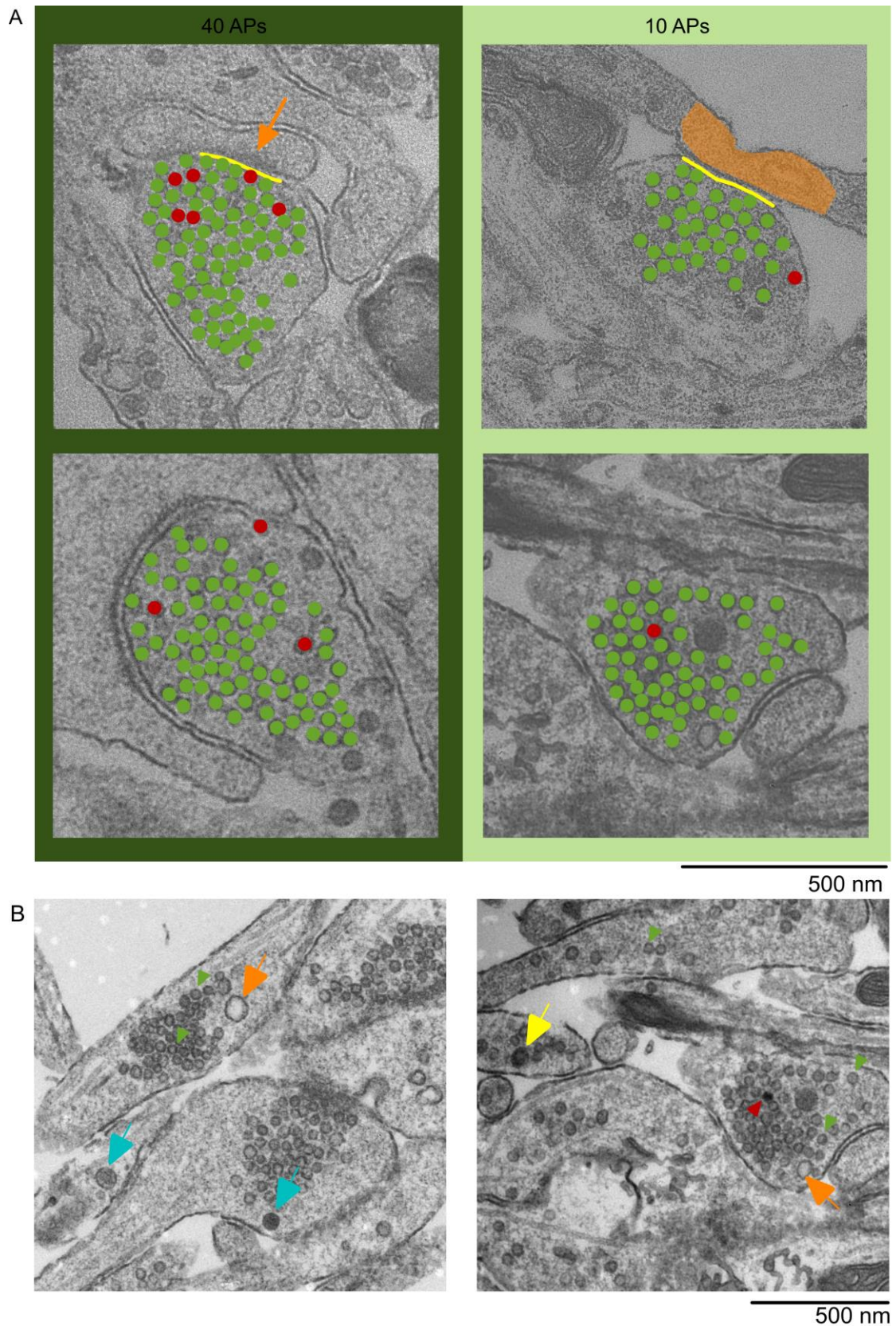


**Figure 5.15 Quantification of PC+ vesicles in 40 APs and 10 APs loaded samples.**  
 A) Representative electron micrographs of synapses from 40 APs and 10 APs loading samples. Orange shade marks postsynaptic region and orange arrow postsynaptic density, yellow line represents AZ, green dots were placed over PC- vesicles and red dots over PC+. Scale bar, 500 nm. B) Various types of vesicles present in presynaptic

terminals: non-photoconverted small synaptic vesicles (green arrowheads), photoconverted SV (red arrowhead), large clear vesicles (orange arrows), dense core vesicles (blue arrows), and electron-dense endosome (yellow arrow). Scale bar 500 nm.

#### 5.4.6 Ultrastructural correlates of synapse-specific behaviour

Being equipped with all the necessary tools, we can finally explore the ultrastructural characteristics of the synapses which exhibited signature functional profiles. Having identified in functional experiments that the size of the total vesicle pool correlated with endocytic kinetics, we wanted to confirm this at the ultrastructural level.

AAV.*sypHy2x* expressing neurons were imaged whilst being stimulated 9 x 4 APs, and detailed DIC images of the region of interest and its surrounding area were collected, in order to aid later relocation of the region as described in detail in section 5.4.3. The sample processing for TEM was carried out as described in Methods 2.12. The synapses for correlative analysis were chosen on the basis of a few criteria: similarity measure, endocytic kinetics, and size measured with *sypHy2x* baseline fluorescence. This ensured that we sampled a range of synapses with different properties. Nevertheless, due to technical reasons we only collected images for full reconstruction of 3 boutons. The 3D models of these synapses are shown in Fig.5.16.A and are accompanied by 1q fluorescence traces from these synapses. From the traces alone, it is apparent that the largest bouton (on the right) was characterized by the fastest vesicle retrieval kinetics. We plotted various functional and structural properties against each other in order to see whether there are any relationships between them. Although we are aware that 3 readouts are not enough to make any concrete conclusions, we decided to fit the points with a function, in order to obtain some indication as to whether various parameters show any signs of scaling together. Nevertheless, we would not have the confidence to

comment on the exact nature (linear or monotonic) of these relationships based on only 3 points.

First, one of the most important results that we were hoping to obtain here, was confirmation of whether sypHy2x baseline correlates with the actual presynaptic size. We saw a very clear positive scaling of the volume and the total number of vesicles with this fluorescence measurement (Fig.5.16.B and C), which further validated our previous attempts to show this (sections 5.2.1 and 5.2.2.2). Second, the established hypothesis, that small synapses might exhibit a much more crowded environment than in large synapses, as far as protein numbers are concerned (Wilhelm et al., 2014), made us hypothesise whether this might also be reflected in the density of the vesicles within boutons. The plot of the relationship of the number of vesicles in the bouton per volume, revealed an interesting result (Fig.5.16.D), which we decided to explore in more synapses (data shown in Fig.5.17). Last but not least, we wanted to explore whether the rate of endocytosis correlates with ultrastructural components. We checked whether in the synapses analysed, endocytic rate scaled with sypHy2x baseline fluorescence, as it had in our previous results (Fig.5.16.E). Although slightly scattered for these 3 synapses, the relationship was maintained. This evidently shows the need for more experiments, as in our larger data sets (Fig.5.1.D), this relationship was very clear. Surprisingly, however, the scaling of the rate with ultrastructural readouts, volume of the synapse and total vesicle count, was very clear (Fig.5.16.F and G). This confirms that the rate of endocytosis correlates with presynaptic properties, specifically, the volume of the bouton and the total number of synaptic vesicles, with larger synapses exhibiting a faster rate of endocytosis than the small synapses.

This data validated our observations from functional experiments regarding the relationship of endocytic retrieval with synaptic size, allowing us to unequivocally measure synaptic volume and the total number of synaptic vesicles. We also uncovered



a potentially interesting relationship between the number of vesicles per bouton and presynaptic volume, which we decided to explore further.

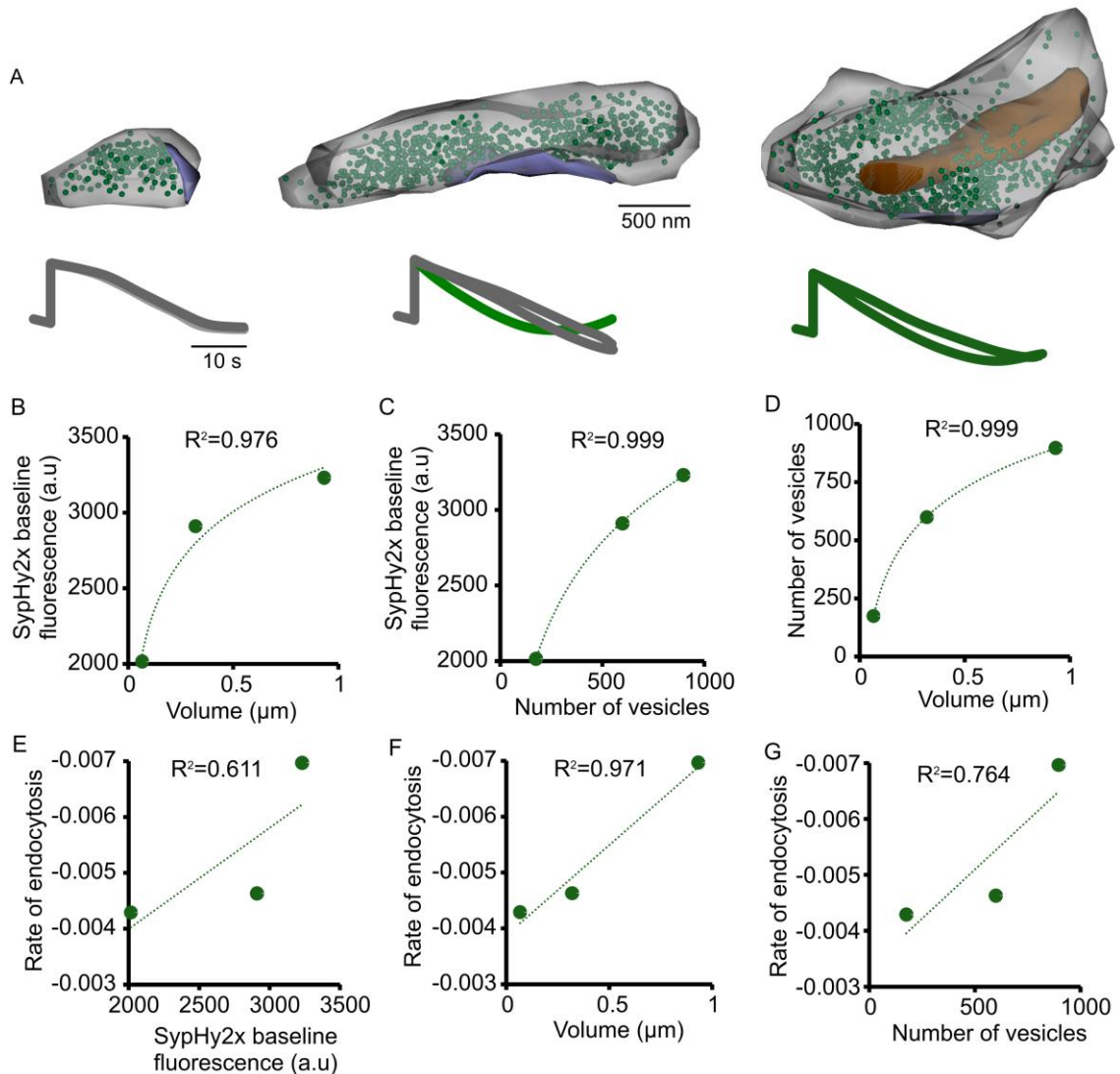


**Figure 5.16 Ultrastructural presynaptic properties that correlate with synaptic behaviour.** A) 3D reconstructions of the chosen terminals (top row). Green circles represent synaptic vesicles, purple area active zone and brown structure mitochondria, only present in the right bouton. Scale bar, 500 nm. Bottom row shows 1q responses from the reconstructed boutons. Grey and green profiles show responses with slower and faster kinetics, respectively. Scale bar 10 s. B-G) Graphs representing relationships between various functional and ultrastructural measurements: syphHy2x baseline fluorescence, volume, number of vesicles and rate of endocytosis. Plots B-D relate various measurements of the size, whereas plots E-G show relationship between the rate of endocytosis and size parameters.

#### **5.4.7 Difference in vesicle density between small and large synapses**

In the correlative TEM experiment, not only did we confirm our functional measurements, but we also uncovered another potential parameter that could influence the kinetics of single vesicle retrieval. In previous sections (5.2.1, 5.2.2.2, 5.2.2.3 and 5.2.2.4), we showed that larger synapses are characterized by a faster rate of endocytic retrieval following single vesicle release events. We reasoned that one possible explanation for this might be the density of synaptic vesicles within synapses.

High variability in vesicle density between synapses has previously been reported in reconstructed Ia presynaptic terminals from the ventral horn (Pierce and Mendell, 1993). Measurements of the total number of vesicles of cultured hippocampal neurons also showed high variability in the count between different synapses (Branco et al., 2010). Despite the fact that the size of the total pool has been previously linked with other structural parameters (Pierce and Mendell, 1993), very little attention has been paid to the effect of density of synaptic vesicles on presynaptic performance. It is important to bear in mind that the presynaptic terminal is a crowded environment with an average of 300,000 proteins per synapse (Wilhelm et al., 2014). Wilhelm et al., 2014, carried out a detailed analysis of the protein composition of hippocampal neurons and using synaptophysin fluorescence as a measure of size they made an interesting observation that small synapses contain more protein per volume than the large ones. This can be as a result of two things. One possibility is that small synapses may simply have a higher copy number of proteins. Alternatively, they could have a higher density of synaptic vesicles, and, resulting from this, a higher copy number of proteins. Our ultrastructural analysis provides us with the opportunity to directly test this using three dimensional reconstructions of hippocampal boutons. We reasoned that a higher density of vesicles, and associated proteins could serve as a spatial hindrance within smaller boutons, contributing to their slower rate of endocytosis in comparison to the large synapses.



In order to accurately measure the density of vesicles within presynaptic volume, we had to set out clear rules for demarcating the boundary of vesicles within the bouton versus those belonging to the axon. We therefore classified vesicles into two groups: i) intrasynaptic vesicles were within the main cluster of vesicles at each synapse, they were in close proximity to each other, and they demarcated the boundary of the presynaptic compartment; ii) extrasynaptic vesicles were the axonal vesicles, away from the main cluster, and, if that distinction was ambiguous, they had to be separated from the intrasynaptic cluster with a distance equivalent to 3 vesicles diameter (Fig.5.17. A and B). The boundary of the bouton area was either established on the basis of the presence of the membrane, or in the case of much wider or unclear ultrastructural boundaries, ~100-120 nm away from the outermost vesicles in the intrasynaptic cluster. The total number of vesicles and the synaptic volume were measured in Reconstruct in fully reconstructed terminals. The analysis revealed a monotonic relationship ( $R^2 = 0.935$ ; linear fit for comparison:  $R^2 = 0.677$ ) between the number of vesicles and synaptic volume ( $n = 18$  3D reconstructed synapses. Spearman correlation test,  $r = 0.963$ ,  $P < 0.0001$ ) (Fig.5.17.C and D), indicating that SVs are less densely packed in large synapses than in the small ones. It may well be that the results were driven by one significantly larger bouton. Nevertheless, when this synapse was excluded from the analysis as an outlier the outcome was still the same ( $n = 17$  3D reconstructed synapses. Spearman correlation test,  $r = 0.9559$ ,  $P < 0.0001$ ). This suggests that the number of vesicles does not scale linearly with the synaptic volume, instead, large boutons are characterized by fewer vesicles per volume than the small ones, which may contribute to their more efficient recycling kinetics.

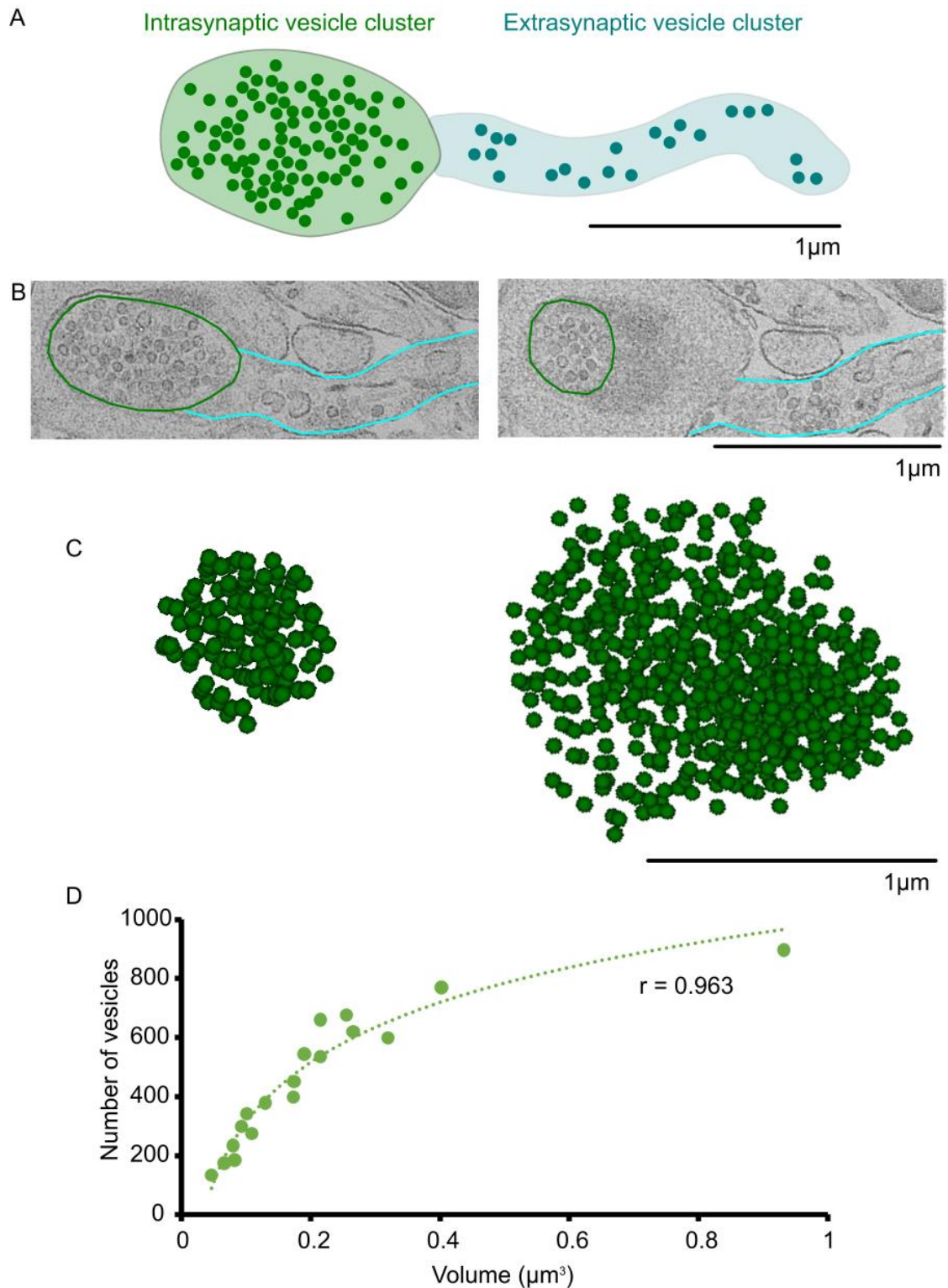


**Figure 5.17 Small and large synapses differ in the density of synaptic vesicles.** A) Example shows vesicles identified on a basis of single sections from the same region. Vesicles from intrasynaptic cluster show much higher density than extrasynaptic vesicles. Scale bar 1  $\mu\text{m}$ . The boundary of the intrasynaptic cluster was assigned based on the outermost vesicles that were within 3 vesicles width away from the main cluster. The boundary for presynaptic volume calculation was drawn within 2 vesicles width from the outermost vesicles in the cluster or if closer, within the ultrastructural boundary of the

synapse. B) TEM images of 2 consecutive section with green lines indicating the area considered for volume analysis and blue lines marking processes with extrasynaptic vesicles. Scale bar 1  $\mu\text{m}$ . C) 3D reconstructions of small (left) and large (right) synapses. Scale bar 1  $\mu\text{m}$ . D) Very strong positive monotonic correlation between the total number of intrasynaptic vesicles and the volume of presynaptic terminal. (Spearman correlation test,  $n = 18$  3D reconstructed synapses,  $r = 0.963$ ,  $P < 0.0001$ ).

## 5.5 Discussion

The functional properties of small central synapses such as release probability, quantal size or plasticity, vary greatly between individual boutons. Underlying this variability must be differences in the structure between synapses such as shape, size, vesicle pool sizes and molecular composition of individual boutons. Nevertheless, there is still limited information on how the behaviour of individual boutons is shaped by their properties. The aim of this chapter was to explore the properties of individual presynaptic terminals that dictate their endocytic behaviour. We successfully identified structural and molecular correlates of the rate of endocytosis at individual boutons.

### 5.5.1 Synaptic size determines presynaptic properties

The efficacy of presynaptic performance has been previously linked with the size of the boutons (Branco et al., 2010; Welzel et al., 2011). We therefore hypothesized that synaptic size might also determine the timing of the retrieval of synaptic vesicles. Firstly we examined whether sypHy2x baseline fluorescence can be used as a measure of synaptic size. Loading synapses with sytI-Oyster550 antibody revealed that the size of the recycling pool correlated with sypHy2x baseline fluorescence, indicating that these parameters were linked and that sypHy2x baseline can be used as a measure of synaptic size. Nevertheless, both these readouts are based on the amount of proteins, synaptotagmin I and synaptophysin, at individual synapses and this result might therefore reflect the relationship in the ratio between the two proteins rather than the

synaptic size per se. However, the correlative TEM experiment confirmed that sypHy2x baseline reflects the overall synaptic volume (section 5.4.6).

Our analysis showed that the kinetics of endocytosis at individual synapses correlated well with their size: larger synapses exhibited faster rates of endocytosis, whereas smaller synapses showed slower kinetics of vesicle retrieval. Next, we explored this result in depth looking for more specific correlates. Is it the overall synaptic volume or perhaps the size of the recycling pool or recycling pool fraction that dictates the endocytic kinetics? The size of the recycling pool has been previously linked with the kinetics of exocytosis at hippocampal synapses (Welzel et al., 2011). Boutons with a larger recycling pool showed slower kinetics of exocytosis measured with FM1-43 (Welzel et al., 2011). However, another study showed that the kinetics of exocytosis was not related to the recycling pool fraction size (Fernandez-Alfonso and Ryan, 2008). We therefore tested whether it is the total pool size, recycling pool size or the recycling fraction, or a combination of these that contribute to the recycling kinetics.

We saw a strong positive correlation between the rate of endocytosis and the size of the total vesicles pool, but there was only moderate correlation between the endocytic rate and the recycling pool. This might appear very surprising considering the fact that the recycling pool scales well with the total vesicle pool. The measurement of the recycling fraction in this study ( $48\% \pm 0.018$ ) corresponds well with previously reported values in the literature (50.3%, 50% and 49% in Kim and Ryan, 2010; Fernandez-Alfonso and Ryan, 2008 and Ratnayaka et al., 2012, respectively). The analysis of the recycling fraction against the total pool size revealed that this parameter is highly variable across synapses. A similar observation was previously made in other studies (Branco et al., 2010; Fernandez-Alfonso and Ryan, 2008; Harata et al., 2001; Marra et al., 2012). This therefore explains the poorer correlation between the endocytic kinetics and the recycling pool or the recycling pool fraction. We explored this further in our homeostatic scaling data.

### **5.5.1.1 Rate of endocytosis scales with synaptic size**

Presynaptic properties such as vesicle trafficking or synaptic strength have been shown to be regulated in order to sustain neurotransmission and to respond and adapt to the levels of changing network activity (Murthy et al., 2001; Turrigiano, 2011; Virmani et al., 2006). In order to further validate our findings on the correlation between synaptic size and vesicle endocytosis we decided to silence synapses for 3 days using CNQX, an AMPA/kainate blocker. This type of silencing induces disuse hypersensitivity and leads to both pre- and postsynaptic changes. Although the mechanisms of this are not fully understood, changes in presynaptic parameters, such as sizes of synaptic vesicle pools, induced by this form of silencing, have been reported (Kim & Ryan, 2010; Murthy et al., 2001).

In an experiment blocking postsynaptic activity by incubating hippocampal cell culture for 2 days with 10  $\mu$ M NBQX Murthy et al., 2001, observed that multiple presynaptic parameters scaled together: total vesicle pool size, synaptic volume, number of docked vesicles and active zone area. These results suggest that although an overall increase in the synaptic size was observed, the relationships between variables were maintained with disuse hypersensitivity. In our study, we observed an increase in the total vesicle pool size accompanied by a decrease in the recycling fraction in CNQX-treated cells. Nevertheless, when synapses of the same size were being compared the recycling fraction in the CNQX group was significantly larger than the control. At first glance this seem like a contradicting result, but we found that the reason for this might be an important presynaptic property. Our investigation showed that small synapses have larger recycling fractions than the larger boutons. It has been previously reported that a larger recycling pool in synapses was associated with a smaller fraction of the RRP, than in those synapses with small recycling pools (Welzel et al., 2011). In a comparable experiment to ours, Fernandez-Alfonso and Ryan, 2008. used the alkaline trapping method with a spH reporter and saw conflicting results. In one experiment, larger

synapses had smaller recycling fraction than the small synapses, whereas the opposite was observed in another experiment, with an extremely slight tendency for the larger synapses to have a larger recycling fraction (Fernandez-Alfonso and Ryan, 2008). The authors did not comment on the discrepancy of their data. A tendency, although not statistically significant, for small synapses to exhibit larger recycling pool fraction than large synapses, can be observed in results from ultrastructural analysis of recycling vesicles (Marra et al., 2012). Our results showing that larger synapses have smaller recycling fraction explain why CNQX-treated synapses, which were larger in terms of their total vesicle pool size, had smaller recycling fractions than the control data. On the other hand, CNQX treated synapses of the same size as the control group exhibited an even larger recycling fraction than the control synapses, indicating that the modulation not only increased the overall size of synapses, but also the recycling fraction in smaller synapses. In this sense, our results are consistent with the study by Murphy et al., 2001, but also with Kim and Ryan, 2010, who showed an increase in the recycling pool size following silencing with TTX. Having established that our modulation worked, we showed that the rate of endocytosis did not scale with the increase in the recycling pool fraction but was correlated with the total vesicle pool size.

How can the total vesicle pool size influence the kinetics of endocytosis? We explore this question further in the sections of this discussion devoted to the results of endophilin I labelling experiment and TEM results, and in the general discussion.

#### **5.5.1.2 Larger synapses exhibit higher variability in their properties**

Larger synapses not only exhibited a faster rate of endocytosis but also potential for greater variability in the retrieval kinetics at individual synapses. From our WSS measurement we found that large synapses can show very similar patterns of single vesicle retrieval kinetics over multiple trials or very variable ones. This suggests that the

regulatory mechanisms and endocytic machinery are not as tightly controlled in large synapses as they are in the small synapses, which show more conserved behaviour over time. If that is the case, the molecular composition of large synapses is likely to reflect this. We tested this hypothesis by measuring the level of one of the most important proteins for endocytosis – endophilin I.

Firstly, however, we sought to determine whether the endocytic kinetics difference between small and large synapses could be explained by varied amounts of endocytic protein present at these synapses. Antibody staining revealed varied expression of important vesicular proteins such as SV2, synaptophysin and synaptotagmin 1 between individual sympathetic varicosities in mice (Knight et al., 2005). A detailed analysis of proteomics of presynaptic terminals revealed that not all the proteins scale linearly with synaptic size measured as the amount of synaptophysin (Wilhelm et al., 2014). We identified endophilin I as a possible target protein responsible for the differences in kinetics between synapses. Endophilin I was found to recruit and stabilize synaptojanin, an important protein involved in triggering clathrin uncoating (Schuske et al., 2003), and more importantly in knock out experiments in mice to be a positive regulator of retrieval kinetics (Milosevic et al., 2011), and of exocytosis (Weston et al., 2011). Our results showed that endophilin I does not scale linearly with synaptic size. Despite the fact that it would be expected that large synapses have more protein than the small ones, large synapses had double the endophilin I than would be expected from the proportional increase of the two variables: endophilin I and size. In other words, we found that large synapses have up to twice as much of this protein than the small synapses when the two measurements are expressed as a function of size. This difference in abundance of endophilin I could be one of the factors contributing to the overall faster endocytic retrieval that we observed at larger boutons.

Not only did we see that larger synapses, proportionally to size, have more endophilin I, but we also observed that the variability in the amount of this protein is considerably

higher in larger boutons. This can offer an explanation of the higher variability in endocytic kinetics within large boutons. Let us assume two situations: a large synapse with little endophilin I and a large synapse with an abundance of endophilin I. Most of this protein is associated with SVs from which it is unbound in an exocytosis-dependent manner, and delivered to the endocytic zones (Bai et al., 2010). It is therefore possible that in large synapses with little endophilin I, the time taken for this protein to be delivered to the endocytic site might be more variable in the consecutive endocytic rounds than in a large synapse where this protein is more abundant. Thus, availability of endophilin I could make the retrieval kinetics across multiple trials more similar and consequently lower the WSS value at large synapses with an abundance of endophilin I in comparison to large synapses with less endophilin I.

This raises the question of how the amount of protein might be regulated at individual synapses. Despite the fact that the roles of many proteins involved in endocytosis, as well as their interactions, have been identified, protein sorting and recycling at presynaptic terminals still remains largely unclear. Nevertheless, a variability in the amount and composition, of exocytic proteins between synapses has been previously reported (Knight et al., 2005). It was hypothesized that this variability might be one of the factors underlying the strength of individual synapses (Knight et al., 2005). It is therefore possible that the amount of endophilin I is regulated locally, based on the strength of a given synapse. Also, hippocampal synapses are extremely plastic with synapse-specific structural changes that occur on a timescale of minutes and affect functional properties of individual boutons such as  $p_r$  (Matz et al., 2010). Perhaps the large synapses with higher functional variability or low endophilin I levels reflect the boutons that are undergoing plasticity.



### **5.5.2 Timing of endocytic kinetics is determined by the fission of the vesicles from the membrane**

The question unresolved so far is whether the variability in the kinetics of fluorescence decay reported with sypHy2x (Chapter 4) is due to different timing of vesicle retrieval between boutons or reacidification kinetics. Rapid quenching of the surface fluorescence with acid has been used to isolate the kinetics of these two processes (Atluri and Ryan, 2006). Nevertheless, this technique was not applicable in our system. It has been estimated with this method that reacidification kinetics were very consistent at 4-5 s following 40-300 APs, 10 Hz stimulus (Atluri and Ryan, 2006). Shorter reacidification time has been reported following single vesicle release events (Gandhi and Stevens, 2003). However, no data was given by these authors that would allow us comment on the variability of this process between synapses. Nevertheless, following their observation of variability in retrieval timing, Gandhi and Stevens, 2003, attributed this variability to the time taken by the endocytic machinery to assemble at the retrieval site. We hypothesized that we can test this by blocking dynamin function at sub-optimal level, which will unify the kinetics of endocytic retrieval across the population of synapses. Using dynasore, we manipulated synapses into behaving in a uniform way and eradicated synapse-specific features of the fluorescence decay, making all the retrieval events at individual synapses more similar to the population of synapses. This demonstrates that the variability in vesicle retrieval is due to differences in the time taken to assemble the endocytic machinery at different synapses, and due to the timing of fission of the vesicles from the membrane.

It is not only the protein composition that may affect synaptic performance (as discussed above), but also lipid composition. Plasma membrane is composed of a variety of different phospholipids, sphingolipids and sterols which will confer various characteristics on the membrane (Rohrbough and Broadie, 2005). The composition of the membrane can influence SVs exo- and endocytosis by regulating membrane fluidity and curvature

(Rohrbough and Broadie, 2005), and by doing so, affecting the function of curvature-sensing proteins such as endophilin I. Moreover, these lipids organize into functional domains called lipid rafts, which many synaptic vesicle proteins have been shown to associate with (Sebastião et al., 2013). For example, endophilin I has been shown to interact with phospholipids before recruiting synaptojanin, which is important for uncoating of newly formed SVs (Kononenko and Haucke, 2015; Schuske et al., 2003). Depletion of PI(4,5)P<sub>2</sub> from neuronal membranes led to accumulation of clathrin-coated pits at the surface (Posor et al., 2013), confirming the importance of protein-lipid interactions. Unlike the modulation of dynamin function with dynasore, which unified all the responses, we hypothesized that disruption of lipid rafts would have the opposite effect, and would increase variability within individual synapses and within the population. Preliminary experiments using methyl- $\beta$ -cyclodextrin (M $\beta$ CD), a drug which extracts cholesterol from the membrane, were performed. M $\beta$ CD was previously shown to impair endocytosis in rat Calyx of Held but it was also found to reduce exocytosis (Yue and Xu, 2015), which we also observed in our system, and further optimization of the experimental conditions would be needed.

### **5.5.3 Density of synaptic vesicles in synapses of various sizes**

Our correlative light-electron microscopy analysis, allowed us to unequivocally verify using sypHy2x baseline fluorescence as a measure of synaptic size. We also showed that the rate of endocytosis increases with synaptic volume and the total number of vesicles, which again strengthens our results from functional data. From this data, we also discovered an interesting relationship between the volume of the boutons and the density of SVs. Further analysis revealed that the density of SVs at large synapses was smaller than in small synapses, which could contribute to the reason for smaller synapses being characterised by slower rates of endocytosis than large ones.

Presynaptic terminals are extremely crowded cellular compartments with hundreds of thousands of proteins interacting together, creating exceedingly efficient machinery.

Detailed analysis of the absolute copy numbers of presynaptic proteins revealed that small synapses contain proportionally more proteins than large synapses (Wilhelm et al., 2014). This could imply that small synapses should be more efficient in their function. However, presumably, it could also work in the opposite way, creating a very crowded environment, which could actually impede effective presynaptic function.

We hypothesized that this higher protein concentration could be caused by a higher density of SVs in small terminals in comparison to the large ones. The size of the measured synapses in our study is highly comparable with the previously reported volume for hippocampal boutons (0.12 to 0.54  $\mu\text{m}^3$ ) (Harris and Sultan, 1995; Yang et al., 2005). Our analysis of 3D reconstructions revealed that the density of SVs does not scale linearly with synaptic volume and that larger synapses are characterized by a lower SV density than small ones. What mechanism could lead to higher SVs density at smaller synapses? It has been shown in an *in vivo* study in *Drosophila* that mechanical tension promotes actin polymerisation which stimulates vesicle clustering at presynaptic terminals of neuromuscular junction (Siechen et al., 2009). Importantly, the opposite was also true: the release of tension led to actin depolymerisation which could lead to dispersion of the vesicle cluster (Hirata et al., 2008; Siechen et al., 2009). The authors concluded that the application of stretch led to tension build-up in the membrane, which in turn promoted actin polymerisation and vesicle clustering (Siechen et al., 2009). It might be therefore possible that the cytoskeletal and membrane forces in small and large synapses are different and therefore lead to various levels of actin polymerisation and lower or higher densities of vesicle clustering. Moreover, actin polymerisation was shown to be increased in hippocampal cultures following intensive stimulation (Colicos et al., 2001). Perhaps the release of a synaptic vesicle, and the following endocytosis in small synapses, brings about bigger changes in membrane tension, and therefore to increased actin polymerisation and denser vesicle clustering as observed in our experiment.

#### 5.5.4 Concluding remarks and future directions

The results presented in this chapter point towards an enormous complexity in the factors influencing presynaptic behaviour. Nevertheless, we identified structural properties that determine endocytic kinetics at individual boutons. We confirmed that the kinetics of retrieval of single synaptic vesicles scales with synaptic size, and we identified precise correlates of endocytic behaviour, including: the total number of vesicles, the presynaptic volume and the amount of endophilin I. All these properties might be shaped by the precise role a given synapse has in the network, and might be substrates for the expression of plasticity associated changes. Future experiments in relation to this, could involve examining the similarity measurements in synapses that had undergone plasticity. If consistency of endocytic behaviour at individual synapses somehow confers functional advantages, or if it is associated with the strength of the synapse, then induction of LTP might be expected to result in a more unified behaviour, across all the boutons. More detailed correlative investigation of ultrastructural-functional properties such as overall synaptic shape, size and position of active zone, number of docked vesicles, and position and number of vesicles recently recycled in the presence of FM dye, could reveal more parameters underlying the basis of the operation of individual boutons. A direct correlation of the level of endophilin I with the behaviour of individual boutons, would also allow us to further verify claims made here regarding the interplay between synaptic size, the amount of endophilin I and the level of similarity in the behaviour of consecutive recycling vesicles at individual synapses. As mentioned earlier in the discussion, manipulation of the constituency of lipid rafts would also be interesting, and it would provide us with another line of enquiry as to what aspects of presynaptic structure affect similarity.

In Chapter 7 we propose a model summarizing the regulation of the endocytic kinetics following single vesicle exocytosis.

## 6 THE EFFECTS OF AMYLOID BETA 1 - 42 ON FUNCTION OF PRESYNAPTIC TERMINALS

---

### HIGHLIGHTS

24 hour treatment with 1  $\mu$ M A $\beta$  1-42 leads to:

- Reduced density of functional synapses
- Impairment in the kinetics of exocytosis during medium and large stimulation trains
- An increased number of vesicles being released in response to small and medium stimulation
- Reduced rate of endocytosis following medium stimulation but does not affect the endocytosis of single synaptic vesicles
- Larger Ca<sup>2+</sup> influx in response to small and medium stimulation
- Larger Ca<sup>2+</sup> influx during repeated stimulation trains in comparison with the controls

## 6.1 Introduction

Alzheimer's disease (AD) is a leading cause of dementia in the elderly, affecting a significant proportion of the population over 65 years of age. The cost of care for the patients in the UK alone, exceeds £26 billion per annum (Alzheimer's society, 2016). Despite huge research efforts, the available drugs, such as acetylcholinesterase inhibitors, offer only symptomatic treatment, with limited effectiveness and common side effects (Galimberti and Scarpini, 2011). Recent therapeutic developments, attempting to halt the disease with encouraging results in animal experiments should be treated with caution as most of them failed to show efficacy at the level of clinical trials (Amanatkar et al., 2016; Davtayan et al., 2016; Karran and Hardy, 2014). The pathogenesis of AD has been strongly linked with the loss of synapses and synaptic dysfunction due to accumulation, and toxicity exerted by A $\beta$  peptide (Murphy and LeVine III, 2010). However, it is not fully understood how this protein leads to synaptic dysfunction and eventually to synaptic degeneration. The postsynaptic mechanisms of A $\beta$  toxicity have been studied in more depth (Hsieh et al., 2006; Renner et al., 2010) in comparison to the presynaptic changes induced by this protein, which will be explored in this work.

Following the first description of the symptoms and the accompanying brain pathology by Alois Alzheimer, the plaques and neurofibrillary tangles he associated with the disease have later been found to contain fibrillar A $\beta$  and hyperphosphorylated tau, respectively (Karran et al., 2011). A $\beta$  is generated by two sequential enzymatic cleavages of amyloid precursor protein (APP) by  $\beta$ -secretase 1 (BACE1) and subsequently by  $\gamma$ -secretase to produce either a 40 or 42 amino acid long A $\beta$  peptide (Pimplikar, 2009). A $\beta$ 1-40 and A $\beta$ 1-42 have been shown to form aggregates of various sizes ranging from small soluble oligomers to larger oligomers, protofibrils and fibrils (Sakono and Zako, 2010). Over the years the consensus as to which is the most toxic A $\beta$  species has changed. Soluble oligomers have been attributed to an extensive range

of cytotoxic effects (Soura et al., 2012) and in the last decade the belief has emerged that they are the major cause of AD pathology (Bieschke et al., 2012; Sakono and Zako, 2010). In human brain samples, the severity of synaptic pathology was strongly correlated with the abundance of soluble A $\beta$ 1-40 and A $\beta$ 1-42, but not the fibrillar form of this protein (Lue et al., 1999). A $\beta$ 1-42 is considered to be the more toxic peptide in comparison to 40 amino acid long A $\beta$ , and it is also thought to have a higher propensity to form toxic oligomers (Walsh and Selkoe, 2007). We therefore chose to carry out our study using small oligomeric A $\beta$ 1-42.

A $\beta$  has been found to have a profound effect on synaptic function, affecting a wide range of synaptic properties. Some of the known, reproducible effects of A $\beta$  on postsynaptic function include: i) impairment of long-term potentiation (Lambert et al., 1998; Walsh et al., 2002) and induction of long term depression mediated by AMPA-R internalization (Sheng et al., 2012); ii) NMDA-Rs dependent overproduction of reactive oxygen species (ROS) and dendritic spine loss (De Felice et al., 2007; Shankar et al., 2007); iii) blockade of inhibitory postsynaptic potentials by inducing GABA<sub>A</sub> receptor internalization (Ulrich, 2015). Other sites of toxicity involve stimulation of mitochondrial apoptotic pathway, impaired cellular metabolism and disrupted Ca<sup>2+</sup> signalling (Sheng et al., 2012). These results show a widespread detrimental effect of A $\beta$  on neuronal homeostasis.

Despite the fact that the presynaptic effects of A $\beta$  have not been extensively examined, there is some indication in the literature of A $\beta$ -induced disturbance in the function of this compartment (Kelly and Ferreira, 2007; J. Park et al., 2013). Nevertheless, it is difficult to draw concrete conclusions regarding the effect of A $\beta$  due to differences in the peptide used (A $\beta$ 1-40 versus A $\beta$ 1-42), concentration and incubation timing in different studies. Here follows a summary on the current knowledge of presynaptic changes induced by A $\beta$ .

It has been demonstrated that the treatment of hippocampal neurons for 24 h with a mixture of fibrillar and oligomeric synthetic A $\beta$ 1-40 (2  $\mu$ M) led to an endocytic deficiency in neurons stimulated with high potassium (90 mM K<sup>+</sup>) (Kelly and Ferreira, 2007). However, this type of stimulation does not allow for precise control of the level of release (Ryan and Smith, 1995). Similar observations were made in another study using hippocampal neurons employing more defined stimulation paradigm. In this case, the cells were incubated with 0.2  $\mu$ M A $\beta$ 1-42 for 2 h (J. Park et al., 2013), a tenfold lower concentration and significantly shorter incubation time than in the other study (Kelly and Ferreira, 2007). Stimulation with 600 APs at 20 Hz led to a significant decrease in the rate of endocytosis measured with vGpH (J. Park et al., 2013) and a longer incubation time (72 h) led to even greater deficit in endocytic timing (J. Park et al., 2013). Despite their experimental differences both studies observed impairment in endocytosis following treatment with A $\beta$ . It was also observed that the size of the resting pool increased in A $\beta$ 1-42 treated cells at an expense of the recycling pool fraction (J. Park et al., 2013). However, the effects of A $\beta$  were explored at large, non-physiological stimulation levels (600 APs at 20Hz). In this study, we exploited the sensitive imaging approaches we developed in previous chapters, to test the toxicity of A $\beta$  at a range of different stimuli, so that we could investigate whether the level of activity influences the functional disturbance caused by this peptide.

Other deleterious effects of A $\beta$  for presynaptic function include: i) disruption in the formation of functionally important presynaptic protein complexes (Russell et al., 2012); ii) disturbance in the function of synaptic mitochondria (Reddy and Beal, 2008); iii) perforation of neuronal membranes (Peters et al., 2014); iv) disruption of the integrity of lipid rafts and proteins associated with it (Rushworth and Hooper, 2010). The disturbance in lipid rafts can be especially damaging for efficient presynaptic function. Proteins such as VAMP2, syntaxin 1A, Munc18, SNAP-25, synaptotagmin and synaptophysin, which are important for synaptic vesicle recycling, have been shown to interact with these



cholesterol-rich domains at the plasma membrane (Chamberlain et al., 2001; Sebastião et al., 2013).

The difficulty in comparing and relating published studies not only comes from the differences in the concentration and the incubation time of the A $\beta$ , but also from the differences in the method used for preparation of the A $\beta$  and the type of the control used (Gilson et al., 2015; J. Park et al., 2013; Peters et al., 2014; Yu et al., 2010). The A $\beta$ 1-42 used in this study was prepared in the same way as described in Marshall et al., 2016 (modified method from Soura et al., 2012) which ensures the presence of small oligomeric A $\beta$ 1-42 species. It is also important that the solvents used during preparation of the peptide, HFIP and DMSO, are removed, as they themselves can be toxic to cells (Soura et al., 2012) or influence the rate with which A $\beta$ 1-42 forms aggregates (Broersen et al., 2011). Some authors do not report taking crucial steps to remove these solvents, which makes the validity of their interpretation of the results ambiguous, and raises the possibility of false positive results.

One of the major limitations of studies using exogenously applied A $\beta$  is the lack of suitable control. The use of reversed, scrambled or rodent A $\beta$ 1-42 has been previously reported, nevertheless, the structural, assembly and toxicity information on these peptides is not available (Marshall et al., 2016). A recently developed vA $\beta$ 1-42 peptide, which differs in only 2 amino acids from A $\beta$ 1-42, offers a new solution to this problem (Marshall et al., 2016). Unlike A $\beta$ 1-42, vA $\beta$ 1-42 did not form oligomers and had no effect on the viability of hippocampal neurons, making it the most suitable control available (Marshall et al., 2016).

Considering the fact that current therapeutic approaches have failed to halt the disease and only offer some symptomatic relief, it is important to further explore mechanisms of A $\beta$  toxicity. As described above, the effects of A $\beta$  on the function of presynaptic terminals

have not been extensively investigated, despite the fact that this structure is critical for the maintenance of effective neurotransmission. We therefore wanted to explore whether A $\beta$  has an effect on crucial parameters of presynaptic performance: exocytosis and endocytosis of synaptic vesicles and stimulus-evoked Ca<sup>2+</sup> influx, this will further expand our knowledge on the A $\beta$ -induced synaptic pathology, and potentially allow us to identify novel treatment targets. We also validated whether recently developed vA $\beta$ 1-42 (Marshall et al., 2016) has an effect on presynaptic function and therefore, whether it is a suitable control for functional studies in hippocampal neurons.

## **6.2 FM dye imaging of cells treated with 1 $\mu$ M A $\beta$ 1-42 for 24 hours**

### **6.2.1 The effect of A $\beta$ 1-42 on the number functional presynaptic terminals**

One of the clinical representations of AD is the loss of neurons, preceded by the loss of synapses (Scheff et al., 2006). Before embarking on a detailed analysis of A $\beta$ 1-42 effects on presynaptic function, we wanted to test whether our oligomeric A $\beta$ 1-42 preparation has any effect on synapses in hippocampal cell culture. The toxicity of A $\beta$ 1-42 would be manifested in lower number of synapses recruited during the stimulation. We also wanted to establish whether, similarly to A $\beta$ 1-42, vA $\beta$  leads to synaptic loss and therefore whether it is a suitable control.

Cells were treated for 24 h with 1  $\mu$ M A $\beta$ 1-42, 1  $\mu$ M vA $\beta$  or a corresponding volume of HEPES based buffer, which was used for the preparation of the two peptides (for protocol refer to section 2.14). The concentration of A $\beta$ 1-42 used here was tenfold lower than in toxicity experiments carried out on the same system by Dr Karen Marshall (Marshall et al., 2016). This ensured that the amount of A $\beta$ 1-42 added and the incubation timing didn't

primarily induce cell death, but led to functional disturbances. The experimenter was blind to the treatment protocol whilst carrying out the experiments and during the analysis. In order to investigate the effects of A $\beta$ 1-42 and vA $\beta$  on the synaptic homeostasis we used FM1-43. Recycling vesicles in treated neurons were subjected to field stimulation (1200 APs at 20 Hz) in the presence of FM-dye (loading protocol summarized in Fig.6.1.A). The labelling procedure was similar to the protocol explained in section 2.8 and 3.2.2. FM1-43 dye was applied to the cell culture, after 1 min of incubation with the dye, then 1200 APs 20 Hz stimulus was delivered in order to label all recycling vesicles. To allow for endocytosis to complete, cells were left for 2 min in the presence of the dye, following which the dye was washed out. Representative images of loaded regions were collected from multiple coverslips for each condition (Fig.6.1.B).

In order to quantify the number of functional synapses that responded to the delivered stimulation, the ImageJ isodata thresholding algorithm was applied on raw, non-filtered maximum intensity projections (4 x 0.5  $\mu$ m image stacks). The number of ROIs identified from the thresholding was summarised for the treatment groups. The results showed that A $\beta$ 1-42 led to a significant decrease in the number of functional synapses recruited during the applied stimulation in comparison to vA $\beta$  or buffer treated cells (n= 20, 30 and 30 images for A $\beta$ 1-42, vA $\beta$  and buffer treated, respectively. Kruskal-Wallis one-way ANOVA with Dunn's multiple comparison test: A $\beta$ 1-42:vA $\beta$ , P = 0.0074; A $\beta$ 1-42:buffer treated, P < 0.0001), whereas there was no difference between the cells incubated with vA $\beta$  and the buffer treated cells (n = 20, 30 and 30 images for A $\beta$ 1-42, vA $\beta$  and buffer treated, respectively. Kruskal-Wallis one-way ANOVA with Dunn's multiple comparison test: vA $\beta$ : buffer treated, P = 0.235) (Fig.6.1.C). These findings are in line with previous work indicating that oligomeric A $\beta$ 1-42 is associated with a loss of functional synapses (Kelly and Ferreira, 2007; Shankar and Walsh, 2009). The results also validate the use of vA $\beta$  as a control in our system.

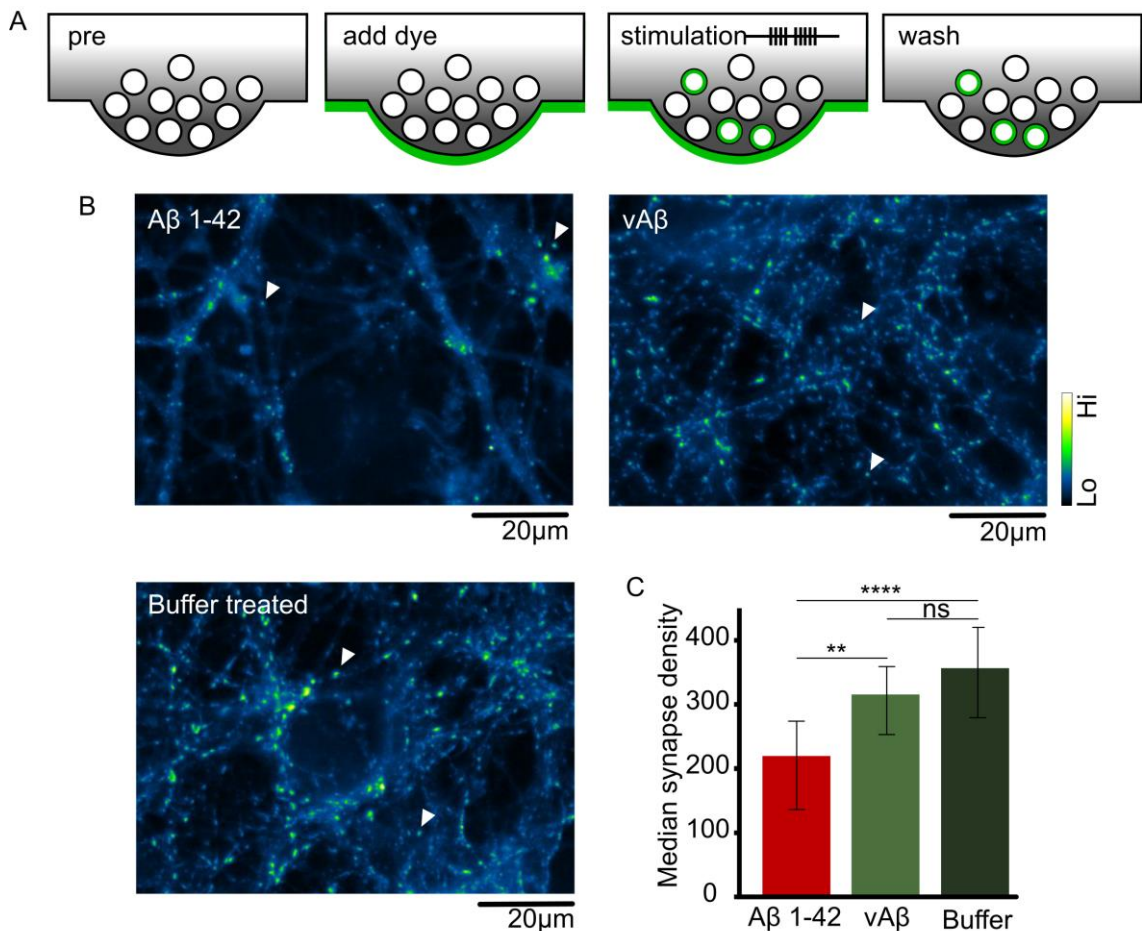


**Figure 6.1 Quantification of functional boutons in Aβ1-42 treated cells.** A) Summary of FM1-43 loading protocol, described in details in Fig 3.2.A. B) Representative images of Aβ1-42 (top left), vAβ (top right) and buffer treated neurons (bottom left), loaded with FM1-43 dye (1200 APs at 20 Hz). Examples of discrete functional terminals are indicated by white arrowheads. Scale bar 20 μm. C) Quantification of the number of functional terminals in the treatment groups. Data showed as media ± IQR (Aβ1-42: 218 IQR 134-273, vAβ1-42: 315 IQR 253-359, buffer: 355 IQR 278-420, n = 20, 30, 30 images, respectively; Kruskal-Wallis one-way ANOVA,  $P < 0.0001$  with Dunn's multiple comparison test: Aβ1-42:vAβ,  $P = 0.0074$ ; Aβ1-42:buffer treated,  $P < 0.0001$ ; vAβ:buffer treated,  $P = 0.235$ ). Figure modified from Marshall et al., 2016, data collected and analysed by Milena Maria Wagner.

## 6.2.2 The effect of Aβ1-42 on synaptic function

FM1-43 not only permits a readout of the number of functional boutons, but also provides information on the behaviour of synapses. In particular, it allows to measure the kinetics of exocytosis during activity-driven FM1-43 dye-loss. Cells loaded with FM1-43 (1200 APs at 20 Hz) were stimulated with 1200 APs at 20 Hz in order to release all recycling

vesicles (Fig.6.2.A). Boutons responding to the stimulation were identified by subtracting the images before and after the destaining. ROIs ( $2.1 \times 2.1 \mu\text{m}$ ) were drawn around fluorescence puncta. Firstly we looked at the % dye loss in each treatment group. In order to quantify this, the background fluorescence was subtracted for each ROI. Traces were normalised to the baseline fluorescence before the stimulation (average of 5 frames) and the average of the last 5 imaging frames was used to calculate the % destaining. We found that the level of dye-loss was significantly less in A $\beta$ 1-42 treated cells than in vA $\beta$  or buffer alone conditions, which were markedly similar to each other ( $n = 218, 428$  and  $560$  synapses for A $\beta$ 1-42, vA $\beta$  and buffer treated, respectively. Kruskal-Wallis one-way ANOVA with Dunn's multiple comparison test: A $\beta$ 1-42:vA $\beta$ ,  $P < 0.0001$ ; A $\beta$ 1-42:buffer treated,  $P < 0.0001$ ; vA $\beta$ :buffer treated,  $P = 0.09$ ) (Fig.6.2.B and C).

These results provide strong evidence that an impairment in synaptic vesicle use occurs in the presence of A $\beta$ 1-42. To investigate the nature of this impairment in more detail, we next sought to examine how A $\beta$ 1-42 might influence the kinetics of vesicle release, in addition to its impact on the number of vesicles that are recruited in response to the stimulation. To do this, data was normalized to the baseline fluorescence (average of 5 frames before the stimulation) and to the average of 5 frames at the end of imaging, allowing a direct comparison of the rate of dye-loss for each condition. Single exponential curves, constrained to the baseline fluorescence for each synapse, were then fitted for each destaining curve. The summary of tau measurements revealed that A $\beta$ 1-42 group had significantly slower destaining rate than the vA $\beta$  and buffer treated samples ( $n = 202, 415$  and  $547$  synapses for A $\beta$ 1-42, vA $\beta$  and buffer treated, respectively. One-way ANOVA with Tukey's post-hock analysis: A $\beta$ 1-42:vA $\beta$ ,  $P < 0.0001$ ; A $\beta$ 1-42:buffer treated,  $P < 0.0001$ ; vA $\beta$ :buffer treated,  $P = 0.35$ ) (Fig.6.2.D and E). Taken together, these results indicate that oligomeric A $\beta$ 1-42-induced deficits in presynaptic function; these might include synaptic vesicle pool organization, synaptic vesicle endocytosis or exocytosis.

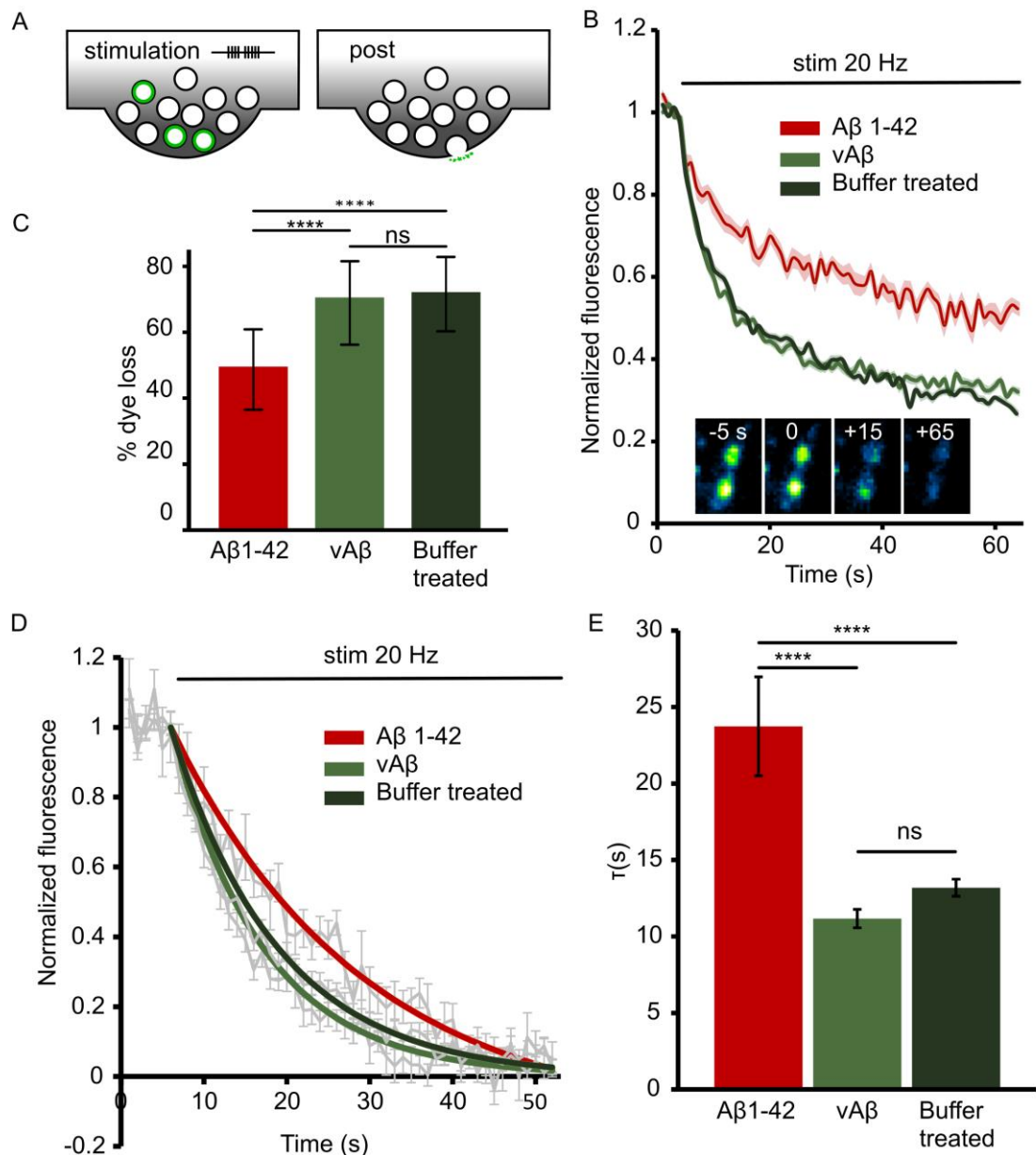


**Figure 6.2 A $\beta$ 1-42 affects synaptic vesicle exocytosis under 1200 APs stimulation protocol.** A) Schematic showing the protocol for FM1-43 destaining. B) FM1-43 destaining profiles (1200 APs at 20 Hz) of normalized fluorescence for the treatment group. Data showed as average of destaining fluorescence of  $n = 218$  for A $\beta$ 1-42,  $n = 428$  for vA $\beta$  and  $n = 560$  synapses for buffer treated group. The inset shows representative images of destaining synapses at various time points of the destain. Shaded area indicates SEM. C) Quantification of % dye loss showed in (B). Data showed as mean  $\pm$  IQR (A $\beta$ 1-42: 50 IQR 36-61, vA $\beta$ 1-42: 71 IQR 56-82, buffer: 72 IQR 60-83,  $n = 218, 428, 560$  synapses, respectively; Kruskal-Wallis one-way ANOVA,  $P < 0.0001$  with Dunn's multiple comparison test: A $\beta$ 1-42:vA $\beta$ ,  $P < 0.0001$ ; A $\beta$ 1-42:buffer treated,  $p < 0.0001$ ; vA $\beta$ :buffer treated,  $P = 0.09$ ). D) Example FM1-43 destaining curves (stim. 1200 APs at 20 Hz) normalized to the frames before and at the end of the stimulation. Data showed as average  $\pm$  SEM ( $n = 8$  synapses for A $\beta$ 1-42, vA $\beta$  and buffer treated, respectively). E) Histogram summary of destaining kinetics expressed as  $\tau$  measurements. Data showed as averages  $\pm$  SEM. Only data with successful fitting of single exponential was included in the analysis ( $n = 202, 415, 547$  synapses for A $\beta$ 1-42, vA $\beta$  and buffer treated, respectively; One-way ANOVA,  $p < 0.0001$  with Tukey's post-hoc).

analysis: A $\beta$ 1-42:vA $\beta$ ,  $P < 0.0001$ ; A $\beta$ 1-42:buffer treated,  $P < 0.0001$ ; vA $\beta$ :buffer treated,  $P = 0.35$ ). Figure modified from Marshall et al., 2016, data collected and analysed by Milena Maria Wagner.

### **6.3 Treatment with 1 $\mu$ M A $\beta$ 1-42 for 24 hours affects synaptic vesicle cycle**

Our FM1-43 data offers some insights into the recycling properties of synapses treated with A $\beta$ 1-42, but interpretation of these results is limited when it comes to a more detailed analysis. There are a number of reasons for this. First, the dye needs to be loaded into synaptic vesicles prior to assaying synaptic function; as such, its internalization will be biased by any underlying deficiencies in synaptic vesicle exocytosis or endocytosis. Only functional vesicles will take up dye, which effectively leads to unintended preselection of recycling vesicles, which can confound interpretation of results. A related issue is that all tests of FM-dye-evoked exocytosis have to necessarily follow a strong stimulation for loading; the specific consequences of such a loading protocol on subsequent release kinetics are unclear. Moreover, although FM1-43 fluorescence is sufficient to observe release events following a limited stimulation protocol such as 10 APs 20 Hz stimulus (cell culture experiments carried out by Milena Maria Wagner, published in Rey et al., 2015), its relatively high photobleach rate makes it less appropriate tool for imaging of smaller events. Therefore, in order to investigate the effect of A $\beta$ 1-42 on the function of presynaptic terminals in more detail, we made use of the genetically-encoded reporter, sypHy2x (described in details in previous chapters), which overcomes these problems. This allowed us to monitor both exocytosis and endocytosis of synaptic vesicles, following protocols mobilising only small number of SVs.

### 6.3.1 A $\beta$ 1-42 affects the kinetics of endocytosis

Primary hippocampal neurons were infected with the AAV-based sypHy2x construct at DIV 4-6, allowed to mature and to establish sufficient expression before being used for experiments DIV 14-17. Cells were treated with 1  $\mu$ M A $\beta$ 1-42 or buffer alone for 24 h prior to imaging. Regions with sypHy2x expression were identified using the baseline fluorescence level. There was no discernible difference in sypHy2x expression between the A $\beta$ 1-42 or buffer only treated cells (Fig.6.3.A). Each region was imaged 4 times during 40 APs, 20 Hz stimulation, however the first trial was discarded as a bleaching trial, but along with other trials was used for identification of functional boutons. The average of all responses for 40 APs, 20 HZ stimulation revealed that cells treated with A $\beta$ 1-42 display larger responses to the same stimulus than buffer treated cells ( $n = 1129$  and  $2171$  responses for A $\beta$ 1-42 and buffer treated, respectively. Two-tailed unpaired Student's t-test,  $P < 0.0001$ ) (Fig.6.3.B). The cumulative distribution of  $\Delta F_{\text{exo}}$  revealed a difference between the two treatment groups, exposing the tendency of A $\beta$ 1-42 treated synapses to respond with a higher number of released vesicles than the buffer control group ( $n = 1129$  and  $2171$  responses for A $\beta$ 1-42 and buffer treated groups, respectively, from 3 independent experiments. Kolmogorov-Smirnov test,  $P < 0.0001$ ) (Fig.6.3.C).

We then explored whether A $\beta$ 1-42 has an effect on the endocytosis of synaptic vesicles following 40 APs, 20 Hz stimulation. All responses were normalized to the peak of the response (average of 10 frames) and the average of 50 frames at the end of each trace. Profiles were then fitted with single exponentials constrained to the average of 5 frames before and after the fitting frame. Due to the appearance of slower and faster component of endocytosis within the profiles, the frame for the beginning of the fit was at a point immediately following the fast endocytic component. A $\beta$ 1-42 was found to decrease the rate of endocytic retrieval of synaptic vesicles following 40 APs 20 Hz stimulation by 21% in relation to buffer treated cells ( $n = 1101$  and  $2130$  responses from A $\beta$ 1-42 and buffer



treated groups from 3 independent experiments. Two-tailed unpaired Student's t-test,  $P < 0.0001$ ) (Fig.6.3.D). Taken together, these results indicate A $\beta$ 1-42 induced impairment in synaptic vesicle recycling.

However, this raises the question of whether this apparent difference in the recycling kinetics of these two treatment groups can be a consequence of the discrepancy in the response sizes in each group. Based on our previous data, this is unlikely under this moderate level of stimulation, nevertheless, we set out to compare endocytic kinetics within data sets with comparable distribution of response sizes. More importantly, we decided to test whether A $\beta$ 1-42 has a different effect on endocytosis when few or multiple vesicles need to be internalised, which might be informative about its mode of toxicity.

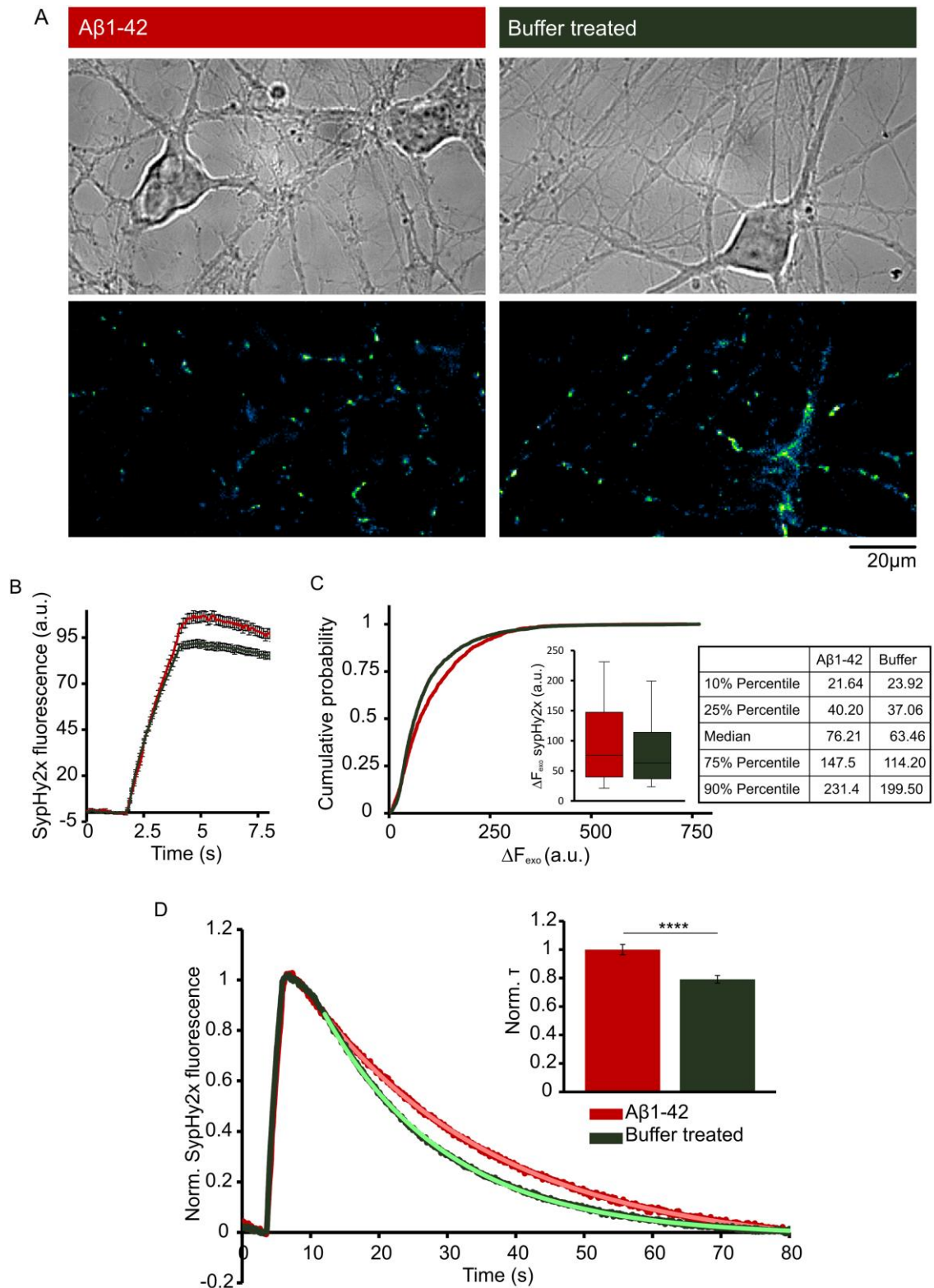


**Figure 6.3 The effect of 24 h 1  $\mu$ M A $\beta$ 1-42 treatment on synaptic vesicle exocytosis and endocytosis.** A) Representative images of A $\beta$ 1-42 and buffer treated cells. Top row DIC images, bottom row syHy2x fluorescence at the peak of response. Scale bar 20  $\mu$ m. B) Average of all responses to 40 APs, 20 Hz stimulation in A $\beta$ 1-42 (red) and buffer treated (green) cells ( $n = 1129$  and  $2171$  responses for A $\beta$ 1-42 and buffer treated groups, respectively  $\pm$  SEM, from 3 experiments). C) Cumulative probability distribution of response sizes following 40 APs, 20 Hz stimulation in A $\beta$ 1-42 (red) and buffer treated

(green) cells ( $n = 1129$  and  $2171$  responses for A $\beta$ 1-42 and buffer treated groups, respectively, from 3 experiments. Kolmogorov-Smirnov test,  $P < 0.0001$ ). Inset represents the variability in the spread of  $\Delta F_{\text{exo}}$  in both groups (A $\beta$ 1-42, red; buffer treated, green) and the table provides the summary of the values. D) Normalized sypHy2x readouts of 40 APs, 20 Hz responses of A $\beta$ 1-42 (red,  $n = 1101$  responses) and buffer treated (green,  $n = 2130$  responses) cells. Light green and light red lines indicate single exponential fit for buffer treated and A $\beta$ 1-42 groups, respectively. The inset shows summary of tau readouts for both groups ( $n = 1101$  and  $2130$  responses from A $\beta$ 1-42 and buffer treated groups from 3 experiments. Two-tailed unpaired Student's t-test,  $P < 0.0001$ ).

### 6.3.2 The effect of A $\beta$ 1-42 is more pronounced in larger responses

In order to address the question whether A $\beta$ 1-42 might differentially affect vesicle retrieval time following responses of various sizes, we split response amplitudes to 40 APs, 20 Hz stimulation into increments of 20 a.u.  $\Delta F_{\text{exo}}$  (Appendix I, Fig. 6). This initial treatment of the data allowed us to independently examine endocytosis following small and large responses to 40 APs, 20 Hz stimulation. Moreover, for each sub-group, we could explore recycling kinetics independently of the number of vesicles recruited. The outcome of this approach was striking; specifically, we revealed that the endocytic rate was not affected in low responding A $\beta$ 1-42-treated synapse, compared to matched controls, but the kinetics of endocytosis of larger fusion events was significantly slower (Appendix I, Fig.6). Based on these incremental graphs, the two ranges of responses were selected for further analysis: low range ( $\Delta F_{\text{exo}}$  0-100 a.u.) and a high range ( $\Delta F_{\text{exo}}$  160-400 a.u.). These fluorescence ranges were applied across the 40 APs, 20 Hz data in order to reveal the population of responses within each range.

The analysis of the low range showed that there was neither a difference in the average size of the responses between A $\beta$ 1-42 and buffer treated groups ( $n = 683$  and  $1549$  responses for A $\beta$ 1-42 and buffer treated. Two-tailed unpaired Student's t-test,  $P = 0.866$ ) (Fig.6.4.A), nor any difference in the distribution of the response amplitudes in these two

groups ( $n = 683$  and  $1549$  responses for A $\beta$ 1-42 and buffer treated, respectively. Kolmogorov-Smirnov test,  $P = 0.1749$ ) (Fig.6.4.B and C). Consistent with this, similar observations were made for the high range responses. There was no difference in the  $\Delta F_{\text{exo}}$  ( $n = 232$  and  $296$  responses for A $\beta$ 1-42 and buffer treated. Two-tailed unpaired Student's t-test,  $P = 0.549$ ) (Fig.6.4.E) and in the distribution of response sizes ( $n = 232$  and  $296$  responses for A $\beta$ 1-42 and buffer treated. Kolmogorov-Smirnov test,  $P = 0.670$ ) (Fig.6.4.F and G). We therefore established 2 sets of data comprised of identical sets of responses for both treatment groups. This allows for unequivocal comparison of the endocytic kinetics between the two treatment groups.

Unexpectedly, we saw that the exocytosis in the high range responses seemed slower in the A $\beta$ 1-42 than in the buffer treated group (Fig.6.4.E) and we decided to further explore this observation. In order to quantify the kinetics of exocytosis, we average fluorescence values for each trace within 20-80% of the total fluorescence rise within the same time frame for A $\beta$ 1-42 and for the buffer treated synapses. We did this in both high and low response groups. The reason for this was to make sure that we captured the same, straight line fluorescence increase for each synapse. The higher the average fluorescence value, the faster the kinetics of exocytosis. We saw that in the low range of responses group there was no difference in the kinetics of exocytosis (Fig.6.4.D) (Two-tailed unpaired Student's t-test,  $P = 0.07$ ), whereas the release time was significantly longer in A $\beta$ 1-42 treated cells in the high range of responses (Fig.6.4.H) (Two-tailed unpaired Student's t-test,  $P < 0.0001$ ), which is consistent with our FM1-43 data.

Going back to endocytosis, the comprehensive investigation of endocytic timing based on response size revealed that although the A $\beta$ 1-42 endocytic kinetics was 13% slower than in the buffer treated group in the low range of responses ( $n = 657$  and  $1501$  responses for A $\beta$ 1-42 and buffer treated. Two-tailed unpaired Student's t-test,  $P = 0.006$ ) (Fig.6.4.I), an even more pronounced effect was observed for data set comprising of high

range of responses (Fig.6.4.J). The retrieval time in A $\beta$ 1-42 was reduced by 45% in comparison to buffer treated group following larger release events ( $n = 231$  and  $295$  for A $\beta$ 1-42 and buffer treated, respectively. Two-tailed unpaired Student's t-test,  $P < 0.0001$ ) (Fig.6.4.J). Moreover, although there was no statistical difference between the endocytic kinetics of low and high range of responses from buffer treated cells ( $n = 1501$  and  $295$  responses for low and high range, respectively. Two-tailed unpaired Student's t-test,  $P = 0.2689$ ), vesicle retrieval time in high range responses from A $\beta$ 1-42 was significantly slower than in the low range ( $n = 657$  and  $231$  responses for low and high range, respectively. Two-tailed unpaired Student's t-test,  $P < 0.0001$ ).

Taken together, this data shows that exocytic and endocytic machinery is less affected by A $\beta$ 1-42 during small release and retrieval events, than when more vesicles are released and recycled back into the presynaptic terminals. As a consequence these results provide an important clue to the possible mode of synaptic impairment induced by A $\beta$ 1-42, which will be discussed later.

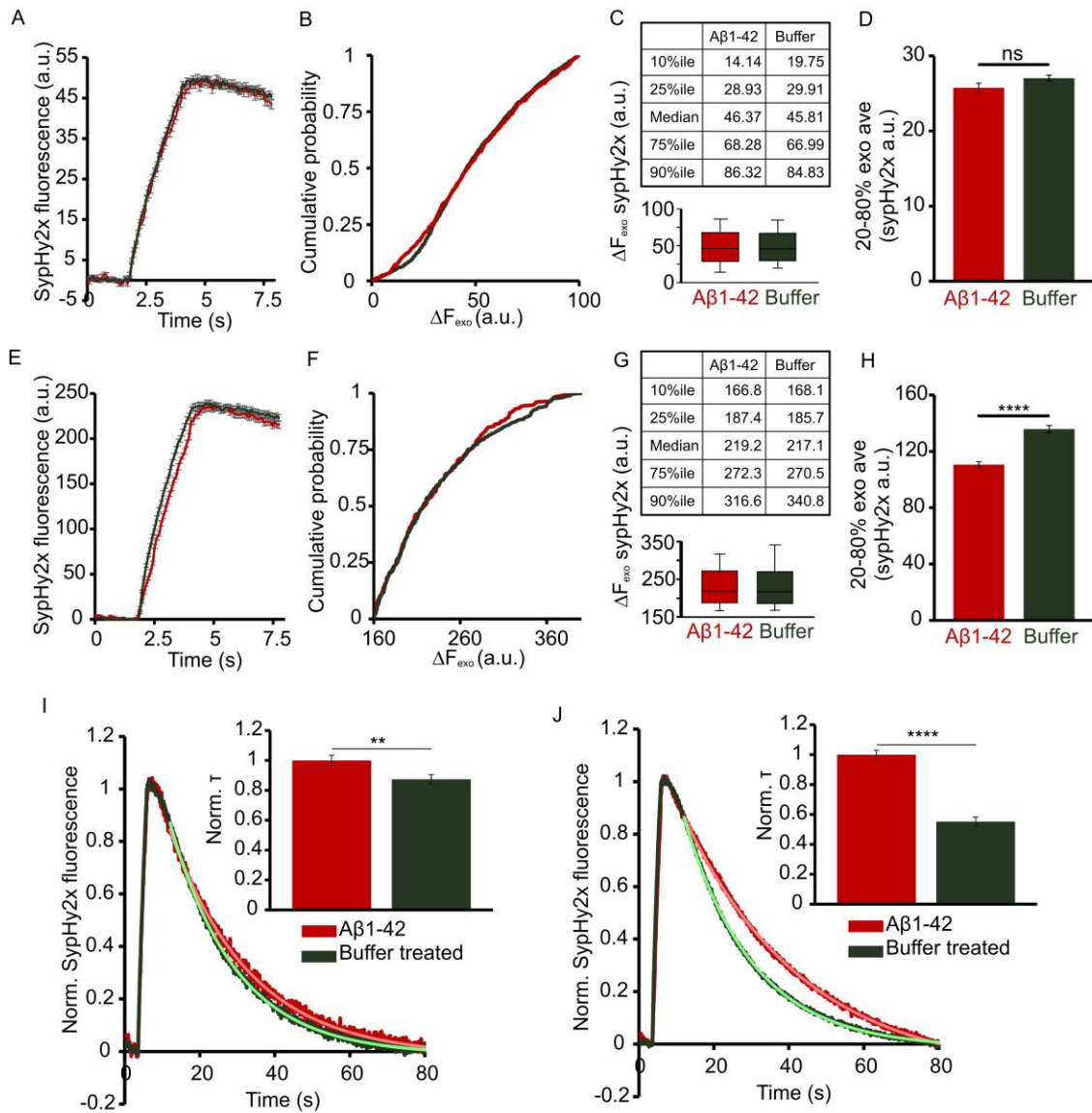


**Figure 6.4 Treatment with 1  $\mu$ M A $\beta$ 1-42 for 24 hours has effect on the kinetics of endocytosis only following larger responses.** A) Average of the exocytic profiles of A $\beta$ 1-42 (red) and buffer treated (green) cells from the lower range ( $\Delta F_{\text{exo}}$  0-100 a.u.) of responses to 40 APs, 20 Hz stimulation (n = 683 and 1549 responses for A $\beta$ 1-42 and buffer treated groups respectively). B) Cumulative probability distribution of  $\Delta F_{\text{exo}}$  response sizes from the synapses from the low range for both groups (n = 683 and 1549 responses for A $\beta$ 1-42 (red) and buffer treated (green) groups, respectively. Kolmogorov-Smirnov test, P = 0.1749). C) Whisker plot represents the variability in the spread between both groups (n = 683 and 1549 responses for A $\beta$ 1-42 (red) and buffer treated (green) groups, respectively). The values are summarized in the table. D) Comparison of the kinetics of exocytosis in A $\beta$ 1-42 (red) and buffer treated (green). Data shown as average  $\pm$  SEM. (n = 683 and 1549 responses for A $\beta$ 1-42 and buffer treated, respectively. Two-tailed unpaired Student's t-test, P = 0.07). Figures E, F, G and H mirror figures A, B, C and D but show data for the high range of response sizes ( $\Delta F_{\text{exo}}$  160-400 a.u.). Within this range there were 232 and 296 analysed responses for A $\beta$ 1-42 and buffer treated groups, respectively. F) Cumulative probability distribution (Kolmogorov-Smirnov test, P = 0.670). H) Comparison of kinetics of exocytosis (Two-tailed unpaired Student's t-test, P < 0.0001). I) and J) Normalized fluorescence profiles of synHy2x

responses to 40 APs, 20 Hz stimulation fitted with single exponential (A $\beta$ 1-42, light red; buffer treated, light green). I) Summary of the low range of response (n = 657 and 1501 responses for A $\beta$ 1-42 (red) and buffer treated (green) groups, respectively). Inset summary of tau readouts (Two-tailed unpaired Student's t-test, P = 0.006). Values were normalized to the average value for the slower treatment group. J) Summary of the high range of responses (n = 231 and 295 for A $\beta$ 1-42 (red) and buffer treated (green) groups, respectively). Inset summarises tau readouts. Values were normalized to the average for the slower group (Two-tailed unpaired Student's t-test, P < 0.0001).

### 6.3.3 vA $\beta$ has no effect on the rate of endocytosis

Next, we examined whether vA $\beta$  has a similar effect to oligomeric A $\beta$ 1-42 on synaptic vesicle endocytosis. As previously described vA $\beta$  was prepared and treated according to the protocol that was identical to A $\beta$ 1-42 protocol (section 2.14). SyphHy2x expressing cells were incubated with 1  $\mu$ M vA $\beta$  and the corresponding volume of buffer for 24 h (Fig.6.5.A). Time-lapse images of syphHy2x expressing and responding to stimulation regions were collected during 40 APs, 20 Hz stimulation. Image analysis was performed as described above. Low ( $\Delta F_{\text{exo}}$  1-50 a.u.) and high range ( $\Delta F_{\text{exo}}$  80-200 a.u.) of responses were determined independently based on the population of collected responses for this experiment.

vA $\beta$  did not have any detrimental effect on the kinetics of endocytosis, at either low (n = 410 and 341 responses for buffer and vA $\beta$  treated cells, respectively. Two-tailed unpaired Student's t-test, P = 0.287) (Fig.6.5.B) or high range of responses (n = 48 and 300 responses for buffer and vA $\beta$  treated groups, respectively. Two-tailed unpaired Student's t-test, P = 0.442) (Fig.6.5.C). It appears that, vA $\beta$  might have slightly accelerated the kinetics of endocytosis in the high range responses. However, this was not significant and could relate to the sampling difference – a relatively small number of responses in the buffer control group for this range. This result shows that vA $\beta$  has no detrimental effect on presynaptic function and further validates the use of vA $\beta$  as a control for oligomeric A $\beta$ 1-42 in functional studies.

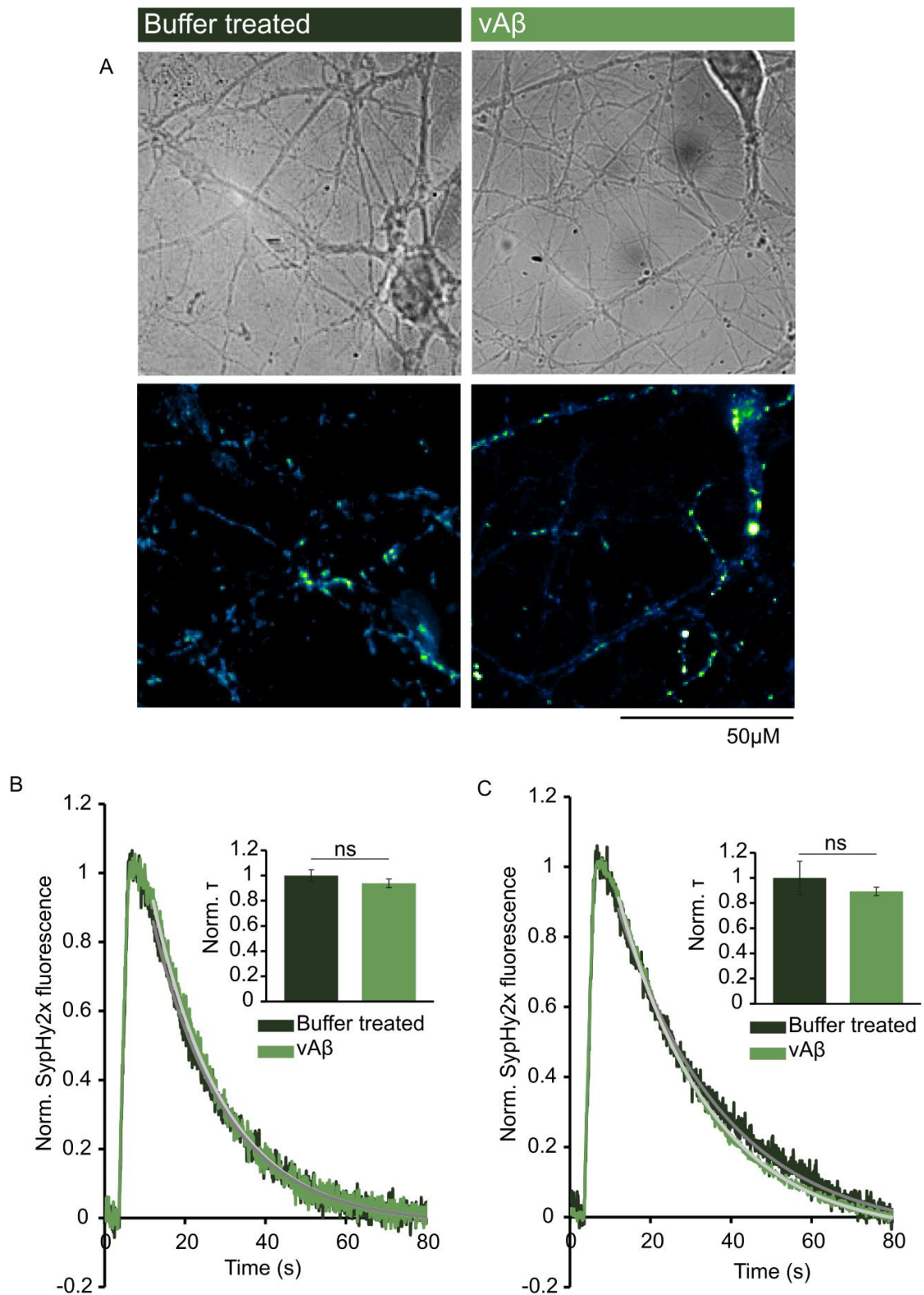


**Figure 6.5 Treatment with 1  $\mu$ M vA $\beta$  for 24 hours had no effect on synaptic vesicles endocytosis.** A) DIC (top row) and syHy2x baseline fluorescence (bottom row) images of buffer and vA $\beta$  treated neurons. Scale bar 50  $\mu$ M. B) SyHy2x profiles (low range,  $\Delta F_{\text{exo}}$  1-50 a.u.) following 40 APs, 20 Hz stimulation. Light grey and dark grey lines indicate single exponential fit for vA $\beta$  and buffer treated cells, respectively. Inset shows summary of tau readouts for both groups ( $n = 410$  and  $341$  responses for buffer treated and vA $\beta$  treated cells, respectively. Two-tailed unpaired Student's t-test,  $P = 0.287$ ). C)



Average of high range of responses ( $\Delta F_{\text{exo}}$  80-200 a.u.) following 40 APs, 20 Hz stimulation with single exponential fits (light grey for vA $\beta$  and dark grey for buffer treated). Inset represents summary of tau readouts within this range of responses ( $n = 48$  and 300 responses for buffer and vA $\beta$  treated groups, respectively. Two-tailed unpaired Student's t-test,  $P = 0.442$ ).

#### **6.4 24 hour treatment with 0.1 $\mu\text{M}$ A $\beta$ 1-42 had no effect on synaptic vesicles endocytosis**

There is a substantial body of research showing that lower than 1  $\mu\text{M}$  concentration of oligomeric A $\beta$ 1-42 had an effect on presynaptic properties (Kelly et al., 2005; J. Park et al., 2013; Russell et al., 2012). We therefore decided to test whether 24 hour treatment with oligomeric A $\beta$ 1-42 at lower concentration (0.1  $\mu\text{M}$ ) has a similar endocytic effect to 1  $\mu\text{M}$  A $\beta$ 1-42. Responses following 40 APs, 20 Hz stimulation were analysed in 24 h 0.1  $\mu\text{M}$  A $\beta$ 1-42 and buffer treated groups. Data analysis and single exponential fitting was identical to the method described above.

Similar to the observation made following 24 hour 1  $\mu\text{M}$  A $\beta$ 1-42 treatment, the analysis of 40 APs, 20 Hz stimulation data revealed that 0.1  $\mu\text{M}$  A $\beta$ 1-42 treated cells showed higher  $\Delta F_{\text{exo}}$  than the buffer only group ( $n = 648$  and 668 responses for A $\beta$ 1-42 and buffer treated group, respectively. Kolmogorov-Smirnov test,  $P = 0.0006$ ) (Fig.6.6.A,B and C). However, the tau measurements of all responses showed no difference in the endocytic kinetics of traces from 0.1  $\mu\text{M}$  A $\beta$ 1-42 group when compared to buffer treated cells ( $n = 610$  and 608 responses for A $\beta$ 1-42 and buffer treated, respectively. Two-tailed unpaired Student's t-test,  $P = 0.850$ ) (Fig.6.6.D). To investigate this result further, the approach of separating data into a low and high range of responses was employed. Tau measurements were made for low ( $\Delta F_{\text{exo}}$  0-10 a.u.) and high range of responses ( $\Delta F_{\text{exo}}$  20-50 a.u.). There was no significant difference in the retrieval time between 0.1  $\mu\text{M}$  A $\beta$ 1-42 and buffer only traces in either low ( $n = 272$  and 318 responses for A $\beta$ 1-42 and buffer treated, respectively. Two-tailed unpaired Student's t-test,  $P = 0.183$ ) (Fig.6.6.E) or high

range responses ( $n = 110$  and  $64$  responses for A $\beta$ 1-42 and buffer treated, respectively). Two-tailed unpaired Student's  $t$ -test,  $P = 0.901$ ) (Fig.6.6.F). Nevertheless, there was some tendency for the A $\beta$ 1-42 traces to exhibit a slower rate of endocytosis than the buffer treated control in the high range of responses (Fig.6.6.F). It can be therefore concluded that, although 24 h treatment with  $0.1 \mu\text{M}$  A $\beta$ 1-42 has some effect on the homeostasis of presynaptic terminals, unlike higher A $\beta$ 1-42 concentration, it does not lead to any dramatic impairment in the recycling of synaptic vesicles.

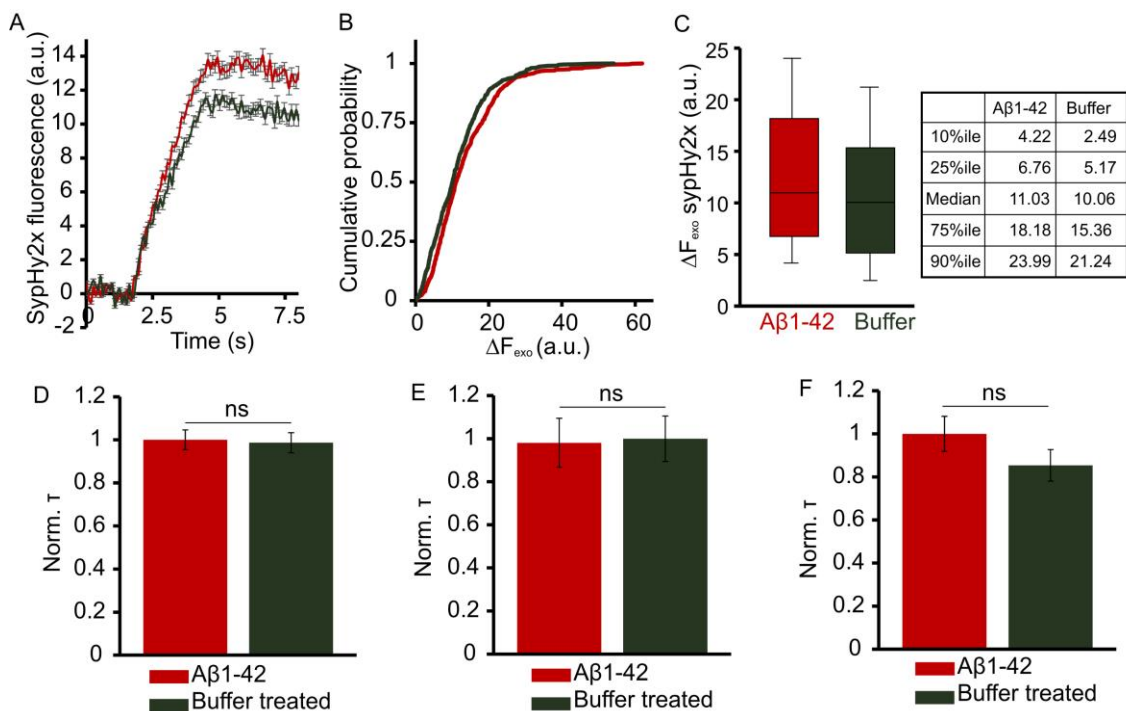


**Figure 6.6 The effect of 24 hour  $0.1 \mu\text{M}$  A $\beta$ 1-42 treatment on synaptic vesicle exocytosis and endocytosis.** A) Profiles representing the average of all 40 APs, 20 Hz responses of A $\beta$ 1-42 (red) and buffer treated (green) cells ( $n = 648$  and  $668$  responses for A $\beta$ 1-42 and buffer treated group, respectively  $\pm$  SEM). B) Cumulative probability distribution of  $\Delta F_{\text{exo}}$  for A $\beta$ 1-42 and buffer treated group ( $n = 648$  and  $668$  responses for A $\beta$ 1-42 and buffer treated group, respectively). Kolmogorov-Smirnov test,  $P = 0.0006$ ). C) Whisker plot represents variability in the spread of  $\Delta F_{\text{exo}}$  data (A $\beta$ 1-42, red; buffer treated, green). Table summarizes the results. D) Summary of tau measurements for A $\beta$ 1-42 (red) and buffer treated (green) groups ( $n = 610$  and  $608$  responses for A $\beta$ 1-42 and buffer treated, respectively). Two-tailed unpaired Student's  $t$ -test,  $P = 0.850$ ). E) Summary of tau measurement for low range of responses ( $\Delta F_{\text{exo}}$  0-10 a.u.) for A $\beta$ 1-42 (red) and buffer treated (green) groups ( $n = 272$  and  $318$  responses for A $\beta$ 1-42 and buffer treated, respectively). Two-tailed unpaired Student's  $t$ -test,  $P = 0.183$ ). F) Summary of tau measurement for high range of responses ( $\Delta F_{\text{exo}}$  20-50 a.u.) for  $\beta$ 1-42 (red) and buffer treated (green) groups ( $n = 110$  and  $64$  responses for A $\beta$ 1-42 and buffer treated, respectively). Two-tailed unpaired Student's  $t$ -test,  $P = 0.901$ ).

## 6.5 The effect of 1 $\mu$ M A $\beta$ 1-42 on single vesicle endocytosis

The results illustrated in Figure 6.4 point towards a very compelling endocytic deficit induced by 24 h treatment with 1  $\mu$ M oligomeric A $\beta$ 1-42 in the larger range of responses elicited by 40 APs, 20 Hz stimulation. The lack of the effect of A $\beta$ 1-42 in the smaller response range might indicate a more global effect of A $\beta$ 1-42 during conditions where the endocytic machinery is overwhelmed. To provide evidence for this idea, we next used our single vesicle fusion approach to test whether A $\beta$ 1-42-driven endocytic defects were visible at the level of quantal event profiles. The aim of this experiment was therefore to further dissect the substrate of A $\beta$ 1-42 related impairment in the recycling kinetics.

The cells were prepared according to the usual protocol and A $\beta$ 1-42 treatment carried out as described elsewhere (sections 2.2, 3.2.1, 6.2.1). AAV.*sypHy2x* expressing cells were stimulated 10 times with 4 APs. The first trial was used to identify the responding region and was discarded as a bleaching trial. In agreement with results for 40 APs, 20 Hz stimulation, A $\beta$ 1-42 treated cells responded with higher number of vesicle released than the buffer treated control ( $n = 510$  and  $725$  responses for A $\beta$ 1-42 and buffer treated, respectively. Kolmogorov-Smirnov test,  $P = 0.48$ ) (Fig.6.7.A, B and C). The lower fluorescence range for 1q size (92.2 a.u.) was used as a limit for the smallest responses included in this analysis. This was to avoid the possibility that many failures to respond in the 4 APs stimulation protocol would have been included in the analysis, and therefore might have contaminated the results. There was no upper limit for the response size.

In order to ascertain whether oligomeric A $\beta$ 1-42 had any effect on the endocytic kinetics of single synaptic vesicles, the established fluorescence value corresponding to 1q release was applied across the data. Due to the possibility of A $\beta$ 1-42 affecting the quantal size, we first examined the quantal size in A $\beta$ 1-42 treated cells. From multiple Gaussian fit in the experiment that exhibited signs of quantal distribution, we found that

the value of fluorescence corresponding to 1 quanta was 87.4-144 (a.u.). It is reasonable to conclude that these values are sufficiently similar to apply the standard in this study value of 92.2-157(a.u.) fluorescence corresponding to single vesicle release.

Single quantum responses were filtered out for the A $\beta$ 1-42 treated and buffer treated groups. The analysis of distribution of sizes within 1 quantum range revealed no difference between these two treatment groups (n = 372 and 224 responses for A $\beta$ 1-42 and buffer treated group, respectively. Kolmogorov-Smirnov test, P = 0.8) (Fig.6.7.D, E and F). The kinetics of responses within individual synapses were calculated using linear fits, starting at the frames just past the peak of the responses and ending with the average of the last 10 imaging frames. This allowed us to establish the slope of the decay. We found that there was no difference in the kinetics of single vesicle endocytosis in A $\beta$ 1-42 and buffer treated cells (n = 61 and 100 synapses in A $\beta$ 1-42 and buffer treated groups, respectively. Two-tailed unpaired Student's t-test, P = 0.64) (Fig.6.7.G, H and I). It can therefore be concluded that A $\beta$ 1-42 has no effect on the endocytosis of single synaptic vesicles and that the endocytic deficit described earlier develops only after larger vesicle recruitment to the membrane, and is presumably associated with increased recycling demand.

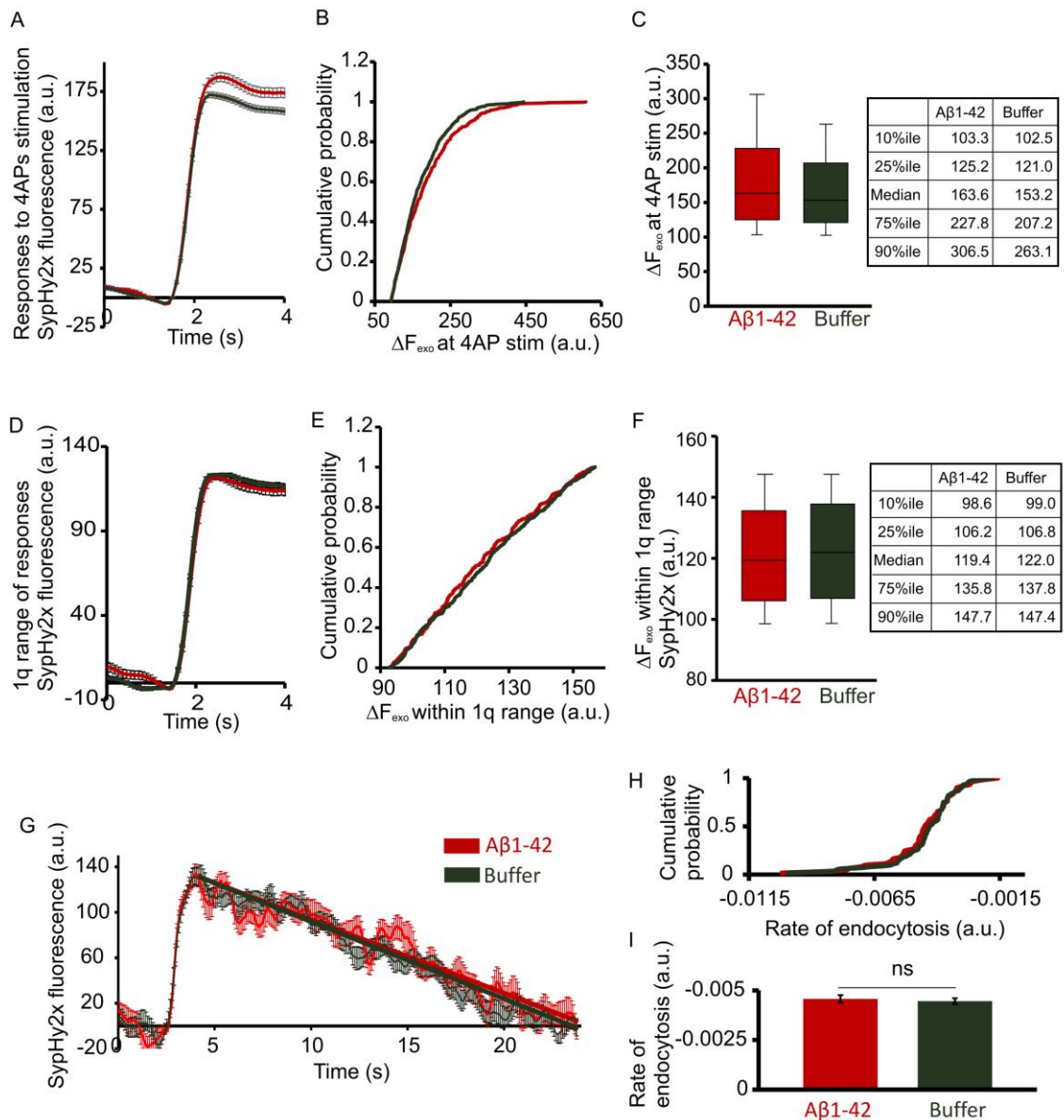


**Figure 6.7 Aβ1-42 does not affect the kinetics of endocytosis following single vesicle release events.** A) Average profiles of responses to 4 AP stimulation at 20 Hz ( $n = 510$  and  $725$  responses for Aβ1-42 (red) and buffer treated (green), respectively  $\pm$  SEM). B) Cumulative probability distribution of  $\Delta F_{\text{exo}}$  in response to 4 AP stimulation ( $n = 510$  and  $725$  responses for Aβ1-42 (red) and buffer treated (green), respectively. Kolmogorov-Smirnov test,  $P = 0.48$ ). C) Whisker plot illustrating the variability of responses to 4 AP in Aβ1-42 (red) and buffer treated (green) groups. Table shows the summary of the data shown. D) Average profiles of 1q responses for buffer (green) and Aβ1-42 (red) treated groups ( $n = 372$  and  $224$  responses for buffer treated and Aβ1-42, respectively  $\pm$  SEM). E) Cumulative probability distribution of the response sizes within 1q range for Aβ1-42 and buffer treated groups ( $n = 372$  and  $224$  responses for Aβ1-42 and buffer treated group, respectively. Kolmogorov-Smirnov test,  $P = 0.8$ ). F) Whisker plot illustrating the variability within 1q range of responses for both Aβ1-42 (red) and buffer treated (green) groups. Table shows the values for both groups. G) Example of endocytic profiles in Aβ1-42 and buffer treated synapses. Data showed as average of 3 profiles for each group  $\pm$  SEM, fitted with linear fit. H) Cumulative probability distribution plot of the endocytic rates within 1q range ( $n = 61$  and  $100$  synapses for Aβ1-42 (red) and buffer treated (green) groups, respectively. Kolmogorov-Smirnov test,  $P = 0.4$ ). I)

Summary of the endocytic rate readouts following single vesicle release events (n=61 and 100 synapses in A $\beta$ 1-42 (red) and buffer treated (green) groups, respectively. Two-tailed unpaired Student's t-test, P = 0.64).

## 6.6 The effect of 1 $\mu$ M A $\beta$ 1-42 on stimulation evoked Ca<sup>2+</sup> influx

The results presented so far indicate that A $\beta$ 1-42 leads to increased release of synaptic vesicles, as a response to medium (40 APs, 20 Hz) and small (4 APs, 20 Hz) stimuli. What factors could underlie the larger vesicle recruitment seen with A $\beta$ 1-42 treatment? This section of the chapter broadens the exploration of A $\beta$ 1-42 – associated changes to include its effect of stimulus-driven Ca<sup>2+</sup> influx into the presynaptic terminal. To test this, we used syGCaMP6f, a reporter of free cytoplasmic calcium, characterized by fast fluorescence rise and decay kinetics (Chen et al., 2013), described in detail in section 3.3.3. This allowed us to address the following questions in relation to A $\beta$ 1-42 induced presynaptic changes: i) is the increase in SV release resulting from elevated Ca<sup>2+</sup> influx?; ii) is the Ca<sup>2+</sup> dependent exo- endocytic coupling disturbed by the A $\beta$ 1-42?

### 6.6.1 The effect of 1 $\mu$ M A $\beta$ 1-42 on Ca<sup>2+</sup> influx at larger stimulations

Cells, A $\beta$ 1-42 and vA $\beta$  preparation were carried out as in previous experiments. In short, primary hippocampal neurons were infected with AAV based syGCaMP6f construct (DIV 4-6), and treated for 24 h with 1  $\mu$ M A $\beta$ 1-42 or vA $\beta$ , applied 10 days later. Representative regions were imaged (13.7 Hz, 70 ms per frame), while being stimulated 4 times with 40 APs, 20 Hz stimulation with 1 min intervals between each stimulation (Fig.6.8.A). Due to the low level of syGCaMP6f baseline fluorescence, the first trial was used for region recognition in order to match sypHy2x based protocols, and was discarded from the analysis

The summary of raw fluorescence values from all responses from the first of the 3 x 40 APs experimental trials showed striking difference between the A $\beta$ 1-42 and the control groups. Figure 6.8.B shows the average profiles for the three treatment groups and the dark grey panel indicates the frames that were used for the analysis of the rise in fluorescent signal. The quantification of the fluorescence amplitude showed that A $\beta$ 1-42 treated neurons had significantly larger Ca $^{2+}$  influx as a result of responses to this stimulation than vA $\beta$  and buffer controls, which showed no difference between one another (n = 315, 232 and 317 synapses for buffer treated, vA $\beta$  and A $\beta$ 1-42, respectively. One-way ANOVA with Tukey's post-hock analysis: buffer: vA $\beta$ , P = 0.054; buffer: A $\beta$ 1-42, P < 0.0001; vA $\beta$ : A $\beta$ 1-42, P < 0.0001) (Fig.6.8.B and C).

The other question to ask was whether this A $\beta$ 1-42 induced increase in Ca $^{2+}$  influx can be sustained over multiple stimulation rounds. In order to investigate this we normalized all responses in the 1<sup>st</sup> and 3<sup>rd</sup> trial for all the groups to the largest response (A $\beta$ 1-42 in the 1<sup>st</sup> trial) (Fig.6.8.D). We then analysed the % decrease in Ca $^{2+}$  influx in the 3<sup>rd</sup> trial in relation to the 1<sup>st</sup> trial, and we found that although a similar decrease was found in buffer treated and vA $\beta$  groups, this decline was significantly smaller in A $\beta$ 1-42 treated cells (One-way ANOVA with Tukey's post-hock analysis: buffer:vA $\beta$ , P = 0.054; buffer:A $\beta$ 1-42, P < 0.0001; vA $\beta$ :A $\beta$ 1-42, P < 0.0001) (Fig.6.8.E). These results indicate that A $\beta$ 1-42 not only leads to more Ca $^{2+}$  influx, but it also sustains this high level of Ca $^{2+}$  during consecutive stimulations.

However, these results need to be treated with caution. A plausible explanation for this could relate to differences in the size of synapses responding in different treatment groups. We therefore decided to carry out more detailed analysis of this data. Firstly, we selected responses from synapses within a certain range of baseline level fluorescence, secondly, we looked at the responses within a given range of the rise in syGCaMP6f fluorescence, which will be discussed in the next sections.

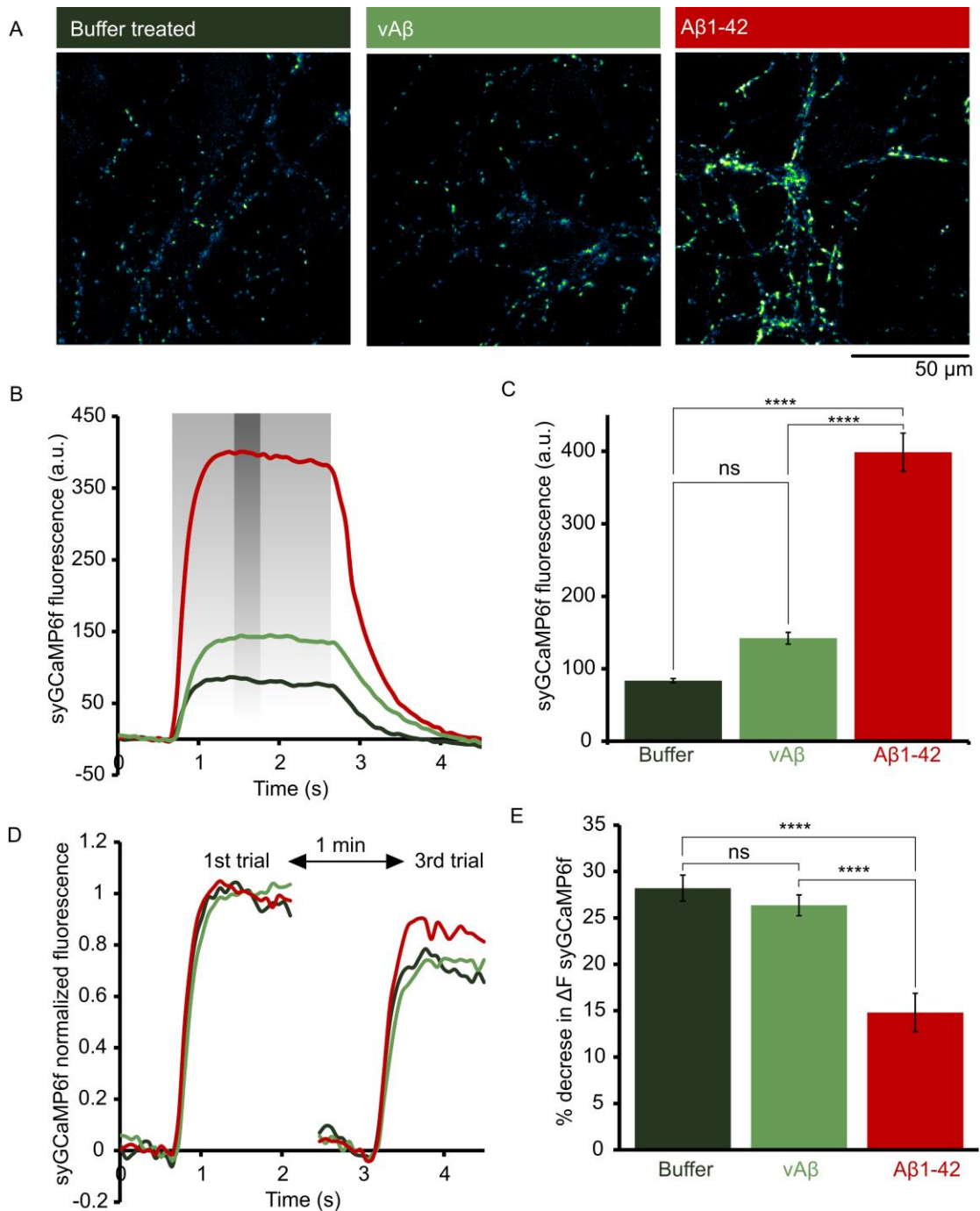


**Figure 6.8 Measurements of Aβ1-42 effect on stimulation evoked presynaptic  $\text{Ca}^{2+}$  influx.** A) syGCaMP6f fluorescence at the peak of responses. Scale bar 50  $\mu\text{m}$ . B) Summary of the size of syGCaMP6f responses to 40 APs, 20 Hz stimulation. Light grey panel indicates the length of the stimulation. Dark green panel indicates the frames used for calculation of  $\Delta F$  ( $n = 315$ , 232 and 317 synapses for buffer treated (dark green), vAβ (light green) and Aβ1-42 (red), respectively). C) Quantification of  $\Delta F$  syGCaMP6f fluorescence ( $n = 315$ , 232 and 317 synapses for buffer treated (dark green), vAβ (light green) and Aβ1-42 (red), respectively  $\pm$  SEM. One-way ANOVA with Tukey's post-hoc analysis: buffer:vAβ,  $P = 0.054$ ; buffer:Aβ1-42,  $P < 0.0001$ ; vAβ:Aβ1-42,  $p < 0.0001$ ). D) syGCaMP6f fluorescence in response to 40 APs, 20 Hz stimulation. The responses in first and 3rd trial were normalized to the peak fluorescence from 1st trial for each synapse ( $n = 315$ , 232 and 317 synapses for buffer treated (dark green), vAβ (light green) and Aβ1-42 (red), respectively). E) Graph showing the average % decrease in fluorescence



between 1st and 3rd trial. ( $n = 315, 232$  and  $317$  synapses for buffer treated (dark green), vA $\beta$  (light green) and A $\beta$ 1-42 (red), respectively  $\pm$  SEM. One-way ANOVA with Tukey's post-hock analysis: buffer:vA $\beta$ ,  $P = 0.054$ ; buffer:A $\beta$ 1-42,  $P < 0.0001$ ; vA $\beta$ :A $\beta$ 1-42,  $P < 0.0001$ ).

#### **6.6.1.1 Sub selection of responses within the same baseline range**

The analysis of the baseline syGCaMP6f fluorescence revealed a big disparity in this parameter between the 3 groups (Fig.6.9.A and B). The results revealed significant differences in the distribution of the baseline fluorescence in the different conditions, with the A $\beta$ 1-42 treated group showing the largest baseline fluorescence and also the largest variability (Coefficient of variation: 15.37%, 15.09% and 40.97% for buffer treated, vA $\beta$  and A $\beta$ 1-42, respectively). In order to more reliably compare the behaviour of similar populations of synapses, we decided to limit our measurements to synapses within a given range of baseline fluorescence (315-415 a.u.) (Coefficient of variation: 6.06%, 5.74% and 5.74% for buffer treated, vA $\beta$  and A $\beta$ 1-42, respectively). SyGCaMP6f baseline fluorescence only moderately correlates with synaptic size (Pearson's correlation test for syGCaMP6f baseline fluorescence and 600 APs, 20 Hz sytl-Oyster 550 loading fluorescence,  $n = 100$  synapses,  $r = 0.49$ ,  $P < 0.0001$ ), hence we can only assume that synapses within this range of baseline fluorescence are approximately of similar size. In this population we again looked at the behaviour of synapses in the 1<sup>st</sup> and 3<sup>rd</sup> 40 APs, 20 Hz stimulation trials. We found that within this group of synapses, the % decrease in syGCaMP6f signal was again smaller in A $\beta$ 1-42 than in buffer treated and vA $\beta$  group, which showed no difference between them ( $n = 245, 148$  and  $121$  synapses buffer treated, vA $\beta$  and A $\beta$ 1-42, respectively. One-way ANOVA with Tukey's post-hock analysis: buffer:vA $\beta$ ,  $P = 0.825$ ; buffer:A $\beta$ 1-42,  $P < 0.0001$ ; vA $\beta$ :A $\beta$ 1-42,  $P < 0.0001$ ) (Fig.6.9.C). The fluorescence decrease in A $\beta$ 1-42 in the population of synapses was even smaller than in the entire population of synapses previously reported in the Figure 6.8.D and E.

A drawback of this approach is that all synapses are assumed to have lower calcium influx in the third trial than in the first one. We therefore decided to test how many synapses in each treatment group displayed activity driven increases in the syGCaMP6f fluorescence amplitude in the 3<sup>rd</sup> trial in comparison to the 1<sup>st</sup> one. We found that only 6.5% and 6.1% of synapses showed this tendency in buffer and vA $\beta$  treated cells, respectively, but as much as 25.6% synapses in A $\beta$ 1-42 group were characterised by this behaviour (Fig.6.9.D). This suggests that the apparently smaller decrease in fluorescence amplitude in A $\beta$ 1-42 is driven by the actual increase in calcium influx in this group. This points toward higher excitability in A $\beta$ 1-42 treated cells and may potentially contribute to the increased excitotoxicity as a result of it.

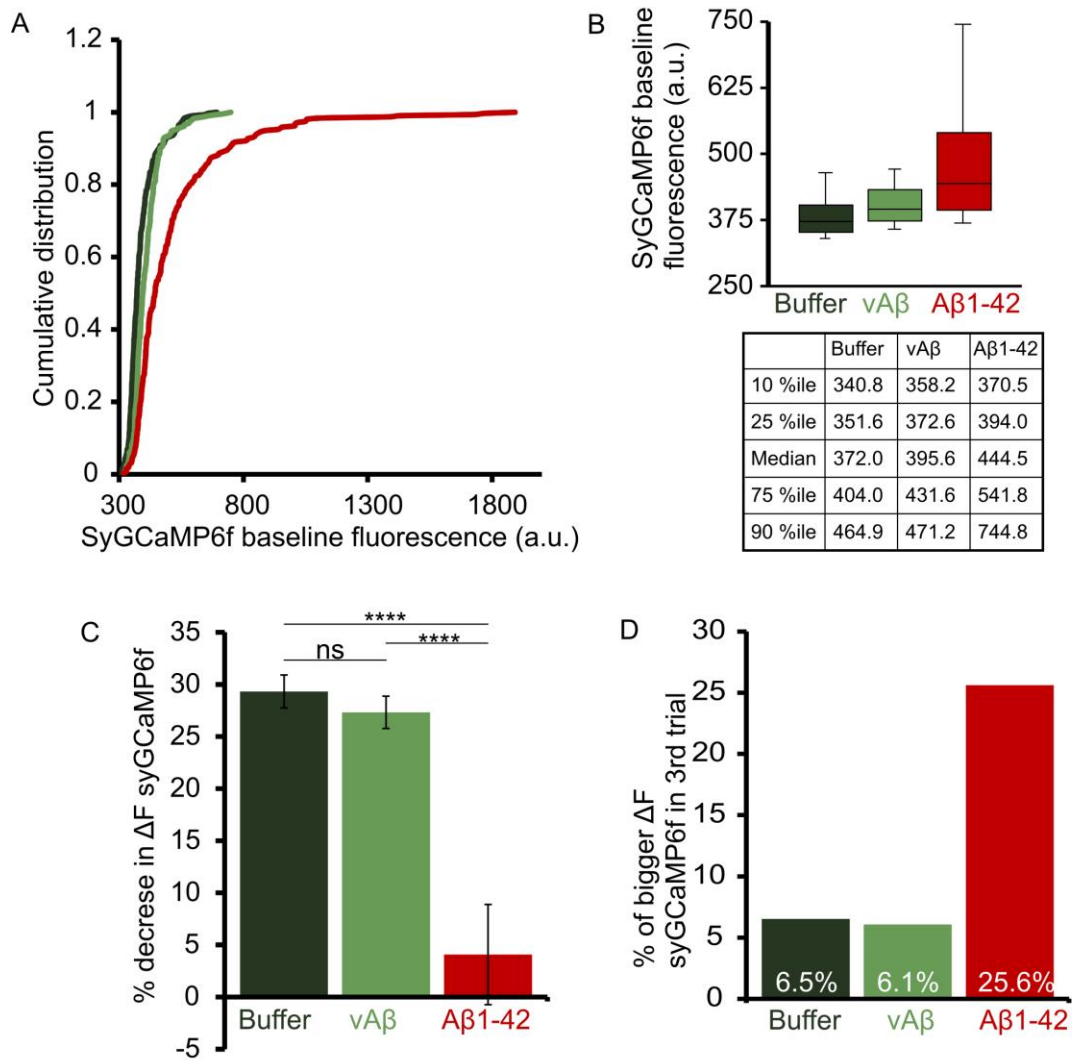


**Figure 6.9 The effect of Aβ1-42 on Ca<sup>2+</sup> influx in population of synapses of similar size.** A) Cumulative probability distribution of syGCaMP6f baseline fluorescence for each experimental group (n = 315, 232 and 317 synapses for buffer treated (dark green), vAβ (light green) and Aβ1-42 (red), respectively. Kolmogorov-Smirnov test: buffer:vAβ, p<0.0001; buffer:Aβ1-42, P < 0.0001; vAβ:Aβ1-42, P < 0.0001). B) Whisker plot summarizing the difference in the distribution of syGCaMP6f baseline fluorescence (n = 315, 232 and 317 synapses for buffer treated (dark green), vAβ (light green) and Aβ1-42 (red), respectively). C) Graph summarizing the % decrease in ΔF syGCaMP6f between 1st and 3rd trial for the data from baseline range 315-415 (a.u.) (n = 245, 148 and 121 synapses buffer treated (dark green), vAβ (light green) and Aβ1-42 (red), respectively ± SEM. One-way ANOVA with Tukey's post-hock analysis: buffer:vAβ, P = 0.825; buffer:Aβ1-42, P < 0.0001; vAβ:Aβ1-42, P < 0.0001). D) Quantification of the number of responses that were bigger in the third trial in comparison to the first trial (16/245, 9/148 and 31/121 synapses for buffer treated (dark green), vAβ (light green) and Aβ1-42 (red), respectively).

### 6.6.1.2 Sub selection of responses with the same response size

As previously mentioned the syGCaMP6f baseline fluorescence doesn't accurately reflect the size of the synapses (section 6.6.1.1). We therefore employed yet another approach and selected population of synapses which fell within  $\Delta F$  1-100 a.u. range of response amplitude in the first trial. This allows us to compare synapses with similar properties, regardless whether the size of the responses was driven by potential effect of A $\beta$ 1-42 on excitability or number of Ca<sup>2+</sup> channels.

There was no difference in the distribution of the fluorescence amplitudes within the defined range between the buffer and vA $\beta$  group, and buffer and A $\beta$ 1-42 (n= 233,112 and 91 synapses for buffer treated, vA $\beta$  and A $\beta$ 1-42, respectively. Kolmogorov-Smirnov test: buffer:vA $\beta$ , P = 0.724; buffer:A $\beta$ 1-42, P = 0.051) (Fig.6.10.A and B). Despite the fact that there was a small difference in the response distribution between vA $\beta$  and A $\beta$ 1-42, we do not think this will have an impact on later measurements as the distribution in A $\beta$ 1-42 is only slightly shifted towards a smaller size responses within this range (n = 112 and 91 synapses for vA $\beta$  and A $\beta$ 1-42, respectively. Kolmogorov-Smirnov test: vA $\beta$ :A $\beta$ 1-42, P = 0.013) (Fig.6.10.A and B).

We carried out similar analysis to the one shown in Figure 6.9 by comparing the amplitude of response from the 3<sup>rd</sup> 40 APs trial to the one from the 1<sup>st</sup> trial. Within our population of synapses we found that despite the fact that there was no difference between buffer and vA $\beta$  treated cells, there were significant differences between these two groups and A $\beta$ 1-42 (n = 233,112 and 91 for buffer treated, vA $\beta$  and A $\beta$ 1-42, respectively. One-way ANOVA with Tukey's post-hock analysis: buffer:vA $\beta$ , P = 0.743; buffer:A $\beta$ 1-42, P < 0.0001; vA $\beta$ :A $\beta$ 1-42, P < 0.0001) (Fig.6.10.C). The average decrease for A $\beta$ 1-42 was negative (-3.5%), which actually suggests a high proportion of larger responses in the 3<sup>rd</sup> trial than in the first one. Indeed, we found that almost 40% of synapses had more Ca<sup>2+</sup> influx in the 3<sup>rd</sup> trial in comparison to the first round of

stimulation, whereas it was 9.4% and 10.7% for buffer control and vA $\beta$  groups, respectively (Fig.6.10.D). This suggests disruption of presynaptic Ca<sup>2+</sup> influx caused by A $\beta$ 1-42.

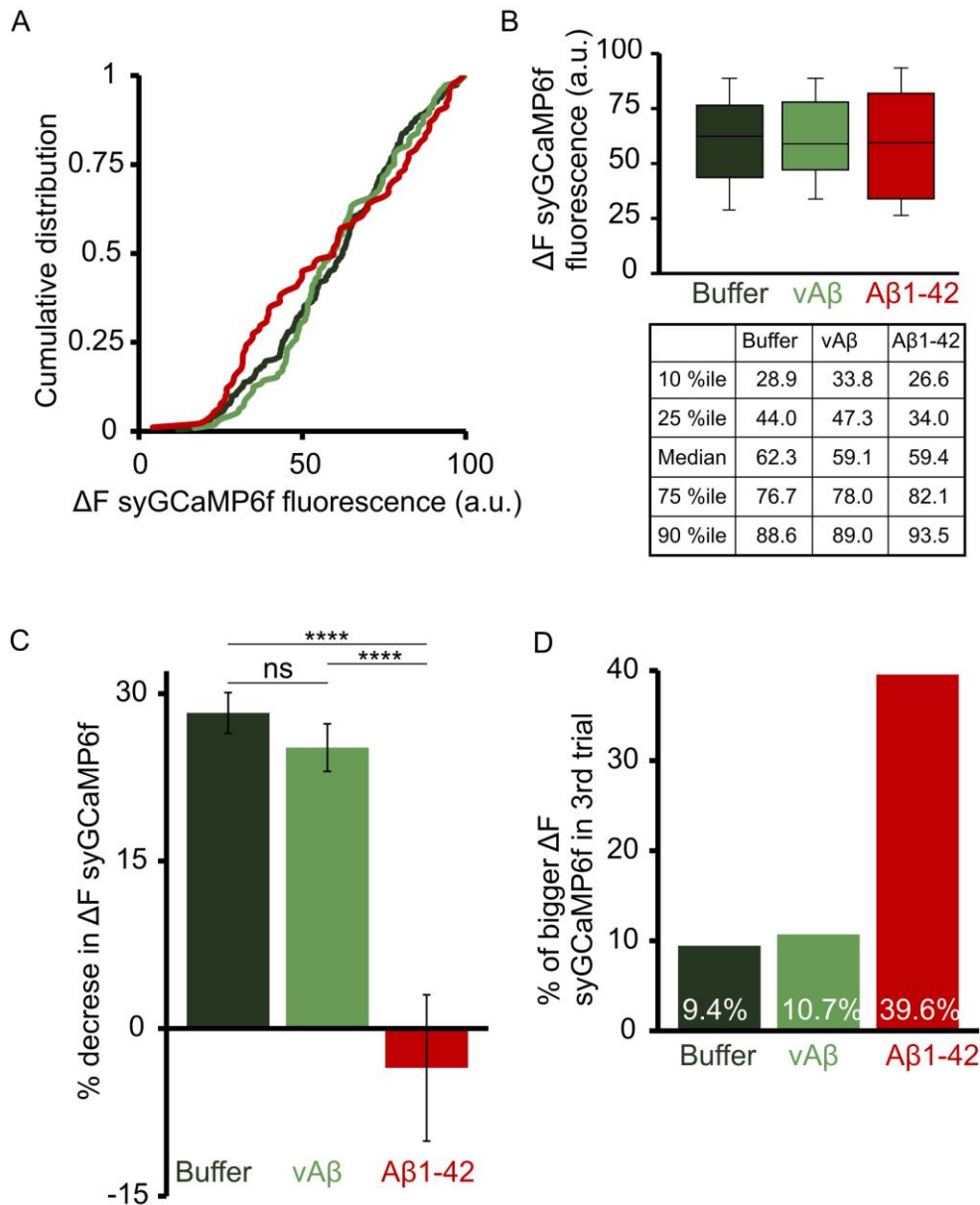


**Figure 6.10 The effect of A $\beta$ 1-42 on Ca<sup>2+</sup> influx in population of synapses of similar response amplitude.** A) Cumulative distribution plot of the syGCaMP6f responses within the range of  $\Delta F$  1-100 ( $n = 233,112$  and 91 synapses for buffer treated (dark green), vA $\beta$  (light green) and A $\beta$ 1-42 (red), respectively). Kolmogorov-Smirnov test: buffer:vA $\beta$ ,  $P = 0.724$ ; buffer:A $\beta$ 1-42,  $P = 0.051$ ; vA $\beta$ :A $\beta$ 1-42,  $P = 0.013$ ). B) Whisker plot showing summarizing the spread of responses within 1-100  $\Delta F$  range ( $n = 233,112$  and 91 for Buffer treated (dark green), vA $\beta$  (light green) and A $\beta$ 1-42 (red), respectively). C) Summary of the % decrease in response size between the 1st and 3rd 40 APs, 20 Hz

stimulation trial ( $n = 233, 112$  and  $91$  for buffer treated (dark green),  $vA\beta$  (light green) and  $A\beta 1-42$  (red), respectively  $\pm$  SEM. One-way ANOVA with Tukey's post-hock analysis: buffer: $vA\beta$ ,  $P = 0.743$ ; buffer: $A\beta 1-42$ ,  $P < 0.0001$ ;  $vA\beta$ : $A\beta 1-42$ ,  $P < 0.0001$ ). D) Graph summarizing the percentage of synapses that showed larger  $\Delta F$  in the third trial in comparison to the first trial ( $22/233$ ,  $12/112$  and  $36/91$  for buffer treated (dark green),  $vA\beta$  (light green) and  $A\beta 1-42$  (red), respectively).

### 6.6.2 The effect of $1 \mu M$ $A\beta 1-42$ on $Ca^{2+}$ influx in response to minimal stimulus

In the previous sections we demonstrated, that under moderate stimulation (40 APs, 20 Hz)  $A\beta 1-42$  treated cells exhibited higher stimulation-related  $Ca^{2+}$  influx than the control synapses (buffer treated and  $vA\beta$ ). We now wanted to test whether the same phenomenon can be observed in response to smaller stimuli. For this purpose, we employed stimulation protocols that were similar to syPhy2x data; we stimulated 5 times with 4 APs, each 1 minute apart.

There was no difference in the baseline fluorescence level between the treatment groups, suggesting that the synapses were of similar size ( $n = 372$ ,  $199$  and  $296$  synapses for buffer: $vA\beta$ ,  $P = 0.899$ ; buffer: $A\beta 1-42$ ,  $P = 0.998$ ;  $vA\beta$ : $A\beta 1-42$ ,  $P = 0.885$ ). Initially we looked at all 5 trials separately and a recurring pattern emerged.  $Ca^{2+}$  influx in response to 4 APs stimulation was always larger in  $A\beta 1-42$  than in the buffer treated and  $vA\beta$  in all 5 trials (Fig.6.11.A and B). For easier comparison, we pulled the data together from all the trials to reveal that  $Ca^{2+}$  influx in  $A\beta 1-42$  treated cells was significantly larger than in buffer treated and  $vA\beta$  controls, which were not different from each other ( $n = 5$  trials, One-way ANOVA with Tukey's post-hock analysis: buffer: $vA\beta$ ,  $P = 0.358$ ; buffer: $A\beta 1-42$ ,  $P = 0.0002$ ;  $vA\beta$ : $A\beta 1-42$ ,  $P < 0.0001$ ) (Fig.6.11.C and D). This strengthens the finding that treatment with  $A\beta 1-42$  leads to increased  $Ca^{2+}$  influx in response to stimulation.

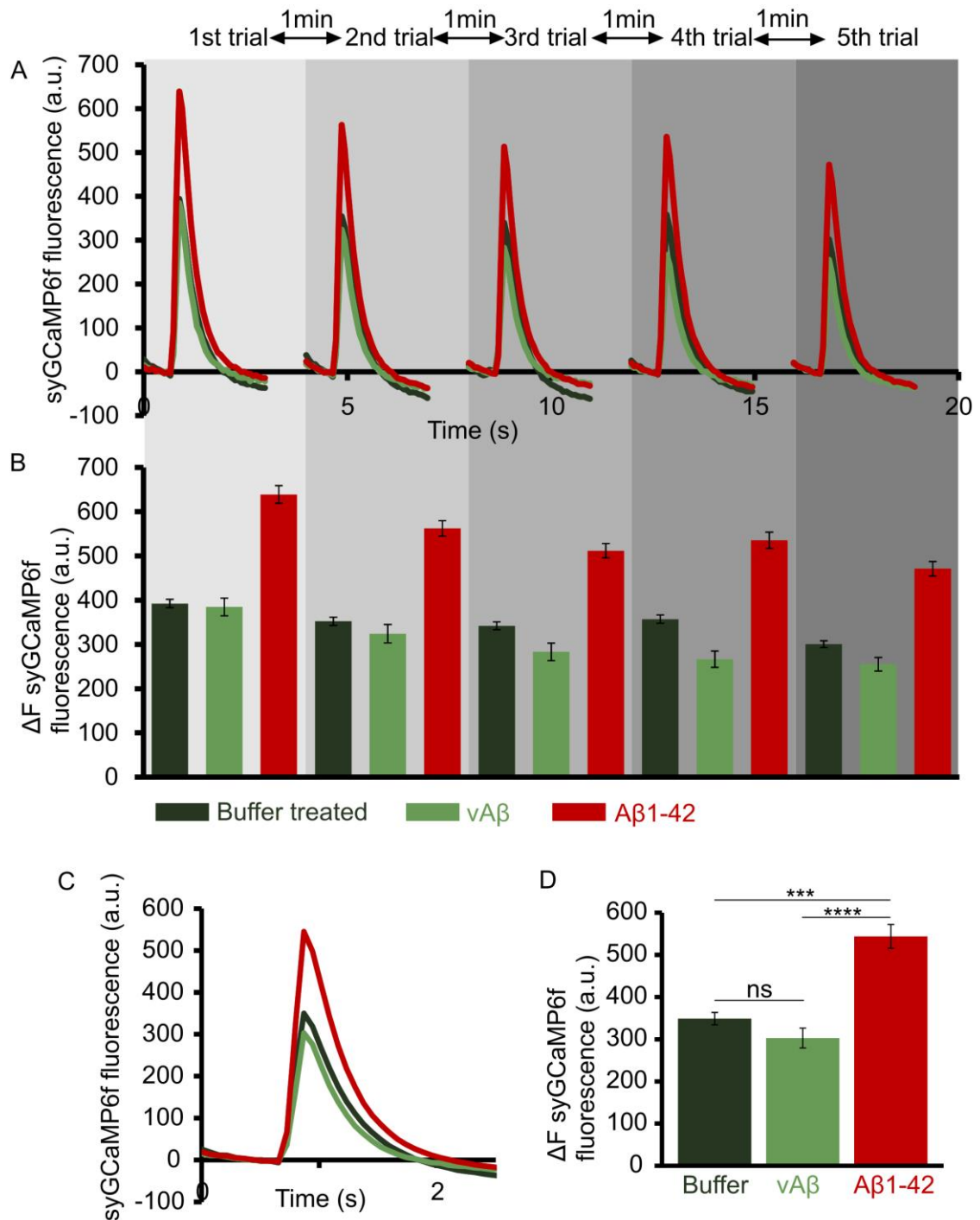


**Figure 6.11 A $\beta$ 1-42 leads to increased Ca<sup>2+</sup> influx in response to 4 APs stimulation.**

A) Baseline subtracted traces of 5 consecutive trials at 4 APs. B) The quantification of the size of the responses in the treatment groups  $\pm$  SEM (n = 590, 199, 532 synapses from 9, 6 and 11 regions for buffer treated, vA $\beta$  and A $\beta$ 1-42 groups, respectively). C) Summary of responses from buffer treated (dark green), vA $\beta$  (light green) and A $\beta$ 1-42 groups (red) across 5 trials. D) Summary of the response sizes across 5 trials  $\pm$  SEM (n = 5 trials, One-way ANOVA with Tukey's post-hock analysis: buffer:vA $\beta$ , p=0.358; buffer:A $\beta$ 1-42, P = 0.0002; vA $\beta$ :A $\beta$ 1-42, P < 0.0001).

## 6.7 Discussion

Despite an enormous body of work, the mechanisms of toxicity of A $\beta$ 1-42 are still largely unknown and highly debated (Benilova et al., 2012). Considering the inconceivable diversity of the targets reported in studies on Alzheimer's Disease, any attempt to identify the main toxicity loci in this disease seems to be utterly bewildering (Fig.6.12). Nevertheless, presynaptic terminals have emerged as an important potential site for expression of the pathogenesis of neurodegenerative disorders. For example, the loss of synapses, and in particular the selective loss of presynaptic terminals, which preceded the atrophy of cell bodies, was identified as an early component leading to behavioural deficits in prion disease (Gray et al., 2009). Proteins aberrantly expressed in familial Parkinson's Disease such as  $\alpha$ -Synuclein, Parkin or Lrrk2 were found to disrupt synaptic vesicle trafficking and to directly bind and regulate presynaptic proteins such as SNARE complex proteins (Esposito et al., 2012). Meta-analysis of 103 studies conducted on post-mortem brain samples from Alzheimer's sufferers, revealed that presynaptic markers were predominantly affected over postsynaptic markers, suggesting strong involvement of presynaptic component in the pathology of this disease (de Wilde et al., 2016).

Here we focused our efforts on understanding how presynaptic properties change in the presence of oligomeric A $\beta$ 1-42. Our main findings on A $\beta$ 1-42 effects on presynaptic terminals in hippocampal neurons include: i) reduced density of functional boutons; ii) possible aberrant sorting of vesicles; iii) impaired kinetics of exocytosis during large stimulation trains; iv) higher numbers of vesicle released at small/medium stimulation levels; v) slower rates of endocytosis following medium release events; vi) larger Ca<sup>2+</sup> influxes in response to small to medium stimulation; vii) larger Ca<sup>2+</sup> influxes over multiple stimulation trains in comparison to the controls. These results suggest a wide range of A $\beta$ 1-42 - induced impairments at different stages of synaptic vesicle cycle, with a



tendency towards a higher degree of presynaptic deficiency during large bursts of activity.

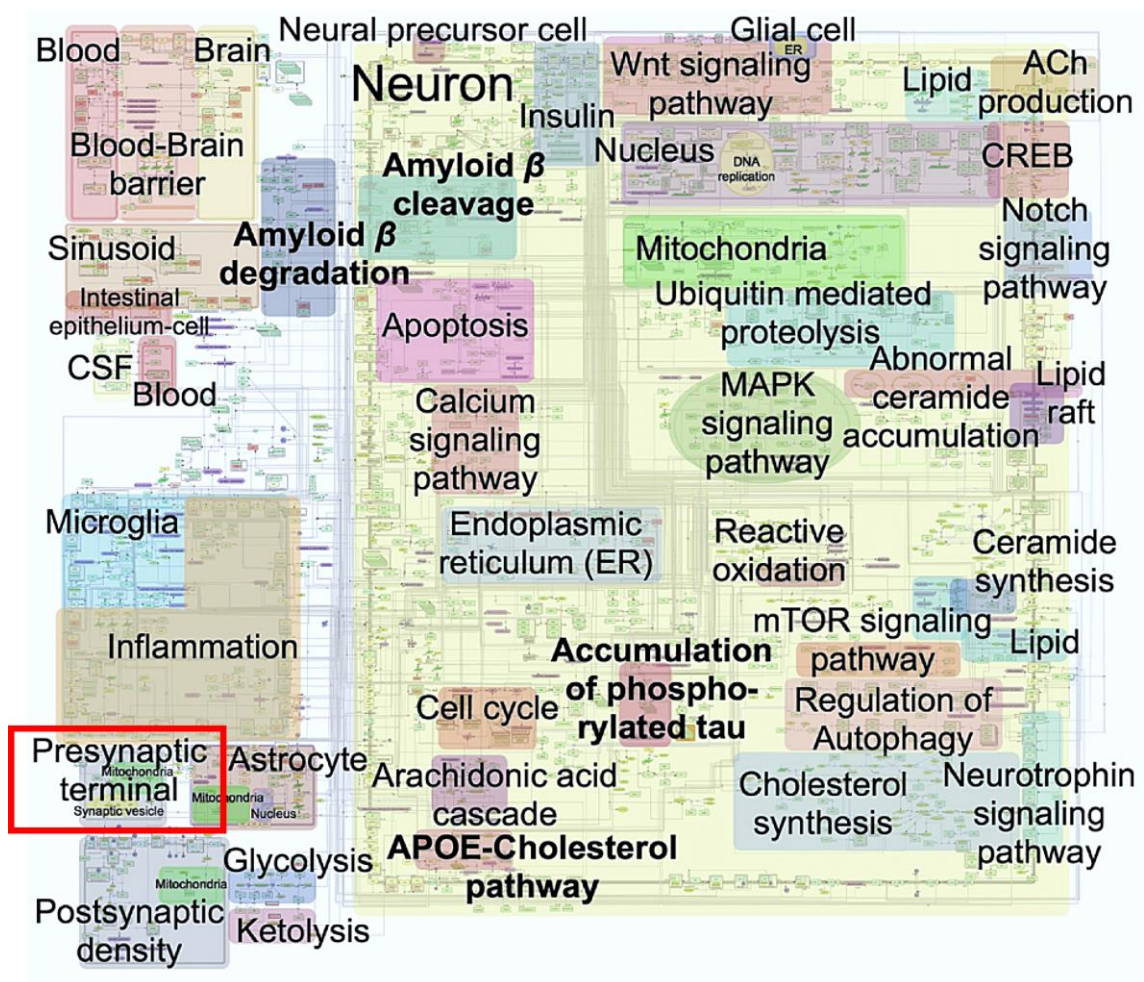


**Figure 6.12 Summary of signalling pathways identified to be affected in Alzheimer's Disease – "AlzPathway".** The map encapsulates intra, inter and extracellular pathways, includes 1347 molecules and 1070 reactions in various cells types and specific cellular compartments demonstrating shear complexity of AD. Presynaptic terminal highlighted with a red frame. Figure modified from Mizuno et al. 2012.

### 6.7.1 Oligomeric A $\beta$ 1-42 reduces the number of functional synapses

Our first observation using FM1-43 dye was that 24 hour treatment with 1  $\mu$ M A $\beta$ 1-42 significantly reduced the number of functional boutons. This suggests that many presynaptic terminals were either lost or simply non-functional. Electron microscopy analysis of synapse density in post-mortem brain samples from the dentate gyrus of patients with AD and mild cognitive impairment (MCI), revealed significantly reduced

numbers of synapses in patients with AD and some level of reduction in MCI (Scheff et al., 2006). A recent meta-analysis concluded that at early stages of AD, oligomeric A $\beta$  affects the presynaptic machinery, including proteins from the SNARE-complex and calcium sensors (de Wilde et al., 2016). Considering the role of these proteins in synaptic vesicle release, impairment in their expression or function could result in a lower number of FM1-43 loaded synapses in our cell culture. In line with our results, a reduction in the number of FM1-43 loaded synapses (600 APs, 20 Hz) was observed in another study (Abramov et al., 2009). This was a very encouraging finding, which validated the concentration and the timing of the incubation with A $\beta$ 1-42 in our system, and gave us confidence for further detailed exploration of its effects on SVs cycle.

### **6.7.2 Oligomeric A $\beta$ 1-42 affects synaptic vesicle exocytosis**

Firstly, we examined whether A $\beta$ 1-42 affects the kinetics of exocytosis. Our results indicate that the level of destaining was lower, and the kinetics of vesicle release slower in A $\beta$ 1-42 treated synapses, than in the vA $\beta$  and buffer treated groups. We hypothesized whether these results could arise due to A $\beta$ 1-42 interfering with departitioning of the FM dye from the membrane. Abnormal lipid membrane profile and increased membrane viscosity was found in tissue from frontal cortex from AD patients (Sebastião et al., 2013). FM1-43 insertion into the membrane and departitioning relies on a hydrophobic reaction of hydrocarbon tail of this dye with the lipids in the bilayer (Cousin, 2008). Hence any interference with the membrane lipids induced by A $\beta$ 1-42 could potentially affect the destaining rate of FM1-43. Nevertheless, a study using liposomes with increasing percentages of cholesterol to influence the membrane fluidity, found that the membrane composition had a minimal influence on the dissociation kinetics of FM dyes (Wu et al., 2009). Similarly, analysis of single vesicle destaining revealed that neither the lipid nor protein composition of the membrane contributed to changes in departitioning kinetics of FM1-43 (Richards et al., 2005). It is therefore unlikely that the difference between the

A $\beta$ 1-42 and the control groups observed in our results arose due to a technical component.

The reduced level of FM1-43 dye loss could result from a combination of 2 factors: impaired sorting of SVs to the vesicles pools upon recycling and/or impeded kinetics of exocytosis. An increase in resting pool fraction at the expense of recycling pool fraction has been reported and linked to A $\beta$ 1-42 – mediated activation of CDK5 activity (J. Park et al., 2013). In addition to this, the recovery of fusion-competent vesicles, specifically their repriming rate, was found to be severely impaired (J. Park et al., 2013). These factors together could explain a significant decrease in destaining level and in the kinetics of exocytosis revealed in our results.

Nevertheless, FM1-43 experiments conducted here used a very high level of stimulation (1200 APs, 20 Hz), which turns over the entire recycling pool. This level of activity would not be observed physiologically, unless perhaps during seizure. We therefore decided to employ smaller stimulation protocols, 40 APs and 4 APs at 20 Hz, in syHy2x experiments, which allowed us to monitor both exo – and endocytosis of SVs under different level of activity. Interestingly, we observed that the kinetics of exocytosis was not affected when few vesicles were released (responses to 4 APs and low amplitude range of responses to 40 APs), but was significantly slower in responses where multiple vesicles were released in response to 40 APs. As well as this, the amplitude of exocytosis was increased in A $\beta$ 1-42 treated cells under this small to medium stimulation. These results at first glance appear to be contradictory to the results obtained with FM1-43 where fewer vesicles were released in response to a large stimulation. Nevertheless, it has been previously found that A $\beta$ 1-42 increased the number of primed vesicles in culture hippocampal neurons (Russell et al., 2012). Moreover, inhibition of degradation of endogenous A $\beta$  was found to be positively regulating the probability of release in hippocampal cultures (Abramov et al., 2009). It is therefore possible that at lower stimulation protocols, when primed vesicles are available in abundance, together with

higher  $p_r$ , the number of vesicles released in A $\beta$ 1-42 treated was higher, whereas the availability of vesicles to be released at high stimulation was limited due to a smaller recycling pool size and slower repriming rate.

We also saw that A $\beta$ 1-42 treated cells were characterized by a significantly higher level of  $\text{Ca}^{2+}$  influx than buffer control or vA $\beta$ , which might have contributed to the higher amplitude of exocytosis in this group. This increased  $\text{Ca}^{2+}$  influx could be due to A $\beta$ 1-42 effect on P/Q-type  $\text{Ca}^{2+}$  currents. Oligomeric A $\beta$ 1-42 was indeed shown to reduce the threshold for opening of P/Q-type  $\text{Ca}^{2+}$  channels and therefore leading to a bigger  $\text{Ca}^{2+}$  influx and facilitation of the number of vesicles released (Mezler et al., 2012). Our results also indicate that with multiple rounds of stimulation, evoked  $\text{Ca}^{2+}$  influx did not decrease in A $\beta$ 1-42 treated cells in a similar fashion to buffer control and vA $\beta$ . This higher  $\text{Ca}^{2+}$  influx could lead to excitotoxicity and loss of functional synapses as it was observed in our FM1-43 experiment.

Despite the increase in the amplitude of exocytosis, we also saw slower kinetics of vesicle release in A $\beta$ 1-42 treated neurons in responses with higher amplitude. The obvious target to consider was proteins associated with SNARE complex. Oligomeric A $\beta$ 1-42 was shown to affect SNARE complex formation, by directly interacting with syntaxin 1 in a dose-dependent manner (Yang et al., 2015). Counterintuitively, the authors saw that vesicle docking was not affected and concluded that A $\beta$ 1-42 inhibits fusion pore formation, allowing only partial SNARE assembly (Yang et al., 2015). This study was carried out in a cell free environment using proteoliposomes. Perhaps, this effect of A $\beta$ 1-42 on the function of SNARE complexes was reflected in our results and aggravated during increased demand on the system.

Our results strongly indicate a deficiency in exocytosis caused by oligomeric A $\beta$ 1-42 which is apparent when higher demand is placed upon exocytic machinery. We make some predictions as to why that is the case in the model of A $\beta$ 1-42 toxicity (section 6.7.4).

### 6.7.3 Oligomeric A $\beta$ 1-42 affects synaptic vesicle endocytosis

After observing that A $\beta$ 1-42 has detrimental effect on synaptic vesicle exocytosis and Ca<sup>2+</sup> influx, we also wanted to explore whether endocytosis is affected by this protein in order to have a full picture of its mode of toxicity. Our results showed a significant decrease in the rate of endocytosis, which was more pronounced as the number of vesicles to be retrieved increased. Notably, the kinetic properties of endocytosis following single vesicle release were not affected at all. Unlike A $\beta$ 1-42, vA $\beta$  had no detrimental effect on SVs endocytosis.

SypHy2x reports reacidification of synaptic vesicles following their internalization. The decrease in the rate of endocytosis in A $\beta$ 1-42 treated synapses could therefore arise due to either delayed endocytic retrieval of plasma membrane, slower reacidification kinetics or a combination of both. Based on our results from minimal stimulation (4 APs) and experiments with Dynasore, we concluded that slower recovery of sypHy2x signals in 40 APs stimulation resulted from delayed vesicle retrieval rather than impaired reacidification kinetics. This is based on the fact that individual vesicles contain a single copy of v-ATPase (Takamori et al., 2006). If the reacidification kinetics were affected by A $\beta$ 1-42, it would be likely that we would observe a slower endocytic decay following single vesicle fusion events, which was not observed in our study. We therefore concluded that the endocytic deficiency is likely due to A $\beta$ 1-42 disturbed vesicle retrieval.

Other studies suggested endocytic deficiency in A $\beta$ 1-40 treated neurons, which was attributed to dynamin 1 depletion (Kelly and Ferreira, 2007). Similarly, a decrease in dynamin 1 was also observed in A $\beta$ 1-42 treated hippocampal neurons and in AD mouse model - Tg2576 (Kelly et al., 2005). Dynamin inhibition was found to have similar endocytic consequences as oligomeric A $\beta$  (Kelly and Ferreira, 2007), strengthening the possibility of dynamin involvement in A $\beta$ 1-42 mediated toxicity in our study. In the experiment in Chapter 5 using a dynamin blocker, Dynasore, we saw a significant

reduction in the endocytic rate. Loss of dynamin or its function, could be therefore responsible for the endocytic deficiency in A $\beta$ 1-42 treated neurons.

Not only was dynamin shown to be affected by oligomeric A $\beta$ , but abnormal cellular redistribution and accumulation of amphiphysin at the plasma membrane was also found (Kelly and Ferreira, 2007). Amphiphysin, similarly to endophilin I, is a BAR domain protein, and together with endophilin, intersectin and syndapin acts to recruit dynamin I to the cell membrane (Haucke et al., 2011; Murthy and De Camilli, 2003). Depletion of amphiphysin or a block of its function was shown to inhibit endocytic retrieval in various systems (Hosoi et al., 2009; Meinecke et al., 2013). Therefore, not only might dynamin be depleted, but also proteins important for dynamin recruitment to the endocytic sites might be affected by A $\beta$ 1-42, resulting in a decrease in the rate of endocytic retrieval.

Despite the fact that the increased stimulation-driven Ca<sup>2+</sup> influx in A $\beta$ 1-42 treated cells was likely to contribute to the increased number of exocytosed vesicles, it did not seem to have any rescue on the rate of endocytosis. What does that tell us about the exo – endocytosis coupling? Elevated intracellular calcium during sustained activity has been linked with an increased rate of endocytosis by its modulatory effect on the number of available endocytic sites (Balaji et al., 2008). Nevertheless, despite increased exocytosis and Ca<sup>2+</sup> influx, endocytosis was slower in A $\beta$ 1-42 suggesting disturbed coupling between exocytosis and endocytic retrieval of SVs. Ca<sup>2+</sup>/calmodulin-dependent phosphatase calcineurin (CaN), which is an important positive regulator of SVs endocytosis by its modulation of activity of dephosphorins (dynamin, amphiphysin or synaptojanin) (Evans and Cousin, 2007), could be a target for A $\beta$ 1-42. However, the effects of A $\beta$ 1-42 on CaN expression and activity are inconclusive (Agostinho et al., 2008; Celsi et al., 2007). SNARE proteins, including syntaxin, have been recently implicated in regulating the rate of endocytosis and in coupling exo- and endocytosis in the calyx of Held (Xu et al., 2013). Considering the possible interaction of A $\beta$ 1-42 with

syntaxin (Yang et al., 2015), the slower rate of endocytosis might be caused by disruption of function of proteins not classically associated with endocytosis.

Taking into account the complexity of cellular effects of A $\beta$ 1-42 and the variety of pathways it has been found to disrupt (Fig.6.12), it is perhaps not surprising that we find it difficult to point towards a single mechanism that would explain our results. Nevertheless, we attempted to unify our findings in a more general model of A $\beta$  toxicity.

#### **6.7.4 Model of A $\beta$ 1-42 toxicity in presynaptic terminals**

So far we considered the effect of A $\beta$ 1-42 on various proteins important for vesicle exocytosis and endocytosis. This however does not inform us on the global mechanism of A $\beta$ 1-42 induced presynaptic impairment. Most studies examining the effects of A $\beta$  average the values across all the responses to a given stimulus. Considering a large variability in presynaptic function emphasized elsewhere in this study, we decided to look at how presynaptic function is affected by A $\beta$ 1-42 depending on the level of activity. The important pattern emerged from this study, which suggests that A $\beta$ 1-42 affected vesicle recycling only during increased demand on exocytic and endocytic machinery, whereas release and retrieval of small number of vesicles occurred with no obvious impediments. We therefore propose a model of A $\beta$ 1-42 mediated presynaptic toxicity, which is based on general effect on the plasma membrane and associated with it exocytic/endocytic machinery.

Before that, we need to consider the site of A $\beta$ 1-42 toxicity: extracellular (membrane bound) or intracellular. Oligomeric A $\beta$ 1-42 applied to our cultured hippocampal neurons was shown to associate with membranes and/or be internalized (Marshall et al., 2016). A $\beta$ 1-42 was found to associate with gangliosides, a glycosphingolipid enriched in the outer leaflet of plasma membrane, leading to the disruption of the integrity of plasma membrane (Williams et al., 2015). Experiments using the neuroblastoma cell line N2A,

showed that A $\beta$ 1-42 internalization was via dynamin-dependent endocytosis (Yu et al., 2010). The effects observed here might therefore arise from both A $\beta$ 1-42 associated with the plasma membrane and from internalized oligomers. It is well known that in the presence of A $\beta$ 1-42 membrane integrity, structure and function of membrane associated proteins are severely affected by a variety of factors: i) A $\beta$ 1-42 insertion into the plasma membrane (Williams et al., 2015, 2010); ii) abnormal cellular distribution and accumulation of proteins at plasma membrane (Kelly and Ferreira, 2007); iii) direct binding of A $\beta$ 1-42 to important presynaptic proteins and a block of their normal function (Yang et al., 2015); iv) disruption of integrity and lipid and protein composition of lipid rafts (Rushworth and Hooper, 2010). We therefore propose that exo-endocytic deficiencies in the presence of A $\beta$ 1-42 might be associated with structural and functional disturbance of the membrane caused by this peptide.

Kelly & Ferreira 2007 only observed endocytic deficiency in the presence of amyloid beta when synapses had to cope with sustained, intense levels of activity, whereas spontaneous activity, which is low in hippocampal neurons, did not lead to similar impairment. It was hypothesized in a different study that at low frequency firing, membranes remain organized and synaptic vesicle proteins clustered, hence the future vesicles retain their identity, whereas during more intense stimulation, the membrane becomes more disorganized and more protein intermixing occurs (Kim and von Gersdorff, 2009). We therefore propose that during low demand on exo-endocytic machinery, assembled patches of lipids with associated proteins from readily retrievable pool are available at the plasma membrane. Perhaps some of these pre-organized “vesicles” are not affected by A $\beta$ 1-42 and would be the first ones to undergo endocytosis at low level activity. With increasing number of vesicles to be retrieved, these patches would become depleted, and further endocytic retrieval would require a high level of protein sorting and trafficking at and in the vicinity of the plasma membrane, which might be impeded by A $\beta$ 1-42 via its disrupting effects on the integrity of the plasma membrane.



In addition to this, the function of individual proteins crucial for exo- and endocytosis might be disrupted by A $\beta$ 1-42 as discussed above. Perhaps during low level activity, neurons can overcome this by recruiting fully functional proteins, whereas at high levels of activity, this distinction cannot be made, leading to functional impairment.

The dose-dependence of the disruptive effects of A $\beta$ 1-42 readily apparent in our study, might be supportive of the model put forward above. At 10-times lower concentration the number of exocytosed vesicles was still increased, whereas the kinetics of endocytosis was not affected. Perhaps this initial increase in the number of released vesicles, combined with membrane deficits induced by A $\beta$ 1-42, leads to a gradual clogging-up of the membrane with proteins, change in membrane curvature and fluidity, which in turn affects endocytic proteins and leads to endocytic impairment. Interestingly, endophilin I expression has been found to be increased in AD brain (Ren et al., 2008), which might be suggestive of some homeostatic mechanism that is activated to maintain sufficient recycling. However, subsequent activation of c-Jun N-terminal kinase (JNK), which is a stress kinase, by endophilin I, might lead to the death of neurons and AD pathology (Ren et al., 2008). Therefore, this potential rescuing mechanism might have unfavourable long term consequences.

### **6.7.5 Summary and future directions**

Our results point towards a wide spread effect of A $\beta$ 1-42 on presynaptic machinery, which is apparent during high level activity. By contrast, vA $\beta$  had no detrimental effects on the synaptic vesicle cycle, making it a suitable control for studies using hippocampal neurons. It is therefore critical to further explore A $\beta$ 1-42 effects on presynaptic homeostasis in order to find causal relationship between different aspects of the synaptic cycle that are affected by A $\beta$ 1-42.

Prevention of A $\beta$ 1-42 binding to the membranes with agents such as europium (Williams et al., 2015) could provide a first step towards elucidating the beginning of the presynaptic cascade, leading to numerous presynaptic dysfunctions. In addition to this, dynamin blockers such as dynasore, could be used during incubation times with A $\beta$ 1-42 in order to distinguish between extracellular versus intracellular effects of A $\beta$ 1-42. Experiments conducted here inform us about the effects of A $\beta$ 1-42 on the synaptic vesicle cycle and calcium influx. The important consequence of these processes is the release of neurotransmitter molecules from the SVs. Additional experiments in our culture system using iGluSnFR, could be performed in order to address the efficiency of transmission in A $\beta$ 1-42 treated cells. In order to further reinforce the findings made here, other widely employed models of Alzheimer's disease, such as Tg2576 mice or ApoE mice model, could be used in a similar set of experiments.

# 7 GENERAL DISCUSSION

---

The events associated with synaptic vesicle recycling have usually been considered to occur in a stochastic way (Balaji and Ryan, 2007; Ribault et al., 2011). The assumption that expression of presynaptic operation is largely random, is both very easily made, due to an enormous variability of parameters, and yet quite puzzling, considering the precision with which the presynaptic processes have to take place in both space (nanometres) and time (milliseconds) to ensure effective neurotransmission. In this work we addressed one of the fundamental questions about the sources of heterogeneous behaviour of the population of synapses, and uncovered rules that underlie the synapse-specific kinetics of endocytosis.

The two main aims of this work were to establish whether individual synapses show signature endocytic behaviour, and to determine to what extent the presynaptic performance is linked to the underlying synaptic characteristics. The results presented here indicate that the endocytic retrieval of synaptic vesicles at individual presynaptic terminals proceeds with signature kinetics, determined by structural and molecular characteristics of the synapses. We identified synaptic size, the size of the total vesicle pool, vesicle density and protein composition as determinants of endocytic kinetics at individual presynaptic terminals. Our findings are summarized in Figure 7.1. Based on these results, in section 7.2, we propose a model of the regulation of the kinetics of endocytosis at individual synapses.

The significance of these results lies in the role of synapses within neuronal networks. Changes in presynaptic function and structure underlie various forms of plasticity; in turn

this modulation of synaptic properties has an effect on the information flow and storage within a given network (Takeuchi et al., 2014). Conversely, the behaviour and characteristics of a given synapse is closely shaped by its function within the network (Evergren et al., 2006). Nevertheless, the regulation and expression of synaptic strengths and precision behind this regulation still remain unknown (Bartol et al., 2015). The finding made here of synapse-specific kinetics of single vesicle endocytosis could reflect adaptation of a given synapse to its role within the network. Perhaps synapses with a more unified endocytic behaviour are the stronger, more reliable synapses, and the consistency of their operation might reflect plasticity-induced adaptation, based upon an individual synapse. If that is the case, the signature behaviour of a given synapse could be a locus for disease associated disturbance of synaptic function, which could be reflected at the level of the entire network.

In addition to synapse-specific timing of vesicle retrieval, we observed that larger synapses are characterized by a faster rate of endocytosis. This again might reflect adaptation to higher functional needs placed upon these boutons. Tonic synapses, in lamprey spinal cord, which are adapted to a continuous high level of activity, showed a greater level of endocytic proteins such as dynamin and amphiphysin, than phasic synapses, which only sporadically release neurotransmitters (Evergren et al., 2006). In line with this, in our study we found that the level of endophilin I, an important regulator of endocytic kinetics, in large synapses was proportionally higher than in the small synapses, which was accompanied by faster kinetics of endocytosis in large boutons. This shows that the efficiency of synaptic machinery is highly linked with the molecular composition of a given synapse. The need for faster vesicle endocytosis in large synapses, might also stem from the fact that despite their overall bigger size, we found that these synapses are characterized by a smaller recycling fraction, relative to the small synapses. As such, they might therefore need a more efficient way of replenishing their

recycling pool of vesicles in order to sustain high levels of activity. Taken together, our findings uncover important functional parameters of hippocampal neurons.

In addition to this, we explored changes inflicted on the synaptic vesicle cycle by oligomeric amyloid beta. Our findings strongly suggest that small A $\beta$ 1-42 oligomers disrupt endocytic machinery under more intense stimulation paradigms, whereas no effect was observed during single vesicle endocytosis. We also observed an increase in the number of exocytosed vesicles and an increase in the stimulation-evoked Ca<sup>2+</sup> influx. Collectively, these presynaptic dysfunctions might be a prerequisite for the synaptic loss observed in Alzheimer's disease (Shankar et al., 2007). We proposed that A $\beta$ 1-42 toxicity is exerted by an overwhelming of the presynaptic machinery, through increasing the release of SVs. This may then serve to disrupt membrane integrity, and the function of endocytic proteins associated with it. Taken together, these findings offer new insight into the on the mechanisms of toxicity evoked by A $\beta$ 1-42 oligomers.

In the first results chapter we validated optical tools suitable for various experimental needs. As far as acutely applied probes are concerned, FM1-43 was most appropriate for monitoring synaptic vesicle exocytosis and dynamics of synaptic vesicle pools and sytl-Oyster550 for unambiguous identification of presynaptic terminals and relating presynaptic properties. Most of the functional experiments were carried out using sypHy2x, which was identified as the most suitable construct for monitoring single vesicle release and recovery events in our system. Ultrastructural analysis of presynaptic terminals allowed to verify our experimental approaches and uncover more properties of synapses that determine their functional behaviour.

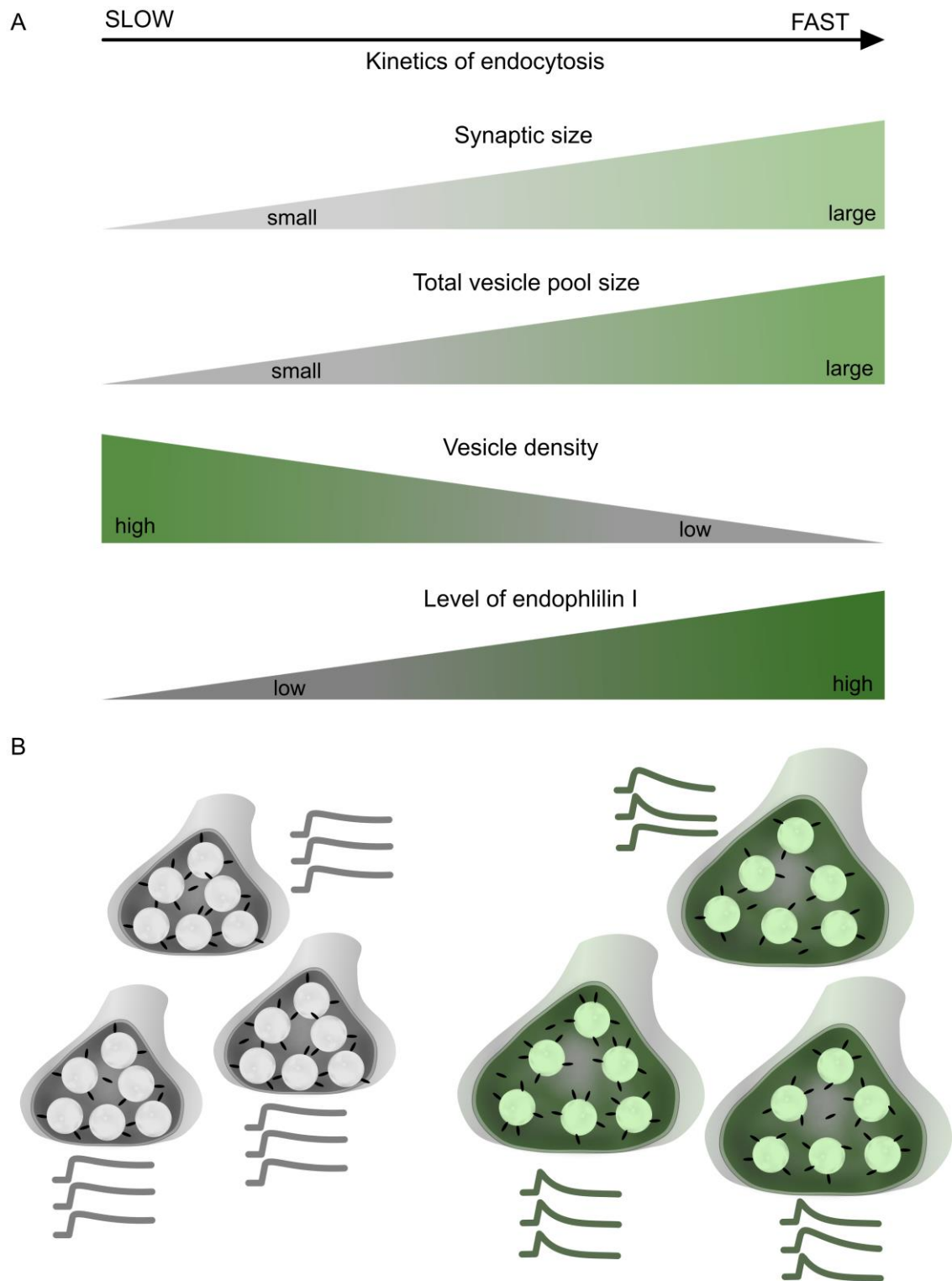


**Figure 7.1 Summary of presynaptic properties and correlates associated with endocytic timing at small and large synapses.** A) Variables associated with slower or faster kinetics included: synaptic size, size of the total pool, vesicle density and level of endophilin I. Despite the fact that the size of the total pool is directly linked to the synaptic size, we listed it separately to highlight the fact that it correlates better with the endocytic rate than the size of the recycling pool or recycling pool fraction. B) In addition to parameters summarized, small synapses were found to be less variable in terms of their endocytic kinetics and endophilin I expression, than large synapses. Examples of three

different scenarios for the behaviour of large synapses (right hand side cluster (green synapses): i) large synapse with low level of endophilin I, comparable to the amount in small synapses, behaving in a more variable way (top); ii) large synapse with more endophilin and more unified behaviour (right); iii) large synapse with high level of endophilin and fast, unified behaviour (left). The basis for this is further extrapolated in discussion in Chapter 5 section 5.5.1.2.

## 7.1 Synapse specific timing of single vesicle retrieval kinetics

We observed in our experiments a large variability in the endocytic kinetics in individual fluorescence profiles originating from the population of synapses. Based on our findings and available literature we established that this variability was not related to experimental conditions (endocytic load, focus, sampled population, and lateral diffusion of sypHy). The possibility that it was due to the differences in reacidification kinetics was also low considering the reported presence of a single v-ATPase per vesicle (Takamori et al., 2006). We therefore concluded that this variability most likely results from heterogeneity in the timing of vesicle endocytosis. Our analysis also revealed that although highly variable across the population of responses endocytic retrieval time was consistent over multiple stimulation rounds at a given synapse. We therefore suggest that individual synapses have a “preferred” mode of endocytosis. This might mean two things: different synapses preferentially recycle vesicles via different endocytic mechanisms for example CME or ultrafast endocytosis or perhaps a given endocytic mechanism is carried out with different level of efficiency at different synapses.

The timing of vesicle retrieval in our system ( $\tau = 9.4$  s following 40 APs, 20 Hz stimulation), excludes the possibility that the endocytosis proceeded via kiss-and-run. The two most likely endocytic mechanisms to operate in our system are CME and ultrafast endocytosis. In ultrafast endocytosis, within milliseconds after a single stimulus, a large portion of the plasma membrane is recovered in the form of endosome, from which individual vesicles are retrieved within 5-6 s with most of the vesicles recovered within 30 s post stimulus (Watanabe et al., 2014, 2013). This recovery of vesicles within

the period of 5-30 seconds perfectly corresponds with our findings, and could explain the general variability between synapses. Nevertheless, these authors also concluded that the endocytosis of a large endosome, equivalent to surface area of 4 vesicles, takes place after every single vesicle release event (Watanabe et al., 2013). Assuming that the entire endosome is resolved into small synaptic vesicles, the fluorescence of sypHy2x in our case should drop below the baseline each time and we only observed a few profiles that might have confirmed this mode of endocytosis as a major endocytic mechanism in this study. Although we did not specifically test this, the most likely endocytic mechanism to occur at our experimental conditions is CME. From our experiment using dynasore we established that the endocytosis is dynamin dependent and, in turn, dynamin is critical for efficient CME (Meinecke et al., 2013; Rizzoli, 2014). This suggests that individual vesicles are recycled directly from the plasma membrane in our system and that the similarity of endocytic timing at a given synapse is due to differences in the efficiency with which CME proceeds at individual boutons.

Is it possible that the similarity within synapses, is simply due to the fact that the same vesicle is recycled multiple times within our 10 trials? 4 APs stimulation used in this study would be expected to mobilize vesicles from the RRP. An investigation carried out in our laboratory, showed, that the level of reuse of RRP vesicles in a subsequent round of RRP-mobilizing stimulation, exceeded the extent of reuse that would be predicted if the same vesicles were mobilized by chance (Rey et al., 2015). In other words, some vesicles were preferentially recycled into the RRP. Precisely, 41.2% of vesicles from a 10 APs loading protocol were recruited during the next RRP-mobilizing stimulus (Appendix I, Fig.7.A-C). This indicates that the same vesicles could potentially have been recycled multiple times during repeated 4 APs stimulation in this study. However, a further experiment in the same study provides an even more definitive test: here, repeated 10 APs stimulus was applied in the presence of bafilomycin (baf), which prevents vesicle reacidification by blocking v-ATPase (Rey et al., 2015; Appendix I,



Fig.7.D). In the consecutive rounds of 10 APs stimulation, recycled vesicles were therefore prevented from undergoing a further round of exocytosis-endocytosis and, as such, this provides a test of the level of reuse. Although the amplitude of the response gradually diminished, this decline was very slow, implying that reuse was low. Moreover, a larger 1200 APs 20 Hz stimulus could still elicit a substantial response (Appendix, Fig.7.D and E). This suggests that the chances of reuse of the same vesicle in multiple 4 APs stimulation is very unlikely. In addition to this, based on the literature discussed in earlier chapters, the chances that it is exactly the same vesicle, understood as exactly the same portion of the membrane being internalized, is very negligible. We therefore propose that endocytic retrieval time is dependent on the structural and molecular characteristics of individual synapses that dictate their signature timing of retrieval.

## **7.2 Presynaptic properties that determine kinetics of single vesicle endocytosis**

We identified numerous presynaptic characteristics that can all underlie the signature endocytic behaviour of a given synapse such as size, total number of vesicles, vesicle density and the level of endophilin I (Fig.7.1). Here we propose a model that consolidates our findings and combines the mechanical and chemical interactions that may explain the differences between the endocytic kinetics at small and large synapses. In designing this model, not only did we consider protein-protein and protein-lipid interactions and composition of the plasma membrane, but also the structure-related forces that may underlie the biochemical processes leading to endocytosis of synaptic vesicles.

Plasma membrane tension, in broad terms, describes the amount of force that is needed to induce membrane deformation (Diz-Muñoz et al., 2013). In various cellular systems it has been shown that the level of exo- and endocytosis is regulated by the membrane tension (Diz-Muñoz et al., 2013). Exocytosis, leads to a decrease in plasma membrane tension, whereas endocytic retrieval, which is induced by low plasma membrane tension, has the opposite effect - it increases membrane tension (Dai et al., 1997; Diz-

Muñoz et al., 2013). Considering the fact that addition of the membrane decreases plasma membrane tension (Gauthier et al., 2009), we hypothesized that small synapses have higher plasma membrane tension than the large ones.

The interactions between proteins and lipids at the plasma membrane initiate spontaneous formation of curved membrane buds, which will later transition into  $\Omega$ -shaped invagination that will be pinched off into a new synaptic vesicle. Important steps during CME involve coating the membrane with adaptor proteins followed by assembly, of the clathrin coat (Fig.1.5). Modelling of the effect of plasma membrane tension on the formation and morphology of clathrin-coated pits, revealed that at low membrane tension, curvature of the membrane was gradually increased, leading to invagination of  $\Omega$ -shaped vesicles (Hassinger et al., 2016). However, under high membrane tension accumulation of a protein coat was observed but the membrane remained mostly flat (Hassinger et al., 2016). Our smallest synapses, therefore, must have had plasma membrane tension under a certain level above which, CME would not progressed at all. How could difference in plasma membrane tension between small and large synapses affect the endocytic retrieval? In the same model it was suggested that actin polymerisation is needed to provide the necessary forces for the transition from open U-shaped invagination to  $\Omega$ -shaped structures (Hassinger et al., 2016). Other groups proposed that clathrin coat provided sufficient force for the development of the membrane bud under low tension, whereas actin polymerisation was needed for this process to occur in a membrane under high tension (Boulant et al., 2011). This additional step in small synapses could therefore lead to a slower retrieval kinetics. Where does endophilin I function fit into this model? BAR-domain proteins (BDPs), such as endophilin or amphiphysin, have both curvature sensing and binding, and membrane-deforming properties (Liu et al., 2010). In addition to endophilin I recruitment of dynamin to endocytosing vesicles (Frost et al., 2009), BDPs were proposed to be involved in phase segregation of lipids, which was proposed to be sufficient, together with dynamin, to drive

scission of the invaginated vesicle off the membrane, making actin dispensable in the process (Liu et al., 2009). High plasma membrane tension, by having a lower propensity for bending as described above, could disrupt BDPs binding to the membrane (Diz-Muñoz et al., 2013; Zhao et al., 2011).

Taken together, we propose that smaller synapses, with higher plasma membrane tension, may need forces from polymerisation of both clathrin and actin for curvature-induction, thereby slowing down generation of an appropriate shape for endophilin I binding and scission of the invaginated vesicle (Fig.7.2). Moreover, the function of amphiphysin was shown to depend on the concentration of that protein on the membrane: mainly curvature sensing at low density and mainly membrane-deforming at high densities (Sorre et al., 2012). Perhaps endophilin I behaves in a similar way, which, considering there is proportionally lower amount of this protein in small synapses, would further slow down the endocytosis. On the other hand, in larger synapses, membrane curvature might be brought about quicker thanks to lower plasma membrane tension, and with proportionally more endophilin would lead to faster recruitment of dynamin and thus the new vesicle could be formed in a much shorter time than in small synapses (Fig.7.2). In addition to this, perhaps the space within small synapses is filled to the maximum capacity with the necessary number of copies of proteins critical for endocytosis, whereas large synapses offer more space for the movement of molecules and for the assembly of necessary protein complexes, which might also accelerate endocytic retrieval of SVs. All these factors therefore make large synapses more optimal for carrying out endocytic retrieval.

How can this model be affected by amyloid beta in our experiments? Firstly, assuming that A $\beta$ 1-42 binds to, or in any other way associates with the proteins or lipids at the membrane, it could lead to overcrowding of the plasma membrane which could itself disturb the invagination of SVs (Hassinger et al., 2016). Moreover, proteins can influence sorting of the lipids in the membrane, those that are directly, but also indirectly associated

with that particular protein (Callan-Jones et al., 2011). Hence the homeostasis at the membrane might be disrupted by A $\beta$ 1-42. Secondly, the role of lipids should not be overlooked as lipid composition plays a crucial role in setting membrane properties such as fluidity, tension or shape, and it is the configuration of different lipids that sets the membrane curvature or stretching (Callan-Jones et al., 2011). As mentioned before, lipids at the membrane associate into nanoscale domains – lipid rafts. The specific composition of these rafts and their distribution can affect membrane curvature and in return the function of curvature sensing proteins such as endophilin I. Binding of A $\beta$ 1-42 at the membrane, precisely to gangliosides within lipid rafts, and its disrupting-effect on membrane integrity (Williams et al., 2010), could lead to the observed endocytic deficiency.

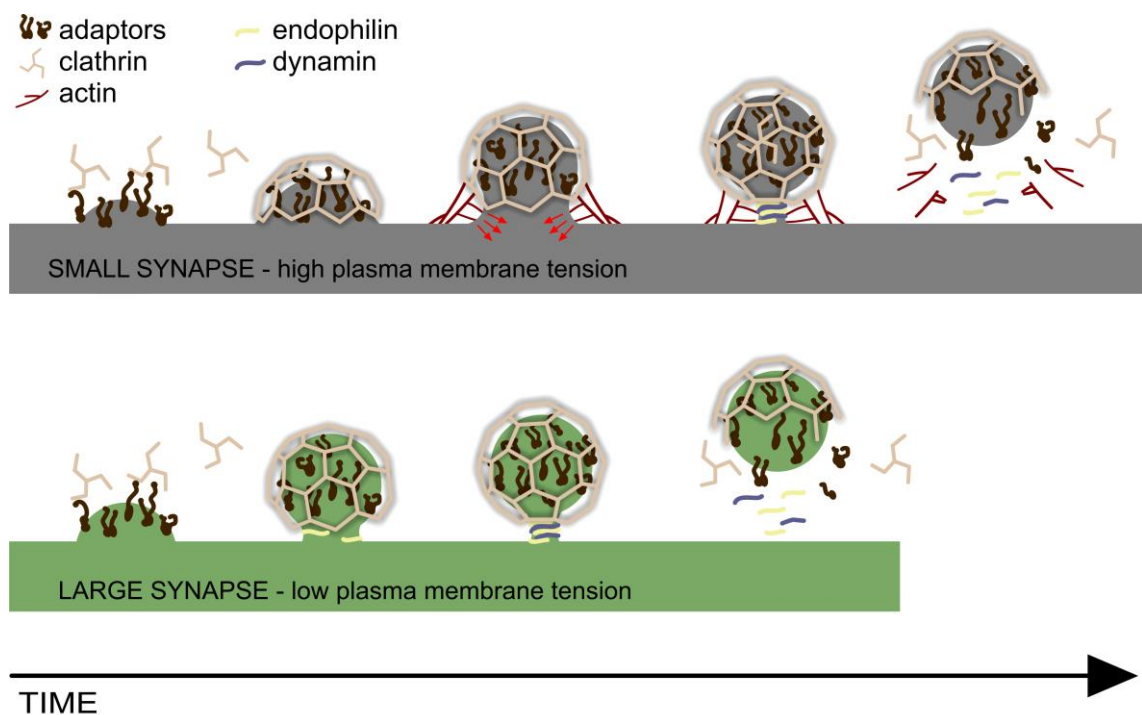


**Figure 7.2 Model summarising the difference in endocytic timing at small and large synapses.** We propose that due to higher membrane tension in small synapses, they employ actin in addition to clathrin to exert enough force for the invagination of the vesicle to proceed. Due to this additional step, the binding of BAR domain proteins such as endophilin, would also be delayed with a knock-on effect on recruitment of dynamin to the scission site. Conversely, binding of endocytic adaptor proteins and formation of clathrin coat in large synapses with lower plasma membrane tension would be sufficient to drive vesicle curvature, allowing for earlier binding of BDPs and dynamin, and faster fission of the vesicles. Graphic components based on figure from Milosevic et al. 2011.

### 7.3 Conclusions and future experiments

Despite the fact that there is an ongoing debate on the predominant mode of endocytosis in hippocampal preparations, we demonstrated that individual synapses operate in a synapse-specific manner. Moreover, the timing of endocytosis was shaped by structural and molecular properties of the presynaptic terminals. These findings offer a new insight into principle rules that govern the behaviour of small central synapses. In addition to expanding our knowledge on presynaptic function, data presented here could be utilized as another variable to be implemented in studies on network modelling and artificial intelligence. Moreover, the synaptic vesicle cycle can be a site for expression of disease associated impairment in synaptic function. We showed that A $\beta$ 1-42 reduces the number of functional synapses and that it decreases the rate of endocytic retrieval, both of which could have disastrous consequences.

The future studies could involve testing whether synapse-specific behaviour is observed in hippocampal slices from sypHy expressing mice or in vivo. This however poses imaging difficulties associated with the depth of the tissue. Currently, fluorescence resulting from stimulation below 40 APs could not be resolved in our confocal system (personal communication with Dr Stephanie Rey).

It has been proposed in the study using an epithelial cell line that under low tension a clathrin coat is sufficient to lead to the formation of a membrane bud, whereas under high tension actin polymerisation was crucial for providing additional force and therefore ensuring the progression of the membrane invagination (Boulant et al., 2011). A suggestion was also made that actin polymerisation takes over the membrane invagination only if clathrin polymerisation mechanisms halts (Boulant et al., 2011). Based on this, the entire mechanochemical model of regulation of endocytic kinetics put forward here could be tested in our cell culture system by modulating actin polymerisation with pharmacological modulators. If the hypothesis is true, latrunculin, which induces actin depolymerisation (Morales et al., 2000), should further decrease, or

perhaps even halt the endocytosis at the smallest synapses, whereas large synapses would not be affected by this treatment or to a lesser extent. The hypothesis that a higher level of vesicle clustering at small synapses, induced by tension-mediated actin polymerisation, could also be tested using this drug in an ultrastructural study.

Despite our expanding knowledge on the function of presynaptic terminals, it is very possible that major functional components of presynaptic machinery have not yet been identified. This is due to the difficulty associated with carrying out isolation of specific presynaptic components with high purity (Boyken et al., 2013). In addition to this, the possibility of the existence of a molecular tag, which would discriminate between various vesicle pools is a very attractive postulate. The method proposed here could improve the confidence of the fractionation, allow to isolate certain presynaptic structures and provide highly anticipated answers regarding the nature of vesicles pools. In short, the experimental procedure could involve loading synaptic vesicles with antibody-tagged nanomagnetic particles in a stimulation dependent manner, followed by the isolation of this tagged material with an electromagnet. Loading with the stimulus targeting different vesicle pools (RRP, RP or no stimulation for spontaneous pool), would allow to discern whether the highly anticipated and sought for molecular tag exists.

The literature spanning the last two decades, points towards a high level of variability in function and structure within hippocampal presynaptic populations. Findings presented in this thesis provide a new insight into the rules that underlie this variability, and uncover crucial presynaptic properties that determine their behaviour, offering an important platform for further exploration of the fundamental workings of central synapses in health and disease.

## Bibliography

- Abramov, E., Dolev, I., Fogel, H., Ciccotosto, G.D., Ruff, E., Slutsky, I., 2009. Amyloid- $\beta$  as a positive endogenous regulator of release probability at hippocampal synapses. *Nat. Neurosci.* 12, 1567–1576.
- Agostinho, P., Lopes, J.P., Velez, Z., Oliveira, C.R., 2008. Overactivation of calcineurin induced by amyloid-beta and prion proteins. *Neurochem. Int.* 52, 1226–1233.
- Akerboom, J., Chen, T.-W., Wardill, T.J., Tian, L., Marvin, J.S., Mutlu, S., Carreras Caldéron, N., Esposti, F., Borghuis, B.G., Sun, X.R., Gordus, A., Orger, M.B., Portugues, R., Engert, F., Macklin, J.J., Filosa, A., Aggarwal, A., Kerr, R.A., Takagi, R., Kracun, S., Shigetomi, E., Khakh, B.S., Baier, H., Lagnado, L., Wang, S.S.-H., Bargmann, C.I., Kimmel, B.E., Jayaraman, V., Svoboda, K., Kim, D.S., Schreiter, E.R., Looger, L.L., 2012. Optimization of a GCaMP Calcium Indicator for Neural Activity Imaging. *J. Neurosci.* 32, 13819–13840.
- Alabi, A.A., Tsien, R.W., 2013. Perspectives on Kiss-and-Run: Role in Exocytosis, Endocytosis, and Neurotransmission. *Annu. Rev. Physiol* 75, 393–422.
- Alzheimer's society - Dementia support and research charity. [online] [Alzheimers.org.uk/](https://www.alzheimers.org.uk/) Available at: <https://www.alzheimers.org.uk/> [Accessed 15 Aug 2016].
- Amanatkar, H.R., Papagiannopoulos, B., Grossberg, G.T., 2016. Analysis of recent failures of disease modifying therapies in Alzheimer's disease suggesting a new methodology for future studies. *Expert Rev. Neurother.* 1–10.
- Anderl, J.L., Redpath, S., Ball, A.J., 2009. A Neuronal and Astrocyte Co-Culture Assay for High Content Analysis of Neurotoxicity. *J. Vis. Exp* 27, 1–6.
- Aravanis, A.M., Pyle, J.L., Harata, N.C., Tsien, R.W., 2003. Imaging single synaptic vesicles undergoing repeated fusion events: kissing, running, and kissing again. *Neuropharmacology* 45, 797–813.
- Armbruster, M., Ryan, T. a, 2011. Synaptic vesicle retrieval time is a cell-wide rather than individual-synapse property. *Nat. Neurosci.* 14, 824–826.
- Atluri, P.P., Ryan, T., 2006. The Kinetics of Synaptic Vesicle Reacidification at Hippocampal Nerve Terminals. *J. Neurosci.* 26, 2313–2320.
- Atwood, H.L., Karunanithi, S., 2002. Diversification of synaptic strength: presynaptic elements. *Nat. Rev. Neurosci.* 3, 497–516.
- Bai, J., Hu, Z., Dittman, J.S., Pym, E.C.G., Kaplan, J.M., 2010a. Endophilin Functions as a Membrane-Bending Molecule and Is Delivered to Endocytic Zones by Exocytosis. *Cell* 143, 430–441.
- Bai, J., Hu, Z., Dittman, J.S., Pym, E.C.G., Kaplan, J.M., 2010b. Endophilin Functions as a Membrane-Bending Molecule and Is Delivered to Endocytic Zones by Exocytosis. *Cell* 143, 430–441.
- Balaji, J., Armbruster, M., Ryan, T.A., 2008. Calcium control of endocytic capacity at a CNS synapse. *J. Neurosci.* 28, 6742–6749.
- Balaji, J., Ryan, T. a, 2007. Single-vesicle imaging reveals that synaptic vesicle exocytosis and endocytosis are coupled by a single stochastic mode. *Proc. Natl Acad. Sci. USA* 104, 20576–20581.

- Banker, G.A., Cowan, W.M., 1977. Rat hippocampal neurons in dispersed cell culture. *Brain Res.* 126, 397–425.
- Bartlett, J.S., Wilcher, R., Samulski, R.J., 2000. Infectious entry pathway of adeno-associated virus and adeno-associated virus vectors. *J. Virol.* 74, 2777–2785.
- Bartol, T.M., Bromer, C., Kinney, J., Chirillo, M.A., Bourne, J.N., Harris, K.M., Sejnowski, T.J., 2015. Nanoconnectomic upper bound on the variability of synaptic plasticity. *Elife* 4, 1–18.
- Benilova, I., Karran, E., De Strooper, B., 2012. The toxic A $\beta$  oligomer and Alzheimer's disease: an emperor in need of clothes. *Nat. Neurosci.* 15, 349–357.
- Bennett, M.R., 1999. The early history of the synapse: From plato to sherrington. *Brain Res. Bull.* 50, 95–118.
- Benoit-Marand, M., Suaud-Chagny, M.-F., Gonon, F., 2007. Presynaptic Regulation of Extracellular Dopamine as Studied by Continuous Amperometry in Anesthetized Animals. In: Michael, A.C., Brland, Laura, M. (Eds.), *Electrochemical Methods for Neuroscience*. CRC Press/Taylor & Francis.
- Benson, D.L., Cohen, P. a, 1996. Activity-independent segregation of excitatory and inhibitory synaptic terminals in cultured hippocampal neurons. *J. Neurosci.* 16, 6424–32.
- Berry, C.T., Sceniak, M.P., Zhou, L., Sabo, S.L., 2012. Developmental Up-Regulation of Vesicular Glutamate Transporter-1 Promotes Neocortical Presynaptic Terminal Development. *PLoS One* 7, e50911.
- Betz, W.J., Bewick, G.S., 1992. Optical analysis of synaptic vesicle recycling at the frog neuromuscular junction. *Science* 255, 200–3.
- Betz, W.J., Mao, F., Bewick, G.S., 1992. Activity-dependent fluorescent staining and destaining of living vertebrate motor nerve terminals. *J. Neurosci.* 12, 363–375.
- Bieschke, J., Herbst, M., Wiglenda, T., Friedrich, R.P., Boeddrich, A., Schiele, F., Kleckers, D., del Amo, J.M.L., Grüning, B., Wang, Q., Schmidt, M.R., Lurz, R., Anwyl, R., Schnoegl, S., Fandrich, M., Frank, R.F., Reif, B., Gunther, S., Walsh, D.M., Wanker, E.E., 2012. Small-molecule conversion of toxic oligomers to nontoxic  $\beta$ -sheet-rich amyloid fibrils. *Nat. Chem. Biol.* 8, 93–101.
- Borghuis, B.G., Marvin, J.S., Looger, L.L., Demb, J.B., 2013. Two-photon imaging of nonlinear glutamate release dynamics at bipolar cell synapses in the mouse retina. *J. Neurosci.* 33, 10972–85.
- Boulant, S., Kural, C., Zeeh, J.-C., Ubelmann, F., Kirchhausen, T., 2011. Actin dynamics counteract membrane tension during clathrin-mediated endocytosis. *Nat. Cell Biol.* 13, 1124–1131.
- Boyken, J., Grønborg, M., Riedel, D., Urlaub, H., Jahn, R., Chua, J., 2013. Molecular profiling of synaptic vesicle docking sites reveals novel proteins but few differences between glutamatergic and GABAergic synapses. *Neuron* 78, 285–297.
- Branco, T., Marra, V., Staras, K., 2010. Examining size-strength relationships at hippocampal synapses using an ultrastructural measurement of synaptic release probability. *J. Struct. Biol.* 172, 203–10.
- Branco, T., Staras, K., 2009. The probability of neurotransmitter release: variability and feedback control at single synapses. *Nature* 10, 373–383.



- Branco, T., Staras, K., Darcy, K.J., Goda, Y., 2008. Local Dendritic Activity Sets Release Probability at Hippocampal Synapses. *Neuron* 59, 475–485.
- Broersen, K., Jonckheere, W., Rozenski, J., Vandersteen, A., Pauwels, K., Pastore, A., Rousseau, F., Schymkowitz, J., 2011. A standardized and biocompatible preparation of aggregate-free amyloid beta peptide for biophysical and biological studies of Alzheimers disease. *Protein Eng. Des. Sel.* 24, 743–750.
- Brumback, A.C., Lieber, J.L., Angleson, J.K., Betz, W.J., 2004. Using FM1-43 to study neuropeptide granule dynamics and exocytosis. *Methods* 33, 287–294.
- Budzinski, K.L., Zeigler, M., Fujimoto, B.S., Bajjalieh, S.M., Chiu, D.T., 2011. Measurements of the acidification kinetics of single Synaptobluorin vesicles. *Biophys. J.* 101, 1580–1589.
- Burgalossi, A., Jung, S., Meyer, G., Jockusch, W.J., Jahn, O., Taschenberger, H., O'Connor, V.M., Nishiki, T. ichi, Takahashi, M., Brose, N., Rhee, J.S., 2010. SNARE Protein Recycling by  $\alpha$ SNAP and  $\beta$ SNAP Supports Synaptic Vesicle Priming. *Neuron* 68, 473–487.
- Burger, P.M., Mehl, E., Maycox, P.R., Baumert, M., Lottspeich, F., De Camilli, P., Jahn, R., 1989. Synaptic Vesicles Immunoisolated from Rat Cerebral Cortex Contain High Levels of Glutamate. *Neuron* 3, 715–720.
- Burré, J., Beckhaus, T., Schägger, H., Corvey, C., Hofmann, S., Karas, M., Zimmermann, H., Volkandt, W., 2006. Analysis of the synaptic vesicle proteome using three gel-based protein separation techniques. *Proteomics* 6, 6250–6262.
- Callan-Jones, A., Sorre, B., Bassereau, P., 2011. Curvature-driven lipid sorting in biomembranes. *Cold Spring Harb. Perspect. Biol.* 3, 1–14.
- Cao, G., Platisa, J., Pieribone, V.A., Raccuglia, D., Kunst, M., Nitabach, M.N., 2013. Genetically Targeted Optical Electrophysiology in Intact Neural Circuits. *Cell* 154, 904–913.
- Ceccarelli, B., Hurlbut, W., Mauro, A., 1973. Turnover of transmitter and vesicles at the frog neuromuscular junction. *J. Cell Biol.* 57, 499–524.
- Ceccarelli, B., Hurlbut, W.P., Mauro, A., 1972. Depletion of vesicles from frog neuromuscular junctions by prolonged tetanic stimulation. *J. Cell Biol.* 54, 30–38.
- Celsi, F., Svedberg, M., Unger, C., Cotman, C.W., Carri, M.T., Ottersen, O.P., Nordberg, A., Torp, R., 2007. Beta-amyloid causes downregulation of calcineurin in neurons through induction of oxidative stress. *Neurobiol. Dis.* 26, 342–352.
- Chamberlain, L.H., Burgoyne, R.D., Gould, G.W., 2001. SNARE proteins are highly enriched in lipid rafts in PC12 cells: implications for the spatial control of exocytosis. *Proc. Natl Acad. Sci. USA* 98, 5619–5624.
- Chen, T.-W., Wardill, T.J., Sun, Y., Pulver, S.R., Renninger, S.L., Baohan, A., Schreiter, E.R., Kerr, R.A., Orger, M.B., Jayaraman, V., Looger, L.L., Svoboda, K., Kim, D.S., 2013. Ultrasensitive fluorescent proteins for imaging neuronal activity. *Nature* 499, 295–300.
- Chen, X., Barg, S., Almers, W., 2008. Release of the styryl dyes from single synaptic vesicles in hippocampal neurons. *J. Neurosci.* 28, 1894–1903.
- Chen, Y., Deng, L., Maeno-Hikichi, Y., Lai, M., Chang, S., Chen, G., Zhang, J.F., 2003. Formation of an endophilin-Ca<sup>2+</sup> channel complex is critical for clathrin-mediated synaptic vesicle endocytosis. *Cell* 115, 37–48.

- Cijssouw, T., Weber, J.P., Broeke, J.H., Broek, J.A.C., Schut, D., Kroon, T., Saarloos, I., Verhage, M., Toonen, R.F., 2014. Munc18-1 redistributes in nerve terminals in an activity- and PKC-dependent manner. *J. Cell Biol.* 204, 759–775.
- Clayton, E.L., Cousin, M.A., 2009. The molecular physiology of activity-dependent bulk endocytosis of synaptic vesicles. *J. Neurochem.* 111, 901–914.
- Colicos, M.A., Collins, B.E., Sailor, M.J., Goda, Y., 2001. Remodeling of Synaptic Actin Induced by Photoconductive Stimulation. *Cell* 107, 605–616.
- Cousin, M.A., 2008. Use of FM1-43 and Other Derivatives to Investigate Neuronal Function. *Curr. Protoc. Neurosci.* Ch.2, 1–12.
- Crawford, D.C., Kavalali, E.T., 2015. Molecular underpinnings of synaptic vesicle pool heterogeneity. *Traffic* 16, 338–364.
- Dai, J., Ting-Beall, H.P., Sheetz, M.P., 1997. The secretion-coupled endocytosis correlates with membrane tension changes in RBL 2H3 cells. *J. Gen. Physiol.* 110, 1–10.
- Dana, H., Mohar, B., Sun, Y., Narayan, S., Gordus, A., Hasseman, J.P., Tsegaye, G., Holt, G.T., Hu, A., Walpita, D., Patel, R., Macklin, J.J., Bargmann, C.I., Ahrens, M.B., Schreiter, E.R., Jayaraman, V., Looger, L.L., Svoboda, K., Kim, D.S., 2016. Sensitive red protein calcium indicators for imaging neural activity. *Elife* 5, e12727.
- Daniels, R.W., Collins, C.A., Chen, K., Gelfand, M. V, Featherstone, D.E., Diantonio, A., 2006. A Single Vesicular Glutamate Transporter Is Sufficient to Fill a Synaptic Vesicle. *Neuron* 49, 11–16.
- Darcy, K.J., Staras, K., Collinson, L.M., Goda, Y., 2006a. Constitutive sharing of recycling synaptic vesicles between presynaptic boutons. *Nat. Neurosci.* 9, 315–321.
- Darcy, K.J., Staras, K., Collinson, L.M., Goda, Y., 2006b. An ultrastructural readout of fluorescence recovery after photobleaching using correlative light and electron microscopy. *Nat. Protoc.* 1, 988–994.
- Davtyan, H., Zagorski, K., Rajapaksha, H., Hovakimyan, A., Davtyan, A., Petrushina, I., Kazarian, K., Cribbs, D.H., Petrovsky, N., Agadjanyan, M.G., Ghochikyan, A., 2016. Alzheimer's disease AdvaxCpG- adjuvanted MultiTEP-based dual and single vaccines induce high-titer antibodies against various forms of tau and A $\beta$  pathological molecules. *Sci. Rep.* 6, 28912.
- De Felice, F.G., Velasco, P.T., Lambert, M.P., Viola, K., Fernandez, S.J., Ferreira, S.T., Klein, W.L., 2007. AB Oligomers Induce Neuronal Oxidative Stress through an N-Methyl-D-aspartate Receptor-dependent Mechanism That Is Blocked by the Alzheimer Drug Memantine. *J. Biol. Chem.* 282, 11590–11601.
- Deák, F., Schoch, S., Liu, X., Südhof, T.C., Kavalali, E.T., 2004. Synaptobrevin is essential for fast synaptic-vesicle endocytosis. *Nat. Cell Biol.* 6, 1102–1108.
- Dean, C., Dunning, F.M., Liu, H., Bomba-Warczak, E., Martens, H., Bharat, V., Ahmed, S., Chapman, E.R., 2012. Axonal and dendritic synaptotagmin isoforms revealed by a pHluorin-syt functional screen. *Mol. Biol. Cell* 23, 1715–1727.
- De Robertis, E.D., Bennett, H.S., 1955. Some features of the submicroscopic morphology of synapses in frog and earthworm. *J. Biophys. Biochem. Cytol.* 1, 47–58.

- de Wilde, M.C., Overk, C.R., Sijben, J.W., Masliah, E., 2016. Meta-analysis of synaptic pathology in Alzheimer's disease reveals selective molecular vesicular machinery vulnerability. *Alzheimer's Dement.* 12, 633–644.
- Del Castillo, J., Katz, B., 1954. Quantal Components of the End-Plate Potential. *J. Physiol* 124, 560–573.
- Delvendahl, I., Vyleta, N.P., Von Gersdorff, H., Hallermann, S., 2016. Fast, Temperature-Sensitive and Clathrin- Independent Endocytosis at Central Synapses Neuron Report Fast, Temperature-Sensitive and Clathrin-Independent Endocytosis at Central Synapses. *Neuron* 90, 492–498.
- Denker, A., Bethani, I., Kröhnert, K., Körber, C., Horstmann, H., Wilhelm, B.G., Barysch, S. V, Kuner, T., Neher, E., Rizzoli, S.O., 2011a. A small pool of vesicles maintains synaptic activity in vivo. *PNAS* 108, 17177–17182.
- Denker, A., Kröhnert, K., Bückers, J., Neher, E., Rizzoli, S.O., 2011b. The reserve pool of synaptic vesicles acts as a buffer for proteins involved in synaptic vesicle recycling. *PNAS* 108, 17183–17188.
- Dittman, J., Ryan, T. a, 2009. Molecular circuitry of endocytosis at nerve terminals. *Annu. Rev. Cell Dev. Biol.* 25, 133–160.
- Diz-Muñoz, A., Fletcher, D.A., Weiner, O.D., 2013. Use the force: Membrane tension as an organized of cell shape and motility. *Trends Cell Biol* 23, 47–53.
- Dobrunz, L.E., Stevens, C.F., 1997. Heterogeneity of release probability, facilitation, and depletion at central synapses. *Neuron* 18, 995–1008.
- Dreosti, E., Odermatt, B., Dorostkar, M.M., Lagnado, L., 2009. A genetically encoded reporter of synaptic activity in vivo. *Nat. Methods* 6, 883–891.
- Eggermann, E., Bucurenciu, I., Goswami, S.P., Jonas, P., 2011. Nanodomain coupling between Ca<sup>2+</sup> channels and sensors of exocytosis at fast mammalian synapses. *Nat. Rev. Neurosci.* 13, 7–21.
- Esposito, G., Ana Clara, F., Verstreken, P., 2012. Synaptic vesicle trafficking and Parkinson's disease. *Dev. Neurobiol.* 72, 134–144.
- Evans, G.J.O., Cousin, M.A., 2007. Activity-Dependent Control of Slow Synaptic Vesicle Endocytosis by Cyclin-Dependent Kinase 5. *J. Neurosci.* 27, 401–411.
- Evergren, E., Zotova, E., Brodin, L., Shupliakov, O., 2006. Differential efficiency of the endocytic machinery in tonic and phasic synapses. *Neuroscience* 141, 123–131.
- Fatt, P., Katz, B., 1952. Spontaneous subthreshold activity at motor nerve endings. *J. Physiol.* 117, 109–128.
- Fernández-Alfonso, T., Kwan, R., Ryan, T.A., 2006. Report Synaptic Vesicles Interchange Their Membrane Proteins with a Large Surface Reservoir during Recycling. *Neuron* 51, 179–186.
- Fernandez-Alfonso, T., Ryan, T.A., 2008. A heterogeneous “resting” pool of synaptic vesicles that is dynamically interchanged across boutons in mammalian CNS synapses. *Brain Cell Biol.* 36, 87–100.
- Fernández-Alfonso, T., Ryan, T.A., 2004. The kinetics of synaptic vesicle pool depletion at CNS synaptic terminals. *Neuron* 41, 943–953.

- Fernández-Busnadiego, R., Zuber, B., Maurer, U.E., Cyrklaff, M., Baumeister, W., Lučić, V., 2010. Quantitative analysis of the native presynaptic cytomatrix by cryoelectron tomography. *J. Cell Biol.* 188, 145–156.
- Fesce, R., Grohovaz, F., Valtorta, F., Meldolesi, J., 1994. Neurotransmitter release: fusion or “kiss-and-run”? *Trends Cell Biol.* 4, 1–4.
- Feuerverger, A., Menzinger, M., Atwood, H.L., Cooper, R.L., Morgan, H., 2000. Statistical methods for assessing the dimensions of synaptic vesicles in nerve terminals. *J. Neurosci. Methods* 103, 181–190.
- Fowler, M.W., Staras, K., 2015. Synaptic vesicle pools: Principles, properties and limitations. *Exp. Cell Res.* 335, 150–156.
- Franks, K.M., Stevens, C.F., Sejnowski, T.J., 2003. Independent Sources of Quantal Variability at Single Glutamatergic Synapses. *J. Neurosci.* 23, 3186–3195.
- Fredj, N. Ben, Burrone, J., 2009. A resting pool of vesicles is responsible for spontaneous vesicle fusion at the synapse. *Nat. Neurosci.* 12, 751–8.
- Frerking, M., Wilson, M., 1996. Saturation of postsynaptic receptors at central synapses? *Curr. Opin. Neurobiol.* 6, 395–403.
- Frost, A., Unger, V.M., De Camilli, P., 2009. The BAR Domain Superfamily: Membrane-Molding Macromolecules. *Cell* 137, 191–196.
- Galimberti, D., Scarpini, E., 2011. Disease-modifying treatments for Alzheimer’s disease. *Ther. Adv. Neurol. Disord.* 4, 203–216.
- Gandhi, S.P., Stevens, C.F., 2003. Three modes of synaptic vesicular recycling revealed by single-vesicle imaging. *Nature* 423, 607–613.
- Gauthier, N.C., Rossier, O.M., Mathur, A., Hone, J.C., Sheetz, M.P., 2009. Plasma Membrane Area Increases with Spread Area by Exocytosis of a GPI-anchored Protein Compartment. *Mol. Biol. Cell* 20, 3261–3272.
- Gilson, V., Mbebi-Liegeois, C., Sellal, F., de Barry, J., 2015. Effects of Low Amyloid- $\beta$  ( $A\beta$ ) Concentration on  $A\beta$ 1-42 Oligomers Binding and GluN2B Membrane Expression. *J. Alzheimers. Dis.* 47, 453–466.
- Glickstein, M., 2006. Golgi and Cajal: The neuron doctrine and the 100th anniversary of the 1906 Nobel Prize. *Curr. Biol.* 16, 147–151.
- Gordon, S.L., Harper, C.B., Smillie, K.J., Cousin, M.A., 2016. A Fine Balance of Synaptophysin Levels Underlies Efficient Retrieval of Synaptobrevin II to Synaptic Vesicles. *PLoS One* 11, e0149457.
- Grabrucker, A., Vaida, B., Bockmann, J., Boeckers, T.M., 2009. Synaptogenesis of hippocampal neurons in primary cell culture 333–341.
- Granseth, B., Lagnado, L., 2008. The role of endocytosis in regulating the strength of hippocampal synapses. *J. Physiol.* 586, 5969–82.
- Granseth, B., Odermatt, B., Royle, S.J., Lagnado, L., 2006. Clathrin-Mediated Endocytosis Is the Dominant Mechanism of Vesicle Retrieval at Hippocampal Synapses. *Neuron* 51, 773–786.
- Gray, B.C., Siskova, Z., Perry, V.H., O’Connor, V., 2009. Selective presynaptic degeneration in the synaptopathy associated with ME7-induced hippocampal pathology. *Neurobiol. Dis.* 35, 63–74.

- Groemer, T.W., Klingauf, J., 2007. Synaptic vesicles recycling spontaneously and during activity belong to the same vesicle pool. *Nat. Neurosci.* 10, 145–147.
- Groffen, A.J., Martens, S., Arazola, R.D., Cornelisse, L.N., Lozovaya, N., Jong, A.P.H. De, Goriounova, N.A., Habets, R.L.P., Takai, Y., Borst, J.G., Brose, N., McMahon, H.T., 2010. Doc2b is a High Affinity  $\text{Ca}^{2+}$  Sensor for Spontaneous Neurotransmitter Release. *Science* 327, 1614–1618.
- Gulyá, A.I., Megías, M., Emri, Z., Freund, T.F., 1999. Total Number and Ratio of Excitatory and Inhibitory Synapses Converging onto Single Interneurons of Different Types in the CA1 Area of the Rat Hippocampus. *J. Neurosci.* 19, 10082–10097.
- Han, Y., Kaeser, P.S., Südhof, T.C., Schneggenburger, R., 2011. RIM determines  $\text{Ca}^{2+}$ -channel density and vesicle docking at the presynaptic active zone. *Neuron* 69, 304–316.
- Harata, N., Ryan, T.A., Smith, S.J., Buchanan, J., Tsien, R.W., 2001. Visualizing recycling synaptic vesicles in hippocampal neurons by FM 1-43 photoconversion. *PNAS* 98, 12748–12753.
- Harata, N.C., Aravanis, A.M., Tsien, R.W., 2006. Kiss-and-run and full-collapse fusion as modes of exo-endocytosis in neurosecretion. *J. Neurochem.* 97, 1546–1570.
- Harris, K.M., Sultan, P., 1995. Variation in the Number, Localization and Size of Synaptic Vesicles Provides an Anatomical Basis for the Nonuniform Probability of Release at Hippocampal CA1 Synapses. *Neuropharmacology* 34, 1387–1395.
- Harris, K.M., Weinberg, R.J., 2012. Ultrastructure of Synapses in the Mammalian Brain. *Cold Spring Harb. Perspect. Biol.* 4, 1–30.
- Hassinger, J.E., Oster, G., Drubin, D.G., Rangamani, P., 2016. Membrane tension is a key determinant of bud morphology in clathrin-mediated endocytosis. *Arxiv* 1604.08629.
- Haucke, V., Neher, E., Sigrist, S.J., 2011. Protein scaffolds in the coupling of synaptic exocytosis and endocytosis. *Nat. Rev. Neurosci.* 12, 127–138.
- Hayashi, Raimondi, O'Toole, Paradise, Collesi, Cremona, Ferguson, Camilli, D., 2008. Cell- and stimulus-dependent heterogeneity of synaptic vesicle endocytic recycling mechanisms revealed by studies of dynamin 1-null neurons. *Proc. Natl Acad. Sci. USA* 105, 2175–2180.
- Henkel, A., Lübke, J., Betz, W., 1996. FM1-43 dye ultrastructural localization in and release from frog motor nerve terminals. *Cell Biol.* 93, 1918–1923.
- Heuser, J.E., Reese, T., 1973. Evidence for recycling synaptic vesicle membrane during neurotransmitter release at the frog neuromuscular junction. *J Cell Biol* 57, 315–344.
- Hirata, H., Tatsumi, H., Sokabe, M., 2008. Mechanical forces facilitate actin polymerization at focal adhesions in a zyxin-dependent manner. *J. Cell Sci.* 121, 2795–2804.
- Holderith, N., Lorincz, A., Katona, G., Rózsa, B., Kulik, A., Watanabe, M., Nusser, Z., 2012. Release probability of hippocampal glutamatergic terminals scales with the size of the active zone. *Nature* 15, 988–997.
- Hopf, F.W., Waters, J., Mehta, S., Smith, S.J., 2002. Stability and Plasticity of Developing Synapses in Hippocampal Neuronal Cultures. *J. Neurosci.* 22, 775–781.

- Horstmann, H., Vasileva, M., Kuner, T., 2013. Photooxidation-Guided Ultrastructural Identification and Analysis of Cells in Neuronal Tissue Labeled with Green Fluorescent Protein. *PLoS One* 8, e64764.
- Hosoi, N., Holt, M., Sakaba, T., 2009. Calcium Dependence of Exo- and Endocytotic Coupling at a Glutamatergic Synapse. *Neuron* 63, 216–229.
- Hsieh, H., Boehm, J., Sato, C., Iwatsubo, T., Tomita, T., Sisodia, S., Malinow, R., 2006. AMPAR Removal Underlies Ab-Induced Synaptic Depression and Dendritic Spine Loss. *Neuron* 52, 831–843.
- Hu, Y., Qu, L., Schikorski, T., 2008. Mean synaptic vesicle size varies among individual excitatory hippocampal synapses. *Synapse* 62, 953–957.
- Hua, Y., Sinha, R., Martineau, M., Kahms, M., Klingauf, J., 2010. A common origin of synaptic vesicles undergoing evoked and spontaneous fusion. *Nat. Neurosci.* 13, 1451–3.
- Hua, Z., Leal-ortiz, S., Foss, S.M., Waites, C.L., Garner, C.C., Voglmaier, S.M., Edwards, R.H., 2011. v-SNARE Composition Distinguishes Synaptic Vesicle Pools. *Neuron* 71, 474–487.
- Ikeda, K., Bekkers, J.M., 2009. Counting the number of releasable synaptic vesicles in a presynaptic terminal. *Proc. Natl Acad. Sci. USA* 106, 2945–2950.
- Ishikawa, T., Sahara, Y., Takahashi, T., 2002. A Single Packet of Transmitter Does Not Saturate Postsynaptic Glutamate Receptors. *Neuron* 34, 613–621.
- Jahn, R., Südhof, T.C., 1994. SYNAPTIC VESICLES AND EXOCYTOSIS. *Annu. Rev. Neurosci* 17, 219–246.
- Jiang, M., Chen, G., 2007. Calcium Phosphate Transfection of Neuronal Cells. Clontech Lab.
- Jin, L., Han, Z., Platisa, J., Wooltorton, J.R.A., Cohen, L.B., Pieribone, V.A., 2012. Single action potentials and subthreshold electrical events imaged in neurons with a novel fluorescent protein voltage probe. *Neuron* 75, 779–785.
- Jung, J., Loy, K., Schilling, E.M., Röther, M., Brauner, J.M., Huth, T., Schlötzer-Schrehardt, U., Alzheimer, C., Kornhuber, J., Welzel, O., Groemer, T.W., 2014. The antidepressant fluoxetine mobilizes vesicles to the recycling pool of rat hippocampal synapses during high activity. *Mol. Neurobiol.* 49, 916–930.
- Kaech, S., Banker, G., 2006. Culturing hippocampal neurons. *Nat. Protoc.* 1, 2406–2415.
- Kaesler, P.S., Deng, L., Wang, Y., Dulubova, I., Liu, X., Rizo, J., Südhof, T.C., 2011. RIM proteins tether Ca<sup>2+</sup> channels to presynaptic active zones via a direct PDZ-domain interaction. *Cell* 144, 282–295.
- Kamin, D., Lauterbach, M.A., Westphal, V., Keller, J., Schönle, A., Hell, S.W., Rizzoli, S.O., 2010. High- and low-mobility stages in the synaptic vesicle cycle. *Biophys. J.* 99, 675–684.
- Kang, R., Swayze, R., Lise, M.F., Gerrow, K., Mullard, A., Honer, W.G., El-Husseini, A., 2004. Presynaptic Trafficking of Synaptotagmin I Is Regulated by Protein Palmitoylation. *J. Biol. Chem.* 279, 50524–50536.
- Karran, E., Hardy, J., 2014. A critique of the drug discovery and phase 3 clinical programs targeting the amyloid hypothesis for Alzheimer disease. *Ann. Neurol.* 76, 185–205.

- Karran, E., Mercken, M., De Strooper, B., 2011. The amyloid cascade hypothesis for Alzheimer's disease: an appraisal for the development of therapeutics.
- Karunanithi, S., Marin, L., Wong, K., Atwood, H.L., 2002. Quantal Size and Variation Determined by Vesicle Size in Normal and Mutant *Drosophila* Glutamatergic Synapses. *J. Neurosci.* 22, 10267–10276.
- Kasprowicz, J., Kuenen, S., Miskiewicz, K., Habets, R.L.P., Smits, L., Verstreken, P., 2008. Inactivation of clathrin heavy chain inhibits synaptic recycling but allows bulk membrane uptake. *J. Cell Biol.* 182, 1007–1016.
- Kavalali, E.T., 2006. Synaptic Vesicle Reuse and Its Implications. *Neurosci.* 12, 57–66.
- Kavalali, E.T., Jorgensen, E.M., 2013. Visualizing presynaptic function. *Nat. Neurosci.* 17, 10–16.
- Kelly, B.L., Ferreira, A., 2007. Beta-Amyloid Disrupted Synaptic Vesicle Endocytosis In Cultured Hippocampal Neurons. *Neuroscience* 147, 60–70.
- Kelly, B.L., Vassar, R., Ferreira, A., 2005.  $\beta$ -Amyloid-induced Dynamin 1 Depletion in Hippocampal Neurons. *J. Biol. Chem.* 280, 31746–31753.
- Kim, J.H., von Gersdorff, H., 2009. Traffic Jams during Vesicle Cycling Lead to Synaptic Depression. *Neuron* 63, 143–145.
- Kim, S., Atwood, Harold, L., Cooper, Robin, L., 2000. Assessing accurate sizes of synaptic vesicles in nerve terminals. *Brain Res.* 877, 209–217.
- Kim, S.H., Ryan, T. a., 2010. CDK5 Serves as a Major Control Point in Neurotransmitter Release. *Neuron* 67, 797–809.
- Klingauf, J., Kavalali, E.T., Tsien, R.W., 1998. Kinetics and regulation of fast endocytosis at hippocampal synapses. *Nature* 394, 581–585.
- Knight, D., Mann, D.L., Jackson, V.M., Trout, S.J., Cunnane, T.C., Lavidis, N.A., 2005. Correlation of non-uniform protein expression with variation in transmitter release probability. *Synapse* 55, 110–121.
- Kononenko, N.L., Diril, M.K., Puchkov, D., Kintscher, M., Koo, S.J., Pfuhl, G., Winter, Y., Wienisch, M., Klingauf, J., Breustedt, J., Schmitz, D., Maritzen, T., Haucke, V., 2013. Compromised fidelity of endocytic synaptic vesicle protein sorting in the absence of stonin 2. *PNAS* 110, E526–35.
- Kononenko, N.L., Haucke, V., 2015. Molecular Mechanisms of Presynaptic Membrane Retrieval and Synaptic Vesicle Reformation. *Neuron* 85, 484–496.
- Kononenko, N.L., Puchkov, D., Classen, G.A., Walter, A.M., Pechstein, A., Sawade, L., Kaempf, N., Trimbuch, T., Lorenz, D., Rosenmund, C., Maritzen, T., Haucke, V., 2014. Clathrin/AP-2 mediate synaptic vesicle reformation from endosome-like vacuoles but are not essential for membrane retrieval at central synapses. *Neuron* 82, 981–988.
- Lambert, M.P., Barlow, A.K., Chromy, B.A., Edwards, C., Freed, R., Liosatos, M., Morgan, T.E., Rozovsky, I., Trommer, B., Viola, K.L., Wals, P., Zhang, C., Finch, C.E., Krafft, G.A., Klein, W.L., Prusiner, S.B., 1998. Diffusible, nonfibrillar ligands derived from A $\beta$ 1–42 are potent central nervous system neurotoxins. *PNAS* 95, 6448–6453.
- Leitz, J., Kavalali, E.T., 2015. Ca<sup>2+</sup> Dependence of Synaptic Vesicle Endocytosis. *Neurosci.* 22, 464–476.

- Lemke, E.A., 2005. Single Synaptic Vesicle Tracking in Individual Hippocampal Boutons at Rest and during Synaptic Activity. *J. Neurosci.* 25, 11034–11044.
- Li, H., Foss, S.M., Dobryy, Y.L., Kevin Park, C., Andrew Hires, S., Shaner, N.C., Tsien, R.Y., Osborne, L.C., Voglmaier, S.M., Garratt, A.N., John Reimer, R., Levitan, E., Bay, M., 2011. Concurrent imaging of synaptic vesicle recycling and calcium dynamics. *Front. Mol. Neurosci.* 4, 1–10.
- Li, Y., Tsien, R.W., 2012. pHTomato, a red, genetically encoded indicator that enables multiplex interrogation of synaptic activity. *Nat. Neurosci.* 15, 1047–1053.
- Li, Z., Burrone, J., Tyler, W.J., Hartman, K.N., Albeanu, D.F., Murthy, V.N., 2005. Synaptic vesicle recycling studied in transgenic mice expressing synaptobluorin. *PNAS* 102, 6131–6136.
- Liu, G., Choi, S., Tsien, R.W., 1999. Variability of Neurotransmitter Concentration and Nonsaturation of Postsynaptic AMPA Receptors at Synapses in Hippocampal Cultures and Slices. *Neuron* 22, 395–409.
- Liu, G., Tsien, R.W., 1995. Properties of synaptic transmission at single hippocampal boutons. *Nature* 375, 404–408.
- Liu, J., Sun, Y., Drubin, D.G., Oster, G.F., 2009. The mechanochemistry of endocytosis. *PLoS Biol.* 7, 1–16.
- Liu, J., Sun, Y., Oster, G., Drubin, D.G., 2010. Mechanochemical crosstalk during endocytic vesicle formation. *Curr Opin Cell Biol* 22, 1–13.
- Llobet, A., Gallop, J.L., Burden, J.J.E., Camdere, G., Chandra, P., Vallis, Y., Hopkins, C.R., Lagnado, L., McMahon, H.T., 2011. Endophilin drives the fast mode of vesicle retrieval in a ribbon synapse. *J. Neurosci.* 31, 8512–8519.
- Lue, L.-F., Kuo, Y.-M., Roher, A.E., Brachova, L., Shen, Y., Sue, L., Beach, T., Kurth, J.H., Rydel, R.E., Rogers, J., 1999. Soluble Amyloid B Peptide Concentration as a Predictor of Synaptic Change in Alzheimer's Disease. *Am. J. Pathol.* 155, 853–862.
- Macia, E., Ehrlich, M., Massol, R., Boucrot, E., Brunner, C., Kirchhausen, T., 2006. Dynasore, a Cell-Permeable Inhibitor of Dynamin. *Dev. Cell* 10, 839–850.
- Mao, T., O'connor, D.H., Scheuss, V., Nakai, J., Svoboda, K., 2008. Characterization and Subcellular Targeting of GCaMP- Type Genetically-Encoded Calcium Indicators. *PLoS One* 3, e1796.
- Marcello, E., Epis, R., Saraceno, C., Di Luca, M., 2012. Synaptic Dysfunction in Alzheimer's Disease. In: Kreutz, M.R., Sala, C. (Eds.), *Synaptic Plasticity*. Springer-Verlag, pp. 573–601.
- Marra, V., Burden, J.J., Thorpe, J.R., Smith, I.T., Smith, S.L., Häusser, M., Branco, T., Staras, K., 2012. A Preferentially Segregated Recycling Vesicle Pool of Limited Size Supports Neurotransmission in Native Central Synapses. *Neuron* 76, 579–589.
- Marshall, K.E., Vadukul, D.M., Dahal, L., Theisen, A., Fowler, M.W., Al-Hilaly, Y., Ford, L., Kemenes, G., Day, I.J., Staras, K., Serpell, L.C., 2016. A critical role for the self-assembly of Amyloid- $\beta$ 1-42 in neurodegeneration. *Sci. Rep.* 6, 30182.
- Marvin, J.S., Borghuis, B.G., Tian, L., Cichon, J., Harnett, M.T., Akerboom, J., Gordus, A., Renninger, S.L., Chen, T.-W., Bargmann, C.I., Orger, M.B., Schreiter, E.R., Demb, J.B., Gan, W.-B., Hires, A.S., Looger, L.L., 2013. An optimized fluorescent probe for visualizing glutamate neurotransmission. *Nat. Methods* 10, 162–174.



- Maschi, D., Klyachko, V.A., 2015. A nanoscale resolution view on synaptic vesicle dynamics. *Synapse* 69, 256–267.
- Matz, J., Gilyan, A., Kolar, A., McCarvill, T., Krueger, S.R., 2010. Rapid structural alterations of the active zone lead to sustained changes in neurotransmitter release. *Proc. Natl Acad. Sci. USA* 107, 8836–41.
- McIntire, L.B.J., Berman, D.E., Myaeng, J., Staniszewski, A., Arancio, O., Di Paolo, G., Kim, T.-W., 2012. Reduction of synaptojanin 1 ameliorates synaptic and behavioral impairments in a mouse model of Alzheimer's disease. *J. Neurosci.* 32, 15271–15276.
- McMahon, H.T., Boucrot, E., 2011. Molecular mechanism and physiological functions of clathrin-mediated endocytosis. *Nat. Rev. Mol. Cell Biol.* 12, 517–533.
- Meinecke, M., Boucrot, E., Camdere, G., Hon, W.C., Mittal, R., McMahon, H.T., 2013. Cooperative recruitment of dynamin and BIN/Amphiphysin/Rvs (BAR) domain-containing proteins leads to GTP-dependent membrane scission. *J. Biol. Chem.* 288, 6651–6661.
- Meinenken, C.J., Borst, J.G.G., Sakmann, B., 2002. Calcium secretion coupling at calyx of held governed by nonuniform channel-vesicle topography. *J. Neurosci.* 22, 1648–1667.
- Melcangi, R.C., Galbiati, M., Messi, E., Magnaghi, V., Cavarretta, I., Riva, M.A., Zanisi, M., 1997. Astrocyte-neuron interactions in vitro: Role of growth factors and steroids on LHRH dynamics. *Brain Res. Bull.* 44, 465–469.
- Mezler, M., Barghorn, S., Schoemaker, H., Gross, G., Nimrich, V., 2012. A $\beta$ -amyloid oligomer directly modulates P/Q-type calcium currents in *Xenopus* oocytes. *Br. J. Pharmacol.* 165, 1572–1583.
- Michel, K., Müller, J.A., Oprea, A.-M., Schoch, S., 2015. The presynaptic active zone: A dynamic scaffold that regulates synaptic efficacy. *Exp. Cell Res.* 335, 157–164.
- Micheva, K.D., Buchanan, J., Holz, R.W., Smith, S.J., 2003. Retrograde regulation of synaptic vesicle endocytosis and recycling. *Nat. Neurosci.* 6, 925–932.
- Miesenböck, G., De Angelis, D.A., Rothman, J.E., 1998. Visualizing secretion and synaptic transmission with pH-sensitive green fluorescent proteins. *Nature* 394, 192–195.
- Miller, T.M., Heuser, J.E., 1984. Endocytosis of synaptic vesicle membrane at the frog neuromuscular junction. *J. Cell Biol.* 98, 685–698.
- Milosevic, I., Giovedi, S., Lou, X., Raimondi, A., Collesi, C., Shen, H., Paradise, S., Toole, E.O., Ferguson, S., Cremona, O., Camilli, P. De, 2011. Recruitment of Endophilin to Clathrin-Coated Pit Necks Is Required for Efficient Vesicle Uncoating after Fission. *Neuron* 72, 587–601.
- Mizuno, S., Iijima, R., Ogishima, S., Kikuchi, M., Matsuoka, Y., Ghosh, S., Miyamoto, T., Miyashita, A., Kuwano, R., Tanaka, H., 2012. AlzPathway: a comprehensive map of signaling pathways of Alzheimer's disease. *BMC Syst. Biol.* 6, 1–10.
- Morales, M., Colicos, M.A., Goda, Y., 2000. Actin-Dependent Regulation of Neurotransmitter Release at Central Synapses. *Neuron* 27, 539–550.

- Moulder, K.L., Jiang, X., Taylor, A.A., Shin, W., Gillis, K.D., Mennerick, S., 2007. Vesicle pool heterogeneity at hippocampal glutamate and GABA synapses. *J. Neurosci.* 27, 9846–9854.
- Murphy, D.D., Rueter, S.M., Trojanowski, J.Q., Lee, V.M., 2000. Synucleins are developmentally expressed, and alpha-synuclein regulates the size of the presynaptic vesicular pool in primary hippocampal neurons. *J. Neurosci.* 20, 3214–3220.
- Murphy, M.P., LeVine III, H., 2010. Alzheimer's Disease and the  $\beta$ -amyloid Peptide. *J. Alzheimers Dis* 19, 1–17.
- Murthy, V.N., De Camilli, P., 2003. Cell Biology Of The Presynaptic Terminal. *Annu. Rev. Neurosci* 26, 701–728.
- Murthy, V.N., Schikorski, T., Stevens, C.F., Zhu, Y., 2001. Inactivity produces increases in neurotransmitter release and synapse size. *Neuron* 32, 673–682.
- Murthy, V.N., Sejnowski, T.J., Stevens, C.F., 1997. Heterogeneous release properties of visualized individual hippocampal synapses. *Neuron* 18, 599–612.
- Murthy, V.N., Stevens, C.F., 1998. Synaptic vesicles retain their identity through the endocytic cycle. *Nature* 392, 497–501.
- Mutch, S.A., Kensel-Hammes, P., Gadd, J.C., Fujimoto, B.S., Allen, R.W., Schiro, P.G., Lorenz, R.M., Kuyper, C.L., Kuo, J.S., Bajjalieh, S.M., Chiu, D.T., 2011. Protein quantification at the single vesicle level reveals that a subset of synaptic vesicle proteins are trafficked with high precision. *J. Neurosci.* 31, 1461–1470.
- Nakai, J., Ohkura, M., Imoto, K., 2001. A high signal-to-noise  $\text{Ca}^{2+}$  probe composed of a single green fluorescent protein. *Nat. Biotechnol.* 19, 137–141.
- Neves, G., Lagnado, L., 1999. The kinetics of exocytosis and endocytosis in the synaptic terminal of goldfish retinal bipolar cells. *J. Physiol.* 181–202.
- Newton, a J., Kirchhausen, T., Murthy, V.N., 2006. Inhibition of dynamin completely blocks compensatory synaptic vesicle endocytosis. *Proc. Natl Acad. Sci. USA* 103, 17955–17960.
- Nicholson-Tomishima, K., Ryan, T. a, 2004. Kinetic efficiency of endocytosis at mammalian CNS synapses requires synaptotagmin I. *Proc. Natl Acad. Sci. USA* 101, 16648–52.
- O'Rourke, N.A., Weiler, N.C., Micheva, K.D., Smith, S.J., 2012. Deep molecular diversity of mammalian synapses: why it matters and how to measure it. *Nat. Rev. Neurosci.* 13, 365–79.
- Okabe, S., 2007. Molecular anatomy of the postsynaptic density. *Mol. Cell. Neurosci.* 34, 503–518.
- Oorschot, D.E., Jones, D.G., 1986. Non-Neuronal Cell Proliferation in Tissue Culture: Implications for Axonal Regeneration in the Central Nervous System. *Brain Res.* 368, 49–61.
- Opazo, F., Punge, A., Bückers, J., Hoopmann, P., Kastrup, L., Hell, S.W., Rizzoli, S.O., 2010. Limited Intermixing of Synaptic Vesicle Components upon Vesicle Recycling. *Traffic* 11, 800–812.
- Orenbuch, A., Shalev, L., Marra, V., Sinai, I., Lavy, Y., Kahn, J., Burden, J.J., Staras, K., Gitler, D., 2012. Synapsin selectively controls the mobility of resting pool vesicles at hippocampal terminals. *J. Neurosci.* 32, 3969–80.

- Palay, S.L., Palade, G.E., 1955. The fine structure of neurons. *J. Biophys. Biochem. Cytol.* 1, 69–88.
- Palay, S.S.L., 1956. Synapses in the central nervous system. *J. Biophys. Biochem. Cytol.* 2, 193–202.
- Pang, Z.P., Bacaj, T., Yang, X., Zhou, P., Xu, W., Südhof, T.C., 2011. Doc2 Supports Spontaneous Synaptic Transmission by a  $\text{Ca}^{2+}$ -Independent Mechanism. *Neuron* 70, 244–251.
- Paredes, R.M., Etzler, J.C., Watts, L.T., Lechleiter, J.D., 2008. Chemical Calcium Indicators.
- Park, H., Li, Y., Tsien, R.W., 2013. Influence of Synaptic Vesicle Position on Release Probability and Exocytic Fusion Mode. *Science* 336, 1362–1366.
- Park, J., Jang, M., Chang, S., 2013. Deleterious effects of soluble amyloid- $\beta$  oligomers on multiple steps of synaptic vesicle trafficking. *Neurobiol. Dis.* 55, 129–39.
- Passafaro, M., Nakagawa, T., Sala, C., Sheng, M., 2003. Induction of dendritic spines by an extracellular domain of AMPA receptor subunit GluR2. *Nature* 424, 677–681.
- Peng, A., Rotman, Z., Deng, P.-Y., Klyachko, V.A., 2012. Differential Motion Dynamics of Synaptic Vesicles Undergoing Spontaneous and Activity-Evoked Endocytosis. *Neuron* 73, 1108–1115.
- Pennuto, M., Bonanomi, D., Benfenati, F., Valtorta, F., 2003. Synaptophysin I Controls the Targeting of VAMP2/Synaptobrevin II to Synaptic Vesicles. *Mol. Biol. Cell* 14, 4909–4919.
- Perkovic, M., Kunz, M., Endesfelder, U., Bunse, S., Wigge, C., Yu, Z., Hodiernau, V.-V., Scheffer, M.P., Seybert, A., Malkusch, S., Schuman, E.M., Heilemann, M., Frangakis, A.S., 2014. Correlative Light- and Electron Microscopy with chemical tags. *J. Struct. Biol.* 186, 205–213.
- Peterka, D.S., Takahashi, H., Yuste, R., 2011. Imaging voltage in neurons. *Neuron* 69, 9–21.
- Peters, C., Espinoza, M.P., Gallegos, S., Opazo, C., Aguayo, L.G., 2014. Alzheimer's A $\beta$  interacts with cellular prion protein inducing neuronal membrane damage and synaptotoxicity. *Neurobiol. Aging* 36, 1369–1377.
- Picconi, B., Piccoli, G., Calabresi, P., 2012. Synaptic Dysfunction in Parkinson's Disease. In: Kreutz, M.R., Sala, C. (Eds.), *Synaptic Plasticity*. Springer-Verlag, pp. 553–572.
- Pierce, J.P., Mendell, L.M., 1993. Quantitative ultrastructure of Ia boutons in the ventral horn: scaling and positional relationships. *J. Neurosci.* 13, 4748–63.
- Pimplikar, S.W., 2009. Reassessing the amyloid cascade hypothesis of Alzheimer's disease. *Int. J. Biochem. Cell Biol.* 41, 1261–1268.
- Popovic, M.A., Foust, A.J., McCormick, D.A., Zecevic, D., 2011. The spatio-temporal characteristics of action potential initiation in layer 5 pyramidal neurons: a voltage imaging study. *J. Physiol. J. Physiol.* 589, 4167–4187.
- Posor, Y., Eichhorn-Gruenig, M., Puchkov, D., Schöneberg, J., Ullrich, A., Lampe, A., Müller, R., Zerbakhsh, S., Gulluni, F., Hirsch, E., Krauss, M., Schultz, C., Schmoranz, J., Noé, F., Haucke, V., 2013. Spatiotemporal control of endocytosis by phosphatidylinositol-3,4-bisphosphate. *Nature* 499, 233–7.

- Puchkov, D., Haucke, V., 2013. Greasing the synaptic vesicle cycle by membrane lipids. *Trends Cell Biol.* 23, 493–503.
- Pulido, C., Trigo, F.F., Llano, I., Marty, A., 2015. Vesicular release statistics and unitary postsynaptic current at single GABAergic synapses. *Neuron* 85, 159–72.
- Pyott, S.J., Rosenmund, C., 2002. The effects of temperature on vesicular supply and release in autaptic cultures of rat and mouse hippocampal neurons. *J. Physiol.* 539, 523–535.
- Qu, L., Akbergenova, Y., Hu, Y., Schikorski, T., 2009. Synapse-to-synapse variation in mean synaptic vesicle size and its relationship with synaptic morphology and function. *J. Comp. Neurol.* 514, 343–352.
- Raimondi, A., Ferguson, S.M., Lou, X., Armbruster, M., Paradise, S., Giovedi, S., Messa, M., Kono, N., Takasaki, J., Cappello, V., O'Toole, E., Ryan, T.A., De Camilli, P., 2011. Overlapping Role of Dynamin Isoforms in Synaptic Vesicle Endocytosis. *Neuron* 70, 1100–1114.
- Ratnayaka, A., Marra, V., Branco, T., Staras, K., 2011. Extrasynaptic vesicle recycling in mature hippocampal neurons. *Nat. Commun.* 2, 511–531.
- Ratnayaka, A., Marra, V., Bush, D., Burden, J.J., Branco, T., Staras, K., 2012. Recruitment of resting vesicles into recycling pools supports NMDA receptor-dependent synaptic potentiation in cultured hippocampal neurons. *J. Physiol.* 590, 1585–97.
- Reddy, P.H., Beal, M.F., 2008. Amyloid beta, mitochondrial dysfunction and synaptic damage: implications for cognitive decline in aging and Alzheimer's disease. *Trends Mol Med* 14, 45–53.
- Regehr, W.G., 2012. Short-Term Presynaptic Plasticity. *Cold Spring Harb. Perspect. Biol.* 4, a005702.
- Ren, Y., Hong, W.X., Davey, F., Taylor, M., Aiton, J., Coote, P., Fang, F., Yao, J., Chen, D., Chen, J.X., Shi, D.Y., Gunn-Moore, F.J., 2008. Endophilin I expression is increased in the brains of Alzheimer disease patients. *J. Biol. Chem.* 283, 5685–5691.
- Renner, M., Lacor, P.N., Velasco, P.T., Xu, J., Contractor, A., Klein, W.L., Triller, A., 2010. Deleterious effects of amyloid beta oligomers acting as an extracellular scaffold for mGluR5. *Neuron* 66, 739–54.
- Rey, S.A., Smith, C.A., Fowler, M.W., Crawford, F., Burden, J.J., Staras, K., 2015. Ultrastructural and functional fate of recycled vesicles in hippocampal synapses. *Nat. Commun.* 6, 1–11.
- Ribrault, C., Sekimoto, K., Triller, A., 2011. From the stochasticity of molecular processes to the variability of synaptic transmission. *Nat. Rev. Neurosci.* 12, 375–387.
- Richards, D.A., 2010. Regulation of exocytic mode in hippocampal neurons by intrabouton calcium concentration. *J Physiol* 58824, 4927–4936.
- Richards, D.A., Bai, J., Chapman, E.R., 2005. Two modes of exocytosis at hippocampal synapses revealed by rate of FM1-43 efflux from individual vesicles. *J. Cell Biol.* 168, 929–939.
- Ringstad, N., Nemoto, Y., De Camilli, P., 2001. Differential Expression of Endophilin 1 and 2 Dimers at Central Nervous System Synapses. *J. Biol. Chem.* 276, 40424–40430.

- Rizzoli, S.O., 2014. Synaptic vesicle recycling: steps and principles. *EMBO J.* 33, 788–822.
- Rohrbough, J., Broadie, K., 2005. Lipid regulation of the synaptic vesicle cycle. *Nat. Rev. Neurosci.* 6, 139–150.
- Rosenmund, C., Stevens, C.F., 1996. Definition of the readily releasable pool of vesicles at hippocampal synapses. *Neuron* 16, 1197–1207.
- Roux, A., Uyhazi, K., Frost, A., De Camilli, P., 2006. GTP-dependent twisting of dynamin implicates constriction and tension in membrane fission. *Nature* 441, 528–531.
- Royle, S.J., Granseth, B., Odermatt, B., Derevier, A., Lagnado, L., 2008. Imaging pHluorin-based probes at hippocampal synapses. *Methods Mol Biol* 457, 293–303.
- Royo, N.C., Vandenberghe, L.H., Ma, J.-Y., Hauspurg, A., Yu, L., Maronski, M., Johnston, J., Dichter, M.A., Wilson, J.M., Watson, D.J., 2008. Specific AAV Serotypes Stably Transduce Primary Hippocampal and Cortical Cultures with High Efficiency and Low Toxicity. *Brain Res.* 1190, 15–22.
- Rushworth, J. V, Hooper, N.M., 2010. Lipid Rafts: Linking Alzheimer's Amyloid- $\beta$  Production, Aggregation, and Toxicity at Neuronal Membranes. *Int. J. Alzheimers. Dis.* 2011, 603052.
- Russell, C.L., Semerdjieva, S., Empson, R.M., Austen, B.M., Beesley, P.W., Alifragis, P., 2012. Amyloid- $\beta$  acts as a regulator of neurotransmitter release disrupting the interaction between synaptophysin and VAMP2. *PLoS One* 7, e43201.
- Ryan, T. a, Reuter, H., Smith, S.J., 1997. Optical detection of a quantal presynaptic membrane turnover. *Nature* 388, 478–482.
- Ryan, T. a, Smith, S.J., 1995. Vesicle pool mobilization during action potential firing at hippocampal synapses. *Neuron* 14, 983–9.
- Saheki, Y., De Camilli, P., 2012. Synaptic Vesicle Endocytosis. *Cold Spring Harb. Perspect. Biol.* 4, 1–30.
- Sakaba, T., Kononenko, N.L., Bacetic, J., Pechstein, A., Schmoranz, J., Yao, L., Barth, H., Shupliakov, O., Kobler, O., Aktories, K., Haucke, V., 2013. Fast neurotransmitter release regulated by the endocytic scaffold intersectin. *Proc. Natl Acad. Sci. USA* 110, 8266–71.
- Sakono, M., Zako, T., 2010. Amyloid oligomers: Formation and toxicity of AB oligomers. *FEBS J.* 277, 1348–1358.
- Sankaranarayanan, S., Ryan, T.A., 2000. Real-time measurements of vesicle- SNARE recycling in synapses of the central nervous system. *Nat. Cell Biol.* 2, 197–204.
- Sankaranarayanan, S., Ryan, T.A., 2001. Calcium accelerates endocytosis of vSNAREs at hippocampal synapses. *Nat. Neurosci.* 4, 129–136.
- Sara, Y., Virmani, T., Deák, F., Liu, X., Kavalali, E.T., 2005. An isolated pool of vesicles recycles at rest and drives spontaneous neurotransmission. *Neuron* 45, 563–573.
- Scheff, S.W., Price, D.A., Schmitt, F.A., Mufson, E.J., 2006. Hippocampal synaptic loss in early Alzheimer's disease and mild cognitive impairment. *Neurobiol. Aging* 27, 1372–1384.
- Schikorski, T., Stevens, C.F., 1997. Quantitative ultrastructural analysis of hippocampal excitatory synapses. *J. Neurosci.* 17, 5858–5867.

- Schikorski, T., Stevens, C.F., 2001. Morphological correlates of functionally defined synaptic vesicle populations. *Nat. Neurosci.* 4, 391–395.
- Schuske, K.R., Richmond, J.E., Matthies, D.S., Davis, W.S., Runz, S., Rube, D.A., 2003. Endophilin Is Required for Synaptic Vesicle Endocytosis by Localizing Synaptotagmin. *Neuron* 40, 749–762.
- Sebastião, A.M., Colino-Oliveira, M., Assaife-Lopes, N., Dias, R.B., Ribeiro, J. a., 2013. Lipid rafts, synaptic transmission and plasticity: Impact in age-related neurodegenerative diseases. *Neuropharmacology* 64, 97–107.
- Serrano-Pozo, A., Frosch, M.P., Masliah, E., Hyman, B.T., 2011. Neuropathological Alterations in Alzheimer Disease. *Cold Spring Harb. Perspect. Med.* 1, 1–23.
- Shankar, G., Walsh, D., 2009. Alzheimer's disease: synaptic dysfunction and A $\beta$ . *Mol. Neurodegener.* 4, 1–13.
- Shankar, G.M., Bloodgood, B.L., Townsend, M., Walsh, D.M., Selkoe, D.J., Sabatini, B.L., 2007. Natural Oligomers of the Alzheimer Amyloid- $\beta$  Protein Induce Reversible Synapse Loss by Modulating an NMDA-Type Glutamate Receptor-Dependent Signaling Pathway. *J. Neurosci.* 27, 2866–2875.
- Sheng, M., Sabatini, B.L., Sudhof, T.C., 2012. Synapses and Alzheimer's Disease. *Cold Spring Harb. Perspect. Biol.* 4, a005777–a005777.
- Shepherd, G.M.G., Harris, K.M., 1998. Three-dimensional structure and composition of CA3- $\rightarrow$ CA1 axons in rat hippocampal slices: implications for presynaptic connectivity and compartmentalization. *J. Neurosci.* 18, 8300–8310.
- Shields, L.Y., Kim, H., Zhu, L., Haddad, D., Berthet, A., Pathak, D., Lam, M., Ponnusamy, R., Diaz-Ramirez, L.G., Gill, T.M., Sesaki, H., Mucke, L., Nakamura, K., 2015. Dynamin-related protein 1 is required for normal mitochondrial bioenergetic and synaptic function in CA1 hippocampal neurons. *Cell Death Dis.* 6, e1725.
- Shupliakov, O., Haucke, V., Pechstein, A., 2011. How synapsin I may cluster synaptic vesicles. *Semin. Cell Dev. Biol.* 22, 393–399.
- Siechen, S., Yang, S., Chiba, A., Saif, T., 2009. Mechanical tension contributes to clustering of neurotransmitter vesicles at presynaptic terminals. *Proc. Natl Acad. Sci. USA* 106, 12611–12616.
- Siksou, L., Rostaing, P., Lechaire, J.-P., Boudier, T., Ohtsuka, T., Fejtova, A., Kao, H.-T., Greengard, P., Gundelfinger, E.D., Triller, A., Marty, S., 2007. Three-Dimensional Architecture of Presynaptic Terminal Cytomatrix. *J. Neurosci.* 27, 6868–6877.
- Singec, I., Knoth, R., Ditter, M., Hagemeyer, C.E., Rosenbrock, H., Frotscher, M., Volk, B., 2002. Synaptic vesicle protein synaptoporin is differently expressed by subpopulations of mouse hippocampal neurons. *J. Comp. Neurol.* 452, 139–153.
- Sinha, R., Ahmed, S., Jahn, R., Klingauf, J., 2011. Two synaptobrevin molecules are sufficient for vesicle fusion in central nervous system synapses. *Proc. Natl Acad. Sci. USA* 108, 14318–14323.
- Smith, S.M., Renden, R., Von Gersdorff, H., 2008. Synaptic vesicle endocytosis: fast and slow modes of membrane retrieval. *Cell* 31, 559–568.
- Sorre, B., Callan-Jones, A., Manzi, J., Goud, B., Prost, J., Bassereau, P., Roux, A., 2012. Nature of curvature coupling of amphiphysin with membranes depends on its bound density. *Proc. Natl Acad. Sci. USA* 109, 173–178.

- Soura, V., Stewart-Parker, M., Williams, T.L., Ratnayaka, A., Atherton, J., Gorringer, K., Tuffin, J., Darwent, E., Rambaran, R., Klein, W., Lacor, P., Staras, K., Thorpe, J., Serpell, L.C., 2012. Visualization of co-localization in A $\beta$ 42-administered neuroblastoma cells reveals lysosome damage and autophagosome accumulation related to cell death. *Biochem. J.* 441, 579–90.
- Speese, S.D., Trotta, N., Rodesch, C.K., Aravamudan, B., Broadie, K., 2003. The Ubiquitin Proteasome System Acutely Regulates Presynaptic Protein Turnover and Synaptic Efficacy. *Curr. Biol.* 13, 899–910.
- Staras, K., Branco, T., 2010. Sharing vesicles between central presynaptic terminals: implications for synaptic function. *Front. Synaptic Neurosci.* 2, 1–6.
- Staras, K., Branco, T., Burden, J.J., Pozo, K., Darcy, K., Marra, V., Ratnayaka, A., Goda, Y., 2010. A Vesicle Superpool Spans Multiple Presynaptic Terminals in Hippocampal Neurons. *Neuron* 66, 37–44.
- Stefanis, L., 2012.  $\alpha$ -Synuclein in Parkinson's disease. *Cold Spring Harb. Perspect. Med.* 2, 1–23.
- Stevens, C.F., Sullivan, J.M., 1998. Regulation of the readily releasable vesicle pool by protein kinase C. *Neuron* 21, 885–893.
- Stevens, C.F., Tsujimoto, T., 1995. Estimates for the pool size of releasable quanta at a single central synapse and for the time required to refill the pool. *Proc. Natl Acad. Sci. USA* 92, 846–849.
- Südhof, T.C., 1995. The synaptic vesicle cycle: a cascade of protein-protein interactions. *Nature*.
- Südhof, T.C., 2004. The Synaptic Vesicle Cycle. *Annu. Rev. Neurosci.* 27, 509–547.
- Südhof, T.C., 2012. The presynaptic active zone. *Neuron* 75, 11–25.
- Südhof, T.C., 2013a. Neurotransmitter release: The last millisecond in the life of a synaptic vesicle. *Neuron* 80, 675–690.
- Südhof, T.C., 2013b. A molecular machine for neurotransmitter release: synaptotagmin and beyond. *Nat. Med.* 19, 1227–1231.
- Südhof, T.C., Rizo, J., 1996. Synaptotagmins: C2-Domain Proteins Review That Regulate Membrane Traffic. *Neuron* 17, 379–388.
- Südhof, T.C., Rizo, J., 2011. Synaptic vesicle exocytosis. *Cold Spring Harb. Perspect. Biol.* 3, 1–14.
- Sun, J.-Y., Wu, X.-S., Wu, L., 2002. Single and multiple vesicle fusion induce different rates of endocytosis at a central synapse. *Nature* 417, 555–559.
- Sun, M., Bernard, L.P., Dibona, V.L., Wu, Q., Zhang, H., 2013. Calcium Phosphate Transfection of Primary Hippocampal Neurons Video Link. *J. Vis. Exp* 81, e50808.
- Takamori, S., Holt, M., Stenius, K., Lemke, E.A., Grønborg, M., Riedel, D., Urlaub, H., Schenck, S., Brü, B., Ringler, P., Mü, S.A., Rammner, B., Grä, F., Hub, J.S., De Groot, B.L., Mieskes, G., Moriyama, Y., Rgen Klingauf, J., Grubmü, H., Heuser, J., Wieland, F., Jahn, R., 2006. Molecular Anatomy of a Trafficking Organelle. *Cell* 127, 831–846.
- Takamori, S., Rhee, J.S., Rosenmund, C., Jahn, R., 2000a. Identification of a vesicular glutamate transporter that defines a glutamatergic phenotype in neurons. *Nature* 407, 189–194.

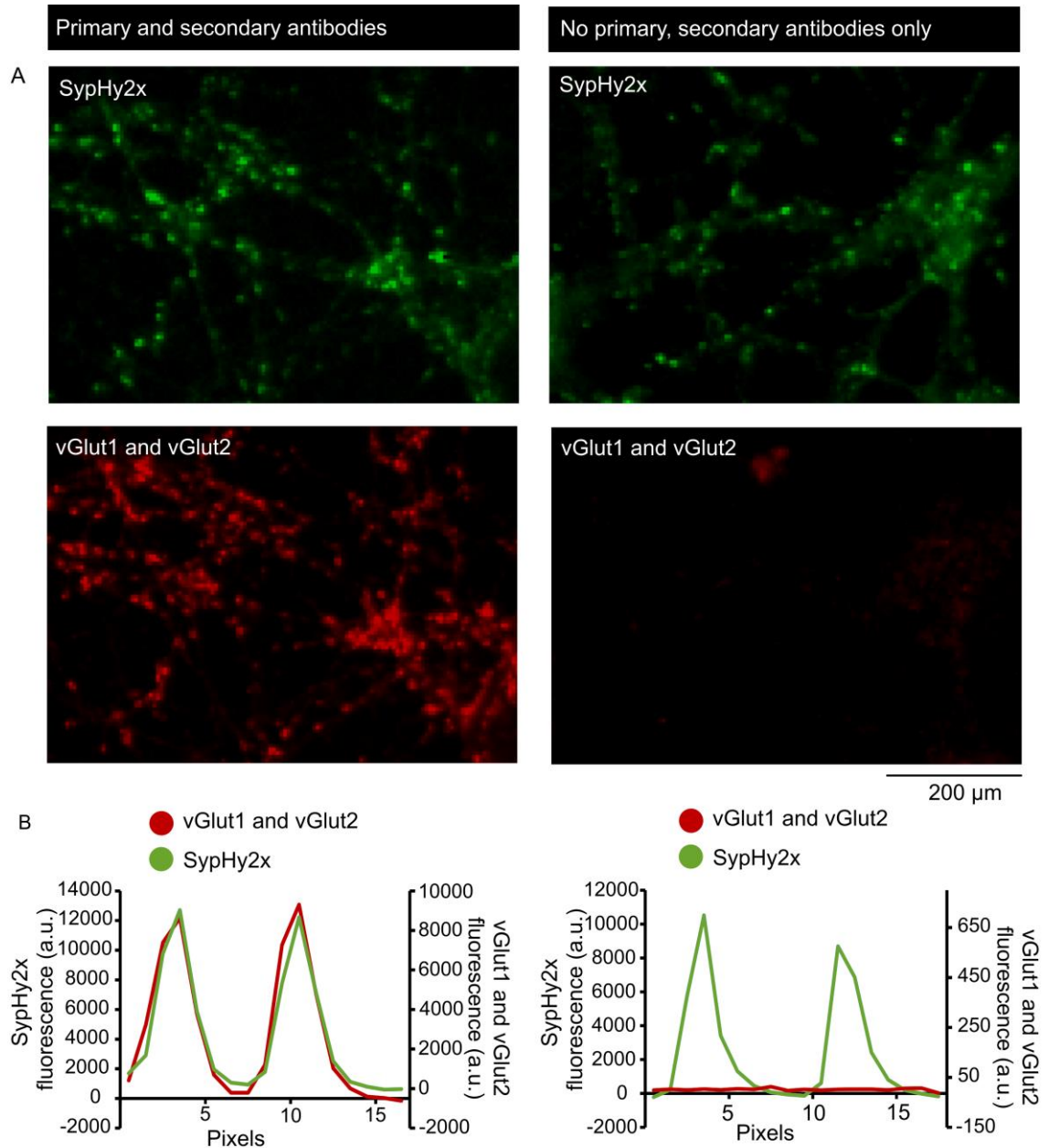
- Takamori, S., Riedel, D., Jahn, R., 2000b. Immunoisolation of GABA-specific synaptic vesicles defines a functionally distinct subset of synaptic vesicles. *J. Neurosci.* 20, 4904–4911.
- Takeuchi, T., Duzsikiewicz, A.J., Morris, R.G.M., 2014. The synaptic plasticity and memory hypothesis: encoding, storage and persistence. *Philos. Trans. R. Soc. Lond. B. Biol. Sci.* 369, 20130288.
- tom Dieck, S., Sanmartí-Vila, L., Langnaese, K., Richter, K., Kindler, S., Soyke, A., Wex, H., Smalla, K.H., Kämpf, U., Fränzer, J.T., Stumm, M., Garner, C.C., Gundelfinger, E.D., 1998. Bassoon, a novel zinc-finger CAG/glutamine-repeat protein selectively localized at the active zone of presynaptic nerve terminals. *J. Cell Biol.* 142, 499–509.
- Turrigiano, G., 2011. Homeostatic synaptic plasticity: Local and global mechanisms for stabilizing neuronal function. *Cold Spring Harb. Perspect. Biol.* 4, 1–17.
- Tyler, W.J., Zhang, X., Hartman, K., Winterer, J., Muller, W., Stanton, P.K., Pozzo-Miller, L., 2006. BDNF increases release probability and the size of a rapidly recycling vesicle pool within rat hippocampal excitatory synapses. *J. Physiol.* 574, 787–803.
- Ulrich, D., 2015. Amyloid- Impairs Synaptic Inhibition via GABAA Receptor Endocytosis. *J. Neurosci.* 35, 9205–9210.
- van den Bogaart, G., Holt, M.G., Bunt, G., Riedel, D., Wouters, F.S., Jahn, R., 2010. One SNARE complex is sufficient for membrane fusion. *Nat. Struct. Mol. Biol.* 17, 358–64.
- Virmani, T., Atasoy, D., Kavalali, E.T., 2006. Synaptic Vesicle Recycling Adapts to Chronic Changes in Activity. *J. Neurosci.* 26, 2197–2206.
- Voglmaier, S.M., Edwards, R.H., 2007. Do different endocytic pathways make different synaptic vesicles? *Curr. Opin. Neurobiol.* 17, 374–380.
- Voglmaier, S.M., Kam, K., Yang, H., Fortin, D.L., Hua, Z., Nicoll, R.A., Edwards, R.H., 2006. Distinct Endocytic Pathways Control the Rate and Extent of Synaptic Vesicle Protein Recycling. *Neuron* 51, 71–84.
- Walsh, D.M., Klyubin, I., Fadeeva, J. V., Cullen, W.K., Anwyl, R., Wolfe, M.S., Rowan, M.J., Selkoe, D.J., 2002. Naturally secreted oligomers of amyloid b protein potently inhibit hippocampal long-term potentiation in vivo. *Nature* 416, 535–539.
- Walsh, D.M., Selkoe, D.J., 2007. AB oligomers - A decade of discovery. *J. Neurochem.* 101, 1172–1184.
- Wang, C., Wang, Y., Hu, M., Chai, Z., Wu, Q., Huang, R., Han, W., Zhang, C.X., Zhou, Z., 2015. Synaptotagmin-11 inhibits clathrin-mediated and bulk endocytosis. *EMBO Rep.* 17, 1–17.
- Watakabe, A., Ohtsuka, M., Kinoshita, M., Takaji, M., Isa, K., Mizukami, H., Ozawa, K., Isa, T., Yamamori, T., 2015. Comparative analyses of adeno-associated viral vector serotypes 1, 2, 5, 8 and 9 in marmoset, mouse and macaque cerebral cortex. *Neurosci. Res.* 93, 144–157.
- Watanabe, S., 2015. Slow or fast? A tale of synaptic vesicle recycling. *Science* 350, 46–7.
- Watanabe, S., Rost, B.R., Camacho-Pérez, M., Davis, M.W., Söhl-Kielczynski, B., Rosenmund, C., Jorgensen, E.M., 2013. Ultrafast endocytosis at mouse hippocampal synapses. *Nature* 504, 242–247.



- Watanabe, S., Trimbuch, T., Camacho-Pérez, M., Rost, B.R., Brokowski, B., Söhl-Kielczynski, B., Felies, A., Davis, M.W., Rosenmund, C., Jorgensen, E.M., 2014. Clathrin regenerates synaptic vesicles from endosomes. *Nature* 515, 228–233.
- Waters, J., Smith, S.J., 2000. Phorbol esters potentiate evoked and spontaneous release by different presynaptic mechanisms. *J. Neurosci.* 20, 7863–7870.
- Waters, J., Smith, S.J., 2002. Vesicle pool partitioning influences presynaptic diversity and weighting in rat hippocampal synapses. *J. Physiol.* 541, 811–823.
- Welzel, O., Henkel, A.W., Stroebel, A.M., Jung, J., Tischbirek, C.H., Ebert, K., Kornhuber, J., Rizzoli, S.O., Groemer, T.W., 2011. Systematic heterogeneity of fractional vesicle pool sizes and release rates of hippocampal synapses. *Biophys. J.* 100, 593–601.
- Weston, M.C., Nehring, R.B., Wojcik, S.M., Rosenmund, C., 2011. Interplay between VGLUT Isoforms and Endophilin A1 Regulates Neurotransmitter Release and Short-Term Plasticity. *Neuron* 69, 1147–1159.
- Wienisch, M., Klingauf, J., 2006. Vesicular proteins exocytosed and subsequently retrieved by compensatory endocytosis are nonidentical. *Nat. Neurosci.* 9, 1019–1027.
- Wilhelm, B.G., Mandad, S., Truckenbrodt, S., Krohnert, K., Schafer, C., Rammner, B., Koo, S.J., Classen, G.A., Krauss, M., Haucke, V., Urlaub, H., Rizzoli, S.O., 2014. Composition of isolated synaptic boutons reveals the amounts of vesicle trafficking proteins. *Science* 344, 1023–1028.
- Williams, T.L., Day, I.J., Serpell, L.C., 2010. The effect of Alzheimer's A $\beta$  aggregation state on the permeation of biomimetic lipid vesicles. *Langmuir* 26, 17260–17268.
- Williams, T.L., Urbanc, B., Marshall, K.E., Vadukul, D.M., Jenkins, A.T.A., Serpell, L.C., 2015. Europium as an inhibitor of Amyloid- $\beta$ (1-42) induced membrane permeation. *FEBS Lett.* 589, 3228–3236.
- Wojcik, S.M., Rhee, J.S., Herzog, E., Sigler, A., Jahn, R., Takamori, S., Brose, N., Rosenmund, C., 2004. An essential role for vesicular glutamate transporter 1 (VGLUT1) in postnatal development and control of quantal size. *PNAS* 101, 7158–7163.
- Wu, X.-S., Xue, L., Mohan, R., Paradiso, K., Gillis, K.D., Wu, L.-G., 2007. The Origin of Quantal Size Variation: Vesicular Glutamate Concentration Plays a Significant Role. *J. Neurosci.* 27, 3046–3056.
- Wu, Y., Yeh, F.L., Mao, F., Chapman, E.R., 2009. Biophysical Characterization of Styryl Dye-Membrane Interactions. *Biophys. J.* 97, 101–109.
- Xia, Z., Dudek, H., Miranti, C.K., Greenberg, M.E., 1996. Calcium Influx via the NMDA Receptor Induces Immediate Early Gene Transcription by a MAP Kinase/ERK-Dependent Mechanism. *J. Neurosci.* 16, 5425–5436.
- Xie, Y., Chan, A.W., McGirr, A., Xue, S., Xiao, D., Zeng, H., Murphy, T.H., 2016. Resolution of High-Frequency Mesoscale Intracortical Maps Using the Genetically Encoded Glutamate Sensor iGluSnFR. *J. Neurosci.* 36, 1261–1272.
- Xu, J., Luo, F., Zhang, Z., Xue, L., Wu, X.S., Chiang, H.C., Shin, W., Wu, L.G., 2013. SNARE Proteins Synaptobrevin, SNAP-25, and Syntaxin Are Involved in Rapid and Slow Endocytosis at Synapses. *Cell Rep.* 3, 1414–1421.

- Xu, J., McNeil, B., Wu, W., Nees, D., Bai, L., Wu, L.-G., 2008. GTP-independent rapid and slow endocytosis at a central synapse. *Nat. Neurosci.* 11, 45–53.
- Yang, G., Gong, Y.-D., Gong, K., Jiang, W.-L., Kwon, E., Wang, P., Zheng, H., Zhang, X.-F., Gan, W.-B., Zhao, N.-M., 2005. Reduced synaptic vesicle density and active zone size in mice lacking amyloid precursor protein (APP) and APP-like protein 2. *Neurosci. Lett.* 384, 66–71.
- Yang, Y., Kim, J., Kim, H.Y., Ryoo, N., Lee, S., Kim, Y., Rhim, H., Shin, Y.K., 2015. Amyloid- $\beta$  Oligomers May Impair SNARE-Mediated Exocytosis by Direct Binding to Syntaxin 1a. *Cell Rep.* 12, 1244–1251.
- Ye, Z.C., Sontheimer, H., 1998. Astrocytes protect neurons from neurotoxic injury by serum glutamate. *Glia* 22, 237–248.
- Yu, C., Nwabuisi-Heath, E., Laxton, K., Ladu, M.J., 2010. Endocytic pathways mediating oligomeric A $\beta$ 42 neurotoxicity. *Mol. Neurodegener.* 5, 1–11.
- Yue, H.-Y., Xu, J., 2015. Cholesterol regulates multiple forms of vesicle endocytosis at a mammalian central synapse. *J. Neurochem.* 134, 247–260.
- Zakharenko, S.S., Zablow, L., Siegelbaum, S.A., 2001. Visualization of changes in presynaptic function during long-term synaptic plasticity. *Nat. Neurosci.* 4, 711–717.
- Zander, J.-F., Münster-Wandowski, A., Brunk, I., Pahner, I., Gómez-Lira, G., Heinemann, U., Gutiérrez, R., Laube, G., Ahnert-Hilger, G., 2010. Synaptic and vesicular coexistence of VGLUT and VGAT in selected excitatory and inhibitory synapses. *J. Neurosci.* 30, 7634–7645.
- Zenisek, D., Steyer, J.A., Feldman, M.E., Almers, W., 2002. A membrane marker leaves synaptic vesicles in milliseconds after exocytosis in retinal bipolar cells. *Neuron* 35, 1085–1097.
- Zhang, Q., 2013. Imaging Single Synaptic Vesicles in Mammalian Central Synapses with Quantum Dots. In: Rosenthal, Sandra, J., Wright, David, W. (Eds.), *Methods in Molecular Biology*. Springer Science + Business Media New York, pp. 57–69.
- Zhang, Q., Fukuda, M., Van Bockstaele, E., Pascual, O., Haydon, P.G., Tsien, R.W., 2004. Synaptotagmin IV regulates glial glutamate release. *PNAS* 101, 9441–9446.
- Zhang, Q., Li, Y., Tsien, R.W., 2009a. Response to Comment on “The Dynamic Control of Kiss-and-Run and Vesicular Reuse Probed with Single Nanoparticles”. *Science* 325, 1499c.
- Zhang, Q., Li, Y., Tsien, R.W., 2009b. The Dynamic Control of Kiss-And-Run and Vesicular Reuse Probed with Single Nanoparticles. *Science* 323, 1448–1453.
- Zhao, H., Kim, Y., Park, J., Park, D., Lee, S.-E., Chang, I., Chang, S., 2014. SCAMP5 Plays a Critical Role in Synaptic Vesicle Endocytosis during High Neuronal Activity. *J. Neurosci.* 34, 10085–10095.
- Zhao, H., Pykäläinen, A., Lappalainen, P., 2011. I-BAR domain proteins: Linking actin and plasma membrane dynamics. *Curr. Opin. Cell Biol.* 23, 14–21.
- Zhu, Y., Xu, J., Heinemann, S.F., 2009. Two Pathways of Synaptic Vesicle Retrieval Revealed by Single-Vesicle Imaging. *Neuron* 61, 397–411.
- Zoghbi, H.Y., Bear, M.F., 2012. Synaptic Dysfunction in Neurodevelopmental Intellectual Disabilities. *Cold Spring Harb. Perspect. Biol.* 4, 1–22.

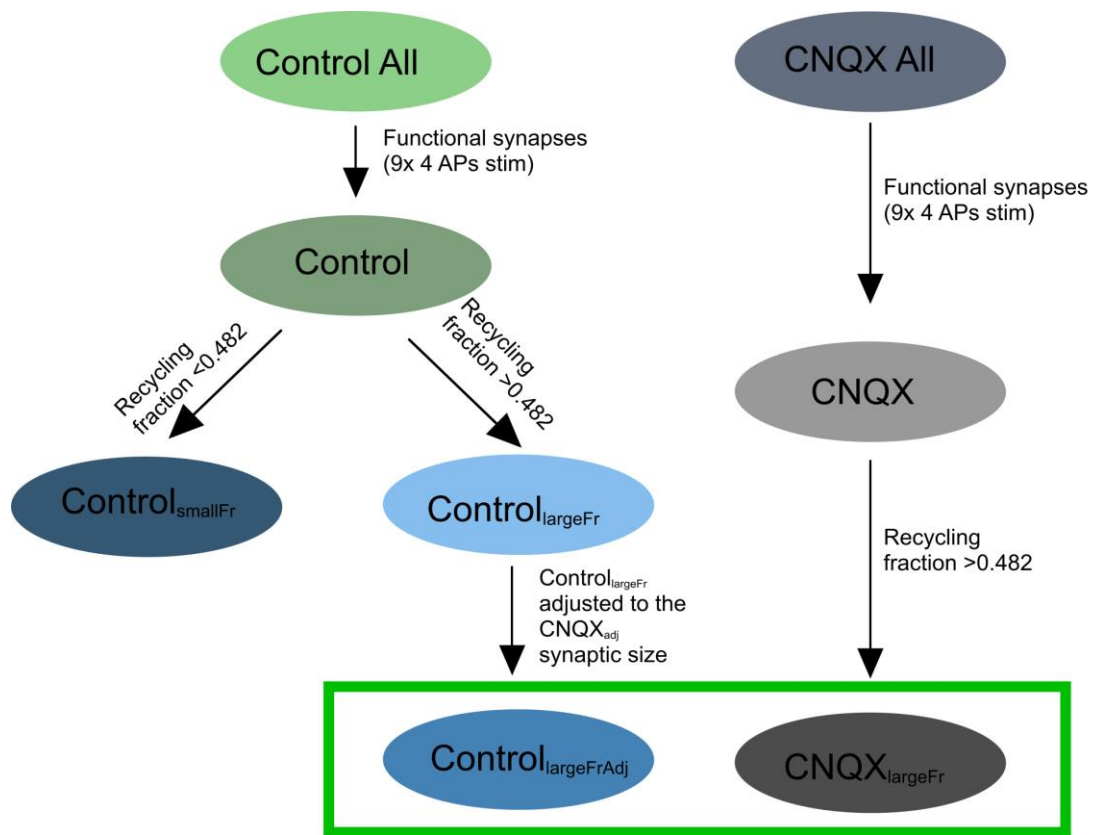
## Appendix I



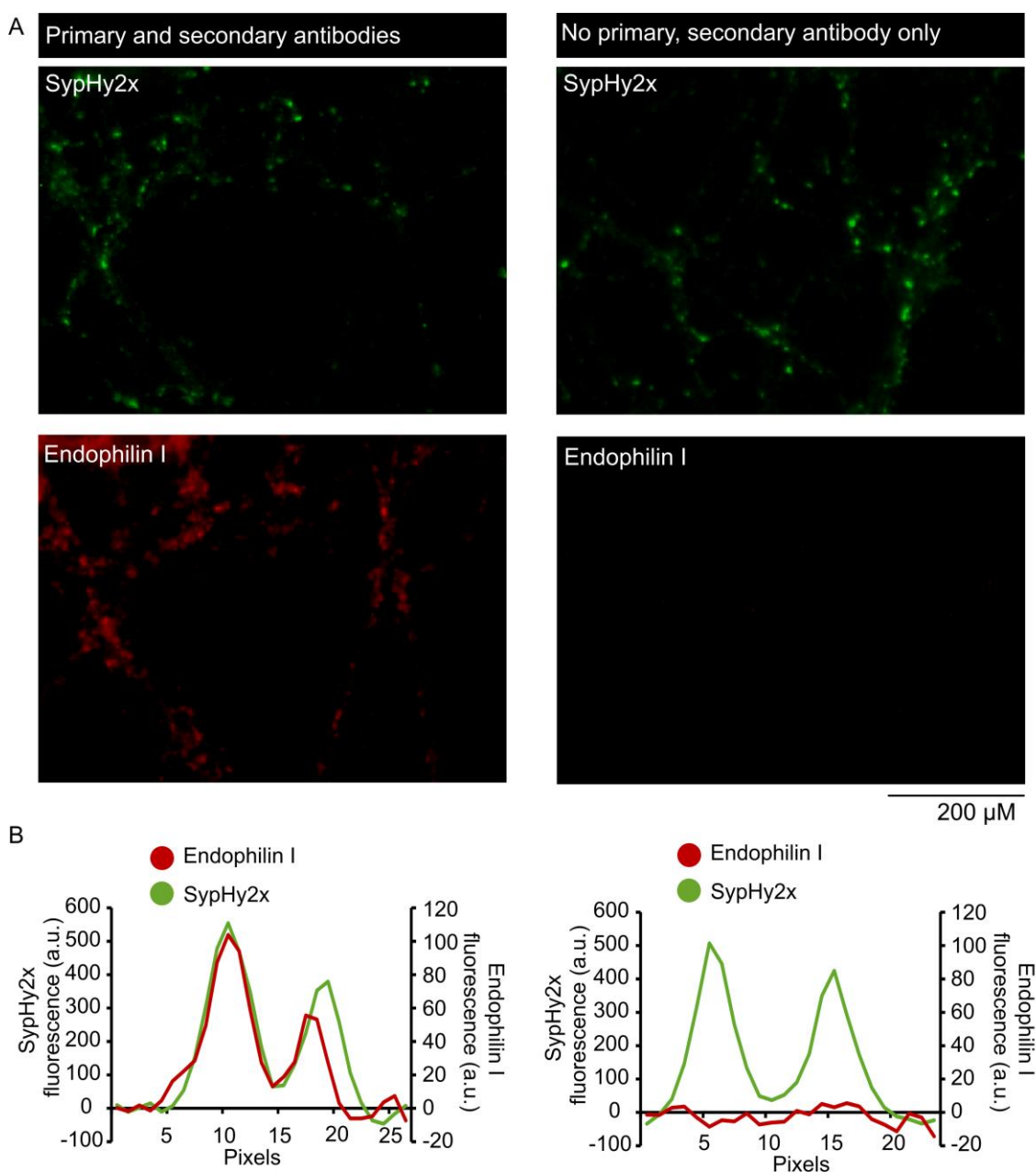
**Appendix I, Figure 1. Secondary antibodies used for vGlut1 and vGlut2 labelling do not show non-specific binding in sypHy2x expressing neurons.** A) Representative images of culture labelled with primary antibodies (Rabbit anti-vGlut1 and Guinea pig anti-vGlut2 antibody) and secondary antibodies (Goat anti-Rabbit Alexa Fluor ® 568 and Goat anti-Guinea pig Alexa Fluor ® 568) (left) or with secondary antibodies only (right). B) Fluorescence intensity profiles were plotted across sypHy2x-expressing neurons in samples labelled with both primary and secondary antibodies (left) or with secondary antibodies only (right). There was no non-specific labelling of secondary antibodies in the presence of sypHy2x.

			trial1	trial2	trial3	trial4	trial5	trial6
	WSS <sub>ave</sub>	RSS <sub>ave</sub>	RSS <sub>trial</sub>	RSS <sub>trial</sub>	RSS <sub>trial</sub>	RSS <sub>trial</sub>	RSS <sub>trial</sub>	RSS <sub>trial</sub>
synapse 1	WSS	RSS <sub>synapse</sub>	RSS	RSS	RSS	RSS	RSS	RSS
synapse 2	WSS	RSS <sub>synapse</sub>	RSS	RSS	RSS	RSS	RSS	RSS
synapse 3	WSS	RSS <sub>synapse</sub>	RSS	RSS	RSS	RSS	RSS	RSS
synapse 4	WSS	RSS <sub>synapse</sub>	RSS	RSS	RSS	RSS	RSS	RSS
synapse 5	WSS	RSS <sub>synapse</sub>	RSS	RSS	RSS	RSS	RSS	RSS
synapse 6	WSS	RSS <sub>synapse</sub>	RSS	RSS	RSS	RSS	RSS	RSS
synapse 7	WSS	RSS <sub>synapse</sub>	RSS	RSS	RSS	RSS	RSS	RSS
synapse 8	WSS	RSS <sub>synapse</sub>	RSS	RSS	RSS	RSS	RSS	RSS
synapse 9	WSS	RSS <sub>synapse</sub>	RSS	RSS	RSS	RSS	RSS	RSS
synapse 10	WSS	RSS <sub>synapse</sub>	RSS	RSS	RSS	RSS	RSS	RSS
synapse 11	WSS	RSS <sub>synapse</sub>	RSS	RSS	RSS	RSS	RSS	RSS
synapse 12	WSS	RSS <sub>synapse</sub>	RSS	RSS	RSS	RSS	RSS	RSS

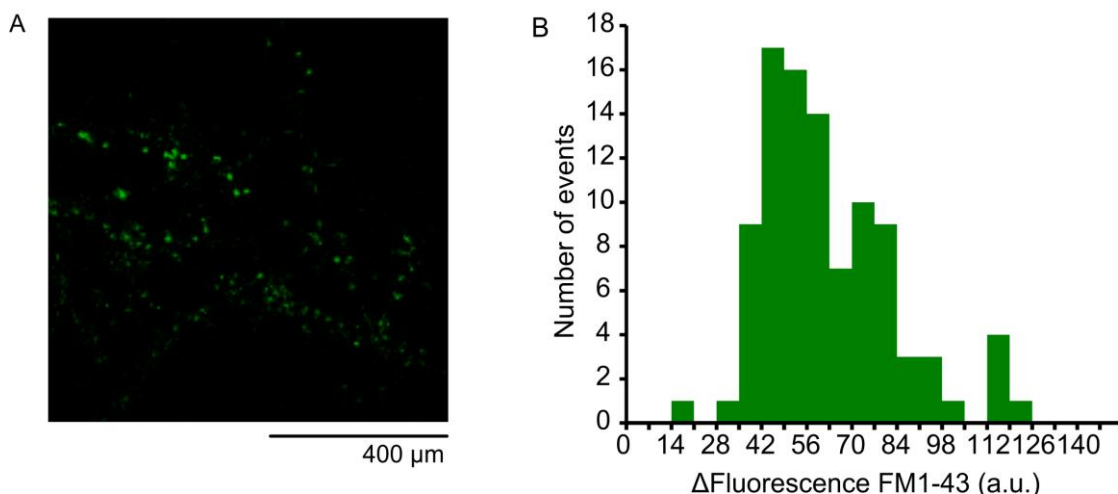
**Appendix I, Figure 2. Representation of the abbreviations and measures used in section 4.3.5.1. exploring the similarity of endocytic profiles within individual synapses.** The rows represent individual synapses and the columns on the right trials. In the experiment, we analysed 372 synapses from 25 experiments and the generated 100 randomized synapses for each experimental synapse. WSS - within synapse similarity is a point-by point measure of the difference in the shapes of endocytic profiles; WSS<sub>ave</sub> - the average of WSS from all experimental synapses; RSS - randomized synapse similarity, is an equivalent measure to WSS but for randomized synapses; RSS<sub>trial</sub> - the average of RSS results from all synapses in a particular randomization trial; RSS<sub>synapse</sub> - is the average of RSS values from 100 trials for a particular synapse; RSS<sub>ave</sub> - the average of all RSS<sub>synapse</sub> values. Double frame around WSS<sub>ave</sub> signifies that this value was used in both 'by trial' and 'by synapse' analysis.



Appendix I, Figure 3. Workflow of analysis of CNQX data.



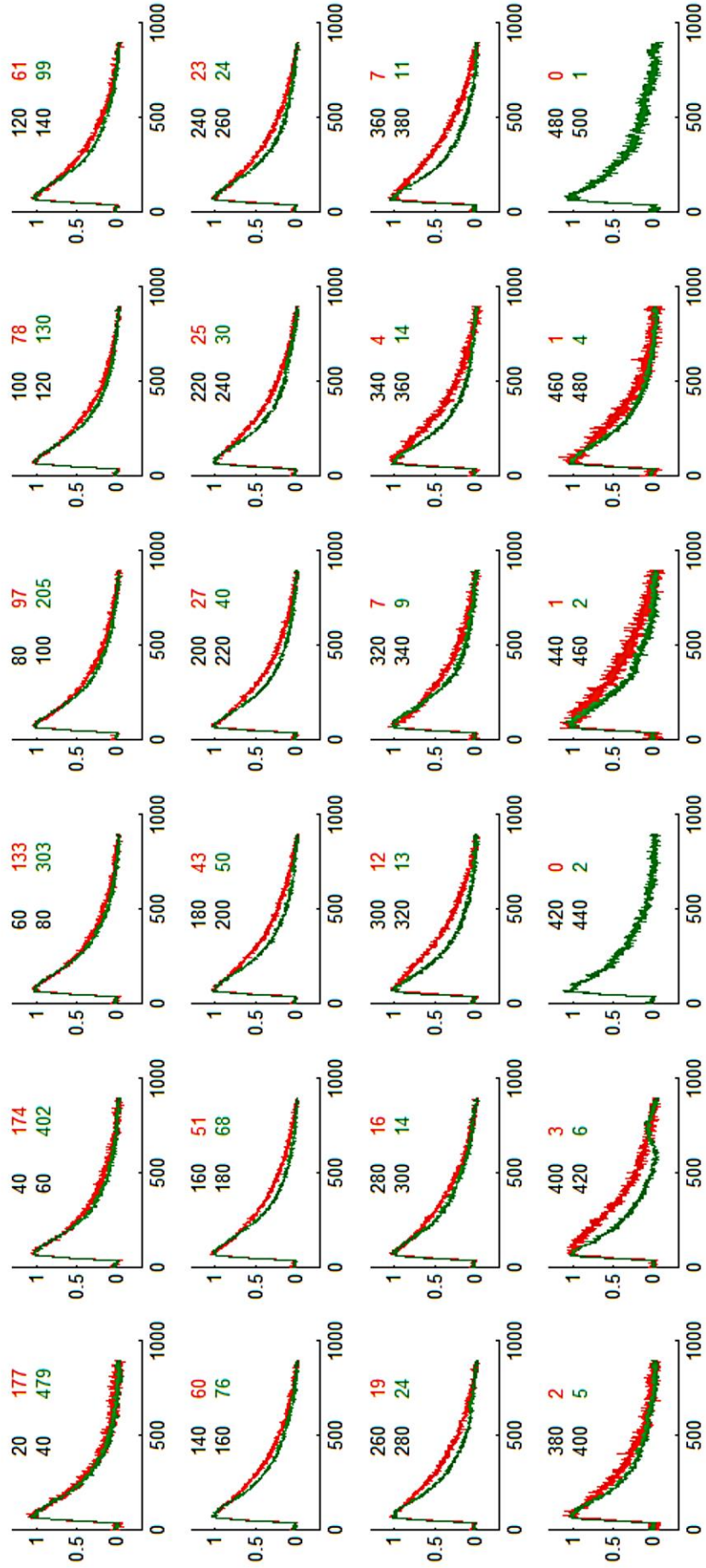
**Appendix I, Figure 4. Secondary Goat anti-Rabbit Alexa Fluor® 568 antibody does not show any non-specific binding.** A) Representative images of sypHy2x and endophilin I fluorescence in culture labelled either with primary (Rabbit anti-Endophilin I antibody) and secondary (Goat anti-Rabbit Alexa Fluor® 568) antibodies (left) or in culture where no primary antibody was used (right). Scale bar 200  $\mu$ M. B) Line profiles were drawn along sypHy2x expressing synapses showing a very good overlay with endophilin I fluorescence (left). There was no fluorescence in the red channel in the sample where no primary antibody was used (right). The measurements were baseline subtracted for each profile. These results show no non-specific binding of secondary antibody in the culture expressing sypHy2x.



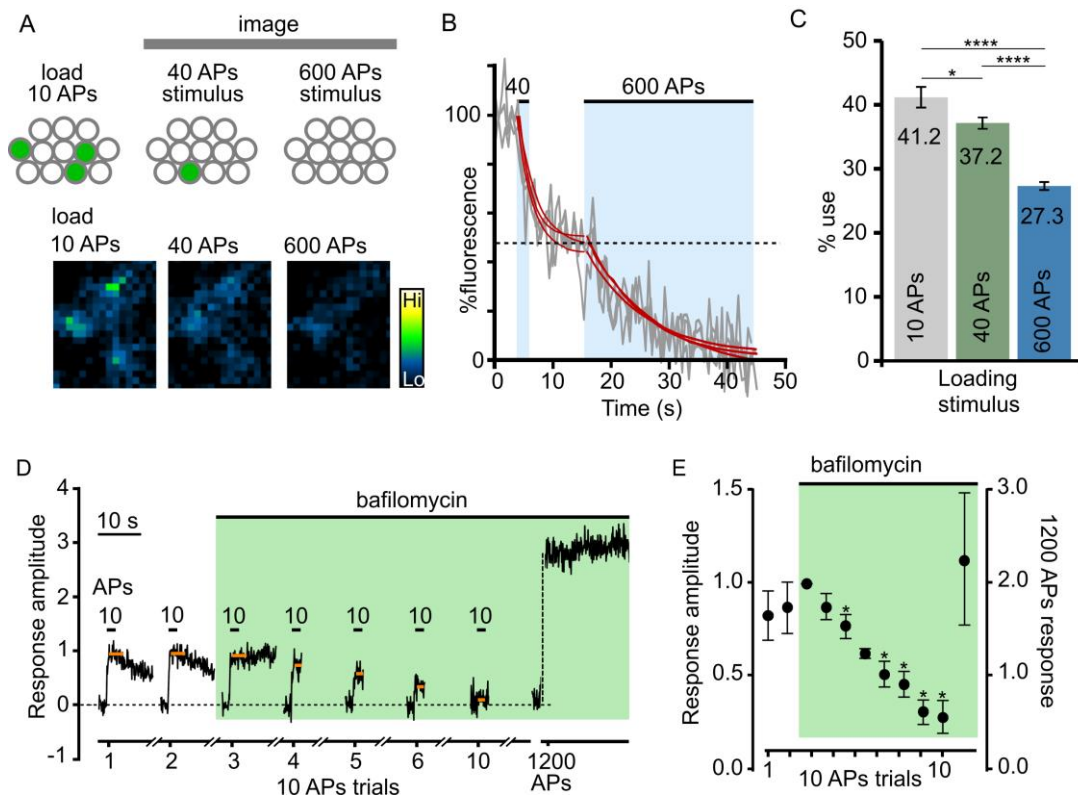
**Appendix I, Figure 5. Quantal profile of FM1-43 destaining.** Fluorescence of 4 APs loaded sample was measured prior to destaining stimulus and after 600 APs, 20 Hz stimulation. The images were subtracted and the resulting fluorescence of the punctate regions (A) measured and plotted on the histogram (B). There is evidence for quantal vesicle release with the fluorescence value corresponding to 1 quanta being 45.5 a.u. Due to the quantification method used there is no 0q peak ( $n = 97$  synapses).

**Appendix I, Figure 6 (below). Summary of responses to 40 APs 20 Hz stimulation from 24 h 1 μM Aβ1-42 (red) and Buffer treated (green) synapses.** Black digits indicate the range of response amplitudes included in the average for a given graph. Red digits give a number of Aβ1-42 traces and green of buffer treated traces found at a given response increment. Data was normalized to the peak and to the end point of each trace,  $n = 1143$ , 2209 responses from 6 (9 regions) and 7(12 regions) coverslips for Aβ1-42 and buffer treated control, respectively.









#### Appendix I, Figure 7. Measurement of vesicles reuse at RRP and 10 APs stimulus.

A) Hippocampal cultures were loaded with FM1-43 during 10 APs, 20 Hz stimulation (loading protocol as described in section 2.8). After 20 min, synapses were stimulated with 40 APs and subsequently with 600 APs in order to measure the level of reuse following the RRP stimulus. B) Destaining curves from 3 sample synapses (grey), fitted with exponential curve (red) for each round of stimulation. C) The analysis of vesicle reuse revealed a significantly greater level of subsequent recruitment of vesicles from small loading stimulus, 10 APs, than after 40 APs or 600 APs stimulus ( $n = 74, 119$  and  $131$  for 10 APs, 40 APs and 600 APs loading, respectively. One-way ANOVA with Bonferroni's multiple comparisons: 10 APs:40 APs,  $P=0.02$ ; 40 APs:600 APs,  $P < 0.0001$ ; 10 APs:600 APs,  $P < 0.0001$ ). This suggests that although most vesicles are sorted in a random fashion, some vesicles preferentially enter the RRP. D) Example profiles from 3 synapses during repeated 10 APs stimulation, 1 min apart, in the presence of  $1 \mu\text{M}$  bafilomycin show gradual depletion of vesicles available for release under 10 APs stimulation, and simultaneous availability of vesicles in RP (1200 APs stimulation). Response amplitudes were normalized to the first round of stimulation in the presence of bafilomycin. E) Quantification of response amplitudes to 10 APs stimulation in the presence of bafilomycin normalized to the first response amplitude in bafilomycin ( $n = 105$  synapses, data showed as mean  $\pm$  SEM. Asterisks indicate where the changes were significantly different from 1 in two-tailed paired Student's t-test,  $P < 0.05$ ). Figure modified from Rey et al., 2015. Results collected and analysed by Milena Maria Wagner.

# A critical role for the self-assembly of Amyloid-β1-42 in neurodegeneration

Karen E. Marshall<sup>1</sup>, Devleek M. Vadukul<sup>1</sup>, Liza Dahaj<sup>1,2</sup>, Alina Theisen<sup>1,3</sup>, Milena W. Fowler<sup>1</sup>, Youssara Al-Hilali<sup>1,2</sup>, Lenzie Ford<sup>1,3,4</sup>, György Kementes<sup>1</sup>, Iain J. Day<sup>1</sup>, Kevin Staras<sup>1</sup> & Louise C. Serpell<sup>1</sup>

Received: 09 June 2016  
Accepted: 28 June 2016  
Published: 22 July 2016

Amyloid β1-42 (Aβ1-42) plays a central role in Alzheimer's disease. The link between structure, assembly and neuronal toxicity of this peptide is of major current interest but still poorly defined. Here, we explored this relationship by rationally designing a variant form of Aβ1-42 (vAβ1-42) differing in two amino acids. Unlike Aβ1-42, we found that vAβ1-42 does not self-assemble in the presence of neuronal cells. Moreover, while Aβ1-42 oligomers impact synaptic function, vAβ1-42 does not. In a living animal model system we demonstrate that only Aβ1-42 leads to memory deficits. Our findings underline a key role for peptide sequence in the ability to assemble and form toxic structures. Furthermore, our non-toxic variant satisfies an unmet demand for a closely related control peptide for Aβ1-42 cellular studies of disease pathophysiology, offering a new opportunity to decipher the mechanisms that accompany Aβ1-42 induced toxicity leading to neurodegeneration.

Alzheimer's disease (AD) is characterised by the deposition of Aβ as amyloid plaques and the intracellular accumulation of tau as neurofibrillary tangles in the brain. Mutations in Aβ and the amyloid precursor protein (APP) are linked to familial AD, hence Aβ is thought to play an important role in the disease process<sup>1,2</sup>. Numerous studies have been carried out to try to better understand how Aβ contributes to the neurodegeneration observed in AD patients and the symptoms of the disease. Self-assembled Aβ has been shown to cause membrane defects<sup>3,4</sup>, disruption to neuronal networks<sup>5,6</sup>, neuronal dysfunction<sup>7,8</sup>, impairment of long-term potentiation<sup>9</sup> and changes in animal behaviour<sup>10,11</sup>. Based on these reports, the current consensus is that Aβ conformation and self-assembly into oligomeric forms is responsible for neuronal death in AD, although the exact role of fibrillar amyloid forms of Aβ and the specific mechanisms of toxicity are still very much debated.

The Aβ peptide is a member of a large group of amyloidogenic peptides and proteins<sup>12</sup> whose toxic properties are believed to be specifically linked to their amyloidogenicity<sup>13</sup>. However, a detailed mechanistic understanding of the link between structure, assembly and toxicity of Aβ remains elusive. One major obstacle to this understanding has been the lack of a suitable peptide against which the toxic properties of Aβ can be rigorously assessed. At present, most researchers typically use a buffer or alternative vehicle solution, but neither takes account of the structural features of Aβ oligomers or other aggregated isoforms that may be responsible for neurotoxic actions. Although scrambled, reversed or rodent Aβ1-42 sequences are occasionally used as controls, the assembly, structure and toxicity of these peptides have never been characterized in detail. Therefore a non-assembling peptide is not available to compare the effects with Aβ1-42. In practice, a peptide with an essentially identical size and sequence to Aβ is required, but which neither assembles nor causes cell death. The importance of using assembly-incompetent peptides cannot be understated if robust conclusions are to be drawn on how self-assembly and amyloidogenesis contributes to disease. A second issue that has hampered progress in delineating Aβ action, is the propensity of the peptide to self-assemble a process that is difficult to control since it is influenced by many factors such as peptide concentration, solvent type, temperature and the presence of seed that can accelerate

<sup>1</sup>School of Life Sciences, University of Sussex, Falmer, BN1 9QJ, UK. <sup>2</sup>College of Sciences, Chemistry Department, Al-Mustansiriyah University, Baghdad, Iraq. <sup>3</sup>Present address: Department of Chemistry, University of Cambridge, Lensfield Road, Cambridge, UK. <sup>4</sup>Present address: Manchester Institute of Biotechnology, University of Manchester, 131 Princess Street, Manchester, M1 7DN, UK. <sup>5</sup>Present address: Department of Neuroscience, Columbia University, 1051 Riverside Drive, New York, NY 10032, USA. <sup>6</sup>Present address: Howard Hughes Medical Institute, Columbia University, 1051 Riverside Drive, New York, NY 10032, USA. Correspondence and requests for materials should be addressed to L.C.S. (email: L.C.Serpell@sussex.ac.uk)

Aβ1-42: DAEFRHDSGYEVHHQKLVFFAEDVGSNKGAIIGLMVGGVVIA  
vAβ1-42: DAEFRHDSGYEVHHQKLVFFAEDVGSNKGAIIGLMVGGVVIA

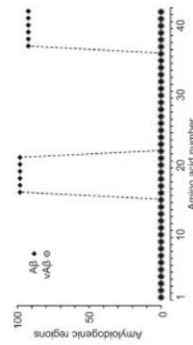


**Figure 1.** The graph produced using WALTZ<sup>18</sup> shows two peaks that indicate two amyloidogenic regions (residues 16–21 and residues 37–42) in Aβ1-42 compared to the trace for vAβ1-42 peptide design showing abolition of the amyloidogenic regions.

assembly<sup>14,15</sup>. As a result, preparation procedures are liable to substantial variability in the type and size of aggregates formed, and the effects of these aggregates on cells and neurons are therefore difficult to interpret. Importantly although monomeric Aβ has not been implicated as playing a role in toxic effects, it has not been previously possible to ensure the preparation of pure monomeric Aβ, and that it remains so for extended periods. For the first time, we have rationally designed and extensively characterized a non-oligomeric peptide, representing a major breakthrough in the ability to dissect which structural species are responsible for Alzheimer's deficits.

Here, we report an approach that addresses two major limitations to AD research; the lack of a non-assembling peptide to compare to, and the need for a preparation method that produces consistent oligomer populations, and provides the basis for tightly-controlled studies of Aβ action. Specifically, we outline the rational design and generation of a non-aggregation prone variant of Aβ, identical to the wild type 1–42 sequence with the exception of two amino acid substitutions. We show that in combination with a protocol designed to remove pre-aggregates and potentially contaminating solvents<sup>16–18</sup> we can produce highly consistent peptide preparations of Aβ1-42 and compare it to vAβ1-42 prepared under identical conditions. To gain insights into how the amyloidogenicity of Aβ1-42 is linked to its structure, we used a range of biophysical techniques to compare the two peptides. Compared to wild-type Aβ, we show that vAβ1-42 is compromised in its ability to aggregate and thus ordered non-toxic. Even over extended periods (7 days), we find that the variant peptide does not assemble into oligomers or fibres or develop any characteristic 3-sheet structure. Furthermore, unlike Aβ1-42 oligomers, vAβ1-42 is not detected associated with or internalised into primary hippocampal neurons and has no effect on the metabolic activity or viability of neuroblastoma cells or neurons. Using optical imaging approaches we show that presynaptic viability and vesicle recycling is compromised in Aβ treated but not vAβ-treated neurons. Using a whole animal model system, which is routinely employed for studying behavioural learning<sup>19</sup>, we show that normal memory formation occurs in vAβ1-42 but not Aβ-treated animals. This peptide illustrates the key role of amino acid sequence in the ability of Aβ1-42 to assemble and form toxic structures. Furthermore it can act as a robust control, providing an indispensable tool for studies on Aβ in AD.

## Results and Discussion

**Rational design of a non-assembling variant of the Aβ1-42 peptide.** WALTZ algorithm<sup>18</sup> was used to predict the effects of amino acid substitutions on the propensity of wildtype (WT) Aβ1-42 to form amyloid. WALTZ identifies two regions of WT Aβ1-42, between 15–22 and 36–42 that have the most amyloid-forming potential (Fig. 1). All possible amino acid substitutions were introduced into these regions and examined for amyloidogenicity using WALTZ<sup>18</sup>. The results were ranked and those substitutions that result in abolition of amyloidogenicity peaks were examined further. Substituting phenylalanine at position 19 (F19) with serine (S) and glycine at position 37 (G37) with aspartic acid (D) results in removal of the amyloidogenic regions in the Aβ1-42 peptide (Fig. 1). Previous studies have shown that phenylalanine and F19 in particular in Aβ plays an important role in driving assembly<sup>20–22</sup> and acid state NMR measurements of Aβ specifically show molecular contacts between F19 and L34<sup>23–24</sup>. Single substitutions of F19 have shown a significant reduction in Aβ assembly<sup>25</sup>. Substitution of F19 for leucine revealed that the F19 residue plays an important role in nucleating cycline formation and in driving assembly<sup>26</sup>. The substitution of F19 with aspartic acid (F19D) with G37D, a mutation that dramatically reduced the toxic effects in cell culture and in vivo in *Cerebrolydin* oligomer<sup>27</sup>. NMR studies have revealed that G37 fits into a solvent accessible turn together with G38 within oligomers<sup>28</sup>. Therefore, G37D was selected to disrupt this architecture. The substitution of hydrophobic F19 for smaller, polar serine and G37, for the negatively charged, bulky aspartic acid was predicted to disrupt the intermolecular contacts that drive and stabilise assembly into oligomers and fibrils.

**F19SG37D substitutions impair assembly of Aβ1-42.** Aβ1-42 F19SG37D, hereafter referred to as vAβ1-42, was characterised alongside WT Aβ1-42 using a range of biophysical techniques that report on the structural changes that take place during assembly. The peptides were prepared using a method that ensures removal



of preformed aggregates and any potentially contaminating solvents as described in detail in the methods<sup>17</sup>. Peptide concentration was measured immediately after preparation and then the solution diluted to 50  $\mu$ M to ensure reproducibility between experiments. We followed the assembly of both peptides over the course of one week using transmission electron microscopy (TEM) as well as spectroscopic and immunological methods to fully examine their assembly properties.

The morphology of the structures was visualised over time using TEM (Fig. 2a). Even at very early time points small spherical assemblies could be observed in the A $\beta$ 1-42 sample (Fig. 2a), consistent with previous reports<sup>22</sup> whilst the A $\beta$ 31-42 sample was free from any aggregates. After 2 hours, very small worm-like structures appear in A $\beta$ 1-42, which resemble protofibrils (Fig. 2a). After 24 hours long fibrils form and are present in abundance by 72 hours. These are similar to those shown in recent studies<sup>22-25</sup>. Conversely, A $\beta$ 31-42 does not form fibrils, even up to one week after preparation.

To further investigate A $\beta$ 1-42 was undergoing any structural reorganisation that could not be detected using TEM, circular dichroism (CD) was used. CD is a secondary structure of the peptide as monitored using circular dichroism (CD) (Fig. 2b). CD spectra confirm that A $\beta$ 1-42 is initially random coil for two to four hours (minima at 200 nm) and converts to  $\beta$ -sheet conformation (maximum at 195 nm and minimum at 218 nm). After 24 hours a clear  $\beta$ -sheet signal is apparent that becomes stronger at 48 hours, concomitant with the appearance of fibrils by TEM. A $\beta$ 31-42 remains in a random coil conformation for the duration of the experiment (7 days). This confirms that the A $\beta$ 31-42 peptide remains soluble and does not assemble into a  $\beta$ -sheet rich structure.

To examine the fibrillogenesis process, a Thioflavin T (ThT) fluorescence assay was carried out to monitor amyloid assembly with time (Fig. 2c). A $\beta$ 1-42 shows some fluorescence intensity even at early time points, indicating the presence of small species able to bind the dye. However this signal significantly increases at 24 hours, when fibrils are visible by TEM and when a  $\beta$ -sheet CD signal predominates. A $\beta$ 31-42 shows negligible intensity at 483 nm. Together these biophysical data suggest that A $\beta$ 1-42 does not self-assemble into amyloid whilst wild-type A $\beta$ 1-42 does form amyloid. To further monitor the change in solubility of A $\beta$  peptides over time<sup>26</sup>, since the signal arising from the soluble peptide disappears as the peptide assembles beyond a certain size. Here, we examined the <sup>1</sup>H NMR spectra from A $\beta$ 31-42 over three days and confirmed that the NMR signal remained strong and identical to time zero indicating that the peptide does not change structure or self-assemble during this time (Supplementary Figure 1).

**A $\beta$ 31-42 does not form oligomers.** Although the data outlined above indicate that A $\beta$ 31-42 is not assembling into species that may contain  $\beta$ -sheet structure, it is possible that it is able to assemble into very small oligomers of a size below the resolution of TEM, and that do not exhibit  $\beta$ -sheet conformation or bind ThT. To explore this further, we used a series of antibodies directed against different conformations and epitopes to determine whether A $\beta$ 1-42 was forming any assemblies resembling those formed by A $\beta$ 1-42. Antibodies that bind to A $\beta$  oligomers were used for dot blotting (Fig. 2d). The anti-oligomer antibody 4G8 (6E10) (6E10) was used for dot blotting (Fig. 2d). A $\beta$ 1-42 and A $\beta$ 31-42 were prepared at the same time point as in Fig. 2a-c. The oligomer-specific antibody (NU1) detected only A $\beta$ 1-42 indicating that A $\beta$ 31-42 does not form antibody detectable oligomers. The N-terminal antibody, 4G8, does not bind to A $\beta$ 31-42 as expected since the epitope overlaps with the F19S substitution. In contrast 6E10 binds to both peptides, confirming that A $\beta$ 31-42 can be detected by dot blotting. Notably there is a decrease in signal for each antibody with A $\beta$ 1-42 incubation time. This is consistent with changes in conformation that accompany assembly to form fibrils which would reduce available epitopes. In contrast, there is no change in 6E10 intensity for A $\beta$ 31-42 over time consistent with the peptide remaining monomeric for up to 7 days.

Although dot blotting provides a useful way of looking at the antigenicity of A $\beta$ 1-42 and A $\beta$ 31-42, due to the dynamic nature of amyloid assembly, the samples applied to the membrane probably contain a heterogeneous mixture of different species. To detect any assembled structures, we ran SDS-PAGE using samples collected at different time points (Fig. 2e). A $\beta$ 1-42 was predominantly in a monomeric conformation (M) and migrated at around 15 kDa, with a significant population of dimers (D, ~9 kDa) and trimers (T, ~13.5 kDa) present. After 2 hours, higher molecular weight oligomers form. These species migrate as a smear and, at later time points, the lower molecular weight monomer and oligomers disappear. After 7 days there are no oligomeric species present at all and fibrils are observed in the well of the gel. A $\beta$ 31-42 remains monomeric and migrates at 4.5 kDa for each incubation time point in the experiment (Fig. 2e).

**A $\beta$ 31-42 is not toxic to primary hippocampal neurons and has no effect on metabolic activity in a human neuroblastoma cell line.** Having established that in contrast to A $\beta$ 1-42, A $\beta$ 31-42 does not assemble into oligomers or fibrils, we sought to determine if there was a corresponding difference in function. There are numerous reports suggesting that pre-formed oligomeric species are the cause of the neurodegeneration observed in Alzheimer's disease<sup>27-29</sup>. To test this hypothesis, we prepared primary hippocampal neurons and neuroblastoma cells (Fig. 3a,b) and treated them with A $\beta$ 1-42 or A $\beta$ 31-42. The peptide preparations were used at this time point. In addition, we chose to carry out these experiments out at a final peptide concentration of 10  $\mu$ M, to ensure that any negative results were not due to low levels of peptide and accelerate the peptide effects within a reasonable time-frame.

A $\beta$ 1-42 oligomers have been shown to be toxic to cultured neuroblastoma cells and neurons<sup>29,32</sup>. In order to investigate this effect of A $\beta$ 1-42 on cells and compare to A $\beta$ 31-42, we conducted cell viability assays on two different cell types, shown in Fig. 3. First, a live/dead cell assay was carried out using primary rat hippocampal neurons (Fig. 3a,b) and second the widely-used 3-(4,5-dimethylthiazol-2-yl)-2,5-diphenyltetrazolium bromide (MTT)

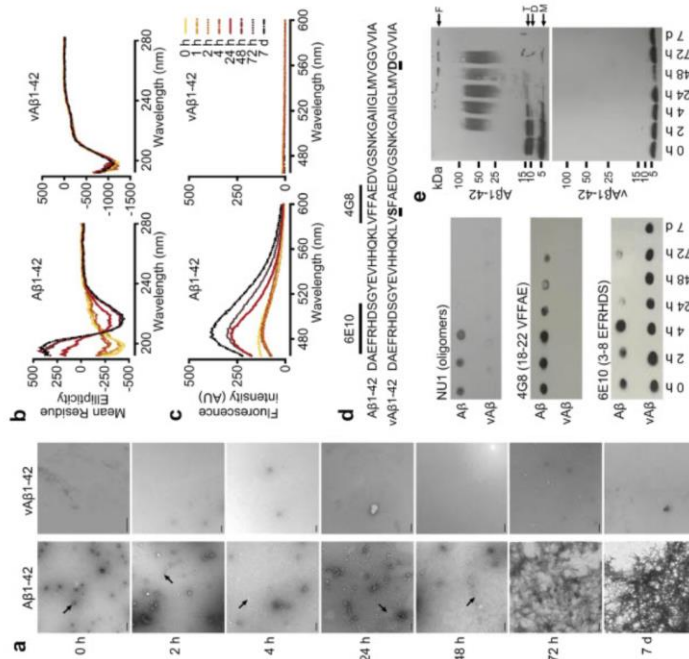


**Figure 2.** (a) Negative stain transmission electron microscopy images of A $\beta$ 1-42 (left panels) and A $\beta$ 31-42 (right panels) showing assembly of A $\beta$ 1-42 into fibrils at around 24 hours, preceded by small spherical assemblies. A $\beta$ 31-42 does not assemble into any structures. (b) CD spectra of A $\beta$ 1-42 and A $\beta$ 31-42 over time showing the formation of  $\beta$ -sheet structures for A $\beta$ 1-42 after around 24 hours whilst A $\beta$ 31-42 remains as random coil structure up to the final time point of 7 days. (c) Thioflavin T fluorescence showing increasing fluorescence at 483 nm of A $\beta$ 1-42 over 7 days, compared to no change in fluorescence of A $\beta$ 31-42. (d) Sequence of A $\beta$ 1-42 (top) and A $\beta$ 31-42 (bottom), showing epitope regions for 4G8 and 6E10 antibodies. The amino acid substitutions are underlined. Dot blots using anti-oligomer antibody, NU1 and anti-A $\beta$  antibodies 4G8 and 6E10 show oligomer reactive species only in A $\beta$ 1-42 samples and not A $\beta$ 31-42. Similarly, 4G8 does not detect A $\beta$ 31-42 due to the F19S substitution in the epitope region. 6E10 binds both A $\beta$ 1-42 and A $\beta$ 31-42 as the epitope is the same in both peptides. (e) Western blot of A $\beta$ 1-42 (top) and A $\beta$ 31-42 (bottom) with 6E10 over time shows monomers (M), dimers (D), trimers (T), higher molecular weight species and fibrils (F) are only formed by the wild-type peptide. A $\beta$ 31-42 runs as a monomer.

assay and CellTiter-Blue (CTB) assays were performed on human SH-SY5Y neuroblastoma cells (Fig. 3c,d) providing two independent verifications of metabolic activity and cell viability.

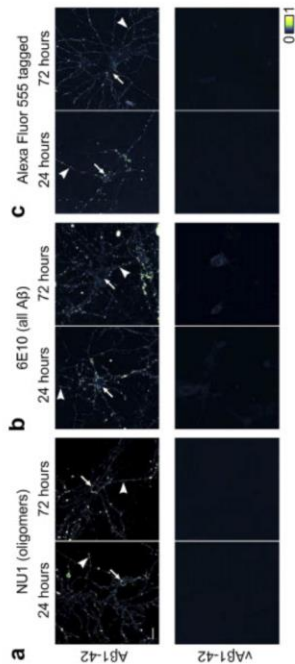


**Figure 4.** Hippocampal neurons treated with oligomeric Aβ1-42 or vAβ1-42 (a,b) or Alexa fluor 555 tagged peptide (c) and imaged by confocal microscopy. Cells in a and b were fixed and stained with anti-oligomer antibody NU1<sup>11</sup> (a) or 6E10 (b). Maximum projection images of six 0.5 μm slices are shown in a and c, b shows one 1 μm slice from the centre of a Z-stack. Scale bars 20 μm.

fluorescent tag was shown not to affect assembly<sup>27</sup>. Cells treated with labeled versions of either Aβ1-42 or vAβ1-42 looked similar to those treated with antibodies, with only fluorescent Aβ1-42 present along neurites and around the cell body and no fluorescent signal for the vAβ1-42 treated neurons, even after three days. Whether antibodies were used or not, there was no evidence that vAβ1-42 either bound to the outside of the cell nor was internalised.

**vAβ1-42 has no effect on hippocampal synaptic function in primary hippocampal neurons.** The function of small central synapses critically relies on the efficient fusion and retrieval of synaptic vesicles (SV). Aβ1-42 oligomers previously have been reported to modulate aspects of both recycling and vesicle pool organization<sup>28</sup>. Here we used FM1-43, a widely employed fluorescent reporter of vesicle turnover to investigate the effects of Aβ1-42 and vAβ1-43 on vesicle recycling parameters<sup>29</sup>. In double-blind experiments, primary hippocampal neurons were loaded with FM1-43 and then subjected to field stimulation (200 APs, 20 Hz) in the presence of FM dye to drive vesicle buffer release, and then subjected to field stimulation (200 APs, 20 Hz) in the presence of FM dye to drive vesicle labelling (Fig. 5a). As a measure of synaptic vesicle recycling for the different treatments, representative images were collected after washing (Fig. 5b) and labelled terminals were quantified using a thresholding method (see Methods). Our analysis revealed that while vAβ1-42 and buffer alone had highly comparable synapse counts, the number of puncta in Aβ1-42-treated neurons was significantly lower (Fig. 5c, see figure legend for quantification). These results reveal that Aβ1-42 treatment leads to a significant deficiency in the recruitment of functional synapses compared to vAβ1-42 peptide or buffer alone conditions. Next, the consequences of the three incubation treatments on activity-driven FM1-43 dye-loss from labelled terminals (a measure of vesicle release) were examined (Fig. 5d). The level of dye-loss was highly comparable for vAβ1-42 and buffer alone conditions but was significantly less in Aβ1-42 treated neurons suggesting an impairment in exocytosis (Fig. 5d). Taken together, these findings indicate a specific deficit in vesicle recycling properties in Aβ1-42 treated synapses, which are not observed in vAβ1-42 or buffer control treatments.

**Behavioural studies on an animal model (Lymnaea stagnalis, pond snail).** To investigate possible effects of vAβ1-42 on whole animal function, we took advantage of a well-characterised model system, the pond snail, *Lymnaea stagnalis*. This system has been used extensively for studies of both behavior and learning and memory, due to its ability to undergo robust classical conditioning and form stable long-term memories (for review, see ref. 18). Recent work had demonstrated that Aβ1-42 significantly impairs recall of long-term memory associated with single-trial food-reward classical conditioning<sup>30</sup>. Here, to investigate whether vAβ1-42 showed the same effect, vAβ1-42 was administered to snails. Briefly, animals were conditioned to associate a chemical stimulus with a food stimulus (Fig. 6a). Conditioned long-term memory can be tested by administering the stimulus without the food stimulus. In this case, the stimulus was the chemical stimulus, vAβ1-42, and the food stimulus was a food pellet. Animals were tested at 0 hours, injected with peptide or controls at 24 hours and tested at 48 hours to determine if vAβ1-42 disrupts consolidated long-term memory (Fig. 6a). Comparison of the peptide effect on the conditioned feeding response following incubation with Aβ1-42 or vAβ1-42 with the vehicle (buffer only) control is shown in Fig. 6b. While Aβ1-42 treated animals display decreased conditioned feeding response to the chemical stimulus in comparison to vehicle treated animals, vAβ1-42 treated animals exhibit a similar conditioned feeding response to the vehicle control, suggesting vAβ1-42 does not disrupt recall of consolidated long-term memory. These findings support our cellular-level results and suggest that vAβ1-42 is largely inconsequential for neural network function.

Our results reveal a striking and important contrast between the activity of wild-type Aβ1-42 peptide and the novel variant vAβ1-42. Here we show that only the wild-type assembles to form Aβ1-42 positive oligomers and

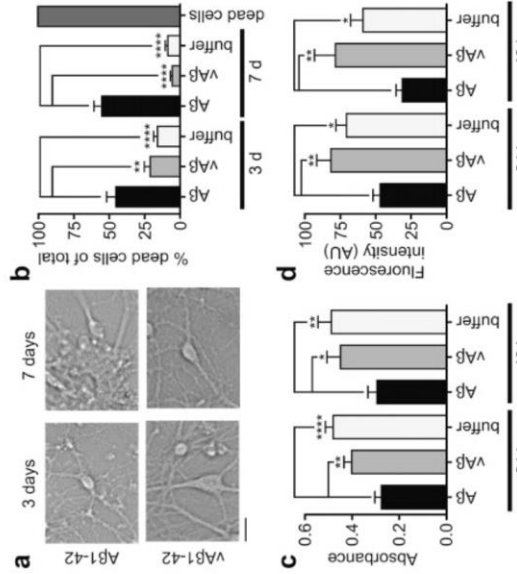


**Figure 3.** (a) DIC widefield images of neurons live in culture following treatment with either Aβ1-42 oligomers or vAβ1-42 after 3 or 7 days. Some live neurons are still clearly visible in the Aβ1-42 culture after 3 days but by 7 days some appear healthy. Scale bar 20 μm. (b) Measurement of proportion of dead cells compared to the total counted in culture by ReadyProbes assay following 3 and 7 days exposure to Aβ1-42 or vAβ1-42 or buffer only (total number of cells counted (number of dead cells in brackets) at 3 days: n = 1163 (545), 1012 (220) and 1661 (279) and 7 days: n = 1002 (610), 684 (27) and 1112 (97) for Aβ1-42, vAβ1-42 and buffer respectively). (c) MTT assay (24 hours) n = 19, 9 and 20, 48 hours: n = 14, 9 and 13 for Aβ1-42, vAβ1-42 and buffer respectively. (d) MTT assay (48 hours) n = 11, 12, 9 and 18 for Aβ1-42, vAβ1-42 and buffer respectively. Error bars represent standard deviation. Unpaired parametric t-test, only significant differences are shown, where  $p < 0.05$  (\*),  $p < 0.01$  (\*\*),  $p < 0.0001$  (\*\*\*). Error bars are expressed as SEM.

The results revealed that oligomeric Aβ1-42 causes death of neurons while vAβ1-42 has no observable effects on cell death in any of the assay periods. In an oligo peptide concentration assay, neurons in culture were visibly affected with treatment of oligomeric Aβ1-42, but not vAβ1-42, after 3 days (Fig. 3a). At 7 days, healthy cells after 7 days. In contrast, neurons treated with vAβ1-42 remain healthy over the time of the experiment (Fig. 3b). The MTT (Fig. 3c) and CTB (Fig. 3d) assays show a decrease in the metabolic activity and viability of neuroblastoma cells treated with Aβ1-42. vAβ1-42 has no effect on cell viability in any of the assays conducted and is comparable to vehicle buffer only.

**vAβ1-42 does not associate with primary hippocampal neurons.** To provide additional insights into the behaviour of vAβ1-42 compared to Aβ1-42, we added each peptide (incubated for 2-4 hours) to primary rat hippocampal neurons and examined their distribution by two methods, immunolabelling with NU1 and 6E10 and using fluorescently tagged peptides (Fig. 4). The antibody labelling to Aβ1-42 is detected in the cell body and along the axons (Fig. 4a, top panels) and persisted for at least 3 days. In contrast, neurons treated with vAβ1-42 resemble the buffer only control (not shown) and show no labelling (bottom panels). Dot-blotting confirmed that 6E10 is able to bind to vAβ1-42 (Fig. 2d,e). Therefore, these results indicate that vAβ1-42 neither binds to the cell body nor axons of primary hippocampal neurons. To confirm that vAβ1-42 does not associate with neurons with the cellular rather than being removable, a variation of the experiment was conducted using Alexa fluor tagged versions of the Aβ peptides. This method has been used by our group previously and the



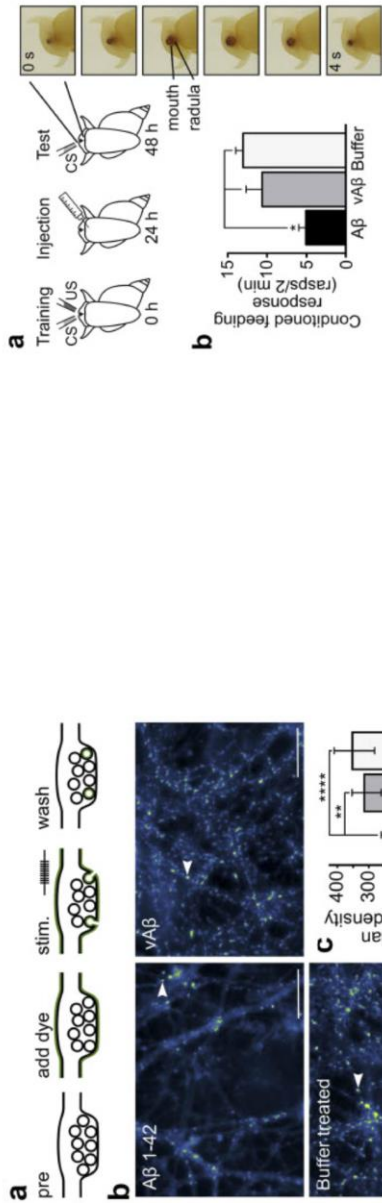


**Figure 5.** (a) Cartoon illustrating functional synaptic readout. Neurons are activated by field stimulation to evoke vesicle turnover in the presence of extracellular FMI-43-dye. Washing in dye-free solution leaves recently recycled vesicles fluorescently labelled. (b) Representative images of FMI-43 loading in neurons treated with Aβ1-42, vAβ1-42 or buffer. Arrowheads indicate discrete functional terminals. Scale bar 20 μm. (c) Histogram (median ± IQR) shows number of functional synapses expressed as the median synapse density per image. (Aβ1-42: 218 IQR 137–262; vAβ1-42: 315 IQR 258–355; buffer: 355 IQR 283–416, n = 20, 30, 30 images, respectively; Kruskal-Wallis one-way ANOVA, p = 0.0002; with Dunnett's multiple comparison test, see Methods for details). (d) Histogram shows percentage of dye loss per image. (Aβ1-42: 60% IQR 48–72; vAβ1-42: 48% IQR 36–61; buffer: 48% IQR 36–61, n = 20, 30, 30 images, respectively; Kruskal-Wallis one-way ANOVA, p = 0.0001; with Dunnett's multiple comparison test, see Methods for details). (e) Line graph shows normalized fluorescence over time (0–60 s) for Aβ1-42, vAβ1-42 or buffer. (Aβ1-42: 0.55 ± 0.05, n = 20; vAβ1-42: 0.55 ± 0.05, n = 30; buffer: 0.55 ± 0.05, n = 30; 2-way ANOVA, p = 0.0001; with Dunnett's multiple comparison test, see Methods for details). (f) Histogram of magnitude of FMI-43 destaining for data in (e), expressed as % dye loss (median ± IQR, Aβ1-42: 50 IQR 36–61; vAβ1-42: 48 IQR 36–61; buffer: 48 IQR 36–61, n = 20, 30, 30 images, respectively; Kruskal-Wallis one-way ANOVA, p = 0.0001; with Dunnett's multiple comparison test, see Methods for details).

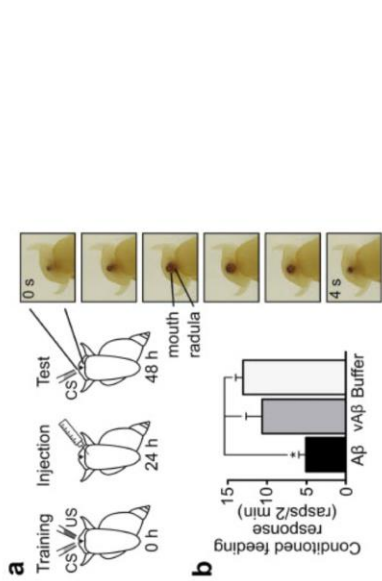


**Figure 6.** (a) Cartoon illustrating conditioned feeding response of *Lymantria stagnalis* treated with Aβ1-42 or vAβ1-42. Animals were classically conditioned using the single-trial food-reward paradigm at 0 hours; injected with 1 μM Aβ1-42 (n = 55), 1 μM vAβ1-42 (n = 20), or vehicle (n = 100) at 24 hours, and tested for the conditioned feeding response at 48 hours. Picture insets show an example of a complete feeding cycle (rasp) on the left, and a complete feeding cycle (rasp) on the right. (b) Bar graph showing the conditioned feeding response (response in rasps/2 min) of the pooled radula, ingestion of food, and drinking of water at 48 h. (b) One-way ANOVA, p < 0.0001. Tukey's multiple comparison with p = 0.05; vAβ1-42 vs. Aβ1-42, Vehicle vs. Aβ1-42. Error bars are shown as ± SEM.

anyfold fibrils. The Aβ1-42 oligomers are able to bind to and internalise into neuronal cells and show accompanying cellular toxicity. In stark contrast, the non-assembling vAβ1-42 is not associated with cell membranes, internalised and nor does it affect neuronal survival. We show that Aβ1-42 oligomers can impair synaptic vesicle recruitment and exocytosis at synapses. Finally, we were able to utilize the peptide in an animal behavior assay and reveal that whilst Aβ1-42 impairs memory recall, vAβ1-42 has no such effect. Only by comparison with this rationally-designed peptide variant can robust conclusions can be drawn and exciting new insights made into the effects of Aβ on neuronal cell function and animal behavior.

### Conclusions

Aβ is known to play an important role in the pathology of Alzheimer's disease (AD), but the link between Aβ self-assembly and neurodegeneration remains elusive. It is clear however that the conformational change that accompanies assembly is a critical factor underlying amyloidogenic protein toxic action. To investigate this further, we rationally designed a non-assembling peptide variant of Aβ1-42 that shares size and sequence with Aβ but does not self-assemble into oligomers or fibrils. The identification of such a peptide is an essential contribution to the field and provides a powerful tool for elucidating structure-toxicity relationships and rigorously assessing the mechanisms of Aβ induced neuronal dysfunction in cellular assays and animal models.

Here, we have examined the potential amyloidogenic regions of Aβ1-42 and rationally designed a peptide variant that does not aggregate over the course of one week, does not cause toxicity in cell culture or behavioural effects in an animal model, nor binds to or is taken up by neuronal cells in culture. The double substitutions, P19S and G37D completely removed amyloidogenicity and the variant peptide was confirmed experimentally as non-amyloidogenic using a range of biophysical and biochemical examples of the rational design strategy are provided, and show that self-assembly is key to Aβ1-42 detrimental effects.

Modelling the neurotoxic properties of Aβ1-42 using cells in culture is challenging but critical if its pathogenic mechanisms are to be understood at a molecular level. In AD, it is likely that a range of Aβ1-42 aggregates are produced that may all contribute to neuronal death and it may not be the case that one species in particular (e.g. dimer, trimer, octamer) is responsible. We sought to replicate this environment as closely as possible, carrying out our functional assays with a heterogeneous Aβ1-42 oligomer preparation in order to simulate how the dynamic nature of amyloid assembly, as well as the assemblies themselves, might be detrimental to cells. To this end, a suitable peptide that is unable to self-assemble is essential since it is not possible to produce a stable monomer of wild-type Aβ1-42.

**Thioflavin T fluorescence.** 10  $\mu$ M of TBT in 50  $\mu$ M A $\beta$  peptide was added to a 10 mm cuvette. An emission scan between wavelength 460–600 nm was performed in a Victor Xp2 Fluorescence Spectrophotometer. The sample compartment temperature was set to 21  $^{\circ}$ C, scan rate was 600 nm/min and three spectra were averaged for each measurement.

**Dot blotting.** 5  $\mu$ l of 50  $\mu$ M A $\beta$  peptide was spotted onto a nitrocellulose membrane and allowed to dry. The membrane was boiled with TBS for three minutes twice and then incubated at room temperature with blocking buffer (10% milk in 0.1% TBS-T) for 1 hour. The blocking buffer was poured off the membrane and replaced with primary antibody overnight at 4  $^{\circ}$ C. The membrane was washed for 10 minutes three times with 1% TBS-T before being probed with secondary antibody. The membrane was then probed with secondary antibody. The membrane was washed with ECL substrate (Millipore) for three minutes before being developed. Antibodies were purchased from Cambridge Bioscience (6E10 and 4G8), NUI was a gift from the William Klein lab<sup>31</sup>.

**Western blotting.** 2  $\mu$ g of peptide in 4x Laemmli Sample Buffer (Bio-Rad) were loaded on a 4–20% Mini-PROTEAN TGS Stain-Free gel (Bio-Rad) and run in 1X running buffer (diluted from 10X stock of 25 mM Tris Base, 192 mM Glycine, 1% SDS) at 100V. The gel was then transferred in 1X transfer buffer (10% 10X stock (25 mM Tris Base, 192 mM Glycine), 10% Methanol, 80% dH<sub>2</sub>O) at 25V for 2 hours on to nitrocellulose 0.45  $\mu$ m membrane. The membrane was blocked with 10% Milk/TBS-T at room temperature for 1 hour then incubated with a 1:10000 dilution of 6B10 antibody overnight at 4  $^{\circ}$ C. The membrane was washed three times for ten minutes with 1% TBS-T before being probed with secondary antibody. The membrane was then probed with secondary antibody at 1:1000 dilution for 1 hour at room temperature. The membrane was washed three times for ten minutes with 1% TBS-T and incubated with ECL substrate for five minutes before being developed.

**Nuclear magnetic resonance.** VA $\beta$ 1–42 was prepared at 200  $\mu$ M concentration in 10% v/v D<sub>2</sub>O standard. 1H NMR spectra (128 scans) were acquired every 30 minutes over a period of 66 hours. The temperature was regulated at 25  $^{\circ}$ C. The spectra were processed with 1.5 Hz line broadening prior to base line correction and Fourier transformation. The residual solvent signal around 4.8 ppm was cut for clarity.

**Cell culture.** SH-SY5Y cells were cultured as described previously<sup>27</sup> in Dulbecco's modified Eagle medium (DMEM) supplemented with 10% Fetal Calf Serum, 1% Penicillin-Streptomycin and 2 mM L-Glutamine. Cells were passed every 4–5 days at around 80% confluency and not used beyond passage 19.

Rats are housed within a specialised facility under Home office guidelines and sacrificed using procedures in accordance with Animals (Scientific Procedures) Act 1986, Amendment Regulations 2012. Primary neurons were prepared from the hippocampus of P0-P1 rats by initially dissecting the tissue into ice cold HBSS containing 0.1 M HEPES. Following washes in pre-warmed Basal Medium Eagle (BME) (Gibco) containing 0.5% glucose, 2% FCS, 1 mM Na-Pyruvate, 0.01 M HEPES pH 7.35, 1% Penicillin-Streptomycin, 1% B27 supplement and 1% Glutamax, tissues were triturated using a 1 ml pipette until fully dissociated. The cell suspension was diluted further with complete BME media and approximately 40,000 cells plated into 2 cm<sup>2</sup> wells containing a coverslip coated in 20  $\mu$ g/ml Poly-D-Lysine with a 1  $\mu$ l of 2.5  $\mu$ M cytosine arabinoside to curb further proliferation of astrocytes. After 2–3 days of treatment with 2.5  $\mu$ M cytosine arabinoside, cells were treated with 10  $\mu$ M Ara-C for 4–5 days. Cells were used 10–14 days after plating.

**Cell viability assay with primary hippocampal neurons.** After the desired incubation time, one drop of each ReadyProbes reagent (Life Technologies) was added per well. The kit contains a blue stain to label all cells, and a green stain to label dead cells only. Cells were incubated for 15 minutes then imaged on a Zeiss CO widefield microscope using DAPI and FITC filters. Images were analysed using Fiji software as follows. Regions of interest were drawn around neuronal cell bodies (astrocytes were excluded) using DIC and DAPI channels, which indicated total cell number (live and dead). Background values in the green channel (dead cells) were determined and any value greater than this was subtracted to positive i.e. dead. Numbers of dead cells are expressed as a percentage of the total number of cells. Between nine and seventeen regions in total per sample were imaged from either two or three coverslips from experiments performed on three separate occasions using newly prepared peptide.

**Cell metabolism assays with neuroblastoma cells.** The Vybrant MTT [3-(4,5-dimethylthiazol-2-yl)-2,5-diphenyl-2H-tetrazolium bromide] cell-proliferation assay (Invitrogen) was used on undifferentiated SH-SY5Y cells according to the manufacturer's protocol. Briefly, SH-SY5Y cells (10<sup>4</sup> cells/well) were seeded on a 96-well plate 2 days prior to the assay. The cells were then incubated with 10  $\mu$ M oligomeric A $\beta$ 1–42 or VA $\beta$ 1–42 for 24 or 48 hours at 37  $^{\circ}$ C. At these time points, 12 mM MTT solution was added to the cells and further incubated for 4 hours at 37  $^{\circ}$ C. The resulting insoluble dye was dissolved with 50  $\mu$ l of DMSO and the absorbance measured at 540 nm with a 600 nm reference filter. For CTS (Cell-Titer Blue), cells were plated as above except 2 hours before adding 20  $\mu$ l of CTS (Cell-Titer Blue) to the cells. Cells were then incubated for 24 hours at 37  $^{\circ}$ C. The assay was carried out to each well and further incubated for 2 hours. Fluorescence was measured at 570 nm. Experiments were carried out in triplicate a minimum of three times and the data pooled. Background absorbance or fluorescence was calculated from a dead cell control. Triplicate values were averaged then subtracted from sample values. This was carried out separately for each time point in each experiment. Statistical analysis was carried out using GraphPad Prism software.

**Immunofluorescent labeling and confocal microscopy.** Primary neuronal cells were treated with 1  $\mu$ M of either A $\beta$ 1–42 or VA $\beta$ 1–42 oligomers, or volume-matched buffer, for 24 and 72 hours. For 6B10 staining, 1  $\mu$ M A $\beta$ 1–42 or 5  $\mu$ M VA $\beta$ 1–42 were added. After removal of media, cells were immediately fixed with 2% paraformaldehyde for 15 minutes. Following a wash with wash buffer (25% Superblock (Thermo Fisher) in PBS), cells were

It is paramount that peptides, and not just buffers or vehicle solutions, are used to compare with wild-type A $\beta$  in AD research. In our experiments, VA $\beta$ 1–42 has the same effect as buffer controls, supporting observations that aggregated, and not monomeric isoforms of A $\beta$ 1–42 are toxic. These conclusions can only be drawn by comparison of A $\beta$ 1–42 with another peptide similar in sequence and, crucially, that has undergone the same preparation method. Solvents such as HTPP are often used to solubilise the peptide and can produce false positive results if not completely removed. By preparing VA $\beta$ 1–42 using the procedure described here, any contaminating effects would be uncovered.

Our data show that VA $\beta$ 1–42 remains in a soluble random coil conformation throughout the course of the experiment and it is likely that for this reason its detrimental effects are abrogated. The structure of A $\beta$ 1–42 oligomers has been shown to play a very important role in their toxic function<sup>30,32</sup> and these results confirm that oligomerisation is required for A $\beta$ 1–42 to associate with neurons, affect neuronal viability and exert behavioural effects.

The data described here outlines an unprecedented characterisation of a novel peptide and show unambiguously in several models that self-assembly is required for neurotoxicity. This novel peptide allows new insight into the pathways of A $\beta$  action, revealing that  $\beta$ -sheet rich, oligomeric A $\beta$ 1–42 accumulates within neuronal cells. Our results show that it is likely that the oligomeric structure is crucial for membrane binding and internalisation. Once inside, it is able to exert detrimental effects on synaptic function in hippocampal neurons and on long-term memory in a model organism. In contrast, the non-assembling VA $\beta$ 1–42 lacks the ability to form  $\beta$ -sheet rich oligomers and is unable to exert any of these effects, providing strong evidence that self-assembly is fundamental for the damaging effects of A $\beta$ .

### Materials and Methods

**Peptide design.** Sequence based design was performed using the WALTZ algorithm<sup>33</sup> to explore the effect of amino-acid substitutions on the predicted amyloidogenicity of the A $\beta$ 1–42 peptide. The graph produced using WALTZ shows two peaks indicating the location of two amyloidogenic regions (residues 16–21 and residues 37–42). VA $\beta$ 1–42 was designed to have the same sequence as A $\beta$ 1–42, but with different amino acid residues in regions to examine the effect on the graphically output prediction. All possible substitutions at positions 19 and 37 were investigated and ranked based on their ability to reduce the amyloidogenicity peak. A number of variants were shown to reduce the predicted amyloidogenicity and two were selected based on previous experimental assembly studies.

**Preparation of peptides.** Hexafluoroisopropanol (HFIP) films of recombinant A $\beta$ 1–42 were purchased from Peptide and VA $\beta$ 1–42 was purchased from IPT. Peptides were prepared using an adapted protocol originally developed in<sup>34</sup>. HEPES buffer (10 mM HEPES, 50 mM NaCl, 1.6 mM KCl, 2 mM MgCl<sub>2</sub>, 3.5 mM CaCl<sub>2</sub>) was used to mimic the culture media as previously described<sup>34,35</sup>. All preparation was conducted using protein LoBind Eppendorf and tips (Alpha Laboratories). Briefly, 0.2 mg A $\beta$ 1–42 (Peptide) was solubilised in 200  $\mu$ L HFIP (Sigma-Aldrich) to disaggregate the peptide. The solution was then vortexed on high for one minute and sonicated in a 5000 Hz bath sonicator for five minutes. HFIP was removed completely using a low stream of nitrogen gas. The peptide was then dissolved in 200  $\mu$ L DMSO and stored at 20  $^{\circ}$ C for up to 24 hours. Solutions were added to a 7K MWCO Zeba buffer exchange column (Thermo Scientific) equilibrated with HEPES buffer with 40  $\mu$ L HEPES as a stacking buffer. The protein solution was kept on ice and the absorbance at 280 nm measured with a NanoDrop spectrophotometer using a molar absorption coefficient of 1490 M<sup>-1</sup> cm<sup>-1</sup>. Solutions were immediately diluted to 50  $\mu$ M with HEPES buffer and incubated where indicated or used immediately in further experiments.

**Generation of Alexa Fluor 555-conjugated peptides.** Peptides were treated as outlined above up to the addition of 200  $\mu$ L dry DMSO. The Alexa Fluor 555 tag was prepared as per manufacturers instructions (Life Technologies). Briefly, 10  $\mu$ L H<sub>2</sub>O was added to the Alexa Fluor TFP ester and kept on ice. This was added to the peptide in 200  $\mu$ L DMSO along with 10  $\mu$ L 1 M sodium bicarbonate pH 8.3, mixed and incubated for 15 minutes at room temperature protected from light. Following this the procedure resumed as above and the solution added to the Zeba buffer exchange column. The calculations for the concentration was adjusted to take into account the absorbance of the dye.

**Transmission electron microscopy.** 4  $\mu$ L of 50  $\mu$ M A $\beta$  was placed on the surface of a Formvar/carbon film coated 400 mesh copper grid (Agar Scientific) and allowed to adsorb for 10 minutes. The grid was then washed with 40  $\mu$ L of milliQ filtered water, then added to the grid and blotted. Immediately after this the grid was repeated once more and the grid was left to air dry. All TEM grids were examined using a Hitachi-7100 TEM at 100 kV and the images were acquired digitally with an axially mounted (2000  $\times$  2000 pixel) Gatan UltraScan 1000 CCD camera. Aliquots of A $\beta$  peptide samples were taken at different time points to monitor the fibrillation state and morphology.

**Circular dichroism.** 300  $\mu$ L of 50  $\mu$ M A $\beta$  peptide (prepared as described above) in phosphate buffer (pH 7.4) was placed into a 1 mm path length quartz cuvette (Hellma) and scanned between 180 nm and 275 nm on a JASCO 1715 Spectropolarimeter. The samples were equilibrated at 20  $^{\circ}$ C using a water bath. Three spectra were averaged for each measurement.



permeabilised with 0.3% Triton-X 100 for 10 minutes then 50 mM glycine added to block unreacted aldehydes. Cells were incubated with Image-IT signal enhancer (Life Technologies) for 30 minutes then cells were blocked using undiluted Superblock for 30 minutes. Primary antibody NU1<sup>®</sup> or 6E10 (Cambridge Biosciences) (both 1:500) diluted in wash buffer was incubated with the cells for one hour. After washing, Alexa Fluor 555 (6E10) or 488 (NU1) conjugated goat anti-mouse secondary antibody (1:500) (Life Technologies) was added for the same period and after a final wash the coverslips were mounted in ProLong Gold (Life Technologies), cured for 2 days then imaged. Cells were imaged using a 63 × 1.2 NA water objective (tagged peptide or NU1 antibody) or a 40 × 1.1 NA water objective (6E10 antibody) on a Leica SP8 confocal microscope. Emission from NU1 stained cells (488 secondary) was collected using a 488 nm excitation laser line between 495 and 540 nm on a PMT detector. Emission from Alexa Fluor-555 tagged peptide treated cells and 6E10 stained cells (555 secondary) was collected using a 561 nm laser line between 555 and 650 nm. Samples were imaged sequentially.

For cells treated with tagged peptides, the cells were fixed, washed and mounted as described above.

**Assessments of synaptic function.** 10 days *in vitro* primary hippocampal neurons grown on coverslips were treated for 24 h with 1.0 μM Aβ1–42 or Aβ1–42 + Aβ1–40. For the control, the same coverslip culture was transferred into external bath solution (in mM: 37 NaCl, 5 KCl, 2.5 CaCl<sub>2</sub>, 1 MgCl<sub>2</sub>, 10 D-glucose, 5 HEPES, 20 mM 6-cyano-7-nitroquinoxaline-2,3-dione and 50 μM di-(2-amino-5-phosphonopentanoic acid) and field stimulation (1200 APs at 20 Hz) applied in the presence of FM1–43 (10 μM) dye to label synapses. After completion of endocytosis, residual surface fluorescence was removed by washing in dye-free saline. The experimenter was blind to the treatment protocol for each coverslip during both imaging and data analysis. All analysis was carried out on non-filtered, raw images in ImageJ. For the quantification of functional synapses ten regions were sampled for each coverslip and converted to maximum intensity projections based on 4 × 0.5 μm image stacks. Terminals were identified using objective automated methods based on isoquant thresholding [1]. IsoData core function, ImageJ, NIH, USA). For activity-evoked dye-loss analysis, we applied a further destaining protocol (1200 APs/20 Hz) to FM1–43 dye-loaded coverslips while imaging. Destaining synapses were identified manually on the basis of fluorescence images acquired during destaining. The destaining curves were normalised to the average value of five points before the onset of the stimulation. The % destaining was calculated using the average of the last five frames from the end of the stimulation. Images were collected on an Olympus BX51WI microscope equipped with a x60 1.0 N.A. dipping objective, excitation and emission filter sets at 480/20 and 520/35, and an Olympus XM10 camera with 2 × 2 binning. Statistical analysis was carried out in GraphPad Prism using Kruskal–Wallis one-way ANOVA followed by Dunn's multiple comparison test.

**Comparison of the effect of the peptides on memory in *Lymanaea stagnalis*.** Pond snails, *Lymanaea stagnalis*, were bred at the University of Sussex and maintained in large holding tanks containing 18–22 °C copper-free water, at a 12:12 hour light-dark cycle. The animals were fed Tetra-Phyll (TETRA Werke) twice a week and lettuce three times a week.

The peptides were administered to the animals directly after preparation. Using a 1 mL syringe with 30 gauge precision gauge needles (Becton Dickinson), 100 μL of the Aβ1–42 or Aβ1–42 + Aβ1–40 was injected into the haemolymph of the animals. The animals were then placed in a 14 cm diameter Petri dish with 90 mL of 18–22 °C copper-free water for ten minutes. After the acclimatisation period, 5 mL of Aβ1–42. As there is no blood-brain barrier in *Lymanaea*<sup>28</sup>, the injected peptides have direct access to the animal's central nervous system. For vehicle-injected control animals, 100 μL of normal saline was injected.

Using well-established methods<sup>29</sup>, four to six-month-old snails were removed from their home tanks and starved in new tanks for two days at the same temperature and light-dark cycle as the home tanks. After the starvation period, the animals underwent single-trial food-reward classical conditioning<sup>30</sup> in which the conditioned stimulus (CS) (amyl acetate; 0.004% final concentration) and the unconditioned stimulus (US) (sucrose; 0.6% final concentration) were paired. Initially, each individual snail was left to acclimatise in a 14 cm diameter Petri dish with 90 mL of 18–22 °C copper-free water for ten minutes. After the acclimatisation period, 5 mL of amyl acetate was added to the dish and after thirty seconds, 5 mL of sucrose was added. The snails were then left in their Petri dishes for two minutes, and then removed to their starvation tanks. Both the vehicle-injected and Aβ1–42-injected groups were trained. CS. Each individual snail was left to acclimatise in a 14 cm diameter Petri dish with 90 mL of 18–22 °C copper-free water for ten minutes. After the acclimatisation period, 5 mL of 18–22 °C copper-free water was added to the dish. Raps, the animals' feeding movements, were manually counted for two minutes to determine a baseline rasping rate (number of rasps per two minutes) for each individual. After two minutes, 5 mL amyl acetate was added to the dish. Rasping was tracked for two minutes. Rasping rates were determined by subtracting the individual animal's baseline rasps from the amyl acetate induced rasps.

One-way analysis of single variance [ANOVA] with Tukey's multiple comparison) to establish significance (crit-terion,  $p < 0.05$ ). GraphPad Prism software was used for all analyses.

References

1. Selkoe, D.J. Toward a comprehensive theory for Alzheimer's disease. Hypothesis: Alzheimer's disease is caused by the central role of amyloid-β peptide in the pathogenesis of the disease. *Neuron* 10, 924–925 (1993).
2. Hardy, J. The amyloid hypothesis for Alzheimer's disease: a critical reappraisal. *Neurodegeneration* 10, 119–124 (2001).
3. Williams, T.L., Day, L.I. & Selkoe, D.J. The effect of Alzheimer's amyloid-β aggregation state on the permeation of biocompatible lipid vesicles. *Langmuir* 26, 17266–17268 (2010).
4. Williams, T.L., Day, L.I. & Selkoe, D.J. The effect of Alzheimer's amyloid-β aggregation state on the permeation of biocompatible lipid vesicles. *Langmuir* 26, 17266–17268 (2010).
5. Williams, T.L., Day, L.I. & Selkoe, D.J. The effect of Alzheimer's amyloid-β aggregation state on the permeation of biocompatible lipid vesicles. *Langmuir* 26, 17266–17268 (2010).

5. Stankovic, G. M. et al. Natural oligomers of the Alzheimer amyloid-beta protein induce reversible synaptic loss by modulating an NMDA-type glutamate receptor-dependent signaling pathway. *The Journal of Neuroscience* 27, 2866–2875 (2007).
6. Stankovic, G. M. et al. Natural oligomers of the Alzheimer amyloid-beta protein induce reversible synaptic loss by modulating an NMDA-type glutamate receptor-dependent signaling pathway. *The Journal of Neuroscience* 27, 2866–2875 (2007).
7. Crayth, J.P. et al. Natural oligomers of the amyloid-beta protein specifically disrupt cognitive function. *Nat Neurosci* 8, 79–84 (2005).
8. Loo, P.N. et al. Natural oligomers of the amyloid-beta protein specifically disrupt cognitive function. *Nat Neurosci* 8, 79–84 (2005).
9. Loo, P.N. et al. Natural oligomers of the amyloid-beta protein specifically disrupt cognitive function. *Nat Neurosci* 8, 79–84 (2005).
10. Loo, P.N. et al. Natural oligomers of the amyloid-beta protein specifically disrupt cognitive function. *Nat Neurosci* 8, 79–84 (2005).
11. Loo, P.N. et al. Natural oligomers of the amyloid-beta protein specifically disrupt cognitive function. *Nat Neurosci* 8, 79–84 (2005).
12. Loo, P.N. et al. Natural oligomers of the amyloid-beta protein specifically disrupt cognitive function. *Nat Neurosci* 8, 79–84 (2005).
13. Loo, P.N. et al. Natural oligomers of the amyloid-beta protein specifically disrupt cognitive function. *Nat Neurosci* 8, 79–84 (2005).
14. Loo, P.N. et al. Natural oligomers of the amyloid-beta protein specifically disrupt cognitive function. *Nat Neurosci* 8, 79–84 (2005).
15. Loo, P.N. et al. Natural oligomers of the amyloid-beta protein specifically disrupt cognitive function. *Nat Neurosci* 8, 79–84 (2005).
16. Loo, P.N. et al. Natural oligomers of the amyloid-beta protein specifically disrupt cognitive function. *Nat Neurosci* 8, 79–84 (2005).
17. Loo, P.N. et al. Natural oligomers of the amyloid-beta protein specifically disrupt cognitive function. *Nat Neurosci* 8, 79–84 (2005).
18. Loo, P.N. et al. Natural oligomers of the amyloid-beta protein specifically disrupt cognitive function. *Nat Neurosci* 8, 79–84 (2005).
19. Loo, P.N. et al. Natural oligomers of the amyloid-beta protein specifically disrupt cognitive function. *Nat Neurosci* 8, 79–84 (2005).
20. Loo, P.N. et al. Natural oligomers of the amyloid-beta protein specifically disrupt cognitive function. *Nat Neurosci* 8, 79–84 (2005).
21. Loo, P.N. et al. Natural oligomers of the amyloid-beta protein specifically disrupt cognitive function. *Nat Neurosci* 8, 79–84 (2005).
22. Loo, P.N. et al. Natural oligomers of the amyloid-beta protein specifically disrupt cognitive function. *Nat Neurosci* 8, 79–84 (2005).
23. Loo, P.N. et al. Natural oligomers of the amyloid-beta protein specifically disrupt cognitive function. *Nat Neurosci* 8, 79–84 (2005).
24. Loo, P.N. et al. Natural oligomers of the amyloid-beta protein specifically disrupt cognitive function. *Nat Neurosci* 8, 79–84 (2005).
25. Loo, P.N. et al. Natural oligomers of the amyloid-beta protein specifically disrupt cognitive function. *Nat Neurosci* 8, 79–84 (2005).
26. Loo, P.N. et al. Natural oligomers of the amyloid-beta protein specifically disrupt cognitive function. *Nat Neurosci* 8, 79–84 (2005).
27. Loo, P.N. et al. Natural oligomers of the amyloid-beta protein specifically disrupt cognitive function. *Nat Neurosci* 8, 79–84 (2005).
28. Loo, P.N. et al. Natural oligomers of the amyloid-beta protein specifically disrupt cognitive function. *Nat Neurosci* 8, 79–84 (2005).
29. Loo, P.N. et al. Natural oligomers of the amyloid-beta protein specifically disrupt cognitive function. *Nat Neurosci* 8, 79–84 (2005).
30. Loo, P.N. et al. Natural oligomers of the amyloid-beta protein specifically disrupt cognitive function. *Nat Neurosci* 8, 79–84 (2005).

Acknowledgements

L.C.S., K.S. and K.M. are supported by funding from Medical Research Council UK (MR/K022105/1). L.C.S. is supported by Alzheimer's society and Alzheimer's research UK. K.S. is supported by funding from the BBSRC (BB/K019015/1). The authors acknowledge the kind gift of NU1 antibody from William Klein.


Author Contributions

K.E.M., D.M.V., L.D., V.A.H., J.I.D. and A.T. conducted the structural experiments. K.E.M., D.M.V. and M.W.E. conducted cellular experiments. M.W.E. analyzed synaptic data. L.C.H. conducted animal studies. L.D. and L.S. designed the peptide. G.J.C. contributed to memory and learning studies. K.S. directed the synaptic work and edited the manuscript and figures. K.E.M. and L.C.S. planned the experiments, managed the work and wrote the manuscript.

**Additional Information****Supplementary Information**

**Competing financial interests:** The variant peptide, a kit including the variant peptide, and their uses, are covered by an International (PCT) patent application PCT/GB2015/02242 filed by the University of Sussex.

**How to cite this article:** Marshall, K. E. *et al.* A critical role for the self-assembly of Amyloid- $\beta$ 1-42 in neurodegeneration. *Sci. Rep.* 6, 30182; doi:10.1038/srep30182 (2016).

 This work is licensed under a Creative Commons Attribution 4.0 International License. The images or other third party material in this article are included in the article's Creative Commons license, unless indicated otherwise in the credit line; if the material is not included under the Creative Commons license, users will need to obtain permission from the license holder to reproduce the material. To view a copy of this license, visit <http://creativecommons.org/licenses/by/4.0/>



ARTICLE

Received 13 May 2015 | Accepted 11 Jul 2015 | Published 21 Aug 2015

DOI: 10.1038/ncomms9043

OPEN

# Ultrastructural and functional fate of recycled vesicles in hippocampal synapses

Stephanie A. Rey<sup>1</sup>, Catherine A. Smith<sup>1</sup>, Milena W. Fowler<sup>1</sup>, Freya Crawford<sup>1</sup>, Jemima J. Burden<sup>2</sup> & Kevin Staras<sup>1</sup>

Efficient recycling of synaptic vesicles is thought to be critical for sustained information transfer at central terminals. However, the specific contribution that retrieved vesicles make to future transmission events remains unclear. Here we exploit fluorescence and time-stamped electron microscopy to track the functional and positional fate of vesicles endocytosed after readily releasable pool (RRP) stimulation in rat hippocampal synapses. We show that most vesicles are recovered near the active zone but subsequently take up random positions in the cluster, without preferential bias for future use. These vesicles non-selectively queue, advancing towards the release site with further stimulation in an actin-dependent manner. Nonetheless, the small subset of vesicles retrieved recently in the stimulus train persist nearer the active zone and exhibit more privileged use in the next RRP. Our findings reveal heterogeneity in vesicle fate based on nanoscale position and timing rules, providing new insights into the origins of future pool constitution.

<sup>1</sup>School of Life Sciences, University of Sussex, Brighton BN1 9QJ, UK. <sup>2</sup>Medical Research Council Laboratory for Molecular Cell Biology, University College London, Gower Street, London WC1E 6BT, UK. Correspondence and requests for materials should be addressed to K.S. (email: k.staras@sussex.ac.uk).

ARTICLE

Synaptic vesicles in presynaptic terminals are classified in terms of their position on the basis of function<sup>1–4</sup>. As such, the properties of these pools, their size, physical organization, availability for release and kinetics of recycling, are critical determinants of synaptic performance and of major interest. Arguably the most significant pool class is the readily releasable pool (RRP); by definition, the subset of synaptic vesicles that are first to undergo fusion in response to stimulation<sup>5,6</sup>. Thanks to the privileged release status of this pool, and therefore its central relevance in signalling, investigations of the RRP have been the subject of substantial research effort.

In small central presynaptic terminals, recent elegant work based on fast fusion approaches has revealed key steps occurring in the immediate aftermath of vesicle fusion<sup>7–10</sup>. However, the longer-term functional and organizational fate of vesicles reclaimed after a defined pool is accessed, remains poorly understood. For example, in case of the RRP, does the fact that these vesicles undergo preferential use, predispose the retrieved pool to also have privileged release properties? This could be a consequence of a specific characteristic of such vesicles, for example a molecular identifier that earmarks them for selective treatment, as suggested for other functionally defined vesicle pools<sup>11</sup>, or perhaps simply reflect the physical positions they adopt after retrieval. Alternatively, such vesicles might exhibit no specific 'tagged' or 'marked' properties once recycled. A third possibility is the vesicle fate might not be determined according to a non-random pecking order<sup>12</sup>. These issues are of major significance, relevant to fundamental ideas about the relationship between functional and organizational properties of vesicles and the rules that govern their future use.

Here we address the issue of vesicle fate and future pool composition directly, using a combination of sensitive imaging and time-stamped function-ultrastructure approaches in acute hippocampal slices and neuronal cultures. We show that vesicles retrieved after recycling of the RRP are endocytosed close to the active zone but their subsequent fate is variable across the pool. Most vesicles are randomly inserted back into the cluster volume, with no privileged status for further release. We demonstrate that additional synaptic activity and actin remodelling are factors in advancing these vesicles towards the active zone. However, a subset of the retrieved pool becomes preferentially organized at positions near the release site, undergoing privileged use in subsequent signalling events. We investigate the basis for this using reduced stimulation protocols, demonstrating that this subset of the pool correlates with vesicles retrieved most recently in the stimulus train. Our findings reveal a tight link between ultrastructural organization and vesicle function. Heterogeneity in the fate of vesicles retrieved after RRP stimulation provides new understanding of the mechanisms that govern vesicle recycling at size-limited central synapses and the origins of future pool composition.

## Results

**Ultrastructural tracking of endocytosed vesicles.** Vesicles recycled after RRP stimulation in acute hippocampal slices were labelled with FM1-43 (refs 16–18) applied to CA1 while activating Schaffer collaterals (40 action potentials (APs) at 20 Hz) with field stimulation<sup>19–21</sup> (Fig. 1a). After loading, confocal imaging revealed discrete punctate staining (Fig. 1b), consistent with dye marking of functional terminals. For ultrastructural investigation we used the capability of FM-dye to drive dimethylenediazine (DAB) polymerization to form an osmophilic precipitate when photoactivated<sup>22–24</sup>. Dye-labelled brain slices were rapidly fixed at three time points (1, 5 and 20 min) after loading.

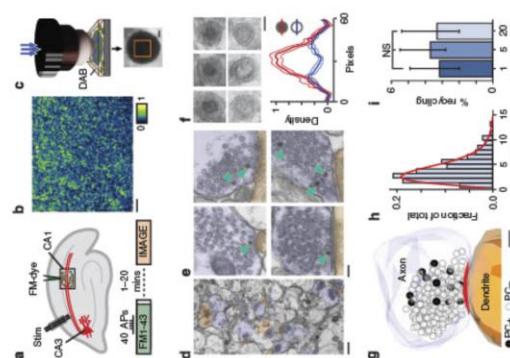


**Figure 1 | Ultrastructural visualization of vesicles retrieved after RRP stimulation in acute hippocampal slices.** (a) Schematic illustrating experimental protocol for labelling recycled vesicles. Extracellular stimulation (40 APs, 20 Hz) of Schaffer collaterals is combined with FM-dye application to CA1. (b) Representative image of fluorescence from dye-labelled synapses in CA1. Scale bar, 10  $\mu$ m. (c) Schematic illustrating approach for photoconversion of labelled vesicles. Dye-loaded fixed target region is photo-illuminated using blue light focused through an objective lens in the presence of DAB (top), producing an electron-dense spot in the slice tissue (bottom). Orange square indicates trimmed target region used for ultrastructural analysis. Scale bar, 200  $\mu$ m. (d) Low magnification electron micrograph showing presynaptic terminals (blue) and postsynaptic structures (brown). Scale bar, 500 nm. (e) Typical images showing terminals with PC+ vesicles (arrowheads). Scale bar, 100 nm. (f) Top: High magnification images of PC+ vesicles with electron-dense lumen and PC- vesicles with clear lumen. Scale bar, 25 nm. (bottom) Cross-sectional density profiles of PC+ and PC- vesicles ( $n=6$ , mean  $\pm$  s.e.m.) illustrating a quantitative approach that allows for the differentiation of vesicle classes. (g) 3D reconstruction showing PC+ vesicles (dark spheres) and PC- vesicles (transparent spheres). Active zone appears red. Scale bar, 100 nm. (h) Frequency histogram of PC+ pool sizes based on ultrastructural analysis of  $n=10$  synapses from 11 slices from 10 animals, assessed as % of total pool. Bar represents gamma function fit. (i) Summary bar chart showing the percentage of total pool for vesicles fixed at different times after loading (1 min: 3.1% (2.0–4.9),  $n=73$  PC+ vesicles from 28 synapses (including  $n=8$  full serial reconstructions) from 3 slices from 3 animals; 5 min: 3.6% (2.5–5.0),  $n=188$  PC+ vesicles from 59 synapses (including  $n=4$  full serial reconstructions) from 3 slices from 3 animals; 20 min: 23% (2.0–54),  $n=455$  PC+ vesicles from 100 synapses (including  $n=10$  full serial reconstructions) from 5 slices from 4 animals, not significant, Kruskal-Wallis one-way ANOVA,  $P=0.378$ ).





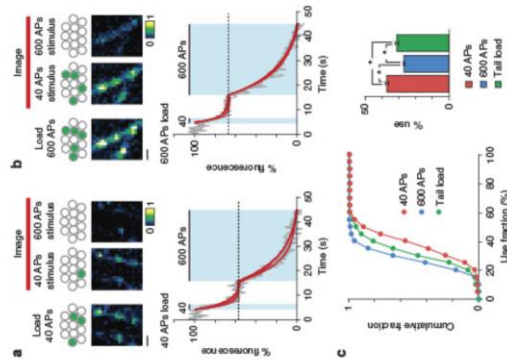


**Figure 5 | Heterogeneity in functional use of recycled vesicles.** (a) (Top) Schematic illustrating experimental approach. The pool recruited from recruitment of the RRP (40 APs) is labeled and 20 min later subjected to two rounds of stimulation (desatting) in the absence of dye while imaging 40 APs to release current RRP and 600 APs to release TRP. The ratio of APs that are recycled (red) versus released (blue) is shown. Note that in not desatting, although 600 APs and 40 APs should have access > 90% of the available pool of vesicles, the RRP is not a non-recycling pool could lead to this value being an overestimate. (Middle) Representative images of 40 APs loading and the two phases of activity-driven dye loss. Scale bar, 2  $\mu$ m. (Bottom) Plot showing three sample desatting curves (grey lines) each fitted with two single exponentials (red lines). Fluorescence is total fluorescence lost during the two-phase desatting protocol, allowing us to make an estimate of the relative proportion of dye loss arising from the 40 APs versus the larger 600 APs desatting protocol. (b) As in (a) for 600 APs loading. Scale bar, 2  $\mu$ m. (c) Mean  $\pm$  s.e.m. histogram summary (right) and cumulative frequency distribution plot (left) of % use for 40 APs stimulation after 40 APs loading (n = 119 from 4 cultures, red) and 600 APs loading in culture (n = 131 from 4 cultures, blue). Green bar (right) and line plot (left) shows a third protocol (tail load) in which only the tail and (< 200 APs) of a 600 APs stimulus train had FM-dye present to allow labelling (n = 131 from 4 cultures). Mean  $\pm$  s.e.m. use fraction was as follows: 40 APs: 37.2  $\pm$  0.9%, 600 APs: 27.1  $\pm$  0.6%, tail load: 31.7  $\pm$  0.9% (one-way ANOVA,  $P < 0.001$ , Bonferroni's multiple comparison: 40 APs versus 600 APs,  $P < 0.05$ , 40 APs versus tail load,  $P < 0.05$ ).

NATURE COMMUNICATIONS | DOI: 10.1038/ncomms5043 | www.nature.com/naturecommunications

© 2015 Macmillan Publishers Limited. All rights reserved.

loading (two-tailed unpaired  $t$ -test, 600 APs versus 40 APs,  $P < 0.0001$ ). Thus, vesicles recruited after the RRP were used in a subsequent stimulus train that was significantly exceeds that expected by chance suggesting some privileged release properties. This could relate to some vesicles being specially designated or alternatively reflect some property related to the timing of their retrieval in the stimulus train. To examine this latter idea, we carried out a further protocol in which we based dye labelling to only the most recently retrieved vesicles in a stimulus train by applying FM-dye at the end (~200 APs) of a maximal 600 APs loading protocol. In the same two-step desatting paradigm, the fraction of vesicle use for this selective loading of the 'tail' of the stimulus (31.7  $\pm$  0.8%,  $n = 131$  from 4 cultures, Fig. 5c, tail load) was intermediate between the 600 APs loading condition and the 40 APs loading protocol (one-way analysis of variance (ANOVA),  $P < 0.001$ , Bonferroni's multiple comparison: 600 APs versus tail loading,  $P < 0.05$ ; 40 APs versus tail loading,  $P < 0.05$ ; 600 APs versus 40 APs,  $P < 0.05$ ). This implies a significant role for the timing of retrieval in contributing to the subsequent use of those vesicles in the next RRP stimulation.

**Privileged use relates to vesicle position in the cluster.** If recent retrieval is important for subsequent use, then vesicles that are limited stimulation might be expected to undergo privileged release. To test this directly we chose a minimal loading stimulus (10 APs, Fig. 6a) that accesses a small vesicle subset representing the most recently recycled vesicles. Consistent with our hypothesis we found that the relative dye loss to the 40 APs desatting stimulus (Fig. 6b, see also Fig. 5a) was significantly larger for this minimal 10 APs loading protocol than for the 40 APs loading condition (10 APs: 41.2%  $\pm$  1.6%, 40 APs: 37.2  $\pm$  0.9%,  $n = 74$ ,  $n = 119$ , two-tailed unpaired  $t$ -test,  $P < 0.02$ , Fig. 6b). This suggests that such a limited loading protocol has a small but significant bias towards recruitment of vesicles that subsequently undergo preferential use.

To provide a further confirmation of this idea we took advantage of the genetically encoded optical reporter syph2<sup>2</sup>, a fusion construct of synaptophysin and two copies of pHluorin, a pH-sensitive fluorophore that provides a readout of vesicle fusion, endocytosis and vesicle re-acidification (Fig. 6c). Compared with FM-dye, this probe offers improved sensitivity close to quantal resolution (Fig. 6d, see also Fig. 6b) permits readout of multiple recycling rounds at short intervals (Fig. 6f). After generating baseline responses using repeated 10 APs stimulations at 1 min intervals we added batholymycin (1  $\mu$ M) to stabilize the vesicle pool. We noted that 1 previously released, now alkaline-trapped, vesicles are used they should not contribute to further fluorescence rises. In this way, we could test if new vesicles were always used on subsequent rounds of 10 APs stimulation, or whether a proportion of the vesicles were the same ones recycled previously. We found that post-batholymycin, repeated 10 APs stimulations led to progressive reductions in stimulus amplitude (Fig. 6f) indicating that larger and larger proportions of the accessed pool were comprised of vesicles that have been recently retrieved. This reduction did not correspond to a depletion of all releasable vesicles since the substitution of a larger maintained stimulus (1,200 APs) could evoke a substantial additional fluorescence rise (Fig. 6g) in the same synapses (Supplementary Fig. 4). Although batholymycin treatment does cause spontaneous alkalization, the long time constant of this process (~60 min<sup>-1</sup>) suggests that it is unlikely to be a significant factor in the minute-to-minute timescale changes that we observe.

NATURE COMMUNICATIONS | DOI: 10.1038/ncomms5043 | www.nature.com/naturecommunications

5

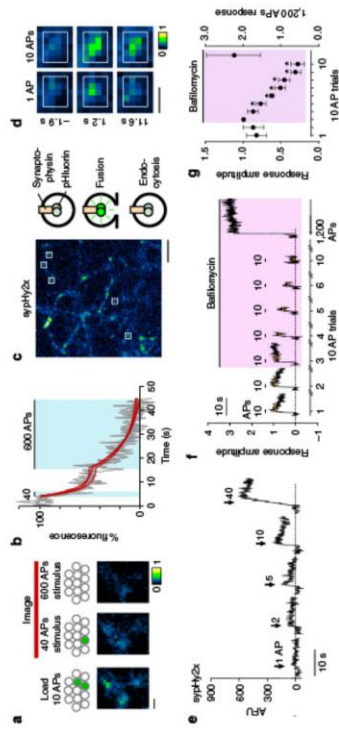


**Figure 6 | Preferential use of vesicles previously recruited by a limited loading protocol.** (a) (Top) Schematic illustrating experimental approach. Vesicles FM-dye labeled with 10 APs are stimulated with two further rounds of stimulation (desatting) in the absence of dye while imaging 40 APs to release current RRP and 600 APs to release TRP. The ratio between dye loss after 40 APs stimulation and total dye loss provides a measure of preferential use of the original loaded pool. (Bottom) Representative images of 10 APs loading and the two phases of activity-driven dye loss. Scale bar, 2  $\mu$ m. (b) Plot showing sample desatting curves for three synapses each fitted with two single exponentials (red lines). Fraction of 10 APs-loaded vesicles used in subsequent stimulus was significantly higher than 40 APs: 41.2%  $\pm$  1.6%, 40 APs: 37.2  $\pm$  0.9%,  $n = 74$  from 7 cultures,  $n = 119$  two-tailed unpaired  $t$ -test,  $P < 0.05$ . (c) (Left) Example image of syph2<sup>2</sup> expression and schematic illustrating mechanism of action as fusion reporter. Image was collected at 40 AP peak response at synapse in response to stimulation (1 AP, left; 10 AP, right). Scale bar, 2  $\mu$ m. (d) Sample syph2<sup>2</sup> images showing fluorescence change at synapse in response to stimulation (1 AP, left; 10 AP, right). Scale bar, 2  $\mu$ m. (e) Traces showing average fluorescence intensity profiles for same single synapse from (d) a range of stimuli. (f) Traces showing average fluorescence responses (3 synapses) with repeated 10 APs stimulations (interval 1 min) before (trials 1 and 2) and after (trials 3–10) the addition of 1  $\mu$ M batholymycin, a VAMP inhibitor that prevents vesicle acidification. Values are normalized relative to the first batholymycin trial response amplitude. The reduction in response amplitude after batholymycin treatment is consistent with the use of alkali-trapped vesicles. A larger maintained stimulus (1,200 APs) can recruit additional non-recycled vesicles, observed as a significant rise in fluorescence intensity. (g) Mean  $\pm$  s.e.m. responses (105 synapses from 4 cultures), normalized to first batholymycin trial. Asterisks indicate significant outcomes ( $P < 0.05$ ) of two-tailed one-sample  $t$ -tests for each time point versus 1. Note 1,200 APs response amplitude is shown on different scale (right).

We note also that the magnitudes of each successive amplitude reduction (~20%), are broadly compatible with what would be predicted on the basis of the previous FM-dye results when scaled down for the smaller 10 AP stimulation protocol used here. These results, consistent with our FM-dye experiments, indicate a small but significant preferential use of the recently retrieved pool.

Does our preferential use of the recently retrieved pool of APs stimulation correspond to the vesicles that are most alkaline-trapped? To address this question we used the previously released, now alkaline-trapped, vesicles are used they should not contribute to further fluorescence rises. In this way, we could test if new vesicles were always used on subsequent rounds of 10 APs stimulation, or whether a proportion of the vesicles were the same ones recycled previously. We found that post-batholymycin, repeated 10 APs stimulations led to progressive reductions in stimulus amplitude (Fig. 6f) indicating that larger and larger proportions of the accessed pool were comprised of vesicles that have been recently retrieved. This reduction did not correspond to a depletion of all releasable vesicles since the substitution of a larger maintained stimulus (1,200 APs) could evoke a substantial additional fluorescence rise (Fig. 6g) in the same synapses (Supplementary Fig. 4). Although batholymycin treatment does cause spontaneous alkalization, the long time constant of this process (~60 min<sup>-1</sup>) suggests that it is unlikely to be a significant factor in the minute-to-minute timescale changes that we observe.

sub-compartment of the terminal (Fig. 7e). Our findings support the idea that the vesicles recovered after RRP stimulation are variable with regard to their functional and ultrastructural fates, some vesicles are randomly positioned in the terminal space and undergo non-preferential use but others, in particular those released by a limited stimulus, tend to re-cluster at sites close to the active zone and preferentially participate in transmission on subsequent stimulation.

**Activity advances recycled vesicles towards the active zone.** Although we established that a subset of vesicles retrieved after RRP stimulation remain close to the active zone for subsequent release, we also show that the majority do not. As such, our findings are different from those previously reported for TRP organization where vesicles preferentially re-cluster at sites near the active zone after recycling<sup>1</sup>. One key difference between RRP and TRP loading protocols is the level of evoked stimulation (40 APs versus > 600 APs) suggesting that the additional activity may be an important factor that shapes vesicle organization. To test this idea directly we labelled the vesicles retrieved after RRP recruitment but carried out a further brief stimulation (3  $\times$  40 APs) before ultrastructural processing at 20 min (Fig. 8a). Notably, the remaining non-released fraction of PC+ vesicles had a highly segregated arrangement compared with the standard 20 min condition without stimulation (Fig. 8b–d), with a

NATURE COMMUNICATIONS | DOI: 10.1038/ncomms5043 | www.nature.com/naturecommunications

© 2015 Macmillan Publishers Limited. All rights reserved.



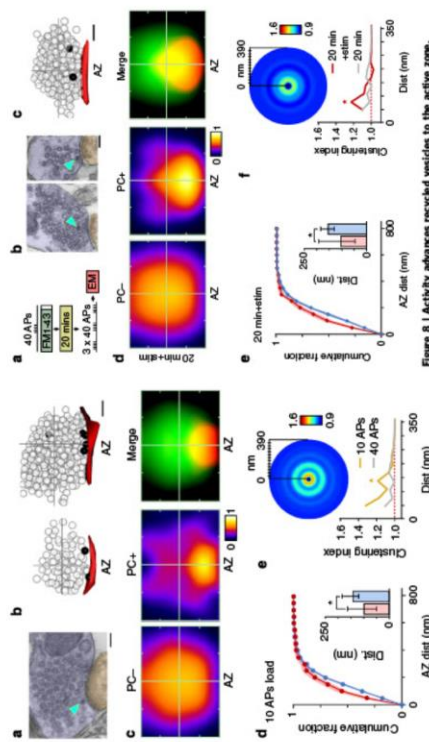


**Figure 7 | Segregated organization of preferentially used vesicles.** (a) Representative electron micrograph after 10 APs loading (PC+ vesicle, arrow). Scale bar, 100 nm. (b) Representative 3D reconstructions showing PC+ vesicles (dark spheres) and PC- vesicles (transparent spheres). Active zone appears red. Grey cross hairs indicate vesicle cluster boundaries. Scale bar, 100 nm. (c) Normalized, smoothed spatial frequency density plots for 10 APs condition (n=59) for PC+ (left panel), PC- (middle panel) and merged (right panel). Active zone centre (AZ) are bottom middle in each plot. In merged plots, green is PC-, red is PC+. (d) Cumulative frequency plots for vesicle active zone distances (n=59) surrounding 10 APs full serial reconstructions from 3 slices from 2 synapses. Red lines/circles: PC+; blue lines/circles: PC-. (e) Histogram shows median distance ± s.e.m. Red lines/circles: PC+; blue lines/circles: PC-. (f) Circular frequency density plot showing vesicle clustering, with colour look-up table corresponding to fraction of PC+ vesicles. (Bottom) Line plot (red) showing clustering ratio with increasing distance from vesicle centre, normalized to ratio for whole synapse. Grey line shows 40 APs 20 min data (from Fig. 4b). Asterisk indicates radial distance where clustering significantly exceeds baseline values (two-tailed one-sample t-test,  $P < 0.05$ ).

significantly shorter mean distance to active zone for its PC+ vesicles versus the population of PC- vesicles in the terminal (Fig. 8a, inset see legend). Moreover, analysis revealed a return to significant clustering of vesicles at a short distance range (Fig. 8b) indicative of a process leading to the condensation of PC+ vesicles into a smaller presynaptic compartment. We also considered whether stimulation might have had some overall impact on the organization of the whole cluster. To examine this we quantified the raw distances of all vesicles to the active zone for the standard 20 min condition (without extra stimulation before fraction), versus the same condition with brief stimulation ( $3 \times 40$  APs), fixation and ultrastructural difference (20 min median (QR), 175 nm (98–259),  $n = 7964$

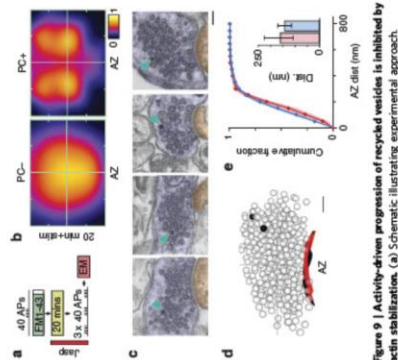


**Figure 9 | Activity-driven progression of recycled vesicles is inhibited by actin stabilization.** (a) Schematic illustrating experimental approach. (b) Normalized and smoothed spatial frequency density plots for 20 min + stimulation condition in presence of 1  $\mu$ M jasplakinolide (n=48 animals) for PC+ (left panel) and PC- (right panel) showing the vesicle positions with respect to the active zone and cluster boundaries. Active zone centres (AZ) are bottom middle in each plot. (c) Representative electron micrographs for same condition. Scale bar, 100 nm. (d) Example 3D reconstruction for same condition (dark spheres: PC+, transparent spheres: PC-). Active zone appears red. Grey cross hairs indicate boundaries of vesicle cluster from active zone centre. Scale bar, 100 nm. (e) Cumulative frequency plots (n=48). Lines and circles are mean values and shaded areas are s.e.m. Red lines/circles: PC+; blue lines/circles: PC-. (Inset) Histogram shows median distance ± s.e.m. for PC+ vesicles (red bar) and PC- vesicles (blue bar) (PC+ versus PC-: 159 (108–223) nm versus 142 (115–166) nm, n=48, Wilcoxon test,  $P = 0.090$ ).

micrographs we observed a robust blockade of the PC+ vesicle segregation at the active zone—seen previously (Fig. 9b–d) such that the median distance between the active zone and PC+ vesicles slightly exceeded that for PC- vesicles (Fig. 9e). However, when we quantified the raw distances of all vesicles to the active zone for the standard 20 min condition (without extra stimulation before fraction), versus the same condition with brief stimulation ( $3 \times 40$  APs), fixation and ultrastructural difference (20 min median (QR), 175 nm (98–259),  $n = 7964$

that this large activation recycles a significant proportion of the functional vesicles, which then become the basis for the cluster becoming stabilized by actin stabilization, consistent with the ultrastructural data. Thus, in subsequent rounds of RRP stimulation these vesicles are not available for recycling and contribute to the decline in response amplitude. Taken together, these findings support a permissive role for synaptic activation and actin in the participation of recently endocytosed vesicles for subsequent transmission events.

## Discussion

Our results provide a nanoscale view of the fate of the vesicle pool retrieved after turnover of the RRP in small native central terminals, addressing fundamental questions about vesicle use and the origins of the current pool composition. At 1 min after stimulation, we show that recycled vesicles (~3–4% of the total pool) are significantly segregated near the active zone, compatible with recent findings<sup>8,9</sup>. Over longer time periods (5–20 min), however, the overall organization of the retrieved pool changes markedly, with labelled vesicles becoming randomly distributed in the cluster, consistent with their non-selective insertion into the presynaptic terminal volume. On the basis of functional readouts, we show that most vesicles do not exhibit prolonged retention episodes and are available for future release after recycling. Nonetheless, our analysis suggests that preceding their further RRP-recycling stimulus, a significant proportion of the level of release expected by chance. Using a reduced magnitude loading stimulus (10 APs) we could also physically closer to the subset, demonstrating that they were also physically closer to the release site than the total RRP-recycled vesicle pool. Our results suggest that the long-term fate of vesicles retrieved after RRP stimulation is heterogeneous across the population, with some non-selectively entering the recycling pool while others are effectively fast-tracked for subsequent use.

We make several key assumptions in interpreting our findings. First, in comparing across a variety of different protocols, we have to assume that synapses recruited by different stimuli are homogeneous. We cannot, of course, fully rule out that potential differences among synapses—in some way selectively recruited under different conditions—could account for aspects of the heterogeneous behaviour we observe. However, our evidence based on the fundamental parameters we measure functionally (for example responses evoked by different stimulation protocols using sytphix, Fig. 6c, Supplementary Fig. 5) or in ultrastructure (for example, the overall morphology of terminals, their total pool size, the average vesicle distance to the active zone and the number of clustered vesicles) indicates that our experiments result in equally representative samples of synaptic dynamics. Second, we need to interpret our vesicle dynamics in the context of a central assumption that vesicles stay intact after endocytosis (unless they undergo further rounds of release) and thus any subsequent changes in locations at different time points therefore represent time-dependent migration. The fact that the numbers of PC+ vesicles are well-conserved between time points suggests that this is likely to be a reasonable supposition.

What is the basis for this heterogeneity? Our experiments indicate that there is a bias towards subsequent preferential use of the pool retrieved after a minimal stimulation (for example, 10 APs). This effect is not large but nonetheless significant. One possibility is that this protocol favours the turnover of a special subset of RRP vesicles with a characteristic identifier, for example a molecular tag, that singles them out for preferential release in subsequent rounds of stimulation. This would place them in a distinct category where their re-use occurs because of attributes that persist over multiple rounds of activity, an idea that appears



that adds with recent findings in the field, an alternative possibility is that vehicle use is a product of their recent experiences. For example, if the vehicle use of the experimental subjects is the simplest idea being their order of retrieval in the stimulus train with the most recently retrieved vehicles predominating, then the higher vehicle use probabilities, in the experimental group, would favor more use of the vehicles in the retrieved pool. In this scenario, the stimulating with 10 APs versus 40 APs would favor more use of the vehicles would, in relative terms, be recently endocytosed. To formalize these ideas, we tested the outcomes of our functional experiments (Supplementary Fig. 7) in a modelled vesicle population with randomly assigned weightings for vesicle use (either heterogeneous or homogeneous across the population). However we cannot definitively rule out more complex scenarios, in which the reverse order of retrieval could—effectively “last in, first out”—in the vesicles that were most recently endocytosed are used for future use, proved to be the most parsimonious conclusion that matched our experimental findings. Such a mechanism predicts some favored use of the vesicles retrieved after RRP stimulation, as we observe, without the need for a lingering identifying characteristic of the previously released pool, for example based on molecular determinants that define pool identity.<sup>38</sup> Such a conclusion is also highly compatible with our ultrastructural findings, which demonstrate that the minimally released pool resides near the active zone and is thus presumably highly proximal to the release site. This implies a high probability of release, and thus a more consistent and consistent use of these vesicles, than those of other pools.

On the basis of our findings here and those of our earlier studies, a proportion of the observed pool of vesicles may be automatically distributed in the active zone. This pool of vesicles is approximately distributed in the active zone of 5 and 20 minis. What drives this? Recent evidence suggests that intersynaptic  $\text{Ca}^{2+}$  waves exist as intersynaptic  $\text{Ca}^{2+}$  transients (23,22,38,40). The release of vesicles from the active zone is dependent on the movement of vesicles can occur over these timescales, even in resting terminals. Such mobility would presumably be quite ineffective in dispensing vesicles in the manner we visualize, however, over tens of minutes. Notably, however, it does not observe such scattering in the case of our limited 10 APs loading over the same time course, perhaps implying that vesicles and associated components lying closest to the active zone remain more effectively anchored. Consistent with this idea, evidence for a stable active zone-associated core scaffold<sup>1</sup> and a subpopulation of vesicles that are resistant to intersynaptic trafficking<sup>2</sup> have been described. We also reveal a role for actin in influencing vesicle organization. First, PC+ vesicles exhibited a small but directed progression forwards to the active zone with respect to the cluster volume as a whole. This might be explained by the fact that PC+ vesicles but could also be non-selective, perhaps simply a consequence of forces created by the insertion of new endocytosed vesicles at the cluster edges, causing a stimulus-driven migration of resident vesicles is subtle, corresponding to a less than one-vesicle-thickness shift in  $\sim 10\text{--}15\%$  of the total pool, observable only thanks to the substructural readout. This may account for the relatively limited role for activity-driven mobilization of vesicles reported in other studies<sup>3</sup>. Moreover, we show that actin contributes to this behavior in the form of a thick band of actin filaments adjacent to the vesicle back with filamentary junctions. This is reminiscent of a decision in the released pool zone. This aligns with our previous findings demonstrating that remodeling of actin is important in facilitating the movement of the TSP towards the active zone after endocytosis<sup>4</sup>. It remains unclear whether actin directly facilitates vesicle movement or alternatively functions as a support scaffold that can help guide other vesicle-associated elements as a signal<sup>5</sup>. Second, we show that stimulation brings about a small but significant condensation of all vesicles towards the release site and this effect is abolished with thapsigargin.

Previous work has characterized a similar activity-driven concentration of axons towards the active zone<sup>26</sup> suggesting that two events could directly interact. However, the heterogeneity in the ultrastructural and functional fate of the presynaptic vesicles observed in the recycled axonal terminals of central synapses, an elegant method by Ryan and Smith<sup>27</sup> exposed the short-term use of vesicles after release, using fluorescent probes based upon the Thy-1 considered relatively long-lasting labels (100 and 36% of the functional pool) and found no direct evidence for a hierarchy of releasability related to their use history over a timescale of ~2 min. Our findings would suggest a similar outcome since these significant 'loading' pools would recycle substantial vesicle populations, and thus make any small preferential bias related to the most recently released vesicles undetectable. Other work has offered an assorted picture of short-term preferential vesicle re-use in central terminals with evidence both in favour<sup>28,29</sup> and against<sup>30,31</sup>. Our long-term tracking of the ultrastructural translocation of vesicle destiny (~20 min) is not inconsistent with these studies, but the fact that we observe differences in functional vesicle fates according to the nature of the stimulus applied (with limiting stimuli tending to favour more or less subsequent use and larger stimuli less use) may help to reconcile some of these findings. With regard to vesicle position, elegant studies using comparable time courses of our work have indicated that small<sup>32</sup> versus mature<sup>33</sup> segregation of recycled vesicles with respect to the active zone. We note that the leading paradigms have been proposed in these papers (40 APs and 10 APs, respectively) would be highly consistent with our observations of re-clustering according to the level of stimulation. In particular, Park *et al.*<sup>32</sup> suggest a link between vesicle position in the terminal and the subsequent release that seems well-matched with our results. It is

It is notable that our findings contrast with the fate of retrieved synapses in the hippocampus, in which synaptic strength is maintained in the face of RRP depletion. In the hippocampus, synaptic strength is maintained by a combination of mechanisms, including the preferential re-use across the population<sup>24</sup>. As such, physical positioning and release are not highly correlated in this system, and other mechanisms—perhaps physical tracks that link vesicles to the active zone—are more important in preserving RRP status over multiple rounds of recycling.

An interesting consequence of the idea that recent ongoing activity favours subsequent use can be considered in the context of low frequency activity. Such a scenario is particularly relevant to *in vivo* where spiking frequencies of CA3 pyramidal neurons average  $\sim 1$  Hz during behavioural tasks, with only occasional higher frequency bursts (5–10 Hz). Our findings would predict that, in this case, there should be a tendency towards recycling and use of the same retrieved population of vesicles. As such, a subset of vesicles, smaller than the whole population of functional vesicles at a single time, would be most relevant to support basal activity. This is consistent with the idea that the basal activity could be based on ultrastructural assessment of vesicles recycled during the previous *in vivo* session, using a variety of preparation types, reports of which have been mixed. For example, in one study, 10% of the total vesicles were recycled, with a very limited fraction (1–5%) of the total were pool<sup>25</sup>.

## Methods

**Acute slice preparation.** Experiments were in accordance with the UK-Animal (Scientific Procedures) Act 1986 and satisfied local institutional regulations at the University of Sussex. Adult transverse hippocampal slices (200 µm) were made from 3- to 4-week-old male (Sprague-Dawley) and maintained in artificial cerebrospinal fluid containing (in mM): 125 NaCl, 2.5 KCl, 2.5 glucose, 1.25 NaH<sub>2</sub>PO<sub>4</sub>, 26 NaHCO<sub>3</sub>, 1 MgCl<sub>2</sub>, 2 CaCl<sub>2</sub>, 20 µM β-cyano-L-nitroquinoline-2,3-dione, 50 µM AP-5 (bubbled with 95% O<sub>2</sub> and 5% CO<sub>2</sub>; pH 7.3; 19.30–20). All experiments were performed at 23–25°C. FM1-43 or FM1-43FXF (Molecular Probes, 20 µM in

CSF) was pressure applied to hippocampal CA1. After 3 min Schaffer collaterals were stimulated at 20 Hz for 2 s (40 A/s) or 10 Hz for 1 s (10 A/s) using a tungsten electrode. Imaging experiments were performed 20 min after loading using an Olympus BX51M microscope ( $\times 60$  NA objective) equipped with a EV 300 confocal system (Olympus UK), a 488 nm ArGa laser and 510 long pass emission filter. Cells were treated with 1  $\mu$ M jasplakinolide (Calbiochem) applied immediately after FM dye-loading.

The biocompatibility and ultrathin optical investigation for intracellular formaldehyde, samples underwent rapid microwave fixation (60% glutaraldehyde, 2% formaldehyde) in PBS at 1, 5 or 20 min after dye loading. Subsequently, samples were transferred to 100 mM phosphate (pH 7.1), rinsed in 100 mM ammonium chloride (pH 7.1) for 1 h, and then fixed in 1% osmium tetroxide (pH 7.1) for 1 h. Samples were then dehydrated through a series of ethanol washes (30%, 50%, 70%, 80%, 90%, 100%) and critical point dried. Samples were then sputter-coated with gold and imaged using a scanning electron microscope (SEM) (Hitachi S-3000N). Samples were also stained with uranyl acetate and lead citrate, and imaged using a transmission electron microscope (TEM) (Hitachi HT-7000). Samples were also stained with uranyl acetate and lead citrate, and imaged using a transmission electron microscope (TEM) (Hitachi HT-7000). Samples were also stained with uranyl acetate and lead citrate, and imaged using a transmission electron microscope (TEM) (Hitachi HT-7000).

[illegible][illegible]

unless the distance between two vesicles was  $> \sim 2$  vesicle diameters, in which case the line entered the vesicle cluster until it reached the next vesicle. The vesicles in contact with this external boundary line defined the edge vesicle population. A second line, one-vesicle-diameter inside the first line, encompassed the vesicle core population. Visual inspection proved these to be a satisfactory definition of the cluster in each case. (Note: the compartment analysis produces a complex polygon that represents the outline of the vesicle cluster; it is not the same as the bounding rectangle used for the generation of spatial frequency density plots.

Fluorescence time-lapse sequences were analysed in ImageJ using 29 frames identified with the aid of a subpixel scale of frames before and after the destaining stimulus, and separated for both destaining phases. In this way, synaptotagmin that underwent destaining in either phase would be isolated. Chosen puncta were limited to those that were fully encapsulated by the ROI and positionally discrete. For analysis of destaining curves, pixel density (LSI for 40 Å, 30 Å for 600 Å) was fitted with a one-phase exponential decay curve (GraphPad Prism). Curve fitting was constrained to the fluorescence value immediately before destaining (start). Start and end curve values were used to estimate the relative fluorescence

For vesicle cluster analysis, we measured the fraction of PC+ vesicles in circular ROIs of increasing size (50 nm radial distance) surrounding individual PC+ vesicles. All values for these circular ROIs were then normalized to the fraction of PC+ vesicles in the grasper achieved when the lin ate encompassed the total vesicle cluster, for the reason the right hand end of all plots was the same. In each case, we compared the results with a control, and found that in all but one case, the results were significantly different for significance against 1 using one sample *t*-tests. We also plotted the fraction of PC+ vesicles in each circular ROI against the radius of the circular ROIs. For all ROIs, the fraction of PC+ vesicles in the ROIs was significantly different (higher or lower) than the overall (baseline) level of clustering of PC+ vesicles in the terminal.

Statistical comparisons used GraphPad Prism. Data sets were tested for normal distribution using the D'Agostino-Pearson test. Where data sets did not conform to the normal distribution, non-parametric comparisons (Wilcoxon) were reported. Median and IQR and applied non-parametric comparisons (Wilcoxon tests for paired, Mann-Whitney tests for unpaired). For parametric comparisons we reported mean  $\pm$  s.e.m. and tests between multiple groups used one-way ANOVA with post-hoc Bonferroni's multiple comparison tests. Two sample comparisons used unpaired or paired *t*-tests. One-sample *t*-tests were used for comparing a sample to a value. Significance was defined as  $P < 0.05$ .

## References

1. Schwartz, F. R. & Ryan, T. A. The synaptic vesicle cycle: exocytosis and endocytosis. *Curr. Opin. Neurobiol.* 16, 298–304 (2006).
2. Alkh, A. A. & Tilton, R. W. (2013). Synaptic vesicle pools and dynamics. *Cold Spring Harb. Perspect. Biol.* 4, a015601 (2013).
3. Alkh, A. A. & Tilton, R. W. (2013). Synaptic vesicle pools as update. *Front. Synaptic Neurosci.* 2, 139 (2010).
4. Rizzoli, S. O. & Betz, W. J. Synaptic vesicle pools. *Nat. Rev. Neurosci.* 6, 57–69 (2005).
5. Südhof, T. C. The synaptic vesicle cycle. *Annu. Rev. Neurosci.* 27, 509–547 (2004).
6. Fowler, M. W. & Saran, K. Synaptic vesicle pools: principles, properties and limitations. *Phys. Cell Res.* 335, 105–106 (2015).
7. Rosenmund, C. & Stevens, C. F. Definition of the readily releasable pool of vesicles at hippocampal synapses. *Neuron* 16, 1197–1207 (1996).
8. Schikorski, T. Readily releasable vesicles at hippocampal synapses. *Neuron* 16, 1197–1207 (1996).
9. Watanabe, S. et al. Ultrafast endocytosis at mouse hippocampal synapses. *Neuron* 50, 243–247 (2013).
10. Watanabe, S. et al. *Chadborn regenerates synaptic vesicles from endosomes.* *Neuron* 515, 259–253 (2014).
11. Watanabe, S. et al. *Ultrafast endocytosis distinguishes synaptic vesicle pools.* *Neuron* 71, 434–447 (2012).
12. Barago, J. et al. VAMP9 directs synaptic vesicles to a pool that selectively maintains asynchronous neurotransmission. *Nat. Neurosci.* 15, 738–745 (2012).
13. Alkh, A. D., Khoshdel, M., Trammann, B. & Kewalram, E. T. VGLUT1 defines a vesicle pool that is functionally distinct from the readily releasable pool of synaptic vesicles. *J. Neurosci.* 32, 121–134 (2012).
14. Bai, M. et al. Insulin modulates a VAMP7-defined synaptic vesicle pool and selectively regulates spontaneous neurotransmission. *Neuron* 80, 934–946 (2013).
15. Alkh, A. D. & Smith, S. J. Vesicle pool mobilization during action potential firing at hippocampal synapses. *Neuron* 14, 983–989 (1995).
16. Betz, W. J. & Reulein, C. Optical analysis of synaptic vesicle recycling at a single frog neuromuscular junction. *Science* 255, 200–203 (1992).
17. Spay, T. et al. The kinetics of synaptic vesicle recycling measured at single hippocampal synapses. *Neuron* 14, 713–724 (1995).
18. Garfield, M. A. & Betz, W. J. Synaptic vesicle recycling: synaptic endocytosis and endocytosis with FM dyes. *Nat. Rev. Physiol.* 1, 2616–2621 (2009).

- This work is licensed under a Creative Commons Attribution 4.0 International license. The images or other third party material in this article are included in the article's Creative Commons license, unless indicated otherwise in the credit line; if the material is not included under the Creative Commons license, users will need to obtain permission from the license holder to reproduce the material. To view a copy of this license, visit <http://creativecommons.org/licenses/by/4.0/>



Available online at [www.sciencedirect.com](http://www.sciencedirect.com)

ScienceDirect

journal homepage: [www.elsevier.com/locate/yecr](http://www.elsevier.com/locate/yecr)

## Review Article

## Synaptic vesicle pools: Principles, properties and limitations

Milena Wagner Fowler, Kevin Staras<sup>a</sup><sup>a</sup> School of Life Sciences, University of Sussex, Brighton BN1 9QJ, UK

## ARTICLE INFORMATION

## Article Chronology:

Received 3 March 2015

Accepted 14 March 2015

Available online 24 March 2015

## Keywords:

Presynaptic terminal

Vesicle pool

Central synapses

## Contents

Vesicle pool categories	151
Total recycling pool (TRP), recycling pool (RP) and resting pool (RIP)	151
Readily releasable pool (RRP)	151
Spontaneous pool	152
Docked pool	153
Superpool	153
Physical organization of defined pools	153
Limits of pool classifications	154
Molecular 'signatures' of vesicle pools	154
Concluding remarks	154
Acknowledgments	154
References	154

It is around three decades since the term 'pool' was first used to refer to a sub-population of presynaptic vesicles differentiated on the basis of their specific functional or structural characteristics. Subsequently, the idea that vesicle clusters can be sub-categorized has been widely embraced, offering an important framework for elucidating elemental principles of synaptic operation and uncovering presynaptic sub-states of modulation. This short review aims to provide a contemporary perspective on the vesicle pool field, identify key remaining questions, and also to consider some of the limitations of the pool concept.

\* Corresponding author.

E-mail address: [k.staras@sussex.ac.uk](mailto:k.staras@sussex.ac.uk) (K. Staras).<http://dx.doi.org/10.1016/j.yecr.2015.03.007>

0014-4827/© 2015 Elsevier Inc. All rights reserved.

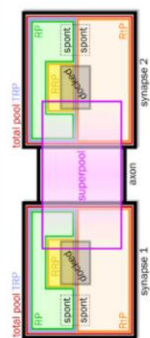


**Fig. 1** – Schematic of principal pool classifications and relationships. The pools shown are total pool, total recycling pool (TRP), recycling pool (RP), resting pool (RIP), readily releasable pool (RRP), docked pool and superpool. The spontaneous pool is indicated by dashed rectangles, reflecting uncertainty in defining its place within existing pool structures. Approximate average magnitudes of pools are indicated by relative box sizes.

In the central nervous system, most information transfer takes place at chemical synapses, ultrastructurally specialized neuron-neuron contact points where pre- and post-synaptic terminals are closely apposed. The presynaptic terminal is characterized by synaptic vesicles, spherical neurotransmitter-containing organelles which are densely clustered around the release site, or active zone. The process of transmission involves the rapid and regulated fusion of vesicles with the membrane and the release of their contents into the synaptic cleft, typically followed by vesicular endocytosis and refilling for subsequent re-use [61].

In electron micrographs, vesicles appear morphologically indistinct, but it is now well-established that their appearance belies substantial heterogeneity, defined on the basis of functional and organizational characteristics. Vesicles that share similar properties are categorized as 'pools', sub-clusters of the total complement of vesicles at a terminal. Such classifications have proved very helpful in unambiguously referencing vesicles participating in particular aspects of synaptic operation, in allowing comparative studies within and across synapse types, and in providing a framework for considering vesicle classes as possible modifiable substrates in plasticity or disease. The aim of this brief review is not to provide an exhaustive summary of pool classifications and properties; this has been done very comprehensively elsewhere [1,4,48,61]. Instead, we review core principles of pools, focusing on small central terminals where substantial and recent research effort has been invested. We also consider deficits in current understanding and explore some of the limits of the pool ideology.

## Vesicle pool categories

Since the concept of the pool emerged, researchers have enthusiastically embraced the idea of sub-categorizing vesicle populations leading to an array of different pool types across a variety of systems. Some pools are defined by functional characteristics, others by structural properties. Some are discrete, some are subsets, and yet others are unions of multiple pools (Fig. 1). This, together with the large range of systems under investigation, has led to some varied descriptions of pool classes and accompanying nomenclature. In a recent review, Alabi and Tsien [1] proposed a

clear and logical rationalization of pool definitions and categories which addresses and clarifies many of these issues. For consistency we will refer to pool categories according to their proposal.

## Total recycling pool (TRP), recycling pool (RP) and resting pool (RIP)

In simple terms, the sum of the total recycling pool and resting pool together describes the full complement of morphologically-defined vesicles in a presynaptic terminal: ~200 in small hippocampal synapses [21,53] (Fig. 2). Operationally, the TRP refers to the total vesicle population that engages in stimulus-evoked recycling. The resting pool is the remainder of the total pool which does not undergo activity-driven fusion, even under saturating stimulation conditions. The recycling pool (RP) or in many studies referred to as the reserve pool defines the residual of the TRP without the readily releasable pool (RRP; see below).

There is a general consensus that the TRP is only a fraction of the total pool [5,11,20,31,32] and that this fraction is highly variable in size within synaptic populations [20,29,32]. Moreover, mean size values also vary widely in different studies from ~15–20% [20,32] to >70% [26,49], in part reflecting differences in measurement approaches, choices of preparation, and recruitment paradigms – in particular the frequency of stimulation (reviewed in [6]). Recent findings suggest that most information transmission in vivo might rely principally on only a sub-division of recycling vesicles (1–5% of the total pool [6]) although higher fractions (5–23%) have also been reported [32]. Given the direct correlation reported between total recycling pool size and synaptic release probability [36,67] – a measure of synaptic efficacy – there has been substantial interest in mechanisms of TRP modulation. For example, inhibition of protein degradation by proteasome has been reported to increase the total recycling pool through increases in cAMP-PKA activity [71] while knockout of secretory carrier membrane protein 5, a candidate gene for autism, causes a reduction in TRP [72].

It follows that if the TRP is a variable subset of the total pool, then RP is often a very sizeable fraction (~15–85% of all vesicles). Why does a large non-functional pool reside at terminals, presumably at considerable energetic cost [26,7]? One suggestion is that these vesicles act as a buffer for soluble accessory proteins involved in vesicle recycling [7]. Another possibility is that the RP operates as a vesicle donor and/or acceptor pool for the TRP. In support of this, evidence suggests that the antidepressant fluoxetine expands the recycling pool at the expense of the resting pool [27]. Similarly, COMS activity has been shown to promote recruitment of vesicles from the RP to the TRP while calcineurin activity has the opposite effect [29,32], and such a mechanism has been implicated in the scaling of the TRP in homeostatic plasticity [29]. A similar conversion of RP into TRP vesicles has been proposed as a mechanistic substrate for a form of NMDA receptor-dependent synaptic potentiation [46]. If the RP acts as a recruitable vesicle reservoir, it offers a possible explanation for why – influenced by activity-driven plasticity – its specific size is highly variable across synaptic populations.

## Readily releasable pool (RRP)

The RRP defines the pool of vesicles that are first to undergo fusion during synaptic activity [10,50]. Estimates suggest that average RRP

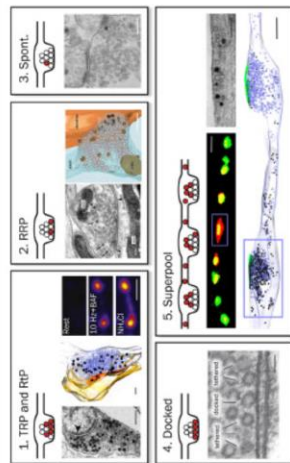


**Fig. 2 – Visual readouts of pool categories.** 1. TRP and RFP. Left, Electron micrograph of synapse from cultured hippocampal neurons after FM1-43-loading and dye photoconversion. FM1-43 is a fluorescent dye that selectively labels vesicles that have undergone activity-driven recycling. Photoconversion allows the visualization of these vesicles by formation of electron-dense precipitate. As such, dark vesicles correspond to the TRP and clear vesicles to the RFP (adapted from [20]). Scale bar, 250 nm. Middle, 3–d reconstruction from acute hippocampal slice using same approach (adapted from [32]). Scale bar, 100 nm. Right, quantification of TRP and RFP using vChart-plotting, a vesicle-associated pH-sensitive reporter. At rest, fluorescence is quenched by the acidic pH of the vesicle. Stimulation evokes a fluorescence rise as pH buffers move onto the extracellular leaflet of the plasma membrane during exocytosis. The presence of halocypin, a blocker of vesicle reacidification, inhibits fluorescence re-quenching after endocytosis, providing a stable readout of the TRP. Addition of  $\text{NH}_4\text{Cl}$  unblocks all pHluorin proteins. The relative differences between stimulation and  $\text{NH}_4\text{Cl}$  steps provides a fractional readout of TRP and RFP (adapted from [29]). Scale bar, 5  $\mu\text{m}$ . 2. RFP. Left, Electron micrograph of RFP based on FM-dye photoconversion. 3–d reconstruction using same approach. RFP vesicles appear brown (adapted from [54]). Scale bars, 100 nm. 3. Spontaneous. Electron micrograph of RFP-labeled vesicle (dark) following spontaneous release (adapted from [51]). Scale bar, 200 nm. 4. Docked pool. Electron micrograph of morphologically docked vesicles (adapted from [65]). Scale bar, 100 nm. 5. Superpool. Middle, Fluorescence image of Synaptophysin 1-Dendra, a photoswitchable fluorophore expressed on vesicles. The protein initially emits green light. A single bouton (blue rectangle) was switched at time 0 to a red-emitting form. The movement of vesicles from the target synapse over 40 min is observed as the spreading of red fluorescence into green neighbors (seen as yellow). Green fluorescence from neighbors also accumulates at the red synapse target. Scale bar, 2  $\mu\text{m}$ . Bottom, 3–d reconstruction of TRP vesicles (black) selectively labeled at target synapse (blue rectangle) spreading along axon to a synaptic neighbour over five minutes (adapted from [57]). Scale bar, 500 nm. Top right, electron micrograph based on FM-dye photoconversion showing appearance of mobile vesicles (TRP, black; resting, clear) trafficking along axon (adapted from [5]). Scale bar, 200 nm.

size is 5–15 vesicles in hippocampal neurons [10,27,58] (Fig. 2). Thanks to the privileged release status of this pool, and therefore its central relevance to signaling properties and synaptic strength determination, the RRP has attracted substantial research interest. Nonetheless, a single defining stimulus paradigm does not exist, sometimes confounding a straightforward interpretation of findings [34,60]. One approach relies on the introduction of hypertonic solution (typically sucrose) evoking calcium-independent vesicle fusion [50] while other paradigms utilize action potential stimulation (typically 10–50 APs at 10–20 Hz, [37,41,68]) triggering vesicle fusion through conventional calcium-dependent processes. Evidence indicates that these methods probably access shared vesicles, but whether the overlap is absolute remains controversial [34,60]. There is an established body of evidence supporting the idea that RRP size and release probability are positively correlated [9,10,33,35] ensuring interest in mechanisms of RRP modulation and its possible role in long-term plasticity. For example, increased activation of protein kinase C induced by phorbol esters is reported to cause the

expansion of the RRP [48,69] and accelerate its refilling rate [58]. A reduction in the size of the RRP has been established in synapses undergoing long-term depression [16] while brain-derived neurotrophic factor (BDNF) has been implicated in pool expansion during long-term potentiation [64].

### Spontaneous pool

Spontaneous neurotransmitter release – which occurs stochastically in synapses at low probability in the absence of stimulation – is thought to play a role in synaptic development, plasticity, homeostasis and excitability [28,63]. A reasonable assumption might be that the vesicles mediating spontaneous transmission are the same as those supporting evoked release. However, in recent years, this idea has been questioned [28,63], researchers instead suggesting that spontaneous release uses a discrete pool of vesicles – effectively a subset of the resting pool which is distinct from those participating

in evoked transmission [14,44,51] (Fig. 2). Consistent with this idea, evidence has accumulated to indicate that this pool has a specific set of postsynaptic targets, distinct fusion machinery, recycling pathways and molecular composition [28]. Other groups, however, propose that the spontaneous pool overlaps with the recycling pool [17,23,70] or a subset of both resting and recycling pools [26]. A possible explanation for these divergent views could be the existence of two pools of vesicles, one released both spontaneously and following stimulus and another undergoing spontaneous recycling exclusively [63], but a final consensus will require further investigation.

### Docked pool

The population of vesicles that are morphologically associated with the active zone forms a special pool category, defined on the basis of their ultrastructural arrangement alone. An attractive feature of the docked pool is that it can be readily quantified in electron micrographs without pre-requisite functional labeling (Fig. 2). At small hippocampal synapses, the mean docked vesicle pool size is ~10 [21,53] and scales with structural parameters including active zone area and post-synaptic density size [53]. Further insight has come with recent developments in high-pressure freezing approaches that offer a substantially enhanced view of the docked pool, revealing that not all vesicles make membrane–membrane contact with the active zone but rather are linked by variable-length tethers [12], perhaps implying heterogeneity in pool composition.

The size of the docked pool is known to correlate with a number of synaptic parameters including synaptic release probability [31] and RRP size [35,54,65]. Nonetheless, the idea that the docked pool is simply the morphological correlate of the RRP is possibly too simplistic. Studies where the TRP (including all RRP vesicles) was maximally labeled before ultrastructural characterization, reveal that the docked pool is only ever partially represented by functional vesicles [5,20,32,46] implying that only a subset of RRP vesicles docked prior to release. Perhaps then, the idea that RRP characteristics scale with a fraction of the morphologically docked pool may be more accurate.

Thanks to the privileged position of its vesicles in the terminal, researchers have identified the docked pool as a possible substrate for disease and plasticity-associated changes in synaptic performance. Leucine-rich repeat kinase 2 (LRRK2) – mutations in which are implicated in inherited Parkinson's disease – has been reported to mediate a reduction in docked pool size in knockdown mice and changes in functional characteristics of synapses [42]. Pharmacological silencing has been demonstrated to bring about increases in docked vesicle number and synaptic release probability [55]. Expansion of the available docking sites in long-term potentiation by conversion of nascent zone into active zone populated with SVs has also recently been reported [7]. One possibility suggested by functional heterogeneity in the docked pool is that rapid changes in release properties might be achievable if docked resting pool vesicles are replaced by functional ones, although this remains to be tested.

### Superpool

In the last decade a new pool classification has emerged which is operationally and organizationally distinct from those outlined

above. The ‘superpool’ defines a vesicle population that is not confined to a synapse, but rather dynamically shared at a high rate (~4% of total pool per minute at each synapse) along axons between multiple presynaptic terminals [57] (Fig. 2). Anterograde and retrograde extrasynaptic vesicle traffic was first established using FM-dyes in somatically-mature hippocampal cultures [53,60] but its relevance to acute brain slices [57] and *in vivo* [12] has since been demonstrated. One important feature of this lateral vesicle traffic is that mobile vesicles can retain their fusion-competence both during transit along the axon [45] thus deviating from conventional modes of point-to-point signaling but also after integration in a new host synaptic terminal [5]. The superpool is comprised of both recycling and resting pool vesicles [5,11] in approximately equal numbers and trafficked along the axon in small mixed vesicle clusters [5,68]. Recent work exploiting super-resolution imaging methodologies has characterized the dynamic trafficking behavior of single superpool vesicles [41,68]. One important consequence of constitutive superpool traffic is its possible impact on the long-term integrity of vesicle clusters, suggesting that specific mechanisms must be present to preserve presynaptic identity [13,57].

Why might such a pool exist? One hypothesis is that the superpool could represent an extrasynaptically recruitable resource that can support dynamic changes in the properties of host terminals [56]. Recent studies have implicated brain-derived neurotrophic factor (BDNF) [57], synapsin [39] and alpha-synuclein [56] as superpool regulators, suggesting possible links between extrasynaptic vesicle traffic and disease-related dysfunction.

### Physical organization of defined pools

The classification of vesicles in functionally-defined pools raises questions about their physical organization in the terminal. In particular, the possibility that the arrangement of vesicles may contribute to or underpin their operational characteristics. Cartoons usually depict the most releasable vesicle pools near the active zone and resting vesicles further back in the cluster but an unequivocal test of this model has proved challenging. Ultrastructural approaches provide the most direct assessment of vesicle organization with respect to other nanoscale elements, but are typically based on selective labeling of recently fused vesicles that are retrieved during endocytosis – either directly from the plasma membrane or through vesicular intermediates [52,65]. As such the labeled vesicles correspond to the pool that has just been accessed but not necessarily those that will be used in a subsequent round of stimulation. Nonetheless, such studies provide interesting insights. Both recycled RRP [32,54] and TRP vesicles [5,20,32] are distributed throughout the terminal after endocytosis albeit with a bias towards the release site [32,54]. Recent evidence based on single vesicle movement and release dynamics using nano-particle labeling of vesicles also reveals a correlation between the apposition of a vesicle to the active zone and its probability of release [41]. Such findings are in general agreement with the idea that physical position of vesicles with respect to the release site may be a determinant of function in small central synapses, and consistent with selective trafficking mechanisms for specific pools based on discrete molecular identifiers (see below). As noted above, a positive relationship between docked pool size and the number of RRP vesicles has been reported [35,54,65] but the assumption that the former is the morphological correlate of



transmission [43]. Vesicles which recycle spontaneously have also been reported to differ from recycling pool vesicles in terms of increased levels of syntaxin 13 and VAMP4, and decreased levels of synaptobrevin 1, synapsin and VAMP2 [47]. It seems plausible, then,

classes. Of course, such n

peptides remain approximately constant in their molecular composition after recycling [38]. Another possible discriminator of  $\alpha$ -synuclein could arise from its interactions with soluble proteins. One candidate is synaptobrevin, which appears to selectively immobilize  $\alpha$ -synuclein [39]. Triple mutants of synaptobrevin covalently increased NP recycling [39]. In addition, interactions with other proteins, such as the superpore [39], DOC2, another soluble protein, has been suggested as a possible tag for the spontaneous pool [39,40]. Taken together, then, a molecular code of sorts – is emerging, but at present is based on often subtle distinctions in multiple protein expression profiles. Improving the sensitivity of these protein assays, and also the precision of our functional pool definitions, will be necessary to take this to the next stage.

## Concluding remarks

ones may include a small subset of highly releasable, pre-purified vesicles [59] as well as a larger complement of more relevant ones [59, 60]. The passage of time is also likely to erode pool integrity. For example, if we operationally define a pool at one point in time, can we assume it has the same vesicular composition at a later time-point? The probable answer is no. One driving force is the substantial redistribution of vesicles between individual synapses and the superpool, with significant turnover across a timescale of minutes [57]. Possible interactions between synapse-specific pools – for example trading of vesicles between resting pool and recycling pools [23, 46] – would also serve to undermine pool identity.

### Acknowledgments

**Molecular 'signatures' of vesicle pools**

## REFERENCES

- What form could a molecular signature take? One possibility is that it could correspond to the number of copies of one or multiple specific proteins or their isoforms expressed on the vesicle membrane. This idea has gained considerable traction in recent years. High levels of VAMP7 have been implicated as a possible identifier of resting vesicles and VGLUT1 and VAMP2 as correlates of the recycling pool [25]. Another synaptic vesicle protein, has been associated with vesits that are mobilized during spontaneous

- [46] A. Ratzupala, V. Marra, D. Bush, J.J. Burden, T. Branco, K. Staras, Recruitment of resting vesicles into recycling pools supports NMDA-receptor dependent synaptic potentiation in cultured hippocampal neurons, *J. Physiol.* 590 (2012) 1585–1597.
- [47] N.H. Borekh, D. Kamin, S. Trachtenbrodt, A.B. Wong, K. Heur-Jensen, E. Beninger, T. Moser, S.O. Rizzoli, A new probe for super-resolution microscopy elucidates trafficking pathways, *J. Cell Biol.* 205 (2014) 591–605.
- [48] S.O. Rizzoli, W.J. Betz, Synaptic vesicle pools, *Nat. Rev. Neurosci.* 6 (2005) 57–69.
- [49] T. Rose, F. Schoenberger, K. Jesek, T.G. Dietner, Developmental refinement of vesicle cycling at Schaffer collateral synapses, *Neuron* 77 (2013) 1109–1121.
- [50] C. Rosenmund, C.F. Stevens, Definition of the readily releasable pool of vesicles at hippocampal synapses, *Neuron* 16 (1996) 207–220.
- [51] Y. Saito, T. Iwamatsu, E. Dohi, X. Liu, E.T. Koyanagi, An isolated pool of vesicles recycles at rest and drives spontaneous neurotransmission, *Neuron* 45 (2005) 563–573.
- [52] T. Schikorski, Readily releasable vesicles recycle at the active zone of hippocampal synapses, *Proc. Natl. Acad. Sci. USA* 111 (2014) 5415–5420.
- [53] T. Schikorski, C.F. Stevens, Quantitative ultrastructural analysis of hippocampal excitatory synapses, *J. Neurosci.* 17 (1997) 5858–5867.
- [54] T. Schikorski, C.F. Stevens, Morphological correlates of functionally defined synaptic vesicle populations, *Nat. Neurosci.* 4 (2001) 157–165.
- [55] D. Scott, S. Ray, alpha-Synuclein inhibits intrasynaptic vesicle mobility and maintains recycling-pool homeostasis, *J. Neurosci.* 32 (2012) 10129–10135.
- [56] K. Staras, T. Branco, Sharing vesicles between central presynaptic terminals: implications for synaptic function, *Front. Synaptic Neurosci.* 10 (2010) 103389/103389fsmv-2010-00020.
- [57] K. Staras, T. Branco, J.J. Burden, K. Poo, K.J. Darcy, V. Marra, A. Ratzupala, Y. Gada, A vesicle superpool spans multiple presynaptic terminals in hippocampal neurons, *Neuron* 66 (2010) 37–46.
- [58] C.F. Stevens, T. Thoreson, Estimates of the readily releasable vesicle pool by protein kinase C, *Neuron* 21 (1988) 885–893.
- [59] C.F. Stevens, T. Thoreson, Estimates for the pool size of releasable quanta at a single central synapse and for the time required to refill the pool, *Proc. Natl. Acad. Sci. USA* 92 (1995) 846–849.
- [60] C.E. Stevens, J.H. Williams, Discharge of the readily releasable pool with action potentials at hippocampal synapses, *J. Neurophysiol.* 98 (2007) 3221–3229.
- [61] T.C. Sudhof, The synaptic vesicle cycle, *Annu. Rev. Neurosci.* 27 (2004) 509–547.
- [62] S. Takamori, M. Held, K. Senjar, E.A. Lemke, M. Grubberg, M. Hecht, H. Urlaub, S. Schenck, B. Brügger, P. Agreier, A. Mayhew, The anatomy of a trafficking organelle, *Cell* 127 (2006) 831–846.
- [63] S. Trachtenbrodt, S.O. Rizzoli, Spontaneous vesicle recycling in the synaptic bouton, *Front. Cell. Neurosci.* 8 (2014) 409.
- [64] W.J. Tyler, X.L. Zhang, K. Hartman, J. Winterer, W. Müller, P.K. Stanton, L. Pozzo-Miller, BDNF increases release probability and the size of a rapidly recycling vesicle pool within rat hippocampal excitatory synapses, *J. Physiol.* 574 (2006) 787–803.
- [65] S. Vatajable, B.K. Rost, M. C. Truchetto-Perez, M.W. Dant, B. Solbiado, Synaptic vesicle recycling and the readily releasable pool at mouse hippocampal synapses, *Nature* 504 (2013) 242–247.
- [66] J. Waters, S.J. Smith, Phorbol esters potentiate evoked and spontaneous release by different presynaptic mechanisms, *J. Neurosci.* 20 (2000) 7863–7870.
- [67] J. Waters, S.J. Smith, Vesicle pool partitioning influences presynaptic diversity and weighting in rat hippocampal synapses, *J. Physiol.* 541 (2002) 811–823.
- [68] V. Weispuhl, S.O. Rizzoli, M.A. Lauterbach, D. Kamin, R. Jahn, S.W. Hell, Video-rate full-field optical tomography dissects synaptic vesicle recycling in hippocampal neurons, *J. Neurosci.* 29 (2009) 1500–1510.
- [69] B.C. Wilheim, S. Mandel, S. Trautwein, K. Kohnert, C. Schuler, B. Renner, S.J. Kim, C.A. Clasen, M. Krauss, V. Hardie, et al., Composition of isolated synaptic boutons reveals the amounts of vesicle trafficking proteins, *Science* 344 (2014) 1023–1028.
- [70] B.C. Wilheim, T.W. Groemer, S.O. Rizzoli, The same synaptic vesicles drive active and spontaneous release, *Nat. Neurosci.* 13 (2010) 1454–1456.
- [71] K. Willmanner, S.M. Pütz, F.E. Schweizer, Proteasome inhibition triggers activity-dependent increase in the size of the recycling pool of vesicles in cultured hippocampal neurons, *J. Neurosci.* 28 (2006) 11333–11341.
- [72] H. Zhao, Y. Kim, J. Park, D. Park, S.E. Lee, L. Chang, S. Chung, SCAMPS plays a critical role in synaptic vesicle endocytosis during high neuronal activity, *J. Neurosci.* 34 (2014) 10085–10095.